

**Novel 3,4-Diazaphospholane Ligands:
Synthesis and Investigation in Rhodium-Catalyzed Hydroformylation**

by
Julia Wildt

A dissertation submitted in partial fulfillment of
the requirements for the degree of

Doctor of Philosophy
(Chemistry)

at the
University of Wisconsin–Madison
2017

Date of final oral examination: Tuesday, December 20, 2016

The dissertation is approved by the following members of the Final Oral Committee:

Clark R. Landis, Professor, Chemistry
Jennifer M. Schomaker, Associate Professor, Chemistry
Steven D. Burke, Professor, Chemistry
John F. Berry, Professor, Chemistry
Ive Hermans, Professor, Chemistry

**Novel 3,4-Diazaphospholane Ligands:
Synthesis and Investigation in Rhodium-Catalyzed Hydroformylation**

Julia Wildt

Under the supervision of Professor Clark R. Landis

University of Wisconsin–Madison

Abstract

Hydroformylation is one of the largest homogeneously catalyzed transformations in industry, leading to important aldehyde products from alkene starting materials. Asymmetric hydroformylation on the other hand is underdeveloped. The challenge is to maintain high regio- and enantioselectivities for the resulting branched aldehyde. Extensive research is performed on the development and synthesis of chelating bisphosphorus ligands to help control the desired selectivities. However, the substrate scope is only limited for any single ligand. With the discovery of the class of bisdiazaphospholane ligands by Landis and coworkers, new paths were opened in addressing a broad scope of substrates over the years. The ligand (S,S,S)-BisDiazaPhos represents a state-of-the-art ligand, that can hydroformylate a variety of substrates with fast rates, while maintaining both high regio- and enantioselectivity. This work focuses on the synthesis of novel 3,4-diazaphospholane ligands to expand the existing library and to address new substrates or improve upon existing selectivities.

Chapter 3 shows that racemic 2,5-phenyl- and naphthyl-substituted bisdiazaphospholanes, containing the acylhydrazine backbone, can be reduced with BH_3 to yield alkylhydrazine-based bisdiazaphospholanes. These reduced ligands have been tested in the rhodium-catalyzed hydroformylation of different substrate classes. Interestingly, the regioselectivity with the reduced ligands was improved compared to their non-reduced analogues. This improvement is considered to come from the conformational change in the ring structure, where an increased torsion angle

within the ring correlates to higher regioselectivities. A steric quadrant model is used to rationalize the improved regioselectivities for the reduced bisdiazaphospholanes.

Chapter 4 describes the development of boronate bearing diazaphospholanes as directing or scaffolding ligands for the purpose of intramolecular hydroformylation of the challenging substrate class of allylic and homoallylic alcohols. This concept takes advantage of functional groups that can coordinate covalently to a substrate and datively to a metal center, leading to improved selectivity and reactivity compared to a non-directed transformations. The synthesis of these novel boronate bearing diazaphospholanes is laid out. The directed hydroformylation of allylic substrates was not observed with mono-diazaphospholanes. The synthesis towards chelating bisdiazaphospholane is described and thought to have the potential to gain further insights into the directing effects of bisdiazaphospholane structures.

DEDICATION

I dedicate this work to my parents, Maria and Christian Wildt, for their constant support in what I do and their endless love. To my brother, Stefan, for believing in me and encouraging me in my live decision. To my wonderful and loving husband and best friend, Travis Sunderland, for the greatest support and motivation in all parts of life we have been through together.

Acknowledgements

I would like to thank my advisor, Professor Clark R. Landis, for mentoring me over the last four and half years. I am very thankful to him for accepting me into his research group when I came to UW Madison as a non-typical first-year student. I appreciate his very patient and kind personality and am grateful for his mentorship as well as him driving my motivation, success and improvement in my scientific development. In addition, I am thankful that he provided me with the opportunity to be part of our industrial collaboration with the Dow Chemical Company, which had a substantial influence on my scientific carrier.

I am very grateful to the members of the Landis group for the supportive and collegial working environment. All previous and current members influenced my scientific, as well as personal, development over the years. Thanks to all group members for their help when I first joined the group, especially to Gene Wong, you are greatly missed. Thank you to my current office-mates Floriana Foarta, Brad Jones and Josephine Eshon for providing a comfortable working atmosphere, the fun and discussion about scientific and non-scientific topics. The rest of the Landis group crew, Anna Brezny, Heather Johnson, Eric Cueny, Katie Ziebarth, Maurus Schmid, Stephanie Blaszczyk and Anna Dunn for their support and encouragement throughout fun times as well as hard and challenging times. Jessica Roberts, why didn't you join UW Madison earlier, my Zumba Buddy! Thank you to Leigh Abrams and Spring Knapp for their motivating discussions about our projects and scientific expertise. To Kristi Heming, for everything she has done for me starting with helping me out from the very beginning.

I appreciate all the time I got to share with Amanda Corcos, Ryan Pakula, Kasia Kornecki and Wes Brogden outside of the chemistry department. Your support and motivation means very much to me. Thank you to my good friends Floriana Foarta, Brandon Kilduff, Julia Nault and Ambar Rana for their friendship outside the department, all the fun times exploring Madison and playing disc golf that we were able to share.

To my best friend Mitra Weber, thank you for going with me through a challenging 5 years of school, for all the laughter and incredibly valuable times together. I am incredibly thankful to my family, my parents Maria and Christian and my brother Stefan. Despite seeing their only daughter and only sister leave the country to be with the love of her life and pursue a scientific carrier, they offered me a tremendous amount of support. They provided me with the strength of continuing and finishing what I have started. For always believing in me and making me to a stronger person. Without you, I would have never been able to be where I am as a person.

To my new family, Nancy and Steve Sr., and Nadine and Steve. I could not have wished for a better substitute for my own family. Thank you for accepting me into the family. I will never forget your support and everything you have done for me and am looking forward for all the times we are going to share.

All of the thank yous in this world are not enough to express my gratefulness to my wonderful and amazing husband Travis Sunderland. Without you, I would not be the person I am to date. Thank you for your unlimited support throughout very important parts of my life. You have made my life better. Thank you to the unlimited support and help coming to a new country and new education system. Without you I would not know what true love is.

Table of Contents

Abstract	i
Dedication	iii
Acknowledgments	iv
Table of Contents	vi

Chapter 1: Wisconsin Initiative for Science Literacy: My Research Explained to a Lay Audience 1

1.1 Chemistry with Transition Metals and Phosphorus Containing Molecules	2
Figure 1.1. The periodic table of the elements.	3
1.2 Catalysis	3
Figure 1.2. Two possible pathways to get to the other side of the mountain (left) and the scientific visualization for energy barriers.	4
Scheme 1.1. Production of aldehydes with a rhodium catalyst (hydroformylation).	5
1.3 Chirality	5
Figure 1.3. Chirality demonstrated by non-superimposable mirror images of our hands (top) and ‘molecules’ (bottom).	6
Figure 1.4. Three sets of chiral pharmaceutical molecules, Ibuprofen (top), Naproxen (middle) and Thalidomide (bottom).	7
1.4 My Specific Research	7
Figure 1.5. General type of diazaphospholane ligand framework (left) and specific structure of interest, the groups to modify are circled in red (right).	9
1.5 How to Know Which Molecule I Made – NMR Spectroscopy	10
Figure 1.6. Proton (^1H) nuclear magnetic resonance (NMR) spectrum of ethanol (EtOH).	11

1.6 References	11
Chapter 2: Rhodium-Catalyzed Hydroformylation of Alkenes with Phosphorus-based Ligands	12
2.1 Introduction	13
Scheme 2.1. Rhodium-catalyzed hydroformylation of alkenes.	13
Figure 2.1. The aldehyde group as an important intermediate in synthesis of bulk chemicals.	14
Figure 2.2. Tolman cone angle (θ) as a characterization method for monophosphines (left) and the bite angle (α) for bidentate phosphorus ligands (right).	15
Figure 2.3. Decrease of hydroformylation rates with increasing substitution on the alkenes.	16
2.2 Bisphosphite Ligands	17
Figure 2.4. Commonly used bisphosphite ligands 1 , 2 and 3 .	17
Table 2.1. Hydroformylation of Benchmark Substrates with Selected Bisphosphite Ligands.	18
2.3 Bisphosphine Ligands	19
Figure 2.5. A selection of bisphosphine ligands used in rhodium-catalyzed hydroformylation.	20
Figure 2.6. High selectivity for 1,1-disubstituted alkenes with ligands 15 and 16 .	20
Table 2.2. Hydroformylation of Benchmark Substrates with Selected Bisphosphine Ligands.	21
2.4 Bisphospholane Ligands	22
Figure 2.7. The bisphospholane classes DuPhos, Ph-BPE and BisDiazaPhos.	22

Scheme 2.2. Synthesis of the bisdiazaphospholane ligand framework.	23
Scheme 2.3. Synthesis of the state-of-the-art ligand (S,S,S)-BisDiazaPhos 20 .	23
Scheme 2.4. Improved synthesis of 20 with propylphosphonic anhydride T3P.	24
Scheme 2.5. Synthesis to chiral 1,2-diacyl cyclohexane backbone bearing bisdiazaphospholane.	24
Figure 2.8. TangPhos ligands 21 and the Bis(TangPhos)-Rh complex.	25
Table 2.3. Hydroformylation of Benchmark Substrates with Selected Phospholane Ligands.	26
Table 2.4. Substrate Scope for (S,S,S)-BisDiazaPhos 20 .	27
2.5 Hybrid Phosphine-Phosphite and Other Phosphorus Ligands	28
Figure 2.9. Hybrid phosphorus ligands 23 , 24 and 25 and other ligands 26 and 27 .	28
Table 2.5. Hydroformylation of Benchmark Substrates of Selected Hybrid Ligands.	30
Figure 2.10. Hydroformylation results of cyclic alkenes with ligand 28 .	31
2.6 Mechanism of Rhodium-Catalyzed Hydroformylation with BisDiazaPhos Ligands	31
Figure 2.11. Mechanism of rhodium-catalyzed hydroformylation of alkenes.	32
Figure 2.12. Dependency of CO-pressure (left) and H ₂ -pressure (right) on regio- (b : l) and stereoselectivity (<i>R</i> : <i>S</i>) with (S,S,S)-BisDiazaPhos ligand 20 .	33
Figure 2.13. Qualitative energetic map with steric and electronic influences on the orientation of alkene bound to the RhH(CO)-ligand complex.	34
2.7 Conclusion	35
2.8 References	36

Chapter 3: Regioselective Rhodium-Catalyzed Hydroformylation of Alkenes

Utilizing Backbone-Modified Bisdiazaphospholanes 40

3.1 Introduction 41

Scheme 3.1. Rhodium-catalyzed hydroformylation of alkenes.	41
Figure 3.1. Ligands (<i>R,R</i>)-Ph-BPE and (<i>S,S,S</i>)-BisDiazaPhos.	42
3.2 Results and Discussion	43
3.2.1 Synthesis of Electronically Reduced Bisdiazaphospholanes	43
Scheme 3.2. Reduction of the acylhydrazine backbone of bisdiazaphospholanes towards an alkylhydrazine red-BDPs using $\text{BH}_3 \cdot \text{THF}$.	43
Figure 3.2. Bisdiazaphospholanes 1, 3, 5 and 7 and their reduced derivatives 2, 4, 6 and 8.	44
Figure 3.3. Methine protons in the ^1H NMR spectra of ligands 1 and 5, coupling constants determined with the WINDNMR simulation program (red: experimental; blue: simulated).	46
Figure 3.4. BDP ligands TPSB BDP 1 (left) and TPSB BDPE 5 (right) indicating the conformational difference due to the bridge between the P-atoms (P–C–C–P shown as spheres).	47
3.2.2. Hydroformylation of Benchmark Substrates Styrene, Vinyl Acetate and Allyl Cyanide	47
Table 3.1. Hydroformylation of Benchmark Substrates Styrene, Vinyl Acetate and Allyl Cyanide.	48
Table 3.2. Hydroformylation of Benchmark Substrates Styrene, Vinyl Acetate and Allyl Cyanide.	50
3.2.3 Hydroformylation of Allylic Alkenes	51
Table 3.3. Screening of Allylic Alkene Substrates.	53
3.2.4. Hydroformylation of Cyclic Heteroatom-Containing Alkenes	54
Table 3.4. Hydroformylation of Cyclic Alkenes.	56
3.2.5. Summary and Conclusions Regarding Reduced Ligands	57
Table 3.5. Total Fold Increase in Branched Regioselectivity of red-BDP Compared	

to BDP; Numbers in () Indicating a Decrease in the Selectivity for the α -Product.	58
3.2.6 Conformational Analysis of Reduced Ligands	58
Figure 3.5. Definition of the torsion angle (θ) within the diazaphospholane moiety.	59
Figure 3.6. Crystal structures of red-TPSB BDP 2 (left, $\theta = 62.1^\circ$) and TPSB BDP 1 (right, $\theta = 19.2^\circ$), oriented along the N–N bond of one of the diazaphospholane rings (blue: nitrogen atoms, orange: phosphorus atoms, red: oxygen atoms).	59
Figure 3.7. Crystal structures of red-TPPB BDP 4 (left, $\theta = 56.0$) and TPPB BDP 3 (right, $\theta = 10.4^\circ$), oriented along the N–N bond of one of the diazaphospholane rings (blue: nitrogen atoms, orange: phosphorus atoms, red: oxygen atoms).	60
Figure 3.8. Calculated structures of red-TPSB BDPE 6 (left, $\theta = 56.4$) and TPSB BDPE 5 (right, $\theta = 14.0^\circ$), oriented along the N–N bond of one of the diazaphospholane rings (blue: nitrogen atoms, orange: phosphorus atoms, red: oxygen atoms).	60
Figure 3.9. Crystal structures of red-TNSB BDP 8 (left, $\theta = 58.9^\circ$) and TNSB BDP 7 (right, $\theta = 33.4^\circ$) oriented along the N–N bond of one of the diazaphospholane rings (blue: nitrogen atoms, orange: phosphorus atoms, red: oxygen atoms).	61
Figure 3.10. Calculated (blue bars, B3LYP/6-31G(d)) and experimental (red bars, X-ray crystallography) torsion angle of diazaphospholane rings in reduced BDPs, Ph-BPE and BDPs.	62
Figure 3.11. Crystal structure of [Rh(acac)(1)] oriented along the N–N bond of one of the diazaphospholane rings with a torsion angle (θ) of 21.7° .	62
Figure 3.12. Relative energies of the steric transition-state model for [RhH(CO)propene(2)] of four orientations in the steric map (right, blue boxes are shaded based on the steric bulk (dark blue: biggest steric bulk). As an example,	

complex [RhH(CO)propene(2)] for the b- <i>Si</i> conformation is depicted (left).	
calculations were performed using B3LYP/LAN2DZ.	64
Figure 3.13. Comparison of relative energies for [RhH(CO)propene(1)] (left)	
and [RhH(CO)propene(2)] (right) for the steric model.	65
3.2.7 Routes to Resolved Reduced Bisdiazaphospholanes	66
Scheme 3.3. Classical resolution of <i>trans</i> -cyclohexane dicarboxylic acid (CHDC)	
with (S)-methylbenzylamine and subsequent chlorination of isolated (S,S)-CHDC.	66
Scheme 3.4. Synthesis of the chiral cyclohexane backbone containing BDP 9 .	67
Scheme 3.5. Borane-reduction of enantiopure TP CHB ligand 10 .	68
3.2.8 Borane Reduction of Tetraamide containing BDPs.	68
Scheme 3.6. Borane-reduction applied to tetraamide containing BDPs 11 and 12 .	68
Figure 3.14. Mixture of three reduced Tetraamide BDPs 12 observed in the	
³¹ P NMR spectrum.	69
3.2.9 Investigation of the Borane-Reduction of Tetracarboxylicacid BDP	70
Scheme 3.7. Reaction of racemic Tetraacid BDP with BH ₃ •THF to yield 13 .	70
Scheme 3.8. Esterification of red-Tetraacid BDP for purification attempts.	71
3.3 Conclusion and Future Work	71
Scheme 3.9. Potential for classical resolution of 2 with	
(1S)-(+)-10-Camphorsulfonic acid.	73
Figure 3.15. Next generation of proposed new reduced BDP ligand.	73
Scheme 3.10. Proposed synthesis to a hybrid red-Diazaphos-Phosphonite ligand.	74
3.4 Experimental Section	74
3.5 References	86

Chapter 4: Diazaphospholane Ligands with Boronate-containing

Directing Groups for Rhodium-Catalyzed Hydroformylation 90

4.1 Introduction 91

Scheme 4.1. Directed epoxidation (top, Henbest) and cyclopropanation (bottom, Winstein). 91

Scheme 4.2. Substrate-directed catalytic hydrogenation (Thomson). 92

Figure 4.1. Intramolecular transformation through a reagent- or catalyst-directing group DG. 92

Scheme 4.3. Synthetic routes towards the “Roche Aldehyde”. 93

Scheme 4.4. Aldehyde products from the hydroformylation of allylic and homoallylic alcohols. 94

4.1.1 Stoichiometric Directing Groups for Regio- and Stereoselective Control in Rhodium-Catalyzed Hydroformylation 94

Scheme 4.5. Intramolecular hydroformylation in the synthesis of (+)-phyllanthocin. 95

Scheme 4.6. High regioselectivity of allylic alcohol substrates controlled by the *o*-DPPB group. 95

Scheme 4.7. Directed branched selective hydroformylation of the phosphine-tethered alkene **E**, in contrast, the control reaction with 1-hexene leads to linear aldehyde. 96

Scheme 4.8. Branched selective hydroformylation through use of a phosphite directing group. 97

4.1.2 Catalytic Catalyst-Directing Groups and Scaffolding Catalysis 97

Figure 4.2. Catalytic cycle with a scaffolding ligand acting as a catalytic catalyst directing group. 98

Scheme 4.9. Branched-selective hydroformylation of homoallylic alcohol with the

catalytic directing group Ph ₂ POMe and the mechanism proposing a six-membered metallacycle.	99
Scheme 4.10. Tan's aminated phospholane ligand L capable of covalent coordination of a substrate and selective hydroformylation towards the branched aldehyde product; the proposed mechanism features a seven-membered cyclic transition state N .	100
Table 4.1. Selective Hydroformylation of Hydroxy Containing Alkenes with Tan Ligand L .	101
Scheme 4.11. Directed hydroformylation of protected allyl amine with enantiopure ligand P .	102
Scheme 4.12. Reversible and facile exchange of alcohols in boronic acids and esters.	102
Figure 4.3. Boronate bearing bisdiazaphospholanes as potential scaffolding ligands in catalysis.	103
4.2 Results and Discussion	103
4.2.1 Synthesis of Boronate Containing Azines	103
Scheme 4.13. 1,2-dihydro-1-hydroxy-2,3-benzodiazaborene 2 as the major product from an intramolecular cyclization reaction of 2-formylphenyl boronic acid and hydrazine.	104
Scheme 4.14. Reaction of 3-formylphenyl boronic acid and hydrazine to form azine 3 .	105
Scheme 4.15. Protection of 2- and 3-formylphenylboronic acid with pinacol and subsequent reaction with hydrazine to the Bpin azines 6 and 7 .	105
4.2.2 Synthesis of Boronate-Bearing Diazaphospholanes	106
Scheme 4.16. Synthesis of <i>o</i> - and <i>m</i> -Bpin DiazaPhos 8 and 9 .	106
Figure 4.4. Crystal structure of <i>o</i> -Bpin DiazaPhos 8 shown with 50% probability ellipsoids. All H atoms, minor components of the disorder, and the DCM solvent molecules are omitted.	107
Scheme 4.17. Deprotection of the pinacol group with diethanolamine followed	

by hydrolysis.	108
Scheme 4.18. Synthesis of the control ligands Me Diazaphos 16 and 17 .	109
Figure 4.5. Crystal structure of <i>o</i> -Me DiazaPhos 16 shown with 50% thermal probability ellipsoids. All H atoms and minor disordered components are omitted for clarity.	109
4.2.3 Rhodium-Catalyzed Hydroformylation of Hydroxy Containing Alkenes	109
Table 4.2. Hydroformylation of Benchmark Substrates with Ligands 12 , 13 , 16 and 17 .	110
Table 4.3. Hydroformylation of Allylic and Homoallylic Alcohols with Ligand 12 , 13 , 16 and 17 .	111
4.2.4 Investigations on the Synthesis of Boronate-Bisdiazaphospholanes	112
Scheme 4.19. Direct reaction of 1,2-bisphosphinobenzene and succinyl chloride to an acyl phospholane when using sterically demanding Bpin Azines 6 and 7 rather than bisdiazaphospholane formation 18 .	113
Figure 4.6. Reaction of 1,2-bisphosphinobenzene, 3 and succinyl chloride leading to a <i>m</i> -B(OH) ₂ BisDiazaPhos isomer mixture in a 8 : 1 : 1 : 8 ratio and challenging to separate.	114
Scheme 4.20. Route to the ethylene glycol protected azine 20 and subsequent reaction with phenylphosphine and succinyl chloride to give ligand 21 .	115
Figure 4.7. Synthesis of <i>m</i> -Bgly BisDiazaPhos 22 (top) and the ¹ H and ³¹ P NMR spectra showing the <i>racemic</i> conformation in the diazaphospholane rings suggested by the splitting pattern.	116
Scheme 4.21. Unselective reaction of glycol ester 23 and hydrazine to form some azine 24 and majorly diazaborine side products.	117
4.2.5 Attempts on the Synthesis of a Boronate-Containing Mimic of the Tan Ligand	117
Scheme 4.22. Potential route for the synthesis to the boronate mimic of the Tan	

Ligand.	117
Scheme 4.23. Synthesis towards the secondary (hydroxyphenyl)phenyl phosphine as the potential precursor to the boronated Tan Ligand mimic.	118
Figure 4.8. ^{11}B (left) and ^{31}P NMR (right) spectra of the reaction of 25 with $\text{B}(\text{OMe})_3$ and NaH .	119
Figure 4.9. Reaction of hydroxy phosphine 25 with BCl_3 and NEt_3 .	120
Scheme 4.24. Proposed future work on the boronate containing Tan Ligand mimic.	120
4.3 Conclusion and Outlook	120
Scheme 4.25. Esterification of the boronic acid with homoallylic alcohol followed by HF .	121
Scheme 4.26. Synthesis towards other boronate containing Bisdiazaphospholanes.	122
Figure 4.10. Boronate phosphine series with varying distance between the P- and B-atom.	123
Scheme 4.27. Potential separation of diastereomers through use of a chiral boronate group.	123
4.4 Experimental Methods	124
4.5 References	134
Appendix 1: A Sterically Reduced Diazaphospholane	137
A1.1 Introduction	138
Figure A1.1. Sterically reduced bis-azaphospholanes with varying ring sizes (top) and sterically reduced, direct analogues to succinyl bisdiazaphospholanes (bottom).	138
A1.2 Results and Discussion	139
A1.2.1 Investigation of Sterically Reduced BiaDiazaPhos	139
Scheme A1.1. Synthesis of 1 via a melt reaction of phenylphosphine with	

Paraformaldehyde.	139
Figure A1.2. Observed retro-addition upon reacting of 1 with hydrazine.	140
Scheme A1.2. Reaction of bis(hydroxymethyl)phosphine and <i>p</i> -TsCl yields product 3 .	140
Scheme A1.3. Monodiazaphospholane 4 synthesis with 1 and 1,2-dimethylhydrazine•2HCl.	141
Figure A1.3. Synthesis of 5 and the ^1H (left) and $^{31}\text{P}\{^1\text{H}\}$ NMR spectrum (right).	142
Figure A1.4. Synthesis and ^1H (left) and ^{31}P NMR spectrum (right) of ligand 6 .	143
A1.2.2 Hydroformylation Results with <i>N,N,N,N</i> -Tetramethyl BisDiazaPhos 6 and Investigation of its Rhodium-Complexes	143
Table A1.1. Hydroformylation Results with Ligand 6 .	144
Figure A1.5. Consumption (circles) and %branched aldehyde formation (triangles) of styrene obtained with the WiHP NMRR (left) using ligand 6 and ^{31}P NMR spectrum (right) after 16 h.	145
Figure A1.6. Reaction between 6 and $[\text{Rh}(\text{acac})(\text{CO})_2]$ yields complexes 7 and 8 (top $^{31}\text{P}\{^1\text{H}\}$ NMR spectrum) and $^{31}\text{P}\{^1\text{H}\}$ NMR spectrum after reaction of 7 and 8 with syngas (bottom).	146
Figure A1.7. Interconversion of complex 8 in the presence (top) or absence (bottom) of CO and 8 proposed as a five-coordinate CO-complex of 7 .	147
Figure A1.8. IR-stretching frequencies of a potential dinuclear Rh-complex with ligand 6 compared to the frequencies of the Wilkinson yellow dimer.	148
A1.3 Conclusion and Future Work	148
Scheme A1.4. Bicyclic BisDiazaPhos ligands of interest and their proposed synthesis.	149
Scheme A1.5. Proposed synthesis of 4- and 6-membered heterocyclic phosphines.	149
A1.4 Experimental Methods	150
A1.5 References	155

Appendix 2: Investigations of P–H Bond Insertion Reactions Into Metal-Carbenoids	156
A2.1 Abstract	157
A2.2 Introduction	157
Scheme A2.1. Reaction of a dirhodium paddlewheel complex and a diazo compound to form a rhodium-carbenoid complex.	158
Figure A2.1. Chiral phosphines potentially produced through carbenoid insertion into P–H-bonds.	159
A2.3 Results and Discussion	159
A2.3.1 Investigation of the Insertion Reaction into the P–H Bond of Diphenylphosphine	159
Scheme A2.3. Reaction of diphenylphosphine and a diazo compound with Rh ₂ (tpa) ₄ .	159
Figure A2.2. Products 3 , 4 and 5 obtained from reaction of phosphine 1 and diazo 2 with or without catalyst and the corresponding ³¹ P NMR spectrum.	161
Figure A2.3. Tested catalysts IrCl ₂ (phebox)(H ₂ O) and IrCl ₂ (tpp)(CH ₃).	162
Scheme A2.4. Switchable phosphination based on the reagent used.	162
A2.3.2 Borane-protected Diphenylphosphines and Reactivity in P–H Insertion Reactions	162
Figure A2.4. NMR splitting pattern for the Ph ₂ PH•BH ₃ 6 adduct.	163
Scheme A2.5. B–H bond insertion preferred over a P–H bond insertion.	164
Scheme A2.6. Borane-phosphine adducts 8 and 9 are too labile under the reaction conditions. As a result, a product mixture from the direct reaction between phosphine 1 and diazo 2 is observed (Figure A2.1).	165
Figure A2.5. Single, unidentified phosphine product in the reaction of 10 and 2 .	165
A2.4 Conclusions and Future Work	166
Scheme A2.7. Proposed synthesis towards a phospholane through a reaction with a <i>bis</i> (diazo).	166
A2.5 Experimental Methods	166

A2.6 References

169

Appendix 3: Supporting Information

171

Chapter 1

Wisconsin Initiative for Science Literacy: My Research Explained to a Lay Audience

1.1 Chemistry with Transition Metals and Phosphorus Containing Molecules

Chemistry is the study, manipulation and application of the chemical elements. All of the elements can be arranged in a systematic way, displayed in what is known as the periodic table seen below in Figure 1.1.¹ The periodic table arranges the elements into different categories in several ways such as periods (rows), groups (columns) or blocks (the different colored sections in Figure 1.1) based on the properties of the elements in those categories. The largest block of the periodic table, where the largest number of elements are found, is the yellow section in Figure 1.1 called the transition metals, or d-block. Transition metals have many common uses in everyday items such as tools and building materials (iron (Fe), nickel (Ni) and copper (Cu)), currency (silver (Ag) and gold (Au)) and jewelry (nickel (Ni), rhodium (Rh), silver (Ag), platinum (Pt) and gold (Au)). While many of the transition metals can be used in their elemental form, such as a 24k gold ring or a solid bar of gold, more commonly chemists and nature incorporate them into parts of molecules. An example of this from nature is hemoglobin, a protein found in all of our red blood cells, which is a large molecule that has the transition metal iron as part of its structure that is responsible for transporting oxygen in our bloodstream. The iron atom in hemoglobin is held in place by being attached (bonded) to other atoms within the molecule, four nitrogen atoms in this example. Transition metals can bind to many types of other atoms, but usually they can be found attached to atoms such as carbon (C), nitrogen (N), oxygen (O), phosphorus (P), sulfur (S) and chlorine (Cl), all found together in the upper right section of the periodic table. The majority of my work found in this thesis has been focused on making new molecules, which have phosphorus atoms in them that will be used to bind to the transition metal rhodium (Rh). Molecules that contain rhodium (often with phosphorus atoms attached to the rhodium atom) are of interest because they often can perform interesting reactions. Even though rhodium is one of the rarest and most expensive elements that exists, often the reactions that it can perform motivate chemists to continue making new molecules that contain it. One factor that can make these expensive molecules more affordable to use is that often they can make a reaction faster and perform the

reaction many times over and over. This type of molecule is usually given a special name, a catalyst.

Periodic Table of the Elements

The periodic table is organized into groups (columns) and periods (rows). The groups are labeled with Roman numerals and letters (IA, IIA, etc.) at the top. The elements are color-coded into categories: Alkali Metal (pink), Alkaline Earth (orange), Transition Metal (yellow), Basic Metal (green), Semimetal (light blue), Nonmetal (blue), Halogen (purple), Noble Gas (light purple), Lanthanide (light orange), and Actinide (light pink).

Legend:

- Alkali Metal
- Alkaline Earth
- Transition Metal
- Basic Metal
- Semimetal
- Nonmetal
- Halogen
- Noble Gas
- Lanthanide
- Actinide

Figure 1.1. The periodic table of the elements.

1.2 Catalysis

Catalysts are special types of molecules that are usually described as molecules neither created nor destroyed during the reaction. Catalysts make the reaction faster by lowering the activation energy of the reaction. This definition can be a little confusing, so we can use a real-life example to better understand what a catalyst can do in a reaction. If we wanted to travel from Germany to Italy, we would have to cross over the Alps, like the people are trying to do in Figure 1.2.² If we were the mountain climber, we would have to climb over the top of each mountain to get to the other side. This pathway to cross the Alps is going to take a lot of time and energy, this pathway would be similar to a reaction with no catalyst. If we look again at the picture in Figure 1.2, we can see there is another pathway to cross the Alps, instead of going over the top of each

mountain, we could use the tunnel and go through the mountains. This alternative pathway will be much faster and save us a lot of energy to get to the other side, this is what can happen when we use a catalyst in a reaction, it can speed up the reaction by opening up a new pathway to perform the desired transformation. In addition to the new pathway being opened, the car in Figure 1.2 is not destroyed by crossing through the mountain, which means it will still be available to carry us through the mountain again and again. Even though it would cost a lot of money to buy the car to drive us through the mountain, rather than climb over the top, if we use the car for numerous trips, the cost of each trip will continue to decrease making it more worth it to use the expensive car route. Turning back to chemistry, if we want a reaction to take place, converting molecules A and B into C for example, adding a catalyst to the mixture can open up a new pathway that didn't exist before. A typical graph of how scientist visualize the energy difference is shown on the right in Figure 1.2.³

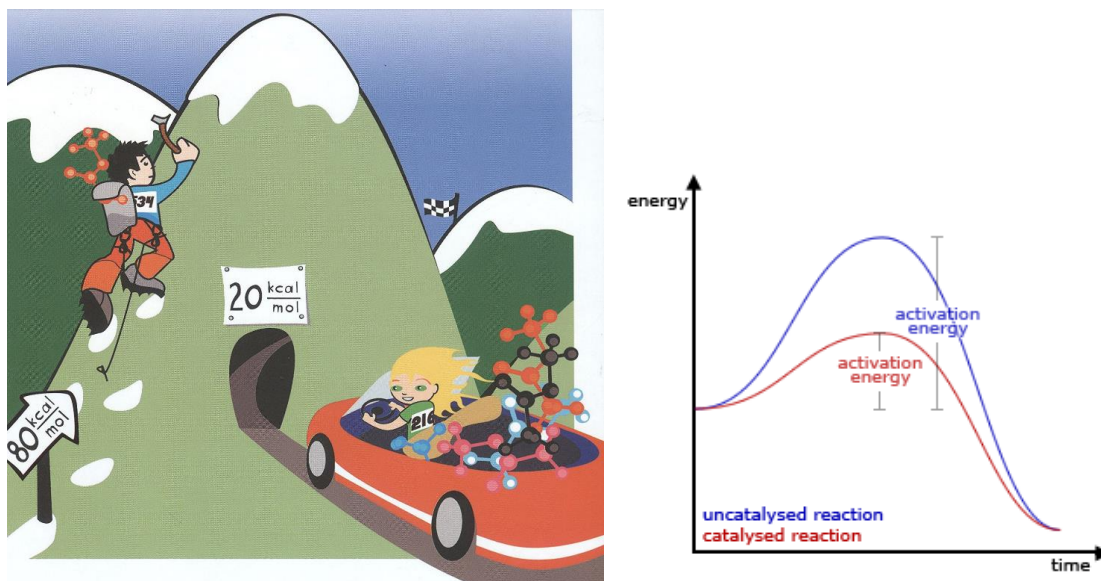
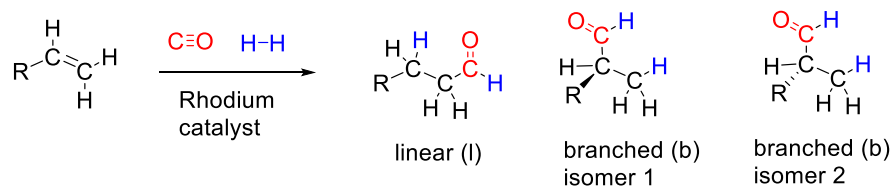


Figure 1.2. Two possible pathways to get to the other side of the mountain (left) and the scientific visualization for energy barriers.

In my research, the rhodium containing molecules I use, are added into the reaction to help bring three different molecules together: hydrogen (H_2), carbon monoxide (CO) and a molecule

with a carbon-carbon double bond (alkene or olefin) to create one new molecule with an aldehyde (CHO) functional group with a rhodium catalyst (Scheme 1.1). This reaction is called hydroformylation. One complication that can occur with the reactions I study, is that there can be multiple versions of each product that is formed (isomers), being able to carefully control which product is formed is important, because the structure of the molecules can have serious consequences on their properties. Aldehyde are important groups found in a variety of other chemicals, such as perfumes and drugs like Ibuprofen and Vitamin C and are necessary to produce other materials such as the Nylon material. Depending on which area this molecule is used in, it is very important to control which isomer is formed, whether the linear or branched isomer is formed. When the branched product is produced, it is also of importance if the branched isomer 1 or isomer 2 is formed.



Scheme 1.1. Production of aldehydes with a rhodium catalyst (hydroformylation).

1.3 Chirality

When we think about the structures of molecules, it is usually easy to quickly distinguish molecules as different from each other, they usually have different types of atoms in them, or the atoms are arranged in a different order that we can quickly see (isomers). Sometimes molecules appear identical in almost every way, but they are still different. A nice example of this can be seen for each of us, our own two hands. When we examine our left and right hands, each is attached to our wrist, each has the same five fingers attached in the same way, they appear identical (ignoring any minor imperfections). If we hold our hands next to each other, as in Figure

1.3, we see that they are mirror images of each other. Now for fun, try to exactly overlay your hands on top of each other, it can't be done, they are different from each other! This concept of non-superimposable mirror images (our hands for example) also exists in molecules, we call it chirality. An example that more closely resembles a molecule can also be seen in Figure 1.3.⁴ The left and right 'molecules' each have one square, circle, oval and triangle attached to a central point, they are mirror images of each other, but if we try to superimpose the two 'molecules' onto each other, it can't be done. These two 'molecules' are chiral and each version is given a special name, an enantiomer. The spatial arrangement of atoms or groups of atoms, called stereochemistry, is an important feature in molecules, especially those we put into our bodies.

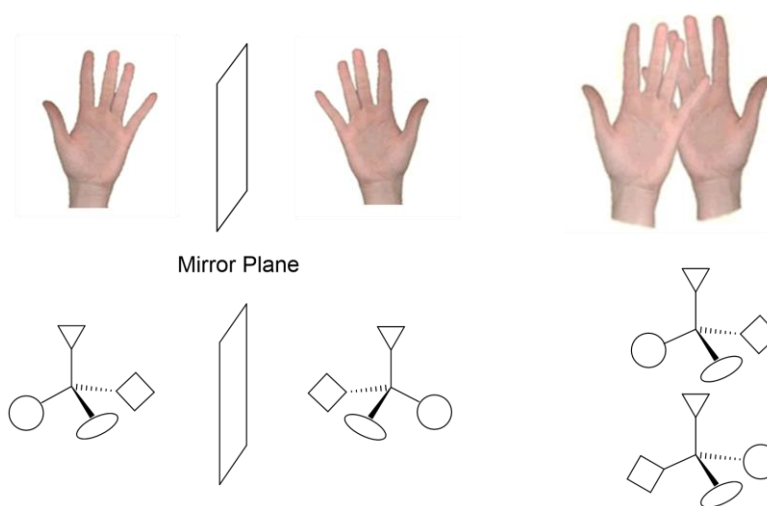


Figure 1.3. Chirality demonstrated by non-superimposable mirror images of our hands (top) and 'molecules' (bottom).

Being aware of the stereochemistry of pharmaceutical drugs we put into our body can be crucial, because the different versions of each drug can interact differently with the proteins and receptors in our bodies. We can look at three examples of common drug molecules to demonstrate how important stereochemistry can be. One example is Ibuprofen, which exists as two enantiomers (just like our right and left hands). It turns out only one version of Ibuprofen is

the active drug, while the other version has no positive or negative effects, which is not always the case. Another drug molecule similar to Ibuprofen is Naproxen, shown in Figure 1.4. While (S)-Naproxen (Figure 1.4, left) is the active version of the anti-inflammatory drug, its mirror image (R)-Naproxen (Figure 1.4, right) is a liver toxin. Another historical example, which had unexpected negative consequences, is Thalidomide (Contergan). This drug was originally developed in West Germany in the 1950's and marketed to pregnant women to treat against morning sickness. Like the other two examples described above, Thalidomide exists as two enantiomers, one helps with morning sickness, however, the other caused severe birth defects and death of thousands of babies. The different effects and consequences that nearly identical molecules can have makes the ability to control their synthesis an important challenge for synthetic chemists.

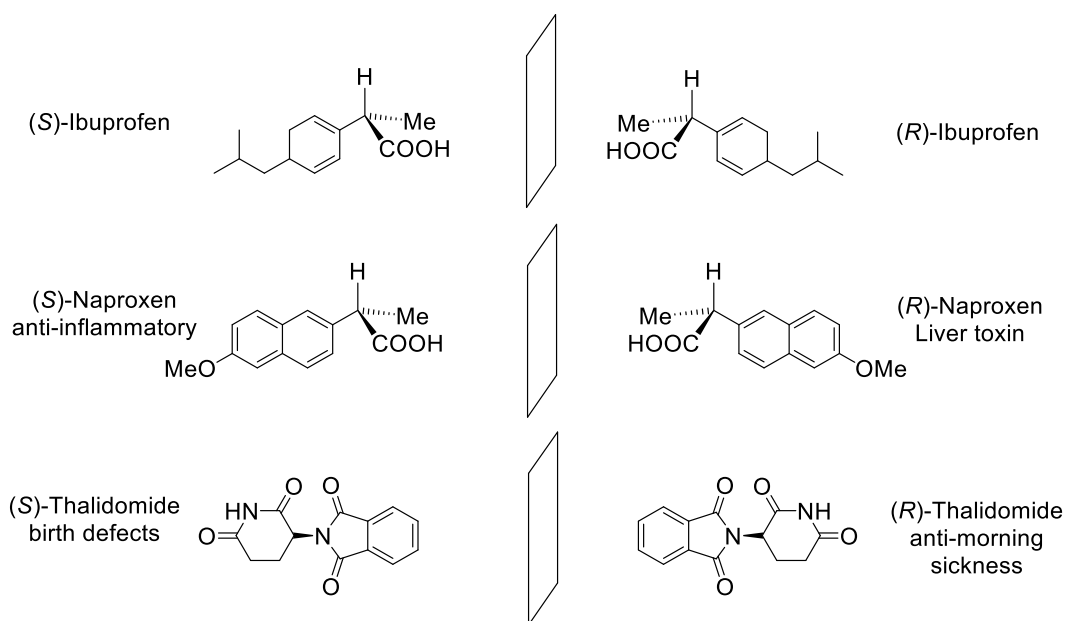


Figure 1.4. Three sets of chiral pharmaceutical molecules, Ibuprofen (top), Naproxen (middle) and Thalidomide (bottom).

1.4 My Specific Research

In general, my research can be described as making new molecules, I am a synthetic chemist. The goal of my research has been to learn about how we can control which products are

formed during catalysis. As described above, being able to control which molecule is formed can have important consequences, such as one version of a molecule being a powerful medicine while a slight change in the structure of the molecule, such as the stereochemistry at one position, can result in the medicine being a toxin instead. The specific chemical transformation I have focused on in the Landis group is hydroformylation, the addition of one equivalent each of hydrogen (H_2) and carbon monoxide (CO) to a carbon-carbon double bond (alkene or olefin), resulting in a new functional group, an aldehyde (Scheme 1.1, see above). To make this transformation occur faster and with less energy, we add a transition metal catalyst to create a new pathway for the reaction to occur, as described above. One of the best transition metals to use for this particular chemical reaction is rhodium. As previously mentioned, the transition metal is usually attached to a larger molecule, this molecule that binds to the rhodium atom and supports it is also called a ligand. One of the best ways to help control which molecule we form during our reaction is to carefully select the ligand that is attached to the rhodium atom. There are generally two key properties that we can change or tune, they are called sterics and electronics. These two key properties can be easily described in general terms. Sterics basically means the size of the ligand and the groups that are attached to it. If the groups attached to the ligand take up a lot of space around the rhodium atom, there will be a limited amount of space available to fit all the other molecules (H_2 , CO, and alkene) around it when our reaction occurs. By tuning the amount of available space around the rhodium atom, this can force the different molecules to twist and turn to fit into the limited space they can find. If the different molecules can only fit into one configuration, this can lead to formation of only one version of our final product (this is our goal). The second key property we can try to control is electronics, which is a little more difficult to describe. To help us understand this, we have to know a little bit more about the bonds in our molecule. Bonds are made by sharing electrons between atoms, but not all atoms share the electrons evenly. We can think about the different bonds kind of like the rope in a tug-of-war and the atoms as the people pulling on the ropes. Depending on which atoms pull harder on the bonds

can cause a shift of the electrons around the molecule, to some degree, changing the distribution of the electrons. Since the reaction to combine the different molecules together into our final product occurs at the rhodium atom, the distribution of the electrons around this atom is the most important in controlling the final products that occur from our reaction. Because our ligand is attached to the rhodium atom at the phosphorus atom, the electron distribution around the phosphorus atom will be a key factor in the electronic tuning of the reaction that occurs. The careful design of the ligand that is attached to the rhodium atom is crucial in controlling our reaction, this is where I have spent the majority of my time in the Landis group, designing and synthesizing new ligands to better control which products are formed from our catalysts. One example of the general framework of the types of ligands I have been working with is shown below in Figure 1.5. The molecules consist of a 5-atom ring including one phosphorus, two carbon and two nitrogen bearing various R-groups (R, R', R''). These R-groups give us the chance to tune the ligand framework using both sterics and electronics to control the environment that is around the rhodium atom where the reaction occurs. In the actual ligand structures, I am focusing on how to specifically change the backbone and introduce new groups in the red circled areas on the ligand. Once I obtain new structures cleanly, I can test them for hydroformylation.

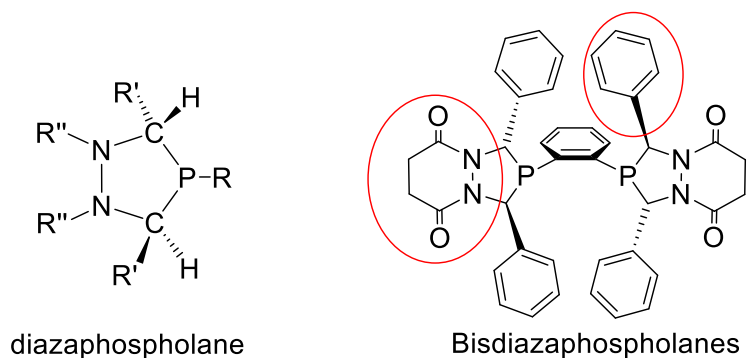


Figure 1.5. General type of diazaphospholane ligand framework (left) and specific structure of interest, the groups to modify are circled in red (right).

1.5 How to know which molecule I Made – NMR Spectroscopy

Since my job each day is focused on synthesizing new molecules, I have to use tools to help me figure out and identify (characterize) what I made. One of the most powerful tools that I can use is nuclear magnetic resonance (NMR) spectroscopy. How I use this powerful tool can be demonstrated by looking at the structure and proton (^1H) spectrum of the ethanol (EtOH) molecule in Figure 1.6.⁵ Because ethanol has hydrogen atoms (protons) in it, we can measure its proton NMR spectrum. The spectrum gives us three key pieces of information that can help us solve the puzzle of what our molecule is. First, it tells us, how many different types of hydrogen atoms we have in our molecule, these are shown in blue, green and red in Figure 1.6. These different types of hydrogen atoms show up at different locations along the x-axis of our spectrum (~ 3.75 , 2.6 and 1.2). The location of each of these signals gives me information about the local environment that each type of hydrogen sits in. Second, it tells me how many hydrogen atoms make up each of the three signals in this example. These numbers are not shown in Figure 1.6, but if we calculate the area under each signal (integrate it), the three signals would show a ratio of $2 : 1 : 3$ from left to right, equal to the number of each type of hydrogen atom in the EtOH molecule. Third, the splitting pattern that each signal forms, tells me about the neighboring atoms. If we look at the EtOH molecule, the signal for the green hydrogen atoms is split into four peaks (quartet) because those hydrogen atoms are next to a carbon atom with three hydrogen atoms connected to it. The signal for the blue hydrogen atoms is split into a three peaks (triplet) because those hydrogen atoms are next to a carbon atom with two hydrogen atoms connected to it. The signal for the red hydrogen atom only shows one peak (singlet) because it is attached directly to an oxygen atom. By combining the three key pieces of information, the number of hydrogen atom environments, the number of hydrogen atoms in each environment, and the splitting patterns of each signal, we can start to piece together the structure of the molecule. In this example, we only looked at the NMR spectrum of the hydrogen atoms, but we could have also looked at the spectrum of the carbon atoms to help us, as well. I am lucky in the types of molecules I work with, because I can use NMR to get

information about several types of atoms that I use (because NMR can't see all types of atoms), including atoms of hydrogen, carbon, boron and phosphorus. One of the favorite saying of my advisor Clark Landis is, "NMR never lies!", because it is a powerful tool in helping us figure out the structure of our molecules.

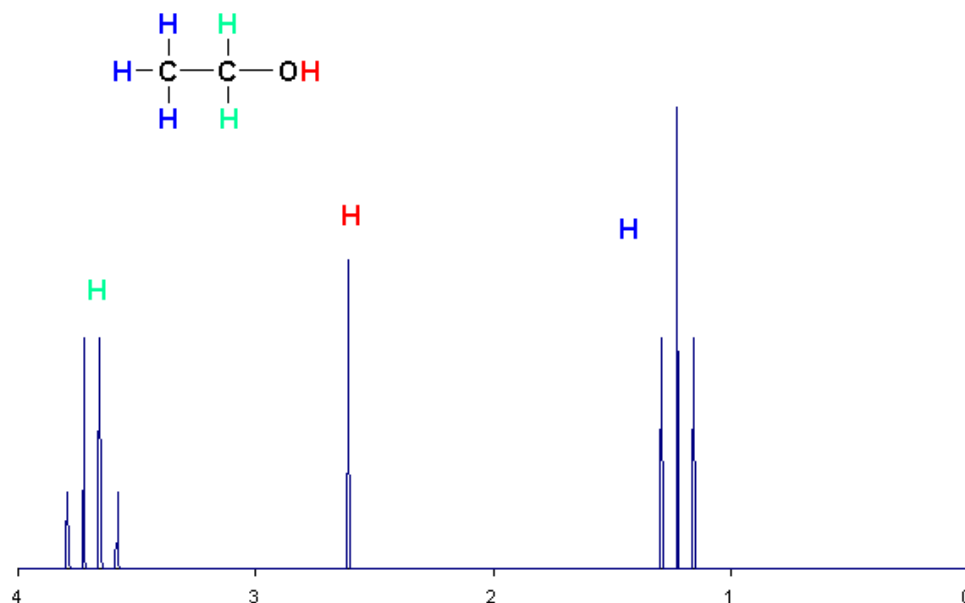


Figure 1.6. Proton (^1H) nuclear magnetic resonance (NMR) spectrum of ethanol (EtOH).

1.6 References

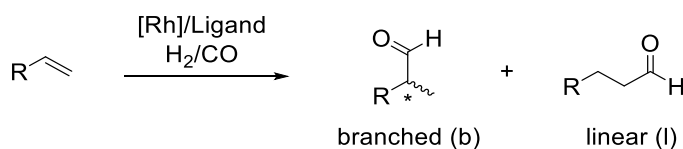
1. <http://sciencenotes.org/printable-periodic-table/>
2. Book Cover: Catalysis: Concepts and Green Application;
<http://onlinelibrary.wiley.com/book/10.1002/9783527621866>
3. <http://www.newworldencyclopedia.org/entry/Catalyst>
4. http://www.chemgapedia.de/vsengine/vlu/vsc/de/ch/8/bc/vlu/chem_grundlagen/chiraliaet.vlu/Page/vsc/de/ch/12/oc/stereochemie/chiralitaet/chiralitaet.vscml.html
5. https://en.wikibooks.org/wiki/Structural_Biochemistry/Organic_Chemistry/Organic_Functional_Group/Hydroxyl

Chapter 2

Rhodium-Catalyzed Hydroformylation of Alkenes with Phosphorus-based Ligands

2.1 Introduction

Hydroformylation is the addition of synthesis gas (“syngas”), a mixture of H₂ and CO in a molar ratio of 1 : 1, across a double bond of an alkene in the presence of a catalyst, leading to a carbon-carbon homologation (Scheme 2.1). This transformation is also known as the “oxo-process” and was discovered by Otto Roelen in 1938.^{1, 2} The branched and linear aldehyde products are produced in a single step and under essentially neutral reaction conditions. With the key attributes of high atom economy, inexpensive reactants, simple purification and high turnover numbers, rhodium-catalyzed hydroformylation is one of the largest homogeneously catalyzed transformations in industry to date, producing over 20 billion pounds (over 10 million metric tons) of oxo-products per year.^{3, 4} Over 80% of hydroformylation is performed with rhodium on the industrial scale, operating with phosphorus-containing ligands. Those types of rhodium catalysts allow for operation at low syngas pressures (260 – 870 psi or 1.8 – 6.0 MPa) and medium temperatures (80 – 130 °C). Even though rhodium is one of the most expensive transition-metals, catalytic activity with rhodium is over 1000 times higher than with cobalt, which is the next most used metal for hydroformylation.⁵



Scheme 2.1. Rhodium-catalyzed hydroformylation of alkenes.

The produced aldehyde group is one of the most versatile and important functional groups, playing an important role as an intermediate in the synthesis of commodity chemicals such as alcohols, esters and amines, as well as other olefins extended by one C-atom-unit upon a reduction-elimination sequence. Furthermore, aldehydes are intermediates on the path of

production of other industrially relevant compounds, such as solvents, plasticizers, detergents and the nylon monomer (Figure 2.1).⁴

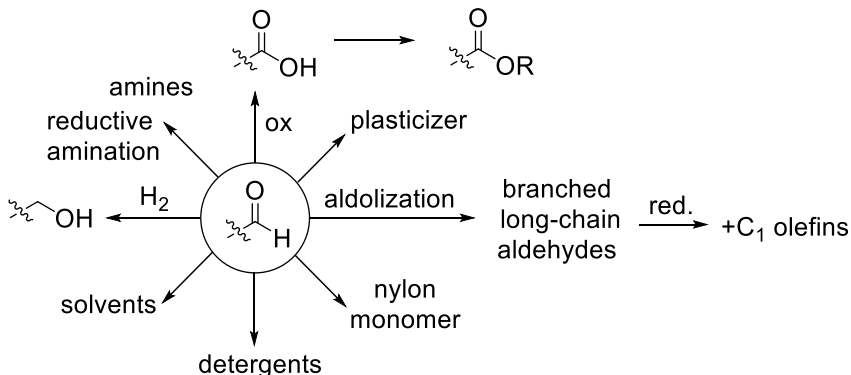


Figure 2.1. The aldehyde group as an important intermediate in the synthesis of bulk chemicals.

The commercial application of hydroformylation is primarily focused on the production of the linear and non-chiral branched aldehyde products. Even though optically active aldehydes derived from the branched products of hydroformylation are important intermediates in the synthesis of fine chemicals, pharmaceuticals, fragrances and agrochemicals,⁶ asymmetric hydroformylation (AHF) is underutilized on the industrial scale. A challenge herein, is to combine high regio- and enantioselectivity for a wide range of alkene substrates. Although research on rhodium-catalyzed asymmetric hydroformylation has advanced, and a variety of new phosphorus-based ligands for AHF have been identified, unmet challenges still exist with the current scope of ligands. One drawback is the limited substrate scope for any single ligand, and the lack of controlling chemo-, regio- and enantioselectivity for a variety of alkene substrates.

Since the discovery of Wilkinson's modified rhodium complexes for highly active and chemoselective hydroformylation with PPh_3 ,⁷ phosphorus compounds were the focus in the application of rhodium-catalyzed hydroformylation. Numerous methods for the analysis of properties and trends that govern selectivity have been developed over the years.⁸⁻¹¹ Trivalent

monophosphorus compounds are typically evaluated by the Tolman cone angle (θ) for steric characterization, and more importantly, the concept of the natural bite angle (α) has been developed for bidentate bisphosphorus ligands in hydroformylation (Figure 2.2). This concept is designed to correlate the ligand's activity and selectivity with a specific bite angle. The steric bite angle is differentiated into a steric and an electronic component, where the latter effect changes based on the hybridization of the metal and can change throughout the catalytic cycle.

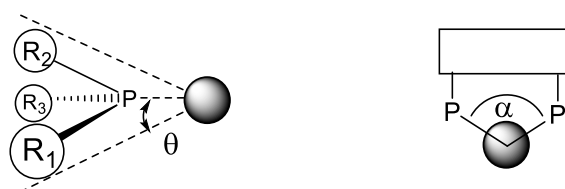


Figure 2.2. Tolman cone angle (θ) as a characterization method for monophosphine ligands (left) and the bite angle (α) for bidentate phosphorus ligands (right).

It is generally found that bisphosphine ligands with a larger distance between the phosphorus atoms, and consequently a greater bite angle (α), bind to the metal center in a di-equatorial fashion. Ligands with bite angles ranging from 100 – 120° have the tendency to form primarily the linear aldehyde products of hydroformylation. In contrast, ligands with an equatorial-axial coordination mode result in a mixture of both branched and linear aldehyde products, with higher branched to linear ratios compared to di-equatorial systems. Three major factors are responsible for increased branched to linear ratios and high enantioselectivity of aldehydes. First, a high preference for the ligands to bind equatorial-axial to the metal center, second, the ligands should contain at least two chiral centers and third, the correct configuration between chiral centers is an important factor.¹²⁻¹⁴

The other factor that determines selectivity in hydroformylation is the alkene itself. First, the rate of reactivity is determined by the substitution pattern, increased number of substituents on

the alkene lead to a decrease in hydroformylation rate (Figure 2.3).^{4, 15} Terminal alkenes are the most common substrates because they only require low temperatures (rt to 80 °C) and pressures (100 – 200 psi) for an effective transformation. Internal alkenes, such as 1,2- and 1,1-disubstituted alkenes are more challenging than terminal alkenes and the reactions need to be performed at higher temperatures than 80 °C to obtain good rates, however, the selectivity suffers from increased temperatures. Catalysts performing under these conditions require a strong π -acceptor ligand, such as bulky phosphites and phosphobenzene systems.^{16, 17} In principal, the addition of another substituent to a trisubstituted sp^2 -hybridized C-atom is un-favored due to the undesired formation of a quaternary carbon-atom (Keulemans' Rule).¹⁸

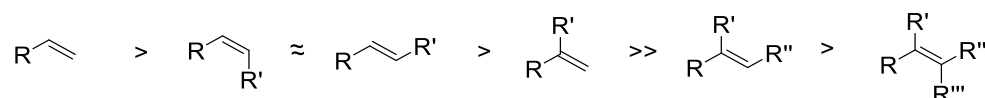


Figure 2.3. Decrease of hydroformylation rate with increasing substitution on the alkene.

Regioselective hydroformylation is also inherent to the substrate's preference. Directing effects are controlled by the functional groups attached to the double bond. Electron-withdrawing substituents favor the formation of the branched aldehyde. This tendency is often unaffected by the catalyst structure. A typical example is styrene, which forms the branched isomer in hydroformylation, whereas 1-octene favors the linear aldehyde product. Another challenge is the design of a ligand that avoids side reactions such as isomerization of the double bond and the possibility for hydrogenation.

The design of active and selective ligands takes advantage of functionalizing, derivatizing and modifying already known ligands, the so-called privileged ligands. Those structures give high selectivities across a broad range of applications and include a limited number of ligands. This chapter summarizes classes of ligands that initially found success as well as other ligands derived from privileged ligands commonly used in asymmetric hydroformylation.

2.2 Bisphosphite Ligands

Bisphosphite ligands have been extensively studied since they provide high levels of selectivity, especially with terminal alkenes¹⁹. Initial success was found with (2*R*,4*R*)-Chiraphite **1** discovered by Union Carbide for the hydroformylation of vinylarenes.²⁰ In regards to the synthesis, a diverse set of phosphite ligands can be accessed easily by varying the bridge between the P-atoms and the chelating substituent, derived from diols. Generally, sterically hindered phosphite moieties lead to higher enantioselectivity. Introduction of bulky *ortho*- and *para*-substituents to the chelating biphenoyl group leads to improved selectivity, but increased steric bulk in the bridging moiety has the opposite effect.¹⁹ Kelliphite ligand **2**, developed by the Dow Chemical Company, contains an achiral biphenol backbone but chirality is introduced through the *tert*-butyl and methyl bearing biphenol (Figure 2.4). A large library derived from furanose was developed and applied to the hydroformylation of vinylarenes, vinyl acetate and vinylethers.^{21, 22}

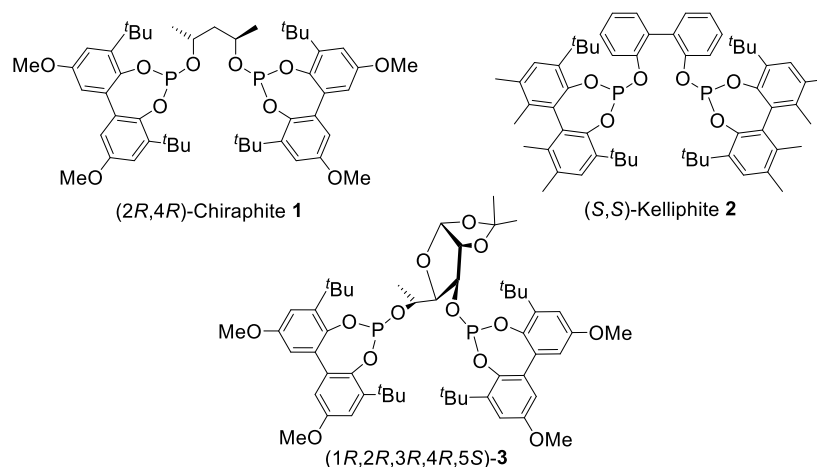
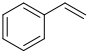
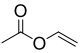
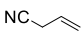


Figure 2.4. Commonly used bisphosphite ligands **1**, **2** and **3**.

The results for hydroformylation of styrene, vinyl acetate and allyl cyanide with ligands **1**, **2** and **3** are compared in Table 2.1. Chiraphite **1** is the most regioselective with vinyl acetate, but cannot maintain good enantioselectivity (entry 1). Kelliphite **2** shows the highest selectivity for

vinyl acetate and allyl cyanide compared to **1** and **3** (entry 2). However, no enantioselective induction is observed with styrene. For commercial application, Kelliphite **2** is highly effective for vinyl acetate and allyl cyanide, and Chiraphite **1** is a good ligand for vinylarenes. Even though furanose-based bisphosphite **3** gives good regio- and enantioselectivity for styrene and vinyl acetate, it is of note that the reaction was performed at lower temperatures compared to entries 1 and 2 (45 vs. 80 °C).

Table 2.1. Hydroformylation of Benchmark Substrates with Selected Bisphosphite Ligands.

Entry Ref	Ligand									
		conv. (%)	b : l	% ee	conv. (%)	b : l	% ee	conv. (%)	b : l	% ee
1 ²³	1 ^a	98	13	56 (<i>R</i>)	95	100	47 (<i>R</i>)	100	6.1	15 (<i>R</i>)
2 ²³	2 ^a	100	17	1 (<i>S</i>)	56	56	77 (<i>R</i>)	100	11	70 (<i>S</i>)
3 ^{21, 22}	3	97 ^b	32	78 (<i>R</i>)	100 ^c	99	65 (<i>R</i>)	---	---	---

^a Reaction performed at 70 °C in acetone with 150 psig of H₂/CO with L/Rh = 1.2, substrate/Rh = 500, 3 h. ^b Reaction performed at 40 °C with 150 psig of H₂/CO with L/Rh = 1.1, substrate/Rh = 1000, 10 h. ^c Reaction performed at 45 °C in toluene with 260 psig of H₂/CO with L/Rh = 1, substrate/Rh = 400, 24 h.

Phosphite moieties are commonly installed into hybrid phosphine-phosphite ligands, which have also shown high selectivity for a variety of substrates. This ligand class is discussed in section 2.5 (*vide infra*).

2.3 Bisphosphine Ligands

Phosphines are defined as an all carbon-atom substituted P-atom. The bisphosphine ligands that finds the most use in hydroformylation are chelating bisphosphines bearing two $P(Ph)_2$ - or $P(alkyl)_2$ groups that are bridged by a variety of functional groups (Figure 2.5). One of the first successful asymmetric rhodium-hydroformylation reaction was carried out with the tartaric acid-derived bisphosphine DIOP **4**.²⁴ DIOP type ligands were used in the hydroformylation of unsaturated nitrogen compounds, aliphatic alkenes, unsaturated carboxylic acids and esters. The rhodium-DIOP complex was found to be effective in the hydroformylation of alkyl α -N-acylaminoacrylates, leading to the single branched product in 60% ee, representing a high enantioselectivity for vinylidene alkenes at that time.²⁵ Glucose-derivate bisphosphine **5** developed by Lu and coworkers, gives high selectivity for vinyl acetate (b : l = 24 : 1, 93% ee) and moderate selectivity for styrene (b : l = 8.1 : 1, 68% ee), but only exhibiting low turnover frequencies (<30/h)²⁶. A library of ligands with a large distance between the P-atoms based on XantPhos **6**⁸ were developed starting in 1990. These ligands became successful in their application in linear hydroformylation, explained by their large bite angles of 100 – 130° and a di-equatorial binding mode in their corresponding metal complexes.²⁷ However, exceptions to this general rule are found. Chiral versions derived from BISBI ligands have been synthesized, for example NAPHOS **9**. Despite its coordination in a di-equatorial fashion, ligand **9** exhibits a high branched to linear ratio of 24 : 1 and an enantioselectivity of 34% at 100 bar and 40 °C for styrene.²⁸ The naphthyl-derived ligands BINAP **10** gives a high branched to linear ratio for vinyl acetate (32 : 1), but only a moderate enantioselectivity.²⁹ BINAP based hybrid ligands are by far more successful than BINAP itself and are discussed further in section 2.5.

Over the years, the development of ligands with a smaller bite angle focused on the improvement of branched selectivity. Despite their simplicity, ligands BDPP **7** and ChiraPhos **8** give high branched to linear ratios with styrene at 116 psi (19 : 1 at 65 °C for **7** and 33 : 1 at 80 °C for **8**), but moderate to low enantioselectivity of 43% and 21%, respectively.³⁰

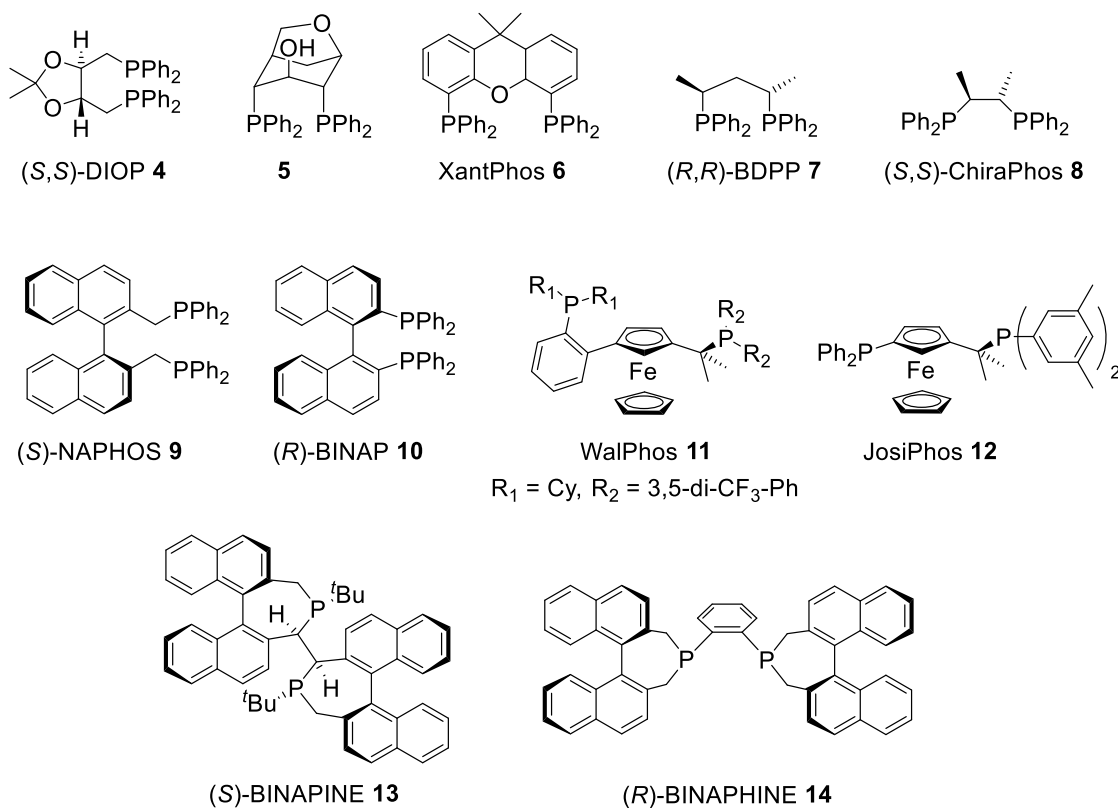


Figure 2.5. A selection of bisphosphine ligands used in rhodium-catalyzed hydroformylation.

Very selective hydroformylation for 1,1-disubstituted alkenes was found with ligands **15** and **16**. Enantioselectivity exceeding 90% with both **15** and **16** while maintaining high regioselectivity to yield exclusively a single aldehyde product was demonstrated (Figure 2.6).^{31, 32}

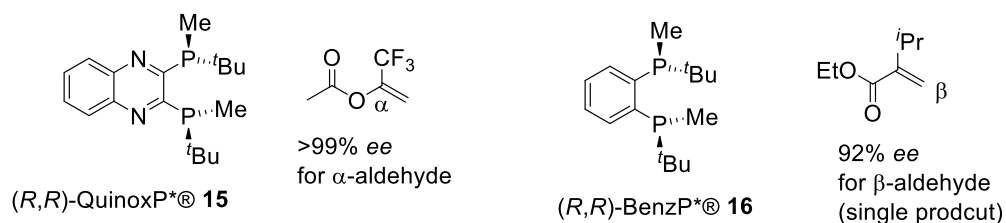
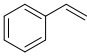
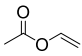
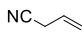


Figure 2.6. High selectivity for 1,1-disubstituted alkenes with ligands **15** and **16**.

A wide range of ligands were evaluated by Klosin and coworkers in the asymmetric hydroformylation of benchmark substrates styrene, vinyl acetate and allyl cyanide. Table 2.2

summarizes the results under industrially relevant reaction conditions of 80 °C, 150 psig and catalyst loadings of 0.03 mol% after 3 h. Styrene can be hydroformylated in a branched to linear ratio of 20 : 1 with JosiPhos **12** (entry 2), however, ligands **7** and **11** show low regio- and enantioselectivity (entry 1 and 3). The best values for vinyl acetate were observed with WalPhos **11** (b : l = 73.1 : 1 and 73% ee, entry 3). High regioselectivity for allyl cyanide was observed with BDPP **7**, followed by JosiPhos **12**. Enantioselectivity varies, with the most simple ligand BDPP **7** leading to the best selectivity for allyl cyanide, which inherently leads to low branched selectivity. Interestingly, BINAPINE **13** affords the highest enantioselectivity for all three substrates within this ligand class under the reaction conditions, especially for allyl cyanide (94%) while still leading to relatively good branched to linear ratios (entry 4). Even though BINAPHANE **14** is structurally similar to **13**, **14** gives poor selectivity for all three substrates (entry 5).

Table 2.2. Hydroformylation of Benchmark Substrates with Selected Bisphosphine Ligands.^a

Entry Ref	L									
		conv. (%)	b : l	% ee	conv. (%)	b : l	% ee	conv. (%)	b : l	% ee
1 ³³	7	22	12.4	48 (S)	22	16.4	31 (S)	82	16.1	70 (S)
2 ³³	12	45	20.1	38 (S)	27	205	17 (S)	92	14.1	22 (S)
3 ³³	11	26	2.7	2 (S)	42	73.1	73 (R)	47	3.5	53 (R)
4 ²³	13	12	9.5	94 (S)	21	32.4	87 (R)	49	6.7	94 (S)
5 ²³	14	17	8.2	34 (R)	21	34	24 (S)	62	5.2	50 (R)

^a Reaction performed at 80 °C in toluene with 150 psig of H₂/CO with L/Rh = 1.2, substrate/Rh = 3000, 3 h.

2.4 Bisphospholane Ligands

Phospholanes are defined as five-membered phosphine cycles with three P–C bonds. Bisphospholanes have received increased attention with the development of DuPhos **17** by Burk (Figure 2.7). This ligand class demonstrated high conversions and enantioselectivity for a broad range of substrates in rhodium-catalyzed hydrogenation.^{34, 35} The success of the DuPhos ligand family stems from the C_2 -symmetric rigid framework, bearing substituents in the 2- and 5-positions of the phospholane ring. One set of the substituents lies in front of the phospholane ring plane, pointing to the bound metal center in the metal-catalyst structure, the other set points behind the plane of the phospholane ring. This steric arrangement leads to strong induction of enantioselectivity. The synthesis towards a large number of DuPhos ligands is challenging. The difficulty lies in the introduction of different substituents in the 2- and 5-positions of the phospholane ring and is limited to alkyl substituents.³⁴ A phenyl-substituted phospholane can only be obtained as an ethylene bridged bisphospholane (Ph-BPE **18**).³⁶ To introduce aryl substituents into a phenylene-bisphospholane, Landis and coworkers have designed a novel route that allows for rapid access to a wide range of 3,4-diazaphospholanes achieved through a mild synthetic route.³⁷ Importantly, ligands with varying substituents in the 2- and 5-positions can be obtained in a two or three step reaction. Furthermore, introduction of a modular functional group as part of the substituent allowed for synthesis of a library of new diazaphospholane ligands.

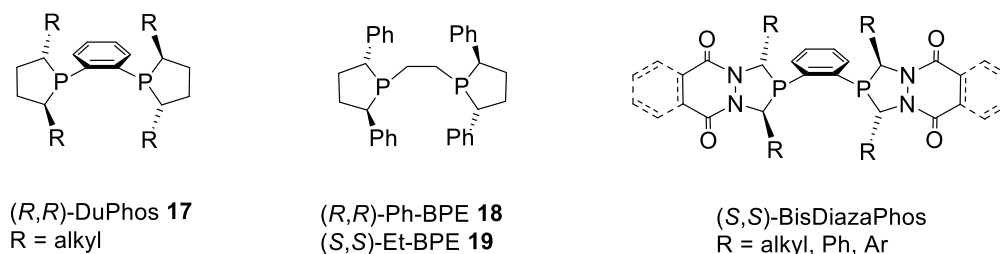
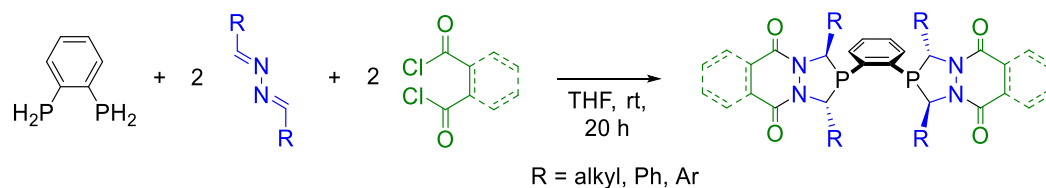


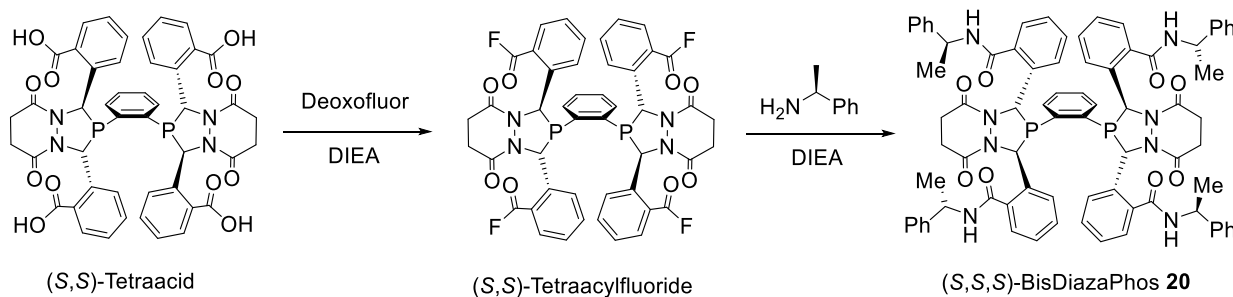
Figure 2.7. The bisphospholane classes DuPhos, Ph-BPE and BisDiazaPhos.

The diazaphospholane framework is synthesized in a one-step Mannich type condensation reaction of a 1,2-disubstituted azine, typically 1,2-benzylidene, 1,2-bisphosphinobenzene and an acyl chloride, which is typically phthaloyl chloride or succinyl chloride. The desired C_2 -symmetric ligand is obtained in moderate yields of around 30% as the racemic mixture (Scheme 2.2).³⁷



Scheme 2.2. Synthesis of the bisdiazaphospholane ligand framework.

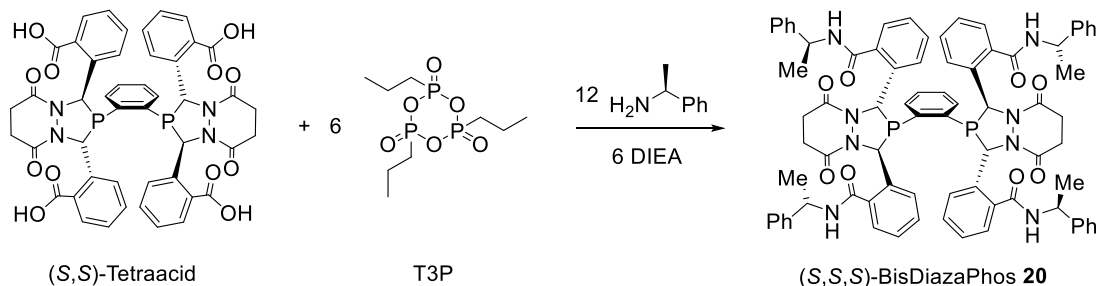
The tetra(methylbenzylamide) state-of-the-art ligand (*S,S,S*)-BisDiazaPhos **20** combines high regio- and enantioselectivity and is obtained by the fluorination of the resolved tetracarboxylic acid and subsequent reaction with methylbenzylamine (Scheme 2.3).³⁸



Scheme 2.3. Synthesis of the state-of-the-art ligand (*S,S,S*)-BisDiazaPhos **20**.

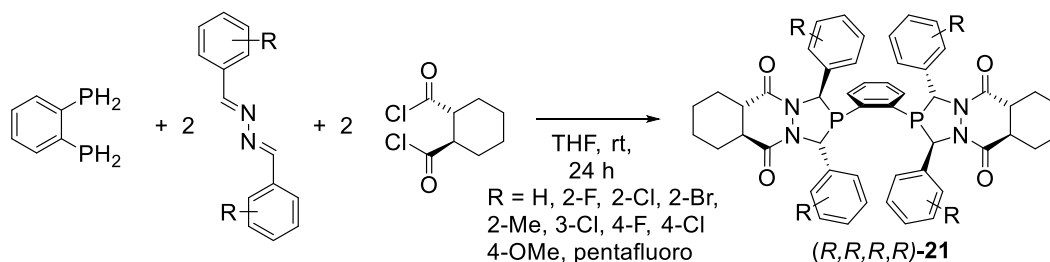
More recently, Jones and Landis have developed an in-house resolution of racemic tetraacid with (+)-pseudoephedrine, avoiding the use of chiral chromatography or specialized equipment. Furthermore, the synthesis of (*S,S,S*)-BisDiazaPhos **20** was improved by utilizing the coupling

reagent propylphosphonic anhydride (T3P) in the amide coupling step allowing for a cleaner coupling reaction and easier purification by recrystallization from acetone (Scheme 2.4).³⁹



Scheme 2.4. Improved synthesis of **20** with propylphosphonic anhydride T3P.

Zhang and coworkers demonstrated a different approach towards enantiopure bisdiazaphospholane derivatives.⁴⁰ By reacting a 1,2-benzylidene azine with 1,2-bisphosphinobenzene and a chiral acyl chloride, the resulting bisdiazaphospholane diastereomers can be separated *via* column chromatography. Of all derivatives, the 2-chlorophenyl substituted ligand shows the highest selectivity for styrene and vinyl acetate (Table 2.3, *vide infra*).



Scheme 2.5. Synthesis of 1,2-diacyl cyclohexane backbone bearing bisdiazaphospholane **21**.

Another representative bisphospholane ligand is TangPhos **22**. It shows relatively good selectivity with the substrates styrene, vinyl acetate and good regioselectivity for allyl cyanide (Table 2.3, entry 7). However, selectivities are very sensitive to the ligand to rhodium ratio. If the

ratio is higher than 1.2 : 1, TangPhos can displace the anionic acac-ligand from the catalyst precursor to form a cationic $[\text{Rh}(\text{TangPhos})_2]\text{acac}$ complex, leading to inactivity throughout the catalytic reaction (Figure 2.8).

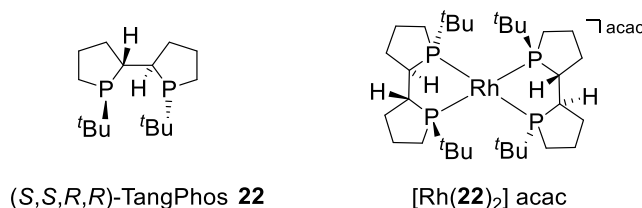
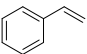
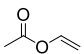
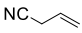


Figure 2.8. TangPhos ligands **22** and the Bis(TangPhos)-Rh complex.

Screening of ligands **17** – **22** was performed in the hydroformylation of the benchmark substrates styrene, vinyl acetate and allyl cyanide (Table 2.3). The stereochemistry is overall determined by the chirality of the phospholane ring. In general, the steric bulk in the 2- and 5-positions determines the regioselectivity. This effect is apparent in the DuPhos and BPE families. The ligands with the largest substituents give the highest regio- and enantioselectivity (entries 1 and 3). In the BPE family, (S,S)-Ph-BPE **18** is the fastest ligand due to the presence of the electron-withdrawing phenyl groups. The ferrocenyl-bridged *iPr*-BPE **iPr5Fc** shows worse selectivities explainable by the ligand bite angle being too large for good performance (entry 4). The combined best results are observed with the bisdiazaphospholane ligands. Good regioselectivity and excellent enantioselectivity are achieved with (S,S,S)-BisDiazaPhos **20** under the same conditions also used with DuPhos and BPE. Very impressive are the conversion results with **20**, exhibiting 9000 turnovers per hour even faster rates than are known with Kelliphite **2** and Chiraphite **1** (*vide supra*).

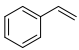
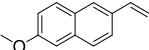
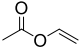
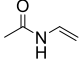
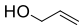
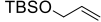
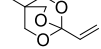
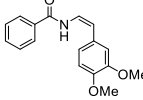
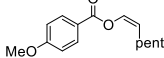
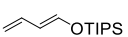
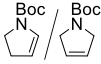

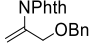
Table 2.3. Hydroformylation of Benchmark Substrates with Selected Phospholane Ligands.

Entry Ref	L									
		conv. (%)	b : l	% ee	conv. (%)	b : l	% ee	conv. (%)	b : l	% ee
1 ⁴¹	<i>i</i> Pr- 17 ^a	15	11.3	83 (S)	29	322	74 (R)	55	7.2	82 (S)
2 ⁴¹	18 ^a	57	45	94 (R)	52	340	82 (S)	96	7.1	90 (R)
3 ⁴¹	19 ^a	10	11.3	55 (R)	23	152	66 (S)	40	6.2	49 (S)
4 ⁴¹	iPr5Fc ^a	9	3.2	15 (R)	22	94	29 (R)	28	3.9	49 (R)
5 ²³	20 ^b	100	6.6	82 (R)	100	37	96 (R)	100	4.1	87 (R)
6 ⁴⁰	2Cl- 21 ^c	99	24	85 (S)	99	53	91 (S)	---	---	---
7 ²³	22 ^a	10	14.9	13 (S)	26	138	81 (R)	49	7.5	6 (S)

^a Reaction performed at 80 °C in toluene with 150 psig of H₂/CO with L/Rh = 1.2, substrate/Rh = 5000, 3 h. ^b Reaction performed at 80 °C in toluene with 150 psig of H₂/CO with L/Rh = 1.2, substrate/Rh = 3000, 3 h, 1 mL of substrates. ^c Reaction performed at 60 °C in toluene with 290 psig of H₂/CO (1 : 3) with L/Rh = 3, substrate/Rh = 3000, 12 h.

This latter screening shows that the ligands with the greatest success and optimal commercial relevance are the bis-3,4-diazaphospholane systems.³⁷ Our group has demonstrated that bis-3,4-diazaphospholanes (BDP) are the most active ligands of all phosphorus-containing ligands, surpassing the activity of bisphosphite ligands. BDPs combine high regio- and enantioselective hydroformylation for a variety of alkene substrates, along with high activity while operating under mild conditions at low catalyst loadings.^{38, 42-45} The substrate scope of (S,S,S)-BisDiazaPhos **20** is summarized in Table 2.4.

Table 2.4. Substrate Scope for (S,S,S)-BisDiazaPhos **20**.

Entry	Substrate	catalyst (mol%)	T (°)	H ₂ /CO (psig)	t (h)	conv. (%)	b : l or α : β	% ee
1 ³⁸		0.0625	60	150	4	100	18.3	87 (<i>R</i>)
2 ⁴³		0.2	40	160 (1:3)	8	100	50 : 1	96 (<i>R</i>)
3 ³⁸		0.0625	60	150	4	100	53 : 1	98 (<i>S</i>)
4 ³⁸		0.5	40	125	4	99	27 : 1	86 (<i>S</i>)
5 ⁴⁴		0.5	40	150	4	99	1 : 3.4	96 (<i>R</i>)
6 ⁴⁴		0.5	40	150	4	99	2.0 : 1	95 (<i>R</i>)
7 ⁴⁶		0.5	40	160 (1:3)	24	100	11.5 : 1	93 (<i>R</i>)
8 ⁴⁵		2	80	150	22	>99	15.4 : 1	98 (<i>S</i>)
9 ⁴⁵		0.3	60	150	24	>99	>50 : 1	99 (<i>S</i>)
10 ⁴⁷		0.5	40	150	4	99	67 : 33 (E : Z)	90 (<i>S</i>)
11 ⁴⁴		0.5	60	140	15 / 18	99 / 99	10.4 : 1 / 1 : 15	97 / 91 ^a
12 ³⁸		0.15	40	150	4	25 / 80	2.8 : 1 / 1 : 15	89 (<i>S</i>) ^a / 86 (<i>R</i>) ^b
13 ⁴⁴		0.5	75	125	38	76	7 : 1 ^c	74 (<i>R</i>)

^a %ee of the major isomer. ^b isomerization to 2,3-dihydrofuran: 18%, ^c branched to isomerization product.

2.5 Hybrid Phosphine-Phosphite and Other Phosphorus Ligands.

Since the discovery of the BINAPHOS ligand **23** by Takaya, Nozaki and coworkers⁴⁸, the design principle of C_1 -symmetric ligands based on two different phosphorus donor groups has thrived.⁴⁹ These ligands combine one phosphorus group known for high activity with another phosphorus group known for high selectivity. Ligands with two distinct groups can affect the orientation and the coordination mode within an Rh-complex and therefore lead to specific selectivities. These ligand classes include phosphine-phosphites ((*R,S*)-BINAPHOS **23**), phosphine-phosphoramidites ((*R,S*)-YanPHOS **24**) and phospholane-phosphites (BobPhos **26**). Additionally discussed are other phosphorus ligands containing only one carbon atom and two heteroatoms showing good to high enantioselectivity (ESPHOS **25** and phosphinite **27**) (Figure 2.9).

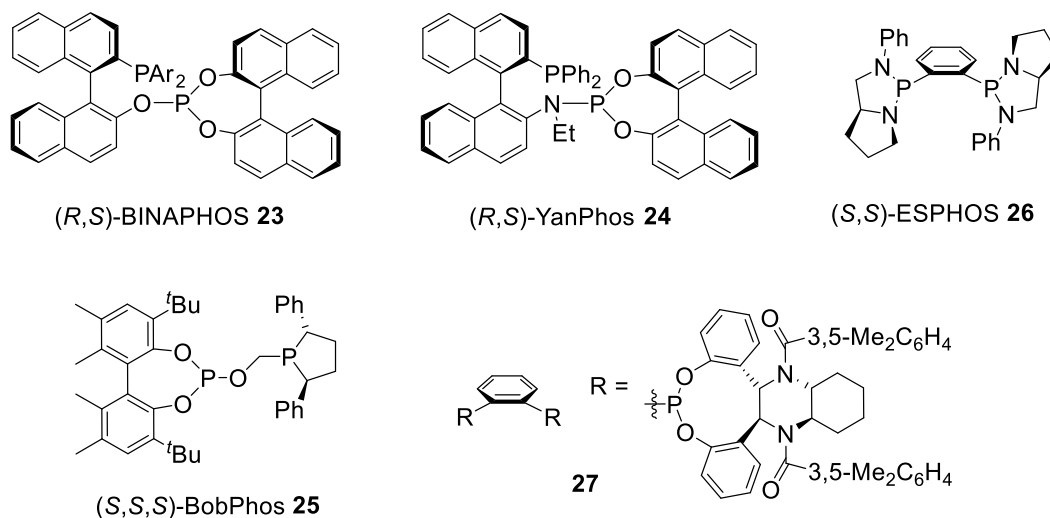
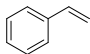
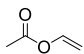
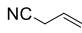


Figure 2.9. Hybrid phosphorus ligands **23**, **24** and **25** and other ligands **26** and **27**.

BINAPHOS **23** and its derivatives were the first ligands to demonstrate high enantioselectivity for several substrates. In a ligand screen study for commercial relevance in AHF by Klosin and coworkers, BINAPHOS **23** provides good enantioselectivity at 80 °C, but poor regioselectivity (Table 2.5, entry 1). BINAPHOS' phosphoramidite analogue YanPhos **24** shows improvements over its parent ligand in enantioselectivity for vinylarenes and vinyl acetate at 60 °C, however, regioselectivities are still poor (entry 2). ESPHOS **26** was one of the first ligands being selective for vinyl acetate, but unfortunately, very unselective in styrene hydroformylation showing no enantiocontrol (entry 3). Quite impressive are the selectivities for all three benchmark substrates with ligand **27** (entry 4), combining high enantio- and regioselectivity with fast rates. One drawback is the operating pressures of 725 and 580 psig, making ligand **27** less attractive for the synthetic bench chemist. BobPhos **25** exhibits very interesting behavior in the hydroformylation of vinylarenes and alkyl alkenes, leading to very high selectivities for styrene and allyl cyanide (entry 5). Of additional note is the high branched selectivity for 1-octene with BobPhos **25** of 3.0 : 1 and 93 %ee after 78% conversion, making it to one of the highest ratios observed. The reaction is performed at 16 °C and 72 psig for 46 h.⁵⁰ BobPhos **25** combines some of the features observed with phospholane Ph-BPE **18** and phosphite ligands. Its high enantioselectivity for aryl and alkyl alkenes can provide the opportunity for further substrate expansion.

Table 2.5. Hydroformylation of Benchmark Substrates with Selected Hybrid Ligands.

Entry Ref	L									
		conv. (%)	b : l	% ee	conv. (%)	b : l	% ee	conv. (%)	b : l	% ee
1 ²³	23 ^a	96	4.5	82 (<i>R</i>)	72	8.2	48 (<i>S</i>)	98	2.1	72 (<i>R</i>)
2 ⁵¹	24 ^b	>99	7.4	98 (<i>R</i>)	75	13.1	96 (<i>S</i>)	---	---	---
3 ⁵²	26	>99 ^c	3.5	0	98 ^d	15.6	89 (<i>S</i>)	---	---	---
4 ⁵³	27	99 ^e	12.2	79 (<i>R</i>)	99 ^e	40.7	91 (<i>S</i>)	99 ^f	3.2	79 (<i>R</i>)
5 ^{50, 54}	25	>99 ^g	46	89 (<i>R</i>)	---	---	---	>99 ^h	8.7	71 (<i>R</i>)

^a Reaction performed at 80 °C in toluene with 150 psig of H₂/CO with L/Rh = 1.2, substrate/Rh = 5000, 3 h. ^b Reaction performed at 60 °C in benzene with 300 psig of H₂/CO with L/Rh = 4.0, substrate/Rh = 1000, 24 h. ^c Reaction performed at 80 °C in toluene with 150 psig of H₂/CO, substrate/Rh = 200, 1.5 h. ^d Reaction performed at 60 °C in toluene with 116 psig of H₂/CO, substrate/Rh = 200, 5 h. ^e Reaction performed at 60 °C in *t*BuOMe with 725 psig of H₂/CO (4:1) with L/Rh = 1.5, substrate/Rh = 500, 2 h, [alkene] = 3 M. ^f Reaction performed at 60 °C in *t*BuOMe with 580 psig of H₂/CO (4:1) with L/Rh = 1.5, substrate/Rh = 500, 4 h, [alkene] = 1 M. ^g Reaction performed at 60 °C, solvent-free with 150 psig of H₂/CO with L/Rh = 2.5, substrate/Rh = 250, 1 h. ^h Reaction performed at 60 °C in toluene, with 150 psig of H₂/CO with L/Rh = 1.25, substrate/Rh = 250, 0.6 h.

The hybrid phosphine-phosphonite ligand **28** with a xanthene-bridge was recently developed by Reek and coworkers. Ligand **28** shows unprecedented regio- and enantioselectivity for dihydrofuran and pyrrolines (Figure 2.10). The ligand in the [RhH(CO)₂**28**]-complex predominantly (at least 80 %) binds in a di-equatorial fashion.⁵⁵

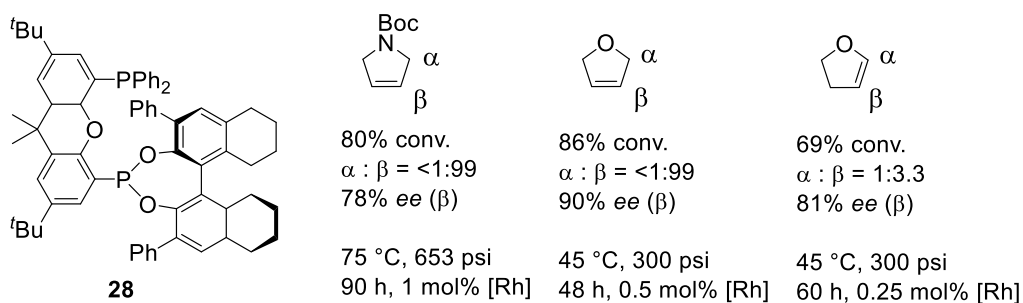


Figure 2.10. Hydroformylation results of cyclic alkenes with ligand **28**.

The hybrid phosphorus ligand classes combine parts of privileged ligands, which are known to exhibit either good selectivity or good reactivity. The recent developments show that hybrid ligands are attractive for hydroformylation for different substrate classes and are (together with the class of phospholanes) the most attractive ligands for asymmetric hydroformylation.

2.6 Mechanism of Rhodium-Catalyzed Hydroformylation with BisDiazaPhos Ligands

The hydroformylation mechanism was first proposed by Heck and Breslow in 1961 and remains the generally accepted mechanism to date.⁵⁶ The catalyst resting state is the off-cycle hydrido-dicarbonyl complex, which loses a CO-ligand to enter the catalytic cycle. From there, the product distribution is determined initially by the orientation of the alkene upon coordination to the Rh-center, leading to a branched and linear alkyl-complex. The acyl-complex is formed upon coordination of another CO-ligand and subsequent CO-insertion between the Rh–C-alkyl-bond. Further addition of H₂ to the Rh-complex and the hydrogenolysis step leads to aldehyde products (Figure 2.11).

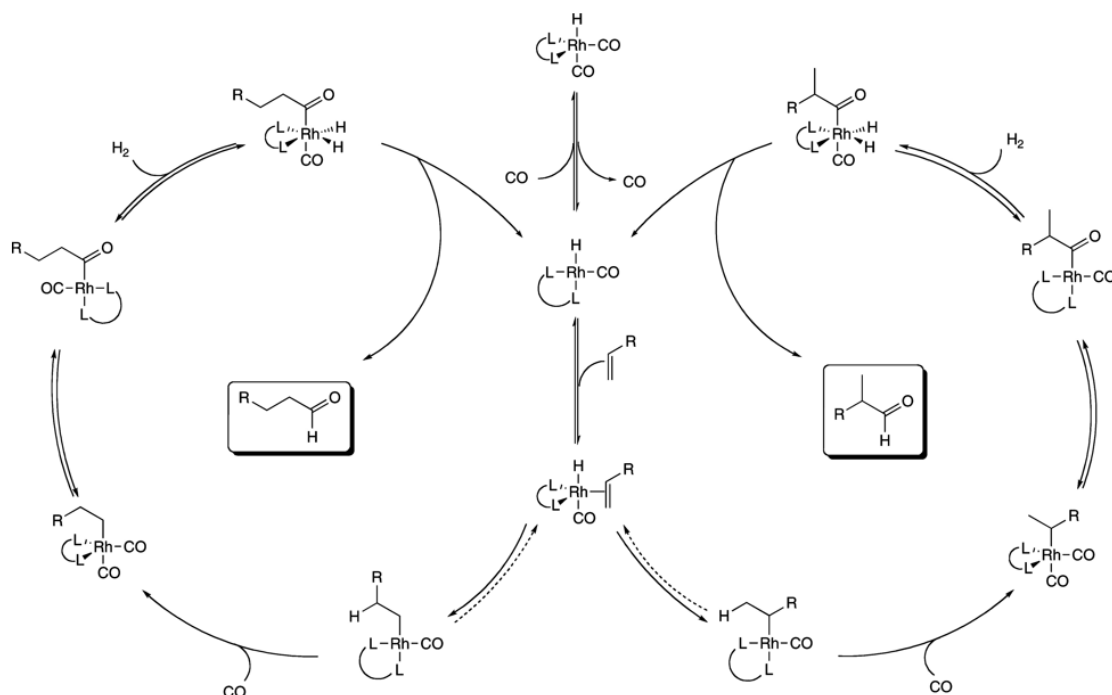


Figure 2.11. Mechanism of rhodium-catalyzed hydroformylation of alkenes.⁵⁷

The mechanism and kinetics of hydroformylation has been extensively studied, investigating the catalytic intermediates along the cycle, as well.⁵⁷⁻⁶⁰ Catalyst speciation is typically only studied and observed under non-catalytic and non-comparable conditions to practical hydroformylation reactions, often including kinetic studies and isotope labeling experiments, for example deuterioformylation.⁵⁷

It is known that the syngas pressure has an influence on the outcome of product ratio distribution. Watkins and Landis have studied the pressure dependence of CO and H₂ on the branched to linear aldehyde ratio and the branched enantiomer distribution for (S,S,S)-BisDiazaPhos **20**.⁵⁷ The pressure of CO has a dramatic effect on the regio- and enantioselectivity for styrene, showing a direct relationship to both. As the CO-pressure increases, the branched to linear ratio and the *R*- to *S*-enantiomer ratio increases, with the largest ratios observed at pressures of at least 190 psia. Above pressures of 190 psia, the selectivity reaches a plateau. In contrast, the H₂ pressure has no effect on the regio- and stereoselectivity (Figure 2.12).

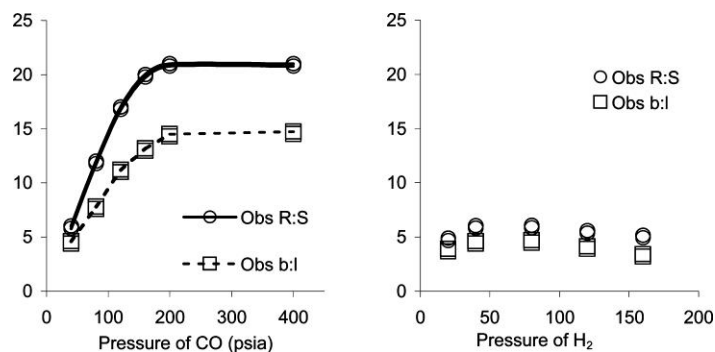
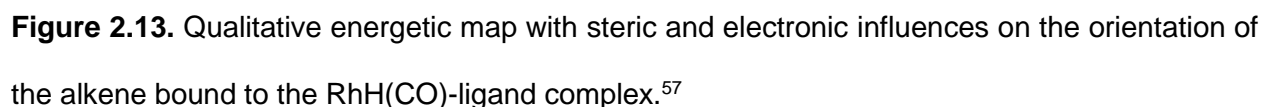


Figure 2.12. Dependency of CO pressure (left) and H₂ pressure (right) on regio- (b : l) and stereoselectivity (R : S) with (S,S,S)-BisDiazaPhos ligand **20**.⁵⁷

Recently, our group has developed the High-Pressure NMR Reactor (WiHP-NMRR),⁶¹ which allows for the monitoring of the hydroformylation reaction progress *in situ* under realistic reaction conditions and the direct observation of catalyst species during catalysis while changing the reaction conditions under active hydroformylation.^{62, 63} Catalyst speciation and the kinetics have been recently studied in depth by Brezny and Landis, explaining the regioselectivity by using the racemic Tetraphenyl BDP ligand. It has been revealed that multiple factors play a role in the selectivity-determining step, taking into account kinetic and thermodynamic preferences for intermediates, competing rates and isomerization preferences under reaction conditions, as well as the role of a fine balance of favored products during the CO-insertion step and the hydrogenolysis step.⁶⁴

For a more simple and qualitative approach to understand the selectivity preferences with bisdiazaphospholane ligands, an energetic map has been developed by Watkins and Landis to visualizes the steric and electronic factors contributing to the regio- and stereoselectivity.⁵⁷ In this map, the bisdiazaphospholane ligand is bound in an equatorial-axial fashion to the pseudo-five-coordinate Rh-center (Figure 2.13). The hydride and the axial P-atom are in the plane of the paper, whereas the CO-ligand and the equatorial P-atom are behind the plane. The coordinated alkene lies coplanar to the Rh–H-bond. Depending on the orientation of the alkene substituent X,



2.7 Conclusion

Rhodium-catalyzed asymmetric hydroformylation of alkenes is an underdeveloped transformation in industry, mainly due to the challenge of controlling both high regio- and enantioselectivity while maintaining high reaction rates. Selectivity can be controlled to some extent by the reaction conditions, but is primarily governed by the nature of the phosphine ligands used. Additionally, an inherent regioselectivity is based on the substituents on the alkene substrates themselves, where more electron withdrawing groups lead to higher amounts of the branched aldehyde product. Considerable effort has been invested into the development and synthesis of chelating chiral bisphosphorus ligands. One of the drawbacks is the limited substrate scope for any single ligand.

The class of bisphosphite ligands gives good regioselectivity for different substrates, however, high enantioselectivity is sensitive to reaction temperature and is dependent on the substrate. A variety of bisphosphines show generally good enantioselectivity, but suffer from poor regioselectivity. (*S*)-Binapine **13** is able to yield some of the highest selectivities within this class.

Bisphospholane ligands stand out in ligands screens compared to all other ligand classes. With both high regio- and enantioselectivity, bisphospholanes are the most promising ligands for asymmetric hydroformylation. The features of the two-carbon linker and the substituents on the 2- and 5-positions of the five-membered phosphacycle play an important role in the induction of high selectivity control. Especially, (*S,S,S*)-BisDiazaPhos **20** and (*R,R*)-Ph-BPE **18** are overall the best ligands for yielding high selectivities at elevated temperatures of 80 °C for high reaction rates for the benchmark substrates styrene, vinyl acetate and allyl cyanide. Bisdiazaphospholanes have been studied to a great extent and found to be selective across a wide scope of substrates and are the most promising ligands for commercial application of asymmetric hydroformylation. These results are encouraging for further ligand designs with the focus on ligands adapted from the bisphospholane structures.

The development of hybrid bisphosphorus ligands was also proven to be quite successful. This strategy focuses on combining two phosphorus groups that are each known for good reactivity and selectivity. New examples of ligands have been created using this concept and were found to be very selective for different alkenes, for example alkyl alkenes.

Future developments will include the modification of the privileged ligands discussed herein, focusing on hybrid ligands and bisphospholane structures, especially the bisdiazaphospholane ligand class. Furthermore, sufficient studies on the models for selectivity prediction are necessary that can explain the coordination geometry and intrinsic steric evaluation of ligands both experimentally and computationally.

2.8 References

1. Roelen, O. Chemische Verwaltungsgesellschaft Oberhausen m.b.H., U.S. Patent 2327066, **1943**, German Patent DE 849548 U.S. Patent 2327066, **1938**.
2. Roelen, O. *Chem. Abstr.* **1944**, 38, 3631.
3. Naqvi, S., Oxo Alcohols. Process Economics Program Report 21E: SRI Consulting: Menlo Park, CA, **2010**.
4. Claver, C.; van Leeuwen, P. W. N. M. *Rhodium Catalyzed Hydroformylation*. Kluwer Academic Publishers: Dordrecht, **2000**.
5. Boerner, A.; Franke, R. *Hydroformylation - Fundamentals, Processes, and Applications on Organic Synthesis*. Wiley-VCH Verlag GmbH, Weinheim, Germany: **2016**.
6. Botteghi, C.; Paganelli, S.; Schionato, A.; Marchetti, M. *Chirality* **1991**, 3, 355–369.
7. Wilkinson, G. *Bull. Soc. Chim. Fr.* **1968**, 5055–5058.
8. Casey, C. P.; Whiteker, G. T. *Isr. J. Chem.* **1990**, 30, 299–304.
9. Casey, C. P.; Whiteker, G. T.; Melville, M. G.; Petrovich, L. M.; Gavney, J. A.; Powell, D. *J. Am. Chem. Soc.* **1992**, 114, 5535–5543.
10. Cuny, G. D.; Buchwald, S. L. *J. Am. Chem. Soc.* **1993**, 115, 2066–2068.

11. Tolman, C. A. *Chem. Rev.* **1977**, 77, 313–348.
12. Gleich, D.; Schmid, R.; Herrmann, W. A. *Organometallics* **1998**, 17, 2141–2143.
13. Gleich, D.; Schmid, R.; Herrmann, W. A. *Organometallics* **1998**, 17, 4828–4834.
14. Gleich, D.; Herrmann, W. A. *Organometallics* **1999**, 18, 4354–4361.
15. Brown, C. K.; Wilkinson, G. *Tetrahedron Lett.* **1969**, 10, 1725–1726.
16. Selent, D.; Wiese, K.-D.; Roettger, D. Boerner, A. *Ang. Chem. Int. Ed.* **2000**, 39, 1639–1641.
17. Breit, B.; Winde, R.; Mackewitz, T.; Paciello, R.; Harms, K. *Chem.Eur. J.* **2001**, 7, 3106–3121.
18. Keulemans, A. I. M.; Kwantes, A.; van Bavel, T. *Recl. Trav. Chim. Pays-Bas* **1948**, 67, 298–308.
19. Diéguez, M.; Pàmies, O.; Claver, C. *Tetrahedron: Asymmetry* **2004**, 15, 2113–2122.
20. Babin, J. E.; Whiteker, G. T. *Asymmetric Catalysis*, World Patent, WO 9303839. **1993**.
21. Diéguez, M.; Pàmies, O.; Ruiz, A.; Castillón, S.; Claver, C. *Chem.Eur. J.* **2001**, 7, 3086–3094.
22. Gual, A.; Godard, C.; Castillón, S.; Claver, C. *Adv. Syn. Cat.* **2010**, 352, 463–477.
23. Klosin, J.; Landis, C. R. *Acc. Chem. Res.* **2007**, 40, 1251–1259.
24. Tanaka, M.; Watanabe, Y.; Mitsudo, T.; Yamamoto, K.; Takegami, Y. *Chem. Lett.* **1972**, 1, 483–485.
25. Gladiali, S.; Pinna, L. *Tetrahedron: Asymmetry* **1991**, 2, 623–632.
26. Lu, S.; Li, X.; Wang, A. *Catalysis Today* **2000**, 63, 531–536.
27. Dierkes, P.; W. N. M. van Leeuwen, P. *Dalton Trans.* **1999**, 1519–1530.
28. Eckl, R. W.; Priermeier, T.; Herrmann, W. A. *J. Organomet. Chem.* **1997**, 532, 243–249.
29. Hoegaerts, D.; Jacobs, P. A. *Tetrahedron: Asymmetry* **1999**, 10, 3039–3043.
30. Masdeu-Bultó, A. M.; Orejón, A.; Castellanos, A.; Castillón, S.; Claver, C. *Tetrahedron: Asymmetry* **1996**, 7, 1829–1834.

31. Wang, X.; Buchwald, S. L. *J. Org. Chem.* **2013**, *78*, 3429–3433.
32. Wang, X.; Buchwald, S. L. *J. Am. Chem. Soc.* **2011**, *133*, 19080–19083.
33. Axtell, A. T.; Klosin, J.; Abboud, K. A. *Organometallics* **2006**, *25*, 5003–5009.
34. Burk, M. J.; Feaster, J. E.; Harlow, R. L. *Organometallics* **1990**, *9*, 2653–2655.
35. Burk, M. J. *Acc. Chem. Res.* **2000**, *33*, 363–372.
36. Pilkington, C. J.; Zanotti-Gerosa, A. *Org. Lett.* **2003**, *5*, 1273–1275.
37. Landis, C. R.; Jin, W.; Owen, J. S.; Clark, T. P. *Ang. Chem. Int. Ed.* **2001**, *40*, 3432–3434.
38. Adint, T. T.; Wong, G. W.; Landis, C. R. *J. Org. Chem.* **2013**, *78*, 4231–4238.
39. Jones, B. R.; Abrams, M. L.; Landis, C. R.; May, S. A.; Campbell, A. N.; Martinelli, J. R.; Calvin, J. R. *J. Org. Chem.* **2016**, *81*, 11965–11970.
40. Xu, K.; Zheng, X.; Wang, Z.; Zhang, X. *Chem. Eur. J.* **2014**, *20*, 4357–4362.
41. Axtell, A. T.; Cobley, C. J.; Klosin, J.; Whiteker, G. T.; Zanotti-Gerosa, A.; Abboud, K. A., *Angew. Chem. Int. Ed.* **2005**, *44*, 5834.
42. Clark, T. P.; Landis, C. R.; Freed, S. L.; Klosin, J.; Abboud, K. A. *J. Am. Chem. Soc.* **2005**, *127*, 5040–5042.
43. Watkins, A. L.; Hashiguchi, B. G.; Landis, C. R. *Org. Lett.* **2008**, *10*, 4553–4556.
44. McDonald, R. I.; Wong, G. W.; Neupane, R. P.; Stahl, S. S.; Landis, C. R. *J. Am. Chem. Soc.* **2010**, *132*, 14027–14029.
45. Abrams, M. L.; Foarta, F.; Landis, C. R. *J. Am. Chem. Soc.* **2014**, *136*, 14583–14588.
46. Risi, R. M.; Burke, S. D. *Org. Lett.* **2012**, *14*, 1180.
47. Watkins, A. L.; Landis, C. R. *Org. Lett.* **2011**, *13*, 164–167.
48. Sakai, N.; Mano, S.; Nozaki, K.; Takaya, H. *J. Am. Chem. Soc.* **1993**, *115*, 7033–7034.
49. Chikkali, S. H.; van der Vlugt, J. I.; Reek, J. N. H. *Coord. Chem. Rev.* **2014**, *262*, 1–15.
50. Noonan, G. M.; Fuentes, J. A.; Cobley, C. J.; Clarke, M. L. *Ang. Chem. Int. Ed.* **2012**, *51*, 2477–2480.

51. Yan, Y.; Zhang, X., *J. Am. Chem. Soc.* **2006**, *128*, 7198–7202.
52. Breeden, S.; Cole-Hamilton, D. J.; Foster, D. F.; Schwarz, G. J.; Wills, M. *Ang. Chem., Int. Ed.* **2000**, *39*, 4106–4108.
53. Zhao, B.; Peng, X.; Wang, Z.; Xia, C.; Ding, K. *Chem. Eur. J.* **2008**, *14*, 7847–7857.
54. Noonan, G. M.; Cobley, C. J.; Mahoney, T.; Clarke, M. L. *J. Chem. Soc. Chem. Comm.* **2014**, *50*, 1475–1477.
55. Chikkali, S. H.; Bellini, R.; de Bruin, B.; van der Vlugt, J. I.; Reek, J. N. H. *J. Am. Chem. Soc.* **2012**, *134*, 6607–6616.
56. Heck, R. F.; Breslow, D. S. *J. Am. Chem. Soc.* **1961**, *83*, 4023–4027.
57. Watkins, A. L.; Landis, C. R. *J. Am. Chem. Soc.* **2010**, *132*, 10306–10317.
58. Brown, J. M.; Kent, A. G. *J. Chem. Soc. Chem. Comm.* **1982**, 723–725.
59. Brown, J. M.; Kent, A. G. *J. Chem. Soc. Per. Trans. 2* **1987**, 1597–1607.
60. Nelsen, E. R.; Landis, C. R. *J. Am. Chem. Soc.* **2013**, *135*, 9636–9639.
61. Beach, N. J.; Knapp, S. M. M.; Landis, C. R. *Rev. Sci. Instr.* **2015**, *86*, 104101.
62. Abrams, M. L. *Dissertation*, University of Wisconsin-Madison, **2014**.
63. Nelsen, E. R.; Brezny, A. C.; Landis, C. R. *J. Am. Chem. Soc.* **2015**, *137*, 14208–14219.
64. Brezny, A. C.; Landis, C. R. *submitted*, **2016**.

Chapter 3

Regioselective Rhodium-Catalyzed Hydroformylation of Alkenes Utilizing Backbone-Modified Bisdiazaphospolanes

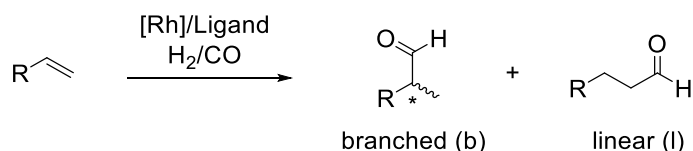
Julia Wildt, Anna Brezny and Clark R. Landis

Department of Chemistry, University of Wisconsin–Madison, 1101 University Avenue, Madison,
Wisconsin 53706

Anna Brezny has synthesized ligands **3**, **7** and **8** and performed hydroformylations of the allylic and cyclic substrates with ligands **3** and **4** and of all substrates with ligands **7** and **8**.

3.1 Introduction

Rhodium-catalyzed hydroformylation of alkenes is one of the largest homogeneously catalyzed transformations, producing over 18 billion pounds of oxo-products annually.¹ Hydroformylation meets all the requirements for an atom economic process, producing chiral aldehydes from inexpensive feed stocks (alkenes and syngas) under neutral reaction conditions.² Even though optically active aldehydes derived from the branched products are important intermediates in the synthesis of fine chemicals, pharmaceuticals and agrochemicals,³ asymmetric hydroformylation (AHF) is underutilized on the industrial scale. A challenge herein is to combine high regio- and enantioselectivities for a wide range of alkene substrates (Scheme 3.1).



Scheme 3.1. Rhodium-catalyzed hydroformylation of alkenes.

Control of regioselectivity alone, outside of catalyst system effects, is inherent to the directing effects exerted by the functional groups on the alkene. Electron-withdrawing groups primarily give rise to the branched product. It is important to control the regioselectivity with the nature of the chelating ligand, aiming for a high branched (b) to linear (l) ratio. The identification of new ligands for AHF has been a goal of much research over the past few decades. Many ligands have been reported for Rh-catalyzed hydroformylation, however, with the primary drawback of limited substrate scope for any single ligand. The ligands with the greatest demonstrated generality are the bisdiazaphospholane systems (Figure 3.1).⁴ Our group has demonstrated that bisdiazaphospholanes (BDP) are the most active ligands of all phosphorus-containing ligands. BDPs combine high regio- and enantioselective hydroformylation for a variety of alkene substrates, along with high activity while operating under mild conditions at low catalyst

loadings.^{5,6, 7,8,9} Ligands with similar key features to bisdiazaphospholanes are bisphospholanes such as (*R,R*)-Ph-BPE ((*R,R*)-1,2-Bis(2,5-diphenylphospholano)ethane) and DuPhos. In a ligand screen, (*R,R*)-Ph-BPE was found to be equally effective in combining high regio- and enantioselectivities for the three benchmark substrates styrene (*b* : *l* = 45 : 1 and 94% ee), vinyl acetate (*b* : *l* = 340 : 1 and 82% ee) and allyl cyanide (*b* : *l* = 7.1 : 1 and 90% ee).¹⁰ One major structural difference between BDPs and Ph-BPE lies in the hybridization of the atoms in the phospholane ring, sp^2 -hybridized N-atoms in the BDP ligand compared to sp^3 -hybridized C-atoms in Ph-BPE, resulting in a change in the phospholane ring conformation. Clearly, this feature seems to have an influence on the regioselectivity of catalytic hydroformylation, even though the phenyl rings in the 2-and 5-positions of the five-membered ring bear no additional substituents.

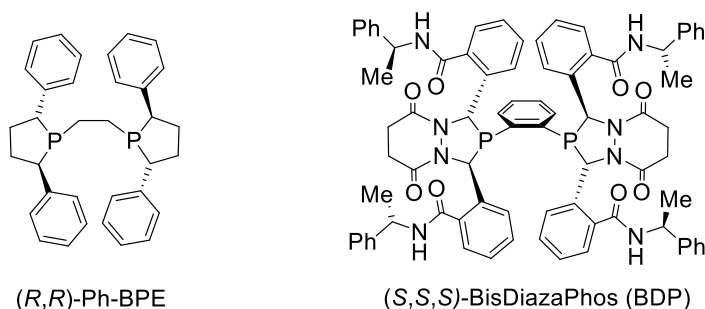


Figure 3.1. Ligands (*R,R*)-Ph-BPE and (*S,S,S*)-BisDiazaPhos (BDP).

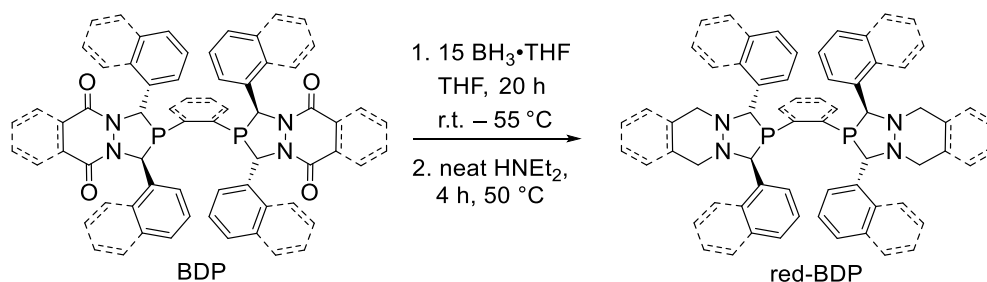
We sought to modify bisdiazaphospholane ligands to contain an all sp^3 -based diazaphospholane ring and investigate the effects primarily on the regioselectivity this structural modification can have. This modification is accomplished by the reduction of the acylhydrazine group to an alkylhydrazine backbone. Herein, we report the synthesis of a collection of reduced, alkylhydrazine-derived bisdiazaphospholanes (red-BDP) containing an all sp^3 -hybridized diazaphospholane ring. Regioselectivity of red-BDPs in the hydroformylation of a range of alkene

substrates are compared to their sp^2 -hybridized acylhydrazine BDPs derivatives, demonstrating the effect of phospholane ring conformation on regioselectivity preferences.

3.2 Results and Discussion

3.2.1 Synthesis of electronically reduced Bisdiazaphospholanes

Conversion of an N,N' -diacyl-3,4-hydrazine to an N,N' -diacyl-3,4-hydrazine is achieved by utilizing $\text{BH}_3 \cdot \text{SMe}_2$ without rupturing the hydrazine bond.¹¹ This reduction method has been previously applied to monodiazaphospholanes by Nelson and Landis.¹² To date, Rh-catalyzed hydroformylation of alkenes with alkylhydrazine-derived diazaphospholanes has not been explored. For this purpose, we have further expanded the borane-reduction towards bisdiazaphospholane ligands. To assure a clean reduction of all acyl groups, we found that $\text{BH}_3 \cdot \text{THF}$ is a more suitable reagent than $\text{BH}_3 \cdot \text{SMe}_2$. Reacting the bisdiazaphospholanes (BDP) with a 2.5-fold excess of borane leads first to the reduced alkylhydrazine phospholane as its phosphine-borane adduct. This adduct is broken by heating the phosphine-borane adduct with HNEt_2 to obtain the desired reduced bisdiazaphospholanes (red-BDPs) (Scheme 3.2).



Scheme 3.2. Reduction of the acylhydrazine backbone of bisdiazaphospholanes towards an alkylhydrazine red-BDPs using $\text{BH}_3 \cdot \text{THF}$.

The bisdiazaphospholanes herein vary in their backbone (succinyl or phthaloyl), the bridge between the phosphorous atoms (phenylene or ethylene) as well as the substituents in the 2- and

5- positions (phenyl or naphthyl) with the purpose of investigating their effect on the regioselectivity in the Rh-catalyzed hydroformylation for a variety of alkenes (Figure 3.2). All bisdiazaphospholanes underwent quantitative reduction to their alkylhydrazine derivative. The reduction of BDPs **1** and **3** was performed at 55 °C for 20 h, whereas the tetranaphthyl derivative has to be reacted at room temperature to prevent from over reduction of the diazaphospholane moiety back to the primary phosphine. The ethylene bridge bearing BDPE **5**, however, is found to be very air sensitive and most of the material was isolated as its phosphine oxide, which was used for the reduction procedure. The reaction with $\text{BH}_3 \cdot \text{THF}$ was conducted at room temperature and to our surprise also reduced the phosphine oxide quantitatively to the tertiary phosphine. Reductions of phosphine oxides typically require reaction with hydrosilanes, such as Ph_3SiH .¹³

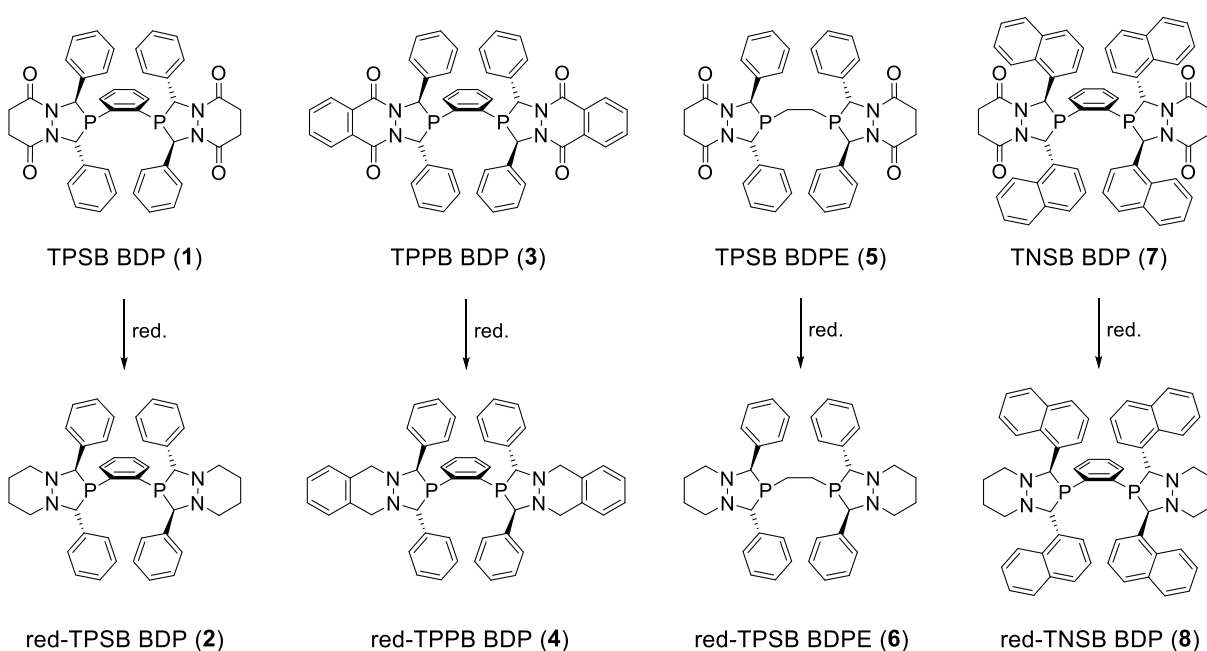


Figure 3.2. Bisdiazaphospholanes **1**, **3**, **5** and **7** and their reduced derivatives **2**, **4**, **6** and **8**.

In the process of NMR-spectroscopic characterization, a difference in the appearances of the H-atom signals in the ^1H NMR spectrum corresponding to the methine-protons in the diazaphospholane ring between the phenylene and ethylene bridge ligands was noted (Figure 3.3). Phenylene bridged BDPs with a racemic configuration are known to contain two inequivalent methine protons. For ligand **1**, the signals are displayed as a broad signal next to a triplet signal (Figure 3.3, top). One would expect only a doublet due to the coupling of the H-atom to the closest P-atom. However, the signal is an apparent triplet, seeming like a first-order pattern, but containing superficially misleading splitting information. This phenomenon is known as virtual coupling. Additional coupling of nuclei arises when the atom of interest (A) is coupled to another atom (B) that has a strong coupling to another atom (C) and the difference in chemical shift between atoms B and C is small. In the BDPs, despite being magnetically equivalent, the two P-atoms are strongly coupled, meaning that $J_{\text{P-P}} > \Delta\nu_{\text{P-P}}$.¹⁴⁻¹⁶ In contrast, the ethylene bridged BDP **5** shows two signals, one as a broad singlet, and one as an apparent doublet of doublets (Figure 3.3, bottom). Comparable virtual splitting patterns have been observed for other ethylene bridged bisphosphines.¹⁷ To get a sense for the coupling pattern and the size of the coupling constant between the phosphorous atoms, the experimental spectra (red) have been simulated for ligands **1** and **5** using the WINDNMR program¹⁸ developed by Hans Reich, starting from a '4-spin' coupling simulation (blue). The splitting pattern can be assigned as AA'XX' and the size for the coupling constant $^3J_{\text{P-P}}$ in **1** is on the order of 200 Hz, whereas the pattern for **5** arises when the coupling constant is on the order of 13 Hz. The height of each peak is sign-sensitive and to obtain the correct height and shape of the peak, the $^5J_{\text{H-P}}$ coupling constants must be negative. In addition, the broadness and overall shape of the peak tops are further adjusted by adding a small coupling constant of 0.8 and 0.9 Hz between the two methine protons, common for a proton-proton-coupling in five-membered rings. Unfortunately, the singlet-shaped signal for H2 in **5** could not be adjusted simultaneously with signal H1, and the overall height and broadness do not line up with the experimental data. This signal can be simulated independently when the

coupling constant $^3J_{P-P}$ is 45.5 Hz, while the doublet of doublets shape of H1 is lost and is converted to a triplet-like pattern.

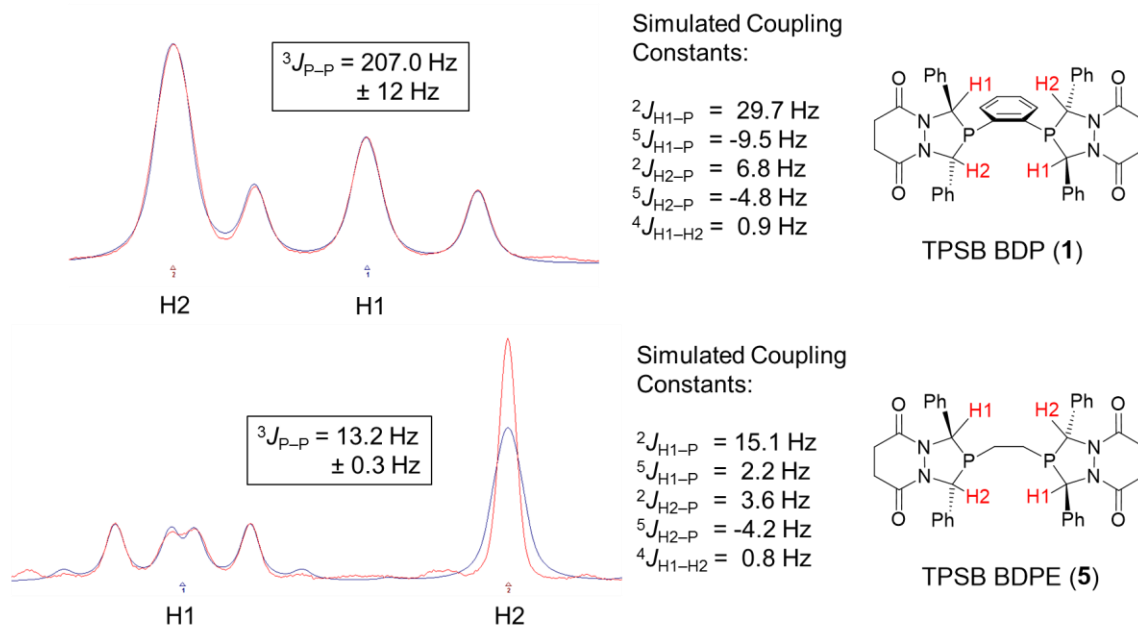


Figure 3.3. Methine protons in the ^1H NMR spectra of ligands **1** and **5**, coupling constants determined with the WINDNMR simulation program (red: experimental; blue: simulated).

The overall difference in P-P-atom coupling can be explained by the relative orientation of the P-atoms towards each other. While the phenylene-bridge is more rigid and forces the P-atoms to be in plane with a $P-C(sp^2)-C(sp^2)-P$ torsion angle of 1° , the ethylene bridge allows for fluctuation with a calculated $P-C(sp^3)-C(sp^3)-P$ torsion angle of 146° (Figure 3.4), resulting in less coupling between the P-atoms.

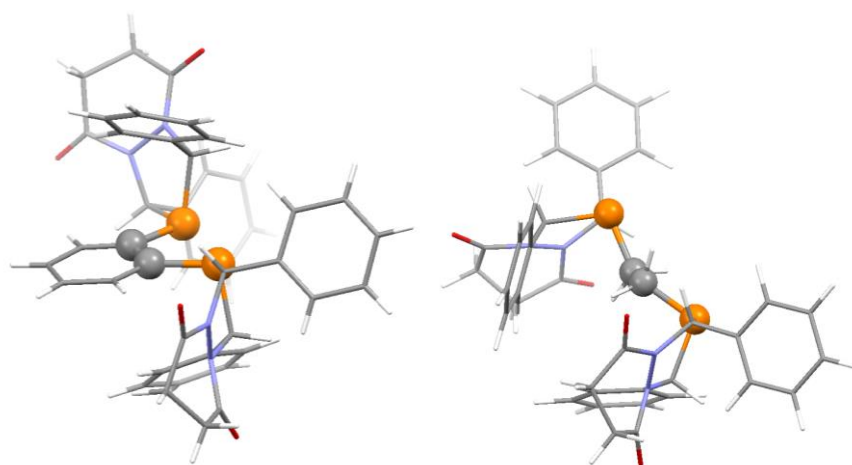


Figure 3.4. BDP ligands TPSB BDP **1** (left) and TPSB BDPE **5** (right) indicating the conformational difference due to the bridge between the P-atoms (P–C–P shown as spheres).

3.2.2 Hydroformylation of Benchmark Substrates Styrene, Vinyl Acetate and Allyl Cyanide

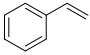
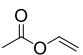
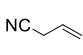
It is known that reduction of the sp^2 -hybridized N-atom to an sp^3 -hybridized N-atom in the diazaphospholane ring has structural effects relative to the ring puckering.¹² These structural changes in the ligand have not been explored in the selectivity control of Rh-catalyzed hydroformylation to this point. The new red-BDP ligands **2**, **4**, **6** and **8** were tested on a variety of substrates and compared to their BDP control ligands **1**, **3**, **5** and **7**. The active catalyst was prepared by mixing a solution of $[\text{Rh}(\text{acac})(\text{CO})]_2$ and 1.5 equiv. of ligand to ensure full rhodium complexation. This solution was pressurized with syngas (H_2/CO (1 : 1 molar ratio)) to 150 psig and heated at 60 °C for at least 1 h under vigorous stirring to give the precatalyst $[\text{RhH}(\text{CO})_2\text{PP}]$.

Initially, hydroformylation of benchmark substrates with ligands **1** – **4** was performed at 80 °C, 150 psig of syngas pressure and 3 h reaction time to have a direct comparison with ligands (*R,R*)-Ph-BPE and (*S,S,S*)-BisDiazaPhos from a previous ligand screening (Table 3.1).¹⁹ Remarkably, the reduced bisdiazaphospholane analogues show a great increase in the regioselectivity (entries 2 and 4), outperforming (*S,S,S*)-BisDiazaPhos (entry 6). Under the test conditions the branched selectivities don't exceed those observed with Ph-BPE in entry 7, however, it becomes clear that the structural changes reflected in **1** – **4** affects the regioselectivities with the reduced ligands

resembling Ph-BPE-like behavior. In addition, the reduced diazaphospholane ligands show higher activity compared to Ph-BPE, as revealed by higher conversions under the trial conditions.

Table 3.1. Hydroformylation of Benchmark Substrates Styrene, Vinyl Acetate and Allyl Cyanide.^a

$$\begin{array}{c}
 \text{R-CH=CH}_2 \\
 \xrightarrow[\text{toluene, 80 } ^\circ\text{C, 3h}]{\begin{array}{l} 0.020 \text{ mol\% [Rhacac(CO)}_2\text{]} \\ 0.024 \text{ mol\% Ligand} \\ 150 \text{ psig H}_2\text{/CO (1 : 1)} \end{array}} \\
 \begin{array}{cc}
 \begin{array}{c} \text{O} \\ \parallel \\ \text{R}-\text{CH}-\text{CH}_2-\text{CHO} \\ \text{branched (b)} \end{array} & + & \begin{array}{c} \text{O} \\ \parallel \\ \text{R}-\text{CH}_2-\text{CH}_2-\text{CHO} \\ \text{linear (l)} \end{array}
 \end{array}
 \end{array}$$

Entry	Ligand	conv. (%)	 b : l	conv. (%)	 b : l	conv. (%)	 b : l
1	TPSB BDP (1)	>99	7.7 : 1	98	8.2 : 1	>99	4.3 : 1
2	red-TPSB BDP (2)	98	30 : 1	89	>50 : 1	98	7.2 : 1
3	TPPB BDP (3)	100	5.7 : 1	95	9.2 : 1	>99	4.6 : 1
4 ^b	red-TPPB BDP (4)	>99	25 : 1	93	>50 : 1	>99	6.4 : 1
5 ^c	(<i>R,R</i>)-Ph-BPE	57	45 : 1	52	370 : 1	96	7.1 : 1
6 ^c	(<i>S,S,S</i>)-BisDiazaPhos	100	6.6 : 1	100	37 : 1	100	4.0 : 1

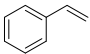
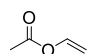
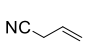
^a Conditions: one pot screen of all 3 substrates, total alkene/Rh = 5000 : 1, [alkene] = 1.5 M, Rh/L = 1 : 1.2, conversions and b : l ratios were determined by ¹H NMR spectroscopy. ^b ligand was used as Rh(acac)(4)-complex. ^c same standard conditions.¹⁹

The benchmark substrates styrene, vinyl acetate and allyl cyanide were further tested at lower reaction temperature, 60 °C, 150 psig syngas pressure, and 0.02 mol% catalyst loading after 16 h with ligands **1** – **8** (Table 3.2). Styrene was hydroformylated competitively with allyl cyanide and vinyl acetate competitively with allyloxy-*tert*-butyldimethylsilane were performed, (*vide infra*, Table 3.3). All ligands show nearly quantitative conversion ranging from 98 to 100% for BDP ligands (entry 1, 3, 5 and 7) and 80 to 100% for red-BDPs (entry 2, 4, 6, and 8) at standard conditions of

60 °C,. The regioselectivity for all benchmark substrates is drastically increased with red-BDPs (entry 2, 4, 6 and 8), relative to the non-reduced ligands, in favor of the branched isomer (Table 3.2). For styrene hydroformylation, BDP ligands exhibit branched to linear ratios on the order of 10 : 1. In contrast, the reduced ligands show high selectivity control for the branched styrene aldehyde product of at least 39 : 1. The most effective ligand is red-TNSB BDP **8** with a >50 : 1 branched to linear ratio (entry 8). Compared to the (S,S,S)-BisDiazaPhos (entry 9), red-TNSB BDP has an over 2.7-fold increase in regioselectivity, favoring the branched isomer. All reduced ligands are highly branched selective for vinyl acetate (b : l = >50 : 1), however, slightly lower conversions are observed with all reduced ligands compared to their non-reduced parents. The only other ligand leading to selectivities of these magnitudes is (*R,R*)-Ph-BPE (at 80 °C: styrene b : l = 45 : 1; vinyl acetate b : l = 370 : 1).²⁰ Regioselectivity control for allyl cyanide is approximately doubled by using the reduced ligands **2**, **4** and **6** (entry 2, 4 and 6) over their non-reduced derivatives **1**, **3** and **5** (entry 1, 3 and 5). Remarkably, red-TNSB BDP **8** exhibits a 5-fold increase of the branched to linear ratio from 4 : 1 to 20 : 1 compared to its control ligand **7** for allyl cyanide. The only other regioselectivities with a branched to linear ratio of around 10 : 1 or higher were found with (*R,R*)-BDPP (b : l = 16 : 1), JosiPhos (b : l = 14.1 : 1) and (S,S)-Kelliphite (b : l = 9.9 : 1) at 80 °C.^{10, 20}

For each substrate, the reduced ligands outperform the BDP control ligands with respect to regioselectivity control. Ligand **8** gives the highest regioselectivities, however, ligand **2** is as selective with styrene and vinyl acetate. The overall lowest regioselectivities are observed with the red-TPPB BDP bearing the more rigid phthaloyl backbone, followed by the ethylene bridged ligand **4** (entry 4).

Table 3.2. Hydroformylation of Benchmark Substrates Styrene, Vinyl acetate and Allyl cyanide.^a

<div style="text-align: center;"> $\begin{array}{c} \text{R}-\text{CH}=\text{CH}_2 \\ \xrightarrow[\text{THF or THF/DCM, 60 } ^\circ\text{C}]{\begin{array}{c} 0.02 \text{ mol\% [Rhacac(CO)}_2\text{]} \\ 0.03 \text{ mol\% Ligand} \\ 150 \text{ psig H}_2\text{/CO (1 : 1)} \end{array}} \\ \begin{array}{c} \text{O} \\ \parallel \\ \text{R}-\text{CH}-\text{CH}_2-\text{CHO} \\ \text{R}^* \\ \text{branched (b)} \end{array} + \begin{array}{c} \text{O} \\ \parallel \\ \text{R}-\text{CH}_2-\text{CH}_2-\text{CHO} \\ \text{linear (l)} \end{array} \end{array}$ </div>							
Entry	Ligand	conv. (%)	 b : l	conv. (%)	 b : l	conv. (%)	 b : l
1 ^b	TPSB BDP (1)	100	13.6 : 1	98	12.3 : 1	100	4.7 : 1
2	red-TPSB BDP (2)	>99	49 : 1	89	>50 : 1	>99	9.4 : 1
3 ^b	TPPB BDP (3)	100	8.5 : 1	98	13.2 : 1	100	5.0 : 1
4	red-TPPB BDP (4)	100	39 : 1	94	>50 : 1	100	7.5 : 1
5 ^b	TPSB BDPE (5)	>99	9.1 : 1	98	16.0 : 1	>99	3.6 : 1
6	red-TPSB BDPE (6)	99	47 : 1	90	>50 : 1	99	7.8 : 1
7 ^b	TNSB BDP (7)	100	10 : 1	100	22 : 1	99	4.0 : 1
8	red-TNSB BDP (8)	80	50 : 1	93	>50 : 1	99	20 : 1
9 ^c	(S,S,S) -BisDiazaPhos	87	18.3 : 1	98	>50 : 1	---	---

^a Conditions: total alkene/Rh = 2500 : 1, [alkene] = 1.5 M, Rh/L = 1 : 1.5 to ensure full ligation of Rh; run as one pot reaction with styrene and allyl cyanide and vinyl acetate with allyloxy *tert*-butyldimethylsilane, branched to linear ratios and conversion were determined by ¹H NMR spectroscopy. ^b ligand added as stock solution in DCM for solubility. ^c standard conditions except of 1600 : 1 total alkene/Rh; 4 h reaction time, run as a one-pot screen with styrene, vinyl acetate and allyloxy-*tert*-butyldimethylsilane.⁸

3.2.3 Hydroformylation of Allylic Alkenes

Regioselective control of allylic substrates commonly is challenging. Due to the improved regioselectivities for allyl cyanide hydroformylation using our reduced ligands, we investigated the hydroformylation of the allylic substrates allyl alcohol, allyloxy-*tert*-butyldimethylsilane and 3-butenic acid (Table 3.3). Previous work has shown an intrinsic preference for the linear aldehyde in the hydroformylation of allyl alcohol. For example, (S,S,S)-BisDiazaPhos yields predominantly the linear aldehyde in a branched to linear ratio of 1 : 3.4 (entry 9).⁷ Nozaki's phosphine-phosphite BinaPhos ligand shows a branched to linear ratio of 1 : 9.²¹ Selectivity of allyl alcohol hydroformylation for the branched aldehyde product was observed for the first time with the cyclic aminated phosphine through directed and intramolecular hydroformylation by Tan and coworkers (b : l = 6.7 : 1).²² Hydroformylation with the non-reduced BDPs **1**, **3** and **7** show a slight preference for the branched aldehyde product (b : l = 1.7 : 1, 1.5 : 1 and 2.0 : 1, respectively). The amount of branched aldehyde product increased with the reduced ligands, in particular with red-TPSB BDP **1** and red-TNSB BDP **8** by 4.4 and 5.0-fold, respectively, giving rise to an outstanding branched to linear ratio of 10 : 1 with red-TNSB BDP. Allyl alcohol can isomerize to propanal under hydroformylation conditions. The reduced ligands have a lower tendency to isomerize allyl alcohol compared to the non-reduced BDP ligands. Propanal is typically formed in around 10% with the BDPs and only to 2% with the reduced ligands. The highest amount of propanal of 10% is observed with ligand **5**. Hydroformylation of allyloxy-*tert*-butyldimethylsilane represents an attractive and alternate route to "Roche Aldehydes", which are very common building blocks in the synthesis of biologically active compounds.^{7, 23-25} Even though (S,S,S)-BisDiazaPhos leads to a higher branched to linear ratio for allyloxy-*tert*-butyldimethylsilane compared to the unprotected allyl alcohol, this trend is not observed with the BDP ligands herein. Non-reduced ligands **1**, **3**, **5**, and **7** give only a 1 : 1 ratio for the aldehyde product (entry 1, 3, 5 and 7). The ratios increase to about 3–4 : 1, with the highest value being obtained by red-TNSB BDP **8** (b : l = 4 : 1, entry 8). Hydroformylation of 3-butenic acid has been

previously reported by Breit and coworkers using a guanidine-substituted monophosphine favoring the linear aldehyde product (b : l = 1 : 23).²⁶ Reek and coworkers also showed a linear preference of 1: 1.9 with the DIMPhos ligand.²⁷ The BDP ligands favor slightly the branched aldehyde product (entries 1, 3, 5 and 7). Hydroformylation with the reduced ligands leads to an increase in regioselectivity to over 5 : 1, the highest selectivity is observed with red-TPPB BDP **4** (b : l = 6.5 : 1) and red-TNSB BDP **8** (b : l = 8.8 : 1).

Table 3.3. Screening of Allylic Alkene Substrates.^a

$\text{R}-\text{CH}=\text{CH}_2 \xrightarrow[\text{THF or THF/DCM}]{\begin{array}{l} 0.02 \text{ mol\% } [\text{Rhacac}(\text{CO})_2] \\ 0.03 \text{ mol\% Ligand} \\ 150 \text{ psig } \text{H}_2/\text{CO} (1 : 1) \end{array}} \begin{array}{c} \text{O} \\ \parallel \\ \text{R}-\text{CH}-\text{CH}_2 \\ \text{branched (b)} \end{array} + \begin{array}{c} \text{O} \\ \parallel \\ \text{R}-\text{CH}_2-\text{CH}_2-\text{CH}_2-\text{CHO} \\ \text{linear (l)} \end{array}$							
		$\text{HO}-\text{CH}_2-\text{CH}=\text{CH}_2 \quad b$		$\text{TBS}-\text{O}-\text{CH}_2-\text{CH}=\text{CH}_2$		$\text{HO}-\text{C}(=\text{O})-\text{CH}_2-\text{CH}=\text{CH}_2 \quad c$	
Entry	Ligand	conv. (%)	b : l	conv. (%)	b : l	conv. (%)	b : l
1	TPSB BDP (1)	39	1.7 : 1	>99	1.1 : 1	>99	2.1 : 1
2	red-TPSB BDP (2)	70	7.4 : 1	98	3.5 : 1	>99	5.8 : 1
3	TPPB BDP (3)	30	1.5 : 1	95	1 : 1	>99	2.6 : 1
4	red-TPPB BDP (4)	70	4.4 : 1	100	3.1 : 1	>99	6.5 : 1
5	TPSB BDPE (5)	34	1 : 1.1	>99	1 : 1.2	>99	1.1 : 1
6	red-TPSB BDPE (6)	67	3.8 : 1	>99	3.5 : 1	99	4.9 : 1
7	TNSB BDP (7)	100	2.0 : 1	83	1 : 1	100	2.3 : 1
8	red-TNSB BDP (8)	65	10.0 : 1	100	4.0 : 1	83	8.8 : 1
9 ^d	(S,S,S) -BisDiazaPhos	99	1 : 3.4	99	2.0 : 1	---	---

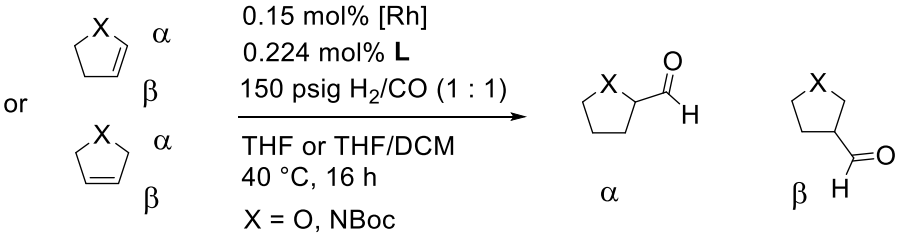
^a Conditions: 60 °C, total alkene/Rh = 2500 : 1, [alkene] = 1.5 M, Rh/L = 1 : 1.5 to ensure full ligation of Rh; ligand added as stock solution in DCM for solubility; allyloxy-*tert*-butyldimethylsilane was run as one pot reaction with vinyl acetate; conversion and b : l ratios determined by ¹H NMR spectroscopy. ^b allyl alcohol was run at 40 °C, hydroformylation products were converted to the pinacolyl acetal; % of 1-propanal of total product mixture formed: BDPs **1**: 7%, **3**: 2%, **5**: 10%, **7**: 2%, red-BDPs **2**: 1%, **4**: <1%, **6**: 3%, **8**: 1%. ^c a few drops of NEt₃ were added to the hydroformylation product mixture before obtaining ¹H NMR spectrum. ^d conditions: [alkene] = 0.75 M in toluene, total alkene/Rh = 200 : 1; 4 h reaction time, 140 psig syngas pressure.⁷

3.2.4 Hydroformylation of Cyclic, Heteroatom-Containing Alkenes

The hydroformylation products of cyclic alkenes, such as *N*-Boc-2,3-dihydropyrrole and 2,3- and 2,5-dihydrofurans are useful precursors and intermediates in organic synthesis.²⁸⁻³² This substrate class was evaluated (Table 3.4) with ligands **1** – **8**. Hydroformylation of *N*-Boc-2,3-dihydropyrrole shows preference for the α -aldehyde (because only branched products are possible for these disubstituted alkenes, the regioisomeric products are labeled as α and β with respect to the heteroatom) product with all tested ligands. Ligands **2**, **4**, and **6** favor the α -product by approximately 1.1 – 1.6 times. The highest regioselectivity is observed with ligands **5** and **6** with $\alpha : \beta = 11.0 : 1$ and $12.2 : 1$, respectively. Interestingly, TNSB BDP **7** shows already good selectivity for the α -aldehyde product with $9.1 : 1$ ratio, but an increase in regioselectivity was not observed using the reduced ligand **8**, rather a drop in the $\alpha : \beta$ ratio to $5.9 : 1$. This result is likely explained by the sterically more bulky naphthyl-substituent. Unlike the selectivity with (S,S,S)-BisDiazaPhos of $2.8 : 1$ in the hydroformylation of 2,3-dihydrofuran (entry 9), BDPs **1**, **2**, **3** and **4** exhibit slight preference for the β -aldehyde product. Under the conditions examined, the highest $\alpha : \beta$ ratio of $2.5 : 1$ is observed with TNSB BDP **7**. In contrast with our observations with previous substrates, all reduced ligands are less selective than their non-reduced equivalents for 2,3-dihydrofuran. Conversions with the reduced ligands are lower for both cyclic 2,3-dihydro substrates and hydroformylation proceed 2 to 4-times slower (entries 2, 4, 6 and 8), red-TNSB BDP is even 20 times slower. Reduced ligands **2**, **4** and **6** give high selectivity for the 2,5-dihydrofuran β -aldehyde product with $\alpha : \beta$ ratios on the order of $1 : 50$, which is better than was reported with (S,S,S)-BisDiazaPhos ($1 : 15$, entry 9). Compared to the tetranaphthyl derivative **7**, red-TNSB BDP **8** exhibits a drop in selectivity from $1 : 14$ to $1 : 6.5$. Ligand **7** yields selectivities comparable to (S,S,S)-BisDiazaPhos. Interestingly, ligand **8** shows again lower selectivity for the β -regioisomer (entry 8). Opposite to the 2,3-dihydro alkenes, the 2,5-dihydrofuran exhibits higher conversion when using the reduced ligands (entries 2, 4, 6, and 8).

Minor formation of 2,3-dihydrofuran through isomerization of the double bond in 2,5-dihydrofuran is observed. As has been already shown in the hydroformylation with allyl alcohol, the reduced ligand **2**, **4**, **6**, and **8** exhibit much lower isomerization. Isomerization product 2,3-dihydrofuran is typically formed in around 6 – 16% with the BDPs and only to 1 – 4% with the reduced ligands.

Table 3.4. Hydroformylation of Cyclic Alkenes.^a

							
Entry	Ligand	conv. (%)	$\alpha : \beta$	conv. (%)	$\alpha : \beta$	conv. (%)	$\alpha : \beta$
1	TPSB BDP (1)	91	5.7 : 1	74	1 : 1.2	42	1 : 50
2	red-TPSB BDP (2)	20	8.2 : 1	11	1 : 1.4	62	<1 : 50
3	TPPB BDP (3)	98	4.6 : 1	90	1 : 1.7	21	1 : 44
4	red-TPPB BDP (4)	15	7.5 : 1	13	1 : 1.9	80	<1 : 50
5	TPSB BDPE (5)	93	11.0 : 1	74	1.6 : 1	24	1 : 30
6	red-TPSB BDPE (6)	55	12.2 : 1	46	1 : 1	58	<1 : 50
7	TNSB BDP (7)	90	9.1 : 1	84	2.5 : 1	3	1 : 14.0
8	red-TNSB BDP (8)	4	5.9 : 1	4	1.6 : 1	6	1 : 6.5
9	(S,S,S)-BisDiazaPhos	99	10.4 : 1 ^b	25	2.8 : 1 ^c	80	1 : 15.0 ^c

^a Conditions: total alkene/Rh = 670 : 1, [alkene] = 1.5 M, Rh/L = 1 : 1.5 to ensure full ligation of Rh; ligand added as stock solution in DCM for solubility; conversion and $\alpha : \beta$ ratios determined by ¹H NMR spectroscopy. ^b conditions: 60 °C, 15 h, 140 psig syngas, total alkene/Rh = 200 : 1, [alkene] = 0.75 M in toluene, Rh/Ligand = 1 : 1.1.⁷ ^c conditions: 40 °C, 4 h, 150 psig syngas, total alkene/Rh = 670 : 1, [alkene] = 2.6 M in toluene/THF, Rh/Ligand = 1 : 1.1.⁸ ^d % of 2,3-dihydrofuran of total product mixture formed: BDPs **1**: 6%, **3**: 16%, **5**: 8%, **7**: 6%, red-BDPs **2**: 1%, **4**: 4%, **6**: 1%, **8**: 1%.

3.2.5 Summary and Conclusions Regarding Reduced Ligands

Overall, the regioselectivity for terminal alkenes increases by using the reduced ligands **2**, **4**, **6** and **8**. An even higher amount of branched aldehyde is observed than when using the state-of-the-art (S,S,S)-BisDiazaPhos. The total changes in regioselectivities are summarized in Table 3.5. The highest branched to linear ratios for all terminal alkenes are observed with red-TNSB BDP **8**. In particular, control towards the branched product of the allylic substrates allyl cyanide, allyl alcohol and 3-butenic acid is by far higher than for any other ligand tested. Ligand **8**, however, is not suitable for selective hydroformylation of the cyclic alkenes. In fact, regioselectivities decline for all cyclic alkenes (entries 7, 8 and 9). In general, ligand **8** shows a drop in conversion for most substrates compared to the other reduced ligands **2**, **4** and **6**, explained by the increased steric bulk of the naphthyl compared to phenyl substituent on the catalyst periphery, as well as lower conversion compared to its control ligand **7**. The next best ligand is red-TPSB BDP **2**, exhibiting generally the best activity for terminal, as well as cyclic alkenes when considering both conversion and regioselectivity. Branched to linear ratios are the lowest with red-TPPB BDP **4**, except with allyl alcohol and 3-butenic acid. Lower selectivity control can be correlated with the small torsion angle of the reduced ligands of 49° compared to all other reduced ligands (*vide infra*). Even though ligand red-TPSB BDPE **6** gives the lowest regioselectivities after ligand **4**, it exhibits the largest total increase, after ligand **8**, in regioselectivity for the alkenes styrene and 3-butenic acid (entries 1 and 6) and the second largest, after ligand **8**, for allyl cyanide, allyloxy silane and 2,5-dihydrofuran (entries 3, 5 and 9). In addition, ligand **6** shows the best regioselectivity for *N*-Boc-2,3-dihydropyrole. Substrate 2,3-dihydrofuran is the most challenging to address with all ligands (entry 8) and the amount of the α -product formed in fact decreases.

Table 3.5. Total Fold Increase in Branched Regioselectivity of red-BDP Compared to BDP; Numbers in () Indicating a Decrease in the Selectivity for the α -Product.

Entry	Substrate	red-TPSB BDP (2)	red-TPPB BDP (4)	red-TPSB BDPE (6)	red-TNSB BDP (8)
1	Styrene	3.7	4.6	5.2	5.0
2	Vinyl acetate	>4.1	>3.8	>3.1	>2.3
3	Allyl cyanide	2.0	1.5	2.2	5.0
4	Allyl alcohol	4.4	2.9	3.8	5.0
5	Allyloxy silane	3.2	3.1	3.6	4.0
6	3-Butenoic acid	2.8	2.5	4.4	3.8
7	<i>N</i> -Boc-2,3-dihydropyrrole	1.4	1.6	1.1	(1.5)
8	2,3-Dihydrofuran	(1.2)	(1.1)	(1.5)	(1.6)
9	2,5-Dihydrofuran	>1	>1	>1.4	(2.2)

3.2.6 Conformational Analysis of Reduced Ligands

To gain more insight into the control of regioselectivity towards the branched aldehyde, the conformation of the diazaphospholane ring of red-BDPs and BDPs were compared. Crystallographic structures of **1** – **4** as well as **7** and **8** were obtained and the C–N–N–C torsion angle (θ) in the diazaphospholane ring of each structure was evaluated. The torsion angle (θ) is the observed dihedral angle when the diazaphospholane ring is oriented in the Newman-projection along the N–N-bond (Figure 3.5).

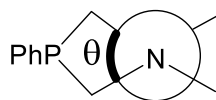


Figure 3.5. Definition of the torsion angle (θ) within the diazaphospholane moiety.

The ligands **1** and **2** in Figure 3.6 are oriented along the N–N-bond of the diazaphospholane ring and the structural changes in the ring conformation are clearly visible. The torsion angle (θ) of the C–N–N–C-connection in the reduced ligands is by far greater than their non-reduced equivalents. The BDP ligands **1** and **3** have a torsion angle of 19.2° and 10.4° , respectively, whereas the red-BDP ligands **2** and **4** show a torsion angle of 62.1° and 56.0° , respectively (Figure 3.6 and Figure 3.7). This torsion angles for the BDPE ligands **5** and **6** were obtained through geometry optimization calculations because the crystallographic structures were not available; the values are 56.4° and 14.0° for the red-BDPE ligand **6** and BDPE **5**, respectively (Figure 3.8). TNSB BDP **7** displays a torsion angle of 33.4° and red-TNSB BDP **8** 58.6° (Figure 3.9). The conformation of the reduced ligands resemble the typical half-chair conformation in cyclopentane-rings.

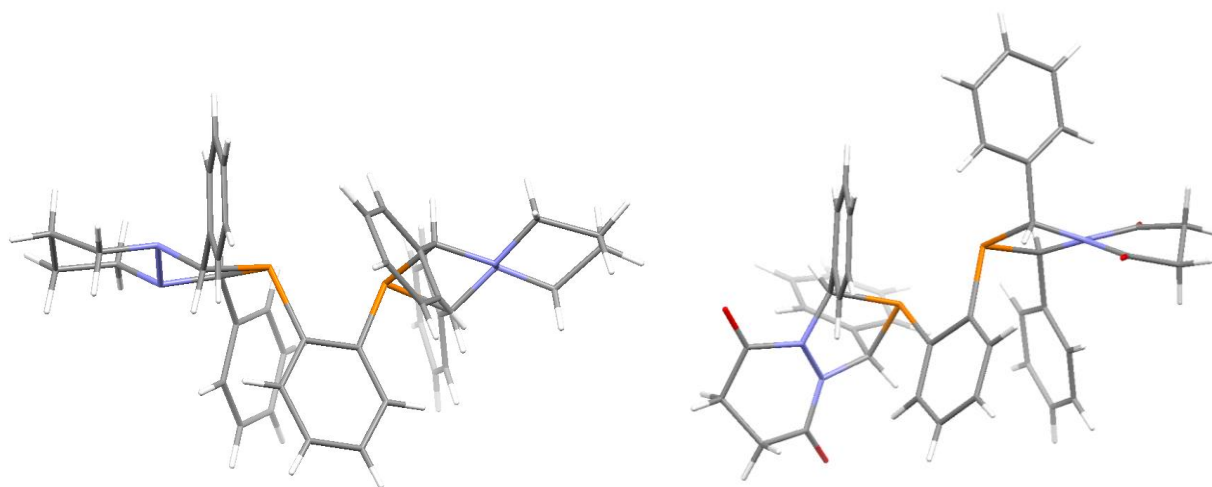


Figure 3.6. Crystal structures of red-TPSB BDP **2** (left, $\theta = 62.1^\circ$) and TPSB BDP **1** (right, $\theta = 19.2^\circ$), oriented along the N–N bond of one of the diazaphospholane rings (blue: nitrogen atoms, orange: phosphorous atoms, red: oxygen atoms).

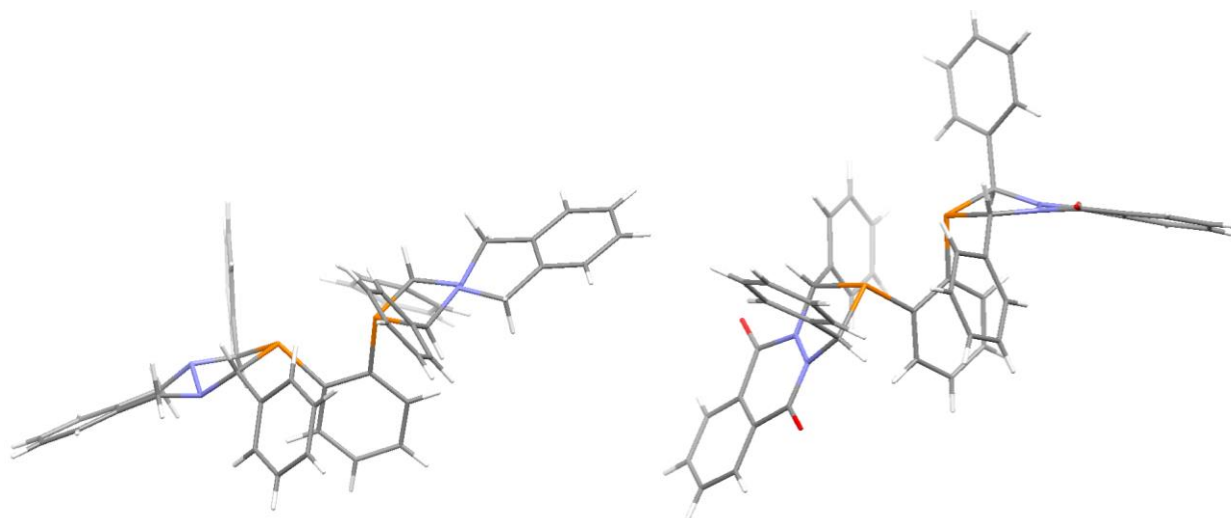


Figure 3.7. Crystal structures of red-TPPB BDP **4** (left, $\theta = 56.0$) and TPPB BDP **3** (right, $\theta = 10.4^\circ$), oriented along the N–N bond of one of the diazaphospholane rings (blue: nitrogen atoms, orange: phosphorous atoms, red: oxygen atoms).

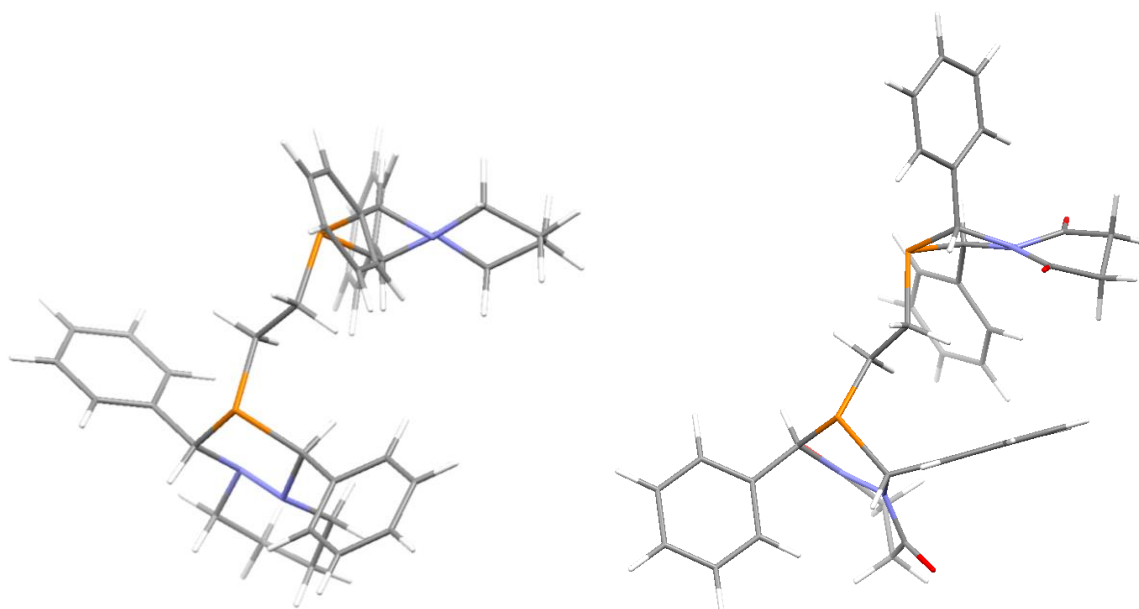


Figure 3.8. Calculated structures of red-TPSB BDPE **6** (left, $\theta = 56.4$) and TPSB BDPE **5** (right, $\theta = 14.0^\circ$), oriented along the N–N bond of one of the diazaphospholane rings (blue: nitrogen atoms, orange: phosphorous atoms, red: oxygen atoms).

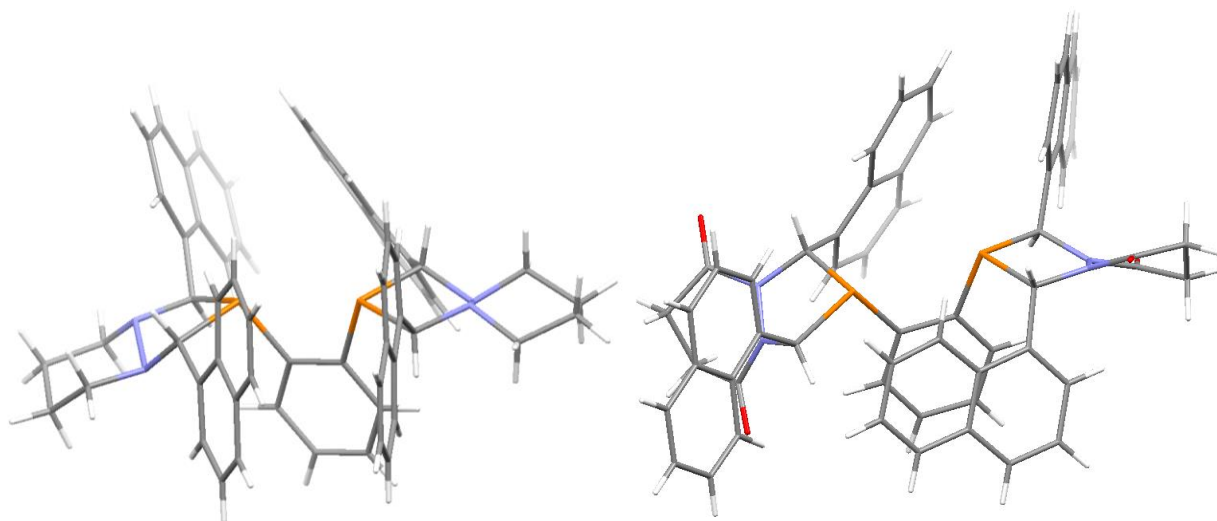


Figure 3.9. Crystal structures of red-TNSB BDP **8** (left, $\theta = 58.9^\circ$) and TNSB BDP **7** (right, $\theta = 33.4^\circ$) oriented along the N–N bond of one of the diazaphospholane rings (blue: nitrogen atoms, orange: phosphorous atoms, red: oxygen atoms).

In addition to the solid state structures, the geometries of **1** – **8** were calculated using *ab initio* calculation (B3LYP/6-31G(d)). These calculations allow for the structural determination of ligands TPSB BDPE **5** and red-TPSB BDPE **6**, whose crystal structures were not obtained. The experimental and calculated torsion angles are visualized in Figure 3.10. The calculated torsion angle for the reduced BDPs ligands is slightly smaller than the experimental value. In contrast, the torsion angle for the BDPs is greater than the experimental value, except for ligand **1**. With the reduction of the acylhydrazine group to the alkylhydrazine, the red-BDPs resemble structurally the class of phospholanes, such as Ph-BPE, which has a calculated torsion angle of 52.2° .

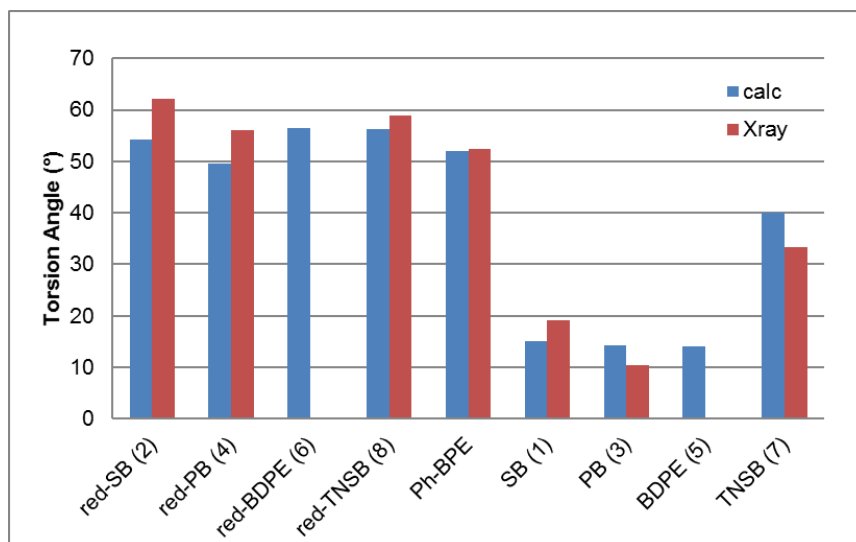


Figure 3.10. Calculated (blue bars, B3LYP/6-31G(d)) and experimental (red bars, X-ray crystallography) torsion angle of diazaphospholane rings in reduced BDPs, Ph-BPE and BDPs.

The crystal structure of the Rh-acac- complex of **1** was also obtained (Figure 3.11). The torsion angle within the phospholane ring is 21.7°, slightly larger compared to the free ligand value of 19.2°, but similar enough to assume that the torsion angle in the diazaphospholane ring of the Rh-complexes can be extrapolated from the free ligand structures.

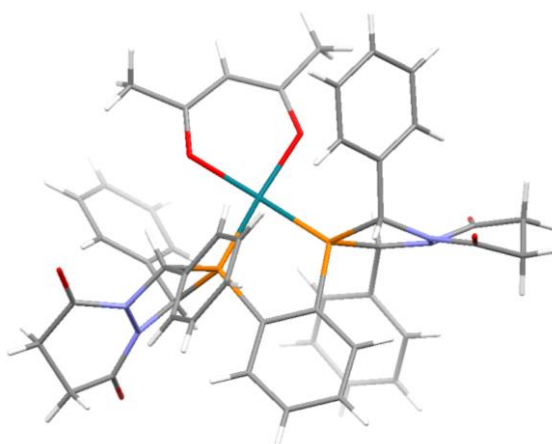


Figure 3.11. Crystal structure of [Rh(acac)(**1**)] oriented along the N–N bond of one of the diazaphospholane rings with a torsion angle (θ) of 21.7°.

As has been demonstrated previously with monodiazaphospholanes,¹² the change from an sp^2 -hybridized N-atom in the acylhydrazine to an sp^3 -hybridized N-atom gives rise to a large change in the puckering of the six-membered diazacyclohexane, as well as the diazaphospholane rings. A subsequent variation in the conformation concerns the orientation of the phenyl rings in the 2- and 5-positions. We have previously developed a quadrant map to visualize the steric and electronic contributions to the transition state energies responsible for the alkene insertion into the Rh–H bond.^{5, 8, 33} For our purposes, we are focusing only on the steric contributions of the map to rationalize the improved control for regioselectivity with the reduced ligands (Figure 3.12). This steric map depicts a pseudo-five coordinate transition-state with one of the P-atoms of the ligand bound in the equatorial position and the other P-atom in the axial position. The alkene is bound so that the double bond of the alkene lies parallel to the Rh–H bond. With the axial P-substituent lying in the plane of the map, the P-substituent has the sterically highest contribution, and the CO ligand has the smallest steric effect. The steric map is colored in different shades of blue indicating the different steric contributions with dark blue having the largest steric effect. The branched aldehyde is formed when the alkene substituent is oriented in the lower two quadrants, either coordinated through its *Si*-face (lower left, branched-*Si*) or *Re*-face (lower right, branched *Re*). We have confirmed this order of steric hindrance by constructing these four transition state model complexes with propene as the alkene and calculated the relative energies of the geometries with the red-TPSB BDP (**2**) as the supporting ligand (Figure 3.12, branched-*Re* depicted, B3LYP/LAN2DZ). We believe that the increased regioselectivity with the reduced ligand can be qualitatively explained by the increased twist in the diazaphospholane ring and the subsequent change in orientation of the phenyl rings in the 2- and 5-positions. As a result, the lower quadrants become sterically more accessible with a reduced ligand compared to when a non-reduced ligand is bound. Predominantly, the lower right quadrant appears to have the biggest influence on the resulting branched product, since the lower left quadrant has the biggest steric

bulk and is highest in energy. The orientation of the alkene in the lower right quadrant is not the determining conformation for our hypothesis

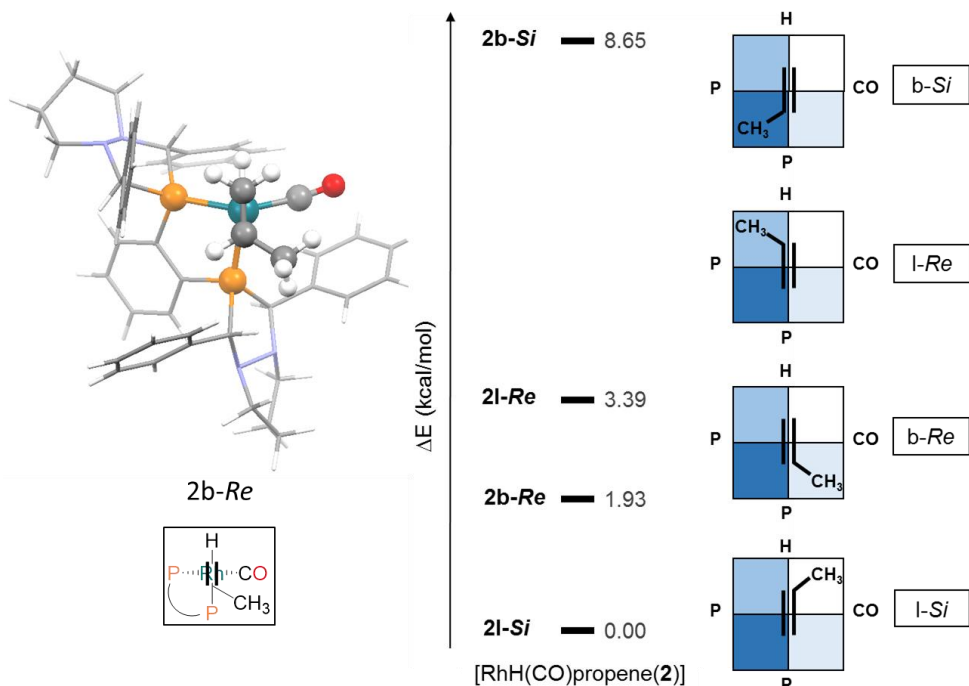


Figure 3.12. Relative energies of the steric transition-state model for $[\text{RhH}(\text{CO})(\text{propene})(\mathbf{2})]$ of four orientations in the steric map (right, blue boxes are shaded based on the steric bulk (dark blue: biggest steric bulk). As an example, complex $[\text{RhH}(\text{CO})(\text{propene})(\mathbf{2})]$ for the $b\text{-Re}$ conformation is depicted (left). Calculations were performed using B3LYP/LAN2DZ.

The same four conformations have been calculated with the TPSB BDP control ligand complex, $[\text{RhH}(\text{CO})(\text{propene})(\mathbf{1})]$. For both ligands, the lowest energy diastereomer is the precursor to the linear aldehyde ($l\text{-Si}$). Taken literally, these models suggest that linear aldehyde should be the main product for both catalysts. The caveat is that this model crudely represents transition states for insertion of the alkene into the Rh-H bond; this model is crude because it is rigid with highly constrained orientations of the atoms in the C=C and Rh-H bonds. The propene-based model does not include any of the electronic effects that are so important in directing the regioselectivity

of more realistic substrates. Nor does the model account for the possibility of reversibility of alkene insertion to form linear or branched Rh-alkyls. Our goal is to see if these rigid models help us to understand the influence of reduced vs. non-reduced diazaphospholanes on the relative regioselectivities. Unfortunately, they do not. The computed data do not show a significant bias for the reduced ligand (**1**) to make branched isomer. For example the model for the lowest energy transition state that generates branched aldehyde is actually more *disfavored* for the reduced ligand than for the non-reduced.

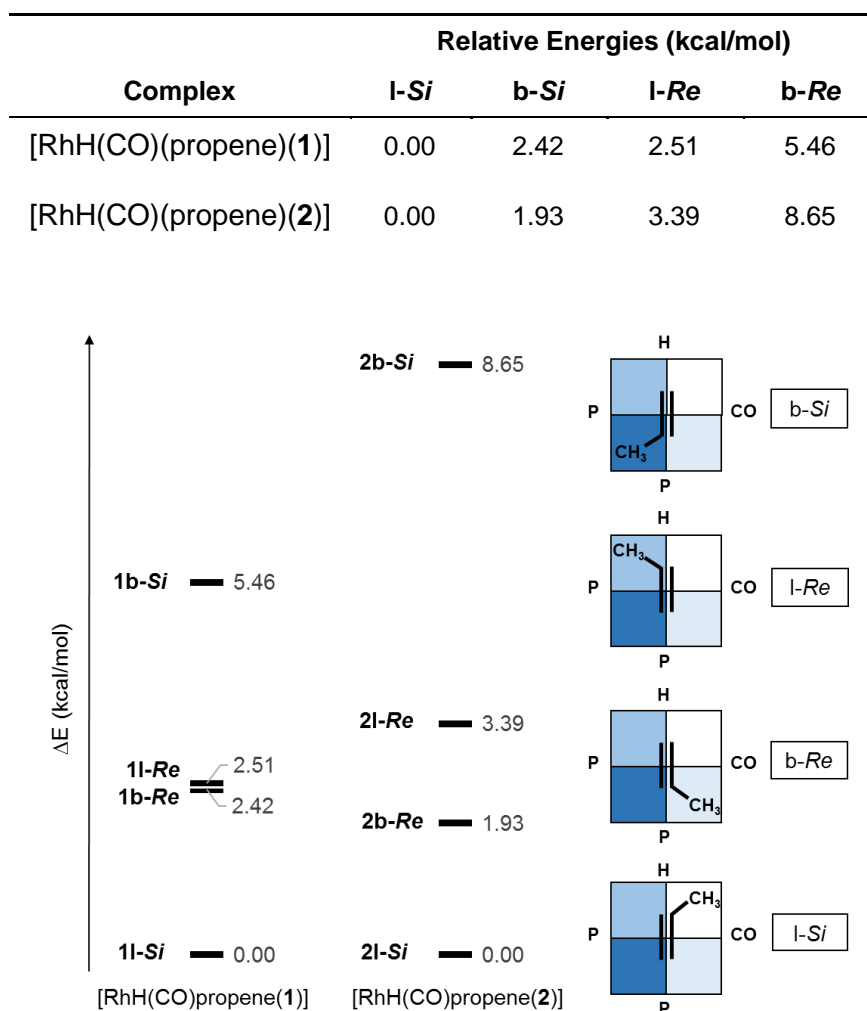
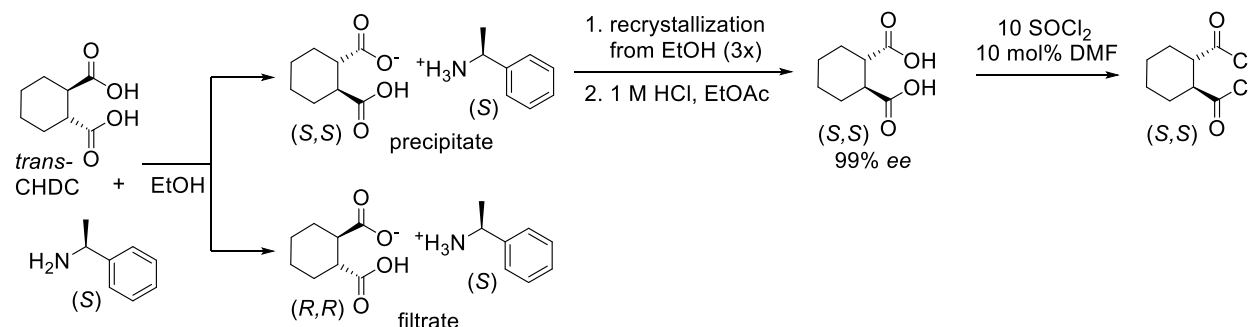


Figure 3.13. Comparison of relative energies for [RhH(CO)propene(**1**)] (left) and [RhH(CO)propene(**2**)] (right) for the steric model.

3.2.7 Routes to Resolved Reduced Bisdiazaphospholanes

We have learned that reduction of the acylhydrazine to the alkylhydrazine groups in the diazaphospholane moiety leads to significant improvements in regioselectivity for a variety of different substrates. Possible effects on enantioselectivity by changing the puckering in the diazaphospholane ring are of great interest. Investigation on the borane reduction of several easily resolvable bisdiazaphospholanes has been undertaken.

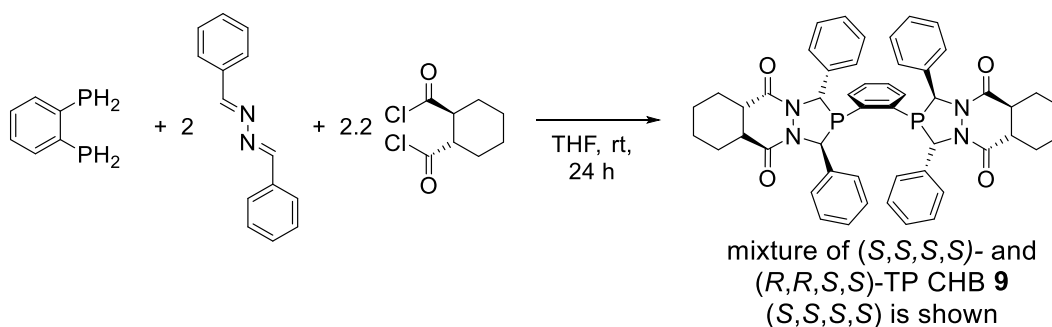
One technique for the separation of enantiomers is the incorporation of a chiral substituent into the diazaphospholane framework. Zhang and coworker separated the bisdiazaphospholane diastereomers by installation of a chiral backbone, specifically an (*S,S*)-1,2-cyclohexane diacyl group.³⁴ Enantiopure (*S,S*)-1,2-cyclohexane diacyl chloride is obtained by the classical resolution of *trans*-CHDC with a chiral amine.^{35, 36} The (*S,S*)-1,2-CHDC is subsequently converted to its acyl chloride using thionylchloride (Scheme 3.3).



Scheme 3.3. Classical resolution of *trans*-cyclohexane dicarboxylic acid (CHDC) with (*S*)-methylbenzylamine and subsequent chlorination of isolated (*S,S*)-CHDC.

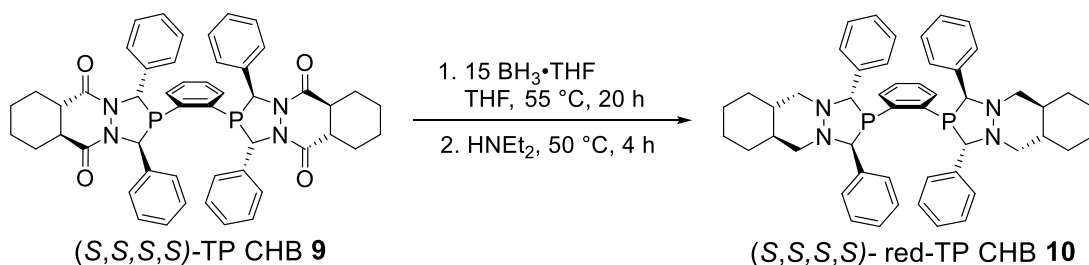
Analogous to the general synthesis of bisdiazaphospholanes by a Mannich-type condensation reaction, 2 equivalents of (*S,S*)-cyclohexane diacyl chloride react with 1,2-bis(phosphino)-benzene and 2 equivalents of 1,2-diphenylazine to yield a mixture of diastereomers of the TPCHB ligand **9**. The two diastereomers of the desired *racemic*, C₂-symmetric ligands with (*S,S*)- and

(*R,R*)- stereochemistry in the phospholane ring can be clearly distinguished by ^{31}P NMR spectroscopy. Furthermore, separation of the diastereomers is now possible using column chromatography, as demonstrated by Zhang and coworkers. Unfortunately, approximately half of the desired material is lost due to oxidation during the separation process, leading to only 10% isolated yield.



Scheme 3.4. Synthesis of the chiral cyclohexane backbone containing BDP **9**.

Borane reduction was carried out with the (*S,S,S,S*)-enantiomers of **9** using the typical reduction procedure (Scheme 3.5). This material is more sensitive to over-reduction back to the primary phosphine compared to other tetraphenyl BDPs (*vide supra*). Over-reduction occurs more readily at 55 °C, and after 20 h results in a mixture that contains approximately 50% of the over-reduced asymmetric side-product where one P-atom resides as the desired diazaphospholane group, while the other P-atom has been converted back to a PH_2 group. The desired reduced compound **10** was isolated in low yields (25%). It can be assumed that the reduction will already occur at room temperature, as has been observed with the TNSB BDP ligand **8** and the TPSB BDPE ligand **6**.

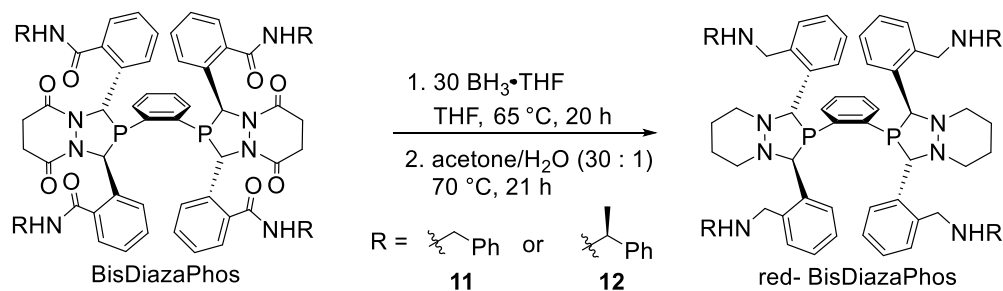


Scheme 3.5. Borane-reduction of enantiopure TP CHB ligand **9**.

3.2.8 Borane Reduction of Tetraamide-containing BDPs.

Borane reduction of other existing chiral BisDiazaPhos ligands is of particular interest. Using enantiopure ligands *ortho*-tetraamide substituted BDPs that are known to give both high regio- and enantioselectivities for the desired branched aldehyde products in Rh-catalyzed hydroformylation is a great starting point. The *S,S,S*-enantiomer of tetra(methylbenzylamide) BDP, in particular, shows the highest enantioselectivities obtained for a variety of substrates to date.⁸ Therefore, we sought to investigate the borane reduction of tetraamide substituted BDPs.

Initially, the borane reduction was applied to the *racemic* tetrabenzylamide and tetramethylbenzylamide BDPs. An excess of 30 equiv. of borane is needed to reduce all eight carbonyl groups simultaneously (Scheme 3.6). To quench all borane byproducts and formed borane-amine adducts, the mixture is heated in wet acetone at 70 °C overnight, after removal of all volatiles under vacuum.



Scheme 3.6. Borane-reduction applied to tetraamide containing BDPs **11** and **12**.

Even though increased temperatures of 65 °C were used in the reduction of tetraamide BDPs, compared to the tetraphenyl-derivatives (*vide supra*), mass spectrometry analysis confirms that full conversion of all carbonyl groups in both tetraamide ligands does not occur, even after reaction times of 24 h or at temperature of 75 °C. Interestingly, all acylhydrazine groups are found to be reduced, as is indicated by the chemical shift of the methine protons in the phospholane ring. The chemical shift of the methine protons in the reduced compounds resonate near 4.5 ppm, whereas the non-reduced diazaphospholane methine protons have a chemical shift around 6 ppm. The ^{31}P NMR spectrum from the reaction to form **12** shows a mixture of three major products (Figure 3.14). Two C_2 -symmetric compounds exhibit equivalent phosphorous atoms, the desired reduced BDP with 8 reduced carbonyl groups (green circle) and one BDP with only 6 reduced carbonyl groups (red triangle). One compound is C_1 -symmetric and gives rise to two doublets in the ^{31}P NMR spectrum with a coupling constant of 203 Hz between the phosphorous atoms (blue square). This pattern suggests that the corresponding compound only contains one amide-carbonyl group. This signal at a chemical shift of -16 ppm lies in the region of a fully reduced phospholane moiety, whereas the signal -3.5 ppm appears when one amide-carbonyl group is still intact.

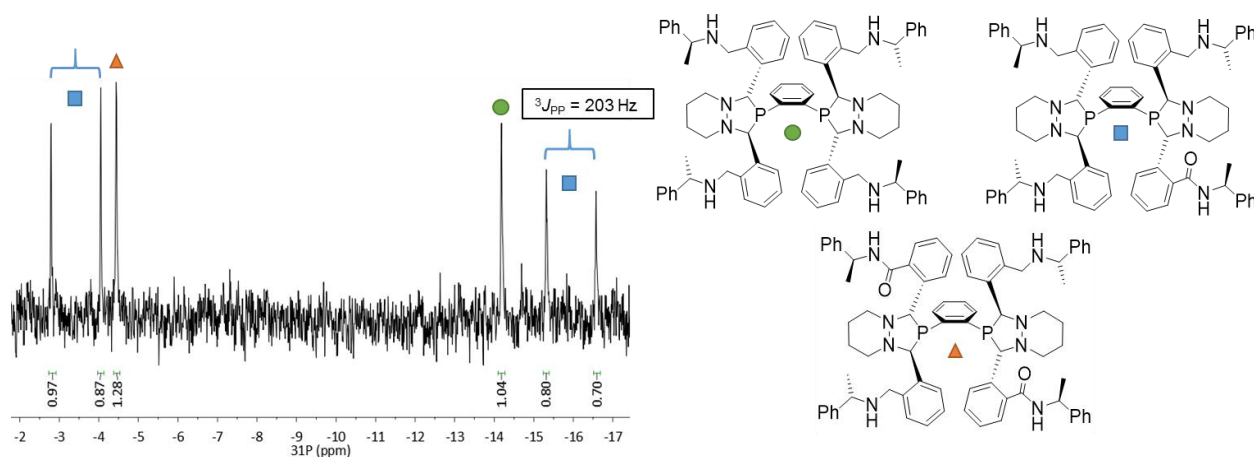
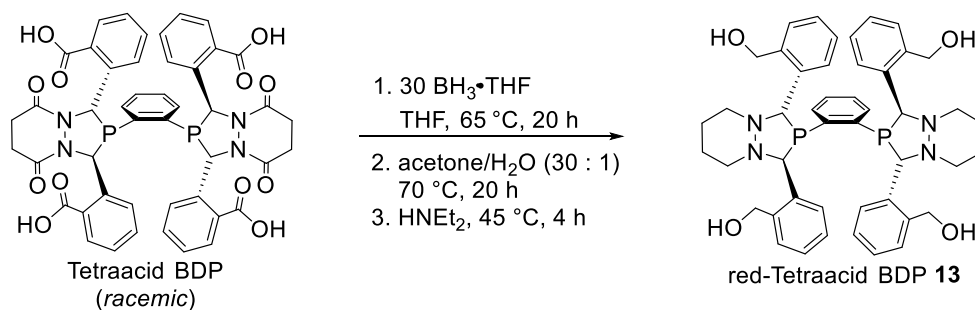


Figure 3.14. Mixture of three reduced tetraamide BDPs **12** observed in the ^{31}P NMR spectrum.

Exceeding reaction temperatures of 65 °C, however, leads to the ring opening reaction of THF, yielding tributoxyborane, and therefore results in loss of the borane reducing agent over time. At elongated reaction times, overreduction is observed. The isolation of the fully reduced ligands **11** and **12** has not been successful to date. Further routes to the complete reduction and purification of these couldn't be investigated in this timeframe.

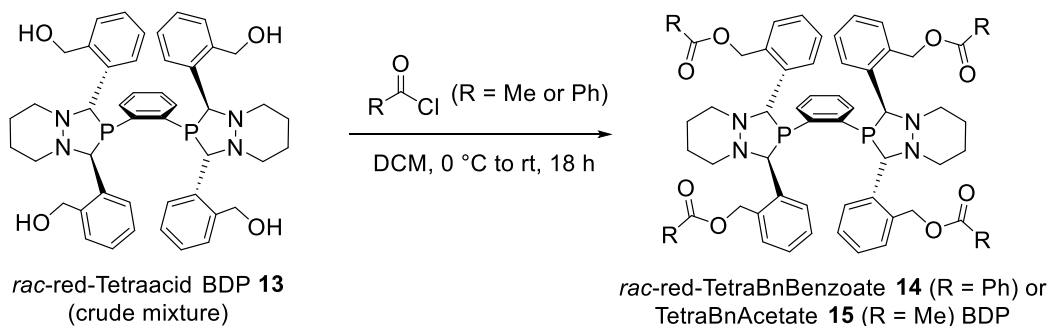
3.2.9 Investigation of the Borane-Reduction of Tetracarboxylicacid BDP

One viable bisdiazaphospholane ligand to test in the reduction procedure is the tetraacid BDP (Scheme 3.7). Tetraacid BDP is the precursor to the state-of-the-art (*S,S,S*)-BisDiazaPhos (*vide supra*) and we have recently demonstrated that separation of the two enantiomers can be performed in house *via* classical resolution using (+)-pseudoephedrine.³⁷ Thus, one is not dependent on separation of enantiomers using SFC (supercritical fluid chromatography) with this new resolution method. Initially, the borane reduction was performed using the *racemic* tetraacid BDP material. As already described for the tetraamide BDPs, tetraacid BDP is reduced with 30 equivalents of $\text{BH}_3\cdot\text{THF}$, resulting in the clean reduction of all 8 carbonyl groups and giving a benzyl alcohol-substituted reduced bisdiazaphospholane. Unlike the tetraamides, the $\text{BH}_3\cdot\text{BDP}$ adduct remains intact after acetone/water treatment. Therefore, both heating with acetone/water as well as with HNEt_2 is necessary to yield the desired red-Tetraacid product (Scheme 3.7).



Scheme 3.7. Reaction of racemic tetraacid BDP with $\text{BH}_3\cdot\text{THF}$ to yield **13**.

Even though the ^{31}P NMR spectrum of the reaction to form **13** only shows one signal at -11.4 ppm, the ^1H NMR and ^{11}B NMR spectra reveals large amounts of boron-containing byproducts obtained from the quenching procedure. These impurities could not be removed through a variety of purification attempts. Therefore, the red-tetraacid ligand **13** was converted to its ester derivatives (Scheme 3.8). The protection of the alcohol groups has the advantage of avoiding acetalization reactions of the alcohols with the aldehyde products during hydroformylation; such reaction would change the nature of the ligand and the hydroformylation result could not be trusted to come from the red-tetraacid. In an attempt to improve purification of red-tetraacid BDP **13**, the benzyl alcohol groups were converted to the benzoate and acetate derivatives **14** and **15**, respectively, by reaction with the corresponding acyl chlorides (Scheme 3.8). Unfortunately, this derivatization still did not result in isolation of pure products.



Scheme 3.8. Esterification of red-tetraacid BDP for purification attempts.

3.3 Conclusion and Future Work

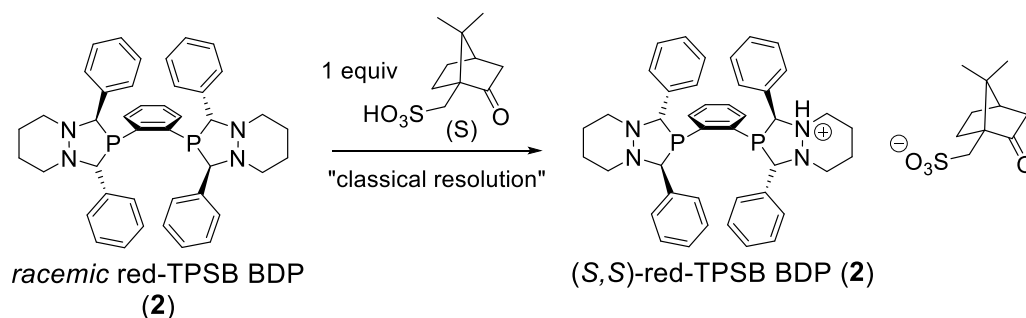
A borane reduction procedure has been applied to four racemic tetraaryl bisdiazaphospholanes varying in the phosphine-bridge, the backbone and the substituents in 2- and 5-positions. The acylhydrazine backbones were converted to alkylhydrazine cycles, leading to a change in the hybridization of the N-atoms from sp^2 to sp^3 . The resulting twist in the diazaphospholane ring leads to both an increased C–N–N–C-torsion angle and reorientation of

the aryl-ring substituents in 2- and 5-positions. This conformational change has drastic effects on the regioselective control in rhodium-catalyzed hydroformylation on a variety of alkenes, including styrene, vinyl acetate, allyl cyanide, allyl alcohol, allyloxy-*tert*-butyldimethylsilane, 3-butenic acid, *N*-Boc-2,3-dihydropyrrole, 2,3- and 2,5 dihydrofuran. Four new reduced diazaphospholanes have been compared to their non-reduced parent-ligand. Indeed, regioselectivities increased by up to 5-fold, with preference for the branched aldehyde product. The tetranaphthyl ligand red-TNSB **8** exhibits the highest regioselectivities for all terminal alkene substrates, however, exhibits slightly lower conversions, correlating with the increased steric bulk. Selectivities for the cyclic alkenes are very challenging. The ligand combining good activity and averaging good regioselectivities for all tested substrate is red-TPSB BDP **6**. Overall, the ligands combining the phenylene bridge and the succinyl backbone red-TPSB BDP **2** and red-TNSB BDP **8** exhibit the best regioselectivities. The torsion angles of the diazaphospholane moieties were analyzed and the selectivity trends were visualized using a qualitative steric map. With the structural changes, the reported reduced ligands resemble the Ph-BPE and DuPhos ligand families, and exhibit enhanced regioselectivities. The reduced ligands have yet to be tested in their enantioselective performance and it will be interesting to see if their performance is similar to the Ph-BPE ligand. The phospholane-like behavior is encouraging and has potential for an increase in enantioselectivities for the branched aldehyde product when using reduced ligand.

The reduction of the more substituted ligands, with carboxylic acid and amide groups, is promising, in particular the tetra-carboxylic acid ligands. Due to the increased number of introduced hetero-atoms, reduction is less clean leading to a higher amount of borane-containing quenching products as impurities, making the purification and isolation of the reduced ligands more challenging. The optimization of the purification would have to be further investigated.

The reduction of the diazaphospholane rings opens a new way to take advantage of the sp^3 -hybridized N-atom. The increased basicity has the potential of protonation with a strong acid.

Reaction with a chiral strong acid like (1*S*)-(+)-10-camphorsulfonic acid could have the potential for classical resolution of the red-BDP enantiomers. Initial results show that reaction of red-TPSB BDP **2** and 1 equivalent of (1*S*)-(+)-10-camphorsulfonic acid leads to a new phosphorous species in the ^{31}P NMR spectrum with a similar chemical shift to the red-TPSB BDP. This result is encouraging and suggest the potential formation of a diastereomeric salt (Scheme 3.9).



Scheme 3.9. Potential for classical resolution of **2** with (1*S*)-(+)-10-Camphorsulfonic acid.

To expand upon the library of reduced ligands, the structures depicted in Figure 3.15 are of interest. The lack of a number of heteroatom-containing substituent is advantageous for the borane-reduction. New steric bulk can be introduced by using xanthene substituents with the potential of increasing regioselectivity for terminal alkenes. Biphenyl as a substituent would allow for formation of rotational isomers and potential for enantioselective hydroformylation.

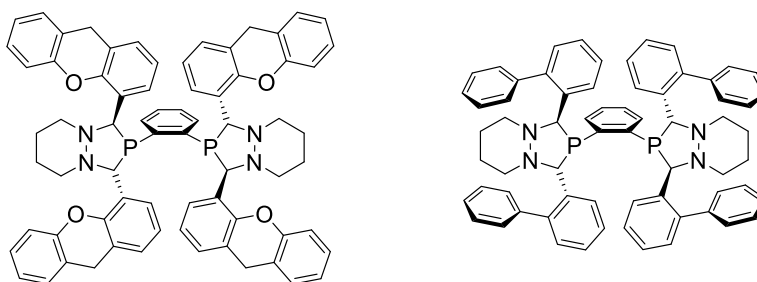
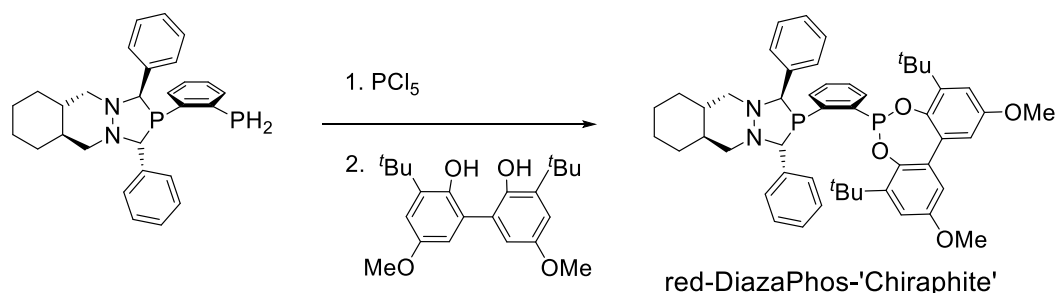


Figure 3.15. Next generation of proposed new reduced BDP ligand.

The hybrid Ph-BPE-Chiraphite ligand called BobPhos found success in the branched-selective hydroformylation of 1-octene.³⁸ The reduced ligands are encouraging starting points to create a mixed Chiraphite derived DiazaPhos-Phosphonite ligand (Scheme 3.10).



Scheme 3.10. Proposed synthesis to a hybrid red-DiazaPhos-Phosphonite ligand.

3.4 Experimental Section

General Considerations

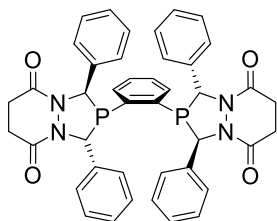
All ligand preparations and manipulations were performed under air-free conditions using standard Schlenk line techniques or an N_2 -filled glovebox. Most workups and flash column chromatography were performed in air. Air-free extractions were performed by sparging the 1 M HCl (aq.) and K_2CO_3 (aq.) vigorously with N_2 for 30 – 40 min prior to use. THF was distilled from Na/benzophenone , DCM was distilled from CaH_2 and sparged with N_2 . CDCl_3 was purchased from Sigma-Aldrich, dried over CaH_2 and stored in a bomb flask over 3 Å molecular sieves under an N_2 atmosphere. $[\text{Rh}(\text{acac})(\text{CO})_2]$ was provided by the Dow Chemical Company and was recrystallized from toluene. Succinyl and phthaloyl chloride were distilled under reduced pressure and stored in an N_2 filled glovebox. All alkenes were purchased from Sigma-Aldrich and purged with N_2 before use. ^1H and ^{31}P NMR spectra were recorded on a Bruker Avance-400 MHz spectrometer. ^{13}C NMR spectra were recorded on a Bruker Avance-500 MHz spectrometer. ^1H and ^{13}C NMR spectra were referenced to the residual proteo-solvent. ^{31}P NMR shifts were referenced from the corresponding ^1H NMR frequency. ^1H splitting patterns are designated as

singlet (s), broad singlet (brs), doublet (d), doublet of doublets (dd), virtual doublet of doublets (vdd), dt (doublet of triplets), triplet (t), triplet of doublets (td), virtual triplet (vt) or multiplet (m). Mass spectra were obtained at the Paul Bender Chemical Instrumentation Center of the Chemistry Department of the University of Wisconsin–Madison using a Thermo Q Exactive™ Plus ESI-MS. Crystallographic data was obtained with Bruker Smart Quazar with an APEX2 detector and a Mo-microsource. The azines and ligand **3** were prepared after known literature procedures.⁴

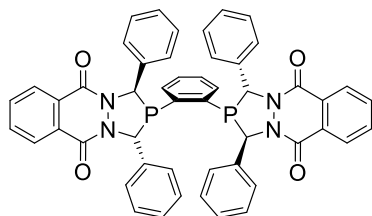
1,2-Bis(phosphino)ethane was prepared after a modified literature procedure.³⁹ A solution of Li[AlH₄] (1 M in ether, 19.56 mL, 8 equiv) in ether (24 mL) was cooled to -78 °C. The phosphine 1,2-bis(dichlorophosphino)ethane (369.1 μL, 2.45 mmol, 1 equiv) was added dropwise *via* syringe over a period of 20 min. The solution was allowed to warm to rt overnight. N₂-sparged water was slowly added dropwise while the reaction mixture was cooled with an ice bath. The white precipitate was filtered off using a Schlenk frit, and the solid was washed with ether (6 x 8 mL). The ether-solution was cannulated into a Schlenk flask containing degassed MgSO₄, which was filtered off using a Schlenk frit and washed with (5 x 3 mL). The product was isolated as a colorless oil (82% yield) by distilling out the lower boiling ether solvent at 40 °C. NMR spectroscopic data is in agreement with the reported values.^{40, 41}

General Synthesis of Tetraaryl-bisdiazaphospholanes **1, **3**, **5** and **7**.**

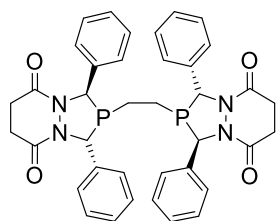
In an oven-dried 50 mL Schlenk flask, the diaryl azine (1.00 g, 4.8 mmol, 2 equiv) and the primary bisphosphine (2.4 mmol, 1 equiv) were combined in THF (30 mL). The corresponding diacyl chloride (5.1 mmol, 2.1 equiv) was added dropwise to the yellow clear solution *via* syringe. The solution turned almost colorless over time. BDP **1**, **3** and **5** precipitate as white solids, BDP **7** stays dissolved in solution.

TPSB BDP (**1**)

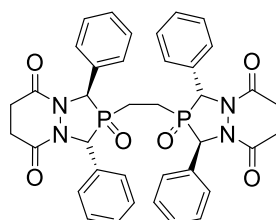
TPSB BDP (1). The product formed as a white solid from the reaction mixture, was filtered off in air and washed with THF (4 x 7 mL)(29% yield). X-ray quality crystals (colorless needles) were obtained from a gas-phase diffusion of pentane into a DCM-solution of **1** at 4 °C. **¹H NMR** (CDCl₃, 400 MHz, ppm): δ 7.45 – 7.30 (m, 8H), 7.16 (d, *J* = 7.5 Hz, 4H), 7.11 – 7.01 (m, 4H), 6.87 (t, *J* = 7.6 Hz, 4H), 6.62 (d, *J* = 7.3 Hz, 4H), 5.75 (brs, 2H), 5.74 (vt, ²*J*_{H-P} = 10.1 Hz, 2H), 2.84 – 2.56 (m, 8H). **¹³C{¹H} NMR** (CDCl₃, 126 MHz, ppm): δ 167.5, 165.1, 138.7 (vt, ²*J*_{C-P} = 2.0 Hz), 137.2 (vt, ²*J*_{C-P} = 9.0 Hz), 135.7, 130.78, 130.1 (vt, ²*J*_{C-P} = 2.1 Hz), 129.2, 128.3, 127.8, 127.2, 126.0 (vt, ¹*J*_{C-P} = 4.4 Hz), 125.9 (vt, ¹*J*_{C-P} = 2.2 Hz), 61.9 (vt, ¹*J*_{C-P} = 18.5 Hz), 57.1 (vt, ¹*J*_{C-P} = 4.3 Hz), 30.3, 29.7. **³¹P{¹H} NMR** (CDCl₃, 162 MHz, ppm): δ -1.4. **HRMS** (ESI, *m/z*): [M+H]⁺ calcd. for C₄₂H₃₇N₄O₄P₂: 723.2285, found: 723.2278 (Δ = 1.0 ppm).

TPPB BDP (**3**)

TPPB BDP (3). All data are in agreement with reported values.⁴

TPSB BDPE (**5**)

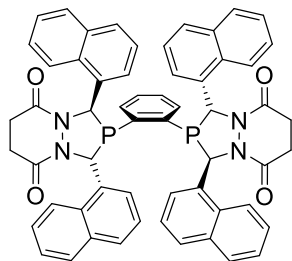
TPSB BDPE (5). The product crashed out of the THF solution, was filtered in air and washed with THF (5 x 3 mL) (333.9 mg, 20% yield). The majority of **5** was recovered from the filtrate as its phosphine oxide derivative. **¹H NMR** (CDCl₃, 400 MHz, ppm): δ 7.40 – 7.27 (m, 12H), 7.17 (d, *J* = 7.5 Hz, 4H), 7.02 (d, *J* = 7.5 Hz, 4H), 5.59 (vdd, ²*J*_{H-P} = 8.7 Hz, 2H), 5.49 (bs, 2H), 3.10 – 2.89 (m, 2H), 2.83 – 2.70 (m, 6H), 1.04–0.94 (m, AA'BB'XX', 2H), 0.54–0.44 (m, AA'BB'XX', 2H). **¹³C{¹H} NMR** (CDCl₃, 126 MHz, ppm): δ 167.9, 165.9, 137.2 (vt, *J*_{C-P} = 7.2 Hz), 133.2, 129.4, 129.2, 128.3, 127.6, 125.7 (vt, *J*_{C-P} = 3.9 Hz), 125.0 (br), 59.8 (vdd, *J*_{C-P} = 14.0 Hz), 59.2 (vt, *J*_{C-P} = 9.3 Hz), 30.8, 29.9. **³¹P{¹H} NMR** (CDCl₃, 162 MHz, ppm): δ 9.8. **HRMS** (ESI, *m/z*): [M+H]⁺ calcd. for C₃₈H₃₇N₄O₄P₂: 675.2285, found: 675.2290 (Δ = 0.7 ppm).



TPSB BDPEO

TPSB BDPEO. The solvent of the filtrate from **5** was removed and the crude solid suspended in EtOAc. The phosphine oxide was filtered and washed with EtOAc (4 x 3 mL) (389.6 mg, 24% yield). **¹H NMR** (CDCl₃, 400 MHz, ppm): δ 7.40 – 7.32 (m, 12H), 7.25 (m, 4H, overlapped with CHCl₃), 7.92 (m, 4H), 5.80 (vdd, ²*J*_{H-P} = 10.0 Hz, 2H), 5.41 (vdd, ²*J*_{H-P} = 16.2 Hz, 2H), 3.95 – 2.82 (m, 2H), 2.81 – 2.62 (m, 6H), 1.85–1.73 (AA'BB'XX', 2H), 1.29–1.16 (m, AA'BB'XX', 2H). **¹³C{¹H} NMR** (CDCl₃, 126 MHz, ppm): δ 167.3, 166.1, 131.4, 131.4, 129.8, 129.5, 129.1, 128.8, 127.0,

125.0, 58.4 (vdd, $J_{C-P} = 31.4$ Hz), 55.4 (vdd, $J_{C-P} = 32.5$ Hz). $^{31}\text{P}\{^1\text{H}\}$ NMR (CDCl_3 , 162 MHz, ppm): δ 54.3. **HRMS** (ESI, m/z): $[\text{M-H}]^-$ calcd. for $\text{C}_{38}\text{H}_{35}\text{N}_4\text{O}_6\text{P}_2$: 705.2037. found: 705.2040 ($\Delta = 0.4$ ppm).

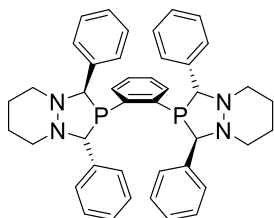


TNSB BDP (**7**)

TNSB BDP (7). **7** was purified via column chromatography (EtOAc:DCM = 9 : 1, $R_f = 0.38$) Colorless needles were obtained by gas-phase diffusion of pentane into a CH_2Cl_2 solution of **7**. (234.2 mg, 20% yield), contains solvents in the crystal lattice. ^1H NMR (CDCl_3 , 400 MHz, ppm): δ 8.25 (d, $J = 8.4$ Hz, 2H), 7.96 (dd, $J = 18.0, 7.8$ Hz, 6H), 7.70 (dt, $J = 19.8, 6.9$ Hz, 4H), 7.48 (t, $J = 7.7$ Hz, 2H), 7.25 (dd, $J = 23.4, 7.6$ Hz, 4H), 7.10 (s, 4H), 6.92 – 6.85 (m, 4H), 6.71 (t, $J = 11.6$ Hz, 2H), 6.57 (t, $J = 7.7$ Hz, 2H), 6.46 (d, $J = 7.2$ Hz, 2H), 6.11 (vt, $^2J_{H-P} = 6.9$ Hz, 2H), 5.86 (s, 2H), 2.78 (td, $J = 15.9, 4.9$ Hz, 2H), 2.49 (dd, $J = 16.7, 3.2$ Hz, 2H), 2.36 (dd, $J = 16.7, 3.2$ Hz, 2H), 2.08 (td, $J = 16.1, 4.7$ Hz, 2H). $^{13}\text{C}\{^1\text{H}\}$ NMR (CDCl_3 , 126 MHz, ppm): δ 167.7, 165.6, 140.0 (vt, $^2J_{C-P} = 1.8$ Hz), 134.53 (vt, $^2J_{C-P} = 10.0$ Hz), 134.3, 132.7, 131.1 (vt, $^2J_{C-P} = 2.0$ Hz), 130.84 (vt, $^2J_{C-P} = 2.1$ Hz), 130.82, 130.4, 129.5, 128.9, 128.6, 128.1, 127.7, 126.6, 126.5, 126.0, 125.7, 125.5, 125.2, 125.1 (vt, $^1J_{C-P} = 8.3$ Hz), 124.31, 123.1 (vt, $^1J_{C-P} = 3.1$ Hz), 121.55, 59.8 (vt, $^1J_{C-P} = 18.5$ Hz), 55.1 (vt, $^1J_{C-P} = 4.2$ Hz), 30.4, 26.9. $^{31}\text{P}\{^1\text{H}\}$ NMR (CDCl_3 , 162 MHz, ppm): δ 3.27. **HRMS** (ESI, m/z): $[\text{M+H}]^+$ calcd. for $\text{C}_{58}\text{H}_{45}\text{N}_4\text{O}_4\text{P}_2$: 923.2911, found: 923.2914 ($\Delta = 0.3$ ppm).

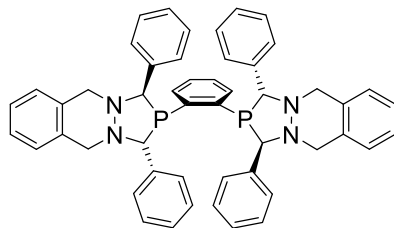
General Borane Reduction Procedures

To a mixture of the BDP ligand (437.9 mg, 0.606 mmol, 1 equiv.) in THF (7 mL), $\text{BH}_3 \cdot \text{THF}$ (1 M in THF, 9.10 mL, 9.10 mmol, 15 equiv.) was added *via* syringe. The Schlenk flask was sealed and the mixture was stirred at 55 °C or at room temperature for 20 h. The reaction mixture was allowed to cool to room temperature and all volatiles were removed *in vacuo*. The remaining solid was dissolved in HNEt_2 (3 mL) and the solution was heated at 50 °C for at least 4 h. Upon cooling, all volatiles were removed *in vacuo*. The crude product was dissolved in EtOAc (15 mL) and aq. HCl (1 M, 10 mL) and the mixture was stirred for at least 30 min. Aq. K_2CO_3 (10 wt%,) was added until the aqueous layer was basic (pH ~ 10). The aqueous layer was extracted and washed with EtOAc (at least 2 x 5 mL). The combined organic layers were washed with aq. K_2CO_3 (10 wt%, 2 x 7 mL) and dried over MgSO_4 . The solvent was removed *in vacuo* to obtain the desired crude product as an off-white solid, which was further purified by column chromatography or recrystallization.

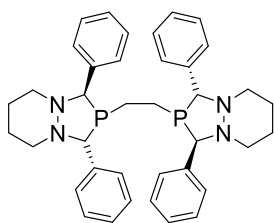


red-TPSB BDP (**2**)

red-TPSB BDP (2). **2** was obtained as colorless block crystals upon slow evaporation of EtOAc (89% yield). ^1H NMR (CDCl_3 , 400 MHz, ppm): δ 7.69 (m, 2H), 7.37 – 7.16 (m, 12H), 6.72 – 6.60 (m, 6H), 6.40 (t, $J = 7.4$ Hz, 4H), 4.09 (vt, $^2J_{\text{H-P}} = 12.5$ Hz, 2H), 3.96 (brs, 2H), 2.94 (dd, $J = 23.5$, 11.4 Hz, 4H), 2.47 (td, $J = 11.4$, 2.9 Hz, 2H), 2.01 (td, $J = 11.4$, 2.9 Hz, 2H), 1.62 – 1.33 (m, 8H). $^{13}\text{C}\{^1\text{H}\}$ NMR (CDCl_3 , 126 MHz, ppm): δ 141.9 (brs), 141.0 (brs), 136.6, 132.8 (vt, $^2J_{\text{C-P}} = 1.9$ Hz), 129.2 (vt, $^1J_{\text{C-P}} = 3.7$ Hz), 128.0, 127.8, 127.5 (brs), 127.0, 126.8 (brs), 71.8 (vt, $^1J_{\text{C-P}} = 10$ Hz), 71.2, 55.4, 54.9, 24.7, 24.0. $^{31}\text{P}\{^1\text{H}\}$ NMR (CDCl_3 , 162 MHz, ppm): δ -0.9. **HRMS** (ESI, m/z): $[\text{M}+\text{H}]^+$ calcd. for $\text{C}_{42}\text{H}_{45}\text{N}_4\text{P}_2$: 667.3114. found: 667.3105 ($\Delta = 1.3$ ppm).

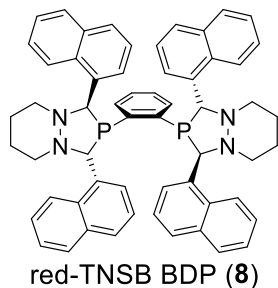
red-TPPB BDP (**4**)

red-TPPB BDP (4). The pure product was obtained by recrystallization from liquid-liquid diffusion of EtOAc and pentane at room temperature (92% yield). **¹H NMR** (CDCl₃, 400 MHz, ppm): δ 7.78 (m, 2H), 7.37 – 7.20 (m, 12H), 7.15 – 7.04 (m, 6H), 6.99 (d, *J* = 7.2 Hz, 2H), 6.89 (d, *J* = 7.2 Hz, 2H), 6.85 (t, *J* = 7.2 Hz, 2H), 6.80 (d, *J* = 7.4 Hz, 4H), 6.64 (t, *J* = 7.7 Hz, 4H), 4.25 (vt, ²*J*_{H-P} = 11.7 Hz, 2H), 4.20 (bs, 2H, overlapped with 4.18 ppm signal), 4.10 (d, *J* = 14.5 Hz, 2H), 3.98 (d, *J* = 14.5 Hz, 2H), 3.51 (d, *J* = 14.5 Hz, 2H). **¹³C{¹H} NMR** (CDCl₃, 126 MHz, ppm): δ 142.1, 141.1 (vt, *J*_{C-P} = 8.6 Hz), 135.8, 133.7, 133.3, 133.2, 128.7 (vt, *J*_{C-P} = 3.5 Hz), 128.4, 128.2, 127.5, 127.0, 126.2, 126.1, 126.0, 125.8, 72.7 (vt, *J*_{C-P} = 9.2 Hz), 71.6, 58.7, 57.6. **³¹P{¹H} NMR** (CDCl₃, 162 MHz, ppm): δ 1.1. **HRMS** (ESI, *m/z*): [M+H]⁺ calcd. for C₅₀H₄₅N₄P₂: 763.3114. found: 763.3105 (Δ = 1.4 ppm).

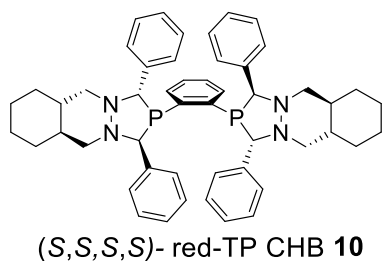
red-TPSB BDPE (**6**)

red-TPSB BDPE (6). Product **6** was obtained through air-free extraction using N₂-sparged EtOAc, aq. HCl (1 M) and aq. K₂CO₃. MgSO₄ was degassed prior to use. The sample also contains small amount of other phosphorous compounds in the ³¹P NMR. **¹H NMR** (CDCl₃, 400 MHz, ppm): δ 7.40 – 7.27 (m, 12H), 7.17 (d, *J* = 7.5 Hz, 4H), 7.02 (d, *J* = 7.5 Hz, 4H), 5.59 (vdd, 2H), 5.49 (bs,

2H), 3.10 – 2.89 (m, 2H), 2.83 – 2.70 (m, 6H), 0.99 (AA'BB'XX', 2H), 0.49 (AA'BB'XX', 2H). $^{31}\text{P}\{^1\text{H}\}$ NMR (CDCl_3 , 162 MHz, ppm): δ 6.5. HRMS (ESI, m/z): $[\text{M}+\text{H}]^+$ calcd. for $\text{C}_{38}\text{H}_{45}\text{N}_4\text{P}_2$: 619.3114, found: 619.3114 ($\Delta = <0.1$ ppm).



red-TNSB BDP (8). (47.5 mg, 76% yield). Colorless needles were obtained by gas-phase diffusion of pentane into a CH_2Cl_2 solution of **8**. ^1H NMR (CDCl_3 , 400 MHz, ppm): δ 8.10 (m, 2H), 7.95 (m, 4H), 7.77 (d, $J = 8.1$ Hz, 2H), 7.54 (t, $J = 7.5$ Hz, 4H), 7.49 – 7.28 (m, 10H), 6.48 (bs, 2H), 6.67 (bs, 6H), 6.40 (bs, 2H), 4.62 (bs, 4H), 2.88 (bd, $J = 11.6$ Hz, 2H), 2.60 (bd, $J = 8.0$ Hz, 2H), 2.47 (bt, $J = 10.4$ Hz, 2H), 1.80 (bt, $J = 11.1$ Hz, 2H), 1.50 – 1.24 (m, 8H). $^{13}\text{C}\{^1\text{H}\}$ NMR (CDCl_3 , 126 MHz, ppm): δ 144.5, 134.0 (br s), 133.7, 13.32 (br s), 133.28, 131.32, 131.29, 130.5, 128.8, 128.8 (vt, $^1J_{\text{C-P}} = 5.0$ Hz), 128.1, 127.3, 127.2, (br s) 126.2, 125.9 (br s), 126.5 (br s), 125.2, 125.0, 124.4, 124.3, 123.6, 122.6 (vt, $^2J_{\text{C-P}} = 2.3$ Hz), 69.6, 55.7, 55.1, 29.9, 25.9, 24.1. $^{31}\text{P}\{^1\text{H}\}$ NMR (CDCl_3 , 162 MHz, ppm): δ -2.2. HRMS (ESI, m/z): $[\text{M}+\text{H}]^+$ calcd. for $\text{C}_{58}\text{H}_{53}\text{N}_4\text{P}_2$: 867.3740, found: 867.3737 ($\Delta = 0.3$ ppm).



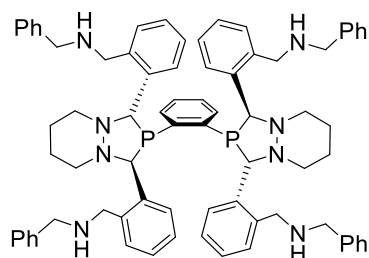
(*S,S,S,S*)-red-TP CHB BDP (**10**). **10** was purified by column chromatography (EtOAc : hexane = 1 : 9, R_f = 0.203) and obtained as a white solid (25% yield). ^1H NMR (CDCl_3 , 400 MHz, ppm): δ 7.55 (d, J = 7.9 Hz, 4H), 7.44 – 7.25 (m, 4H), 7.32 (d, J = 4.7 Hz, 2H), 7.20 – 7.13 (m, 2H), 6.98 – 6.93 (m, 2H), 6.86 (d, J = 7.5 Hz, 4H), 6.63 (t, J = 7.3 Hz, 2H), 6.40 (d, J = 7.7 Hz, 4H), 5.34 (vt, $^2J_{\text{H-P}}$ = 14.1 Hz, 2H), 5.24 (brs, 2H), 2.87 (t, J = 11.3 Hz, 2H), 2.68 (dd, J = 13.1, 4.1 Hz, 2H), 2.56 (t, J = 11.3 Hz, 2H), 2.39 (td, J = 11.4, 3.0 Hz, 2H), 2.01 (td, J = 11.4, 2.9 Hz, 2H), 1.76 – 1.67 (m, 8H), 1.47 – 1.42 (m, 5H), 1.33 – 1.27 (m, 5H), 1.01 (td, J = 12.1, 2.9 Hz, 2H), 0.80 (td, J = 12.1, 2.9 Hz, 2H). $^{31}\text{P}\{^1\text{H}\}$ NMR (CDCl_3 , 162 MHz, ppm): δ 1.8.

General Hydroformylation Procedure

Inside an N_2 -filled glovebox, a solution of $[\text{Rh}(\text{acac})(\text{CO})_2]$ in THF (20 mM), a solution of the bisdiazaphospholane ligand in DCM (5 – 20 mM) or the reduced bisdiazaphospholane in THF (20 mM) and THF were combined into an oven-dried 15 mL Ace Glass pressure bottle equipped with a magnetic stir bar using 1000 μL and 200 μL Eppendorf® pipets. The pressure bottle was attached to a pressure reactor and removed from the glovebox. In a fume hood, the reactor was purged with syngas (3 x 120 psig) and then filled to 150 psig of syngas. The yellow solution was vigorously stirred at 60 °C for at least 60 min. Upon cooling, the reactor was depressurized to 10 psig and the alkene was injected *via* a gas-tight syringe. Solid alkenes were injected as a solution in THF. The reactor was then purged with syngas (3 x 120 psig) and filled to 150 psig of syngas. The reaction was heated at 40, 60 or 80 °C. After the desired reaction time, the reactor was allowed to cool to room temperature and vented to atmospheric pressure. NMR spectra of the crude reaction mixture were taken in CDCl_3 or toluene- d_8 to obtain conversions of the alkenes and branched to linear ratios of the produced aldehydes.

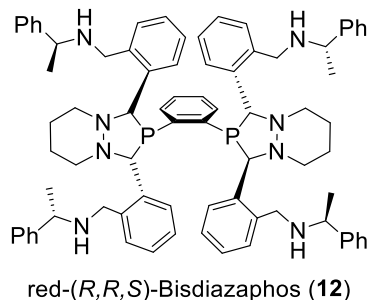
General Procedure for Tetraamide Borane-Reduction

To a solution of the BDP ligand (347.3 mg, 0.265 mmol, 1 equiv.) in THF (4 mL), $\text{BH}_3 \cdot \text{THF}$ (1 M in THF, 7.95 mL, 7.945 mmol, 30 equiv.) was added *via* syringe. The Schlenk flask was sealed and the mixture was stirred at 65 °C for 20 h. The reaction mixture was allowed to cool to room temperature and all volatiles were removed *in vacuo*. The remaining solid was dissolved in an N_2 -sparged acetone/water mixture (30 : 1, 20 mL) and the solution was heated at 70 °C for 21 h. Upon cooling, all volatiles were removed *in vacuo*. The crude product was dissolved in EtOAc (20 mL) and sat. aq. NaHCO_3 (10 mL). The aqueous layer was extracted and washed with EtOAc (10 mL) and DCM (10 mL). The combined organic layers were dried over MgSO_4 . The solvent was removed *in vacuo* to obtain the crude product as a yellow-brown or orange waxy oil.



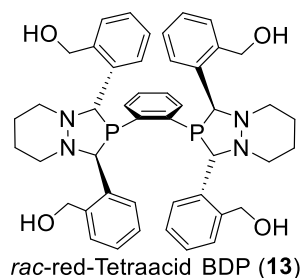
rac-red-TetraBnAmide BDP (11)

rac-red-TetraBnAmide BDP (11). Mixture of multiple species present since not all carbonyl groups were fully reduced under these conditions. $^1\text{H NMR}$ (CDCl_3 , 400 MHz, ppm): most signals are not assignable; all acylhydrazine groups were reduced, methine signals can be found between 4.55 and 4.20 ppm when comparing the ^1H and $^1\text{H}\{^{31}\text{P}\}$ NMR spectra. $^{31}\text{P}\{^1\text{H}\}$ NMR (CDCl_3 , 162 MHz, ppm): δ -14.2 ppm.



red-(R,R,S)-BisDiazaPhos (12). Three major species were present in solution, two with equivalent phosphorous atoms (fully reduced BDP, and one with only six acyl groups reduced), one with inequivalent phosphorous atoms (only seven acyl groups reduced, not all amide groups were fully reduced under these conditions. ^1H NMR (CDCl_3 , 400 MHz, ppm): most signals are not assignable; all acylhydrazine groups were reduced, methine signals can be found between 4.59 and 4.47 ppm when comparing the ^1H and $^1\text{H}\{^{31}\text{P}\}$ NMR spectra. $^{31}\text{P}\{^1\text{H}\}$ NMR (CDCl_3 , 162 MHz, ppm): δ -14.4 ppm. HRMS (ESI, m/z): $[\text{M}+\text{H}]^{2+}$ calcd. for $\text{C}_{78}\text{H}_{89}\text{N}_8\text{P}_2$: 600.3376, found: 600.3378 ($\Delta = 0.3$ ppm).

Synthesis of rac-red-Tetraacid BDP (**13**)



To a suspension of Tetraacid (365 mg, 0.396 mmol, 1 equiv.) in THF (7 mL), $\text{BH}_3\cdot\text{THF}$ (1 M in THF, 11.9 mL, 11.9 mmol, 30 equiv.) was added *via* syringe. The Schlenk flask was sealed and the mixture was stirred at 60 °C for 24 h. The reaction mixture was allowed to cool to room temperature and all volatiles were removed *in vacuo*. The remaining solid was dissolved in an N_2 -sparged acetone/water mixture (30 : 1, 10 mL) and the solution was heated at 70 °C for 22 h. Upon cooling, all volatiles were removed *in vacuo*. The crude product was dissolved in EtOAc

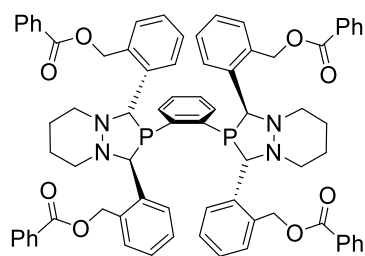
(20 mL) and aq. K_2CO_3 (10 wt%, 15 mL). The aqueous layer was extracted and washed with EtOAc (10 mL) and DCM (10 mL). The combined organic layers were dried over MgSO_4 . The solvent was removed *in vacuo* to obtain the crude product as an orange waxy oil. In a Schlenk flask, the crude product was then dissolved in N_2 -sparged HNEt_2 (4 mL) and the mixture was heated at 45 °C for 16 h. Upon cooling, all volatiles were removed *in vacuo*. The remaining yellow oil was dissolved in EtOAc (20 mL) and aq. HCl (1 M, 10 mL) and the mixture was stirred for at least 30 min. Aq. K_2CO_3 (10 wt%) was added until the aqueous layer was basic (pH ~ 10). The organic layer was washed with aq. K_2CO_3 (10 mL). The combined aqueous layers were extracted and washed with EtOAc (10 mL) and DCM (10 mL). The combined organic layers were dried over MgSO_4 . The solvent was removed *in vacuo* to obtain the desired product as a yellow waxy oil.

Attempts to further isolate the desired product through column chromatography were unsuccessful. The material is clean in the ^{31}P NMR spectrum, but contains boron-containing impurities visible in the ^1H NMR spectrum. **^1H NMR** (CDCl_3 , 400 MHz, ppm): δ 7.69 (m, 2 H), 7.47 (d, J = 7.3 Hz, 2 H), 7.41 (t, J = 7.3 Hz, 2 H), 7.34 – 7.22 (m, 4 H), 6.86 (d, J = 7.5 Hz, 2 H), 6.56 (t, J = 7.4 Hz, 2 H), 6.46 (t, J = 7.4 Hz, 2 H), 6.30 (d, J = 7.6 Hz, 2 H), 5.90 (d, J = 7.6 Hz, 2 H), 5.32 (dt, J = 12.9, 3.1 Hz, 2 H), 4.54 – 4.46 (m, PCHN overlapped with benzyprotons, 8 H), 4.07 (bs, PCHN , 2 H), 3.08 (d, J = 9.9 Hz, 2 H), 2.94 (d, J = 11.4 Hz, 2 H), 2.50 (td, J = 12.2, 1.8 Hz, 2 H), 2.04 (td, J = 12.2, 2.0 Hz, 2 H), 1.65 (d, J = 13.7 Hz, 2 H), 1.55 – 1.30 (m, 8 H). **$^{31}\text{P}\{^1\text{H}\}$ NMR** (CDCl_3 , 162 MHz, ppm): δ -11.2. HRMS (ESI, m/z): $[\text{M}+\text{H}]^+$ calcd. for $\text{C}_{46}\text{H}_{38}\text{N}_4\text{O}_4\text{P}_2$: 787.3537, found: 787.3531 (Δ = 0.8 ppm).

General Procedure for the Esterification of red-Tetraacid 13.

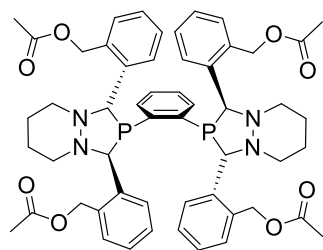
Crude red-Tetraacid (343.2 mg, 0.44 mol, 1 equiv) was dissolved in DCM (15 mL) and NEt_3 (254.4 μL , 2.2 mmol, 5 equiv) was added *via* syringe. The solution was cooled to 0 °C using an ice bath. The acyl chloride (2.2 mmol, 5 equiv) was added dropwise. The orange solution turns

even darker within 30 min. The reaction mixture was allowed to warm to room temperature overnight. All volatiles were removed *in vacuo* after stirring the reaction for 16 h. The crude thick oil was dissolved in EtOAc (20 mL) and aq. HCl (1 M, 20 mL) and the phases were separated. The organic layer was washed with aq. HCl (2 x 10 mL) and the combined aqueous phase with EtOAc (2 x 10 mL). The combined organic phase was washed with aq. NaHCO₃ (2 x 15 mL) and with brine (20 mL), followed by drying over MgSO₄. The solvent was removed *in vacuo* to yield the crude product as a thick orange oil.



rac-red-TetraBnBenzoate (**14**)

rac-red-TetraBnBenzoate (**14**): ¹H NMR (CDCl₃, 400 MHz, ppm): δ methine protons are found in the chemical shift range of 4.59 – 4.44 ppm. ³¹P{¹H} NMR (CDCl₃, 162 MHz, ppm): δ -4.3.



rac-red-TetraBnAcetate (**15**)

rac-red-TetraBnAcetate (**15**): ¹H NMR (CDCl₃, 400 MHz, ppm): δ methine protons are found in the chemical shift range of 4.36 – 4.27 ppm. ³¹P{¹H} NMR (CDCl₃, 162 MHz, ppm): δ -4.2.

3.5 References

1. Claver, C.; van Leeuwen, P. W. N. M. *Rhodium Catalyzed Hydroformylation*. Kluwer Academic Publishers: Dodrecht, **2000**.
2. Trost, B. M. *Science* **1991**, *254*, 1471–1477.
3. Botteghi, C.; Paganelli, S.; Schionato, A.; Marchetti, M. *Chirality* **1991**, *3*, 355–369.
4. Landis, C. R.; Jin, W.; Owen, J. S.; Clark, T. P. *Angew. Chem. Int. Ed.* **2001**, *40*, 3432–3434.
5. Clark, T. P.; Landis, C. R.; Freed, S. L.; Klosin, J.; Abboud, K. A. *J. Am. Chem. Soc.* **2005**, *127*, 5040–5042.
6. Watkins, A. L.; Hashiguchi, B. G.; Landis, C. R. *Org. Lett.* **2008**, *10*, 4553–4556.
7. McDonald, R. I.; Wong, G. W.; Neupane, R. P.; Stahl, S. S.; Landis, C. R. *J. Am. Chem. Soc.* **2010**, *132*, 14027–14029.
8. Adint, T. T.; Wong, G. W.; Landis, C. R. *J. Org. Chem.* **2013**, *78*, 4231–4238.
9. Abrams, M. L.; Foarta, F.; Landis, C. R. *J. Am. Chem. Soc.* **2014**, *136*, 14583–14588.
10. Axtell, A. T.; Klosin, J.; Abboud, K. A. *Organometallics* **2006**, *25*, 5003–5009.
11. Feuer, H.; Brown, F. *J. Org. Chem.* **1970**, *35*, 1468–1471.
12. Landis, C. R.; Nelson, R. C.; Jin, W.; Bowman, A. C. *Organometallics* **2006**, *25*, 1377–1391.
13. Herault, D.; Nguyen, D. H.; Nuel, D.; Buono, G. *Chem. Soc. Rev.* **2015**, *44*, 2508–2528.
14. Reich, H. J. <http://www.chem.wisc.edu/areas/reich/nmr/notes-5-hmr-16-virtual-coupling.pdf>.
15. Fackler, J. P.; Fetchin, J. A.; Mayhew, J.; Seidel, W. C.; Swift, T. J.; Weeks, M. *J. Am. Chem. Soc.* **1969**, *91*, 1941–1947.
16. Pidcock, A. *Chem. Comm.* **1968**, 92–92.
17. Hersh, W. H. *J. Chem. Ed.* **1997**, *74*, 1485.

18. Reich, H. J. <http://www.chem.wisc.edu/areas/reich/plt/windnmr.htm>.
19. Klosin, J.; Landis, C. R. *Acc. Chem. Res.* **2007**, *40*, 1251–1259.
20. Axtell, A. T.; Cobley, C. J.; Klosin, J.; Whiteker, G. T.; Zanotti-Gerosa, A.; Abboud, K. A., *Angew. Chem. Int. Ed.* **2005**, *44*, 5834.
21. Nozaki, K.; Li, W.; Horiuchi, T.; Takaya, H. *Tetrahedron Lett.* **1997**, *38*, 4611.
22. Lightburn, T. E.; De Paolis, O. A.; Cheng, K. H.; Tan, K. L. *Org. Lett.* **2011**, *13*, 2686–2689.
23. Koskinen, A. M. P.; Karisalmi, K. *Chem. Soc. Rev.* **2005**, *34*, 677–690.
24. Fürstner, A.; Nevado, C.; Waser, M.; Tremblay, M.; Chevrier, C.; Teplý, F.; Aïssa, C.; Moulin, E.; Müller, O. *J. Am. Chem. Soc.* **2007**, *129*, 9150–9161.
25. Smith, A. B.; Brandt, B. M. *Org. Lett.* **2001**, *3*, 1685–1688.
26. Šmejkal, T.; Breit, B. *Angew. Chem. Int. Ed.* **2008**, *47*, 311–315.
27. Dydio, P.; Dzik, W. I.; Lutz, M.; de Bruin, B.; Reek, J. N. H. *Angew. Chem. Int. Ed.* **2011**, *50*, 396–400.
28. List, B. *Tetrahedron* **2002**, *58*, 5573–5590.
29. Woodward, R. B.; Logusch, E.; Nambiar, K. P.; Sakan, K.; Ward, D. E.; Au-Yeung, B. W.; Balaram, P.; Browne, L. J.; Card, P. J.; Chen, C. H. *J. Am. Chem. Soc.* **1981**, *103*, 3210–3213.
30. Stemmler, R. *Synlett* **2007**, *6*, 997–998.
31. Carley, S.; Brimble, M. A. *Org. Lett.* **2009**, *11*, 563–566.
32. Stepan, A. F.; Karki, K.; McDonald, W. S.; Dorff, P. H.; Dutra, J. K.; DiRico, K. J.; Won, A.; Subramanyam, C.; Efremov, I. V.; O'Donnell, C. J.; Nolan, C. E.; Becker, S. L.; Pustilnik, L. R.; Sneed, B.; Sun, H.; Lu, Y.; Robshaw, A. E.; Riddell, D.; O'Sullivan, T. J.; Sibley, E.; Capetta, S.; Atchison, K.; Hallgren, A. J.; Miller, E.; Wood, A.; Obach, R. S. *J. Med. Chem.* **2011**, *54*, 7772.
33. Watkins, A. L.; Landis, C. R. *J. Am. Chem. Soc.* **2010**, *132*, 10306–10317.

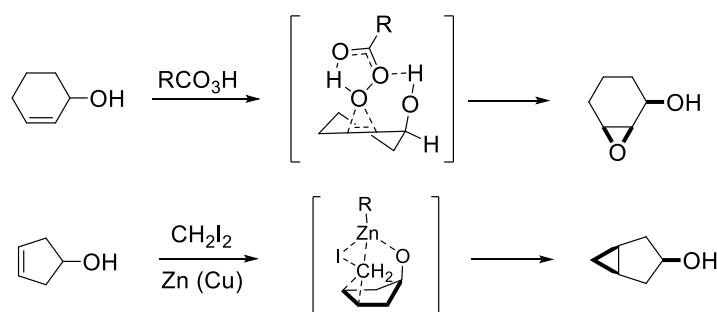
34. Xu, K.; Zheng, X.; Wang, Z.; Zhang, X. *Chem. Eur. J.* **2014**, *20*, 4357–4362.
35. Longeau, A.; Durand, S.; Spiegel, A.; Knochel, P. *Tetrahedron: Asymmetry* **1997**, *8*, 987–990.
36. Kimura, K.; Watanabe, Y.; Suda, T.; Senda, H.; Hosoi, S.; Ohta, T.; Kunimoto, K. *Analytical Sciences* **1999**, *15*, 609–610.
37. Jones, B. R.; Abrams, M. L.; Landis, C. R.; May, S. A.; Campbell, A. N.; Martinelli, J. R.; Calvin, J. R. *J. Org. Chem.* **2016**, *81*, 11965–11970.
38. Noonan, G. M.; Fuentes, J. A.; Cobley, C. J.; Clarke, M. L. *Angew. Chem. Int. Ed.* **2012**, *51*, 2477–2480.
39. Reiter, S. A.; Nogai, S. D.; Karaghiosoff, K.; Schmidbaur, H. *J. Am. Chem. Soc.* **2004**, *126*, 15833–15843.
40. Maier, L. *Helvetica Chimica Acta* **1966**, *49*, 842–851.
41. Marzano, C.; Gandin, V.; Pellei, M.; Colavito, D.; Papini, G.; Lobbia, G. G.; Del Giudice, E.; Porchia, M.; Tisato, F.; Santini, C. *J. Med. Chem.* **2008**, *51*, 798–808.

Chapter 4

Diazaphospholane Ligands with Boronate-containing Directing Groups for Rhodium-Catalyzed Hydroformylation

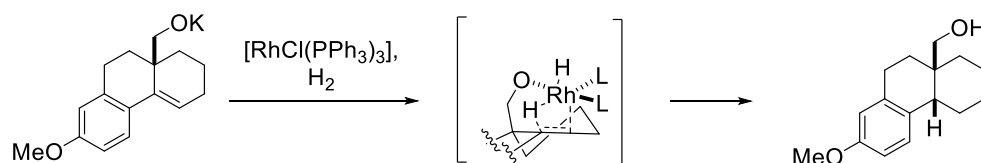
4.1 Introduction

Selectivity control in organic and organometallic transformations is still a great challenge for the synthetic chemist. One approach to addressing this challenge is through the use of intramolecular directing groups. This strategy was first discovered with the hydroxy-directed epoxidation reported by Henbest and Wilson in 1959¹ and the alkoxy-directed Simmons-Smith cyclopropanation by Winstein and Sonnenberg in 1961² (Scheme 4.1). These reactions are thought to proceed through a highly-ordered transition state and give primarily the *cis*-stereoisomer product. The selectivity control is considered to be substrate-directed, where the substrate bears a functional group capable of coordinating to the reagent.



Scheme 4.1. Directed epoxidation (top, Henbest) and cyclopropanation (bottom, Winstein).

An early example of a catalytic reaction utilizing substrate-directing effects is the rhodium-catalyzed hydrogenation shown in Scheme 4.2.³ The hydroxyl group in the substrate is capable of binding to the Rh-center, allowing for the ordered coordination of the alkene functional group. After the hydrogenation step, the product can dissociate from the metal-center. This step is essential for the next turnover to occur and to enable catalysis.



Scheme 4.2. Substrate-directed catalytic hydrogenation (Thompson).

Exploitation of the directing effects of typical functional groups has increased over the years, with the goal of installing new functionalities and stereochemistry in organic molecules. One can take advantage of the already installed groups within the substrate. Substrate with group incapable of directing ability can be modified by installing a group able to bind to the reagent or catalyst the substrate.⁴ Conceptually, a substrate-attached directing group (DG) can be reagent (R)- or catalyst (C)-directing (Figure 4.1). This group is capable of coordinating to the reagent or catalyst, thus allowing for a pre-associated and ordered conformation, which stays present in the transition state of the selectivity-controlling reaction step. Effectively this pre-association converts passage through a bimolecular transition state into a unimolecular step. Indicators of the effectiveness of a directing group include increased selectivity and an enhancement in the reaction rate caused by lowering of the activation entropy.^{2,4} Catalyst-directing groups need the property of reversible binding to the catalyst to allow for turnover. Even when the binding is reversible, the presence of a catalyst-directing group can lead to product inhibition.⁴⁻⁹

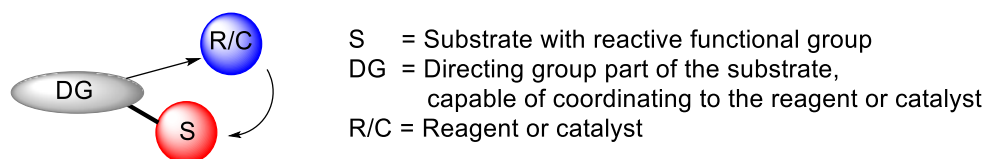
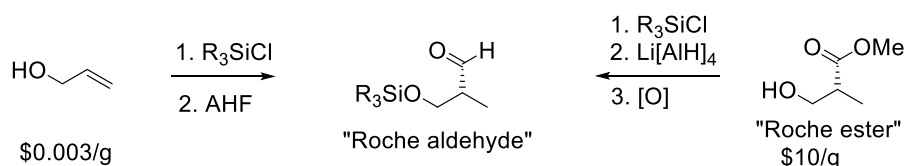


Figure 4.1. Intramolecular transformation through a reagent- or catalyst-directing group DG.

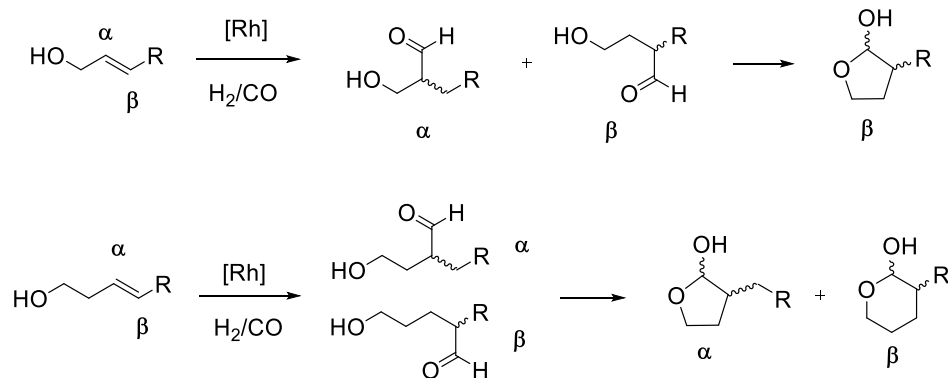
Directing groups have been applied in rhodium-catalyzed hydroformylation to access the branched isomer product in useful levels. Alkenes with hydroxy functionalities are of particular

focus since hydroxy-aldehydes are industrially important aldehyde intermediates. For example, hydroxyaldehydes are produced in the hydroformylation of allyl alcohols for the synthesis of 1,4-butanediol that is mainly used as monomers in the polyester polybutyleneterephthalate (PBT) and in the conversion to tetrahydrofuran (THF).^{10,11,12} Selectivity for the branched aldehyde regioisomer remains a challenge due to the inherent electronic preference towards the linear aldehyde of alkenes lacking strong electron-withdrawing groups. One prominent example important branched aldehydes is the “Roche Aldehyde” (Scheme 4.3), which is commonly used in the synthesis of polyketides and other natural products.^{13,14,15} Typically, the Roche aldehyde is obtained from the expensive “Roche ester” by a multiple step sequence comprising protection of the hydroxyl group, reduction of the ester group, and final oxidation to the aldehyde. Alternatively, a route towards the Roche aldehyde utilizing hydroformylation has been demonstrated, which produces the aldehyde from the silyl-protected allyl alcohol, offering a more affordable and scalable way towards the Roche aldehyde.^{16,17}



Scheme 4.3. Synthetic routes towards the “Roche Aldehyde”.

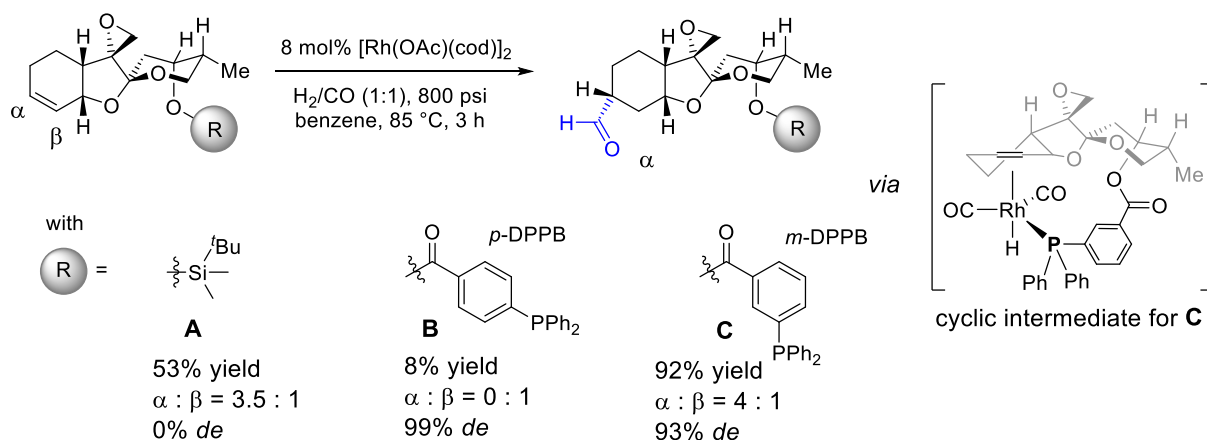
Allylic and homoallylic alcohol hydroformylation products include both branched (or α -product) and linear aldehyde (or β -product) both of which may spontaneously cyclize to the corresponding hemiacetals (Scheme 4.4). The lactol hemiacetals may be further derivatized by oxidation to lactones, reaction with alcohols to form cyclic acetals, or through reduction to yield cyclic ethers.¹⁸



Scheme 4.4. Aldehyde products from the hydroformylation of allylic and homoallylic alcohols.

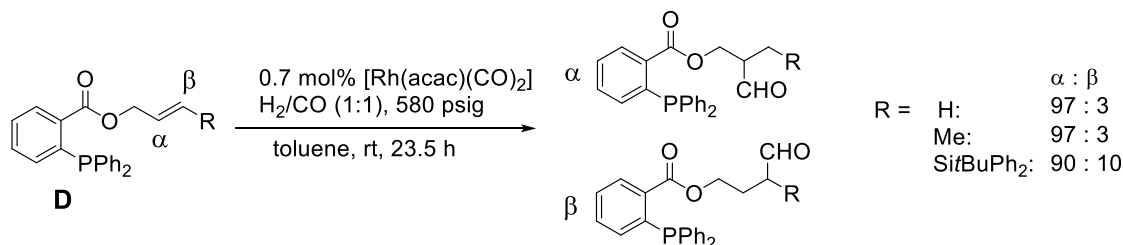
4.1.1 Stoichiometric Directing Groups for Regio- and Stereoselective Control in Rhodium-Catalyzed Hydroformylation

Burke *et al.* demonstrated the regio- and diastereoselectivity induced hydroformylation in the synthesis of (+)-Phyllanthocin (Scheme 4.5).¹⁹ Three substituents have been investigated as the alcohol protecting group in the alkene precursor. First, the silyl ether protected precursor **A** led to 53% yield of the α -aldehyde product, while no preference for either diastereomer of the α -aldehyde was observed (0% *de*). Incorporation of a protecting group that can act as a directing group through reversible binding to the catalyst has a dramatic change on the product distribution: *p*-(diphenylphosphino)benzoate (*p*-DPPB) (precursor **B**) led primarily to the β -aldehyde with 99% *de*, which turns out to be undesired regioisomer. Furthermore, the reaction is slow and gave only 8% yield, which is consistent with observed product-inhibition. To test this theory, the incorporation of the shorter phosphine-tether *m*-DPPB (**C**) was investigated. Surprisingly, the desired α -aldehyde product was majorly formed in 92% yield and in a high diastereomeric excess of 93% *de*. The ring size of the cyclic intermediate formed with the *m*-DPPB group turns out to be ideal to combine good regio- and diastereoselectivity. This example of intramolecular hydroformylation demonstrates the influence and importance on the ring size of the phosphine-Rh-alkene-chelate intermediates.



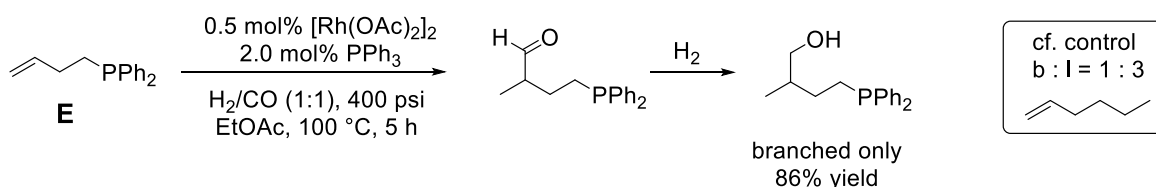
Scheme 4.5. Intramolecular hydroformylation in the synthesis of (+)-phyllanthocin.

Inspired by the work of Burke, Breit *et al.* reported the use of *o*-DPPB to control the regioselectivity in the hydroformylation of mono- and disubstituted allyl alcohol derivatives.²⁰ Preference towards the branched aldehyde, which is disfavored in the absence of directing group effects, was achieved in good yields and high regioselectivities with the *o*-DPPB directing group (Scheme 4.6, **D**). This directing group is also powerful in hydroformylating 1,1-disubstituted^{21,20} as well as trisubstituted allylic alcohols,²² selectively yielding the difficult to synthesize α -isomer. Breit suggests that a well-defined conformation in the cyclic transition state induces a selective hydrometallation step, in which the hydride is rather delivered to the β -position.



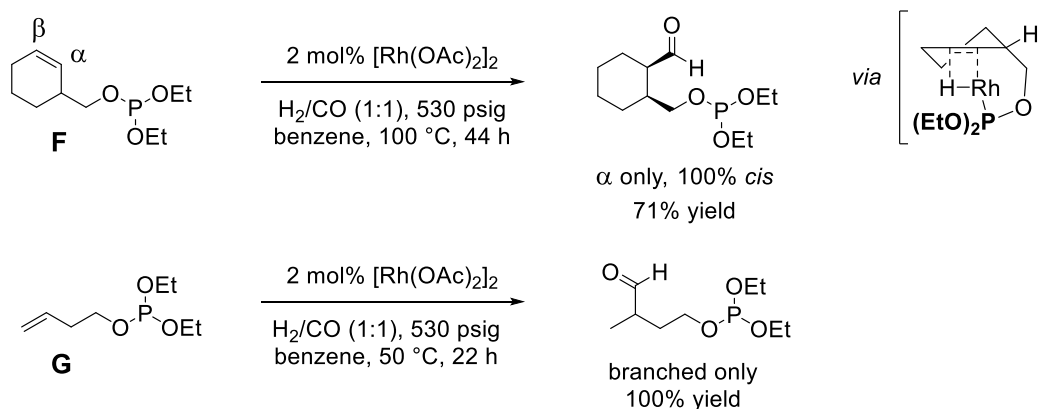
Scheme 4.6. High regioselectivity of allylic alcohol substrates controlled by the *o*-DPPB group.

The importance of a phosphine moiety as a directing group was demonstrated by Jackson *et al.* in 1987.²³ In comparison to a non-directed hydroformylation of 1-hexene, starting with a phosphine-tethered alkene **E**, regioselectivity preference switches to yield primarily the branched aldehyde product, which was isolated as its corresponding hydrogenated product (Scheme 4.7). This example shows how the increased tendency of a metal-center to bind to phosphines over carbon monoxide induces formation of a cyclic phosphine-Rh-alkene complex. Installation of the formyl group occurs on the higher substituted C-atom, leading to the branched aldehyde product. Reversible exchange of the monophosphine ensures constant turnover and lessens product inhibition of the catalytic rate.



Scheme 4.7. Directed branched selective hydroformylation of the phosphine-tethered alkene **E**, in contrast, the control reaction with 1-hexene leads to linear aldehyde.

The first use of a phosphite-directing group was reported by Jackson *et al.* in 1990 for Rh-catalyzed hydroformylation of the acyclic and cyclic homoallylic alkenes **F** and **G** (Scheme 4.8).²⁴ The coordination of the phosphite and the double bond of the alkene to the Rh-center induces a six-membered intermediate, allowing for the addition of the hydride to the terminal C-atom (β -position) and forming exclusively the branched, α -aldehyde products.



Scheme 4.8. Branched selective hydroformylation through use of a phosphite directing group.

4.1.2 Catalytic Catalyst-Directing Groups and Scaffolding Catalysis

Increased research focuses on finding systems with non-stoichiometric directing groups, *i. e.*, directing groups that are an integral component of the substrate and/or catalyst. The advantage of this strategy is that it eliminates extra synthetic steps of installing and removing the directing group. As has been introduced previously (*vide supra*), efficient directing groups enable reversible binding to a reagent or catalyst. The ideal catalytic directing groups should be capable of binding to the substrate covalently, but also reversibly to allow for substrate-product exchange. The concept of the catalytic catalyst-directing groups is often referred to as “scaffolding ligands and scaffolding catalysis”.²⁵ A simplified catalytic cycle on scaffolding catalysis is depicted in Figure 4.2.^{4,26,7} The scaffolding manifold has a domain that can bind to the catalyst datively (blue) and one domain that binds to the substrate covalently and reversibly (red). Initially, the scaffold binds a substrate, followed by coordination to the catalyst. Substrate and catalyst are brought in close proximity and the catalytic reaction can be performed in an intramolecular and directed fashion, leading to selective product formation (green). The scaffold, now bearing the product, can de-coordinate from the catalyst and subsequent exchange with the substrate allows the scaffold-substrate to re-enter the catalytic cycle.

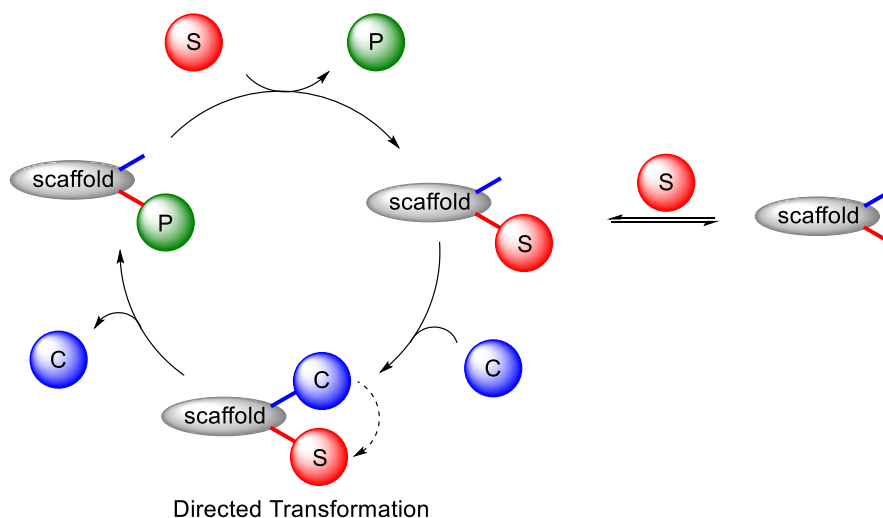
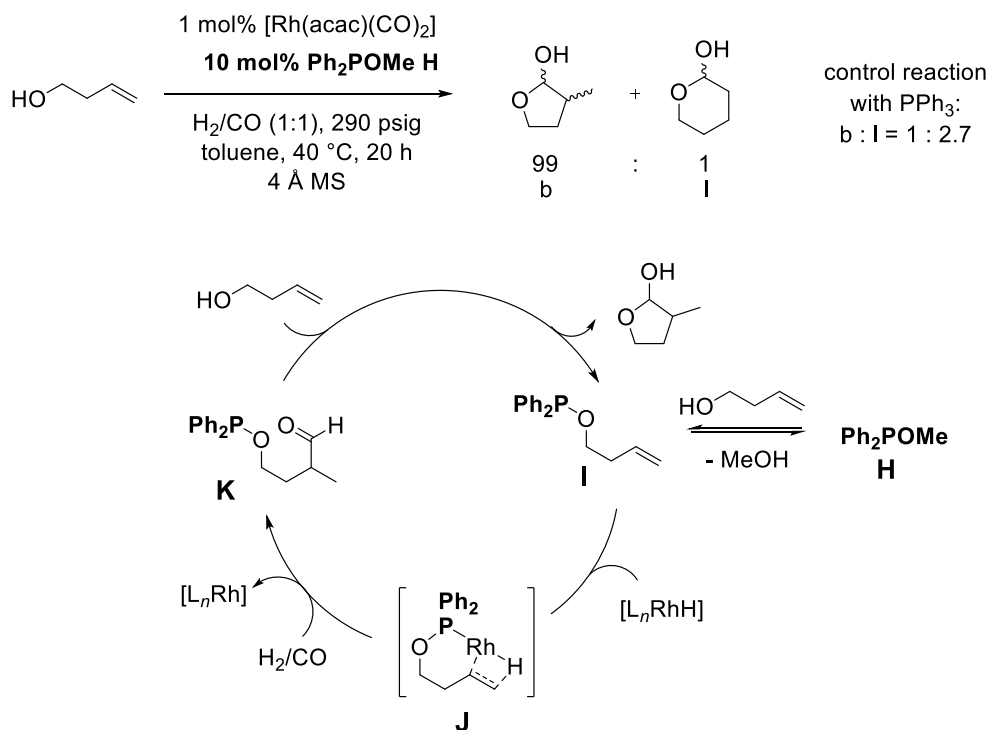


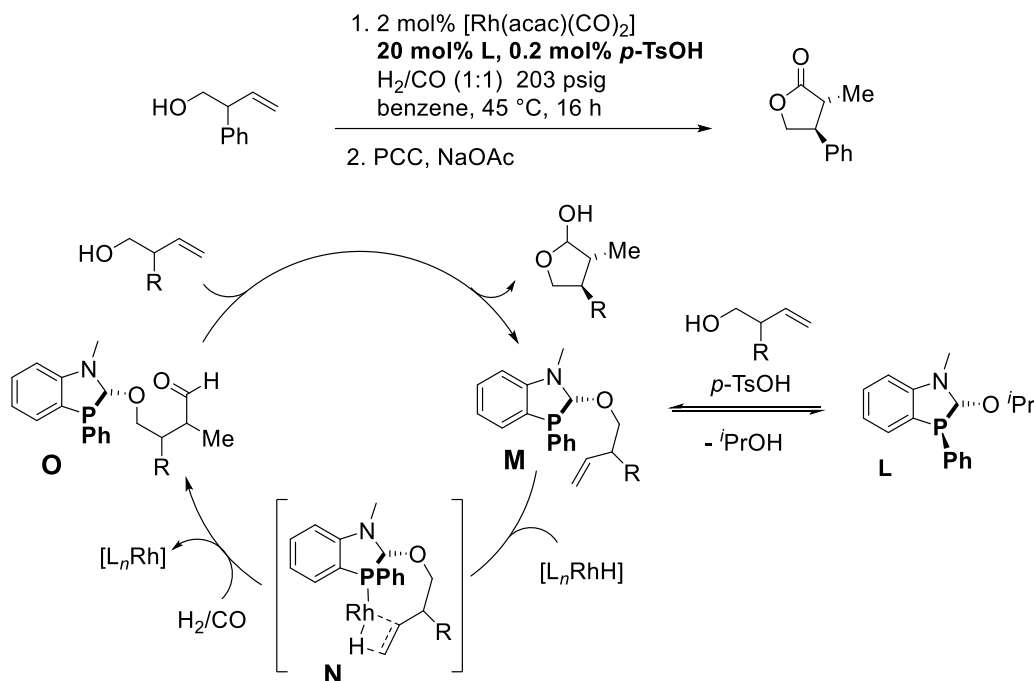
Figure 4.2. Catalytic cycle with a scaffolding ligand acting as a catalytic catalyst directing group.

Successful representatives of scaffolding ligands in the hydroformylation of allylic alcohol substrates are phosphine-based. The phosphinite Ph_2POMe **H**, reported by Breit and coworkers was utilized in as low as 10 mol% for the branched selective hydroformylation of homoallylic alcohols (Scheme 4.9).²⁷ This phosphinite **H** reacts with the substrate with subsequent elimination of MeOH in the presence of 4 Å molecular sieves. The now substrate-attached phosphinite **I** enters the catalytic cycle, binding to the metal-center through the phosphorus atom and the alkene group, forming the chelating complex **J**. Addition of the hydride to the terminal C-atom across the double bond proceeds *via* a six-membered metallacycle, leading to the installation of the formyl group in the branched position. Once the aldehyde product **K** is formed, the phosphine decoordinates from the metal center. Transesterification with another homoallylic alcohol liberates the γ -lactol and reforms a new phosphinite-substrate **I**, making it available for the next turnover in the catalytic cycle (Scheme 4.9). This concept was further expanded towards 1,2-disubstituted homoallylic alcohols,²⁷ and bishomoallylic alcohol substrates²⁸.



Scheme 4.9. Branched-selective hydroformylation of homoallylic alcohol with the catalytic directing group Ph_2POMe and the mechanism proposing a six-membered metallacycle.

Tan and coworkers have found that the aminor containing phospholane **L** also selectively addresses hydroxy containing alkenes (Scheme 4.10).²⁶ Ligand **L** undergoes transacetalization with the hydroxy alkene involving the *iso*-propoxy group in the presence of catalytic amount of *p*-TsOH to **M**. By attachment of the substrate to the phosphorus ligand, chelating coordination to the Rh-metal-center can occur, forming the preferred seven-membered metallacycle **N**, delivering the hydride group to the terminal C-atom of the double bond. Once the formyl group is installed, transacetalization of **O** with the substrate releases the desired product as its lactol to reform **M** (Scheme 4.10).



Scheme 4.10. Tan's aminor phospholane ligand **L** capable of covalent coordination of a substrate and selective hydroformylation towards the branched aldehyde product; the proposed mechanism features a seven-membered cyclic transition state **N**.

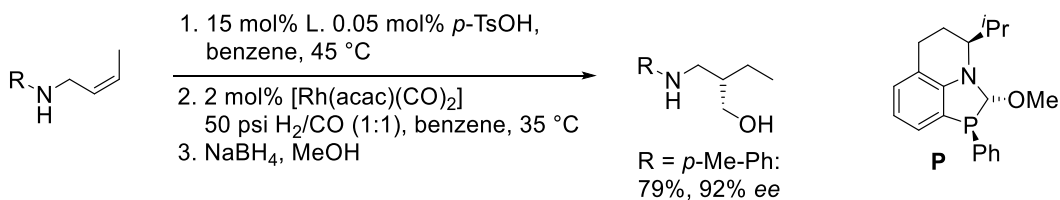
Tan's ligand **L** showed furthermore success in addressing a wide range of hydroxy containing alkene substrates. A selection of substrates is shown in Table 4.1. Good selectivity towards the branched aldehyde was obtained for the homoallylic substrate in entry 1, while using only PPh_3 shows preference for the linear aldehyde (entry 2). In addition, increased diastereoselectivity was also observed with this substrate. A similar trend is observed with 1,2-disubstituted homoallylic alcohol, where the even higher ratio in α to β products can be explained with the sterically less bulky methyl substituent (entry 3 and 4). The 1,2-disubstituted allylic substrate in entry 5 shows a great selectivity for the α -aldehyde, despite the fact that typically styrenyl positions have a high preference for the formyl-addition α to the phenyl ring. Formation of only one diastereomer is observed with the usually challenging trisubstituted allylic alcohol in entry 6. The other challenging substrate class is 1,1-disubstituted alkenes. Hydroformylation using simply PPh_3 leads exclusively

to the β -formyl product, however, with the directing effect of the Tan ligand **L** the production of a quaternary center is strongly favored (entry 7 and 8).

Table 4.1. Selective Hydroformylation of Hydroxy Containing Alkenes with Tan Ligand **L**.

Entry	Ligand	Substrate	Yield (%)	$\alpha : \beta$	<i>dr</i>	Ref.
1	PPh ₃		98	1 : 3	42 : 58	26
2	L		94	6.2 : 1	88 : 12	
3	PPh ₃		n/a	1 : 1.5	n/a	26
4	L		69	15.6 : 1	78 : 22	
5	L		90	20 : 1	--	29
6	L		87	only		
7	PPh ₃		66	<1 : 49	--	30
8	L		73	32 : 1	--	

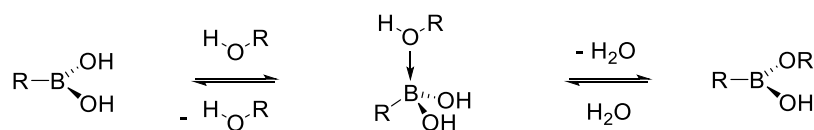
Even though ligand **L** contains two stereogenic centers, the phosphorus center does not stay in this conformation. Under the acidic substrate exchange conditions necessary, the phosphorus stereogenic center can flip during transacetalization. Therefore, Tan and coworkers developed an enantiopure version **P** of their original ligand. Ligand **P** was found to undergo directed hydroformylation, demonstrated on the protected allyl amines (Scheme 4.11).³¹



Scheme 4.11. Directed hydroformylation of protected allyl amine with enantiopure ligand **P**.

These types of cyclic aminal phosphines, however, also have challenges that have not been solved to date. The ligands are not stable to hydrolysis and can degrade over time through ring opening reactions, requiring the use of ligand loadings on the order of 15 – 20 mol%. In addition, only substrate functional groups with high affinity to bind to the ligand generally show improved selectivities over substrates with low binding affinity.³² One other downside is the use of acidic or basic additives necessary for the reversible substrate exchange to proceed.

Directing groups that can solve all of these challenges are thought to be boronic acids and their corresponding boronate esters. These functional groups are known to undergo reversible as well as facile exchange on the order of seconds with alcohol groups, known as transesterification (Scheme 4.12).^{33,34}



Scheme 4.12. Reversible and facile exchange of alcohols in boronic acids and esters.

Boronic acids and boronate esters are sought to possess all the advantages to act as an ideal directing group: 1) the ability to rapidly exchange their oxygen bearing substituents without the use of any additive to ensure reversible exchange; 2) boronates contain two exchange sites per B-atom for binding substrates simultaneously, increasing the chance for substrate binding. This

feature can hypothetically lead to enhanced reaction rates and decrease the potential for product inhibition.

We sought to design a novel scaffolding ligand that can address these challenges and improve upon selectivities of hydroxy-functionalized alkene substrates in directed hydroformylation. With their excellent ability to afford aldehydes in high regio- and enantioselectivities, diazaphos ligands are thought to be modified to function as a scaffolding ligand. The goal of this work is to install boronate directing group functionality onto the diazaphospholane structure that specifically targets hydroxy-alkene substrates (Figure 4.3). Scaffolding catalysis has also not been investigated using bisphosphines. A bisphosphine-metal-complex already containing a directing group allows for a more defined and stable catalyst throughout the catalyzed reaction.

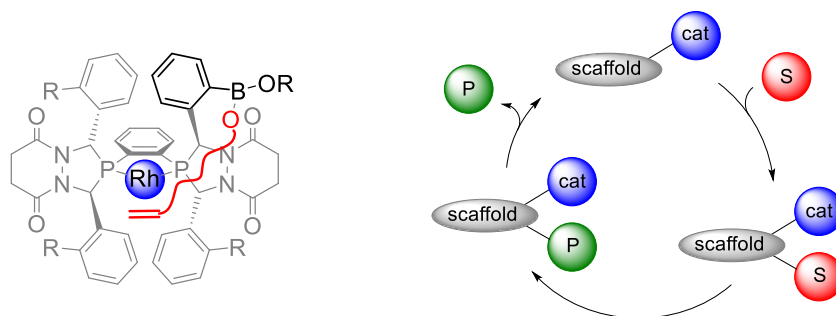


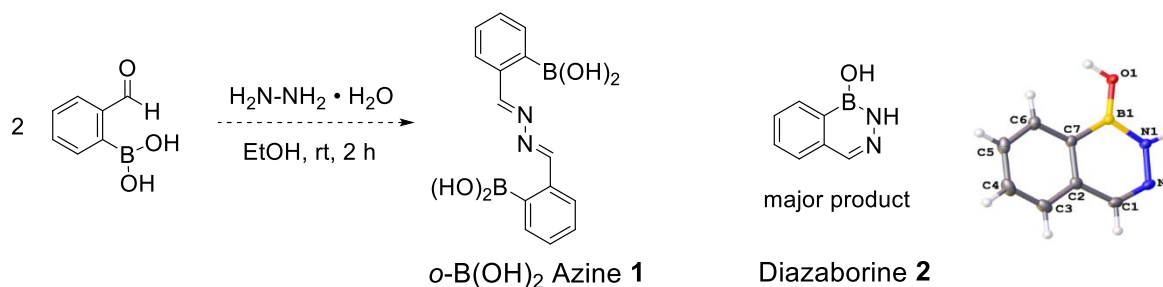
Figure 4.3. Boronate bearing bisdiazaphospholanes as potential scaffolding ligands in catalysis.

4.2 Results and Discussion

4.2.1 Synthesis of Boronate Containing Azines

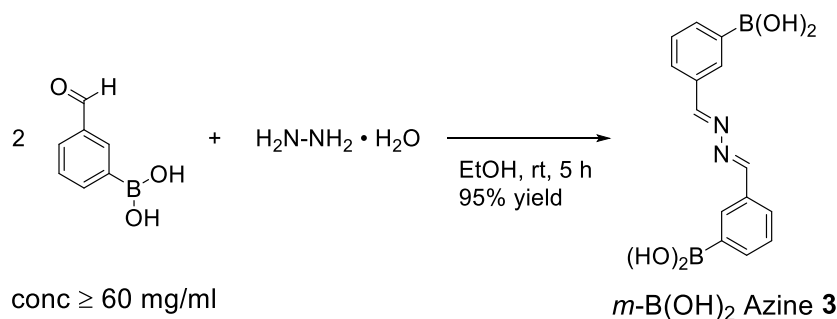
Diazaphospholane ligands are synthesized through a Mannich-type condensation reaction of a primary phosphine, an acyl chloride and commonly 1,2-dibenzylidene hydrazine (azine). In order to synthesize boronic acid containing diazaphospholane ligands, the synthesis of 1,2-di(boronic acid benzylidene)hydrazines (B(OH)_2 Azine) as essential starting materials for the

diazaphospholane framework formation was investigated. The aldehyde 2-formylphenyl boronic acid was reacted with hydrazine monohydrate. Unfortunately, *o*-B(OH)₂ azine **1** is only formed in around 30% based on ¹H NMR spectroscopy analysis. The major product is 1,2-dihydro-1-hydroxy-2,3-benzodiazab-1-borine³⁵ **2**, formed by an intramolecular cyclization reaction of the aldehyde and hydrazine (Scheme 4.13). This structure was confirmed by ¹H and ¹¹B NMR spectroscopy as well as by X-ray crystallography. In addition, a ¹¹B NMR resonance at 1.4 ppm is observed, corresponding to a four-coordinate species that stems from the adduct formation of either EtOH or water to the boronate group in the azine or the diazaborine.



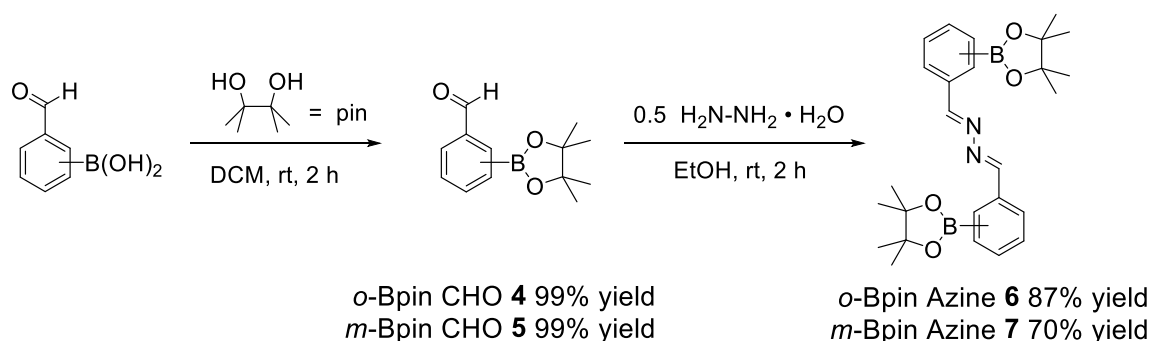
Scheme 4.13. 1,2-dihydro-1-hydroxy-2,3-benzodiazab-1-borine **2** as the major product from an intramolecular cyclization reaction of 2-formylphenyl boronic acid and hydrazine.

To obtain a clean reaction to a boronate containing azine, 3-formylphenyl boronic acid was utilized instead, since the boronic acid substituents in *meta*-positions will avoid the cyclization reaction to a six-membered diazaborine structure. It was found that the reaction between 2 equivalents of 3-formylphenyl boronic acid and hydrazine only proceeds cleanly to a yellow solid **3** when the concentration of 3-formylphenyl boronic acid is greater than 60 mg/mL in EtOH (Scheme 4.14). More diluted reaction conditions result in a complex product mixture in the form of a sticky yellow oil. Azine **3** has poor solubility in most solvents except of MeOH and difficulties in the synthesis towards a bisdiazaphospholane were encountered (*vide infra*).



Scheme 4.14. Reaction of 3-formylphenyl boronic acid and hydrazine to form azine **3**.

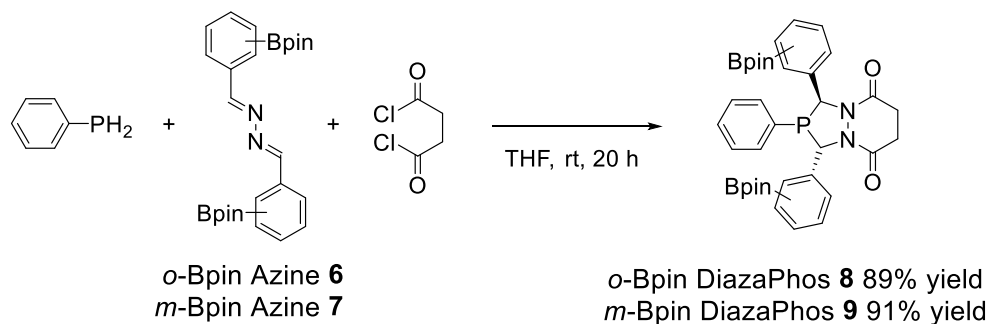
One route that has been utilized to achieve an *ortho*-boronate containing azine, is through the protection of the boronic acid group with pinacol (pin). For the convenience of increasing solubility for the *meta*-substituted B(OH)₂ azine, both starting materials 2- and 3-formylphenylboronic acid were protected with pinacol *via* modified literature procedures.^{36,37} The resulting boronic acid pinacolyl esters **4** and **5** were obtained as colorless oils in high yields (95%). The reaction of **4** and **5** with hydrazine in EtOH at room temperature yields both Bpin azines **6** and **7** as light yellow powders in high yields (**3**: 77% and **4**: 96%) (Scheme 4.15). The azines were characterized by ¹H, ¹³C and ¹¹B NMR spectroscopy and are in agreement with reported values for other azines³⁸ and pinacol boronates³⁹.



Scheme 4.15. Protection of 2- and 3-formylphenylboronic acid with pinacol and subsequent reaction with hydrazine to the Bpin azines **6** and **7**.

4.2.2 Synthesis of Boronate-Bearing Diazaphospholanes

Initially, the synthesis towards the boronate monodiazaphospholane framework was investigated with a monophosphine. The reaction of one equivalent each of azines **6** and **7** with phenylphosphine and succinyl chloride at room temperature yields the diazaphos ligands *o*-Bpin DiazaPhos **8** and *m*-Bpin DiazaPhos **9**, respectively (Scheme 4.16). After stirring the reaction solution overnight, all phenylphosphine was fully converted into primarily one diastereomer (*rac* : *meso* = 95 : 5). The mesomeric isomer was removed by recrystallization with THF/ether at room temperature. ^1H , ^{31}P , ^{11}B and ^{13}C NMR spectroscopic characterizations were obtained. Compound **8** is structurally confirmed by X-ray crystallographic analysis (Figure 4.4). The ^1H NMR spectra display two signals for the inequivalent methine-protons in the phospholane ring with chemical shifts of 6.25 and 7.22 ppm for **8** and 6.54 and 5.78 ppm for **9**. One of the signals is a doublet, showing a significant coupling to the phosphorus atom (**8**: $^2J_{\text{H-P}} = 15.2$ Hz; **9**: $^2J_{\text{H-P}} = 18.5$ Hz). Interestingly, the methyl pinacolyl resonances are observed as four singlets around 1 ppm in the ^1H NMR spectrum. The chemical shift in the ^{31}P NMR spectra (**8**: $\delta = 19.2$ ppm; **9**: $\delta = 10.9$ ppm) are in agreement with other known monodiazaphospholane resonances.⁴⁰ The ^{11}B NMR resonances are in the typical region for boronates with chelating diol substituents.³⁹



Scheme 4.16. Synthesis of *o*- and *m*-Bpin DiazaPhos **8** and **9**.

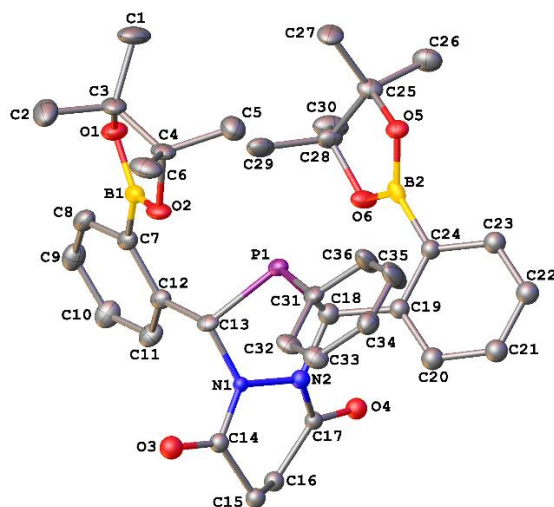
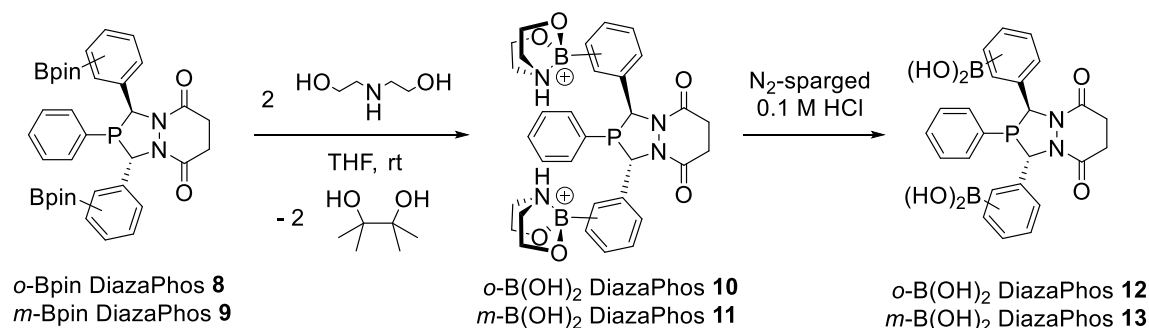


Figure 4.4. Crystal structure of *o*-Bpin DiazaPhos **8** shown with 50% probability ellipsoids. All H atoms, minor components of the disorder, and the DCM solvent molecule are omitted.

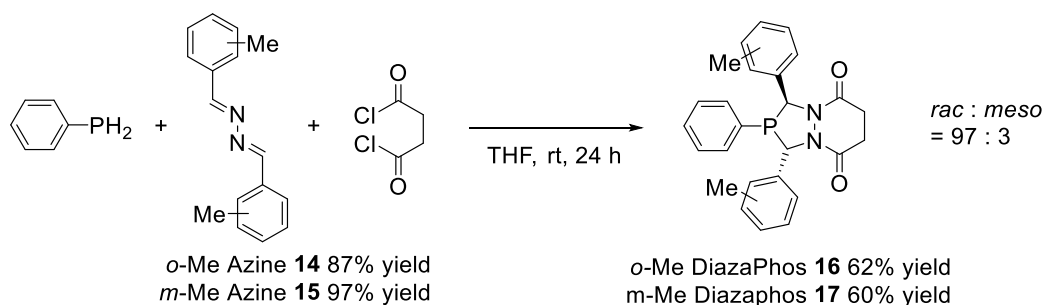
Pinacol is known to be a very stable boronic acid protecting group.⁴¹ Spontaneous exchange with water or alcohols is minimal. For the purposes of using the boronate diazaphospholane ligands in hydroformylation other more labile alkyl esters or boronic acid are necessary. For the Bpin transformation to its boronic acid, Santos' deprotection procedure was applied to *rac*-**5** and *rac*-**6**. Bpin Diazaphos **8** and **9** were treated with N₂-sparged diethanolamine for exchange with the pinacolyl group to yield the entropically driven four coordinate boron adducts Bdea DiazaPhos **10** and **11** (Scheme 4.17). The zwitterionic compounds were filtered off and rinsed with THF to fully wash out the residual pinacol and unreacted starting material.

The obtained ¹¹B NMR chemical shifts of 10.5 ppm for **10** and 10.1 ppm for **11** are in agreement with comparable known compounds from the literature.^{39,42} The colorless solid was suspended in N₂-sparged 0.1 M HCl to hydrolyze the borate to the boronic acid diazaphos **12** and **13** (Scheme 4.17), which were characterized by ¹H and ³¹P NMR spectroscopy. For each species, similar shifts for the phosphorus atoms are observed for all new compounds and all ²J_{P-H} coupling constants are found to be of the typical size as in other *racemic* monodiazaphospholane ligands.³⁸



Scheme 4.17. Deprotection of the pinacol group with diethanolamine followed by hydrolysis.

The goal is to utilize those novel boronic acid diazaphospholanes in rhodium-catalyzed hydroformylation. To evaluate if ligands **12** and **13** act as scaffolding ligands with a directing effect, catalysis must be compared to control ligands. *Ortho*- and *meta*-methyl diazaphospholane ligands have been synthesized (Scheme 4.18). The methyl groups act as a substituent that is sterically comparable to the boronic acid group, but are incapable of coordinating any alcohol containing alkene substrates. As in the boronate diazaphospholane synthesis, reaction of phenylphosphine, the according Me azine **14** or **15** and succinyl chloride affords primarily the racemic diazaphospholane isomers **16** and **17** (Scheme 4.18). The methine protons in the diazaphospholane ring are inequivalent and are observed as two signals in the ^1H NMR spectrum, one as a doublet with a coupling constant $^2J_{\text{H-P}}$ of 19.2 Hz, the other as a broad singlet. Two different signals for inequivalent methyl resonances are present as well. The structure of **17** was confirmed with X-ray crystallography (Figure 4.5).



Scheme 4.18. Synthesis of the control ligands Me DiazaPhos **16** and **17**.

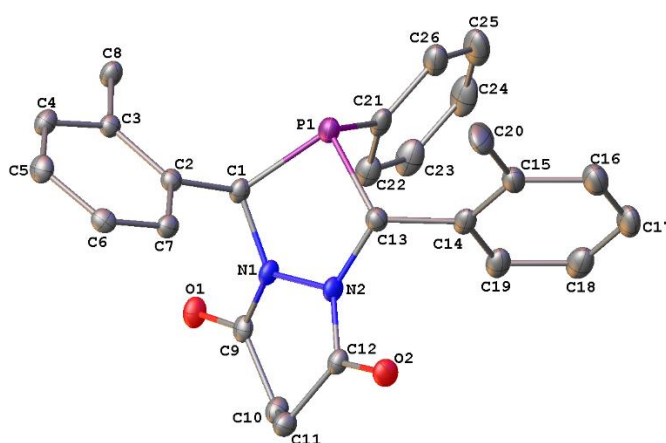


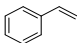
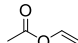
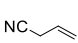
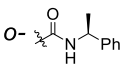
Figure 4.5. Crystal structure of *o*-Me DiazaPhos **16** shown with 50% thermal probability ellipsoids. All H atoms and minor disordered components are omitted for clarity.

4.2.3 Rhodium-Catalyzed Hydroformylation of Hydroxy Containing Alkenes

With the desired boronic acid containing diazaphospholane ligands in hand, hydroformylation reactions were performed. Initially, the bench mark substrates styrene, vinyl acetate and allyl cyanide were tested to ensure that the ligands show reactivity comparable to other known monodiazaphospholanes (Table 4.2). Indeed, the borononate ligands behave similar to other know monodiazaphospholanes in regards to their regioselectivity. The *m*-B(OH)₂ ligand **13** shows lower conversions compared to all other ligands. This observation can stem from impurities in the

ligand sample not visible by NMR spectroscopy. One possibility is the presence of HCl, since aq. HCl is used in the synthesis as the hydrolysis step to yield the B(OH)₂-group.

Table 4.2. Hydroformylation of Benchmark Substrates with Ligands **12**, **13**, **16** and **17**.^a

	$ \begin{array}{c} \text{R-CH=CH}_2 \xrightarrow[\text{THF, 60 } ^\circ\text{C, 20 h}]{\begin{array}{c} 0.020 \text{ mol\% [Rh(acac)(CO)}_2\text{]} \\ 0.042 \text{ mol\% Ligand} \end{array}} \begin{array}{c} \text{O} \\ \parallel \\ \text{R-CH-CH}_2\text{-CH}_2\text{-CHO} \\ \text{b} \end{array} + \begin{array}{c} \text{O} \\ \parallel \\ \text{R-CH}_2\text{-CH}_2\text{-CH}_2\text{-CHO} \\ \text{l} \end{array} \end{array} $					
Ligand						
	conv (%)	b : l	conv (%)	b : l	conv (%)	b : l
<i>o</i> -B(OH) ₂	96	3.1 : 1	87	36 : 1	99	1.2 : 1
<i>o</i> -Me	83	4.7 : 1	53	50 : 1	90	1.1 : 1
<i>m</i> -B(OH) ₂	34	2.7 : 1	23	40 : 1	68	1 : 1
<i>m</i> -Me	99	3.8 : 1	98	31 : 1	>99	1.2 : 1
	^b 28	1.1 : 1	31	39 : 1	93	1.3 : 1

^a conditions: total Rh : substrate = 1 : 5000; 2.5 M in substrate, conversions and b : l ratios were determined with ¹H NMR spectroscopy; ^b conditions: 80 °C in toluene, 3 h reaction time.⁴³

Hydroformylation of the allylic alcohols allyl alcohol and crotyl alcohol, as well as the homoallylic alcohol *trans*-3-hexen-1-ol has been investigated using the boronate ligands **12** and **13** and their control ligands **16** and **17** (Table 4.3). Unfortunately, no significant difference in the regioselectivities between the scaffolding ligands and their control ligands is observable, meaning that a directed, intramolecular reaction is not taking place under the conditions listed. Increasing

the alkene starting concentration to 4.2 M, as well as increasing the ligand loading to 10.5 equiv. has no effect on the regioselectivities.

Table 4.3. Hydroformylation of Allylic and Homoallylic Alcohols with Ligands **12**, **13**, **16** and **17**.^a

Ligand	HO-CH ₂ -CH=CH ₂		HO-CH ₂ -CH ₂ -CH=CH ₂		HO-CH ₂ -CH ₂ -CH ₂ -CH=CH ₂	
	conv (%)	α : β : i	conv (%)	α : β : i	conv (%)	α : β
<i>o</i> -B(OH) ₂	> 99	45:52:3	94	17:81:2 ^b	99	57 : 43
<i>o</i> -Me	> 99	42:53:5	91	11:88:1 ^b	94	52 : 48
<i>m</i> -B(OH) ₂	---	---	65	12:87:1 ^c	---	---
<i>m</i> -Me	---	---	76	14:84:2 ^c	---	---
<i>S,S,S</i> BDP ^d	99	25 : 75	---	---	---	---

^a conditions: [alkene] = 2.5 M, conversions and regioisomer ratios were determined by ¹H NMR spectroscopy. ^bhydroformylation of crotyl alcohol has also been performed at 4.2 M, comparable regioselectivities have been observed. ^c hydroformylation using 10.5 equiv. of ligand show no improvement in regioselectivities.

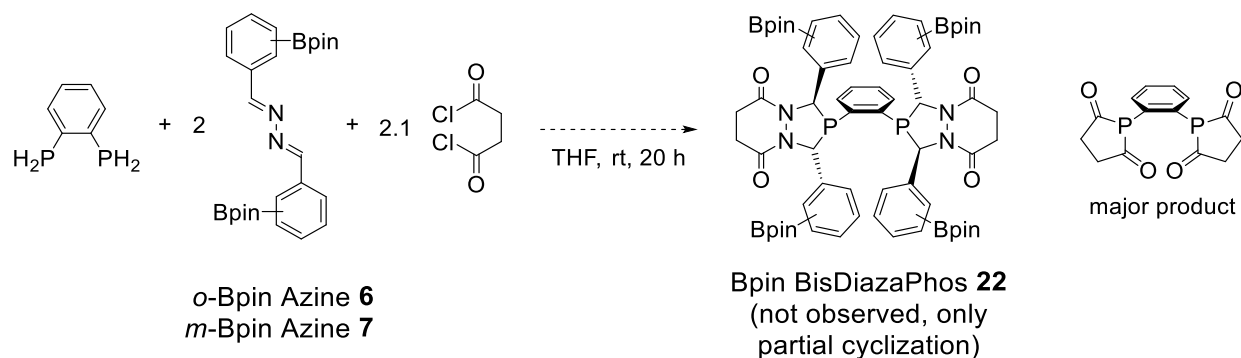
The following hypotheses could be responsible for the lack of non-directed hydroformylation:

- 1) transesterification of the allyl alcohol on the boronic acid occurs on a slower timescale than hydroformylation turnover. Estimating that alcohol exchange is typically on the order of seconds, turnover observed under these reaction conditions are on the order of 1 turnover in approximately

3 minutes. It is assumed that more transesterification events happened before a turnover of the alkene happens. Experiments such as exchange spectroscopy studies (EXSY) are necessary, to ensure that transesterification is fast enough with these ligand structures. However, experimental data on the alcohol exchange rates with these ligands has not been collected yet. 2) the distance between the alkene functional group and the P-atom is too far or too close to form an ideal cyclic intermediate for an intramolecular reaction. Varying the tether length of the alcohol substrate and testing ligands with *ortho*- and *meta*-boronic acid substitution had no significantly outcome on regioselectivity. 3) monophosphines typically form more labile and less well-defined Rh-catalyst complexes throughout catalysis than bisphosphines do. To be able to study a well-defined catalyst species and further apply the procedures optimized for the boronate diazaphospholane ligand, synthesis of boronate bearing bisdiazaphospholane was investigated first. In addition, bisdiazaphospholane are known for greater branched to linear selectivities than their corresponding monodiazaphospholanes.⁴⁴

4.2.4 Investigations on the Synthesis of Boronate-Bisdiazaphospholanes

When reacting 1,2-bisphosphinobenzene with two equivalents each of Bpin azines **6** or **7** and succinyl chloride, the formation of the diazaphospholane framework is not observed. Instead, the direct cyclization of 1,2-bisphosphinobenzene with succinyl chloride occurs as the competitive reaction to give the acyl phospholane in Scheme 4.19, as was seen in previous reactions with sterically bulky azines (e.g. *i*-propyl azine).⁴⁵ To avoid this cyclization reaction, our group reported a 2-step-synthesis for sterically bulky diazaphos ligands. The initial step includes the addition of dry HCl to a mixture of a primary phosphine and an azine. The resulting product is reacted further with the acid chloride derivative to obtain the full diazaphos framework.³⁸



Scheme 4.19. Direct reaction of 1,2-bisphosphinobenzene and succinyl chloride to an acyl phospholane when using sterically demanding Bpin Azines **6** and **7** rather than bisdiazaphospholane formation **18**.

When reacting *m*-Bpin azine **7** and 1,2-bisphosphinobenzene and dry HCl (1 M in diethylether) at room temperature, only partial Mannich-reaction was initially obtained. Clearly, this reaction occurs only slowly. After heating the reaction for several hours in refluxing THF, a greater amount of signals in the ^{31}P NMR spectrum with chemical shifts between 20 and -10 ppm started to appear, indicating some diazaphospholanes framework formation, along with signals around -40 to -50 ppm, representative for a secondary phosphine. The reduction of the solution volume led to the formation of a white solid, comprising a mixture of isomers with both tertiary and secondary phosphines that we have been unable to separated or identify. Even less successful was the reaction between *o*-Bpin azine **6**, 1,2-bisphosphinobenzene and dry HCl in ether, which led to only trace amount formation of the diazaphospholane framework. At this point, the -Bpin substituent is found to be sterically too demanding.

Despite the poor solubility of *m*-B(OH) $_2$ azine **3**, reaction with 1,2-bisphosphinobenzene and succinyl chloride was tested. Formation of the desired bisdiazaphospholanes is observed only to a small amount, starting materials are still present to a major amount. Four major regioisomers were formed, with 80% of the products having a racemic configuration in the diazaphospholane ring. The racemic isomers are a 1 : 1 mixture having equivalent P-atoms based on the ^{31}P NMR

signals, suggesting that one isomer has C_2 - and other C_s -symmetry (Figure 4.6). Attempts to separate the different isomers were unsuccessful.

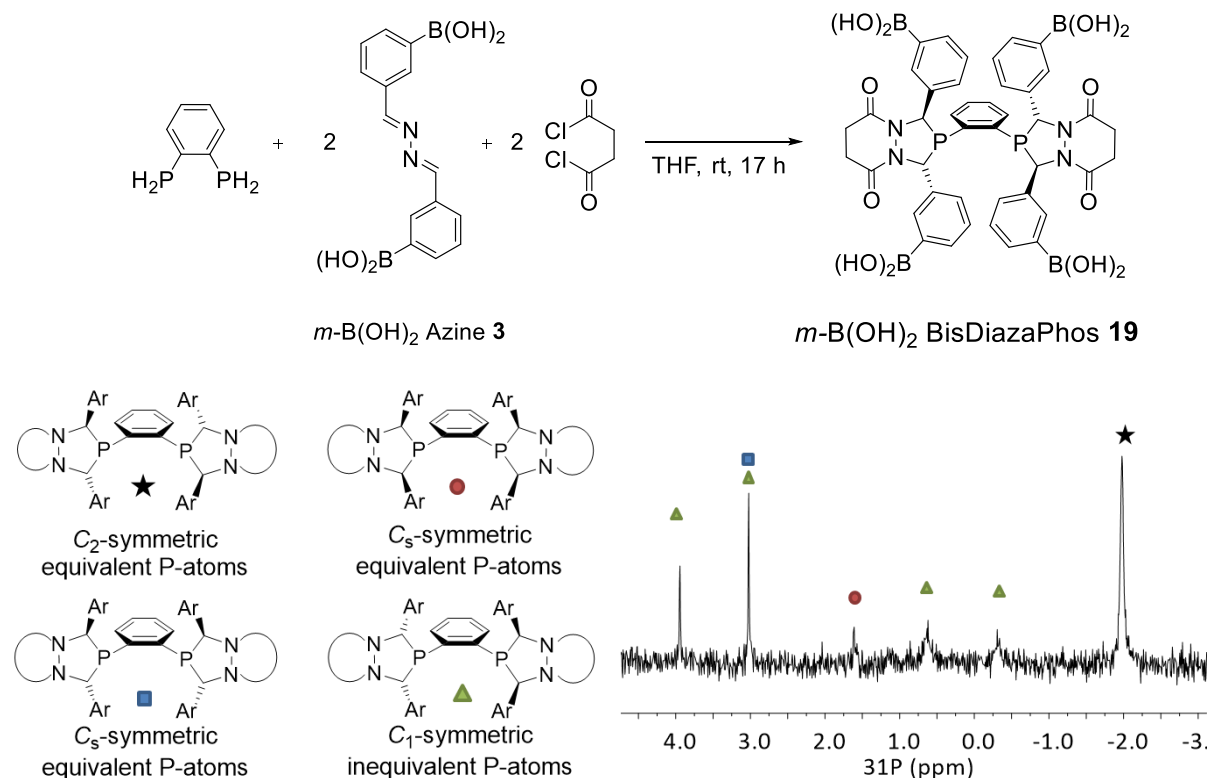
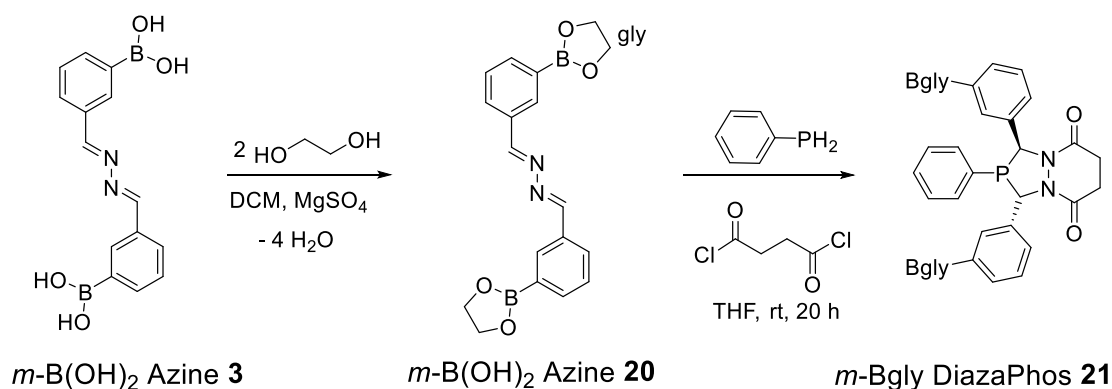


Figure 4.6. Reaction of 1,2-bisphosphinobenzene, **3** and succinyl chloride leading to a *m*-B(OH)₂ BisDiazaPhos isomer mixture in a 8 : 1 : 1 : 8 ratio and challenging to separate.

To overcome the separation problem, a potential approach would be to protect the boronic acid with a chelating diol. This attempt would make the compounds more soluble and allow for separation *via* column chromatography. However, the diol must be stable toward hydrolysis. A weak diol can be opened and even displaced partially in the presence of water, back to the boronic acid. In addition, it has to be considered that a choice of a very stable diol like pinacol should be avoided, since those groups will require additional steps in installing and removing the diol.

To help with solubility and full conversion of the azine starting material *m*-B(OH)₂ azine **3** (*vide supra*), azine **3** was protected with ethylene glycol to yield azine *m*-Bgly azine **20** (Scheme 4.20). Azine **20** was initially tested in the diazaphospholane framework formation with monophenylphosphine, which is indeed leading to *m*-Bgly DiazaPhos **21** (Scheme 4.20). It has also been shown that the glycol group can be cleaved either with acetone or acidic water to yield the boronic acid **13**, providing a faster and more efficient way to a boronic acid diazaphospholane compared to the two-step deprotection route starting with the pinacolyl boronate ligand **9** (Scheme 4.17, *vide supra*).



Scheme 4.20. Route to the ethylene glycol protected azine **20** and subsequent reaction with phenylphosphine and succinyl chloride to give ligand **21**.

The azine *m*-Bgly BisDiazaPhos **20** was also reacted with 1,2-bisphosphinobenzene and succinyl chloride (Figure 4.7). This reaction leads to two major *m*-Bgly BisDiazaPhos **22** isomers, C₂- and C_S-symmetric *racemic* diastereomers, suggested by the splitting pattern of the methine phospholane protons. These protons are inequivalent, leading to two signals in the ¹H NMR spectrum. Those signals are displayed as virtual triplet and as a broad singlet. Since the signals in the ³¹P NMR are singlets, only possible when the P-atoms are equivalent, the ligands have to be C₂- and C_S-symmetric. Even though only two isomers formed, their separation and purification

was found to still be challenging due to the labile ethylene glycol diol group. Handling this compound mixture slowly gave rise to a complicated mixture indicating the deprotection of boronate glycol-group.

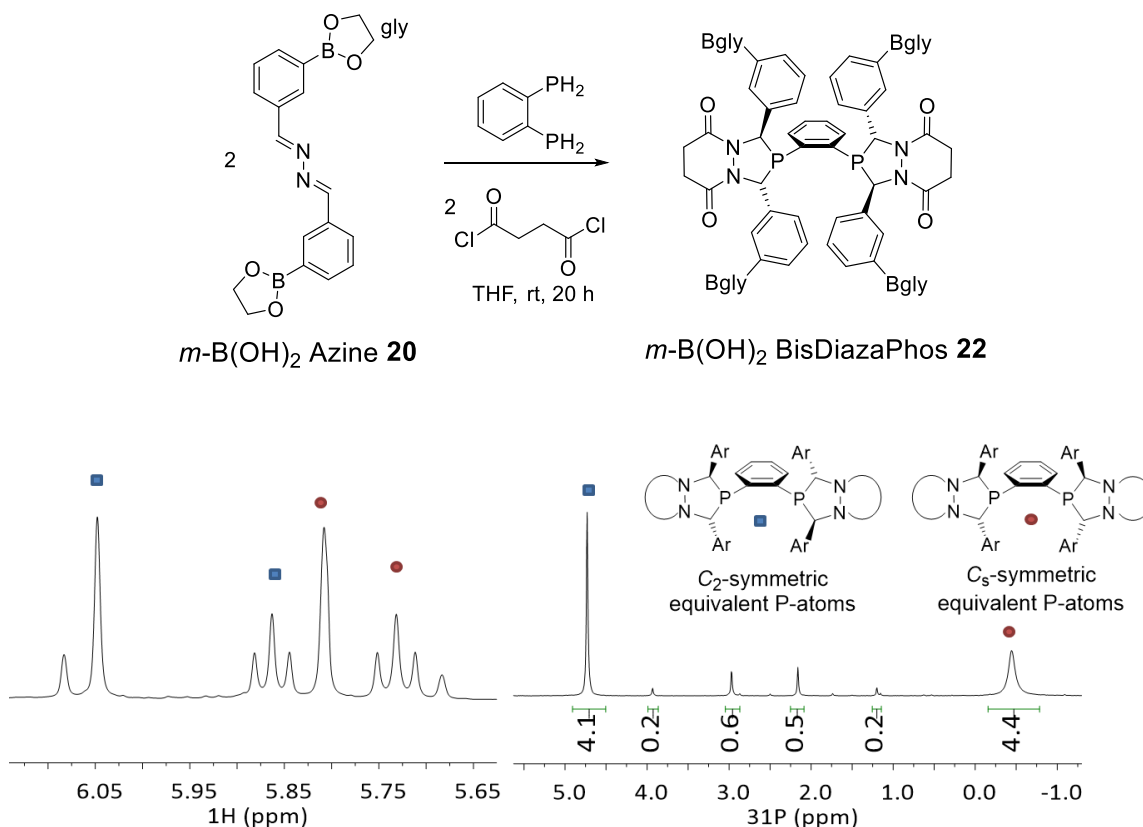
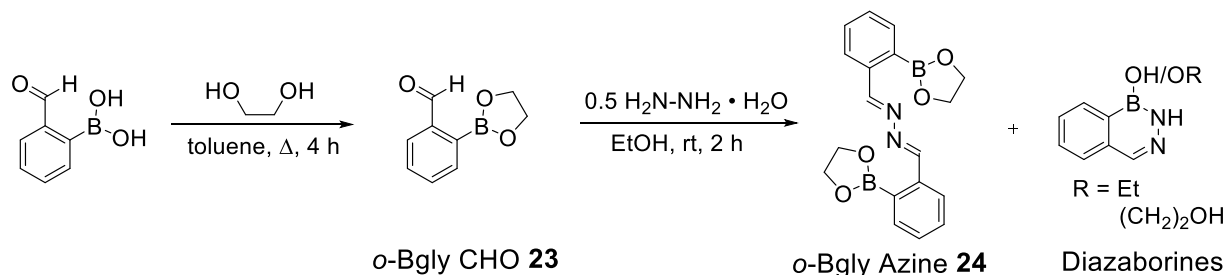


Figure 4.7. Synthesis of *m*-Bgly BisDiazPhos **22** (top) and the ¹H and ³¹P NMR spectra showing the *racemic* conformation in the diazaphospholane rings suggested by the splitting pattern.

With the potential to access the *ortho*-substituted boronate bisdiazaphospholane by using the smaller glycol protecting group, 2-formylphenylboronic acid was treated with ethylene glycol to obtain the aldehyde **23**. Reaction with hydrazine, however, gives a mixture of products and remaining starting material. The lability of the glycol group leads to exchange with the reaction solvent EtOH, leading to a variety of ethoxy glycolyl boronate and the isolation of the desired

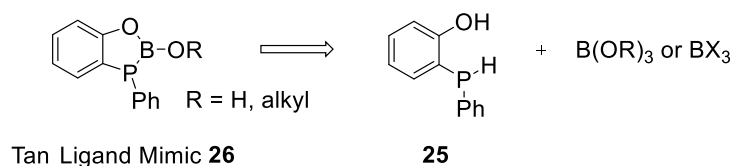
azine very challenging. Furthermore, this property of being a labile diol also leads to intramolecular cyclization benzodiazaborine products (Scheme 4.21).



Scheme 4.21. Unselective reaction of glycol ester **23** and hydrazine to form some azine **24** and majorly diazaborine side products.

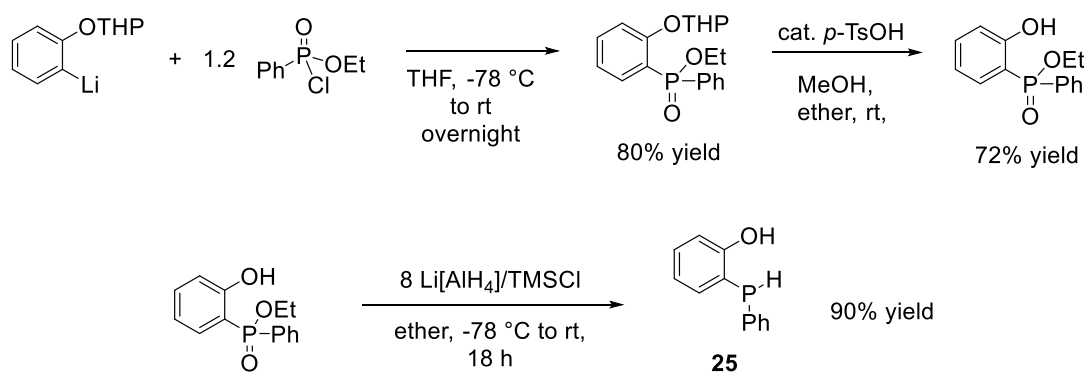
4.2.5 Attempts on the Synthesis of a Boronate-Containing Mimic of the Tan Ligand.

We sought to investigate the synthesis of a mimic to the Tan Ligand that would contain a boronate moiety (Scheme 4.22). Tan's studies on the hydroformylation of a variety of allylic and homoallylic alcohol substrates revealed that the distance between the alkene double bond and the P-atom in the cyclic aminal-phosphine Tan Ligand is ideal to form an intramolecular intermediate allowing for selective and directed aldehyde product formation (*vide supra*). Incorporation of a boronate group would avoid the use of any additives to facilitate a reversible exchange of alcohol groups. We sought to investigate the synthetic route towards the mimic of the Tan Ligand **26** by reacting the secondary 2-hydroxyphenylphosphine **25** and a boron reagent (Scheme 4.22).



Scheme 4.22. Potential route for the synthesis to the boronate mimic of the Tan Ligand.

Hydroxy phosphine **25** has been previously used in the synthesis towards a mixed diazaphospholane-phosphite ligand.⁴⁶ To obtain the hydroxy containing secondary phosphine, tetrahydropyran protected phenol was used as the precursor. Those structures are known to direct towards an *ortho*-lithiation product, which can further be reacted with a phosphonite chloride. Next, the THP-group is deprotected in the *ortho*-phosphorylated product to recover the hydroxyl group. Reduction of the hydroxy phosphonite with a LiAlH₄/TMSCl mixture yields the secondary (hydroxyphenyl)phenylphosphine (Scheme 4.23).



Scheme 4.23. Synthesis towards the secondary (hydroxyphenyl)phenyl phosphine as the potential precursor to the boronated Tan Ligand mimic.

The following synthesis attempts have been tested to install the boronate group and create a phosphorus-boron bond. Reaction of the secondary phosphine with B(OMe)₃ in the presence of NaH leads to a new phosphorus signal at -56 ppm in the ³¹P NMR spectrum (Figure 4.8). This signal however, is still a doublet with a ¹J_{P-H} coupling constant of 225 Hz, indicating that the P-H bond is still intact. It is assumed that the boronate group reacted with the phenoxy group, suggested by the shoulder next to the B(OMe)₃ signal in the ¹¹B NMR spectrum (Figure 4.8).

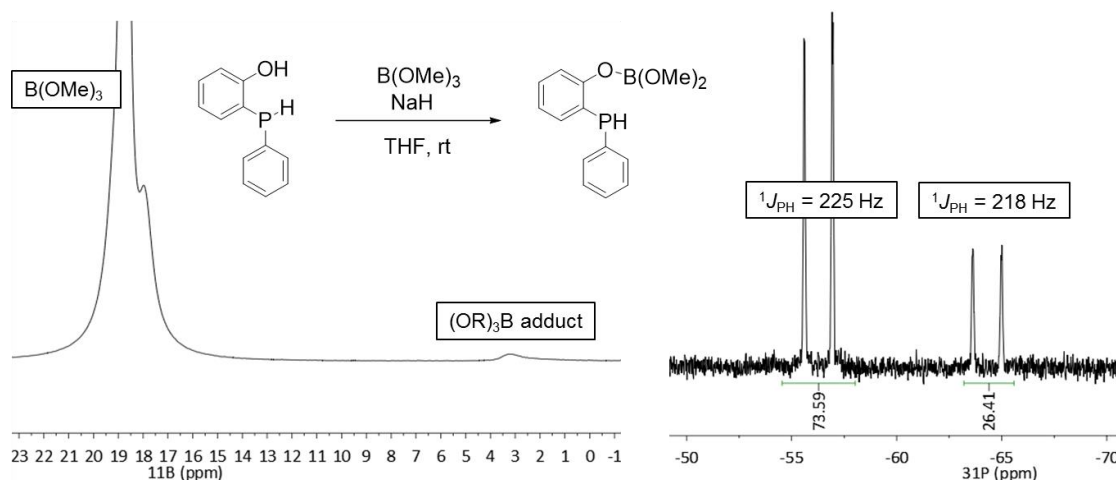


Figure 4.8. ^{11}B (left) and ^{31}P NMR(right) spectra of the reaction of **25** with B(OMe)_3 and NaH .

More promising results were observed when BCl_3 was reacted with the hydroxy phosphine in the presence of NEt_3 (Figure 4.9). The ^{31}P NMR spectrum has a new signal around -60 ppm of a species that does not contain a P–H bond, suggesting that a P–B bond was formed. Signals in the ^{11}B NMR spectrum at around 20 and 1 ppm are observed, where 20 ppm could be interpreted as the desired P–B product. However, non-cyclic P–B-compounds typically display a coupling constant of the size of 100 Hz between the P- and the B-atom.⁴⁷ This missing observed coupling constant of the compounds at -60 ppm in the ^{31}P NMR spectrum raises some doubts about the nature of the synthesized major species. A borane-amine adduct might be the compound assigned to the signal at 1 ppm, a typical chemical shift for four-coordinate boron-species.

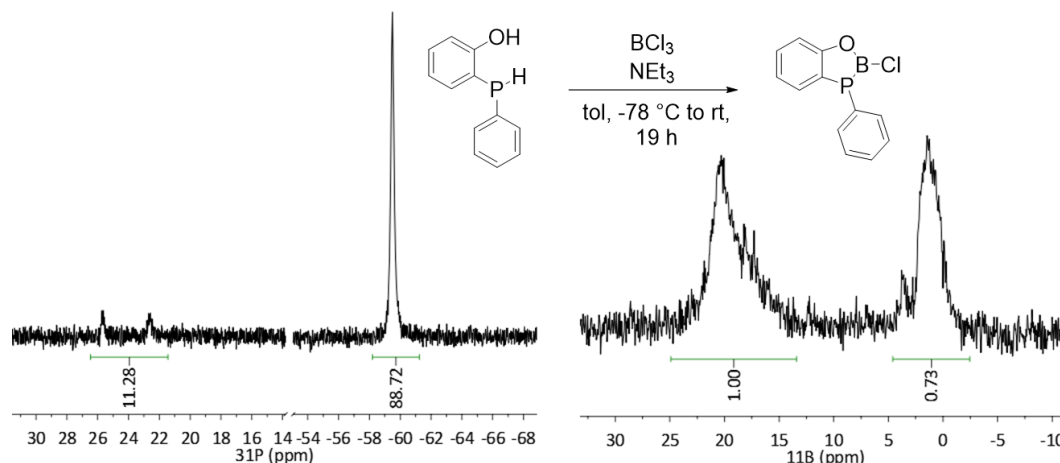
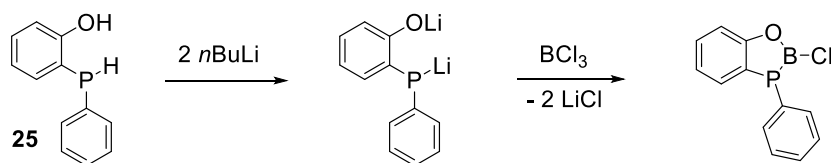


Figure 4.9. Reaction of hydroxy phosphine **25** with BCl_3 and NEt_3 .

Another generally used method to create P–B bond, is the transmetalation between a lithium phosphide and a boron halide.⁴⁷ This transformation has not been investigated to this point and would be the next logical step to pursue to investigate the Tan Ligand mimic (Scheme 4.24).



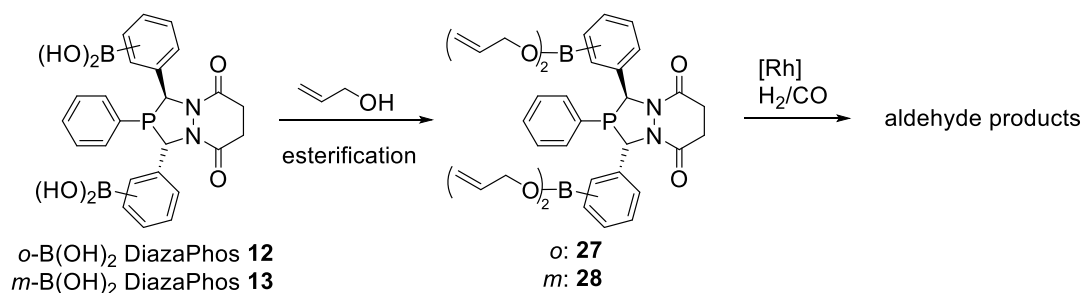
Scheme 4.24. Proposed future work on the boronate containing Tan Ligand mimic.

4.3 Conclusion and Outlook

The incorporation of boronate substituents into diazaphospholane ligands has been investigated for the use as scaffolding ligands, in which the boronate moieties are thought to act as directing groups for allylic alcohol in selective Rh-catalyzed hydroformylation. Both *ortho*- and *meta*-phenyl boronic acid bearing diazaphospholane ligands have been tested in the hydroformylation of allyl alcohol, crotyl alcohol and 3-hexen-1-ol. The outcome has been compared to methyl substituted control ligands. Unfortunately, a directed hydroformylation has

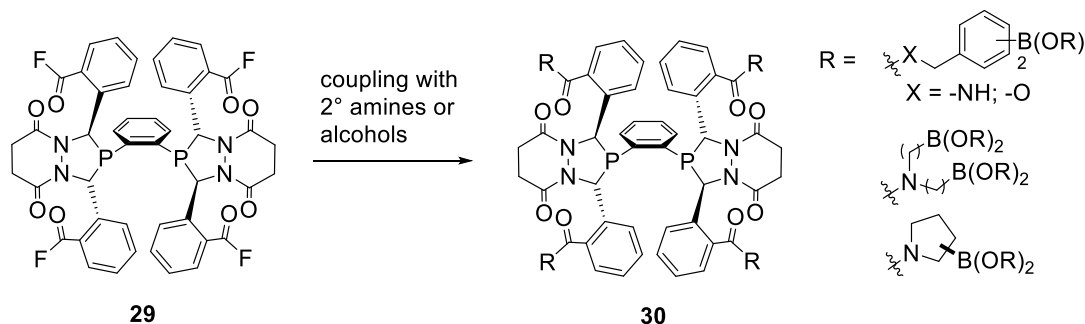
not been observed under the tested hydroformylation conditions. To obtain more insights and form a well-defined catalyst-species that can be studied through potentially stoichiometric hydroformylation reactions, the synthesis of bisdiazaphospholanes has been investigated. However, we ran into the challenge of the isolation and purification of the bisdiazaphospholanes and, thus, hydroformylation of allylic alcohols with boronate bisdiazaphospholanes has not been explored yet. The following strategies are proposed to gain more insights and potentially improve upon directed hydroformylation:

The distance between the alkene and the P-atom is an important feature to assure a directed intramolecular reaction. It is not clear to this extent if the distance between the P-atom and the alkene group is ideal to lead to intramolecular hydroformylations. This issue can be likely evaluated by studying the boronate-alkene ligands **27** and **28** synthesized from boronic acid ligand **12** and **13** (Scheme 4.25). Exposing **27** and **28** to hydroformylation reaction conditions will give insights to whether hydroformylation the potential preference to one aldehyde product can occur. Another necessary study with these structure is the actual exchange rate of the boronic acid group in **12** and **13** with allylic alcohols and the allyloxy group in **27** and **28** with another substrate. It has not been investigated yet, if exchange occurs fast enough on the hydroformylation time scale.



Scheme 4.25. Esterification of the boronic acid with homoallylic alcohol followed by HF.

Challenges in the synthesis and purification of the boronate bisdiazaphospholanes discussed above have been encountered. One way to overcome issues of separating multiple isomers would be to start with only one ligand isomer. Tyler Adint has previously shown that a library of tetraamide ligand can be accessed by a coupling procedure of tetraacyl fluoride **29** with a variety of amines.⁴⁸ This approach is a promising way of incorporating boron-containing amines or alcohols into a diazaphos ligands like structure **30** and brings the following advantages: first, distances between the phosphorus and boron atom can be easily varied by using the appropriate amine or alcohol reagent; second, installation of multiple boronate groups can lead to increased substrate binding sites and faster reaction rates while decreased product inhibition; lastly, the installation of a chiral boronate bearing substituent is possible through this synthetic route (Scheme 4.26).



Scheme 4.26. Synthesis towards other boronate containing bisdiazaphospholanes.

Another way to investigate which type of ligand structure is suitable for scaffolding catalysis, moving away from diazaphospholane based ligands, is to synthesize a series of boronate phosphine with varying distances between the phosphorus and boron-atom (Figure 4.10). In particular, structure **31** is of interest, since it represents a mimic of the Tan ligand **L**. The Tan ligand structure is already known to allow for a directing effect in hydroformylation. The same is true for structure **33**, which is a mimic to *o*-(diphenyl)phosphino benzoate discussed in

Chapter 4.1.1. It would be of great interest to investigate if the boronate moiety will contribute differently and which effect the known facile transesterification property would provide.

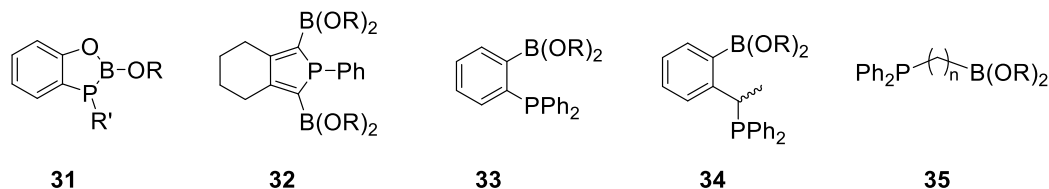
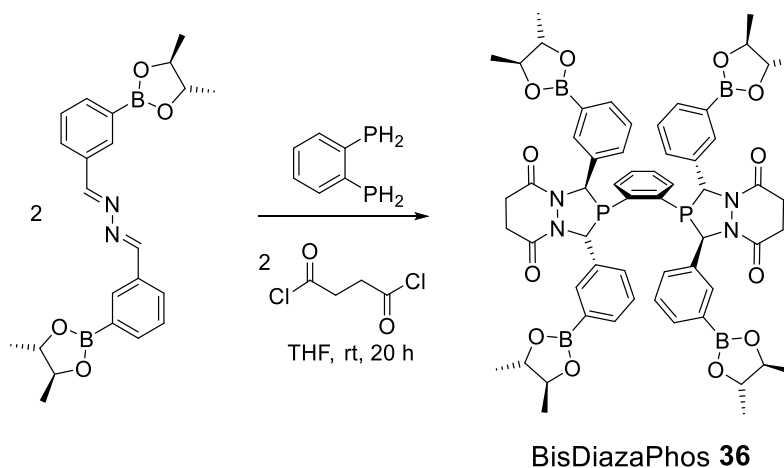


Figure 4.10. Boronate Phosphine Series with varying distance between the P- and B-atom.

On another note, now that the synthesis of boronate bisdiazaphospholane has been explored, the boronate group can be derivatized with a chiral diol, allowing for formation of diastereomers of the diazaphospholane ligand and the potential separation. For example, (2*S*,3*S*)-butanediol could be reacted with the boronic acid azine **3**, which can be subsequently reacted with bisphosphinobenzene and succinyl chloride to ligand **36** (Scheme 4.27).



Scheme 4.27. Potential separation of diastereomers through use of a chiral boronate group.

4.1 Experimental Methods

General Considerations

If not noted differently, all air- and moisture-sensitive reactions were carried out under an N₂ atmosphere using standard Schlenk line techniques or a circulating N₂-filled glovebox. All glassware was oven dried, set under vacuum while hot and cooled to room temperature under vacuum. Work ups and recrystallization were performed using standard Schlenk line techniques. 2-Formylphenylboronic acid and 3-formylphenylboronic acid were purchased from Sigma-Aldrich and Alfa Aesar, respectively, and used as obtained. Succinyl chloride was distilled and degassed under vacuum to remove all volatile impurities before use and stored under an N₂ atmosphere. Primary phosphines were purchased from Strem and stored in an N₂-filled glovebox. THF, diethyl ether, toluene and hexanes were distilled from sodium/benzophenone; CDCl₃ was purchased from Sigma-Aldrich, distilled from CaH₂, freeze-pump-thawed to remove oxygen and stored over 3 Å molecular sieves in an air-tight bomb flask. Other liquid commodity chemicals were degassed by sparging with N₂ prior to usage and solid chemicals were dried overnight under vacuum at room temperature.

Routine NMR-spectroscopical measurements (¹H, ¹³C, ³¹P and ¹¹B) were carried out in perdeuterated solvents on Bruker Avance III-400 and Avance III-500 spectrometers. The chemical shifts δ are reported in ppm, coupling constants *J* in Hz. Splitting patterns were assigned as singlet (s), doublet (d), triplet (t), virtual triplet (vt), quartet (q), multiplet (m), broad (br) and not observed (n.o.). If not noted additionally, further assignments were done using the correlation experiments ¹H-¹H-COSY, HSQC and HMBC experiments. ¹H and ¹³C NMR spectra were referenced internally to tetramethylsilane (0.00 ppm) or to the residual proton signals of the deuterated solvents ($\delta(^1\text{H})$; (¹³C) = 7.26; 77.16 ppm (CDCl₃); 2.50, 39.52 ppm (DMSO-*d*₆), 4.87, 49.00 ppm (CD₃OD)). ³¹P and ¹¹B NMR spectra were referenced to an external standard of 85% phosphoric acid (H₃PO₄) and bortriflouride-diethyletherate (BF₃·OEt₂), respectively. Mass spectra were recorded on a

Waters (Micromass) LCT® for electrospray ionization (ESI) experiments with a sample cone voltage of 20. Crystallographic data was obtained with Bruker Smart Quazar with an APEX2 detector and a Mo-microsource.

Azine and Diazaphospholane Syntheses

Formylphenylboronic acid pinacolyl ester (4) and (5) (after a modified version of the literature procedure^{36,37}). In a 100 mL round bottom flask, formylphenyl boronic acid (1.244 g, 8.285 mmol, 1.0 equiv) was dissolved in DCM (30 mL) and pinacol (1.176 g, 9.954 mmol, 1.2 equiv) was added. The clear solution was stirred at room temperature for 2.5 h. To the slightly cloudy and colorless solution H₂O (10 mL) was added and the phase were separated. The organic phase was further washed with brine solution (2 x 5 mL), the aqueous phase was washed with DCM (2 x 5 mL). The organic phases were combined and dried over MgSO₄. The solvent was removed using a rotary evaporator to obtain the product as a thick, colorless oil (1.829 g, 95.0% yield). Spectral data agree with the reported values.^{36,37}

o-Formylphenylboronic acid glycolyl ester (**23**). (after a modified version of the literature procedure³⁷) A suspension of 2-formylphenyl boronic acid (504.6 mg, 3.370 mmol, 1.0 equiv) ethylene glycol (188 μ L, 3.370 mmol, 1.0 equiv) in toluene (30 mL) was refluxed in a Dean-Stark-Apparatus for 4 h. The clear solution was filtered through a MgSO₄ plug and the solvent was removed *in vacuo* to yield the product as a colorless oil (589 mg, 99.0% yield).

¹H NMR (400 MHz, CDCl₃): δ 10.49 (s, 1H, CHO), 7.96 (dd, J = 7.3, 1.8 Hz, 1H, H^{Ar}), 7.87 (dd, J = 6.9, 2.1 Hz, 1H, H^{Ar}), 7.65–7.55 (m, 2H, H^{Ar}), 4.45 (s, 4H, CH₃CH₂); **¹¹B NMR** (128 MHz, CDCl₃): δ 31.8 (br, $h_{1/2}$ = 151 Hz).

General Synthesis of Azines 3, 6, 7, 14, 15 and 20.

In a 50 mL round bottom flask, the corresponding aldehyde (0.504 mg, 3.36 mmol, 2.0 equiv) was dissolved in EtOH (13 mL) and hydrazine monohydrate (81.5 μ L, 1.720 mmol, 1.02 equiv) was added dropwise. Immediately, the solution turned yellow. The reaction mixture was stirred for 2 h. A light yellow precipitate formed over time. The mixture was cooled with an ice bath for 30 min. The precipitate was filtered off, the residue was washed with cold EtOH (2 x 1.5 mL) and dried *in vacuo*. A second crop of product was collected by reducing the volume of the filtrate, cooling the solution in the fridge overnight and collecting the formed yellow solid.

o-B(OH)₂ Azine (**1**). only partial formation of the desired azine, major product is 1,2-dihydro-1-hydroxy-2,3-benzodiaza-1-borine

m-B(OH)₂ Azine (**3**). Reaction has to be performed in a concentration greater than 60 mg/mL in the 3-formylphenyl boronic acid, 79% yield; ¹H NMR (400 MHz, DMSO-*d*₆): δ 8.72 (s, 2H, NCHAr), 8.30 (s, 2H, H^{Ar}), 8.23 (s, 4H, B(OH)₂), 7.92 (t, *J* = 6.2 Hz, 4H, H^{Ar}), 7.49 (t, *J* = 7.5 Hz, 2H, H^{Ar}); ¹¹B NMR (128 MHz, DMSO-*d*₆): δ 28.4 (br, *h*_{1/2} = 324 Hz); ¹³C{¹H} NMR (100 MHz, DMSO-*d*₆): δ 161.7, 137.0, 135.0 (br, BC^{ipso}), 134.2, 132.9, 130.1, 128.0.

o-Bpin Azine (**6**). 77% yield; ¹H NMR (400 MHz, CDCl₃): δ 9.29 (s, 2H, NCH), 8.27 (d, *J* = 7.6 Hz, 2H, H^{Ar}), 7.88 (dd, *J* = 7.3 Hz, *J* = 1.0 Hz, 2H, H^{Ar}), 7.52 (td, *J* = 7.5 Hz, *J* = 1.1 Hz, 2H, H^{Ar}), 7.44 (td, *J* = 7.4 Hz, *J* = 1.2 Hz, 2H, H^{Ar}), 1.38 (s, 24H, CH₃); ¹¹B NMR (128 MHz, CDCl₃): δ 31.3 (br, *h*_{1/2} = 410 Hz); ¹³C{¹H} NMR (100 MHz, CDCl₃): δ = 25.1 (CH₃), 84.2(C(CH₃)₂), 126.8, 129.9, 132.0, 133.2, 136.1, 162.2 (NCH), n.o (BC^{ipso}).

m-Bpin Azine (**4**). (97% yield); $^1\text{H NMR}$ (400 MHz, CDCl_3): δ 8.68 (s, 2H, NCH), 8.22 (s, 2H, H^{Ar}), 8.00 (d, $J = 7.8$ Hz, 2H, H^{Ar}), 7.90 (d, $J = 7.3$ Hz, 2H, H^{Ar}), 7.46 (t, $J = 7.6$ Hz, 2H, H^{Ar}), 1.37 (s, 24H, CH_3); $^{11}\text{B NMR}$ (128 MHz, CDCl_3): δ 30.8 (br, $h_{1/2} = 502$ Hz).

m-Bgly Azine (**20**). *m*-B(OH)₂ azine **3** (0.505 mg, 1.705 mmol, 1.0 equiv) was suspended in DCM (25 mL). Ethylene glycol (190.2 mL, 3.401 mmol, 2.0 equiv) was added and the solution turns yellow overtime. The reaction mixture was stirred over MgSO_4 overnight. The MgSO_4 was filtered off, the solvent was removed to obtain the product as a yellow solid (569 mg, 96% yield).

$^1\text{H NMR}$ (400 MHz, CDCl_3): δ 8.68 (s, 2H, NCH), 8.23 (s, 2H, H^{Ar}), 8.02 (d, $J = 7.8$ Hz, 2H, H^{Ar}), 7.91 (d, $J = 7.3$ Hz, 2H, H^{Ar}), 7.48 (t, $J = 7.6$ Hz, 2H, H^{Ar}), 4.41 (s, 8H, CH_3CH_2); $^{11}\text{B NMR}$ (128 MHz, CDCl_3): δ 30.6 (br, $h_{1/2} = 563$ Hz).

o-Me Azine (**14**). Spectroscopic data agrees with the reported literature values.³⁸

m-Me Azine (**15**). Spectroscopic data agrees with the reported literature values.³⁸

General Synthesis of *ortho*- and *meta*-substituted Diazaphos **8**, **9**, **16**, **17** and **22**.

In a N_2 -filled glovebox, the azine (0.268 mg, 0.582 mmol, 1.0 equiv) was dissolved in THF (8 mL) and phenylphosphine (64 μL , 0.582 mmol, 1.0 equiv) was added *via* Hamilton® syringe. After stirring the yellow clear solution for 5–10 min, succinyl chloride (64 μL , 0.582 mmol, 1.0 equiv) was added dropwise *via* Hamilton® syringe. The yellow color starts fading within 5 – 10 min. The reaction solution was stirred for 24 h at room temperature. The reaction mixture appears clear to light yellow. The solvent was removed *in vacuo* yielding a crude, light yellow solid.

o-Bpin DiazaPhos (**8**). Full conversion to *rac* : *meso* = 95 : 5 mixture, the crude solid was recrystallized from THF/ether (1 : 2) at rt to obtain the product as a white solid in 89% yield.

¹H NMR (400 MHz, CDCl₃): δ 7.91 (d, *J* = 7.0 Hz, 1H, H^{Ar}), 7.71 (d, *J* = 7.7 Hz, 1H, H^{Ar}), 7.47 (t, *J* = 7.7 Hz, 1H, H^{Ar}), 7.30 (t, *J* = 7.5 Hz, 1H, H^{Ar}), 7.22 (d, ²*J*_{HP} = 2 Hz, 1H, P(CH)N), 7.20 (t, *J* = 7.5 Hz, 1H, H^{Ar}), 7.15–6.99 (m, 2H, H^{Ar}), 6.89 (t, *J* = 7.8 Hz, 1H, H^{Ar}), 6.78 (t, *J* = 7.2 Hz, 2H, H^{Ar}), 6.58 (d, ²*J*_{HP} = 15.2 Hz, 1H, P(CH)N), 6.26 (d, *J* = 8.0 Hz, 1H, H^{Ar}), 2.75–3.06 (m, 4H, (CH₂)₂), 1.13 (s, 24H, CH₃), 1.11 (s, 6H, CH₃), 1.04 (s, 6H, CH₃), 0.97 (s, 6H, CH₃); **³¹P{¹H} NMR** (162 MHz, CDCl₃): δ 19.2; **¹¹B NMR** (128 MHz, CDCl₃): δ 30.8 (br, *h*_{1/2} = 961 Hz); **¹³C{¹H} NMR** (100 MHz, CDCl₃): δ 168.9, 166.1, 144.7 (d, *J*_{CP} = 15.9 Hz), 140.1, 136.8, 135.6, 132.1 (d, *J*_{CP} = 17.7 Hz), 131.6 (m), 130.4, 127.9 (d, *J*_{CP} = 6.0 Hz), 126.6, 125.4, 124.4, 122.5, 84.0 ((CH₂)₂), 83.7, 60.24 (d, *J*_{CP} = 31.6 Hz), 56.6 (d, *J*_{CP} = 21.6 Hz), 31.4, 29.8, 25.2 (CH₃), 24.7, 24.3, 24.2; **HRMS** (ESI, *m/z*) [M+H]⁺ calcd. for C₃₆H₄₃B₂N₂O₆P: 651.3191, found: 651.3201 (Δ = 1.5 ppm).

m-Bpin DiazaPhos (**9**). Full conversion to *rac* : *meso* = 95 : 5 mixture, the crude solid was recrystallized from hot THF/hexane (1 : 4) to obtain the product as a white solid in 89% yield.

¹H NMR (400 MHz, CDCl₃): δ 7.82–7.73 (m, 2H, H^{Ar}), 7.48–7.35 (t, *J* = 7.5 Hz, 4H, H^{Ar}), 7.24 (t, *J* = 7.4 Hz, 1H, H^{Ar}), 7.13 (t, *J* = 7.2 Hz, 2H, H^{Ar}), 6.96 (m, 3H, H^{Ar}), 6.65 (d, *J* = 7.5 Hz, 1H, H^{Ar}), 6.54 (brs, 1H, P(CH)N), 5.78 (d, ²*J*_{HP} = 18.5 Hz, 1H, P(CH)N), 2.98–2.73 (m, 4H, (CH₂)₂), 1.34 (s, 12H, CH₃), 1.30 (s, 6H, CH₃), 1.29 (s, 6H, CH₃); **³¹P{¹H} NMR** (162 MHz, CDCl₃): δ 10.9; **¹¹B NMR** (128 MHz, CDCl₃): δ 30.3 (br, *h*_{1/2} = 856 Hz).

o-Me DiazaPhos (**16**). *rac* : *meso* = 97 : 3, contains around 5% of its phosphine oxide (**³¹P{¹H} NMR** (161.9 MHz, CDCl₃): δ = 45.6 ppm) X-ray quality crystals were grown from a THF/ether recrystallization, crystals obtain both **16** and its oxide in the lattice (62% yield). **¹H NMR** (400 MHz, CDCl₃): δ 7.30–7.21 (m, overlapped with CHCl₃ 2H, H^{Ar}), 7.14 (td, *J* = 7.9 Hz, *J* = 1.2 Hz, 2H,

H^{Ar}), 7.07–6.88 (m, 5H, H^{Ar}), 6.64 (t, $J = 7.6$ Hz, 1H, H^{Ar}), 6.53 (d, $^2J_{\text{HP}} = 2.0$ Hz, 1H, P(CH)N), 6.24 (d, $J = 7.7$ Hz, 1H, H^{Ar}), 5.90 (d, $^2J_{\text{HP}} = 17.5$ Hz, 1H, P(CH)N), 2.96–2.74 (m, 4H, (CH₂)₂), 2.44 (s, 3H, CH₃), 2.42 (brs, 3H, CH₃); **³¹P{¹H} NMR** (162 MHz, CDCl₃): δ -0.6.

m-Me Diazaphospholane (**17**). *rac* : *meso* = 97 : 3, recrystallized from THF/ether (60% yield)

¹H NMR (400 MHz, CDCl₃): δ 7.33–7.23 (m, 2H, H^{Ar}), 7.20–7.08 (m, 4H, H^{Ar}), 7.27–7.20 (m, overlapped with CHCl₃, 1H, H^{Ar}), 6.97 (td, $J = 7.8$ Hz, $J = 1.1$ Hz, 2H, H^{Ar}), 6.61 (t, $J = 7.7$ Hz, 1H, H^{Ar}), 6.83 (d, $^2J_{\text{HP}} = 7.6$ Hz, 1H, H^{Ar}), 6.53 (d, $^2J_{\text{HP}} = 7.7$ Hz, 1H, H^{Ar}), 6.46 (bs, 1H, P(CH)N), 5.76 (d, $^2J_{\text{HP}} = 19.2$ Hz, 1H, P(CH)N), 2.95–2.71 (m, 4H, (CH₂)₂), 2.38 (s, 3H, CH₃), 2.08 (brs, 3H, CH₃); **³¹P{¹H} NMR** (162 MHz, CDCl₃): δ 10.4; **HRMS** (ESI, *m/z*): [M+H]⁺ calcd. for C₂₆H₂₆N₂O₂P: 429.1727, found: 429.1727 ($\Delta = <1$ ppm).

m-Bgly Diazaphos (**22**). *rac* : *meso* = 98 : 2, used without further purification; **¹H NMR** (400 MHz, THF): δ 7.82 (s, 1H, H^{Ar}), 7.70 (d, $J = 7.0$ Hz, 1H, H^{Ar}), 7.50 (d, $J = 7.4$ Hz, 1H, H^{Ar}), 7.38 (d, $J = 7.4$ Hz, 2H, H^{Ar}), 7.32 (s, 1H, H^{Ar}), 7.18 (t, $J = 7.1$ Hz, 1H, H^{Ar}), 7.07 (t, $J = 7.0$ Hz, 2H, H^{Ar}), 6.98 (t, $J = 7.0$ Hz, 2H, H^{Ar}), 6.89 (t, $J = 7.7$ Hz, 1H, H^{Ar}), 6.72 (d, $J = 7.7$ Hz, 1H, H^{Ar}), 6.54 (brs, 1H, P(CH)N), 5.72 (d, $^2J_{\text{HP}} = 18.8$ Hz, 1H, P(CH)N), 4.25 (s, 4H, B(OCH₂)₂), 4.17 (s, 4H, B(OCH₂)₂), 2.92–2.71 (m, 2H, (CH₂)₂), 2.67–2.50 (m, 4H, CH₂)₂); **³¹P{¹H} NMR** (162 MHz, THF): δ 12.7; **¹¹B NMR** (128 MHz, THF): δ 31.5 (br, $h_{\frac{1}{2}} = 1529$ Hz). **¹³C{¹H} NMR** (100 MHz, THF): δ 167.4, 165.1, 137.6 (d, $J_{\text{CP}} = 15.9$ Hz), 134.3, 133.8, 132.7 (d, $J_{\text{CP}} = 19.5$ Hz), 132.6, 131.8 (m), 131.3, 131.1, 129.4, 128.6 (d, $J_{\text{CP}} = 8.1$ Hz), 128.3, 128.1 (m), 126.9, 66.0 (B(OCH₂)₂), 65.8 (B(OCH₂)₂), 61.5 (d, $J_{\text{CP}} = 33.3$ Hz), 57.2 (d, $J_{\text{CP}} = 20.1$ Hz), 30.4, 29.5.

General Procedure for the Pinacol Deprotection.

Bpin DiazaPhos **8** or **9** (0.389 g, 0.596 mmol, 1.0 equiv) was dissolved in THF (11 mL), diethanolamine (N₂-sparged) (286 μ L 2.98 mmol, 5 equiv) was added dropwise *via* Hamilton® syringe. After stirring the clear and colorless solution for 4 h, a white precipitate formed, which was filtered off *via* Schlenk filtration. The residue was washed with THF (4 \times 3 mL) to remove any pinacol and unreacted starting material. The pinacolyl deprotected product B(dea) DiazaPhos **10** and **11** were obtained as a white solid (yield was not determined). Aqueous HCl (0.1 M, N₂-sparged, 6 mL) was added to B(dea) DiazaPhos. The suspension was stirred overnight. The white solid changed from clumpy to fluffy. It was then filtered off *via* Schlenk filtration. After washing with H₂O (N₂ sparged, 5 \times 1.5 mL) the product was obtained as a fine powdered white solid.

o-Bdea DiazaPhos (**10**). ¹H NMR (400 MHz, DMSO-*d*₆): δ 7.54 (d, J = 7.2 Hz, 1H, H^{Ar}), 7.10–7.35 (m, 5H, H^{Ar}), 7.06 (d, ²J_{HP} = 3.8 Hz, 1H, P(CH)N), 6.94 (m, 3H, H^{Ar}), 6.82 (d, ²J_{HP} = 15.9 Hz, 1H, P(CH)N), 6.80 (t, J = 7.2 Hz, 1H, H^{Ar}), 6.64 (brt, ²J_{HP} = 6.2 Hz, 1H, H^{Ar}), 6.50 (t, J = 7.8 Hz, 1H, H^{Ar}), 6.26 (d, J = 8.0 Hz, 1H, H^{Ar}), 4.51 (br, 2H, NH), 2.74–3.30 (m, 20H, (CH₂)₂); ³¹P{¹H} NMR (162 MHz, DMSO-*d*₆): δ 19.5; ¹¹B NMR (128 MHz, DMSO-*d*₆): δ 10.5 (br, $h_{1/2}$ = 1150 Hz).

m-B(dea) DiazaPhos (**11**). ¹H NMR (400 MHz, CDCl₃): δ 7.13–7.45 (m, 7H, H^{Ar}), 7.08 (d, J_{HH} = 7.0 Hz, 1H, H^{Ar}), 6.99 (m, 3H, H^{Ar}), 6.76 (m, 2H, H^{Ar}), 6.29 (s, 1H, P(CH)N), 5.60 (d, ²J_{HP} = 17.7 Hz, 1H, P(CH)N), 3.65–3.95 (m, 10H, (CH₂)₂), 2.72–3.14 (m, 10H, (CH₂)₂); ³¹P{¹H} NMR (162 MHz, DMSO-*d*₆): δ 10.5; ¹¹B NMR (128 MHz, DMSO-*d*₆): δ 10.1 (br, $h_{1/2}$ = 912 Hz).

o-B(OH)₂ DiazaPhos (**12**). 39% yield. ¹H NMR (400 MHz, CD₃OD): δ 8.15 (br, 2H, B(OH)), 8.03 (br, 2H, B(OH)), 7.77 (d, J = 7.5 Hz, 2H, H^{Ar}), 7.51–7.03 (m, 8H, H^{Ar}), 6.95–6.82 (m, 2H, H^{Ar}), 6.73

(t, $J = 7.5$ Hz, 1H, H^{Ar}), 6.48 (d, $^2J_{HP} = 17.4$ Hz, 1H, P(CH)N), 6.31 (d, $J = 7.7$ Hz, 1H, H^{Ar}), 2.70–2.55 (m, 4H, $(CH_2)_2$); $^{31}P\{^1H\}$ NMR (162 MHz, CD_3OD): δ 17.2; ^{11}B NMR (128 MHz, CD_3OD): δ 29.1 (br, $h_{1/2} = n.d.$).

m-B(OH) $_2$ DiazaPhos (**13**). 1H NMR (400 MHz, CD_3OD): δ 8.15 (s, 2H, B(OH)), 7.80–7.66 (m, 2H, H^{Ar} , B(OH)), 7.53–7.24 (m, 6H, H^{Ar}), 7.18 (m, 2H, H^{Ar}), 7.09–6.88 (m, 3H, H^{Ar}), 6.77 (m, 1H, H^{Ar}), 6.38 (s, 1H, P(CH)N), 5.71 (d, $^2J_{HP} = 18.4$ Hz, 1H, P(CH)N), 3.22–2.56 (m, 4H, $(CH_2)_2$), $^{31}P\{^1H\}$ NMR (162 MHz, CD_3OD): δ 10.5; ^{11}B NMR (128 MHz, CD_3OD): δ 28.1 (br, $h_{1/2} = 830$ Hz).

Glycol Deprotection Procedure from *m*-Bgly DiazaPhos **22** to *m*-B(OH) $_2$ Diazaphos **13**.

Method A. *m*-Bgly DiazaPhos **22** (148 mg, 0.274 mmol) was suspended in dinitrogen-sparged aqueous HCl (0.5 M, 10 mL) and the reaction mixture was stirred overnight. The solution was decanted off, the residual white solid was washed with dinitrogen-sparged H_2O (6 x 3 mL) and THF (3 x 2 mL) and dried *in vacuo* to yield the product as a fine white solid.

Method B. *m*-Bgly Diazaphos **22** (253 mg, 0.468 mmol) was dissolved in dinitrogen-sparged acetone (2 mL), dinitrogen-sparged H_2O was added slowly until the solution turns milky. The Schlenk flask was sealed and the reaction mixture was kept in the fridge overnight. More the white solid precipitated and stuck to the side of the glass walls. The clear solution was decanted off and the residual white solid was washed with dinitrogen-sparged H_2O (3 x 3 mL) and THF (3 x 2 mL) and dried *in vacuo* to yield the product as a fine colorless solid.

General Hydroformylation Procedure

Inside a N_2 -purged glovebox, a solution of $[Rh(acac)(CO)_2]$ in THF (20 mM), a solution of the diazaphospholane ligand in THF (5–20 mM) were combined into an oven-dried 15 mL Ace Glass pressure bottle equipped with a magnetic stir bar using 1000 μL and 200 μL Eppendorf® pipets.

The pressure bottle was attached to a pressure reactor and removed from the glovebox. In a fume hood, the reactor was purged with syngas (3 x 120 psig) and then filled to 150 psig of syngas. The yellow solution was vigorously stirred at 60 °C for at least 60 min. Upon cooling, the reactor was depressurized to 10 psig and the alkene was injected with a gas-tight syringe. Solid alkenes were injected as a solution in THF. The reactor was then purged with syngas (3 x 120 psig) and filled to 150 psig of syngas. The reaction was heated at 40 or 60 °C. After the desired reaction time, the reactor was allowed to cool to room temperature and vented to atmospheric pressure. NMR spectra of the crude reaction mixture were taken in CDCl₃ to obtain conversions of the alkenes and branched to linear ratios of the produced aldehydes.

Procedure to Boronate BisDiazaPhos **19** and **22**.

m-B(OH)₂ BisDiazaPhos (**19**). In a N₂-filled glovebox, the *m*-B(OH)₂ azine **3** (0.131 mg, 0.450 mmol, 2.0 equiv) was suspended in THF (20 mL) and 1,2-bisphosphinobenzene (28.7 μL, 0.223 mmol, 1.0 equiv) was added *via* Hamilton® syringe, followed by dropwise succinyl chloride (122.5 μL, 1.113 mmol, 2.5 equiv) addition *via* Hamilton® syringe. The reaction mixture was stirred for 45 h at room temperature. The yellow solid was filtered off using a Schlenk frit and washed with THF (3 x 3 mL). The crude material is identified as a mixture of four bisdiazaphospholane isomers in a ratio of 8 : 1 : 1 : 8 (*racemic*-C₂ : *racemic*-C_S : *mesomeric*-C_S : *mesomeric-racemic*-C₁). All isomers were assigned by ¹H–³¹P-HMBC.

Desired rac-C₂-isomer. ¹H NMR (400 MHz, CD₃OD): δ 7.52, 7.38, 7.21, 7.04, 5.72 (s, 2H, P(CH)N), 5.67 (vt, ²J_{HP} = 9.9 Hz, 2H; P(CH)N); ³¹P{¹H} NMR (162 MHz, CD₃OD): δ = -1.9.

rac-C_S-isomer. ¹H NMR (400 MHz, CD₃OD): δ = 6.93, 6.54 (s, 2H, P(CH)N); ³¹P{¹H} NMR (162 MHz, CD₃OD): δ = 3.0.

meso-C_S-isomer. ¹H NMR (400 MHz, CD₃OD): δ 7.00, 6.40 (s, 2H, P(CH)N), ³¹P{¹H} NMR (162 MHz, CD₃OD): δ = 1.6.

meso-rac-C₁-isomer. **¹H NMR** (400 MHz, CD₃OD): δ 7.67, 7.51, 7.37, 6.55 (s, 2H, P(CH)N), 5.93 (d, $^2J_{\text{H-P}} = 9.9$ Hz, P(CH)N), 5.71 (s, P(CH)N); **³¹P{¹H} NMR** (162 MHz, CD₃OD): $\delta = 3.58$ and 0.27 (d, $^3J_{\text{P-P}} = 190$ Hz).

¹¹B NMR (128 MHz, CD₃OD): $\delta = 27.9$, all isomers are overlapped, 18.6 (RB(OH)₂•CD₃OD).

m-Bgly BisDiazaPhos (22). In a N₂-filled glovebox, the *m*-Bgly azine **24** (0.106 mg, 0.310 mmol, 2.0 equiv) was dissolved in THF (9 mL) and 1,2-bisphosphinobenzene (20.0 μ L, 0.155 mmol, 1.0 equiv) was added *via* Hamilton® syringe. Succinyl chloride (40.5 μ L, 0.37 mmol, 2.4 equiv) was added dropwise *via* Hamilton® syringe and the reaction mixture was stirred for 18 h at room temperature. The solvent was removed *in vacuo* to yield the crude product mixture as a light yellow solid. A mixture of 3 major bisdiazaphospholane isomers in a ratio of *racemic-C₂* : *racemic-C_S* : *C₁* = 4 : 4 : 2 is formed; the isomers were assigned by ¹H–³¹P-HMBC.

rac-C₂-isomer. **¹H NMR** (400 MHz, CDCl₃): $\delta = 7.77$, 7.67, 7.47, 7.40, 7.30, 7.08, 5.81 (s, 2H, P(CH)N), 5.73 (vt, $^2J_{\text{H-P}} = 10.1$ Hz, 2H, P(CH)N); **³¹P{¹H} NMR** (162 MHz, CD₃OD): $\delta = -0.44$.

rac-C_S-isomer. **¹H NMR** (400 MHz, CDCl₃): $\delta = 7.74$, 7.70, 7.43, 7.14, 6.97, 6.79, 6.05 (s, 2H, P(CH)N), 5.86 (vt, $^2J_{\text{H-P}} = 9.1$ Hz, 2H, P(CH)N); **³¹P{¹H} NMR** (162 MHz, CD₃OD): $\delta = 4.75$.

C₁-isomer. **¹H NMR** (400 MHz, CDCl₃): $\delta = 7.83$, 7.77, 7.58, 7.46, 7.37, 7.28, 6.86, 6.65 (s, P(CH)N), 6.06 (d, $^2J_{\text{H-P}} = 17.3$ Hz, P(CH)N), 5.68 (s, P(CH)N); **³¹P NMR** (162 MHz, CD₃OD): $\delta = 2.57$ (ABq). **¹¹B{¹H} NMR** (128 MHz, CDCl₃): $\delta = 31.5$, all isomers are overlapped.

Synthesis Attempts of Boronate Tan Ligand Mimic

Reaction of **25** and B(OMe)₃

The phosphine **25** (19 mg, 0.0097 mmol, 1 equiv) was weighted into a Schlenk flask containing 4 Å molecular sieves and C₆D₆ (0.5 mL) was added. B(OMe)₃ (11.2 μ L, 1.1 equiv) was added with a syringe and the mixture was stirred for 2 d. Only 8% of a new species formed. The mixture was

further heated at 50 °C for 4 h, leading to an increase in the amount of the new species to 66%. One more equivalent of B(OMe)₃ was added and the reaction heated for 2 more days leading to 77% of the new species. NaH (3 mg) was added and the mixture was heated for 5 h at 60 °C. No loss of the P–H bond was observed.

Reaction of **25** and BCl₃

The phosphine **25** (20 mg, 0.0098 mmol, 1 equiv) was weighted into a Schlenk flask and dissolved in toluene (1 mL). NEt₃ (30 µL, 0.0221 mmol, 2.2 equiv) was added with a syringe and the reaction was cooled to 0 °C with an ice bath. The phosphine-amine mixture was slowly added dropwise to a solution of BCl₃ (1 M in hexanes, 109 µL, 0.001 mmol, 1.1 equiv) in toluene (1 mL) was slowly to 0 °C. A white precipitate forms after 20 min. The reaction was stirred for 4 h and allowed to warm to rt. The solid was filtered off using a syringe filter and NMR spectra of the crude mixture were collected in CDCl₃.

4.5 References

1. Henbest, H. B.; Wilson, R. A. L., *J. Chem. Soc.* **1959**, 1958–1965.
2. Winstein, S.; Sonnenberg, J., *J. Am. Chem. Soc.* **1961**, 83, 3235–3244.
3. Thompson, H. W.; McPherson, E., *J. Am. Chem. Soc.* **1974**, 96, 6232–6233.
4. Rousseau, G.; Breit, B. *Angew. Chem. Int. Ed.* **2011**, 50, 2450–2494.
5. Sawamura, M.; Ito, Y. *Chem. Rev.* **1992**, 92, 857–871.
6. Breit, B., *Top. Curr. Chem.* **2007**, 279, 139.
7. Sun, X.; Worthy, A. D.; Tan, K. L. *Angew. Chem. Int. Ed.* **2011**, 50, 8167–8171.
8. Zhang, M.; Zhang, Y.; Jie, X.; Zhao, H.; Li, G.; Su, W. *Org. Chem. Front.* **2014**, 1, 843.
9. Chen, Z.; Wang, B.; Zhang, J.; Yu, W.; Liu, Z.; Zhang, Y. *Org. Chem. Front.* **2015**, 2, 1107–1295.

10. Claver, C.; van Leeuwen, P. W. N. M. *Rhodium Catalyzed Hydroformylation*. Kluwer Academic Publishers: Dordrecht, **2000**.
11. Pittman, C. U. J.; Honnick, W. D. *J. Org. Chem.* **1980**, *45*, 2132–2139.
12. Tic, W. J.; Zoltanski, A. *Curr. Cat.* **2015**, *4*, 155–165.
13. Koskinen, A. M. P.; Karisalmi, K. *Chem. Soc. Rev.* **2005**, *34*, 677–690.
14. Fürstner, A.; Nevado, C.; Waser, M.; Tremblay, M.; Chevrier, C.; Teplý, F.; Aïssa, C.; Moulin, E.; Müller, O. *J. Am. Chem. Soc.* **2007**, *129*, 9150–9161.
15. Smith, A. B.; Brandt, B. M. *Org. Lett.* **2001**, *3*, 1685–1688.
16. McDonald, R. I.; Wong, G. W.; Neupane, R. P.; Stahl, S. S.; Landis, C. R. *J. Am. Chem. Soc.* **2010**, *132*, 14027–14029.
17. Wong, G. W.; Adint, T. T.; Landis, C. R. *Org. Synth.* **2012**, *89*, 243–254.
18. Lundt, I. *Glycoscience* **2001**, 501–531.
19. Burke, S. D.; Cobb, J. E.; Takeuchi, K. *J. Org. Chem.* **1990**, *55*, 2138–2151.
20. Breit, B.; Grünanger, C. U.; Abillard, O. *Eur. J. Org. Chem.* **2007**, *2007*, 2497–2503.
21. Breit, B. *Ang. Chem.* **1996**, *108*, 3021–3023.
22. Breit, B.; Heckmann, G.; Zahn, S. K. *Chem. Eur. J.* **2003**, *9*, 425–434.
23. Jackson, W. R.; Parlmutter, P.; Suh, G.-H. *J. Chem. Soc. Chem. Comm.* **1987**, 724–725.
24. Jackson, W. R.; Parlmutter, P.; Tasdelen, E. E. *J. Chem. Soc. Chem. Comm.* **1990**, 763–764.
25. Yeung, C. S.; Dong, V. M. *Angew. Chem. Int. Ed.* **2011**, *50*, 809–812.
26. Lightburn, T. E.; Dombrowski, M. T.; Tan, K. L. *J. Am. Chem. Soc.* **2008**, *130*, 9210–9211.
27. Grünanger, C. U.; Breit, B. *Angew. Chem. Int. Ed.* **2008**, *47*, 7346–7349.
28. Grünanger, C. U.; Breit, B. *Angew. Chem. Int. Ed.* **2010**, *49*, 967.
29. Lightburn, T. E.; De Paolis, O. A.; Cheng, K. H.; Tan, K. L. *Org. Lett.* **2011**, *13*, 2686–2689.
30. Sun, X.; Frimpong, K.; Tan, K. L. *J. Am. Chem. Soc.* **2010**, *132*, 11841–11843.

31. Worthy, A. D.; Joe, C. L.; Lightburn, T. E.; Tan, K. L. *J. Am. Chem. Soc.* **2010**, *132*, 14757.
32. Joe, C. L.; Tan, K. L. *J. Org. Chem.* **2011**, *76*, 7590.
33. Hall, D. G., *Boronic Acids: Preparation and Applications in Organic Synthesis, Medicine and Materials*. WILEY-VCH Verlag GmbH & Co. KGaA, Weinheim: **2005**.
34. Heyes, R.; Lockhart, J. C. *J. Chem. Soc. A*, **1968**, 326–328.
35. Groziak, M. P.; Chen, L.; Yi, L.; Robinson, P. D. *J. Am. Chem. Soc.* **1997**, *119*, 7817–7826.
36. Oehlke, A. *Dissertation*, Technische Universitaet Chemnitz, **2010**.
37. Lautens, M.; Mancuso, J. *J. Org. Chem.* **2004**, *69*, 3478–3487.
38. Landis, C. R.; Jin, W.; Owen, J. S.; Clark, T. P. *Angew. Chem. Int. Ed.* **2001**, *40*, 3432–3434.
39. Noeth, H.; Wrackmeyer, B. *Nuclear Magnetic Resonance Spectroscopy of Boron Compounds*. Springer Verlag Berlin Heidelberg: **1978**.
40. Clark, T. P.; Landis, C. R. *J. Am. Chem. Soc.* **2003**, *125*, 11792–11793.
41. Roy, C. D.; Brown, H. C. *J. Organomet. Chem.* **2007**, *692*, 784–790.
42. Sun, J.; Perfetti, M. T.; Santos, W. L. *J. Org. Chem.* **2011**, *76*, 3571–3575.
43. Thomas, P. J.; Axtell, A. T.; Klosin, J.; Peng, W.; Rand, C. L.; Clark, T. P.; Landis, C. R.; Abboud, K. A. *Org. Lett.* **2007**, *9*, 2665–2668.
44. Clark, T. P.; Landis, C. R.; Freed, S. L.; Klosin, J.; Abboud, K. A. *J. Am. Chem. Soc.* **2005**, *127*, 5040–5042.
45. Nelson, R. C. *Dissertation*, University of Wisconsin-Madison, **2006**.
46. Hashiguchi, B. G. *Dissertation*, University of Wisconsin-Madison, **2008**.
47. Geier, S. J.; Gilbert, T. M.; Stephan, D. W. *Inorg. Chem.* **2011**, *50*, 336–344.
48. Adint, T. T.; Wong, G. W.; Landis, C. R. *J. Org. Chem.* **2013**, *78*, 4231–4238.

Appendix 1

Sterically Reduced Diazaphospholanes

A1.1 Introduction

Due to the constant need of aldehyde functionalities derived from a variety of alkenes, the design of new ligands for rhodium-catalyzed hydroformylation is important. One of the challenges is the limited substrate scope for any single ligand. With the discovery of the bisdiazaphospholanes by Landis and coworkers, a new successful ligand class was introduced that combines good regio- and high enantioselectivity and activity for a variety of substrates compared to other ligand classes, such as bisphosphines and bisphosphites.¹⁻⁷

Alkenes with higher substitution, such as 1,2-disubstituted and especially 1,1-disubstituted alkenes, require higher temperatures to achieve reasonable rates in rhodium-catalyzed hydroformylation and find fewer applications. There are no reports of hydroformylation of tri- and tetrasubstituted alkenes. To address this issue, we thought to investigate the synthesis of diazaphospholane derived ligands that are sterically less congested, and unlike the current phospholane ligands, would not contain any substituents in the 2- and 5-position of the diazaphospholane ring. In addition, the investigation of azaphospholanes with varying ring sizes is of interest (Figure A1.1).

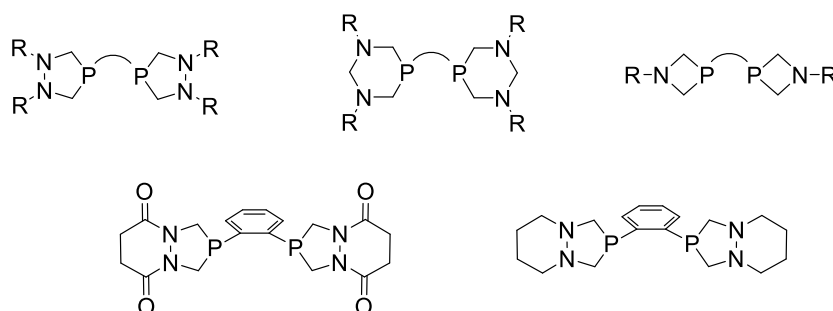
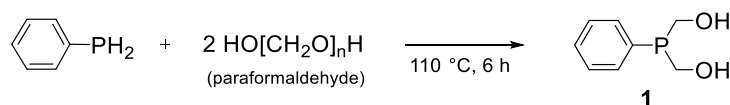


Figure A1.1. Sterically reduced bis-azaphospholanes with varying ring sizes (top) and sterically reduced, direct analogues to succinyl bisdiazaphospholanes (bottom).

A1.2 Results and Discussion

A1.2.1 Investigation of Sterically Reduced BiaDiazaPhos

The synthesis of sterically reduced bisdiazaphospholanes has to be approached by a non-traditional way than is commonly used for 2,5-disubstituted bisdiazaphospholanes. Methylidene azines would have to be utilized as the azine-precursor, but this azine tends to polymerize spontaneously.⁸ Instead, hydrido-phosphines are known to undergo P–C-bond formation with formaldehyde to yield hydroxymethylphosphines.⁹ All reactions were initially optimized on monophosphines. Reaction of phenylphosphine and aqueous formaldehyde was found to be not reproducible. The solution has to be sparged with N₂ to avoid phosphine oxide formation, and it is assumed that the formaldehyde gets removed from the solution, making the concentration of the reagents inconsistent across different runs. Instead, use of paraformaldehyde as the formaldehyde is successful. In a melt-reaction, phenylphosphine is heated with paraformaldehyde at 110 °C for 6 h to yield bis(hydroxymethyl)phosphine **1** (Scheme A1.1).¹⁰



Scheme A1.1. Synthesis of **1** via a melt reaction of phenylphosphine with paraformaldehyde.

In 1980, Jin and Märkl reported the reaction of hydroxymethylphosphines and alkyl hydrazines.¹¹⁻¹³ For our purposes, we were interested in obtaining diazaphospholane **2** (Figure A1.2), since phospholane hydrazines react further with acyl chlorides,¹ giving the option of rapidly derivatizing the backbones on the sterically reduced ligands. Unfortunately, reaction of **1** and hydrazine monohydrate reduced the phosphine to a secondary phosphine by a retro-addition reaction (Figure A1.2). The secondary phosphine is observed both as the hydridophosphine (singlet in the ³¹P NMR spectrum) and the deuterophosphine (1:1:1-triplet in the ³¹P NMR),

suggesting the scrambling of the H- and D-atoms throughout the retro-addition process. One of the secondary phosphines is believed to be the mono-hydroxymethylphosphine at -45 ppm, whereas the signal at -65 ppm could be assigned as a mono-hydrazinemethyl derived phosphine (Figure A1.2, NMR spectrum).

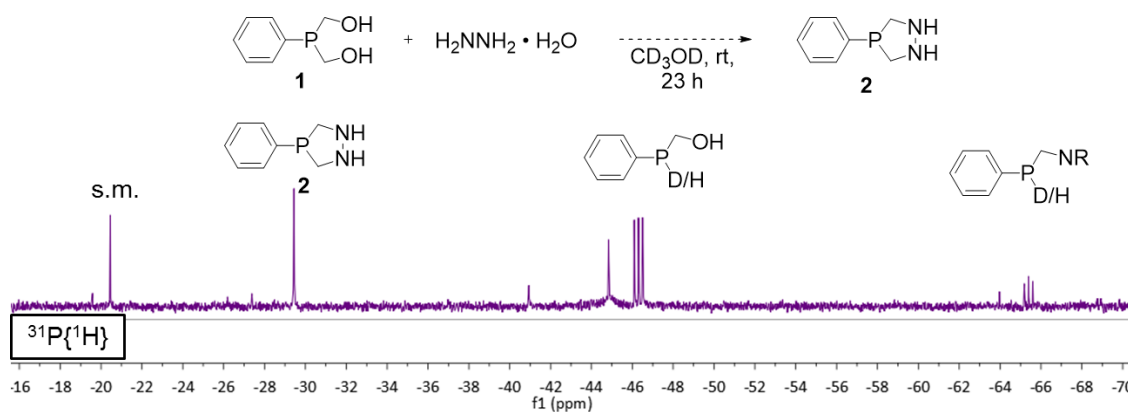
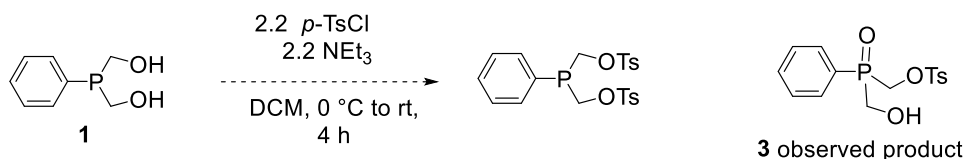


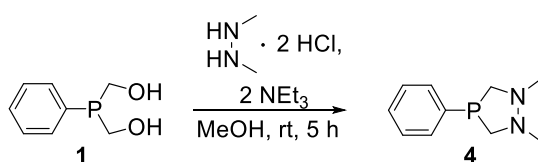
Figure A1.2. Observed retro-addition upon reacting of **1** with hydrazine.

Alternatively, product **2** could be obtained through the reaction of a tosylmethylphosphine and hydrazine. Interestingly, the desired product is not formed by reaction of **1** with *para*-tosyl chloride in the presence of a base. The observed major product **3** is a phosphine oxide containing one hydroxymethyl and one tosylmethyl group (Scheme A1.2). Despite vigorously airfree conditions, the phosphine oxide **3** is always formed as confirmed by both NMR spectroscopy and mass spectrometry.



Scheme A1.2. Reaction of bis(hydroxymethyl)phosphine and *p*-TsCl yields product **3**.

The reaction with substituted hydrazines was investigated to achieve the formation of a diazaphospholane framework. Diaryl-substituted hydrazines do not react with **1** in MeOH at room temperature or elevated temperatures. Interestingly, even monosubstituted hydrazines are not suitable in the reaction with **1** and lead to formation of the secondary phosphines through a retro-addition reaction (*cf.* Figure A1.2, *vide supra*). Successful diazaphospholane ring formation was achieved with 1,2-dimethylhydrazine in the reaction with its corresponding salt and in the presence of a base to yield product **4** (Scheme A1.3).



Scheme A1.3. Monodiazaphospholane **4** synthesis with **1** and 1,2-dimethylhydrazine•2HCl.

With the successful demonstration of a viable synthetic route to a sterically reduced monodiazaphospholane, synthesis of the corresponding bisdiazaphospholane was investigated next. Indeed, reaction of 1,2-bisphosphinobenzene with paraformaldehyde proceeds analogous to the monophosphine route. Bisphosphine **5** displays an interesting splitting pattern in the ^1H NMR spectrum for the diastereotopic methine-protons (Scheme A1.3). Each of the peaks of the AB-quartet (blue trace) is split into a virtual triplet (red trace) with a different coupling constant ($^2J_{\text{H-P}} = 2.8$ and 4.8 Hz) as is typically found in diazaphospholane rings. This behavior suggests that a ring structure through an intramolecular hydrogen-bond is formed.

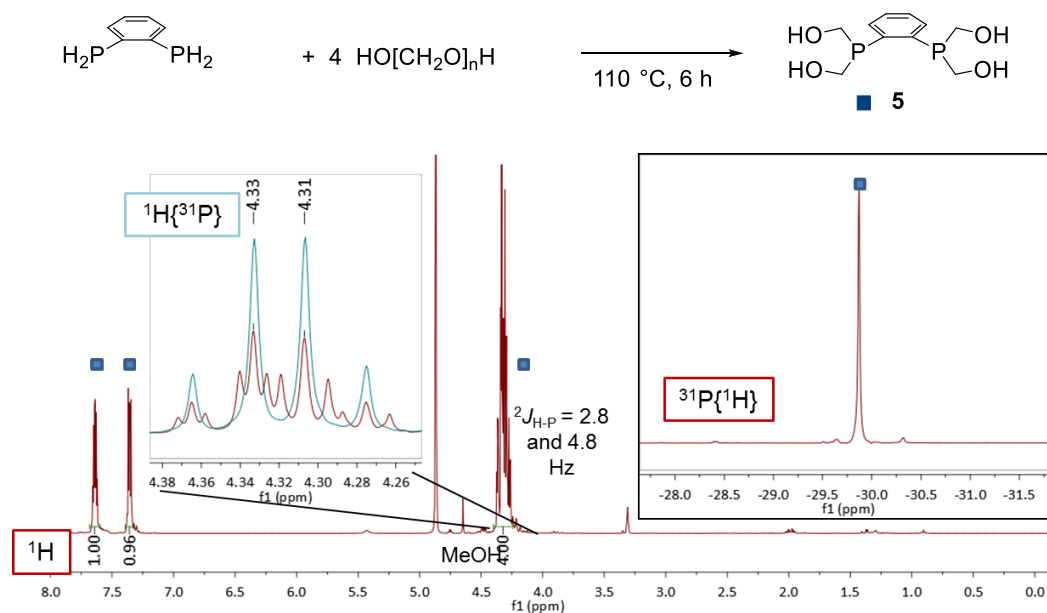


Figure A1.3. Synthesis of **5** and the ¹H (left) and ³¹P{¹H} NMR spectrum (right).

Subsequent reaction of **5** with the 1,2-dimethylhydrazine-HCl salt in the presence of a base yields the desired bisdiazaphospholane **6**. Similar to the starting material **5**, the diastereotopic methine protons in **6** resonate as an AB-quartet. Each of the peaks is split into a virtual triplet, with different ²J_{H-P} coupling constants of 12.9 and 1.4 Hz (Figure A1.4).

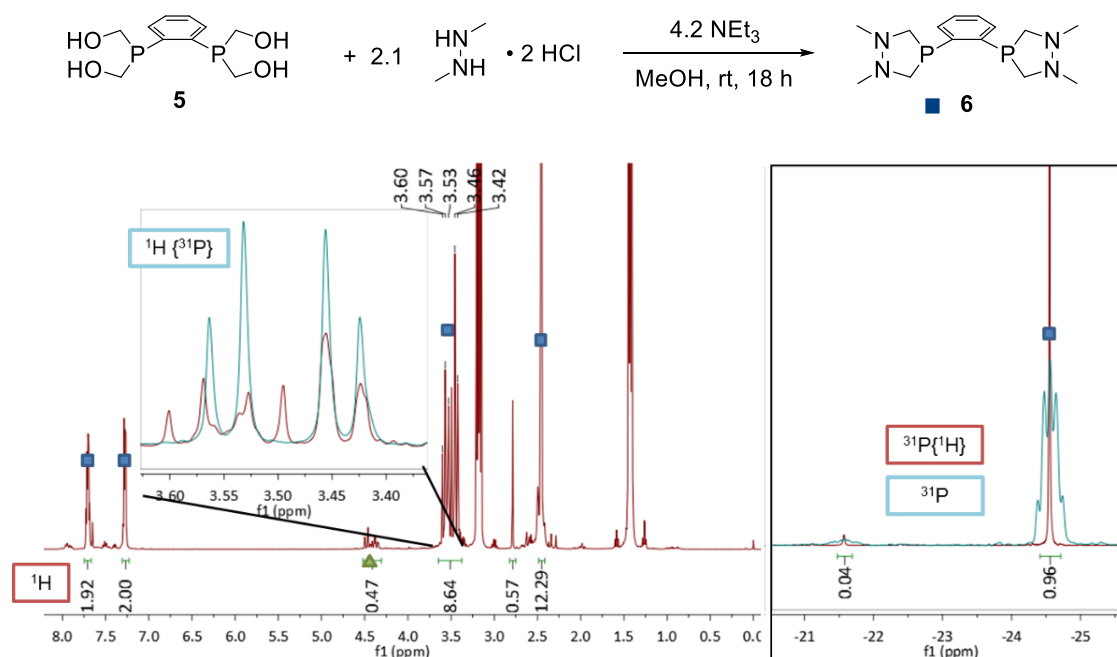


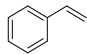
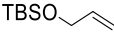
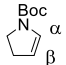
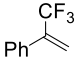
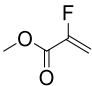
Figure A1.4. Synthesis and ^1H (left) and ^{31}P NMR spectrum (right) of ligand **6**.

A1.2.2 Hydroformylation Results with *N,N,N',N'*-Tetramethyl BisDiazaPhos **6** and Investigation of its Rhodium-Complexes.

To test the hypothesis that a sterically reduced ligand will lead to hydroformylation of substrates at an increased rate, ligand **6** was tested in the hydroformylation of several substrates, including the typical benchmark substrate styrene, bulkier substrates allyloxy-*tert*-butyldimethylsilane, *N*-Boc-2,3-dihydropyrrole and the 1,1-disubstituted alkenes (1-(Trifluoromethyl)vinyl)benzene and methyl 2-fluoroprop-2-enoate (Table A1.1). To our surprise, conversion for all substrates is very low. Regioselectivities for benchmark substrate styrene and bulkier substrates allyloxy-*tert*-butyldimethylsilane and *N*-Boc-2,3-dihydropyrrole are on the low side (entries 1, 2 and 3). Interestingly, (1-(Trifluoromethyl)vinyl)benzene shows preference for the branched quaternary aldehyde (b/l = 6.7) and forms minimal amounts of the hydrogenation product (entry 4). Typically, the tendency for this substrate is to form the linear aldehyde.¹⁴ Even though

the substrate methyl 2-fluoroprop-2-enoate gives rise to the branched aldehyde product only, the amount of the hydrogenation product could not be reduced (entry 5).

Table A1.1. Hydroformylation Results with Ligand **6**.^a

Entry	Substrate	cat. loading (mol %)	solvent	t (h)	conv. (%)	b / l or α : β	hydrogenation (%)
1 ^b		0.15	tol	16	38	12	---
2 ^b	TBSO-CH=CH ₂ 	0.1	THF/tol	17	3	1.8	---
3 ^b		0.5	THF/tol	24	8	2.3	---
4 ^c		1.0	tol	94	40	6.7	1
5 ^c		1.0	tol	94	45	>50	22

^a Conditions: reaction performed at 60 °C, Rh/L = 1 : 1.1, conversions and b : l ratios were determined by ¹H NMR spectroscopy. ^b [alkene] = 1.5 M. ^c [alkene] = 1.0 M.

The activity of ligand **6** was further investigated using our group's Wisconsin High Pressure NMR-Reactor (WiHP-NMRR).¹⁵ I would like to thank Dr. Spring Knapp for her help in setting up the reaction in the reactor and collecting the following data. The conversion of styrene and the production of the branched aldehyde was followed *in situ* at 60 °C and 190 psig of syngas (Figure A1.5). The branched to linear ratio is 12 : 1 after a reaction time of 16 h and a conversion of 38%, the observed half-life is 17.3 h. After 16 h, a ³¹P NMR spectrum was collected to obtain potential

catalyst intermediates, showing unusual signals around 40 ppm (Figure A1.5). The undertaken experiments to learn about the nature of this species are discussed below.

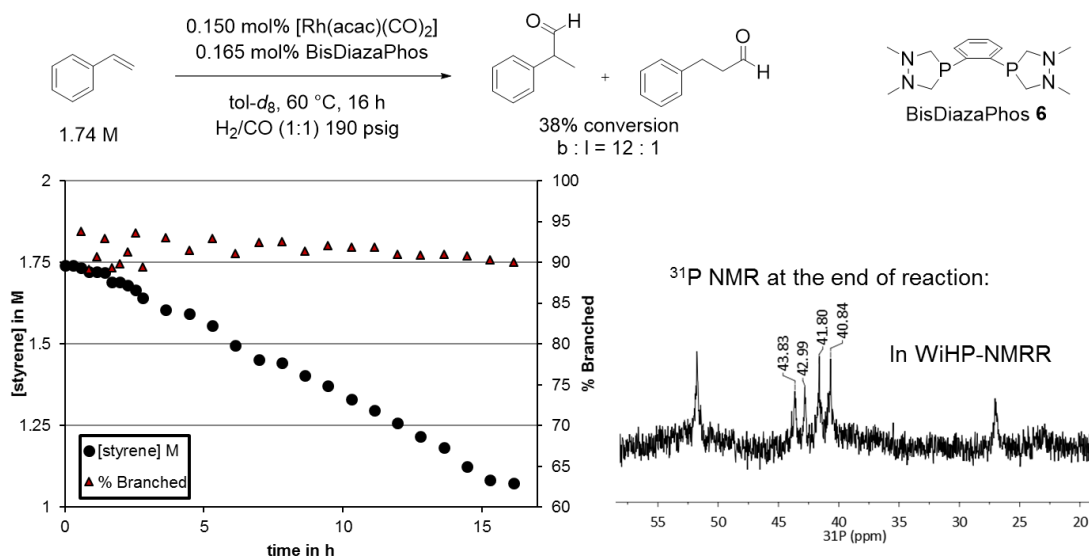


Figure A1.5. Consumption (circles) and %branched aldehyde formation (triangles) of styrene obtained with the WiHP NMRR (left) using ligand **6** and ³¹P NMR spectrum (right) after 16 h.

Ligand **6** was reacted with [Rh(acac)(CO)₂] to analyze the corresponding Rh-acac-complex. Of note, is that the solution turns red-brown even though other Rh-BDP complexes are known to be yellow. Interestingly, the ³¹P NMR spectrum reveals that in addition to the Rh-acac-complex ($\delta = 78.4$ ppm), another species **8** with a chemical shift of 41.3 ppm formed, that is based on a Rh-ligand **6** complex (Figure A1.6). This signal displays a second order-type splitting pattern and can be found with fluctuating 5-coordinate Rh-phosphine-complexes. This product mixture of **7** and **8** together with the internal standard Ph₃PO, were exposed to syngas under typical preactivation-condition of 150 psig at 60 °C for 30 min (Figure A1.6, bottom spectrum). The Rh-acac-complex **7** reacts with syngas to yield the hydrido-dicarbonyl species, which existence is only confirmed by ¹H NMR spectroscopy. However, the corresponding P-signal in the ³¹P NMR spectrum seems to be broadened out and could not be identified. Species **8**, however, does not react with syngas and is still present in solution. Also of notice is the loss of mass balance

indicated by the integrals of all P-containing signals compared to the internal standard. Over time, formation of a red-brown solid is observed, which also explains the loss of P-containing compounds before and after the reaction with syngas.

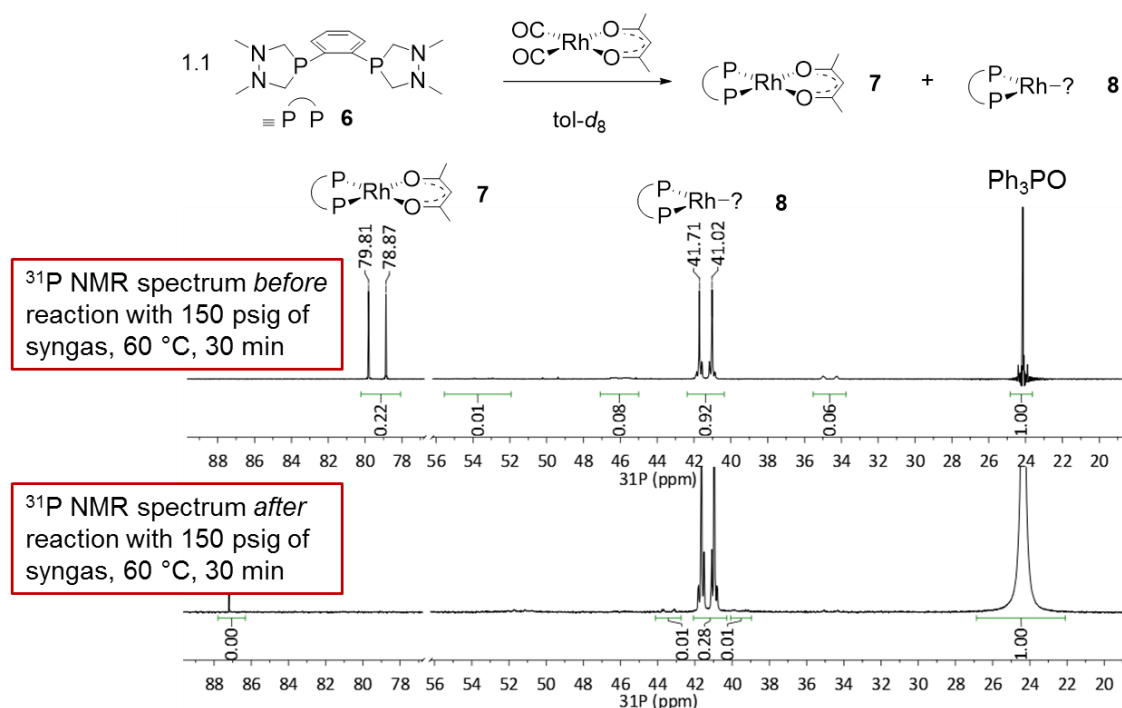


Figure A1.6. Reaction between **6** and $[\text{Rh}(\text{acac})(\text{CO})_2]$ yields complexes **7** and **8** (top $^{31}\text{P}\{^1\text{H}\}$ NMR spectrum) and $^{31}\text{P}\{^1\text{H}\}$ NMR spectrum after reaction of **7** and **8** with syngas (bottom)

The nature of **8** has further been examined. When a mixture of **6** and $[\text{Rh}(\text{acac})(\text{CO})_2]$ is vigorously stirred under N_2 at $60\text{ }^\circ\text{C}$, the desired complex **7** is observed as the only complex in the ^{31}P NMR spectrum (Figure A1.7, top spectrum). Once this sample of clean **7** is reacted with syngas at $60\text{ }^\circ\text{C}$, the same spectrum is observed as shown in the bottom spectrum of Figure A1.6 (*vide supra*). The relationship between **7** and **8** was tested by exposing **7** to an CO atmosphere only. Indeed, complex **8** appears in the ^{31}P NMR, when a solution of clean compound **7** is sparged with CO. The signal for **8** disappears again, when the sample is heated under an N_2 -atmosphere or when the solvent of the sample is removed under vacuum, consequently, also removing CO

(Figure A1.7, bottom spectrum). This data shows that compound **7** and **8** seem to be in equilibrium, suggesting that **8** could be a five-coordinate CO-complex of **7**.

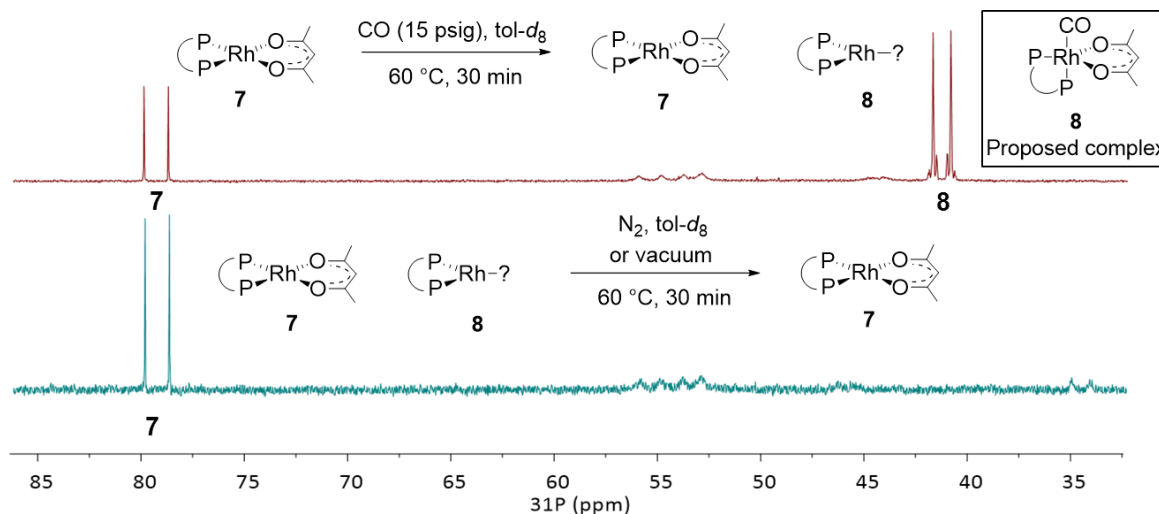


Figure A1.7. Interconversion of complex **8** in the presence (top) or absence (bottom) of CO and **8** proposed as a five-coordinate CO-complex of **7**.

The loss of mass balance in the ^{31}P NMR spectrum mentioned earlier was further examined by IR spectroscopy. The IR-spectrum of the mixture of **7** and **8** after the reaction of syngas (bottom spectrum of Figure A1.6, *vide supra*) was obtained. Interestingly, stretching frequencies of CO were observed that correspond to CO ligands in multinuclear Rh-complexes (Figure A1.8), containing both bridging and non-bridging CO-ligands. For example, Wilkinson reported a Rh-dimer formation with PPh_3 as a ligand (yellow dimer, Figure A1.8), which precipitates out of solution.¹⁶ This dimer formation is observed in the presence of syngas and is in equilibrium with its hydrido-dicarbonyl-phosphine complex. We believe that similar behavior is taken place with the hydrido-dicarbonyl-Rh-complex of **6**. This result explains first the loss of mass balance in the ^{31}P NMR spectrum, and second, the low conversion in the hydroformylation with ligand **6**, since this ligand is trapped in the complex **8** and as a dimeric or even multinuclear Rh-complex.

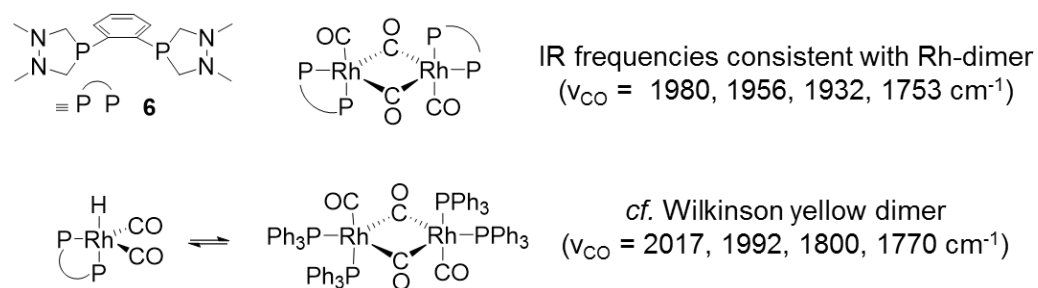
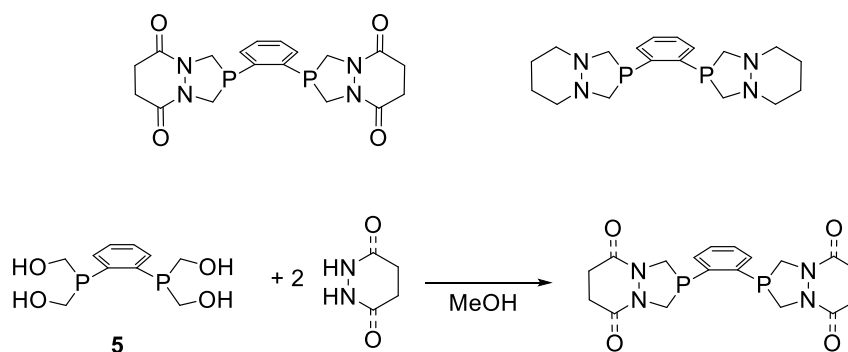


Figure A1.8. IR-stretching frequencies of a potential dinuclear Rh-complex with ligand **6** compared to the frequencies of the Wilkinson yellow dimer.

A1.3 Conclusion and Future Work

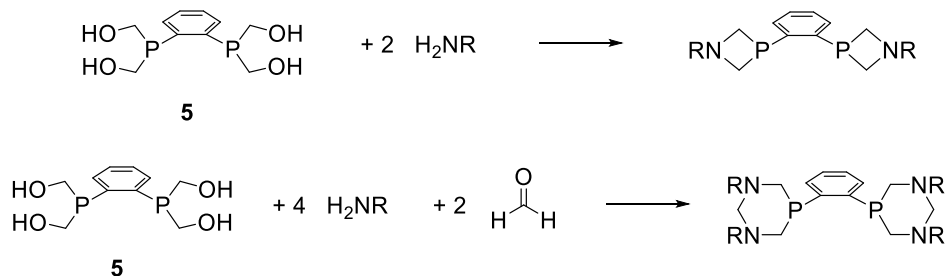
The synthesis of sterically reduced bisdiazaphospholanes was explored. *N,N,N,N*-Tetramethyl BisDiazaPhos **6** was successfully synthesized through the reaction of bis(dihydroxymethyl)-phosphine **5** and 1,2-dimethyl hydrazine. The synthesis towards sterically reduced BDPs is limited to alkyl-substituents on the nitrogen-atoms. The reaction of bis(dihydroxymethyl)-phosphine **1** and hydrazine leads the retro-addition back to the primary phosphine. *N,N,N,N*-Tetramethyl BisDiazaPhos **6** was tested in the hydroformylation of the typical benchmark substrate styrene and the bulky substrates allyloxy-*tert*-butyldimethylsilane, *N*-Boc-2,3-dihydropyrrole and the 1,1-disubstituted alkenes (1-(Trifluoromethyl)vinyl)benzene and methyl 2-fluoroprop-2-enoate. Conversions were found to be low (e.g. 38% for styrene after 16h). Investigations show that the Rh-acac complex **7** is likely in equilibrium with its five-coordinate CO-complex **8**. Furthermore, IR-spectroscopy suggests the presence of inactive, dinuclear or multinuclear rhodium-complexes upon exposure of syngas to complex **7**. The low conversions in hydroformylation are explained by the presence of multiple inactive species. Ligand **6** might be suitable for other H_2 - and CO-free non-enantioselective transformations.

The ligand structures in Scheme A1.4 are of interest and thought to be synthesized by the reaction of **5** and a cyclic hydrazine derivative. This strategy would also allow for the introduction of a stereocenter incorporated into the hydrazine backbone.



Scheme A1.4. Bicyclic BisDiazaPhos ligands of interest and their proposed synthesis.

Azaphospholanes of other ring sizes can be potentially obtained by reaction of **5** with primary amines (Scheme A1.5). With the use of 2 equivalents of amine, a four-membered 3-azaphospholane ring can be achieved. A six-membered 3,5-diazaphospholane cycle can be obtained by reacting **5** with 4 equivalents of amine and subsequent reaction with a formaldehyde source to install the CH_2 -group between the amine substituents. A comparable synthesis has recently been achieved by Musina *et. al* with 2-pyridylphosphines.¹⁷ It needs to be first investigated if these ligands would be able to exclusively form an Rh-acac complex (and consequently avoid formation of inactive Rh-species) before testing them in hydroformylation.



Scheme A1.5. Proposed synthesis of 4- and 6-membered heterocyclic phosphines.

A1.4 Experimental Methods

General Considerations

If not noted otherwise, all air- and moisture-sensitive reactions were carried out under an N₂ atmosphere using standard Schlenk line techniques or a circulating N₂-filled glovebox. All glassware was oven dried, set under vacuum while hot and cooled to room temperature under vacuum. Diphenylphosphine, paraformaldehyde, hydrazine monohydrate, CD₃OD, CDCl₃ and toluene-*d*₈ were purchased from Sigma-Aldrich. Paraformaldehyde was degassed under vacuum for at least 30 minutes. Substituted hydrazines or their HCl salts were purchased from Oakwood Chemicals. CDCl₃ was distilled from calcium hydride, freeze-pump-thawed to remove oxygen and stored over 3 Å molecular sieves in an air-tight bomb flask. Toluene-*d*₈ was dried and stored over 3 Å molecular sieves and sparged with N₂. MeOH was distilled from Mg/MgO. Other liquid commodity chemicals were degassed by sparging with N₂ prior to usage.

Routine NMR-spectroscopic measurements (¹H, and ³¹P) were carried out in perdeuterated solvents on Bruker Avance III-400 and Avance III-500 spectrometers. The chemical shift δ are reported in ppm, coupling constants *J* in Hz. Splitting patterns were assigned as singlet (s), doublet (d), doublet of virtual triplets (dvt), doublet of quartets (dq), triplet (t), quartet (q) multiplet (m), broad (br) and ABX- and ABX₂-quartets. If not noted additionally, further assignments were done using the correlation experiments ¹H-¹H-COSY, HSQC and HMBC experiments. ¹H and ¹³C NMR spectra were referenced internally to tetramethylsilane (0.00 ppm) or to the residual proton signals of the deuterated solvents ($\delta(^1\text{H}); (^{13}\text{C}) = 7.26; 77.16$ ppm (CDCl₃); ³¹P NMR spectra were referenced to an external standard of 85% phosphoric acid (H₃PO₄). Mass spectra were obtained at the Paul Bender Chemical Instrumentation Center of the Chemistry Department of the University of Wisconsin–Madison using a Thermo Q Exactive™ Plus ESI-MS.

Synthesis of **1**, **2**, **3**, **4**, **5** and **6**.

PhP(CH₂OH)₂ (**1**). In a 10 mL Schlenk flask, paraformaldehyde (112 mg, 3.73 mmol, 2.05 equiv) was degassed under vacuum for 1 h. Phenylphosphine (200 μ L, 1.82 mmol, 1.0 equiv) was added *via* syringe. The suspension was heated under N₂ at 110 °C for 6 h, resulting in a colorless liquid. Upon cooling to room temperature, product **5** was obtained as a thick colorless oil, and used as obtained. The sample contained 7% of PhPH(CH₂OH) and some other unidentified P-containing compounds. ¹H NMR (400 MHz, CD₃OD, ppm): δ = 7.58 (td, *J* = 6.8, 1.3 Hz, 2H, H^{Ar}), 7.39 – 7.32 (m, 3H, H^{Ar}), 4.30 – 4.14 (m, 4H, PCH₂N), 2.63 (b, 2H, OH); ³¹P{¹H} NMR (162 MHz, CD₃OD, ppm): δ = -20.4.

N,N'-Dimethyl DiazaPhos (**2**). In an NMR tube, product **1** (9.2 mg, 0.055 mmol, 1.0 equiv) was dissolved in CD₃OD (0.75 mL). Hydrazine-monohydrate (5.4 μ L, 0.056 mmol, 1.05 equiv) was added and the reaction progress was monitored by collecting NMR spectra after 1.5, 2.5, 4, 23 and 29 h. Retro-addition products were observed and made up approximately 70% of the total product mixture. ¹H NMR (400 MHz, CD₃OD, ppm): most signals are overlapped and not identified, methylene protons are in the range of 4.28 – 4.21 ppm. ³¹P{¹H} NMR (162 MHz, CD₃OD, ppm): δ = -29.4.

The equivalent reaction was tried with other substituted hydrazines (1,2-diphenylhydrazine) however, no reaction was observed. Mono-substituted hydrazines (o-methoxyphenyl hydrazine, isopropyl hydrazine) gave rise to a retro-addition to the secondary phosphine.

PhP(O)(CH₂OH)(CH₂OTs) (**3**). Product **1** (85.5 mg, 0.602 mmol, 1.0 equiv) was dissolved in DCM (3 mL). *p*-TsCl (252.4 mg, 1.32 mmol, 2.2 equiv) was degassed and added as a solution in DCM (3 x 4 mL). The mixture was cooled to 0 °C with an ice bath. Pyridine (184.5 μ L, 1.32 mmol,

2.0 equiv) was added dropwise *via* syringe and the reaction mixture was stirred overnight. The crude mixture contains majorly product **3**. **¹H NMR** (500 MHz, CDCl₃, ppm): δ = 7.89 – 7.80 (m, 2H, H^{Ar}), 7.59 – 7.52 (m, 2H, H^{Ar}) 4.58 (A of ABX, J = 12.3 Hz, $^2J_{\text{H-P}}$ = 8.5 Hz, 1H, PCH₂(OTs)), 4.48 (B of ABX, J = 12.8 Hz, $^2J_{\text{H-P}}$ = 5.6 Hz, 1H, PCH₂(OTs)), 3.91 (A of ABX, J = 13.9 Hz, $^2J_{\text{H-P}}$ = 4.8 Hz, 1H, PCH₂OH), 3.85 (B of ABX, J = 13.9 Hz, $^2J_{\text{H-P}}$ = 7.6 Hz, 1H, PCH₂OH) 2.45 (s, 2H, Ts-CH₃); **³¹P{¹H} NMR** (203 MHz, CDCl₃, ppm): δ = 28.6. **HRMS** (ESI, m/z): [M+H]⁺ = 341.0 and [M+NH₄]⁺ 359.0.

N,N'-Dimethyl DiazaPhos (**4**). In a 10 mL Schlenk flask, product **1** (9.6 mg, 0.56 mmol, 1.0 equiv) was dissolved in CD₃OD (0.75 mL). 1,2-dimethylhydrazine•2HCl (6.4 mg, 0.56 mmol, 2.1 equiv) was added as a solid followed by the addition of NEt₃ (15.7 μ L, 1.13 mmol, 2 equiv). NMR spectra of the crude product were obtained. The mixture contained 10% of the starting material and residual HNEt₃Cl. Yield was not determined. **¹H NMR** (400 MHz, CD₃OD, ppm): δ = 7.63 (td, J = 8.0, 1.8 Hz, 2H, H^{Ar}), 7.43 – 7.36 (m, 3H, H^{Ar}), 3.88 – 3.72 (m, 4H, PCH₂N), 2.79 (s, 6H, CH₃); **³¹P{¹H} NMR** (162 MHz, CD₃OD, ppm): δ = -30.2.

Ph(P(CH₂OH)₂)₂ (**5**). In a 10 mL Schlenk flask, paraformaldehyde (149 mg, 5.02 mmol, 4.0 equiv) was degassed under vacuum for 40 min. 1,2-bisphosphinobenzene (161.3 mL, 1.25 mmol, 1.0 equiv) was added *via* syringe. The suspension was heated under N₂ at 110 °C for 6 h, resulting in a colorless liquid. Upon cooling to room temperature, product **5** was obtained as a thick colorless oil (327.8 mg, >99% yield) **¹H NMR** (400 MHz, CD₃OD, ppm): δ = 7.74 – 7.66 (m, 2H, H^{Ar}), 7.29 – 7.23 (m, 2H, H^{Ar}), 4.34 (A of ABX₂, J = 12.7 Hz, $^2J_{\text{H-P}}$ = 2.8 Hz, 4H, PCH₂N), 4.29 (B of ABX₂, J = 12.7 Hz, $^2J_{\text{H-P}}$ = 4.8 Hz, 4H, PCH₂N); **³¹P{¹H} NMR** (162 MHz, CD₃OD, ppm): δ = - 29.9.

N,N,N',N'-Tetramethyl BisDiazaPhos (**6**). Product **5** (327.8 mg, 1.25 mmol, 1.0 equiv) was dissolved in MeOH (2 mL). 1,2-dimethylhydrazine•2HCl (298.3 mg, 2.55 mmol, 2.1 equiv) was added to the phosphine as an N₂-sparged solution in MeOH (3 mL), followed by the dropwise addition of NEt₃ (735.4 μ L, 5.1 mmol, 4.2 equiv). The reaction mixture was stirred overnight and diethylether was added (10 mL). The white precipitate was filtered off and washed with diethylether (3 x 3 mL). The solvent was removed under vacuum to obtain **6** as a light yellow oil (308 mg, 79.4% yield). ¹H NMR (400 MHz, CDCl₃, ppm): δ = 7.67 – 7.61 (m, 2H, H^{Ar}), 7.38 – 7.33 (m, 2H, H^{Ar}), 3.55 (A of ABX₂, J = 12.8 Hz, ²J_{H-P} = 12.9 Hz, 4H, PCH₂N), 3.44 (B of ABX₂, J = 12.8 Hz, ²J_{H-P} = 1.4 Hz, 4H, PCH₂N); ³¹P{¹H} NMR (162 MHz, CDCl₃, ppm): δ = -24.5.

Rhodium-Complexes of **6**.

*Reaction of [Rh(acac)(CO)₂] and **6**.*

Method 1: Inside an N₂-filled glove box, [Rh(acac)(CO)₂] (150 μ L, 75.96 mM in toluene-*d*₈, 1 equiv) and **6** (335 μ L, 37.64 mM in toluene-*d*₈, 1.1 equiv) were combined into an NMR tube. The solution turned red-brown. Ph₃PO (19 mg) was added as an internal standard. NMR spectra were obtained, showing a mixture of products **7** and **8**.

Method 2: A clean sample of **7** was obtained by heating a solution of [Rh(acac)(CO)₂] (150 μ L, 75.96 mM in toluene-*d*₈, 1 equiv) and **6** (335 μ L, 37.64 mM in toluene-*d*₈, 1.1 equiv) under vigorous stirring at 60 °C for 30 min. However, upon pre-activation with syngas, species **8** reappears.

[Rh(acac)**6**] (**7**). ¹H NMR (400 MHz, tol-*d*₈, ppm): δ = 8.11 – 8.00 (m, 2H, H^{Ar}), n.o. (m, 2H, H^{Ar}), 5.37 (s, 1H, acac-methine), 3.54 (dvt, J = 12.6 Hz, ²J_{H-P} = 3.4 Hz, 4H, PCH₂N), 3.54 (dvt, J = 12.6 Hz, ²J_{H-P} = 3.3 Hz, 4H, PCH₂N), 2.56 (s, 12H, NCH₃), 1.90 (s, 6H, acac-CH₃), ³¹P{¹H} NMR (162 MHz, tol-*d*₈, ppm): δ = 79.2 (d, ¹J_{P-Rh} = 191.5 Hz).

[Rh(acac)(CO)6] (**8**). **¹H NMR** (500 MHz, *tol-d*₈, ppm): Listed signals were observed through ¹H-³¹P-HMBC correlation experiments. δ = 8.42 – 8.32 (m, 2H, H^{Ar}), 7.13 (m, 2H, H^{Ar}), 3.60 (m, 4H, PCH₂N), 3.18 (brd, *J* = 11.5 Hz, 4H, PCH₂N), **³¹P{¹H} NMR** (162 MHz, *tol-d*₈, ppm): δ = 79.2 (d (second order), ¹*J*_{P-Rh} = 139.8 Hz).

The red-brown solution was injected into a hydroformylation reactor. The mixture was pre-activated with syngas at 60 °C for 30 min. The dark red-brown solution was transferred into an NMR tube attached to an NMR-tube Schlenk adapter.

[RhH(CO)6]. The hydride signal was visible in the ¹H NMR spectrum, however, no correlation to a P-atom was found. **¹H NMR** (500 MHz, *tol-d*₈, ppm): δ = -8.10 (td, ¹*J*_{H-Rh} = 58.2, ²*J*_{H-P} 10.9 Hz)

General Hydroformylation Procedure

Inside an N₂-filled glovebox, a solution of [Rh(acac)(CO)₂] in toluene (20 mM) and BisDiazaPhos **6** in toluene (20 mM) and THF were combined into an oven-dried 15 mL Ace Glass pressure bottle equipped with a magnetic stir bar using 1000 μ L and 200 μ L Eppendorf® pipets. The pressure bottle was attached to a pressure reactor and removed from the glovebox. In a fume hood, the reactor was purged with syngas (3 x 120 psig) and then filled to 150 psig of syngas. The yellow solution was vigorously stirred at 60 °C for at least 60 min. Upon cooling, the reactor was depressurized to 10 psig and the alkene was injected *via* a gas-tight syringe. The reactor was then purged with syngas (3 x 120 psig) and filled to 150 psig of syngas. The reaction was heated to 60 °C. After the desired reaction time, the reactor was allowed to cool to room temperature and vented to atmospheric pressure. NMR spectra of the crude reaction mixture were taken in CDCl₃ to obtain conversions of the alkenes and branched to linear ratios of the produced aldehydes.

A1.5 References

1. Landis, C. R.; Jin, W.; Owen, J. S.; Clark, T. P. *Angew. Chem. Int. Ed.* **2001**, *40*, 3432–3434.
2. Clark, T. P.; Landis, C. R.; Freed, S. L.; Klosin, J.; Abboud, K. A. *J. Am. Chem. Soc.* **2005**, *127*, 5040–5042.
3. Klosin, J.; Landis, C. R. *Acc. Chem. Res.* **2007**, *40*, 1251–1259.
4. Watkins, A. L.; Hashiguchi, B. G.; Landis, C. R. *Org. Lett.* **2008**, *10*, 4553–4556.
5. McDonald, R. I.; Wong, G. W.; Neupane, R. P.; Stahl, S. S.; Landis, C. R. *J. Am. Chem. Soc.* **2010**, *132*, 14027–14029.
6. Adint, T. T.; Wong, G. W.; Landis, C. R. *J. Org. Chem.* **2013**, *78*, 4231–4238.
7. Abrams, M. L.; Foarta, F.; Landis, C. R. *J. Am. Chem. Soc.* **2014**, *136*, 14583–14588.
8. Neureiter, N. P. *J. Am. Chem. Soc.* **1959**, *81*, 2910–2910.
9. Hellmann, H.; Bader, J.; Birkner, H.; Schumacher, O. *Justus Liebigs Ann. Chem.* **1962**, *659*, 49–63.
10. Rampal, J. B.; Macdonell, G. D.; Edasery, J. P.; Berlin, K. D.; Rahman, A.; Van der Helm, D.; Pietrusiewicz, K. M. *J. Org. Chem.* **1981**, *46*, 1156–1165.
11. G. Märkl, V.; Jin, G. Y.; Schoerner, C. *Tetrahedron Letters* **1980**, *21*, 1409–1412.
12. Märkl, G.; Jin, G. Y. *Tetrahedron Letters* **1980**, *21*, 3467–3470.
13. Märkl, G.; Jin, G. Y. *Tetrahedron Letters* **1981**, *22*, 229–232.
14. Information provided by *Floriana Foarta*.
15. Beach, N. J.; Knapp, S. M. M.; Landis, C. R. *Rev. Sci. Instr.* **2015**, *86*, 104101.
16. Singer, H.; Wilkinson, G. *J. Am. Chem. Soc. A* **1968**, 2516–2520.
17. Musina, E. I.; Khrizanforova, V. V.; Strelnik, I. D.; Valitov, M. I.; Spiridonova, Y. S.; Krivolapov, D. B.; Litvinov, I. A.; Kadirov, M. K.; Lönnecke, P.; Hey-Hawkins, E.; Budnikova, Y. H.; Karasik, A. A.; Sinyashin, O. G. *Chem. Eur. Jour.* **2014**, *20*, 3169–3182.
18. Safari, J.; Gandomi-Ravandi, S. *Synth. Comm.* **2011**, *41*, 645–651.

Appendix 2

Investigations of P–H Bond Insertion Reactions into Metal-Carbenoids

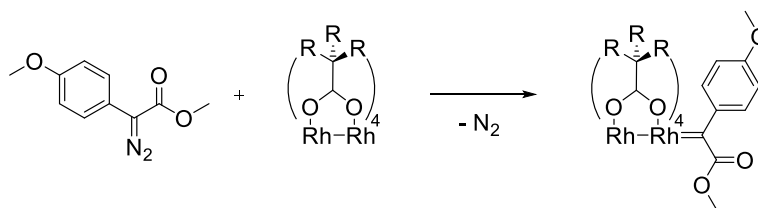
Julia Wildt and Travis Sunderland

A2.1 Abstract

The continued development of synthetic routes to novel organophosphorus compounds is of great importance, especially due to the wide application of chiral phosphorus containing ligands in catalysis. The insertion of metal-carbenoids (derived from diazoesters) into P–H bonds is an attractive route towards the formation of P–C bonds. The reaction of diphenylphosphine and diazoacetate, with or without a catalyst, results in formation of the desired product **3** in minor amounts, in addition to two other major products: the phosphinamide **4** obtained by a P–N bond formation and the subsequent ylide product **5**. The reaction has also been investigated with various diphenylphosphine-borane adducts. Interestingly, the insertion of the metal-carbenoid into the B–H bond was observed with $\text{Ph}_2\text{PH}\cdot\text{BH}_3$ **6**. The use of phosphine adducts with $\text{B}(\text{C}_6\text{F}_5)_3$, BF_3 and BBr_3 did not lead to the production of the desired P–H insertion product.

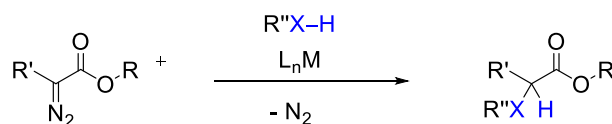
A2.2 Introduction

The functionalization of nonactivated C–H bonds is one of the most challenging transformations in organic chemistry. A great amount of research has been dedicated to the selective activation of C–H bonds through organometallic reactions. One successful route is the metal-carbenoid driven insertion into a C–H bond.^{1, 2} Dirhodium tetracarboxylate paddlewheel complexes have been extensively studied and applied as catalysts in the decomposition of diazo containing compounds, resulting in the formation of a metal-carbenoid species along with the loss of N_2 (Scheme A2.1).^{3, 4}



Scheme A2.1. Reaction of a dirhodium paddlewheel complex and a diazo compound to form a rhodium-carbenoid complex.

This concept of selective insertion into a C–H bond was further expanded towards X–H bonds, e.g. Si–H, S–H, O–H as well as N–H bonds (Scheme A2.1).^{5, 6}



Scheme A2.1. X–H bond insertion reaction based on catalytic carbenoid formation.

Exploration of catalytic P–H-bond insertion reactions has been scarce. Installation of P–C bonds into molecules is of great importance, in particular in the preparation of insecticides, agricultural chemicals, flame retardants, medicinal agents and reagents for olefination reactions, but also in the development of new phosphorus based ligands for metal-catalyzed reactions. The utilization of chiral phosphorus ligands for stereoselective transformations is especially significant due to the ever rising use of enantiomerically pure reagents and pharmaceutically important drugs.⁷ The majority of organophosphorus compounds are synthesized by reaction starting with phosphinylidene precursors (P(=O)H) or other phosphine oxides to create new P–C-bonds.⁸ Insertion reactions into P–H-bonds have been performed previously, however, also utilizing phosphinylidene as the reagents.^{9–12} Insertion reactions *via* metal-carbenoid catalysis and use of P–H bonds directly from primary and/or secondary phosphines would open a new and rapid route to chiral organophosphorus compounds as such as those shown in Figure A2.1.

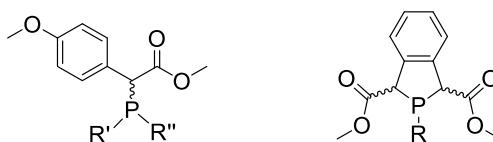


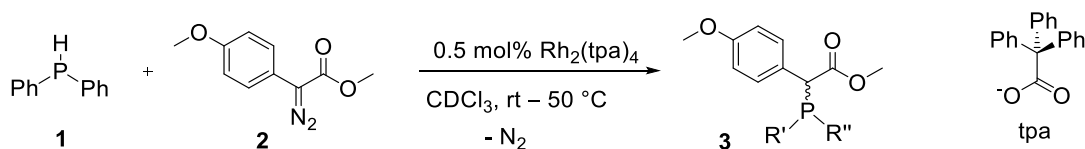
Figure A2.1. Chiral phosphines potentially produced through carbenoid insertion into P–H-bonds.

This project was initially started with the interest of an intra-departmental collaboration. The Landis group has the expertise and interest in the synthesis of chiral phosphine ligands and the Berry group has been investigating dirhodium paddlewheel complexes in the context of C–H-bond insertion chemistry as part of the *Center for Selective C-H Functionalization*. Initial exploration of combining the knowledge of dirhodium paddlewheel complexes along with the phosphine ligand synthesis and handling of this project was started by Dr. Kasia Kornecki (Berry group) and Dr. Ian Tonks (Landis group).

A2.3 Results and Discussion

A2.3.1 Investigation of the Insertion Reaction into the P–H Bond of Diphenylphosphine

Initial experiments towards the synthesis of phosphine **3** by reaction of diphenylphosphine **1** and the *p*-methoxy-phenyldiazoacetate **2** in the presence of a dirhodium tetracarboxylate catalyst were promising and produced the desired compound (Scheme A2.2), however, this reaction is *extremely* sensitive to the chosen conditions and reproducibility has proven very challenging.



Scheme A2.2. Reaction of diphenylphosphine and a diazo compound with Rh₂(tpa)₄.

Herein, we sought to perform a systematic investigation on the product distribution outcome by varying reaction conditions to try to optimize the desired product. Upon addition of diazo **2** to a mixture of the catalyst and phosphine **1** and heating under 50 °C, a mixture of products is observed with only about 50% conversion of the phosphine starting material **1**. The same types of products are observed when reacting **1** and **2** in the *absence* of catalyst, meaning that those identical products are formed by the direct reaction of the starting materials alone.

The desired product is identified as the compound with a chemical shift of 1 ppm in the ^{31}P NMR spectrum (Figure A2.2). Product **4** was isolated and confirmed through ^1H and ^{31}P NMR spectroscopy, 2-dimensional NMR spectroscopic experiments, as well as through ESI-mass spectrometry. This side product is formed by the direct reaction through nucleophilic attack of the phosphine on the terminal nitrogen atom of the diazo compound. It is hypothesized that a subsequent reaction of **4** occurs with another equivalent of diazo **2** to what is believed to be a tertiary phosphine ylide **5**, explaining the loss of the diazo compound over time and presence of leftover phosphine starting material **2**.

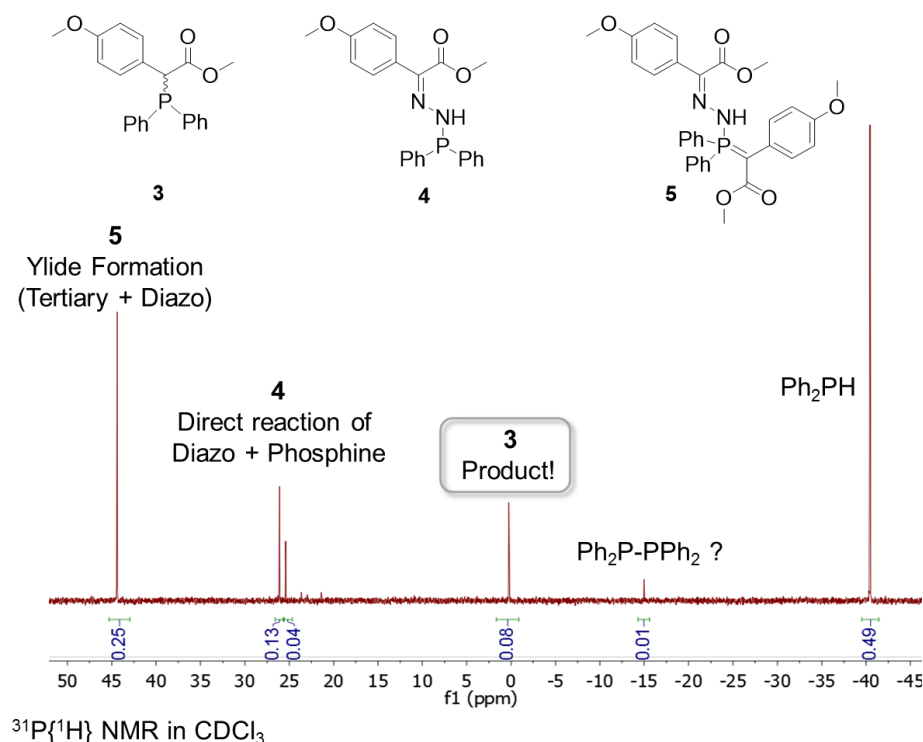


Figure A2.2. Products **3**, **4** and **5** obtained from reaction of phosphine **1** and diazo **2** with or without catalyst and the corresponding ^{31}P NMR spectrum.

Despite the testing of a variety of reaction conditions, the procedure could not be optimized to completely avoid the formation of the side products **4** and **5**. Reaction conditions included varying the order of addition of the reagents, neat and diluted addition, different temperature and reaction times and a variety of concentration conditions. The most successful reaction with the highest amount of product **3** was achieved when diazo **2** was added dropwise as a solution in DCM to a refluxing mixture of the Rh-catalyst and the phosphine **1**. Furthermore, two other catalysts, $\text{IrCl}_2(\text{phebox})(\text{H}_2\text{O})$ and $\text{Ir}(\text{tpp})(\text{CH}_3)$ (Figure A2.3), have been tested, which also led to the product distribution as shown in the ^{31}P NMR spectrum in Figure A2.2.

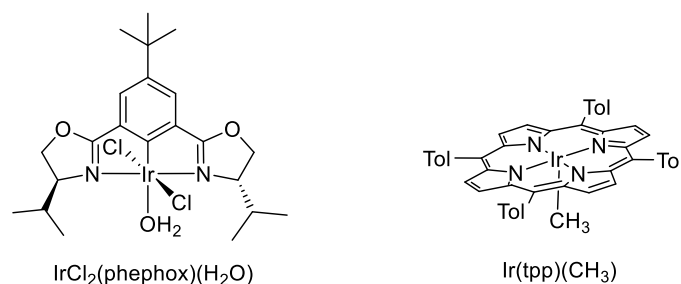
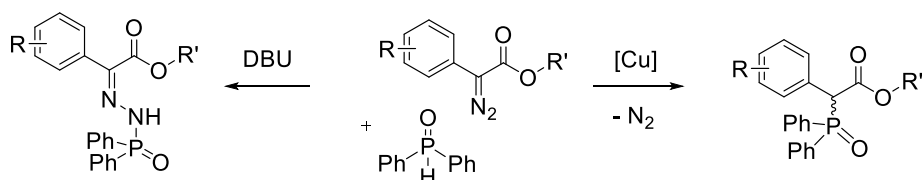


Figure A2.3. Tested catalysts $\text{IrCl}_2(\text{phephox})(\text{H}_2\text{O})$ and $\text{IrCl}_2(\text{tpp})(\text{CH}_3)$.

Evidence for the direct reaction between the a diazo compound and a phosphine compound was also recently demonstrated by Zhu and coworkers using secondary phosphine oxides and aryl diazoacetate derivatives.¹² They found that nucleophilic addition to the terminal N-atom is observed in the presence of catalytic base (DBU), however, when CuBr is used instead, the P–H insertion reaction is favored (Scheme A2.3). The successful P–H insertion reaction demonstrated with phosphine oxides suggested that blocking of the phosphorus lone pair could play a pivotal role in helping prevent significant formation of the direct reaction with the diazo compound and promoting the desired compound instead. Although examples with phosphine oxides have been shown, we sought an alternative route that would avoid the use of phosphine oxides, which would require additional reduction steps to afford our desired compounds.



Scheme A2.3. Switchable phosphination based on the reagent used.

A2.3.2 Borane-protected Diphenylphosphines and Reactivity in P–H Insertion Reaction

Our hypothesis was that borane-protected phosphine compounds should exhibit similar reactivity to the phosphine oxides described above, but be easily deprotected to give the desired

products. Diphenylphosphine was reacted with $\text{BH}_3 \cdot \text{THF}$ to form the phosphine-borane adduct **6** to prevent the nucleophilic attack of the phosphine onto the diazo functional group. The adduct displays interesting splitting patterns in the ^1H , ^{31}P and ^{11}B NMR spectra (Figure A2.4). The H-atom on the phosphorus atom resonates as a doublet of quartets with coupling constants of 396 and 6.9 Hz. The P-atom is observed as a broad doublet with additional couplings to the B- and H-atoms and the B-atom is displayed as a quartet of doublets.

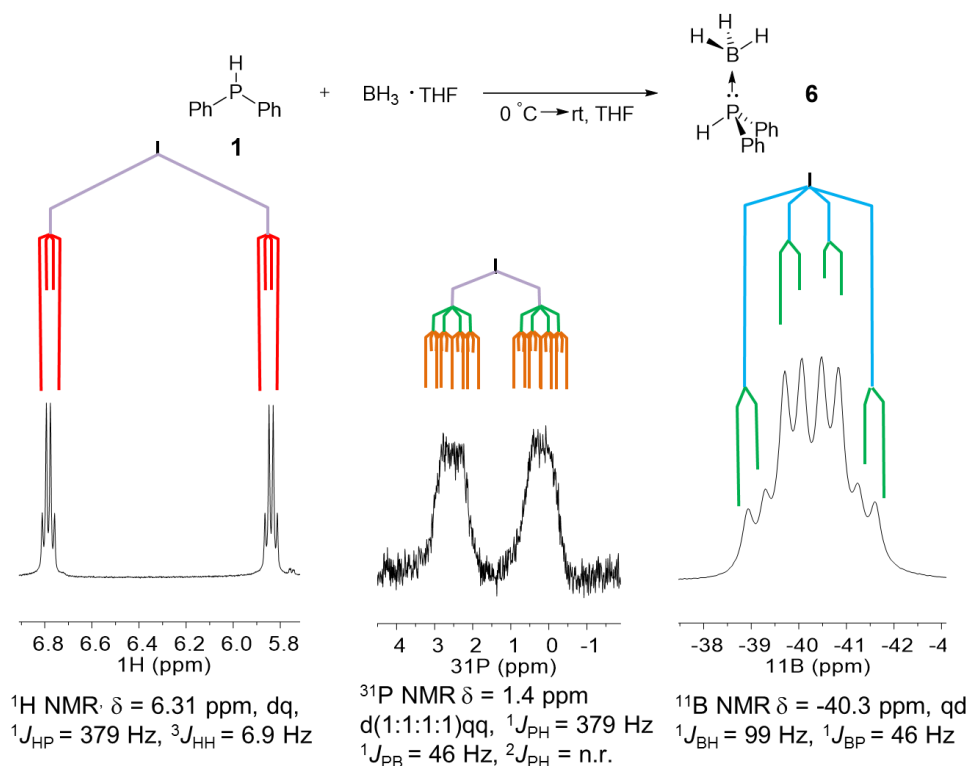
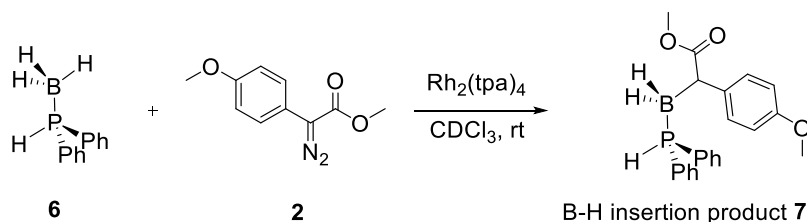


Figure A2.4. NMR splitting pattern for the $\text{Ph}_2\text{PH} \cdot \text{BH}_3$ **6** adduct.

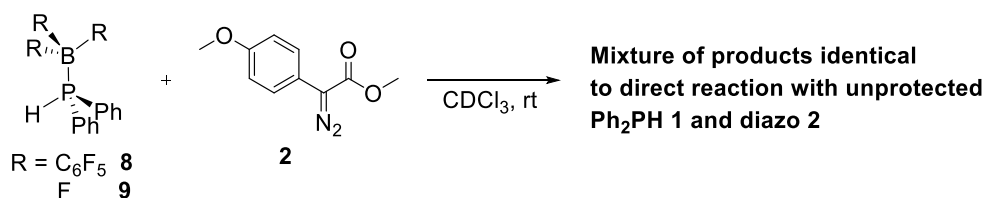
To test our hypothesis that a borane-protected phosphine would not directly react with the diazo compound of interest, a control reaction was conducted that indeed showed that $\text{Ph}_2\text{PH} \cdot \text{BH}_3$ **6** does not react with diazo **2** in CDCl_3 at room temperature. The catalyst was then added to the starting material mixture to promote the desired carbenoid insertion reaction into the P–H bond. Interestingly this leads to carbenoid insertion into the B–H bond instead of giving compound **7**

(Scheme A2.4). The B–H insertion product is displayed as a broad doublet with a chemical shift of -1.8 ppm in the ^{31}P NMR spectrum and as a broad signal at -25 ppm in the ^{11}B NMR spectrum. Concurrent with this result, Zhou and coworkers published a study on carbenoid insertion reactions into B–H bonds of borane-amine adducts, as well as phosphine adducts using a $[\text{Cu}(\text{MeCN})_4]\text{PF}_6$ -catalyst and diazo compounds and expanded it towards production of new chiral organoboranes using chiral nitrogen-based ligands.¹³



Scheme A2.4. B–H bond insertion preferred over a P–H bond insertion.

To avoid this side reaction, other non-hydrido-boranes were used for the phosphine protection. Adduct formation of the phosphine with BPh_3 was not observed, but with $\text{B}(\text{C}_6\text{F}_5)_3$ instead. When $\text{Ph}_2\text{PH} \cdot \text{B}(\text{C}_6\text{F}_5)_3$ **8** was reacted with the diazo compound and the Rh-catalyst, the adduct turns out to be too labile. Products from the direct reaction of the diazo and the Ph_2PH are formed over time. Boranes that would result in stronger P–B-adducts were sought to be utilized instead. Next, BF_3 was also tested and the phosphine-adduct **9** is even weaker than **8**. Already by adding the diazo compound the direct reaction of Ph_2PH **1** and diazo **2** is observed, even in the absence of catalyst (Scheme A2.5).



Scheme A2.5. Borane-phosphine adducts **8** and **9** are too labile under the reaction conditions. As a result, a product mixture from the direct reaction between phosphine **1** and diazo **2** is observed (see Figure A2.1).

With BBr_3 as the protection group for Ph_2PH , the adduct **10** remains intact when performing the reaction with the diazo and the $\text{Rh}_2(\text{tpa})_4$ catalyst. To our surprise, after 15 h, only a single new product is formed in ~30% NMR-yield with a chemical shift at 72 ppm in the ^{31}P NMR spectrum and does not contain a P–H bond (Figure A2.5). However, after letting this reaction run for 24 h, no additional conversion towards this product was observed. The product was not isolated or identified.

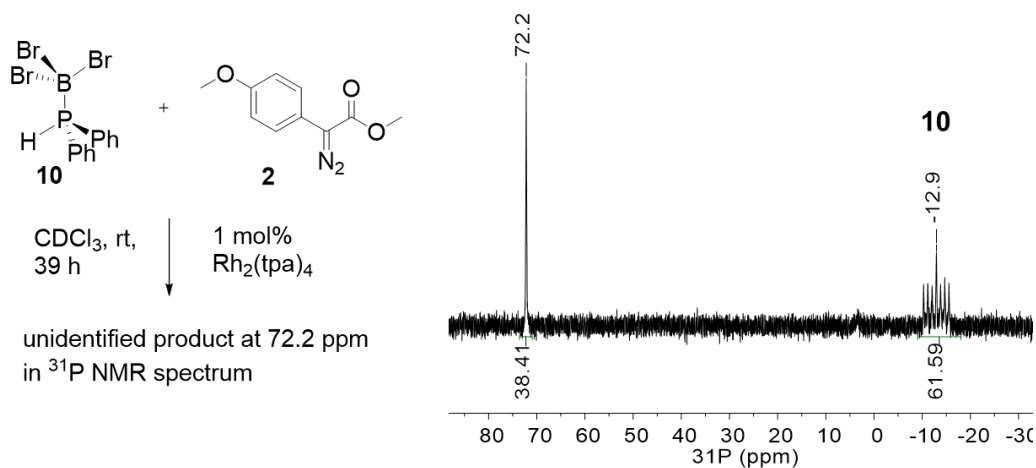
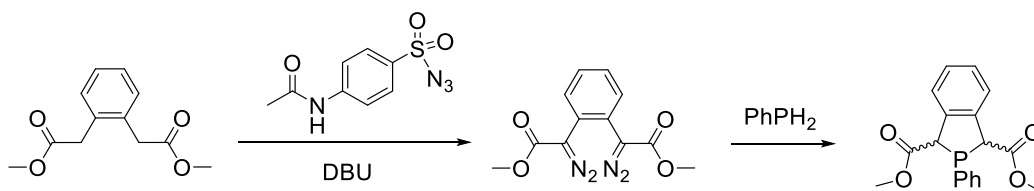


Figure A2.5. Single, unidentified phosphine product in the reaction of **10** and **2**.

A2.4 Conclusion and Future Work

A more detailed and systematic study on the concentration dependence is needed to determine the optimal conditions. One reaction procedure that has yet to be tested that can potentially improve the product formation towards the desired P–H insertion product **3**: the controlled and simultaneous dropwise addition of the phosphine and the diazo as separate solutions to the catalyst. This approach would avoid a high concentration of phosphine when the diazo is added and with that the side reaction to form products **4** and **5** can be minimized.

When the reaction conditions are optimized, the route towards the synthesis of a cyclic phosphine in the proposed route in Scheme A2.6 is to be investigated. This would open routes to new types of phospholane structures to act as phosphine ligands in catalysis.



Scheme A2.6. Proposed synthesis towards a phospholane through a reaction with a *bis*(diazo).

A2.5 Experimental Methods

General Considerations

If not noted otherwise, all air- and moisture-sensitive reactions were carried out under an N₂ atmosphere using standard Schlenk line techniques or a circulating N₂-filled glovebox. All glassware was oven dried, set under vacuum while hot and cooled to room temperature under vacuum. Diphenylphosphine **1** and all boranes were purchased from Sigma-Aldrich and used as obtained. CDCl₃ was purchased from Sigma-Aldrich, distilled from calcium hydride, freeze-pump-thawed to remove oxygen and stored over 3 Å molecular sieves in an air-tight bomb flask. Other

liquid commodity chemicals were degassed by sparging with N₂ prior to usage and solid chemicals were dried for at least 2 h or overnight under vacuum at room temperature.

Routine NMR-spectroscopic measurements (¹H, ¹³C, ³¹P and ¹¹B) were carried out in perdeuterated solvents on Bruker Avance III-400 and Avance III-500 spectrometers. The chemical shifts δ are reported in ppm, coupling constants J in Hz. Splitting patterns were assigned as singlet (s), doublet (d) doublet of quartets (dq), triplet (t), quartet (q or q (1:1:1:1)) quartet of doublet (qd), multiplet (m), broad (br). If not noted additionally, further assignments were done using the correlation experiments ¹H-¹H-COSY, HSQC and HMBC experiments. ¹H and ¹³C NMR spectra were referenced internally to tetramethylsilane (0.00 ppm) or to the residual proton signals of the deuterated solvents ($\delta(^1\text{H})$; (¹³C) = 7.26; 77.16 ppm (CDCl₃); ³¹P and ¹¹B NMR spectra were referenced to an external standard of 85% phosphoric acid (H₃PO₄) and borotriethylfluoride-diethyletherate (BF₃·OEt₂), respectively.

Diazoester **2**¹⁴, Rh₂(tpa)₄¹⁵ and IrCl₂(phebox)(H₂O)¹⁶ were synthesized according to literature procedures. Ir(tpp)(CH₃) was provided by Dr. Bernie J. Anding and the Woo group.

General Procedure for the Reaction of **1** and **2**.

Diphenylphosphine (12.5 μL , 0.072 mmol, 1.0 equiv) was placed in an NMR tube and dissolved in CDCl₃ (0.2 mL) and the NMR tube attached to a Schlenk NMR tube adapter. Diazo compound **2** (15.4 mg, 0.0735 mmol, 1.03 equiv) was dissolved in CDCl₃ (0.3 mL) and added dropwise to the NMR tube *via* syringe. The NMR tube adapter was sealed and heated at 50 °C. NMR spectra were collected upon cooling.

General Procedure for the Reaction of **1**, **2** and Catalyst

Rh₂(tpa)₄•2 MeOH (1 mol%) was heated under vacuum at 130 °C for 2 h until it turned yellow and was then dissolved in CDCl₃ (0.25 mL). Diphenylphosphine (12.5 μL , 0.072 mmol, 1.0 equiv)

was added to the yellow solution. Diazo compound **2** (15.4 mg, 0.0735 mmol, 1.03 equiv) was dissolved in CDCl_3 (0.3 mL) and added dropwise to the reaction mixture. The orange solution was heated at 50 °C. Aliquots were taken to obtain NMR spectra typically after 1, 4 and 20 h. This reaction has also been repeated in a total of 3 mL volume. One other modification included the addition of diazo **2** as a solution in DCM, while the catalyst and the phosphine were heated to reflux in DCM.

P–H insertion Product (3): not all signal can be assigned due to overlap. ^1H NMR (400 MHz, CDCl_3 , ppm): δ = 7.58 (H^{Ar}), 7.38 (H^{Ar}), 7.31 (H^{Ar}), 7.17 (H^{Ar}), 4.40 (d, $^2J_{\text{H-P}}$ = 5.1 Hz, 1H, ArC(H)COOMe); $^{31}\text{P}\{^1\text{H}\}$ NMR (162 MHz, CDCl_3 , ppm): δ = 0.2.

Phosphinamide (4). Isolated through flash column chromatography (EtOAc), contains $\text{Ph}_2\text{P(O)H}$ as an impurity (42%) ^1H NMR (400 MHz, CDCl_3 , ppm): δ = 7.90–7.82 (m, 4H, H^{Ar}), 7.58–7.55 (m, 2H, H^{Ar}), 7.53–7.48 (m, 4H, H^{Ar}), 7.37 (d, J = 20.9 Hz, 1H, NH), 7.24 (d, J = 8.8 Hz, 2H, H^{Ar}), 7.00 (d, J = 8.8 Hz, 2H, H^{Ar}), 3.83 (s, 3H, OCH_3), 3.67 (s, 3H, COOCH_3); $^{31}\text{P}\{^1\text{H}\}$ NMR (162 MHz, CDCl_3 , ppm): δ = 25.5; ^{11}B NMR (128 MHz, CDCl_3 , ppm): δ = -25.1 (br, $h_{1/2}$ = 267 Hz).

B–H Insertion Product (7). ^1H NMR (400 MHz, CDCl_3 , ppm): δ = 7.61–7.52 (m, 4H, H^{Ar}), 7.51–7.36 (m, 6H, H^{Ar}), 7.20 (d, J = 8.7 Hz, 2H, H^{Ar}), 6.74 (d, J = 8.7 Hz, 2H, H^{Ar}), 5.98 (dt, $^1J_{\text{H-P}}$ = 386.7 Hz, J = 15.8 Hz, 1H, PH), 3.75 (s, 3H, OCH_3), 3.50 (s, 3H, COOCH_3), 3.19 (dt, J = 12.4, 5.8 Hz, 1H, ArC(H)COOMe), 2.09 (brq (1:1:1:1), $^1J_{\text{H-B}}$ = n.r., 2H, BH); ^{31}P NMR (162 MHz, CDCl_3 , ppm): δ = -1.8 (brd, $^1J_{\text{P-H}}$ = 392 Hz); ^{11}B NMR (128 MHz, CDCl_3 , ppm): δ = -25.1 (br, $h_{1/2}$ = 267 Hz).

General Synthesis of Ph₂PH-Borane Adducts

Diphenylphosphine (40 μ L, 0.230 mmol, 1.0 equiv) was placed in a Schlenk flask. The borane was added via syringe (0.253 mmol, 1.1 equiv) directly to the flask, solid borane reagents were dissolved first in CDCl₃ (0.2 mL). The reaction mixture was stirred overnight and all volatiles were removed under vacuum. The obtained product was typically used without further purification.

Ph₂PH•BH₃ (**6**). **¹H NMR** (400 MHz, CDCl₃, ppm): δ = 7.61–7.51 (m, 4H, H^{Ar}), 7.44–7.2 (m, 6H, H^{Ar}), 6.20 (dq, ¹J_{H-P} = 379.2 Hz, *J* = 7.0 Hz, 1H, *PH*), 1.01 (q (1:1:1:1), ¹J_{H-B} = 99 Hz, 3H, *BH*); **³¹P NMR** (162 MHz, CDCl₃, ppm): δ = -0.4 (brdd, ¹J_{P-H} = 379.2 Hz, ¹J_{P-B} = 46 Hz); **¹¹B NMR** (128 MHz, CDCl₃, ppm): δ = -40.1 (qd, ¹J_{B-H} = 99 Hz, ¹J_{B-P} = 46 Hz).

Ph₂PH•B(C₆F₅)₃ (**8**). **¹H NMR** (400 MHz, CDCl₃, ppm): δ = 7.55 (t, *J* = 7.6 Hz, 4H, H^{Ar}), 7.43–7.28 (m, 6H, H^{Ar}), 6.97 (d, ¹J_{H-P} = 416 Hz, 1H, *PH*); **³¹P NMR** (162 MHz, CDCl₃, ppm): δ = -0.4 (brd, ¹J_{P-H} = 416 Hz); **¹¹B NMR** (128 MHz, CDCl₃, ppm): δ = -12.8; **¹⁹F NMR** (377 MHz, CDCl₃, ppm): δ = n.d.

Ph₂PH•BF₃ (**9**). **¹H NMR** (400 MHz, CDCl₃, ppm): δ = 7.48–7.34 (m, 4H, H^{Ar}), 7.30–7.19 (m, 6H, H^{Ar}), 5.21 (brd, ¹J_{H-P} = 136 Hz, 1H, *PH*); **³¹P NMR** (162 MHz, CDCl₃, ppm): δ = -40.3 (brd, ¹J_{P-H} = 136 Hz); **¹¹B NMR** (128 MHz, CDCl₃, ppm): δ = -0.7; **¹⁹F{¹H} NMR** (377 MHz, CDCl₃, ppm): δ = -148.1.

A2.6 References

1. Doyle, M. P.; Duffy, R.; Ratnikov, M.; Zhou, L. *Chem. Rev.* **2010**, *110*, 704–724.
2. Davies, H. M. L.; Manning, J. R., *Nature* **2008**, *451*, 417–424.

3. Cotton, F. A.; DeBoer, B. G.; Laprade, M. D.; Pipal, J. R.; Ucko, D. A., *J. Am. Chem. Soc.* **1970**, *92*, 2926–2927.
4. Doyle, M. P. *J. Org. Chem.* **2006**, *71*, 9253–9260.
5. Zhu, S.-F.; Zhou, Q.-L. *Acc. Chem. Res.* **2012**, *45*, 1365–1377.
6. Gillingham, D.; Fei, N. *Chem. Soc. Rev.* **2013**, *42*, 4918–4931.
7. Engel, R.; Cohen, J. L. I. *Synthesis of Carbon-Phosphorus Bonds, Second Edition*. CRC Press LLC: Boca Raton, Florida, **2003**.
8. Coudray, L.; Montchamp, J.-L. *Eur. J. Org. Chem.* **2008**, *2008*, 3601–3613.
9. Polozov, A. M.; Polezhaeva, N. A.; Mustaphin, A. H.; Khotinen, A. V.; Arbuzov, B. A. *Synthesis* **1990**, *6*, 515–517.
10. Bartrum, H. E.; Blakemore, D. C.; Moody, C. J.; Hayes, C. J. *Tetrahedron* **2013**, *69*, 2276–2282.
11. Chen, Z.-S.; Zhou, Z.-Z.; Hua, H.-L.; Duan, X.-H.; Luo, J.-Y.; Wang, J.; Zhou, P.-X.; Liang, Y.-M. *Tetrahedron* **2013**, *69*, 1065–1068.
12. Jiang, H.; Jin, H.; Abdukader, A.; Lin, A.; Cheng, Y.; Zhu, C. **2013**, *11*, 3612–3615.
13. Cheng, Q.-Q.; Zhu, S.-F.; Zhang, Y.-Z.; Xie, X.-L.; Zhou, Q.-L. *J. Am. Chem. Soc.* **2013**, *135*, 14094–14097.
14. Chan, W.-W.; Yeung, S.-H.; Zhou, Z.; Chan, A. S. C.; Yu, W.-Y. *Org. Lett.* **2010**, *12*, 604–607.
15. Hashimoto, S.-i.; Watanabe, N.; Ikegami, S. *Tetrahedron Letters* **1992**, *33*, 2709–2712.
16. Owens, C. P.; Varela-Alvarez, A.; Boyarskikh, V.; Musaev, D. G.; Davies, H. M. L.; Blakey, S. B. *Chem. Sci.* **2013**, *4*, 2590–2596.
17. Oehlke, A. Chromophore Arylboronsaeureester und ihr Komplexbildungsverhalten gegenueber LEWIS-Basen. *Dissertation*, Technische Universitaet Chemnitz, **2010**.
18. Lautens, M.; Mancuso, J. *J. Org. Chem.* **2004**, *69*, 3478–3487.

Appendix 3

Supporting Information

Table of Contents

A3.1	NMR Spectra from Chapter 3	173
A3.2	Crystallographic Data from Chapter 3	188
A3.2.1	Crystallographic Data for TPSB BDP 1	188
A3.2.2	Crystallographic Data for red-TPSB BDP 2	207
A3.2.3	Crystallographic Data for red-TPPB BDP 4	219
A3.2.4	Crystallographic Data for TNSB BDP 7	227
A3.2.5	Crystallographic Data for red-TNSB BDP 8	252
A3.2.6	Crystallographic Data for [Rh(acac)(TPSB BDP 1)]	263
A3.3	NMR Spectra from Chapter 4	278
A3.4	Crystallographic Data from Chapter 4	292
A3.4.1	Crystallographic Data for Diazaborine 2	292
A3.4.2	Crystallographic Data for o-Bpin DiazaPhos 8	302
A3.4.3	Crystallographic Data for o-Me DiazaPhos 16	318
A3.5	NMR Spectra from Appendix 1	344
A3.6	NMR Spectra from Appendix 2	352

A3.1 NMR Spectra from Chapter 3

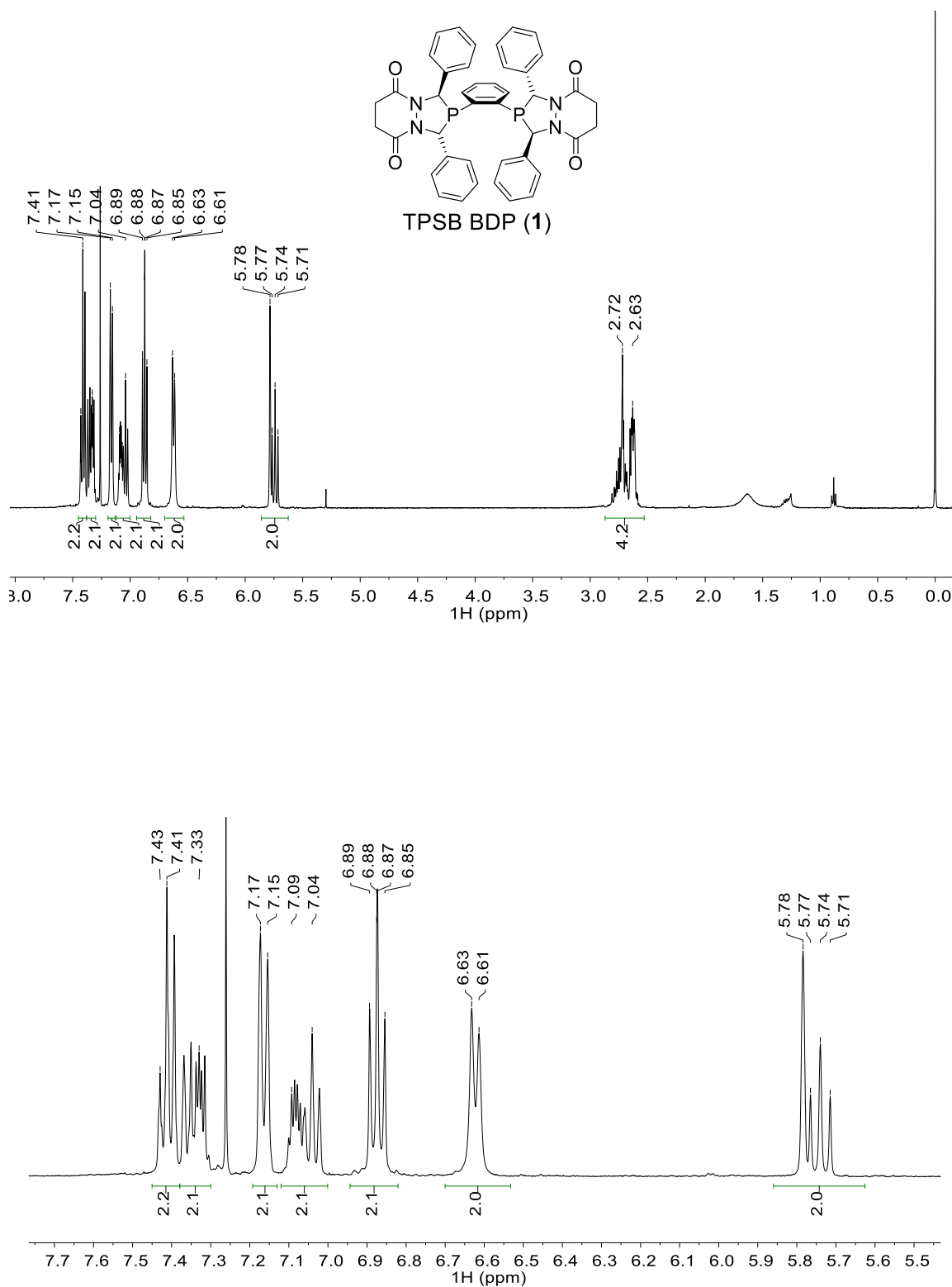


Figure A3.1. ^1H NMR spectrum of **1** in CDCl_3 (top: full spectrum, bottom: zoom).

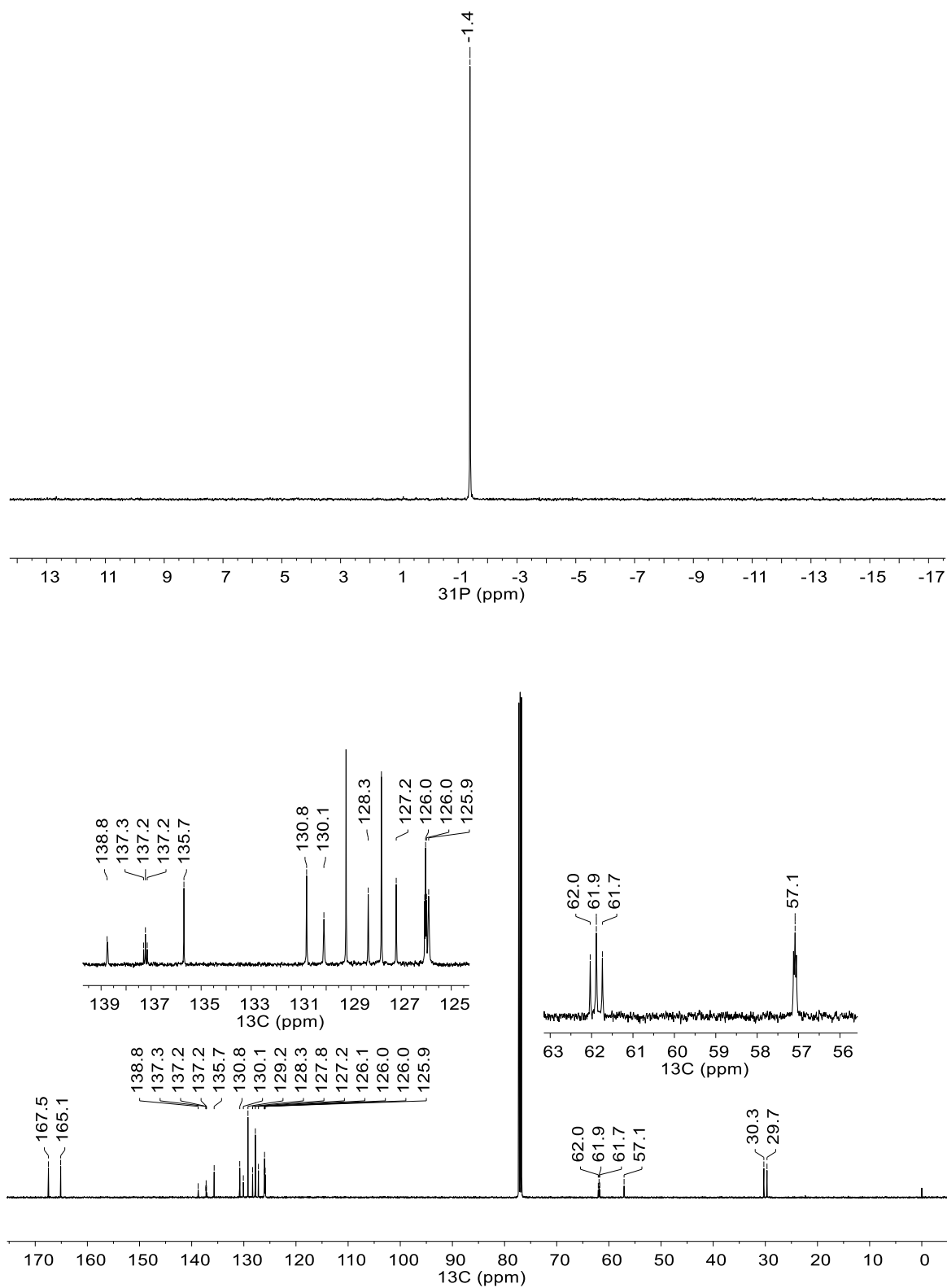


Figure A3.2. NMR spectra of **1** in CDCl_3 (top: $^{31}\text{P}\{^1\text{H}\}$, bottom: $^{13}\text{C}\{^1\text{H}\}$ bottom).

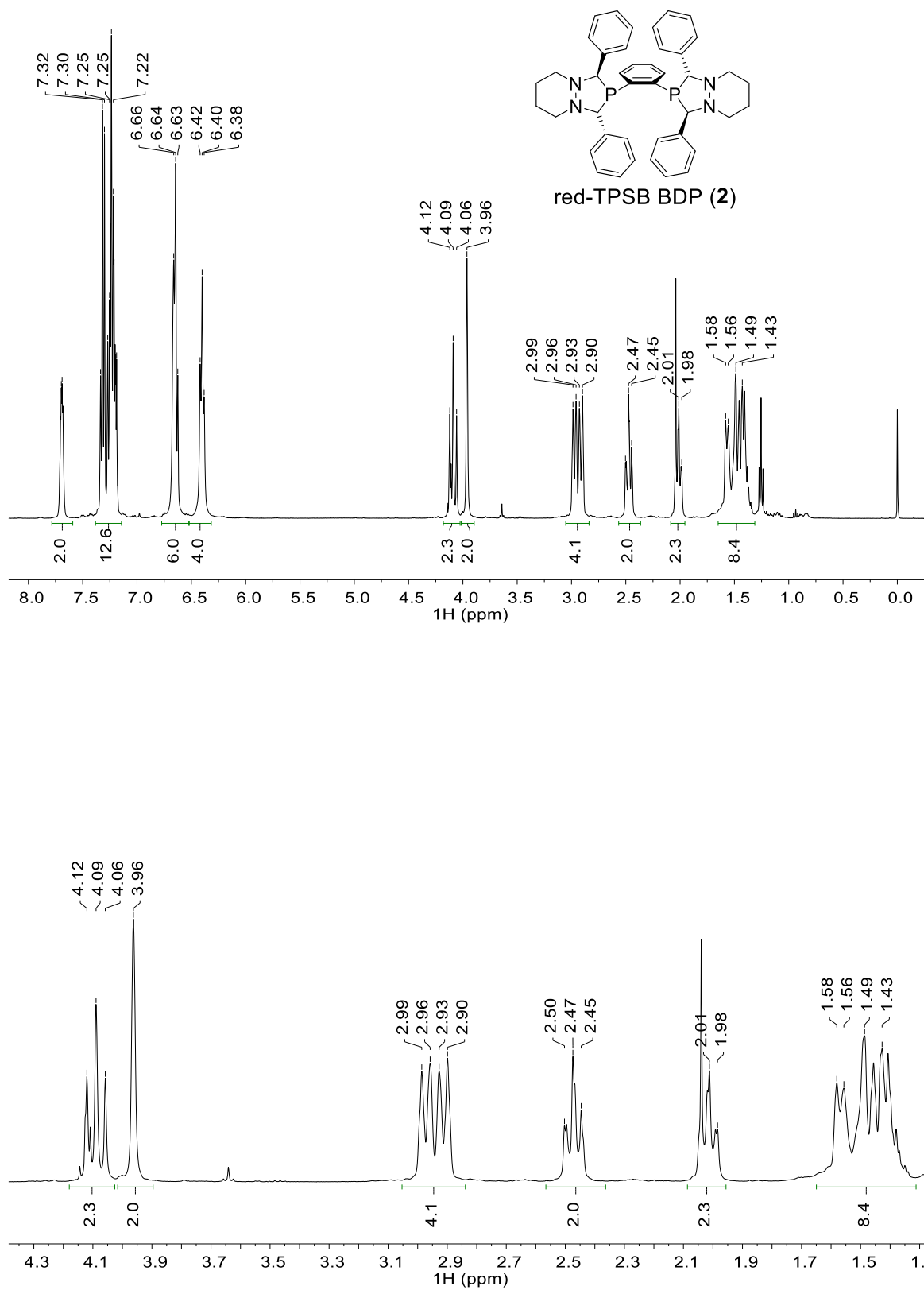


Figure A3.3. ^1H NMR spectrum of **2** in CDCl_3 (top: full spectrum, bottom: zoom).

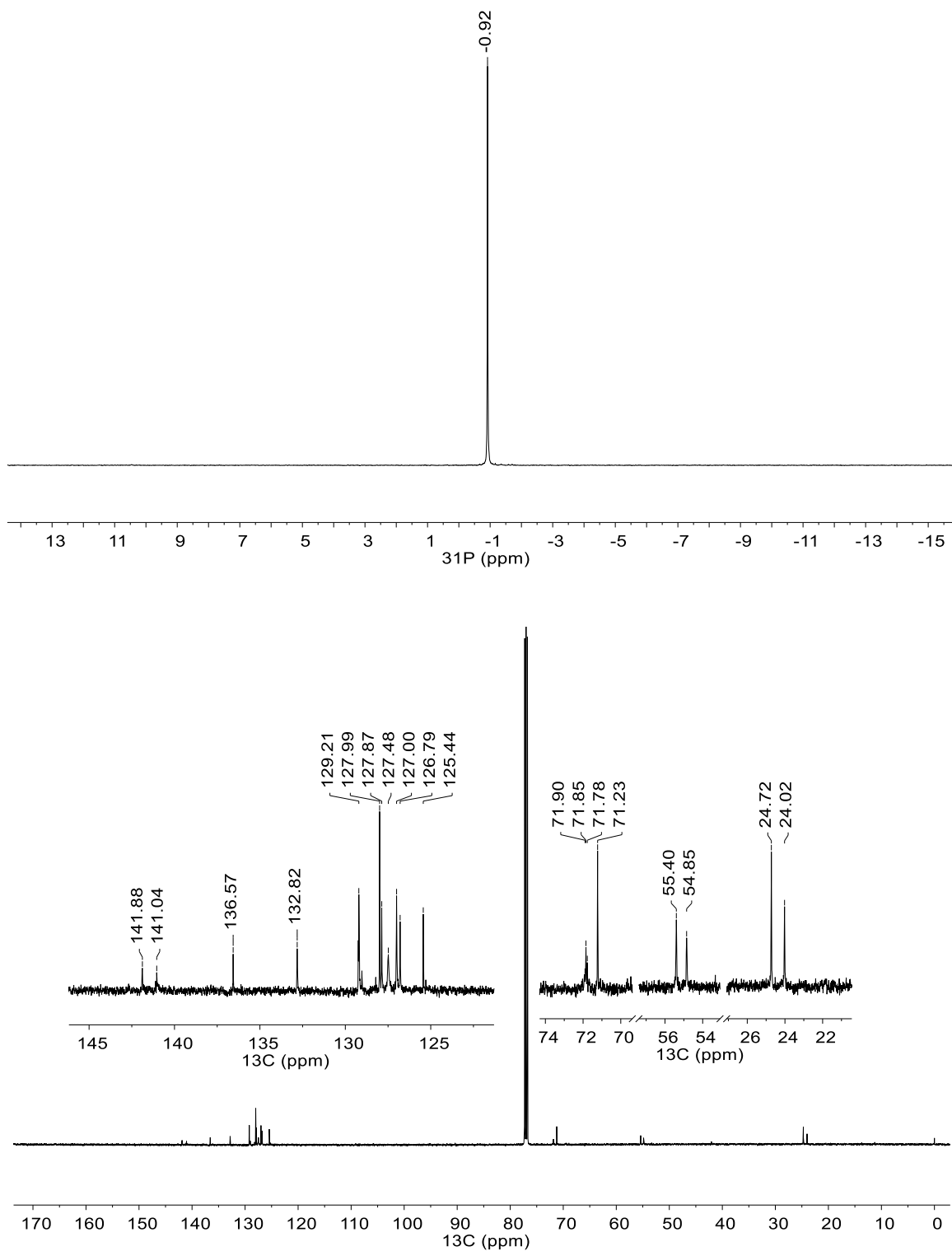


Figure A3. 4. NMR spectra of **2** in CDCl_3 (top: $^{31}\text{P}\{^1\text{H}\}$, bottom: $^{13}\text{C}\{^1\text{H}\}$ bottom).

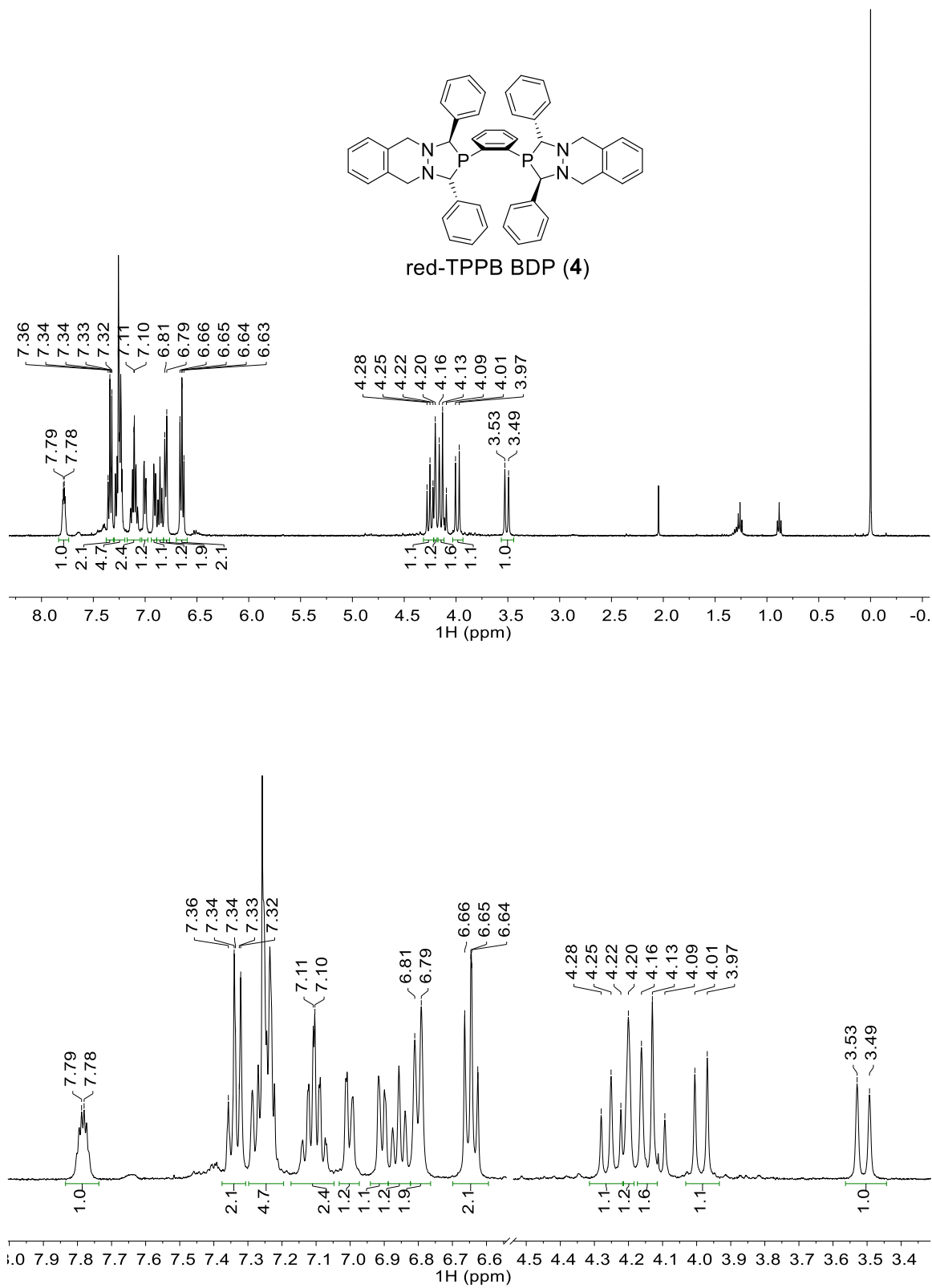


Figure A3.5. ^1H NMR spectrum of **4** in CDCl_3 (top: full spectrum, bottom: zoom).

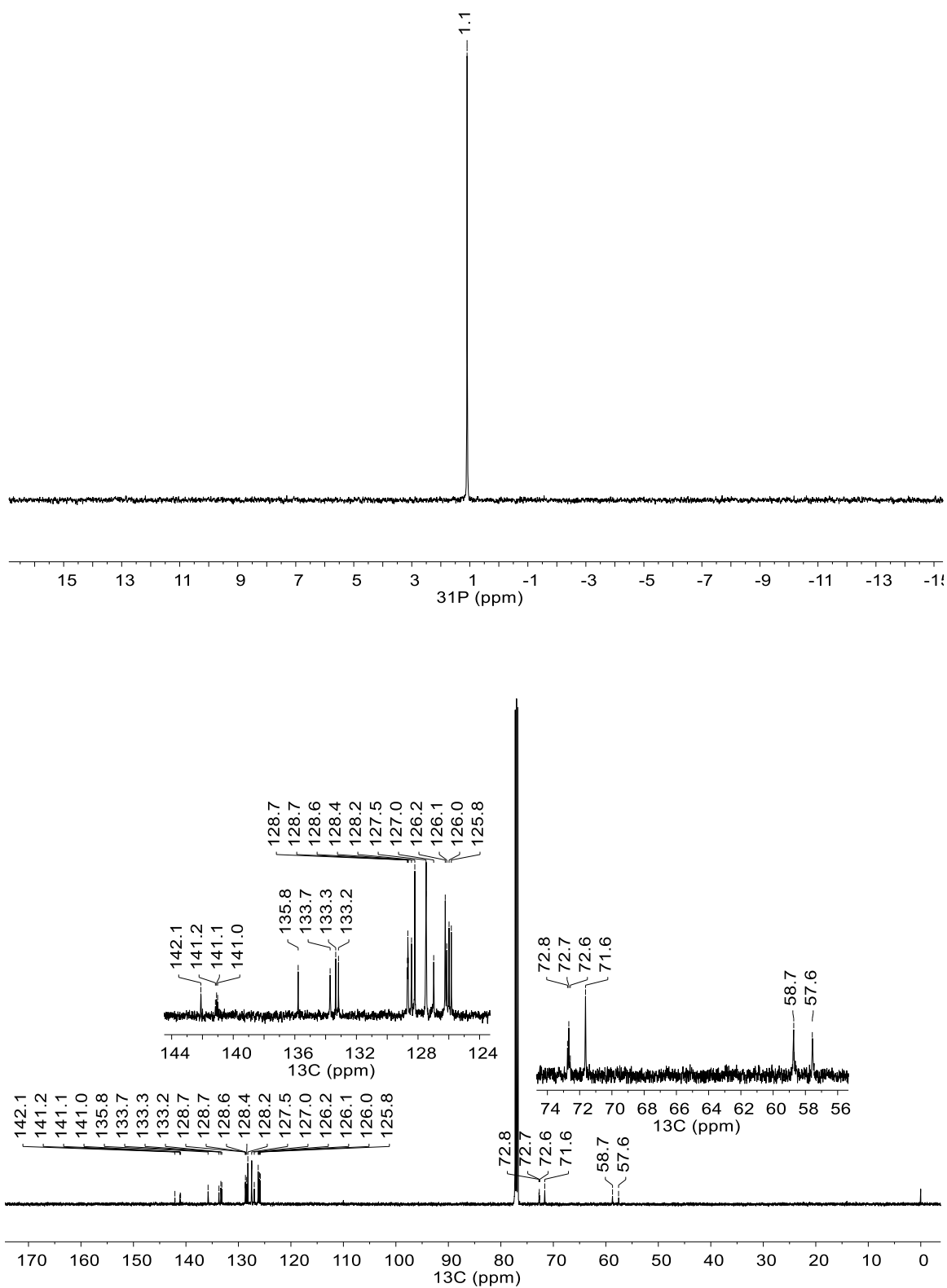


Figure A3.6. NMR spectra of **4** in CDCl_3 (top: $^{31}\text{P}\{^1\text{H}\}$, bottom: $^{13}\text{C}\{^1\text{H}\}$ bottom).

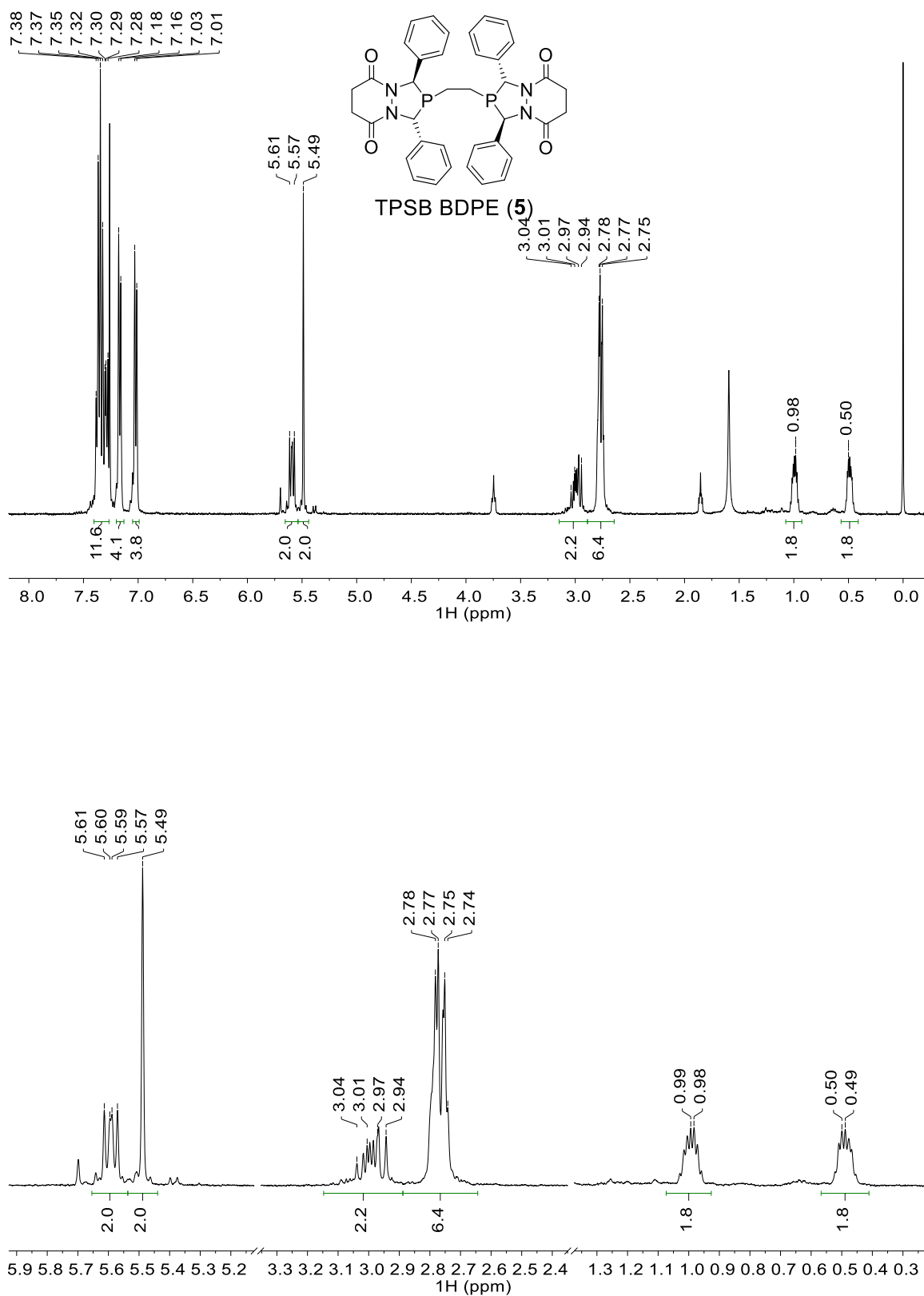


Figure A3.7. ^1H NMR spectrum of **5** in CDCl_3 (top: full spectrum, bottom: zoom).

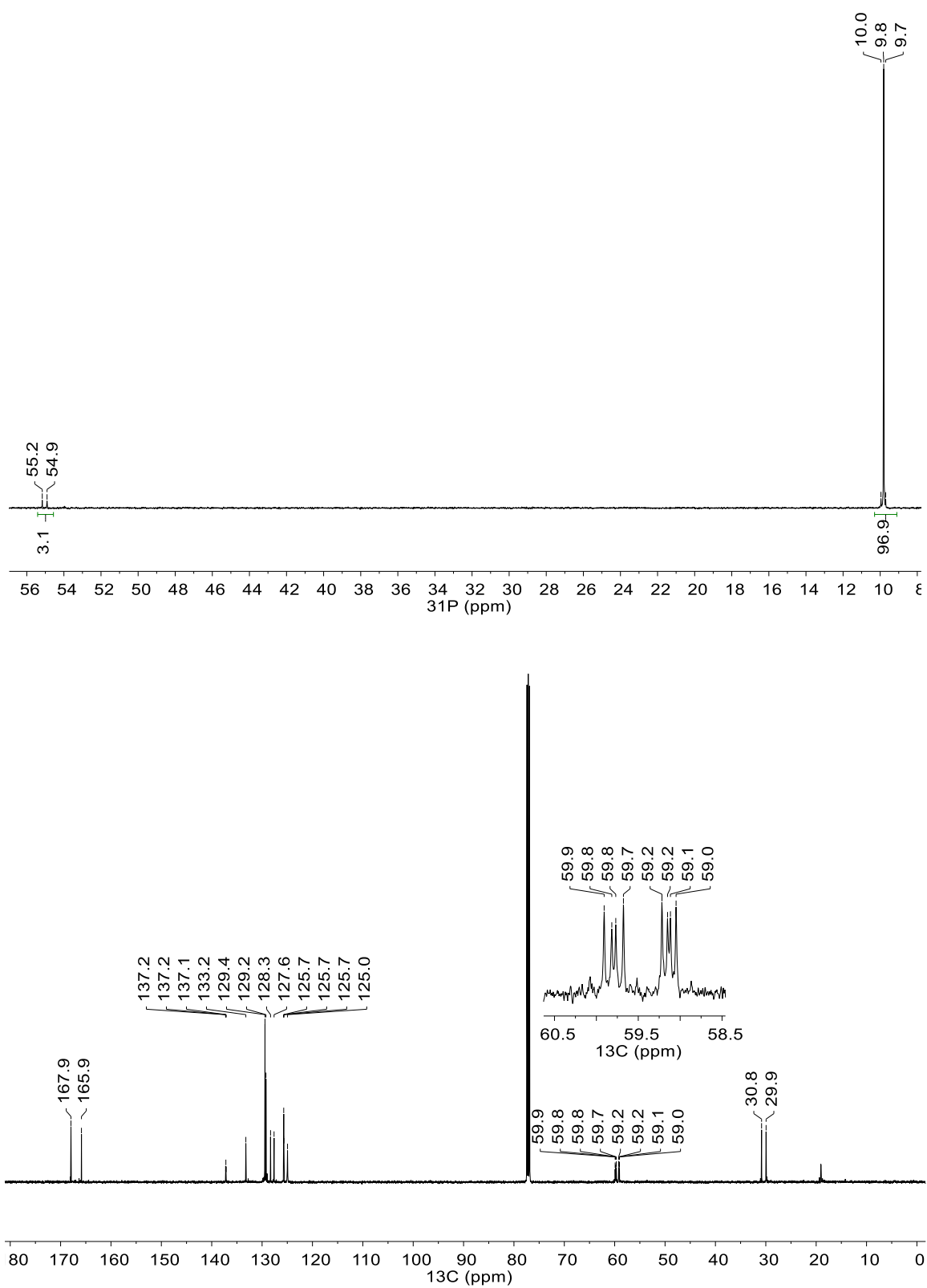


Figure A3.8. NMR spectra of **5** in CDCl_3 (top: $^{31}\text{P}\{^1\text{H}\}$, bottom: $^{13}\text{C}\{^1\text{H}\}$ bottom).

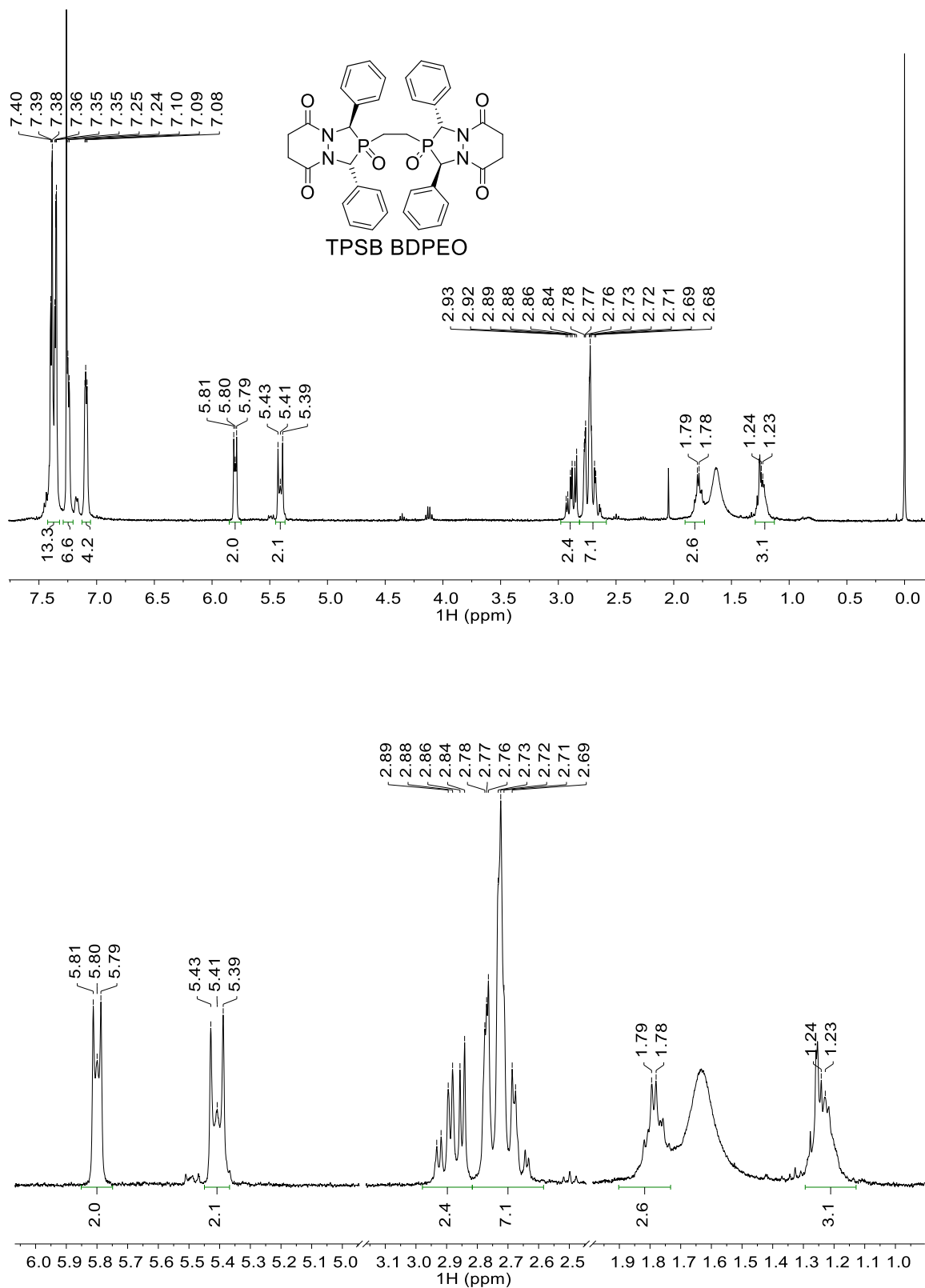


Figure A3.9. ^1H NMR spectrum of TPSB BDPEO in CDCl_3 (top: full spectrum, bottom: zoom).

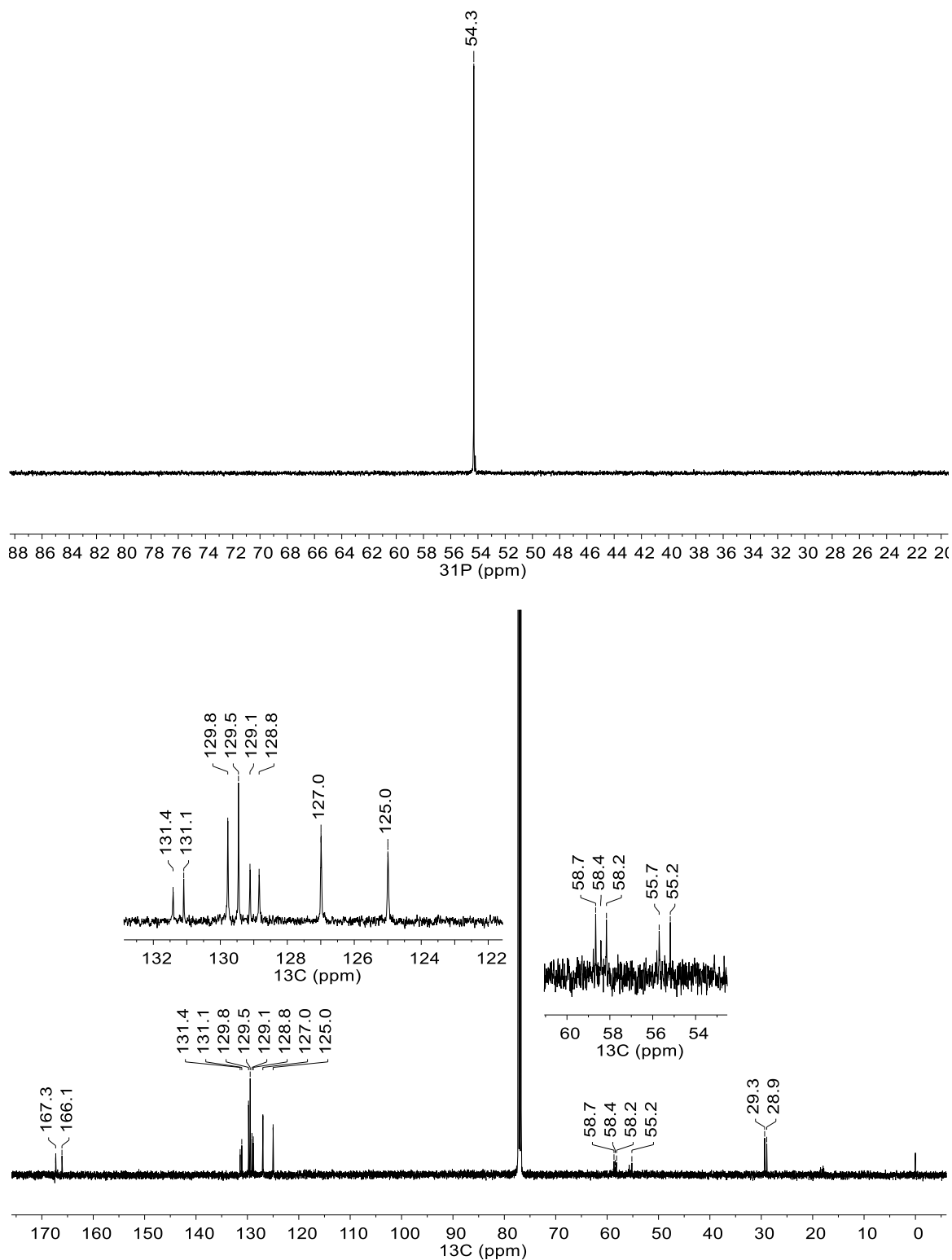


Figure A3.10. NMR spectra of TPSB BDPEO in CDCl_3 (top: $^{31}\text{P}\{^1\text{H}\}$, bottom: $^{13}\text{C}\{^1\text{H}\}$ bottom).

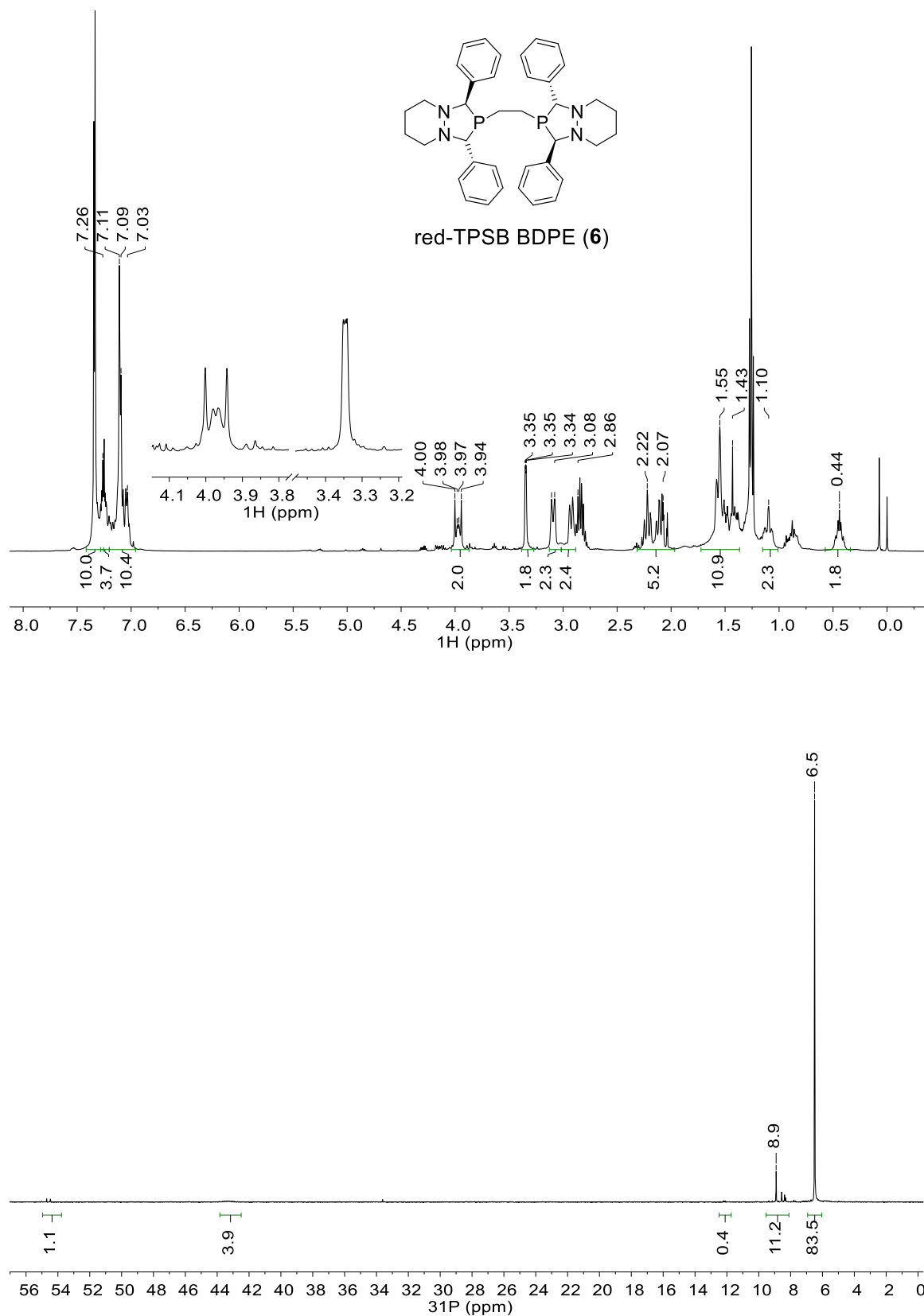


Figure A3.11. NMR spectra of red-TPSB BDPE **6** in CDCl₃ (top:¹H, bottom:³¹P{¹H} bottom).

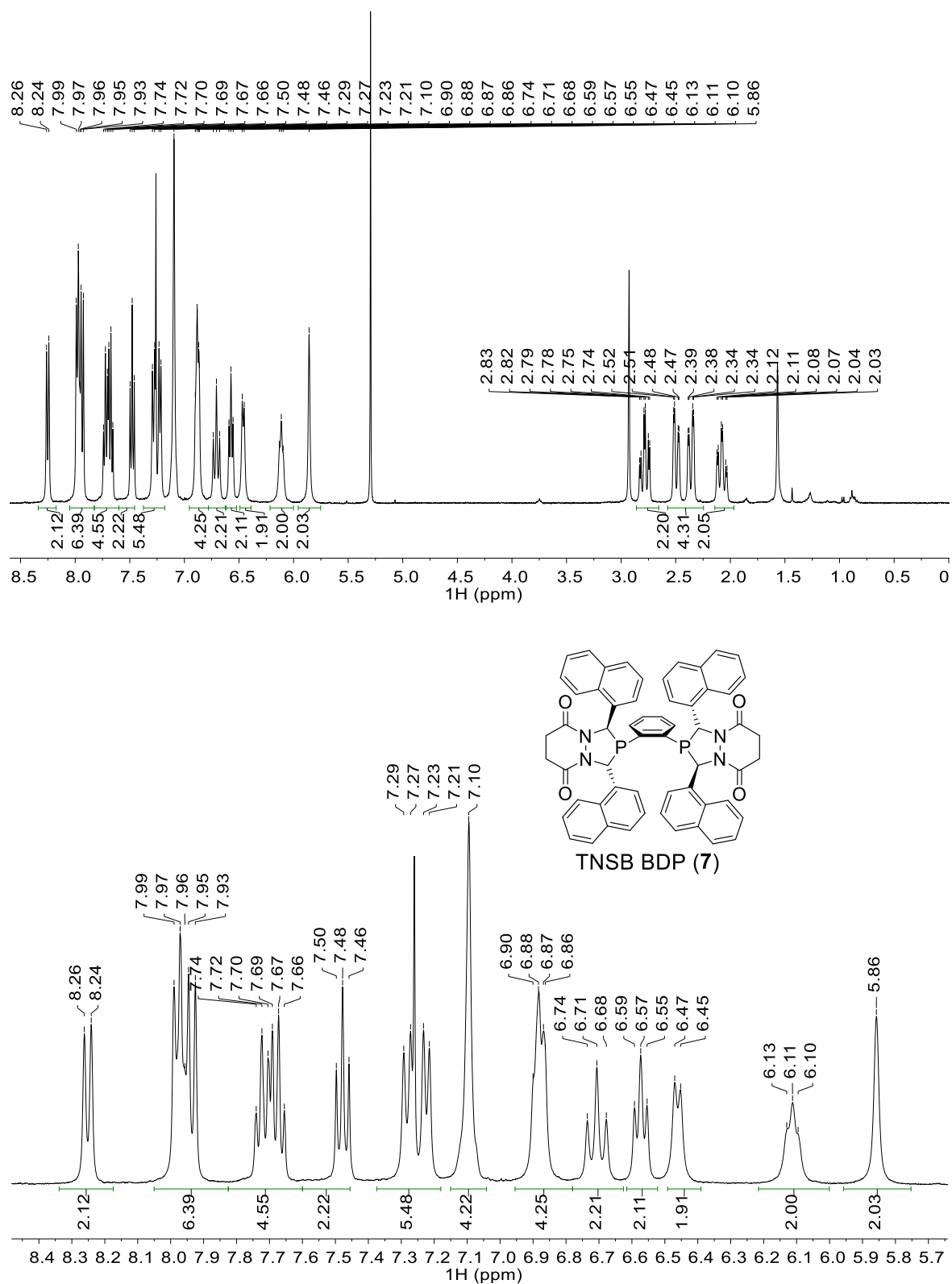


Figure A3.12. ^1H NMR spectrum of TNSB BDP **7** in CDCl_3 (top: full spectrum, bottom: zoom).

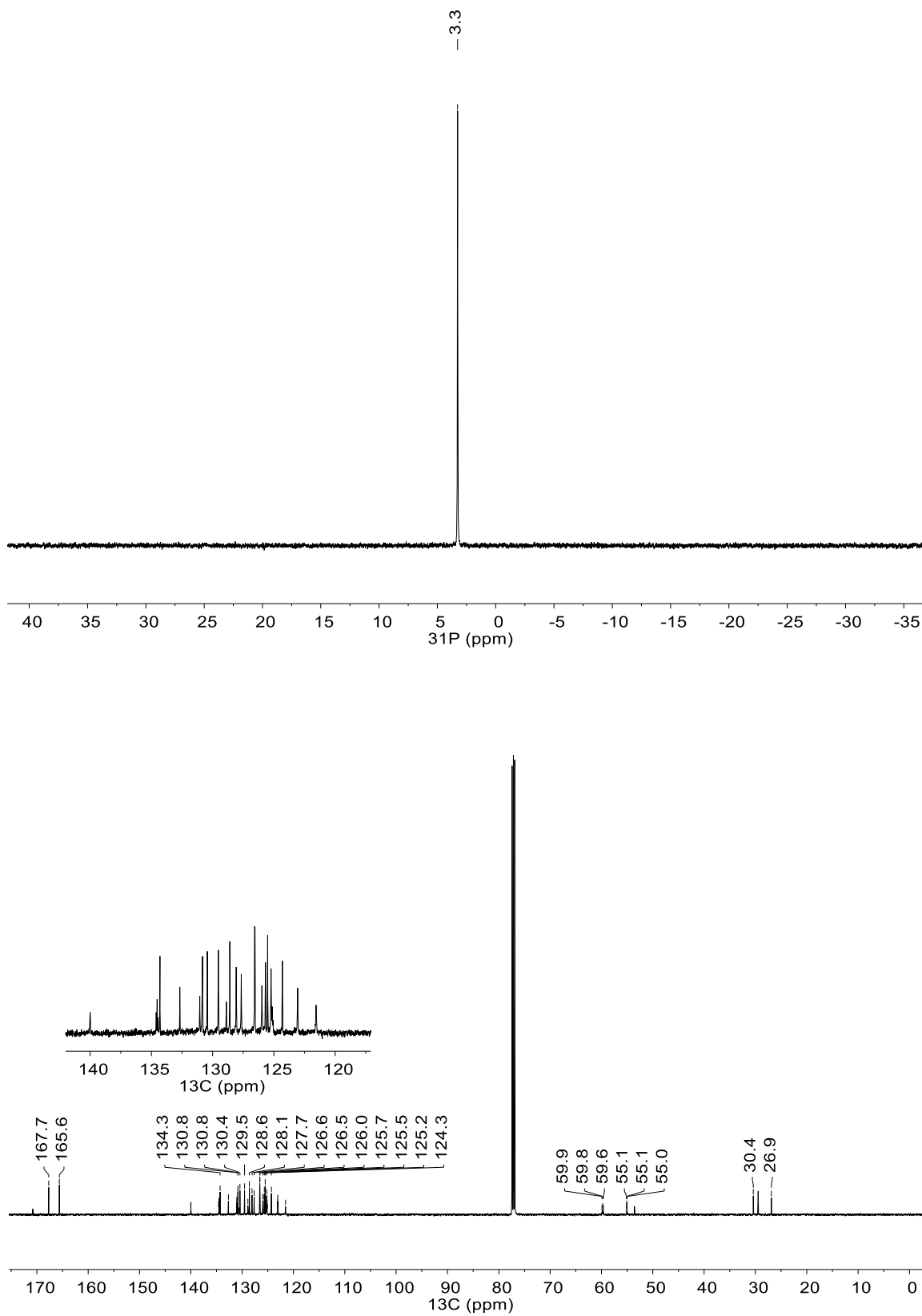


Figure A3.13. NMR spectra of TNSB BDP 7 in CDCl₃ (top: ³¹P{¹H}, bottom: ¹³C{¹H} bottom).

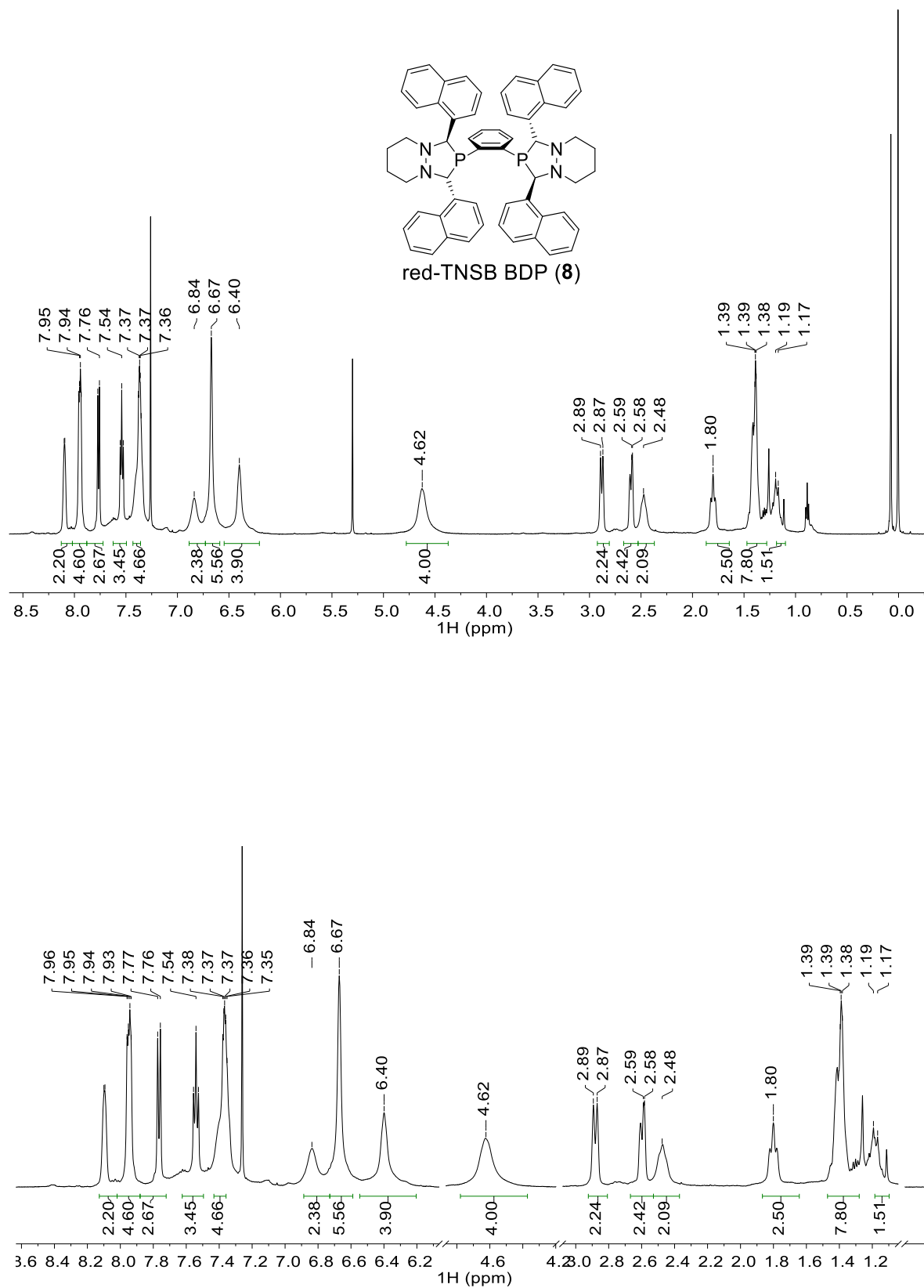


Figure A3.14. ^1H NMR spectrum of red-TNSB BDP **8** in CDCl_3 (top: full spectrum, bottom: zoom).

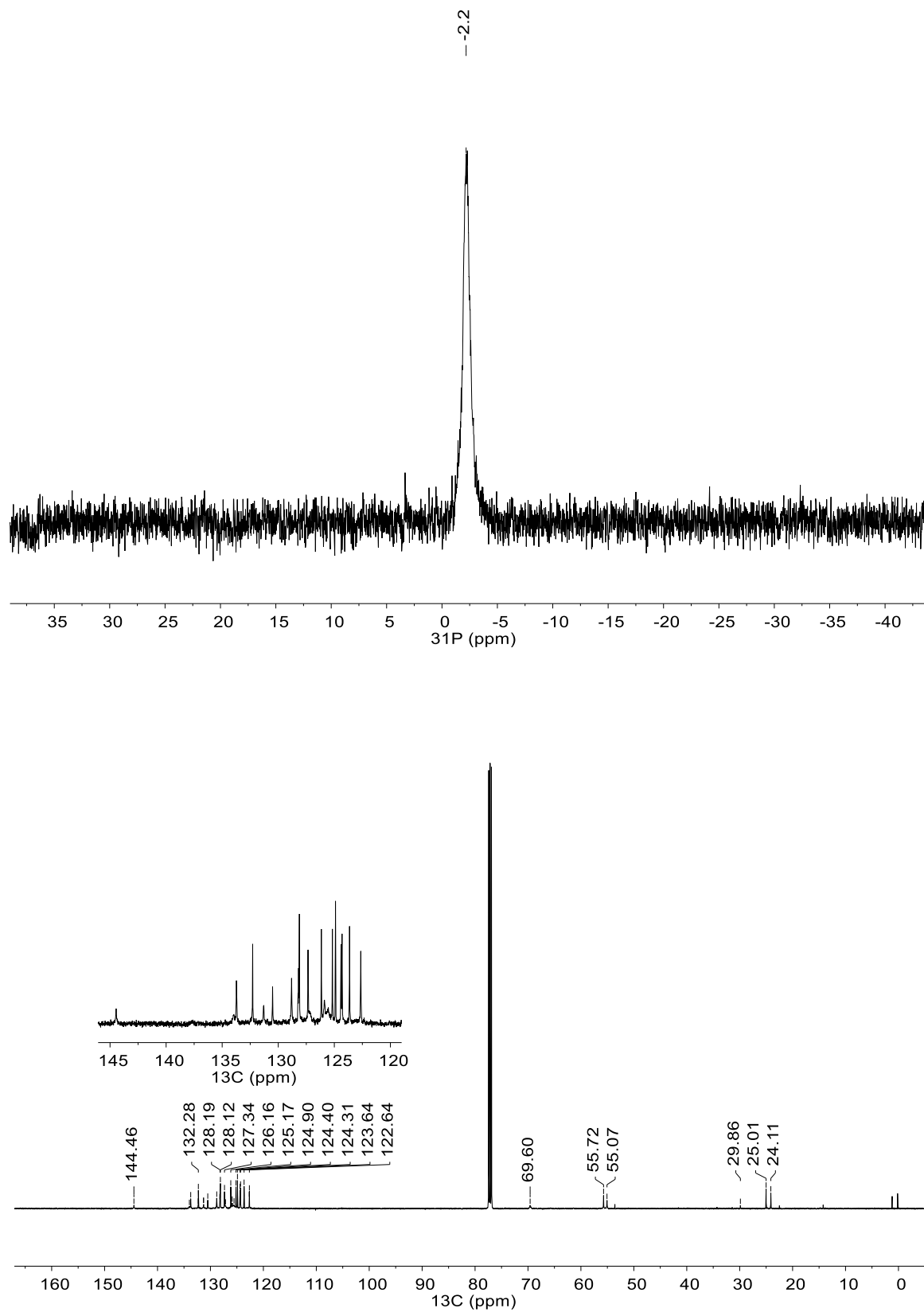


Figure A3.15. NMR spectra of red-TNSB BDP **8** in CDCl_3 (top: $^{31}\text{P}\{^1\text{H}\}$, bottom: $^{13}\text{C}\{^1\text{H}\}$ bottom).

A3.2 Crystallographic Data from Chapter 3

A3.2.1 Crystallographic Data for TPSB BDP 1

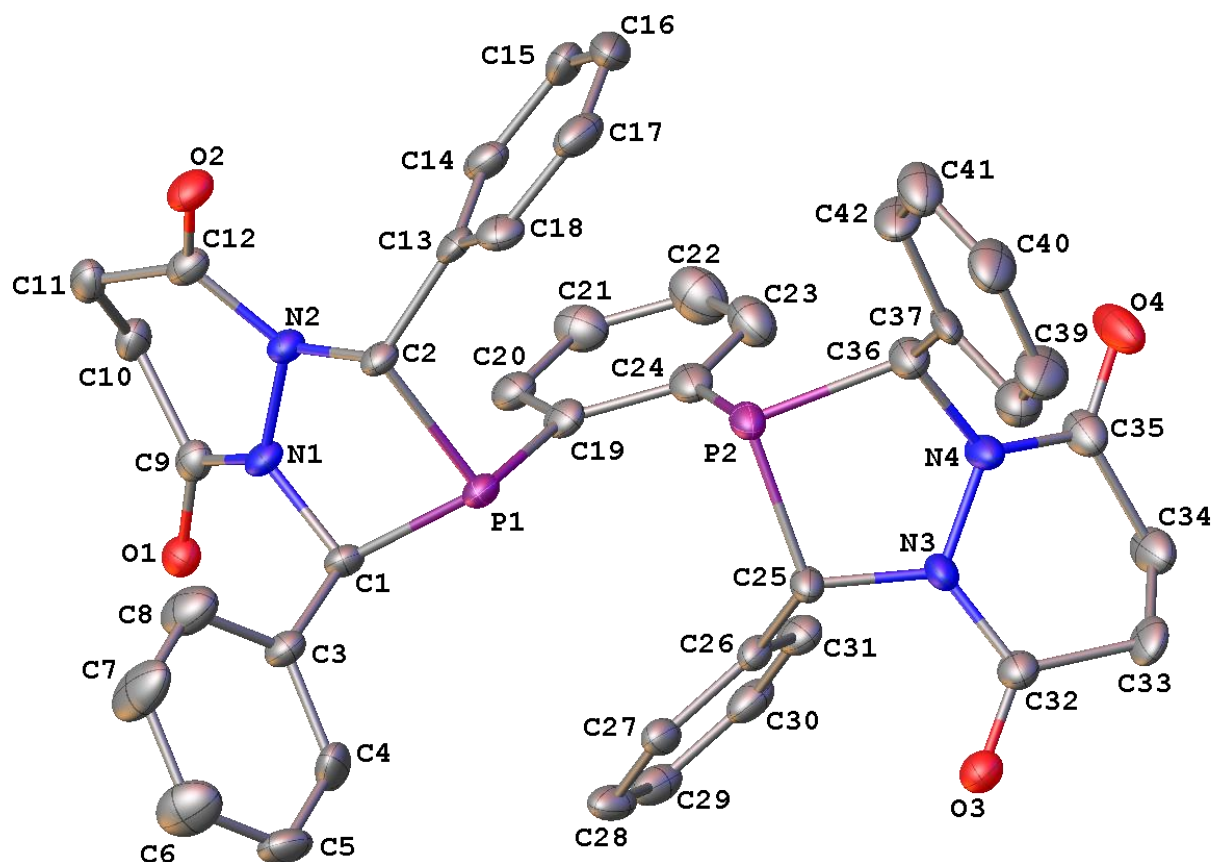


Figure A3.16. A molecular drawing of the first diposphine molecule in TPSB BDP 1 shown with 50% probability ellipsoids. All H atoms are omitted.

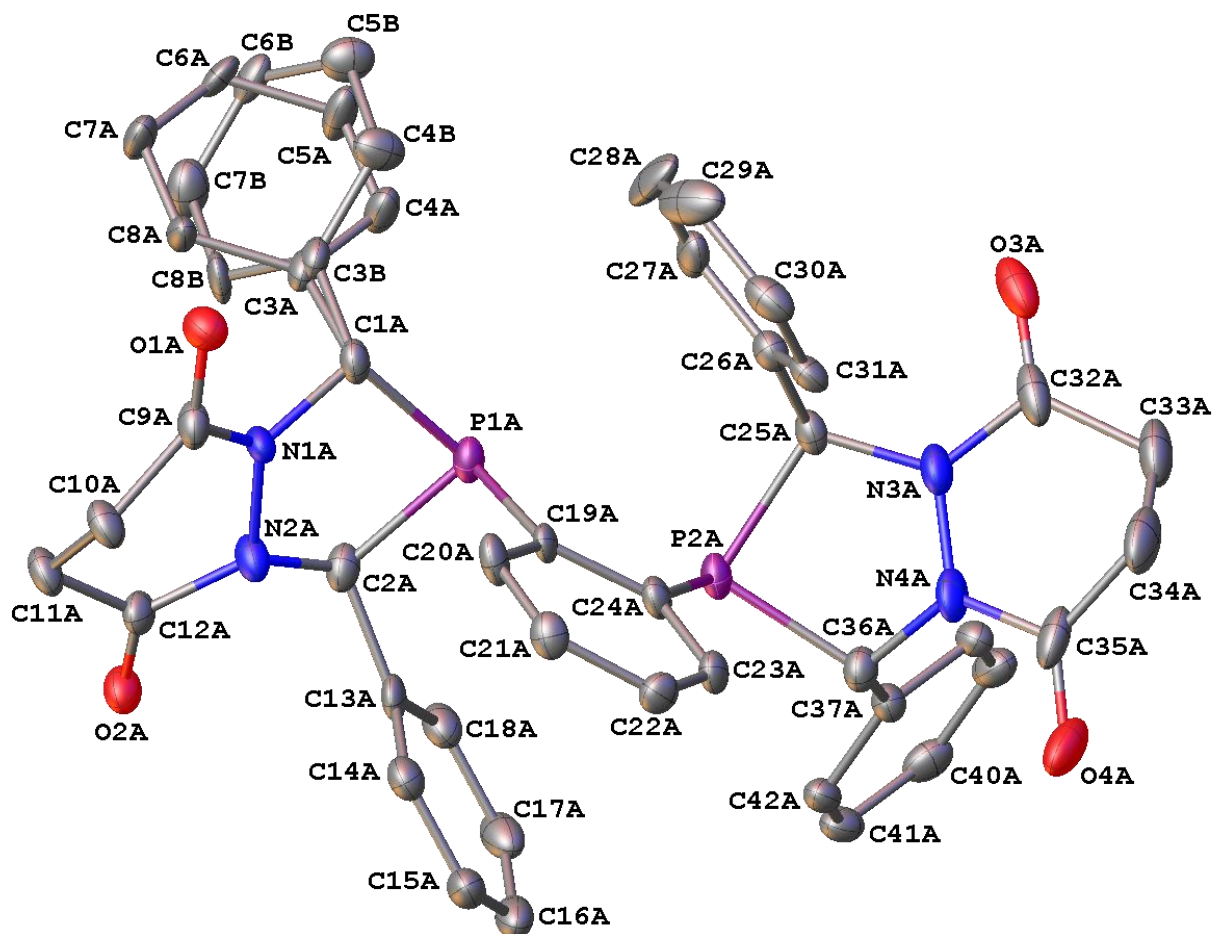


Figure A3.17. A molecular drawing of the second diposphine molecule in TPSB BDP **1** shown with 50% probability ellipsoids. All H atoms are omitted but both positions of the disordered Ph ring are shown.

Data Collection

A colorless crystal with approximate dimensions $0.37 \times 0.05 \times 0.046 \text{ mm}^3$ was selected under oil under ambient conditions and attached to the tip of a MiTeGen MicroMount®. The crystal was mounted in a stream of cold nitrogen at 100(1) K and centered in the X-ray beam by using a video camera.

The crystal evaluation and data collection were performed on a Bruker Quazar SMART APEXII diffractometer with Mo K_α ($\lambda = 0.71073 \text{ \AA}$) radiation and the diffractometer to crystal distance of 4.96 cm [1].

The initial cell constants were obtained from three series of ω scans at different starting angles. Each series consisted of 12 frames collected at intervals of 0.5° in a 6° range about ω

with the exposure time of 20 seconds per frame. The reflections were successfully indexed by an automated indexing routine built in the APEXII program suite. The final cell constants were calculated from a set of 9854 strong reflections from the actual data collection.

The data were collected by using the full sphere data collection routine to survey the reciprocal space to the extent of a full sphere to a resolution of 0.70 Å. A total of 107270 data were harvested by collecting 4 sets of frames with 0.6° scans in ω and φ with exposure times of 90/120 sec per frame. These highly redundant datasets were corrected for Lorentz and polarization effects. The absorption correction was based on fitting a function to the empirical transmission surface as sampled by multiple equivalent measurements. [2]

Structure Solution and Refinement

The systematic absences in the diffraction data were consistent for the space group $Pca2_1$ that yielded chemically reasonable and computationally stable results of refinement [3-8].

A successful solution by the direct methods provided most non-hydrogen atoms from the *E*-map. The remaining non-hydrogen atoms were located in an alternating series of least-squares cycles and difference Fourier maps. All non-hydrogen atoms were refined with anisotropic displacement coefficients. All hydrogen atoms were included in the structure factor calculation at idealized positions and were allowed to ride on the neighboring atoms with relative isotropic displacement coefficients.

There are two symmetry-independent diphosphine molecules in the asymmetric unit. The phenyl ring at atom C1a is disordered over two positions with the major component contribution of 0.574(12).

The crystal appears to be a racemic twin with the minor component contribution of 0.40(6).

There were several partially occupied solvent molecules present in the asymmetric unit. A significant amount of time was invested in identifying and refining the disordered molecules. Bond length restraints were applied to model the molecules but the resulting isotropic displacement coefficients suggested the molecules were mobile. In addition, the refinement was computationally unstable. Option SQUEEZE of program PLATON [9] was used to correct the diffraction data for diffuse scattering effects and to identify the solvate molecule. PLATON calculated the upper limit of volume that can be occupied by the solvent to be 1494 Å³, or 18% of the unit cell volume. The program calculated 539 electrons in the unit cell for the diffuse species. This approximately corresponds to 2.5 molecules of CH₂Cl₂ and ¾ molecules of THF per two diphosphines in the asymmetric unit (540 electrons). The solvent molecules are disordered over

several positions. All derived results in the following tables are based on the known contents. No data are given for the diffusely scattering species.

The diphosphine molecules were refined with restraints and constraints.

The final least-squares refinement of 878 parameters against 16646 data resulted in residuals R (based on F^2 for $I \geq 2\sigma$) and wR (based on F^2 for all data) of 0.0685 and 0.1799, respectively.

Summary

Crystal data for $C_{42}H_{36}N_4O_4P_2$ ($M = 722.69$ g/mol): orthorhombic, space group $Pca2_1$ (no. 29), $a = 23.708(8)$ Å, $b = 13.125(5)$ Å, $c = 26.110(8)$ Å, $V = 8125(5)$ Å³, $Z = 8$, $T = 100.02$ K, $\mu(\text{Mo K}\alpha) = 0.151$ mm⁻¹, $D_{\text{calc}} = 1.182$ g/cm³, 107270 reflections measured ($3.102^\circ \leq 2\theta \leq 52.82^\circ$), 16646 unique ($R_{\text{int}} = 0.0821$, $R_{\text{sigma}} = 0.0611$) which were used in all calculations. The final R_1 was 0.0685 ($I > 2\sigma(I)$) and wR_2 was 0.1799 (all data).

References

- [1] Bruker-AXS (2016). *APEX3*. Version 2016.5-0. Madison, Wisconsin, USA.
- [2] Krause, L., Herbst-Irmer, R., Sheldrick, G. M. & Stalke, D. (2015). *J. Appl. Cryst.* 48, 3-10.
- [3] Sheldrick, G. M. (2013b). *XPREF*. Version 2013/1. Georg-August-Universität Göttingen, Göttingen, Germany.
- [4] Sheldrick, G. M. (2013a). The *SHELX* homepage, <http://shelx.uni-ac.gwdg.de/SHELX/>.
- [5] Sheldrick, G. M. (2015a). *Acta Cryst. A*, 71, 3-8.
- [6] Sheldrick, G. M. (2015b). *Acta Cryst. C*, 71, 3-8.
- [7] Dolomanov, O. V., Bourhis, L. J., Gildea, R. J., Howard, J. A. K. & Puschmann, H. (2009). *J. Appl. Crystallogr.* 42, 339-341.
- [8] Guzei, I. A. (2007-2013). Programs *Gn*. University of Wisconsin-Madison, Madison, Wisconsin, USA.
- [9] Spek, A. L. (2015). *Acta Cryst. C*, 71, 9-18.

Table A3.1. Crystal data and structure refinement for TPSB BDP 1.

Empirical formula	$C_{42}H_{36}N_4O_4P_2$
Formula weight	722.69
Temperature/K	100.02
Crystal system	orthorhombic
Space group	$Pca2_1$
$a/\text{\AA}$	23.708(8)
$b/\text{\AA}$	13.125(5)
$c/\text{\AA}$	26.110(8)
$\alpha/^\circ$	90
$\beta/^\circ$	90

$\gamma/^\circ$	90
Volume/ \AA^3	8125(5)
Z	8
$\rho_{\text{calc}}/\text{g/cm}^3$	1.182
μ/mm^{-1}	0.151
F(000)	3024.0
Crystal size/ mm^3	$0.37 \times 0.05 \times 0.046$
Radiation	Mo K α ($\lambda = 0.71073$)
2 θ range for data collection/ $^\circ$	3.102 to 52.82
Index ranges	$-29 \leq h \leq 25$, $-16 \leq k \leq 16$, $-32 \leq l \leq 32$
Reflections collected	107270
Independent reflections	16646 [$R_{\text{int}} = 0.0821$, $R_{\text{sigma}} = 0.0611$]
Data/restraints/parameters	16646/947/878
Goodness-of-fit on F^2	1.040
Final R indexes [$ I \geq 2\sigma(I)$]	$R_1 = 0.0685$, $wR_2 = 0.1679$
Final R indexes [all data]	$R_1 = 0.0908$, $wR_2 = 0.1799$
Largest diff. peak/hole / $e \text{ \AA}^{-3}$	1.34/-0.41
Flack parameter	0.40(6)

Table A3.2. Fractional Atomic Coordinates ($\times 10^4$) and Equivalent Isotropic Displacement Parameters ($\text{\AA}^2 \times 10^3$) for TPSB BDP 1. U_{eq} is defined as 1/3 of the trace of the orthogonalised U_{ij} tensor.

Atom	x	y	z	U(eq)
P1	5201.8(6)	1152.0(15)	5123.7(6)	27.1(4)
P2	5972.1(7)	1507.1(16)	4203.2(6)	30.7(4)
O1	4385.7(19)	-1046(4)	6207.4(17)	29.8(10)
O2	3292.8(19)	1227(4)	4836.3(19)	36.7(12)
O3	7785.4(19)	1976(4)	4775.9(19)	35.0(11)
O4	7149(3)	181(6)	3033(2)	56.0(18)
N1	4359(2)	176(5)	5609(2)	27.6(12)
N2	4108(2)	599(4)	5153(2)	25.5(11)
N3	7111(2)	1440(5)	4231(2)	31.8(13)
N4	6953(2)	1081(5)	3738(2)	34.2(14)
C1	4918(3)	601(5)	5730(2)	26.5(13)
C2	4448(2)	1402(5)	4919(2)	25.5(13)
C3	4904.8(18)	1434(3)	6131.0(17)	28.8(14)
C4	5396.8(14)	1666(4)	6396.0(19)	43.2(18)
C5	5403.2(17)	2469(4)	6743.4(19)	42.9(18)
C6	4918(2)	3039(4)	6826(2)	58(2)
C7	4425.6(18)	2807(4)	6561(2)	64(3)
C8	4419.2(15)	2004(4)	6213(2)	51(2)
C9	4148(3)	-665(5)	5833(2)	26.1(13)
C10	3605(3)	-1012(6)	5595(3)	30.2(14)

C11	3232(3)	-111(5)	5465(3)	30.4(15)
C12	3523(3)	632(5)	5128(3)	28.6(13)
C13	4403.9(19)	1509(3)	4344.9(11)	28.1(13)
C14	4327.4(18)	675(3)	4024.3(16)	34.4(15)
C15	4338(2)	804(4)	3496.0(15)	41.5(17)
C16	4425(2)	1766(4)	3288.2(12)	50.9(19)
C17	4502(2)	2600(3)	3608.8(17)	44.7(18)
C18	4491.0(19)	2472(3)	4137.2(16)	34.2(15)
C19	5361(3)	27(6)	4730(3)	29.5(15)
C20	5147(3)	-948(6)	4815(3)	34.4(15)
C21	5258(3)	-1734(7)	4474(3)	41.2(17)
C22	5592(4)	-1565(7)	4062(3)	54(2)
C23	5815(4)	-617(7)	3967(3)	44.3(18)
C24	5722(3)	188(6)	4284(3)	35.0(15)
C25	6645(3)	1522(6)	4604(2)	27.1(14)
C26	6683.4(18)	699(3)	5008.5(13)	25.5(13)
C27	6558.2(18)	953(3)	5512.6(15)	30.0(14)
C28	6595(2)	219(4)	5894.9(11)	37.4(16)
C29	6757(2)	-769(3)	5773.2(15)	38.3(16)
C30	6882.3(19)	-1024(3)	5269.1(17)	38.4(16)
C31	6845.4(19)	-290(3)	4886.7(12)	33.9(15)
C32	7655(3)	1636(6)	4359(3)	31.0(15)
C33	8072(3)	1317(7)	3951(3)	39.5(17)
C34	7882(3)	366(7)	3685(3)	44.6(19)
C35	7299(3)	498(6)	3451(3)	38.0(17)
C36	6396(3)	1435(6)	3592(3)	36.8(16)
C37	6394.1(19)	2480(3)	3334.6(17)	35.2(15)
C38	6839.6(16)	3162(4)	3378.5(18)	48.4(19)
C39	6793.4(19)	4135(4)	3172(2)	55(2)
C40	6302(2)	4424(3)	2921(2)	52(2)
C41	5856.1(17)	3741(4)	2877.1(19)	50(2)
C42	5902.3(17)	2769(4)	3083.9(18)	48(2)
P1A	7255.7(7)	6096.5(14)	5043.9(7)	28.3(4)
P2A	6464.7(7)	6542.9(15)	5951.5(7)	28.9(4)
O1A	8010(2)	3803(4)	3970.5(19)	36.8(12)
O2A	9167.3(19)	6054(4)	5305.7(18)	35.9(12)
O3A	4647(2)	7020(5)	5405(3)	49.0(14)
O4A	5290(3)	5400(6)	7178(2)	57.0(17)
N1A	8058(2)	5046(4)	4568(2)	26.4(12)
N2A	8336(2)	5471(5)	5007(2)	31.8(13)
N3A	5323(2)	6436(5)	5931(2)	35.7(13)
N4A	5496(2)	6138(5)	6426(2)	36.5(14)
C1A	7515(3)	5498(5)	4438(3)	28.2(13)
C2A	8007(3)	6289(6)	5242(3)	31.1(15)
C3A	7588(3)	6326(6)	4032(3)	28.4(15)

C4A	7163(3)	7046(7)	3974(3)	40(4)
C5A	7171(4)	7707(7)	3558(3)	46(4)
C6A	7604(4)	7648(7)	3201(3)	32(3)
C7A	8030(3)	6929(7)	3259(3)	40(4)
C8A	8022(3)	6268(6)	3675(3)	36(3)
C3B	7510(4)	6287(8)	4005(4)	28.4(15)
C4B	7030(4)	6427(8)	3708(5)	39(4)
C5B	7014(4)	7197(9)	3343(4)	39(4)
C6B	7479(5)	7828(8)	3275(4)	32(4)
C7B	7960(4)	7688(8)	3572(5)	45(5)
C8B	7975(4)	6917(9)	3937(4)	35(4)
C9A	8267(3)	4205(6)	4336(3)	31.8(15)
C10A	8817(3)	3833(6)	4543(3)	33.5(16)
C11A	9203(3)	4752(6)	4658(3)	34.6(16)
C12A	8923(3)	5488(6)	5015(3)	30.5(14)
C13A	8052.0(19)	6321(3)	5829.9(12)	29.5(14)
C14A	8127.6(19)	5450(3)	6124.6(16)	34.9(15)
C15A	8095(2)	5507(3)	6655.4(15)	40.7(17)
C16A	7988(2)	6437(4)	6891.4(12)	43.2(18)
C17A	7912(2)	7308(3)	6596.7(17)	46.4(18)
C18A	7944.2(19)	7250(3)	6066.0(16)	35.9(16)
C19A	7055(2)	5004(5)	5452(3)	24.7(14)
C20A	7262(3)	4023(6)	5380(3)	32.8(15)
C21A	7152(3)	3271(6)	5737(3)	30.4(15)
C22A	6815(3)	3477(6)	6161(3)	30.2(14)
C23A	6581(3)	4437(6)	6221(3)	29.6(14)
C24A	6705(2)	5216(5)	5868(3)	26.6(13)
C25A	5779(3)	6533(5)	5569(3)	27.6(14)
C26A	5756.2(18)	5729(3)	5149.9(14)	30.1(14)
C27A	5901(2)	5999(3)	4652.2(17)	37.9(17)
C28A	5890(2)	5272(4)	4265.2(13)	58(2)
C29A	5733(2)	4275(4)	4375.8(16)	61(2)
C30A	5588(2)	4006(3)	4873.4(19)	39.7(17)
C31A	5599.6(18)	4733(3)	5260.5(13)	29.5(14)
C32A	4775(3)	6684(7)	5828(4)	44.7(18)
C33A	4369(3)	6428(7)	6258(4)	54(2)
C34A	4560(3)	5466(8)	6527(4)	57(2)
C35A	5133(3)	5652(7)	6750(3)	45.8(19)
C36A	6042(3)	6532(6)	6565(3)	30.5(14)
C37A	6035.7(17)	7603(3)	6789.9(16)	28.1(13)
C38A	5572.7(14)	8240(3)	6726.5(16)	29.6(14)
C39A	5587.6(16)	9230(3)	6915.6(17)	36.7(15)
C40A	6065(2)	9582(3)	7168.2(17)	37.1(16)
C41A	6528.5(15)	8945(3)	7231.6(17)	35.3(15)
C42A	6513.5(14)	7955(3)	7042.4(17)	31.2(14)

Table A3.3. Anisotropic Displacement Parameters ($\text{\AA}^2 \times 10^3$) for TPSB BDP 1. The Anisotropic displacement factor exponent takes the form: $-2\pi^2[h^2a^{*2}U_{11}+2hka^*b^*U_{12}+\dots]$.

Atom	U_{11}	U_{22}	U_{33}	U_{23}	U_{13}	U_{12}
P1	16.7(7)	39.3(10)	25.3(8)	1.4(8)	-3.2(6)	-1.6(7)
P2	23.4(8)	48.3(12)	20.3(8)	3.9(8)	0.0(6)	9.2(8)
O1	24(2)	37(3)	28(2)	0(2)	0.5(18)	4(2)
O2	23(2)	47(3)	40(3)	6(2)	-7(2)	4(2)
O3	25(2)	46(3)	34(2)	2(2)	-2.4(19)	2(2)
O4	52(3)	88(5)	27(3)	-6(3)	-1(2)	35(3)
N1	15(2)	40(3)	29(3)	0(2)	-4(2)	3(2)
N2	17(2)	35(3)	24(3)	3(2)	-3.9(19)	1(2)
N3	24(2)	55(4)	16(2)	2(2)	2(2)	6(3)
N4	24(3)	58(4)	21(3)	-2(3)	-4(2)	13(3)
C1	19(3)	35(4)	25(3)	-2(3)	-5(2)	-4(3)
C2	16(3)	34(4)	27(3)	4(3)	-5(2)	2(2)
C3	19(3)	37(4)	31(3)	-1(3)	-5(2)	1(3)
C4	24(3)	66(5)	39(4)	-8(4)	9(3)	-15(3)
C5	34(4)	56(5)	38(4)	-2(3)	-15(3)	-11(3)
C6	53(5)	47(5)	72(6)	-19(5)	-11(4)	6(4)
C7	31(4)	69(6)	91(7)	-35(5)	-3(4)	15(4)
C8	34(4)	57(5)	62(5)	-12(4)	-10(4)	10(4)
C9	23(3)	27(3)	29(3)	-4(3)	3(2)	4(2)
C10	22(3)	38(4)	31(3)	-2(3)	4(3)	-4(3)
C11	25(3)	36(4)	30(3)	-9(3)	6(3)	-1(3)
C12	21(3)	32(4)	33(3)	-5(3)	-4(2)	2(2)
C13	11(3)	42(4)	32(3)	-2(3)	-3(2)	2(3)
C14	20(3)	44(4)	39(3)	-8(3)	-6(3)	0(3)
C15	20(3)	67(5)	37(3)	-8(3)	3(3)	-10(3)
C16	29(4)	101(6)	22(3)	2(3)	-1(3)	-3(4)
C17	24(3)	62(5)	47(4)	15(3)	-9(3)	-8(3)
C18	27(3)	44(4)	32(3)	5(3)	-10(3)	5(3)
C19	19(3)	37(4)	32(3)	-1(3)	-4(3)	9(3)
C20	22(3)	47(4)	34(4)	-3(3)	-6(3)	5(3)
C21	45(4)	39(4)	39(4)	-3(3)	-6(3)	10(3)
C22	66(6)	51(5)	45(4)	-2(4)	1(4)	14(4)
C23	49(5)	53(4)	31(4)	3(3)	3(3)	13(4)
C24	26(3)	51(4)	28(3)	5(3)	-5(3)	12(3)
C25	21(3)	42(4)	19(3)	7(3)	0(2)	6(3)
C26	17(3)	36(3)	23(3)	7(3)	-1(2)	-1(3)
C27	24(3)	41(4)	25(3)	4(3)	-3(3)	-6(3)
C28	34(4)	53(4)	25(3)	12(3)	-10(3)	-10(3)
C29	29(4)	45(4)	41(4)	17(3)	-11(3)	-10(3)
C30	21(3)	47(4)	48(4)	10(3)	-7(3)	-2(3)

C31	25(3)	43(4)	34(4)	-1(3)	-5(3)	7(3)
C32	25(3)	42(4)	27(3)	3(3)	-3(2)	7(3)
C33	21(3)	57(5)	41(4)	6(3)	3(3)	16(3)
C34	36(4)	66(5)	32(4)	-3(4)	-1(3)	25(4)
C35	37(4)	48(5)	29(3)	4(3)	1(3)	19(3)
C36	28(3)	56(5)	27(3)	3(3)	0(3)	12(3)
C37	26(3)	68(5)	12(3)	4(3)	3(2)	12(3)
C38	38(4)	71(5)	36(4)	7(4)	0(3)	8(3)
C39	50(4)	76(6)	40(4)	27(4)	-2(4)	6(4)
C40	44(4)	76(6)	35(4)	25(4)	3(3)	10(4)
C41	42(4)	75(6)	34(4)	19(4)	4(3)	19(4)
C42	30(4)	81(6)	33(4)	21(4)	-6(3)	14(4)
P1A	20.4(8)	31.6(10)	32.9(9)	2.5(8)	8.2(7)	0.6(7)
P2A	17.2(8)	34(1)	35.5(9)	1.0(8)	5.7(7)	-1.0(7)
O1A	31(3)	45(3)	35(3)	-3(2)	-3(2)	1(2)
O2A	24(2)	47(3)	36(3)	-7(2)	4(2)	-8(2)
O3A	23(3)	57(4)	67(3)	-25(3)	-1(2)	3(2)
O4A	47(3)	87(5)	36(3)	-10(3)	17(2)	-30(3)
N1A	13(2)	41(3)	24(3)	-4(2)	0(2)	1(2)
N2A	19(2)	39(3)	37(3)	-10(3)	3(2)	0(2)
N3A	18(2)	47(4)	41(3)	-8(3)	6(2)	-5(2)
N4A	20(3)	45(4)	45(3)	-8(3)	9(2)	-11(2)
C1A	17(3)	34(4)	34(3)	2(3)	6(2)	-1(3)
C2A	25(3)	34(4)	34(3)	-3(3)	9(3)	-4(3)
C3A	21(3)	41(4)	24(3)	-3(3)	8(3)	-1(3)
C4A	33(6)	57(9)	30(6)	16(6)	13(5)	14(6)
C5A	39(8)	59(10)	40(7)	24(7)	22(6)	18(7)
C6A	39(7)	42(8)	15(5)	4(5)	12(5)	-2(5)
C7A	30(6)	64(9)	27(6)	18(6)	13(5)	10(5)
C8A	18(5)	68(10)	23(5)	13(5)	4(4)	12(5)
C3B	21(3)	41(4)	24(3)	-3(3)	8(3)	-1(3)
C4B	37(7)	40(10)	39(9)	12(7)	-9(6)	-11(7)
C5B	47(9)	34(10)	36(9)	8(7)	-4(7)	-3(7)
C6B	40(8)	30(9)	27(9)	2(7)	18(6)	6(6)
C7B	35(8)	46(11)	53(11)	10(8)	12(7)	-1(7)
C8B	11(6)	47(10)	47(10)	9(7)	10(6)	4(5)
C9A	21(3)	39(4)	35(3)	-4(3)	8(2)	-1(3)
C10A	18(3)	39(4)	44(4)	-6(3)	-2(3)	-3(3)
C11A	16(3)	44(4)	44(4)	-6(3)	-1(3)	-2(3)
C12A	19(3)	43(4)	30(3)	0(3)	5(2)	-9(3)
C13A	13(3)	42(4)	33(3)	0(3)	8(2)	-4(3)
C14A	20(3)	49(4)	35(3)	-1(3)	-1(3)	-2(3)
C15A	24(3)	68(5)	30(3)	6(3)	0(3)	4(3)
C16A	25(4)	76(5)	28(3)	-11(3)	1(3)	0(3)
C17A	29(4)	72(5)	38(4)	-22(3)	-5(3)	7(4)

C18A	23(3)	49(4)	36(3)	-9(3)	-2(3)	-2(3)
C19A	11(3)	37(4)	26(3)	4(3)	4(2)	-3(2)
C20A	15(3)	37(4)	47(4)	3(3)	7(3)	-2(3)
C21A	25(3)	28(4)	39(4)	0(3)	3(3)	-1(3)
C22A	29(3)	35(4)	27(3)	8(3)	3(3)	-5(3)
C23A	16(3)	42(4)	31(3)	5(3)	5(2)	-3(3)
C24A	13(3)	33(3)	33(3)	3(3)	3(2)	-2(2)
C25A	17(3)	30(4)	36(3)	3(3)	3(2)	2(3)
C26A	20(3)	39(3)	32(3)	3(3)	0(3)	2(3)
C27A	22(3)	54(5)	37(3)	14(3)	8(3)	14(3)
C28A	69(6)	81(5)	25(4)	10(4)	23(4)	40(5)
C29A	74(6)	71(5)	37(4)	-15(4)	-10(4)	42(5)
C30A	29(4)	42(4)	49(4)	-4(3)	-11(3)	5(3)
C31A	18(3)	39(4)	32(3)	2(3)	-7(3)	1(3)
C32A	20(3)	52(5)	63(4)	-22(4)	10(3)	-2(3)
C33A	25(4)	71(6)	66(5)	-20(4)	18(3)	-10(4)
C34A	35(4)	80(6)	56(5)	-16(4)	22(3)	-26(4)
C35A	38(4)	56(5)	43(4)	-15(3)	24(3)	-14(3)
C36A	23(3)	37(4)	32(3)	0(3)	6(2)	-4(3)
C37A	19(3)	38(4)	27(3)	2(3)	1(2)	0(2)
C38A	23(3)	42(4)	23(3)	0(3)	-2(2)	3(3)
C39A	39(4)	48(4)	24(3)	2(3)	2(3)	11(3)
C40A	50(4)	37(4)	24(3)	7(3)	4(3)	-5(3)
C41A	28(3)	52(4)	26(3)	6(3)	-6(3)	-10(3)
C42A	21(3)	49(4)	23(3)	8(3)	-3(2)	-2(3)

Table A3.4. Bond Lengths for TPSB BDP 1.

Atom	Atom	Length/Å	Atom	Atom	Length/Å
P1	C1	1.867(7)	P2A	C25A	1.907(7)
P1	C2	1.893(6)	P2A	C36A	1.890(7)
P1	C19	1.839(8)	O1A	C9A	1.250(9)
P2	C24	1.843(9)	O2A	C12A	1.210(8)
P2	C25	1.909(6)	O3A	C32A	1.227(11)
P2	C36	1.889(7)	O4A	C35A	1.226(11)
O1	C9	1.234(8)	N1A	N2A	1.433(8)
O2	C12	1.221(8)	N1A	C1A	1.460(8)
O3	C32	1.216(8)	N1A	C9A	1.353(9)
O4	C35	1.223(9)	N2A	C2A	1.463(9)
N1	N2	1.442(8)	N2A	C12A	1.391(8)
N1	C1	1.474(8)	N3A	N4A	1.411(9)
N1	C9	1.345(9)	N3A	C25A	1.443(8)
N2	C2	1.461(8)	N3A	C32A	1.365(9)
N2	C12	1.389(8)	N4A	C35A	1.364(9)
N3	N4	1.420(8)	N4A	C36A	1.442(9)

N3	C25	1.476(8)	C1A	C3A	1.528(8)
N3	C32	1.359(9)	C1A	C3B	1.532(8)
N4	C35	1.350(9)	C2A	C13A	1.540(7)
N4	C36	1.450(8)	C3A	C4A	1.3900
C1	C3	1.514(7)	C3A	C8A	1.3900
C2	C13	1.510(7)	C4A	C5A	1.3900
C3	C4	1.3900	C5A	C6A	1.3900
C3	C8	1.3900	C6A	C7A	1.3900
C4	C5	1.3900	C7A	C8A	1.3900
C5	C6	1.3900	C3B	C4B	1.3900
C6	C7	1.3900	C3B	C8B	1.3900
C7	C8	1.3900	C4B	C5B	1.3900
C9	C10	1.501(9)	C5B	C6B	1.3900
C10	C11	1.516(10)	C6B	C7B	1.3900
C11	C12	1.482(10)	C7B	C8B	1.3900
C13	C14	1.3900	C9A	C10A	1.494(10)
C13	C18	1.3900	C10A	C11A	1.543(10)
C14	C15	1.3900	C11A	C12A	1.498(10)
C15	C16	1.3900	C13A	C14A	1.3900
C16	C17	1.3900	C13A	C18A	1.3900
C17	C18	1.3900	C14A	C15A	1.3900
C19	C20	1.394(11)	C15A	C16A	1.3900
C19	C24	1.459(11)	C16A	C17A	1.3900
C20	C21	1.387(11)	C17A	C18A	1.3900
C21	C22	1.354(12)	C19A	C20A	1.391(10)
C22	C23	1.375(13)	C19A	C24A	1.395(9)
C23	C24	1.360(11)	C20A	C21A	1.382(10)
C25	C26	1.514(7)	C21A	C22A	1.392(9)
C26	C27	1.3900	C22A	C23A	1.386(10)
C26	C31	1.3900	C23A	C24A	1.407(9)
C27	C28	1.3900	C25A	C26A	1.521(8)
C28	C29	1.3900	C26A	C27A	1.3900
C29	C30	1.3900	C26A	C31A	1.3900
C30	C31	1.3900	C27A	C28A	1.3900
C32	C33	1.513(10)	C28A	C29A	1.3900
C33	C34	1.497(12)	C29A	C30A	1.3900
C34	C35	1.520(10)	C30A	C31A	1.3900
C36	C37	1.527(9)	C32A	C33A	1.518(11)
C37	C38	1.3900	C33A	C34A	1.514(14)
C37	C42	1.3900	C34A	C35A	1.498(12)
C38	C39	1.3900	C36A	C37A	1.523(8)
C39	C40	1.3900	C37A	C38A	1.3900
C40	C41	1.3900	C37A	C42A	1.3900
C41	C42	1.3900	C38A	C39A	1.3900
P1A	C1A	1.870(7)	C39A	C40A	1.3900

P1A	C2A	1.872(7)	C40A	C41A	1.3900
P1A	C19A	1.849(7)	C41A	C42A	1.3900
P2A	C24A	1.846(7)			

Table A3.5. Bond Angles for TPSB BDP 1.

Atom	Atom	Atom	Angle/°	Atom	Atom	Atom	Angle/°
C1	P1	C2	88.1(3)	C36A	P2A	C25A	89.6(3)
C19	P1	C1	103.7(3)	N2A	N1A	C1A	115.7(5)
C19	P1	C2	100.1(3)	C9A	N1A	N2A	120.5(5)
C24	P2	C25	102.5(3)	C9A	N1A	C1A	123.4(6)
C24	P2	C36	102.8(4)	N1A	N2A	C2A	112.1(5)
C36	P2	C25	91.0(3)	C12A	N2A	N1A	118.6(5)
N2	N1	C1	113.8(5)	C12A	N2A	C2A	121.0(6)
C9	N1	N2	121.5(5)	N4A	N3A	C25A	114.0(5)
C9	N1	C1	123.4(5)	C32A	N3A	N4A	121.6(6)
N1	N2	C2	113.3(5)	C32A	N3A	C25A	124.2(7)
C12	N2	N1	117.5(5)	N3A	N4A	C36A	113.1(5)
C12	N2	C2	120.7(5)	C35A	N4A	N3A	120.9(6)
N4	N3	C25	115.2(5)	C35A	N4A	C36A	125.4(7)
C32	N3	N4	122.5(5)	N1A	C1A	P1A	105.3(4)
C32	N3	C25	122.2(5)	N1A	C1A	C3A	110.5(5)
N3	N4	C36	111.8(5)	N1A	C1A	C3B	116.9(6)
C35	N4	N3	122.0(6)	C3A	C1A	P1A	109.0(5)
C35	N4	C36	126.1(6)	C3B	C1A	P1A	109.7(6)
N1	C1	P1	106.7(4)	N2A	C2A	P1A	107.0(5)
N1	C1	C3	113.8(5)	N2A	C2A	C13A	113.7(6)
C3	C1	P1	108.3(4)	C13A	C2A	P1A	110.2(4)
N2	C2	P1	106.2(4)	C4A	C3A	C1A	118.5(5)
N2	C2	C13	116.4(5)	C4A	C3A	C8A	120.0
C13	C2	P1	111.2(4)	C8A	C3A	C1A	120.7(5)
C4	C3	C1	119.0(4)	C5A	C4A	C3A	120.0
C4	C3	C8	120.0	C6A	C5A	C4A	120.0
C8	C3	C1	120.9(4)	C5A	C6A	C7A	120.0
C5	C4	C3	120.0	C6A	C7A	C8A	120.0
C4	C5	C6	120.0	C7A	C8A	C3A	120.0
C7	C6	C5	120.0	C4B	C3B	C1A	120.4(7)
C6	C7	C8	120.0	C4B	C3B	C8B	120.0
C7	C8	C3	120.0	C8B	C3B	C1A	119.4(7)
O1	C9	N1	120.5(6)	C3B	C4B	C5B	120.0
O1	C9	C10	126.6(6)	C6B	C5B	C4B	120.0
N1	C9	C10	112.8(6)	C5B	C6B	C7B	120.0
C9	C10	C11	110.9(6)	C8B	C7B	C6B	120.0
C12	C11	C10	111.9(5)	C7B	C8B	C3B	120.0
O2	C12	N2	119.7(6)	O1A	C9A	N1A	120.6(6)

O2	C12	C11	125.6(6)	O1A	C9A	C10A	124.4(6)
N2	C12	C11	114.7(6)	N1A	C9A	C10A	115.1(6)
C14	C13	C2	122.2(4)	C9A	C10A	C11A	109.4(6)
C14	C13	C18	120.0	C12A	C11A	C10A	111.3(6)
C18	C13	C2	117.5(4)	O2A	C12A	N2A	120.0(6)
C13	C14	C15	120.0	O2A	C12A	C11A	125.1(6)
C16	C15	C14	120.0	N2A	C12A	C11A	115.0(6)
C15	C16	C17	120.0	C14A	C13A	C2A	122.6(4)
C18	C17	C16	120.0	C14A	C13A	C18A	120.0
C17	C18	C13	120.0	C18A	C13A	C2A	116.9(4)
C20	C19	P1	125.0(6)	C13A	C14A	C15A	120.0
C20	C19	C24	118.2(7)	C16A	C15A	C14A	120.0
C24	C19	P1	116.8(6)	C17A	C16A	C15A	120.0
C21	C20	C19	120.8(7)	C16A	C17A	C18A	120.0
C22	C21	C20	119.9(8)	C17A	C18A	C13A	120.0
C21	C22	C23	121.0(8)	C20A	C19A	P1A	123.3(5)
C24	C23	C22	122.1(8)	C20A	C19A	C24A	120.0(6)
C19	C24	P2	114.6(6)	C24A	C19A	P1A	116.6(5)
C23	C24	P2	127.4(6)	C21A	C20A	C19A	120.2(7)
C23	C24	C19	117.9(7)	C20A	C21A	C22A	120.4(7)
N3	C25	P2	105.2(4)	C23A	C22A	C21A	119.8(6)
N3	C25	C26	111.3(5)	C22A	C23A	C24A	120.2(6)
C26	C25	P2	115.1(4)	C19A	C24A	P2A	117.6(5)
C27	C26	C25	118.4(4)	C19A	C24A	C23A	119.3(6)
C27	C26	C31	120.0	C23A	C24A	P2A	123.0(5)
C31	C26	C25	121.6(4)	N3A	C25A	P2A	107.3(5)
C28	C27	C26	120.0	N3A	C25A	C26A	112.6(5)
C29	C28	C27	120.0	C26A	C25A	P2A	114.4(4)
C28	C29	C30	120.0	C27A	C26A	C25A	119.2(4)
C31	C30	C29	120.0	C27A	C26A	C31A	120.0
C30	C31	C26	120.0	C31A	C26A	C25A	120.8(4)
O3	C32	N3	122.1(6)	C28A	C27A	C26A	120.0
O3	C32	C33	124.5(6)	C27A	C28A	C29A	120.0
N3	C32	C33	113.2(6)	C28A	C29A	C30A	120.0
C34	C33	C32	111.2(6)	C29A	C30A	C31A	120.0
C33	C34	C35	111.3(6)	C30A	C31A	C26A	120.0
O4	C35	N4	120.8(7)	O3A	C32A	N3A	120.0(7)
O4	C35	C34	125.8(7)	O3A	C32A	C33A	126.0(7)
N4	C35	C34	113.3(6)	N3A	C32A	C33A	113.9(8)
N4	C36	P2	106.2(4)	C34A	C33A	C32A	109.7(7)
N4	C36	C37	114.0(6)	C35A	C34A	C33A	108.4(7)
C37	C36	P2	109.0(5)	O4A	C35A	N4A	119.9(7)
C38	C37	C36	122.7(4)	O4A	C35A	C34A	126.0(7)
C38	C37	C42	120.0	N4A	C35A	C34A	114.1(8)
C42	C37	C36	117.1(4)	N4A	C36A	P2A	105.4(5)

C37	C38	C39	120.0	N4A	C36A	C37A	114.7(5)
C38	C39	C40	120.0	C37A	C36A	P2A	108.9(4)
C41	C40	C39	120.0	C38A	C37A	C36A	121.2(4)
C42	C41	C40	120.0	C38A	C37A	C42A	120.0
C41	C42	C37	120.0	C42A	C37A	C36A	118.7(4)
C1A	P1A	C2A	88.7(3)	C39A	C38A	C37A	120.0
C19A	P1A	C1A	104.3(3)	C40A	C39A	C38A	120.0
C19A	P1A	C2A	101.0(3)	C41A	C40A	C39A	120.0
C24A	P2A	C25A	101.2(3)	C40A	C41A	C42A	120.0
C24A	P2A	C36A	104.8(3)	C41A	C42A	C37A	120.0

Table A3.6. Torsion Angles for TPSB BDP 1.

A	B	C	D	Angle/°	A	B	C	D	Angle/°
P1	C1	C3	C4	-81.9(5)	P1A	C19A	C24A	C23A	-173.9(5)
P1	C1	C3	C8	94.2(4)	P2A	C25A	C26A	C27A	-95.5(4)
P1	C2	C13	C14	87.4(5)	P2A	C25A	C26A	C31A	83.7(5)
P1	C2	C13	C18	-87.2(4)	P2A	C36A	C37A	C38A	100.3(4)
P1	C19	C20	C21	175.2(5)	P2A	C36A	C37A	C42A	-76.9(5)
P1	C19	C24	P2	1.4(7)	O1A	C9A	C10A	C11A	138.2(7)
P1	C19	C24	C23	-175.6(5)	O3A	C32A	C33A	C34A	141.1(9)
P2	C25	C26	C27	-100.2(4)	N1A	N2A	C2A	P1A	22.3(7)
P2	C25	C26	C31	80.6(5)	N1A	N2A	C2A	C13A	144.1(5)
P2	C36	C37	C38	99.2(4)	N1A	N2A	C12A	O2A	161.3(6)
P2	C36	C37	C42	-75.5(5)	N1A	N2A	C12A	C11A	-20.3(9)
O1	C9	C10	C11	137.0(7)	N1A	C1A	C3A	C4A	-160.4(6)
O3	C32	C33	C34	140.3(8)	N1A	C1A	C3A	C8A	30.0(9)
N1	N2	C2	P1	25.1(6)	N1A	C1A	C3B	C4B	151.9(7)
N1	N2	C2	C13	149.5(5)	N1A	C1A	C3B	C8B	-33.0(11)
N1	N2	C12	O2	158.7(6)	N1A	C9A	C10A	C11A	-40.5(8)
N1	N2	C12	C11	-22.8(8)	N2A	N1A	C1A	P1A	-22.6(6)
N1	C1	C3	C4	159.6(5)	N2A	N1A	C1A	C3A	95.0(7)
N1	C1	C3	C8	-24.3(7)	N2A	N1A	C1A	C3B	99.5(8)
N1	C9	C10	C11	-40.2(7)	N2A	N1A	C9A	O1A	176.3(6)
N2	N1	C1	P1	-21.1(6)	N2A	N1A	C9A	C10A	-5.0(9)
N2	N1	C1	C3	98.3(6)	N2A	C2A	C13A	C14A	-31.6(7)
N2	N1	C9	O1	176.2(6)	N2A	C2A	C13A	C18A	156.1(4)
N2	N1	C9	C10	-6.5(8)	N3A	N4A	C35A	O4A	-179.9(7)
N2	C2	C13	C14	-34.4(7)	N3A	N4A	C35A	C34A	0.8(11)
N2	C2	C13	C18	151.1(4)	N3A	N4A	C36A	P2A	-34.7(7)
N3	N4	C35	O4	178.5(7)	N3A	N4A	C36A	C37A	85.1(7)
N3	N4	C35	C34	-5.8(11)	N3A	C25A	C26A	C27A	141.8(5)
N3	N4	C36	P2	-33.3(7)	N3A	C25A	C26A	C31A	-39.1(6)
N3	N4	C36	C37	86.7(7)	N3A	C32A	C33A	C34A	-34.2(10)
N3	C25	C26	C27	140.2(4)	N4A	N3A	C25A	P2A	-14.3(7)

N3	C25	C26	C31	-39.0(6)	N4A	N3A	C25A	C26A	112.3(6)
N3	C32	C33	C34	-35.2(9)	N4A	N3A	C32A	O3A	174.0(7)
N4	N3	C25	P2	-17.7(7)	N4A	N3A	C32A	C33A	-10.3(11)
N4	N3	C25	C26	107.6(6)	N4A	C36A	C37A	C38A	-17.5(7)
N4	N3	C32	O3	177.5(7)	N4A	C36A	C37A	C42A	165.3(5)
N4	N3	C32	C33	-6.8(10)	C1A	P1A	C2A	N2A	-29.5(5)
N4	C36	C37	C38	-19.2(7)	C1A	P1A	C2A	C13A	-153.5(5)
N4	C36	C37	C42	166.1(5)	C1A	P1A	C19A	C20A	21.4(6)
C1	P1	C2	N2	-30.9(5)	C1A	P1A	C19A	C24A	-162.7(5)
C1	P1	C2	C13	-158.4(5)	C1A	N1A	N2A	C2A	0.3(8)
C1	P1	C19	C20	17.8(7)	C1A	N1A	N2A	C12A	-148.3(6)
C1	P1	C19	C24	-164.7(5)	C1A	N1A	C9A	O1A	4.2(10)
C1	N1	N2	C2	-3.0(7)	C1A	N1A	C9A	C10A	-177.0(6)
C1	N1	N2	C12	-151.1(6)	C1A	C3A	C4A	C5A	-169.7(9)
C1	N1	C9	O1	10.0(10)	C1A	C3A	C8A	C7A	169.5(9)
C1	N1	C9	C10	-172.6(6)	C1A	C3B	C4B	C5B	175.0(11)
C1	C3	C4	C5	176.2(5)	C1A	C3B	C8B	C7B	-175.1(11)
C1	C3	C8	C7	-176.1(5)	C2A	P1A	C1A	N1A	28.9(5)
C2	P1	C1	N1	29.2(5)	C2A	P1A	C1A	C3A	-89.6(5)
C2	P1	C1	C3	-93.6(4)	C2A	P1A	C1A	C3B	-97.7(6)
C2	P1	C19	C20	-72.7(6)	C2A	P1A	C19A	C20A	-70.1(6)
C2	P1	C19	C24	104.8(5)	C2A	P1A	C19A	C24A	105.8(5)
C2	N2	C12	O2	13.0(10)	C2A	N2A	C12A	O2A	15.6(10)
C2	N2	C12	C11	-168.6(6)	C2A	N2A	C12A	C11A	-166.0(6)
C2	C13	C14	C15	-174.4(5)	C2A	C13A	C14A	C15A	-172.0(5)
C2	C13	C18	C17	174.7(4)	C2A	C13A	C18A	C17A	172.5(5)
C3	C4	C5	C6	0.0	C3A	C4A	C5A	C6A	0.0
C4	C3	C8	C7	0.0	C4A	C3A	C8A	C7A	0.0
C4	C5	C6	C7	0.0	C4A	C5A	C6A	C7A	0.0
C5	C6	C7	C8	0.0	C5A	C6A	C7A	C8A	0.0
C6	C7	C8	C3	0.0	C6A	C7A	C8A	C3A	0.0
C8	C3	C4	C5	0.0	C8A	C3A	C4A	C5A	0.0
C9	N1	N2	C2	-170.3(6)	C3B	C4B	C5B	C6B	0.0
C9	N1	N2	C12	41.5(8)	C4B	C3B	C8B	C7B	0.0
C9	N1	C1	P1	146.0(5)	C4B	C5B	C6B	C7B	0.0
C9	N1	C1	C3	-94.6(8)	C5B	C6B	C7B	C8B	0.0
C9	C10	C11	C12	55.8(8)	C6B	C7B	C8B	C3B	0.0
C10	C11	C12	O2	154.9(7)	C8B	C3B	C4B	C5B	0.0
C10	C11	C12	N2	-23.4(8)	C9A	N1A	N2A	C2A	-172.3(6)
C12	N2	C2	P1	172.2(5)	C9A	N1A	N2A	C12A	39.1(9)
C12	N2	C2	C13	-63.4(8)	C9A	N1A	C1A	P1A	149.8(6)
C13	C14	C15	C16	0.0	C9A	N1A	C1A	C3A	-92.6(8)
C14	C13	C18	C17	0.0	C9A	N1A	C1A	C3B	-88.1(9)
C14	C15	C16	C17	0.0	C9A	C10A	C11A	C12A	55.9(8)
C15	C16	C17	C18	0.0	C10A	C11A	C12A	O2A	152.7(7)

C16	C17	C18	C13	0.0	C10A	C11A	C12A	N2A	-25.7(9)
C18	C13	C14	C15	0.0	C12A	N2A	C2A	P1A	170.0(5)
C19	P1	C1	N1	-70.7(5)	C12A	N2A	C2A	C13A	-68.1(8)
C19	P1	C1	C3	166.5(4)	C13A	C14A	C15A	C16A	0.0
C19	P1	C2	N2	72.7(5)	C14A	C13A	C18A	C17A	0.0
C19	P1	C2	C13	-54.8(5)	C14A	C15A	C16A	C17A	0.0
C19	C20	C21	C22	1.9(11)	C15A	C16A	C17A	C18A	0.0
C20	C19	C24	P2	179.1(5)	C16A	C17A	C18A	C13A	0.0
C20	C19	C24	C23	2.1(10)	C18A	C13A	C14A	C15A	0.0
C20	C21	C22	C23	-1.3(13)	C19A	P1A	C1A	N1A	-72.1(5)
C21	C22	C23	C24	1.3(13)	C19A	P1A	C1A	C3A	169.3(5)
C22	C23	C24	P2	-178.2(6)	C19A	P1A	C1A	C3B	161.3(5)
C22	C23	C24	C19	-1.6(12)	C19A	P1A	C2A	N2A	74.8(5)
C24	P2	C36	N4	-83.8(6)	C19A	P1A	C2A	C13A	-49.2(5)
C24	P2	C36	C37	152.9(4)	C19A	C20A	C21A	C22A	2.4(10)
C24	C19	C20	C21	-2.2(10)	C20A	C19A	C24A	P2A	178.0(5)
C25	P2	C24	C19	87.7(5)	C20A	C19A	C24A	C23A	2.1(10)
C25	P2	C24	C23	-95.6(7)	C20A	C21A	C22A	C23A	1.1(10)
C25	P2	C36	N4	19.2(6)	C21A	C22A	C23A	C24A	-3.0(10)
C25	P2	C36	C37	-104.0(5)	C22A	C23A	C24A	P2A	-174.3(5)
C25	N3	N4	C35	-146.1(7)	C22A	C23A	C24A	C19A	1.4(10)
C25	N3	N4	C36	35.0(8)	C24A	P2A	C36A	N4A	-80.2(5)
C25	N3	C32	O3	-6.5(11)	C24A	P2A	C36A	C37A	156.2(4)
C25	N3	C32	C33	169.2(6)	C24A	C19A	C20A	C21A	-4.0(10)
C25	C26	C27	C28	-179.2(4)	C25A	P2A	C24A	C19A	90.5(5)
C25	C26	C31	C30	179.2(5)	C25A	P2A	C24A	C23A	-93.8(6)
C26	C27	C28	C29	0.0	C25A	P2A	C36A	N4A	21.3(5)
C27	C26	C31	C30	0.0	C25A	P2A	C36A	C37A	-102.3(5)
C27	C28	C29	C30	0.0	C25A	N3A	N4A	C35A	-155.1(7)
C28	C29	C30	C31	0.0	C25A	N3A	N4A	C36A	33.6(8)
C29	C30	C31	C26	0.0	C25A	N3A	C32A	O3A	-0.6(12)
C31	C26	C27	C28	0.0	C25A	N3A	C32A	C33A	175.1(7)
C32	N3	N4	C35	30.1(11)	C25A	C26A	C27A	C28A	179.2(5)
C32	N3	N4	C36	-148.7(7)	C25A	C26A	C31A	C30A	-179.2(5)
C32	N3	C25	P2	166.0(6)	C26A	C27A	C28A	C29A	0.0
C32	N3	C25	C26	-68.6(8)	C27A	C26A	C31A	C30A	0.0
C32	C33	C34	C35	57.0(8)	C27A	C28A	C29A	C30A	0.0
C33	C34	C35	O4	139.3(9)	C28A	C29A	C30A	C31A	0.0
C33	C34	C35	N4	-36.2(10)	C29A	C30A	C31A	C26A	0.0
C35	N4	C36	P2	147.9(7)	C31A	C26A	C27A	C28A	0.0
C35	N4	C36	C37	-92.1(9)	C32A	N3A	N4A	C35A	29.7(11)
C36	P2	C24	C19	-178.3(5)	C32A	N3A	N4A	C36A	-141.6(7)
C36	P2	C24	C23	-1.6(7)	C32A	N3A	C25A	P2A	160.7(6)
C36	N4	C35	O4	-2.8(13)	C32A	N3A	C25A	C26A	-72.6(9)
C36	N4	C35	C34	172.8(7)	C32A	C33A	C34A	C35A	61.1(9)

C36	C37	C38	C39	-174.6(5)	C33A	C34A	C35A	O4A	136.2(9)
C36	C37	C42	C41	174.8(5)	C33A	C34A	C35A	N4A	-44.5(10)
C37	C38	C39	C40	0.0	C35A	N4A	C36A	P2A	154.5(7)
C38	C37	C42	C41	0.0	C35A	N4A	C36A	C37A	-85.7(9)
C38	C39	C40	C41	0.0	C36A	P2A	C24A	C19A	-177.0(5)
C39	C40	C41	C42	0.0	C36A	P2A	C24A	C23A	-1.2(6)
C40	C41	C42	C37	0.0	C36A	N4A	C35A	O4A	-9.7(13)
C42	C37	C38	C39	0.0	C36A	N4A	C35A	C34A	171.0(7)
P1A	C1A	C3A	C4A	-45.2(7)	C36A	C37A	C38A	C39A	-177.1(5)
P1A	C1A	C3A	C8A	145.2(5)	C36A	C37A	C42A	C41A	177.2(5)
P1A	C1A	C3B	C4B	-88.3(8)	C37A	C38A	C39A	C40A	0.0
P1A	C1A	C3B	C8B	86.7(8)	C38A	C37A	C42A	C41A	0.0
P1A	C2A	C13A	C14A	88.4(5)	C38A	C39A	C40A	C41A	0.0
P1A	C2A	C13A	C18A	-83.8(5)	C39A	C40A	C41A	C42A	0.0
P1A	C19A	C20A	C21A	171.7(5)	C40A	C41A	C42A	C37A	0.0
P1A	C19A	C24A	P2A	2.0(7)	C42A	C37A	C38A	C39A	0.0

Table A3.7. Hydrogen Atom Coordinates ($\text{\AA}\times 10^4$) and Isotropic Displacement Parameters ($\text{\AA}^2\times 10^3$) for TPSB BDP 1.

Atom	<i>x</i>	<i>y</i>	<i>z</i>	U(eq)
H1	5172.58	40.1	5848.94	32
H2	4329.42	2064.03	5074.74	31
H4	5728.73	1276.67	6339.7	52
H5	5739.42	2627.43	6924.53	51
H6	4921.88	3587.38	7063.27	69
H7	4093.65	3196.58	6617.16	76
H8	4082.96	1845.83	6032.32	61
H10C	3404.26	-1468.74	5835.25	36
H10D	3687.92	-1403.07	5279.2	36
H11C	2886.8	-358.22	5290.84	36
H11D	3115.82	233.71	5784.98	36
H14	4267.81	17.73	4166.33	41
H15	4285.78	233.5	3276.87	50
H16	4432.52	1853.41	2927.12	61
H17	4561.29	3257.56	3466.83	54
H18	4543.31	3041.81	4356.3	41
H20	4921.92	-1075.06	5109	41
H21	5100.76	-2390.24	4530.6	49
H22	5672.65	-2111.1	3834.24	64
H23	6040.6	-520.35	3670.29	53
H25	6673.72	2199.56	4777.73	33
H27	6447.46	1628.77	5595.81	36
H28	6509.55	393.26	6239.45	45
H29	6782.35	-1270.88	6034.47	46

H30	6993.06	-1699.53	5185.86	46
H31	6930.97	-464.03	4542.22	41
H33C	8112.07	1871.84	3696.49	47
H33D	8445.16	1199.13	4109.52	47
H34C	7873.67	-203.55	3933.98	54
H34D	8154.99	189.43	3412.37	54
H36	6219.61	925.65	3357.03	44
H38	7175.71	2964.58	3549.79	58
H39	7097.91	4601.31	3201.59	66
H40	6270.05	5088.59	2779.56	62
H41	5519.99	3939.13	2705.73	60
H42	5597.78	2302.39	3053.93	57
H1A	7245.29	4963.65	4316.79	34
H1AA	7249.68	4935.95	4343.44	34
H2A	8140.95	6955.78	5101.45	37
H4A	6866.64	7085.61	4217.84	48
H5A	6880.28	8198.53	3517.81	55
H6A	7609.9	8100.08	2916.31	38
H7A	8325.89	6888.72	3014.83	48
H8A	8312.26	5775.79	3714.85	43
H4B	6711.74	5996.38	3755.19	47
H5B	6685.8	7293.06	3140.58	47
H6B	7468.81	8354.03	3025.56	39
H7B	8277.76	8118.31	3525.14	54
H8B	8303.7	6821.64	4139.76	42
H10A	9000.67	3380.14	4289.72	40
H10B	8752.17	3437.48	4860.51	40
H11A	9558.69	4507.62	4813.35	42
H11B	9296.74	5103.76	4333.77	42
H14A	8201.24	4814.71	5963.32	42
H15A	8147	4911.95	6856.82	49
H16A	7965.56	6475.99	7254.18	52
H17A	7838.35	7942.78	6758.04	56
H18A	7892.58	7845.56	5864.53	43
H20A	7480.69	3869.26	5084.66	39
H21A	7306.67	2609.13	5692.07	36
H22A	6745.8	2961.03	6408.24	36
H23A	6336.71	4569.69	6501.58	36
H25A	5741.89	7213.41	5400.64	33
H27A	6008.31	6679.9	4576.63	46
H28A	5988.78	5456.39	3925.03	70
H29A	5725.1	3778.78	4111.23	73
H30A	5480.95	3324.66	4949.03	48
H31A	5500.48	4548.15	5600.64	35
H33A	4354.61	6998.88	6505.81	65

H33B	3984.89	6328.83	6116.98	65
H34A	4290.21	5287.18	6802.64	69
H34B	4574.78	4893.79	6280.83	69
H36A	6224.54	6056.66	6815.18	37
H38A	5246.08	7999.6	6553.88	35
H39A	5271.19	9665.48	6872.31	44
H40A	6075.67	10258.33	7297.45	45
H41A	6855.06	9185.3	7404.18	42
H42A	6829.96	7519.41	7085.76	37

Table A3.8. Atomic Occupancy for TPSB BDP 1.

Atom	Occupancy	Atom	Occupancy	Atom	Occupancy
H1A	0.574(12)	H1AA	0.426(12)	C3A	0.574(12)
C4A	0.574(12)	H4A	0.574(12)	C5A	0.574(12)
H5A	0.574(12)	C6A	0.574(12)	H6A	0.574(12)
C7A	0.574(12)	H7A	0.574(12)	C8A	0.574(12)
H8A	0.574(12)	C3B	0.426(12)	C4B	0.426(12)
H4B	0.426(12)	C5B	0.426(12)	H5B	0.426(12)
C6B	0.426(12)	H6B	0.426(12)	C7B	0.426(12)
H7B	0.426(12)	C8B	0.426(12)	H8B	0.426(12)

A3.2.2 Crystallographic Data for red-TPSB BDP 2

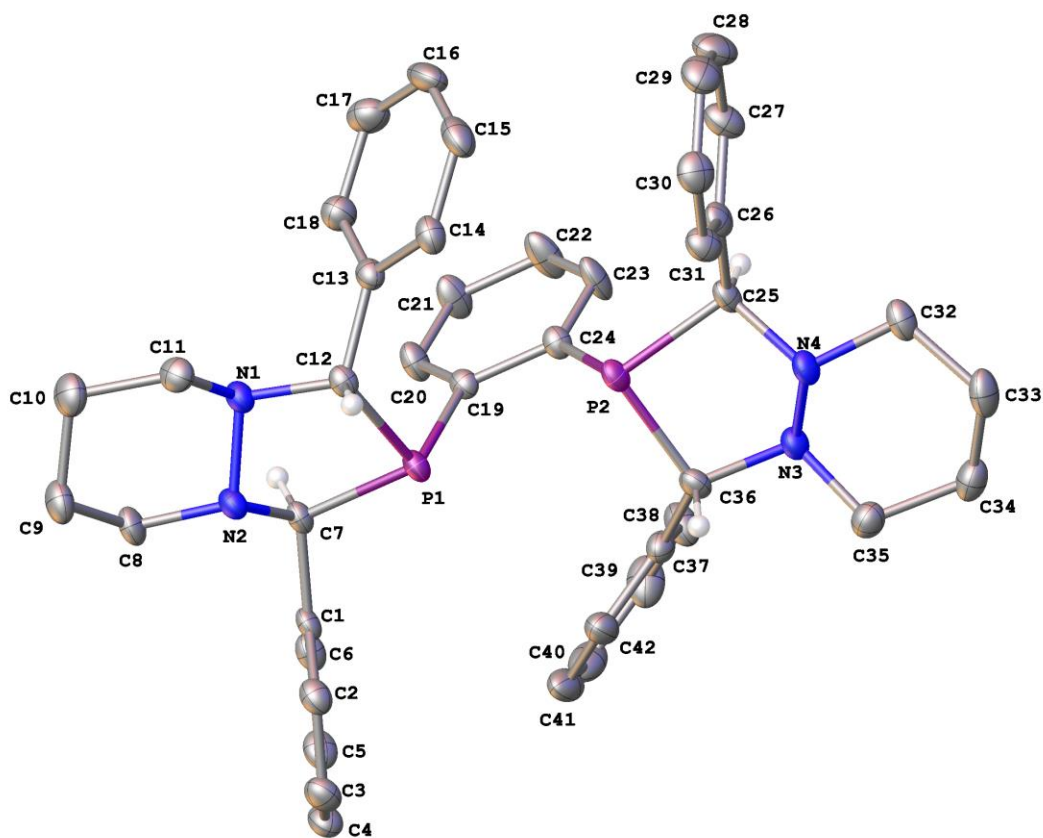


Figure A3.18. A molecular drawing red-TPSB BDP 2. All atoms are drawn as 50% thermal probability ellipsoids. All H atoms except those on chiral carbons are omitted for clarity.

Data Collection

A colorless crystal with approximate dimensions 0.096 x 0.080 x 0.051 mm³ was selected under oil under ambient conditions and attached to the tip of a MiTeGen MicroMount©. The crystal was mounted in a stream of cold nitrogen at 100(1) K and centered in the X-ray beam by using a video camera.

The crystal evaluation and data collection were performed on a Bruker Quazar SMART APEXII diffractometer with Mo K α (λ = 0.71073 Å) radiation and the diffractometer to crystal distance of 4.96 cm.

The initial cell constants were obtained from three series of ω scans at different starting angles. Each series consisted of 12 frames collected at intervals of 0.5° in a 6° range about ω with the exposure time of 20 seconds per frame. The reflections were successfully indexed by an automated indexing routine built in the APEXII program suite. The final cell constants were calculated from a set of 3193 strong reflections from the actual data collection.

The data were collected by using the full sphere data collection routine to survey the reciprocal space to the extent of a full sphere to a resolution of 0.70 Å. A total of 22928 data were harvested by collecting 4 sets of frames with 0.5° scans in ω and ϕ with exposure times of 40 sec per frame. These highly redundant datasets were corrected for Lorentz and polarization effects. The absorption correction was based on fitting a function to the empirical transmission surface as sampled by multiple equivalent measurements. [1]

Structure Solution and Refinement

The systematic absences in the diffraction data were consistent for the space groups $P1$ and $P\bar{1}$. The E -statistics strongly suggested the centrosymmetric space group $P\bar{1}$ that yielded chemically reasonable and computationally stable results of refinement [2-4].

A successful solution by the direct methods provided most non-hydrogen atoms from the E -map. The remaining non-hydrogen atoms were located in an alternating series of least-squares cycles and difference Fourier maps. All non-hydrogen atoms were refined with anisotropic displacement coefficients. All hydrogen atoms were included in the structure factor calculation at idealized positions and were allowed to ride on the neighboring atoms with relative isotropic displacement coefficients.

The structure contains stereocenters at carbons C7, C12, C25, and C36. The relative configuration of these stereocenters is S, S, S, S. Since this is a centrosymmetric spacegroup, the crystals are racemic.

The final least-squares refinement of 433 parameters against 7224 data resulted in residuals R (based on F^2 for $I \geq 2\sigma$) and wR (based on F^2 for all data) of 0.0492 and 0.1256, respectively. The final difference Fourier map was featureless.

Summary

Crystal Data for $C_{42}H_{44}N_4P_2$ ($M = 666.75$ g/mol): triclinic, space group $P\bar{1}$ (no. 2), $a = 10.340(3)$ Å, $b = 11.392(4)$ Å, $c = 15.662(5)$ Å, $\alpha = 75.80(2)^\circ$, $\beta = 82.291(19)^\circ$, $\gamma = 86.231(16)^\circ$, $V = 1771.5(11)$ Å³, $Z = 2$, $T = 100.0$ K, $\mu(\text{MoK}\alpha) = 0.159$ mm⁻¹, $D_{\text{calc}} = 1.250$ g/cm³, 22997 reflections measured ($2.702^\circ \leq 2\theta \leq 52.812^\circ$), 7245 unique ($R_{\text{int}} = 0.0580$, $R_{\text{sigma}} = 0.0674$) which were used in all calculations. The final R_1 was 0.0492 ($I > 2\sigma(I)$) and wR_2 was 0.1256 (all data).

References

- [1] Bruker-AXS. (2007-2014) APEX2 (Ver. 2014.1-1), SADABS (2014-3), and SAINT+ (Ver. 8.32A) Software Reference Manuals. Bruker-AXS, Madison, Wisconsin, USA.
- [2] Sheldrick, G. M. (2008) SHELXL. *Acta Cryst.* **A64**, 112-122.
- [3] Dolomanov, O.V.; Bourhis, L.J.; Gildea, R.J.; Howard, J.A.K.; Puschmann, H. "OLEX2: a complete structure solution, refinement and analysis program". *J. Appl. Cryst.* (2009) **42**, 339-341.
- [4] Guzei, I.A. (2013). Internal laboratory computer programs Gn.
- [5] Guzei, I. A. (2014). *J. Appl. Cryst.* **47**, 806-809.

Table A3.9. Crystal Data and Structure Refinement for red-TPSB BDP 2.

Empirical formula	C ₄₂ H ₄₄ N ₄ P ₂
Formula weight	666.75
Temperature/K	100.0
Crystal system	triclinic
Space group	<i>P</i> $\bar{1}$
a/Å	10.340(3)
b/Å	11.392(4)
c/Å	15.662(5)
α /°	75.80(2)
β /°	82.291(19)
γ /°	86.231(16)
Volume/Å ³	1771.5(11)
Z	2
ρ_{calc} /g/cm ³	1.250
μ /mm ⁻¹	0.159
F(000)	708.0
Crystal size/mm ³	0.096 × 0.08 × 0.051
Radiation	MoK α (λ = 0.71073)
2 θ range for data collection/°	2.702 to 52.812
Index ranges	-12 ≤ h ≤ 12, -14 ≤ k ≤ 14, -19 ≤ l ≤ 19
Reflections collected	22928
Independent reflections	7224 [<i>R</i> _{int} = 0.0578, <i>R</i> _{sigma} = 0.0669]
Data/restraints/parameters	7224/0/433
Goodness-of-fit on F ²	1.017
Final R indexes [<i>I</i> >= 2 σ (<i>I</i>)]	<i>R</i> ₁ = 0.0492, <i>wR</i> ₂ = 0.1099
Final R indexes [all data]	<i>R</i> ₁ = 0.0826, <i>wR</i> ₂ = 0.1256
Largest diff. peak/hole / e Å ⁻³	0.82/-0.33

Table A3.10. Fractional Atomic Coordinates ($\times 10^4$) and Equivalent Isotropic Displacement Parameters ($\text{\AA}^2 \times 10^3$) for red-TPSB BDP **2**. U_{eq} is defined as 1/3 of the trace of the orthogonalised U_{ij} tensor.

Atom	x	y	z	U(eq)
P(1)	792.5(6)	6825.0(6)	3365.8(4)	17.57(15)
P(2)	-1519.1(6)	7670.9(6)	2348.2(4)	18.43(16)
N(1)	1901.8(19)	4590.0(17)	3759.9(12)	19.8(4)
N(2)	2246.4(18)	5291.1(17)	4375.2(12)	19.2(4)
N(3)	-2711.9(18)	9877.0(17)	1972.5(12)	19.9(4)
N(4)	-3602.4(18)	8979.5(18)	1854.9(12)	20.5(4)
C(1)	2686(2)	7415(2)	4317.2(14)	17.7(5)
C(2)	2015(2)	7379(2)	5157.0(15)	23.3(5)
C(3)	2267(2)	8182(2)	5639.5(16)	26.7(6)
C(4)	3182(2)	9061(2)	5278.1(16)	26.2(6)
C(5)	3836(2)	9122(2)	4444.3(16)	25.9(6)
C(6)	3602(2)	8297(2)	3971.7(15)	22.7(5)
C(7)	2409(2)	6526(2)	3801.4(14)	18.2(5)
C(8)	3501(2)	4805(2)	4677.6(16)	24.1(6)
C(9)	3404(3)	3487(2)	5185.2(17)	28.4(6)
C(10)	2947(3)	2756(2)	4601.6(17)	31.0(6)
C(11)	1692(2)	3335(2)	4265.6(16)	24.5(6)
C(12)	650(2)	5155(2)	3478.3(14)	18.1(5)
C(13)	329(2)	4772(2)	2678.6(15)	19.9(5)
C(14)	-953(2)	4519(2)	2621.0(16)	24.4(6)
C(15)	-1274(3)	4201(2)	1876.9(17)	32.5(6)
C(16)	-331(3)	4148(2)	1181.5(17)	34.8(7)
C(17)	943(3)	4408(2)	1225.5(17)	32.6(6)
C(18)	1278(3)	4705(2)	1973.0(16)	26.5(6)
C(19)	1176(2)	7439(2)	2159.6(14)	17.0(5)
C(20)	2421(2)	7527(2)	1703.1(15)	23.9(6)
C(21)	2628(2)	7963(2)	791.0(16)	28.4(6)
C(22)	1581(2)	8347(3)	321.7(16)	33.2(7)
C(23)	328(2)	8290(2)	770.6(15)	28.2(6)
C(24)	100(2)	7847(2)	1682.2(14)	18.7(5)
C(25)	-2715(2)	8079(2)	1515.2(15)	19.7(5)
C(26)	-3431(2)	6999(2)	1460.3(15)	21.4(5)
C(27)	-3341(2)	6653(2)	664.6(16)	28.5(6)
C(28)	-3982(3)	5650(3)	609.1(18)	35.1(7)
C(29)	-4725(3)	4994(3)	1336.6(18)	33.3(6)
C(30)	-4829(2)	5324(2)	2135.5(17)	29.1(6)

C(31)	-4181(2)	6317(2)	2197.1(16)	25.0(6)
C(32)	-4413(2)	9594(2)	1164.0(16)	25.4(6)
C(33)	-5274(2)	10583(2)	1466.0(17)	31.4(6)
C(34)	-4442(3)	11473(2)	1705.0(17)	30.3(6)
C(35)	-3519(2)	10782(2)	2346.7(16)	26.1(6)
C(36)	-1891(2)	9172(2)	2639.2(14)	20.4(5)
C(37)	-726(2)	9853(2)	2713.7(16)	21.4(5)
C(38)	-43(3)	10594(2)	1978.8(18)	31.5(6)
C(39)	1053(3)	11168(2)	2063(2)	37.8(7)
C(40)	1481(3)	11008(3)	2878(2)	39.0(7)
C(41)	817(3)	10275(3)	3616.1(19)	35.1(7)
C(42)	-282(2)	9698(2)	3538.0(17)	27.7(6)

Table A3.11. Anisotropic Displacement Parameters ($\text{\AA}^2 \times 10^3$) for red-TPSB BDP **2**. The Anisotropic displacement factor exponent takes the form: $-2\pi^2[h^2a^{*2}U_{11}+2hka^*b^*U_{12}+\dots]$.

Atom	U_{11}	U_{22}	U_{33}	U_{23}	U_{13}	U_{12}
P(1)	15.2(3)	20.4(3)	16.4(3)	-0.7(2)	-5.6(2)	-2.3(2)
P(2)	12.9(3)	24.5(4)	17.5(3)	-2.8(2)	-4.0(2)	-2.2(2)
N(1)	20.3(11)	19.5(11)	20.1(10)	-2.8(8)	-7.3(8)	-0.8(8)
N(2)	19.9(10)	19.2(11)	18.9(10)	-2.5(8)	-7.3(8)	-1.3(8)
N(3)	15.9(10)	22.5(11)	21.5(10)	-4.3(8)	-5.3(8)	0.6(8)
N(4)	13.9(10)	24.5(11)	22.8(10)	-3.6(8)	-5.8(8)	0.3(8)
C(1)	14.4(11)	20.1(13)	18.5(11)	-1.4(9)	-7.8(9)	-0.5(9)
C(2)	22.2(13)	23.4(13)	23.9(12)	-1.7(10)	-7(1)	-3.7(10)
C(3)	27.4(14)	32.8(15)	20.1(12)	-5.6(11)	-4.9(11)	-1.5(12)
C(4)	27.2(14)	25.6(14)	29.6(14)	-8.9(11)	-11.6(11)	-2.5(11)
C(5)	19.5(13)	24.3(14)	34.1(14)	-3.8(11)	-7.7(11)	-5.2(10)
C(6)	17.8(12)	26.9(14)	21.4(12)	-0.6(10)	-4.2(10)	-1.1(10)
C(7)	15.8(12)	21.6(13)	16.2(11)	-1.0(9)	-5.1(9)	-0.5(10)
C(8)	17.6(12)	28.3(14)	25.7(13)	-1.8(11)	-9.4(10)	1.7(10)
C(9)	25.9(14)	24.4(14)	31.7(14)	2.3(11)	-10.6(11)	2.2(11)
C(10)	33.5(15)	23.1(14)	33.1(14)	1.0(11)	-8.1(12)	3.0(12)
C(11)	28.8(14)	18.9(13)	25.0(12)	-2.5(10)	-4.9(11)	-2.2(11)
C(12)	15.3(12)	20.7(13)	16.9(11)	-1.1(9)	-2.5(9)	-3(1)
C(13)	21.5(13)	16.8(12)	21.7(12)	-3(1)	-6.6(10)	-1(1)
C(14)	21.6(13)	22.9(14)	27.2(13)	-0.8(10)	-7.9(11)	-0.8(10)
C(15)	32.0(15)	29.6(15)	38.1(15)	-4.0(12)	-19.6(13)	-2.0(12)
C(16)	52.6(19)	31.8(16)	25.5(14)	-10.8(12)	-18.9(13)	2.1(14)
C(17)	42.6(17)	31.9(16)	23.5(13)	-8.8(11)	-1.3(12)	-0.5(13)
C(18)	26.3(14)	27.9(15)	25.7(13)	-7.0(11)	-4.0(11)	0.4(11)

C(19)	18.4(12)	14.9(12)	17.2(11)	-1.3(9)	-4.0(9)	-2.5(9)
C(20)	16.7(12)	29.8(14)	23.4(12)	-0.1(10)	-7.1(10)	-1.8(10)
C(21)	14.6(12)	43.4(17)	23.3(13)	-0.4(11)	-1.2(10)	-3.2(11)
C(22)	21.1(14)	56.7(19)	16.0(12)	3.3(12)	-1.9(10)	-5.3(13)
C(23)	15.7(12)	45.5(17)	19.8(12)	1.6(11)	-7.4(10)	-1.4(11)
C(24)	16.7(12)	18.9(13)	19.4(11)	-1.1(9)	-4.1(10)	-2.8(10)
C(25)	13.9(12)	28.4(14)	16.7(11)	-3.7(10)	-4.3(9)	-1.1(10)
C(26)	12.3(11)	27.4(14)	25.2(12)	-5.8(10)	-6.4(10)	0.6(10)
C(27)	24.6(14)	37.8(16)	24.9(13)	-8.4(11)	-5.2(11)	-6.6(12)
C(28)	33.2(16)	46.4(18)	33.3(15)	-19.8(13)	-10.4(13)	-4.3(13)
C(29)	27.9(15)	34.4(16)	42.4(16)	-13.5(13)	-12.0(13)	-4.4(12)
C(30)	19.5(13)	32.4(16)	34.0(14)	-5.2(12)	-1.8(11)	-3.8(11)
C(31)	19.5(13)	31.4(15)	25.4(13)	-8.2(11)	-3.5(10)	-3.7(11)
C(32)	18.0(12)	30.5(15)	24.9(13)	0.8(11)	-6.5(10)	-1.6(11)
C(33)	17.9(13)	37.7(16)	32.8(14)	1.6(12)	-3.7(11)	4.5(11)
C(34)	27.5(14)	26.6(15)	33.7(14)	-4.5(12)	-1.4(12)	7.0(12)
C(35)	25.4(14)	26.4(14)	25.9(13)	-6.9(11)	-1.5(11)	2.4(11)
C(36)	19.9(12)	26.9(14)	14.7(11)	-4.8(10)	-3.5(10)	-1(1)
C(37)	18.0(12)	20.3(13)	27.5(13)	-8.1(10)	-6(1)	2.2(10)
C(38)	29.2(15)	29.1(15)	35.0(15)	0.9(12)	-13.2(12)	-5.6(12)
C(39)	27.6(15)	26.6(16)	56.0(19)	-0.9(13)	-8.3(14)	-4.8(12)
C(40)	26.5(15)	33.4(17)	68(2)	-27.1(15)	-17.2(15)	1.7(13)
C(41)	24.3(14)	47.5(18)	44.5(17)	-28.1(15)	-15.4(13)	8.3(13)
C(42)	24.2(14)	34.9(16)	28.3(13)	-15.0(12)	-7.6(11)	5.7(12)

Table A3.12. Bond Lengths for red-TPSB BDP 2.

Atom	Atom	Length/Å	Atom	Atom	Length/Å
P(1)	C(7)	1.869(2)	C(13)	C(18)	1.389(3)
P(1)	C(12)	1.881(3)	C(14)	C(15)	1.388(3)
P(1)	C(19)	1.845(2)	C(15)	C(16)	1.371(4)
P(2)	C(24)	1.845(2)	C(16)	C(17)	1.383(4)
P(2)	C(25)	1.873(2)	C(17)	C(18)	1.387(3)
P(2)	C(36)	1.879(3)	C(19)	C(20)	1.383(3)
N(1)	N(2)	1.484(3)	C(19)	C(24)	1.413(3)
N(1)	C(11)	1.469(3)	C(20)	C(21)	1.385(3)
N(1)	C(12)	1.479(3)	C(21)	C(22)	1.377(3)
N(2)	C(7)	1.478(3)	C(22)	C(23)	1.387(3)
N(2)	C(8)	1.468(3)	C(23)	C(24)	1.386(3)
N(3)	N(4)	1.479(3)	C(25)	C(26)	1.502(3)
N(3)	C(35)	1.468(3)	C(26)	C(27)	1.387(3)

N(3)	C(36)	1.481(3)	C(26)	C(31)	1.392(3)
N(4)	C(25)	1.480(3)	C(27)	C(28)	1.384(4)
N(4)	C(32)	1.469(3)	C(28)	C(29)	1.368(4)
C(1)	C(2)	1.395(3)	C(29)	C(30)	1.381(4)
C(1)	C(6)	1.386(3)	C(30)	C(31)	1.381(4)
C(1)	C(7)	1.505(3)	C(32)	C(33)	1.518(4)
C(2)	C(3)	1.378(3)	C(33)	C(34)	1.515(4)
C(3)	C(4)	1.386(4)	C(34)	C(35)	1.520(3)
C(4)	C(5)	1.376(4)	C(36)	C(37)	1.508(3)
C(5)	C(6)	1.381(3)	C(37)	C(38)	1.386(3)
C(8)	C(9)	1.519(3)	C(37)	C(42)	1.395(3)
C(9)	C(10)	1.515(4)	C(38)	C(39)	1.382(4)
C(10)	C(11)	1.516(3)	C(39)	C(40)	1.374(4)
C(12)	C(13)	1.506(3)	C(40)	C(41)	1.376(4)
C(13)	C(14)	1.393(3)	C(41)	C(42)	1.383(4)

Table A3.13. Bond Angles for red-TPSB BDP 2.

Atom	Atom	Atom	Angle/°	Atom	Atom	Atom	Angle/°
C(7)	P(1)	C(12)	89.83(10)	C(16)	C(15)	C(14)	120.2(3)
C(19)	P(1)	C(7)	105.28(10)	C(15)	C(16)	C(17)	119.8(2)
C(19)	P(1)	C(12)	103.67(10)	C(16)	C(17)	C(18)	120.5(3)
C(24)	P(2)	C(25)	104.83(10)	C(17)	C(18)	C(13)	120.3(2)
C(24)	P(2)	C(36)	104.24(11)	C(20)	C(19)	P(1)	124.91(17)
C(25)	P(2)	C(36)	89.65(10)	C(20)	C(19)	C(24)	118.8(2)
C(11)	N(1)	N(2)	108.01(17)	C(24)	C(19)	P(1)	116.32(17)
C(11)	N(1)	C(12)	109.37(18)	C(19)	C(20)	C(21)	121.5(2)
C(12)	N(1)	N(2)	104.46(17)	C(22)	C(21)	C(20)	119.9(2)
C(7)	N(2)	N(1)	103.01(16)	C(21)	C(22)	C(23)	119.4(2)
C(8)	N(2)	N(1)	108.28(18)	C(24)	C(23)	C(22)	121.5(2)
C(8)	N(2)	C(7)	109.77(17)	C(19)	C(24)	P(2)	115.46(16)
N(4)	N(3)	C(36)	104.17(17)	C(23)	C(24)	P(2)	125.64(17)
C(35)	N(3)	N(4)	107.30(18)	C(23)	C(24)	C(19)	118.8(2)
C(35)	N(3)	C(36)	109.46(18)	N(4)	C(25)	P(2)	102.72(14)
N(3)	N(4)	C(25)	103.89(17)	N(4)	C(25)	C(26)	111.87(19)
C(32)	N(4)	N(3)	107.76(18)	C(26)	C(25)	P(2)	112.17(16)
C(32)	N(4)	C(25)	108.93(18)	C(27)	C(26)	C(25)	120.0(2)
C(2)	C(1)	C(7)	120.6(2)	C(27)	C(26)	C(31)	118.4(2)
C(6)	C(1)	C(2)	118.1(2)	C(31)	C(26)	C(25)	121.6(2)
C(6)	C(1)	C(7)	121.2(2)	C(28)	C(27)	C(26)	120.5(2)
C(3)	C(2)	C(1)	121.2(2)	C(29)	C(28)	C(27)	120.4(3)

C(2)	C(3)	C(4)	119.6(2)	C(28)	C(29)	C(30)	120.0(3)
C(5)	C(4)	C(3)	119.9(2)	C(29)	C(30)	C(31)	119.9(3)
C(4)	C(5)	C(6)	120.3(2)	C(30)	C(31)	C(26)	120.8(2)
C(5)	C(6)	C(1)	120.8(2)	N(4)	C(32)	C(33)	110.5(2)
N(2)	C(7)	P(1)	101.21(14)	C(34)	C(33)	C(32)	110.0(2)
N(2)	C(7)	C(1)	111.74(18)	C(33)	C(34)	C(35)	109.3(2)
C(1)	C(7)	P(1)	113.01(15)	N(3)	C(35)	C(34)	111.2(2)
N(2)	C(8)	C(9)	111.1(2)	N(3)	C(36)	P(2)	105.90(15)
C(10)	C(9)	C(8)	109.3(2)	N(3)	C(36)	C(37)	112.64(19)
C(9)	C(10)	C(11)	109.0(2)	C(37)	C(36)	P(2)	115.84(16)
N(1)	C(11)	C(10)	110.4(2)	C(38)	C(37)	C(36)	121.9(2)
N(1)	C(12)	P(1)	105.51(15)	C(38)	C(37)	C(42)	118.6(2)
N(1)	C(12)	C(13)	111.35(19)	C(42)	C(37)	C(36)	119.4(2)
C(13)	C(12)	P(1)	117.02(15)	C(39)	C(38)	C(37)	120.6(2)
C(14)	C(13)	C(12)	119.9(2)	C(40)	C(39)	C(38)	120.3(3)
C(18)	C(13)	C(12)	121.4(2)	C(39)	C(40)	C(41)	120.0(3)
C(18)	C(13)	C(14)	118.6(2)	C(40)	C(41)	C(42)	120.1(2)
C(15)	C(14)	C(13)	120.7(2)	C(41)	C(42)	C(37)	120.4(3)

Table A3.14. Torsion Angles for red-TPSB BDP 2.

A	B	C	D	Angle/°	A	B	C	D	Angle/°
P(1)	C(12)	C(13)	C(14)	-98.5(2)	C(12)	C(13)	C(14)	C(15)	178.0(2)
P(1)	C(12)	C(13)	C(18)	79.0(3)	C(12)	C(13)	C(18)	C(17)	-176.8(2)
P(1)	C(19)	C(20)	C(21)	177.9(2)	C(13)	C(14)	C(15)	C(16)	-0.9(4)
P(1)	C(19)	C(24)	P(2)	-1.0(2)	C(14)	C(13)	C(18)	C(17)	0.8(4)
P(1)	C(19)	C(24)	C(23)	-178.48(19)	C(14)	C(15)	C(16)	C(17)	0.3(4)
P(2)	C(25)	C(26)	C(27)	-120.2(2)	C(15)	C(16)	C(17)	C(18)	0.9(4)
P(2)	C(25)	C(26)	C(31)	59.0(3)	C(16)	C(17)	C(18)	C(13)	-1.5(4)
P(2)	C(36)	C(37)	C(38)	84.8(3)	C(18)	C(13)	C(14)	C(15)	0.4(3)
P(2)	C(36)	C(37)	C(42)	-92.5(2)	C(19)	P(1)	C(7)	N(2)	-132.92(14)
N(1)	N(2)	C(7)	P(1)	55.95(17)	C(19)	P(1)	C(7)	C(1)	107.45(17)
N(1)	N(2)	C(7)	C(1)	176.48(17)	C(19)	P(1)	C(12)	N(1)	100.95(15)
N(1)	N(2)	C(8)	C(9)	-62.0(2)	C(19)	P(1)	C(12)	C(13)	-23.5(2)
N(1)	C(12)	C(13)	C(14)	140.0(2)	C(19)	C(20)	C(21)	C(22)	1.5(4)
N(1)	C(12)	C(13)	C(18)	-42.4(3)	C(20)	C(19)	C(24)	P(2)	179.17(18)
N(2)	N(1)	C(11)	C(10)	-64.0(2)	C(20)	C(19)	C(24)	C(23)	1.7(3)
N(2)	N(1)	C(12)	P(1)	37.46(18)	C(20)	C(21)	C(22)	C(23)	-0.1(4)
N(2)	N(1)	C(12)	C(13)	165.39(18)	C(21)	C(22)	C(23)	C(24)	-0.5(4)
N(2)	C(8)	C(9)	C(10)	57.1(3)	C(22)	C(23)	C(24)	P(2)	-177.5(2)
N(3)	N(4)	C(25)	P(2)	52.33(17)	C(22)	C(23)	C(24)	C(19)	-0.3(4)

N(3)	N(4)	C(25)	C(26)	172.83(17)	C(24)	P(2)	C(25)	N(4)	-128.96(15)
N(3)	N(4)	C(32)	C(33)	-64.2(2)	C(24)	P(2)	C(25)	C(26)	110.76(17)
N(3)	C(36)	C(37)	C(38)	-37.3(3)	C(24)	P(2)	C(36)	N(3)	96.35(16)
N(3)	C(36)	C(37)	C(42)	145.4(2)	C(24)	P(2)	C(36)	C(37)	-29.30(19)
N(4)	N(3)	C(35)	C(34)	-63.9(2)	C(24)	C(19)	C(20)	C(21)	-2.3(4)
N(4)	N(3)	C(36)	P(2)	40.16(19)	C(25)	P(2)	C(24)	C(19)	-172.25(18)
N(4)	N(3)	C(36)	C(37)	167.74(18)	C(25)	P(2)	C(24)	C(23)	5.0(3)
N(4)	C(25)	C(26)	C(27)	125.0(2)	C(25)	P(2)	C(36)	N(3)	-8.87(16)
N(4)	C(25)	C(26)	C(31)	-55.8(3)	C(25)	P(2)	C(36)	C(37)	-134.52(18)
N(4)	C(32)	C(33)	C(34)	56.9(3)	C(25)	N(4)	C(32)	C(33)	-176.29(19)
C(1)	C(2)	C(3)	C(4)	1.4(4)	C(25)	C(26)	C(27)	C(28)	179.1(2)
C(2)	C(1)	C(6)	C(5)	-0.5(3)	C(25)	C(26)	C(31)	C(30)	-179.7(2)
C(2)	C(1)	C(7)	P(1)	71.9(2)	C(26)	C(27)	C(28)	C(29)	0.7(4)
C(2)	C(1)	C(7)	N(2)	-41.5(3)	C(27)	C(26)	C(31)	C(30)	-0.5(3)
C(2)	C(3)	C(4)	C(5)	-0.3(4)	C(27)	C(28)	C(29)	C(30)	-0.7(4)
C(3)	C(4)	C(5)	C(6)	-1.2(4)	C(28)	C(29)	C(30)	C(31)	0.0(4)
C(4)	C(5)	C(6)	C(1)	1.6(4)	C(29)	C(30)	C(31)	C(26)	0.6(4)
C(6)	C(1)	C(2)	C(3)	-1.1(3)	C(31)	C(26)	C(27)	C(28)	-0.1(4)
C(6)	C(1)	C(7)	P(1)	-107.5(2)	C(32)	N(4)	C(25)	P(2)	166.97(16)
C(6)	C(1)	C(7)	N(2)	139.1(2)	C(32)	N(4)	C(25)	C(26)	-72.5(2)
C(7)	P(1)	C(12)	N(1)	-4.75(15)	C(32)	C(33)	C(34)	C(35)	-51.3(3)
C(7)	P(1)	C(12)	C(13)	-129.19(18)	C(33)	C(34)	C(35)	N(3)	56.5(3)
C(7)	P(1)	C(19)	C(20)	5.5(2)	C(35)	N(3)	N(4)	C(25)	-177.64(16)
C(7)	P(1)	C(19)	C(24)	-174.36(17)	C(35)	N(3)	N(4)	C(32)	66.9(2)
C(7)	N(2)	C(8)	C(9)	-173.7(2)	C(35)	N(3)	C(36)	P(2)	154.65(16)
C(7)	C(1)	C(2)	C(3)	179.5(2)	C(35)	N(3)	C(36)	C(37)	-77.8(2)
C(7)	C(1)	C(6)	C(5)	179.0(2)	C(36)	P(2)	C(24)	C(19)	94.28(19)
C(8)	N(2)	C(7)	P(1)	171.11(15)	C(36)	P(2)	C(24)	C(23)	-88.4(2)
C(8)	N(2)	C(7)	C(1)	-68.4(2)	C(36)	P(2)	C(25)	N(4)	-24.31(15)
C(8)	C(9)	C(10)	C(11)	-53.9(3)	C(36)	P(2)	C(25)	C(26)	-144.59(18)
C(9)	C(10)	C(11)	N(1)	59.1(3)	C(36)	N(3)	N(4)	C(25)	-61.6(2)
C(11)	N(1)	N(2)	C(7)	-179.05(17)	C(36)	N(3)	N(4)	C(32)	-177.10(18)
C(11)	N(1)	N(2)	C(8)	64.7(2)	C(36)	N(3)	C(35)	C(34)	-176.3(2)
C(11)	N(1)	C(12)	P(1)	152.87(16)	C(36)	C(37)	C(38)	C(39)	-177.4(2)
C(11)	N(1)	C(12)	C(13)	-79.2(2)	C(36)	C(37)	C(42)	C(41)	177.4(2)
C(12)	P(1)	C(7)	N(2)	-28.79(15)	C(37)	C(38)	C(39)	C(40)	0.2(4)
C(12)	P(1)	C(7)	C(1)	-148.42(17)	C(38)	C(37)	C(42)	C(41)	0.0(4)
C(12)	P(1)	C(19)	C(20)	-88.2(2)	C(38)	C(39)	C(40)	C(41)	-0.2(4)
C(12)	P(1)	C(19)	C(24)	92.01(19)	C(39)	C(40)	C(41)	C(42)	0.1(4)
C(12)	N(1)	N(2)	C(7)	-62.7(2)	C(40)	C(41)	C(42)	C(37)	0.0(4)
C(12)	N(1)	N(2)	C(8)	-178.91(17)	C(42)	C(37)	C(38)	C(39)	-0.1(4)

C(12) N(1) C(11) C(10) -177.2(2)

Table A3.15. Hydrogen Atom Coordinates ($\text{\AA} \times 10^4$) and Isotropic Displacement Parameters ($\text{\AA}^2 \times 10^3$) for red-TPSB BDP 2.

Atom	x	y	z	U(eq)
H(2)	1373	6790	5401	28
H(3)	1815	8134	6216	32
H(4)	3358	9620	5606	31
H(5)	4451	9734	4192	31
H(6)	4075	8335	3403	27
H(7)	3123	6520	3304	22
H(8A)	3769	5289	5065	29
H(8B)	4177	4871	4158	29
H(9A)	4268	3167	5361	34
H(9B)	2779	3422	5731	34
H(10A)	2795	1913	4946	37
H(10B)	3624	2734	4094	37
H(11A)	1387	2864	3882	29
H(11B)	1008	3326	4774	29
H(12)	-53	4860	3976	22
H(14)	-1614	4566	3096	29
H(15)	-2148	4019	1849	39
H(16)	-552	3935	671	42
H(17)	1594	4382	740	39
H(18)	2159	4863	2003	32
H(20)	3150	7282	2023	29
H(21)	3491	7997	490	34
H(22)	1717	8648	-304	40
H(23)	-392	8562	446	34
H(25)	-2255	8465	918	24
H(27)	-2836	7107	153	34
H(28)	-3905	5416	62	42
H(29)	-5170	4311	1292	40
H(30)	-5344	4869	2641	35
H(31)	-4249	6537	2749	30
H(32A)	-4965	8998	1033	30
H(32B)	-3844	9953	613	30
H(33A)	-5787	11014	985	38
H(33B)	-5893	10218	1989	38
H(34A)	-5008	12047	1983	36

H(34B)	-3934	11944	1162	36
H(35A)	-2946	11359	2482	31
H(35B)	-4032	10373	2909	31
H(36)	-2442	9015	3229	24
H(38)	-331	10708	1412	38
H(39)	1512	11676	1554	45
H(40)	2237	11402	2933	47
H(41)	1113	10165	4180	42
H(42)	-738	9194	4049	33

A3.2.3 Crystallographic Data for red-TPPB BDP 4

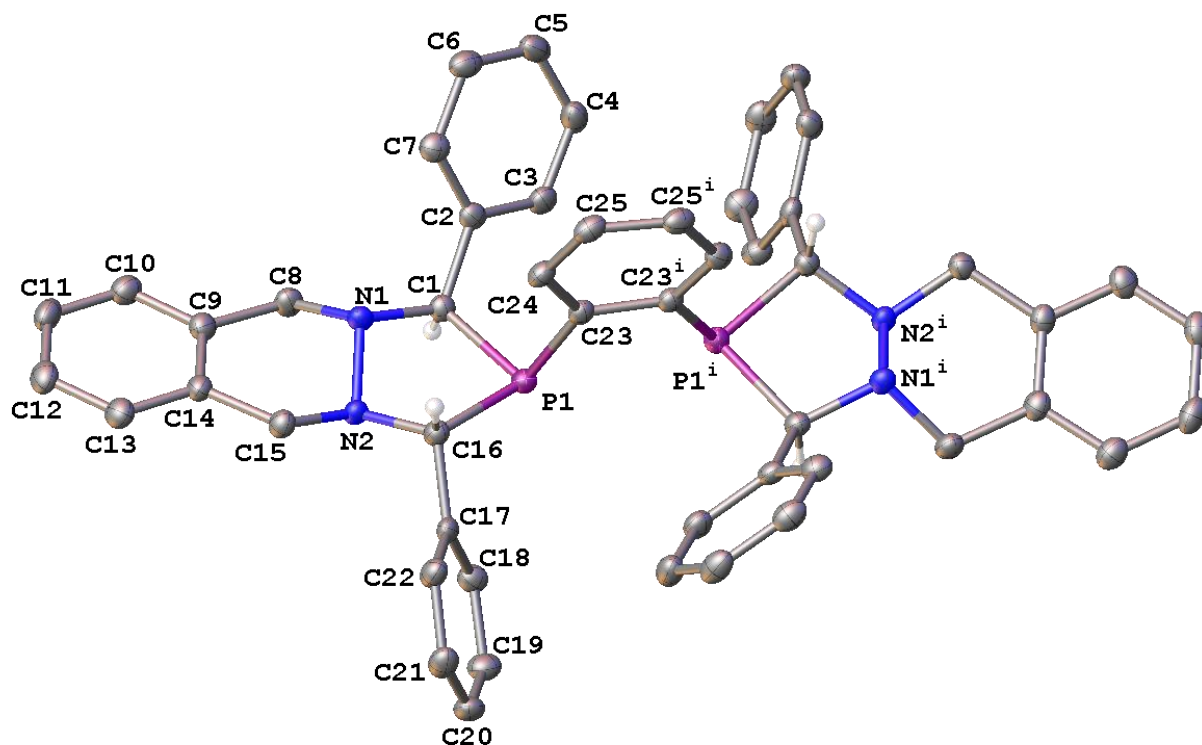


Figure A3.19. A molecular drawing of red-TPPB BDP 4 shown with 50% probability ellipsoids. All H atoms except those on anomeric C atoms are omitted. Symmetry code: i = 1-x, 1-y, z.

Data Collection

A colorless crystal with approximate dimensions $0.55 \times 0.243 \times 0.03 \text{ mm}^3$ was selected under oil under ambient conditions and attached to the tip of a MiTeGen MicroMount©. The crystal was mounted in a stream of cold nitrogen at 100(1) K and centered in the X-ray beam by using a video camera.

The crystal evaluation and data collection were performed on a Bruker Quazar SMART APEXII diffractometer with Mo K α ($\lambda = 0.71073 \text{ \AA}$) radiation and the diffractometer to crystal distance of 7.00 cm [1].

The initial cell constants were obtained from three series of ω scans at different starting angles. Each series consisted of 12 frames collected at intervals of 0.5° in a 6° range about ω with the exposure time of 3 seconds per frame. The reflections were successfully indexed by an automated indexing routine built in the APEXII program suite. The final cell constants were calculated from a set of 9893 strong reflections from the actual data collection.

The data were collected by using the full sphere data collection routine to survey the reciprocal space to the extent of a full sphere to a resolution of 0.80 \AA . A total of 22130 data were harvested by collecting 9 sets of frames with 0.6° scans in ω with exposure times of 15 sec per frame. These highly redundant datasets were corrected for Lorentz and polarization effects. The absorption correction was based on fitting a function to the empirical transmission surface as sampled by multiple equivalent measurements. [2]

Structure Solution and Refinement

The systematic absences in the diffraction data were uniquely consistent for the space group *Fdd2* that yielded chemically reasonable and computationally stable results of refinement [3-8].

A successful solution by the direct methods provided most non-hydrogen atoms from the *E*-map. The remaining non-hydrogen atoms were located in an alternating series of least-squares cycles and difference Fourier maps. All non-hydrogen atoms were refined with anisotropic displacement coefficients. All hydrogen atoms were included in the structure factor calculation at idealized positions and were allowed to ride on the neighboring atoms with relative isotropic displacement coefficients.

The diphosphine resides on a crystallographic twofold axis and only one half of it is symmetry-independent. Both unique anomeric carbons C1 and C16 have the same configuration,

arbitrarily shown as R. In the lattice there are two stereoisomers; in one all chiral carbons are R, whereas in the other S.

The final least-squares refinement of 253 parameters against 47953 data resulted in residuals R (based on F^2 for $I \geq 2\sigma$) and wR (based on F^2 for all data) of 0.0339 and 0.0940, respectively. The final difference Fourier map was featureless.

Summary

Crystal data for $C_{50}H_{44}N_4P_2$ ($M = 762.83$ g/mol): orthorhombic, space group Fdd2 (no. 43), $a = 12.554(6)$ Å, $b = 54.22(2)$ Å, $c = 11.598(6)$ Å, $V = 7894(6)$ Å³, $Z = 8$, $T = 100.0$ K, $\mu(\text{MoK}\alpha) = 0.152$ mm⁻¹, $D_{\text{calc}} = 1.284$ g/cm³, 47953 reflections measured ($3.004^\circ \leq 2\theta \leq 52.774^\circ$), 4043 unique ($R_{\text{int}} = 0.0592$, $R_{\text{sigma}} = 0.0289$) which were used in all calculations. The final R_1 was 0.0339 ($I > 2\sigma(I)$) and wR_2 was 0.0940 (all data).

References

- [1] Bruker-AXS (2016). *APEX3*. Version 2016.5-0. Madison, Wisconsin, USA.
- [2] Krause, L., Herbst-Irmer, R., Sheldrick, G. M. & Stalke, D. (2015). *J. Appl. Cryst.* 48, 3-10.
- [3] Sheldrick, G. M. (2013b). *XPREF*. Version 2013/1. Georg-August-Universität Göttingen, Göttingen, Germany.
- [4] Sheldrick, G. M. (2013a). The *SHELX* homepage, <http://shelx.uni-ac.gwdg.de/SHELX/>.
- [5] Sheldrick, G. M. (2015a). *Acta Cryst. A*, 71, 3-8.
- [6] Sheldrick, G. M. (2015b). *Acta Cryst. C*, 71, 3-8.
- [7] Dolomanov, O. V., Bourhis, L. J., Gildea, R. J., Howard, J. A. K. & Puschmann, H. (2009). *J. Appl. Crystallogr.* 42, 339-341.
- [8] Guzei, I. A. (2007-2013). Programs *Gn*. University of Wisconsin-Madison, Madison, Wisconsin, USA.

Table A3.16. Crystal Data and Structure Refinement for red-TPPB BDP 4.

Empirical formula	C ₅₀ H ₄₄ N ₄ P ₂
Formula weight	762.83
Temperature/K	100.0
Crystal system	orthorhombic
Space group	Fdd2
a/Å	12.554(6)
b/Å	54.22(2)
c/Å	11.598(6)
α/°	90
β/°	90
γ/°	90
Volume/Å ³	7894(6)
Z	8
ρ _{calc} /g/cm ³	1.284
μ/mm ⁻¹	0.152
F(000)	3216.0
Crystal size/mm ³	0.55 × 0.243 × 0.03
Radiation	MoKα (λ = 0.71073)
2θ range for data collection/°	3.004 to 52.774
Index ranges	-15 ≤ h ≤ 15, -67 ≤ k ≤ 67, -14 ≤ l ≤ 14
Reflections collected	47953
Independent reflections	4043 [R _{int} = 0.0592, R _{sigma} = 0.0289]
Data/restraints/parameters	4043/1/253
Goodness-of-fit on F ²	1.000
Final R indexes [I >= 2σ (I)]	R ₁ = 0.0339, wR ₂ = 0.0930
Final R indexes [all data]	R ₁ = 0.0355, wR ₂ = 0.0940
Largest diff. peak/hole / e Å ⁻³	0.34/-0.17
Flack parameter	-0.09(5)

Table A3.17. Fractional Atomic Coordinates (×10⁴) and Equivalent Isotropic Displacement Parameters (Å²×10³) for red-TPPB BDP 4. U_{eq} is defined as 1/3 of the trace of the orthogonalised U_{ij} tensor.

Atom	x	y	z	U(eq)
P1	5557.6(4)	5255.3(2)	1718.9(5)	18.02(17)
N1	7437.2(14)	5495.5(3)	1997.1(18)	19.6(4)
N2	6631.7(14)	5677.7(3)	1585.0(18)	18.3(4)
C1	7046.5(17)	5254.3(4)	1579(2)	18.7(5)
C2	7568.1(17)	5034.2(4)	2134(2)	19.2(5)
C3	7350.0(17)	4802.2(4)	1672(2)	23.2(5)
C4	7796.9(18)	4591.6(5)	2147(3)	27.9(6)
C5	8485.0(18)	4611.9(5)	3086(3)	28.4(6)
C6	8703.1(19)	4841.3(5)	3540(2)	26.4(6)

C7	8243.3(19)	5052.5(5)	3077(2)	23.0(5)
C8	8426.7(18)	5553.7(4)	1369(2)	22.8(5)
C9	8782.9(18)	5815.1(4)	1577(2)	21.8(5)
C10	9839.1(19)	5884.5(5)	1432(2)	26.6(6)
C11	10145.9(19)	6126.7(5)	1602(2)	28.1(5)
C12	9394.4(18)	6304.3(5)	1904(2)	26.8(6)
C13	8349.8(19)	6236.1(5)	2053(2)	25.7(5)
C14	8034.3(17)	5991.4(5)	1895(2)	20.7(5)
C15	6900.5(17)	5915.1(4)	2118(2)	20.8(5)
C16	5589.5(15)	5593.4(4)	2043(2)	18.8(5)
C17	4691.6(17)	5731.1(4)	1449(2)	19.5(5)
C18	4410.9(17)	5676.8(5)	312(2)	22.9(5)
C19	3583.1(19)	5799.7(5)	-226(2)	27.2(6)
C20	3035.7(18)	5983.1(5)	358(3)	26.9(6)
C21	3310.0(19)	6041.8(5)	1477(2)	26.3(6)
C22	4129.5(18)	5913.4(4)	2026(2)	24.1(5)
C23	5294.6(16)	5110.6(4)	3125(2)	18.0(5)
C24	5617.7(17)	5212.2(4)	4181(2)	20.5(5)
C25	5314.8(17)	5105.4(5)	5213(2)	22.5(5)

Table A3.18. Anisotropic Displacement Parameters ($\text{\AA}^2 \times 10^3$) for red-TPPB BDP **4**. The Anisotropic Displacement Factor Exponent Takes the Form: $-2\pi^2[h^2a^{*2}U_{11}+2hka^*b^*U_{12}+\dots]$.

Atom	U_{11}	U_{22}	U_{33}	U_{23}	U_{13}	U_{12}
P1	16.8(3)	17.4(3)	19.8(3)	0.8(2)	-1.3(2)	0.5(2)
N1	15.6(9)	17.2(9)	26.0(11)	1.9(8)	0.3(8)	2.2(7)
N2	13.4(9)	16.6(9)	25.0(11)	0.5(8)	-0.6(8)	0.8(7)
C1	16.8(10)	18.4(11)	20.8(12)	-0.7(9)	2.3(9)	0.5(8)
C2	14.7(10)	20.7(11)	22.3(11)	1.4(9)	4.2(9)	2.0(8)
C3	15.0(11)	25.2(12)	29.5(13)	1.3(11)	0.5(10)	1.7(8)
C4	19.8(11)	20.2(12)	43.6(16)	2.1(11)	2.2(11)	0.0(9)
C5	21.1(12)	26.9(13)	37.0(16)	12.3(12)	3.7(11)	3.3(10)
C6	20.3(12)	33.9(14)	25.1(14)	6.2(11)	0.5(10)	2.8(10)
C7	21.4(11)	25.4(13)	22.2(12)	0.4(10)	3.2(10)	1.6(9)
C8	16.7(11)	21.9(12)	29.9(13)	0.2(10)	3.5(9)	2.4(9)
C9	20.5(11)	22.3(12)	22.7(13)	3.6(10)	0.4(9)	-1.7(8)
C10	20.6(12)	30.9(13)	28.4(14)	3.8(11)	0(1)	0.3(10)
C11	19.7(11)	34.0(13)	30.5(14)	4.8(11)	-2(1)	-7.3(10)
C12	27.3(13)	27.3(13)	25.7(14)	-0.9(11)	-4.5(10)	-6.9(9)
C13	26.0(12)	24.5(12)	26.6(14)	-1.5(10)	-4.5(10)	-2.3(10)
C14	18.6(11)	20.5(12)	22.9(13)	2.6(10)	-3.2(9)	-2.5(8)
C15	18.9(11)	19.7(12)	23.8(13)	-2.6(10)	-1.0(9)	-0.3(8)
C16	16.7(11)	18.2(11)	21.6(13)	-0.9(9)	-0.9(9)	0.3(8)
C17	13.9(10)	18.1(11)	26.4(13)	3.6(9)	-0.7(9)	-3.1(8)
C18	20.6(12)	23.3(13)	24.8(13)	2.4(10)	2.7(10)	3.0(9)

C19	25.2(12)	30.4(13)	25.9(14)	3.9(11)	-3.9(10)	2.7(10)
C20	20.6(11)	24.0(13)	36.2(14)	6.2(11)	-5.9(10)	3.4(9)
C21	18.9(11)	21.9(12)	38.1(16)	-4.1(11)	0.6(10)	3.5(9)
C22	19.2(10)	21.2(12)	31.9(14)	-3.5(10)	-3.9(10)	-0.4(9)
C23	13.8(10)	19.1(12)	21.2(12)	-0.1(9)	0.1(9)	1.5(8)
C24	15.5(11)	23.4(11)	22.7(13)	-2.8(10)	-3.1(9)	0.7(8)
C25	17.1(11)	30.2(14)	20.3(12)	-4(1)	-1.8(10)	3.5(9)

Table A3.19. Bond Lengths for red-TPPB BDP 4.

Atom	Atom	Length/Å	Atom	Atom	Length/Å
P1	C1	1.876(2)	C9	C14	1.390(3)
P1	C16	1.872(3)	C10	C11	1.383(4)
P1	C23	1.839(3)	C11	C12	1.393(4)
N1	N2	1.492(3)	C12	C13	1.373(3)
N1	C1	1.479(3)	C13	C14	1.397(4)
N1	C8	1.474(3)	C14	C15	1.505(3)
N2	C15	1.467(3)	C16	C17	1.518(3)
N2	C16	1.484(3)	C17	C18	1.396(4)
C1	C2	1.506(3)	C17	C22	1.387(3)
C2	C3	1.395(4)	C18	C19	1.383(3)
C2	C7	1.387(4)	C19	C20	1.386(4)
C3	C4	1.387(3)	C20	C21	1.380(4)
C4	C5	1.394(4)	C21	C22	1.396(4)
C5	C6	1.378(4)	C23	C23 ¹	1.409(4)
C6	C7	1.390(4)	C23	C24	1.403(3)
C8	C9	1.505(3)	C24	C25	1.383(4)
C9	C10	1.389(3)	C25	C25 ¹	1.390(5)

Table A3.20. Bond Angles for red-TPPB BDP 4.

Atom	Atom	Atom	Angle/°	Atom	Atom	Atom	Angle/°
C16	P1	C1	89.94(10)	C11	C10	C9	120.4(2)
C23	P1	C1	104.74(11)	C10	C11	C12	120.2(2)
C23	P1	C16	104.10(11)	C13	C12	C11	119.5(2)
C1	N1	N2	104.82(17)	C12	C13	C14	120.7(2)
C8	N1	N2	105.71(17)	C9	C14	C13	119.7(2)
C8	N1	C1	107.86(18)	C9	C14	C15	119.7(2)
C15	N2	N1	106.86(17)	C13	C14	C15	120.5(2)
C15	N2	C16	108.81(18)	N2	C15	C14	112.75(19)
C16	N2	N1	106.19(16)	N2	C16	P1	104.40(14)
N1	C1	P1	107.42(14)	N2	C16	C17	109.92(18)
N1	C1	C2	114.6(2)	C17	C16	P1	112.01(15)
C2	C1	P1	113.48(16)	C18	C17	C16	120.8(2)
C3	C2	C1	117.7(2)	C22	C17	C16	120.6(2)

C7	C2	C1	123.1(2)	C22	C17	C18	118.6(2)
C7	C2	C3	119.2(2)	C19	C18	C17	120.9(2)
C4	C3	C2	120.7(2)	C18	C19	C20	119.8(3)
C3	C4	C5	119.8(2)	C21	C20	C19	120.1(2)
C6	C5	C4	119.5(2)	C20	C21	C22	119.9(2)
C5	C6	C7	120.9(3)	C17	C22	C21	120.6(2)
C2	C7	C6	120.0(2)	C23 ¹	C23	P1	117.21(7)
N1	C8	C9	111.87(19)	C24	C23	P1	123.67(18)
C10	C9	C8	121.3(2)	C24	C23	C23 ¹	119.08(14)
C10	C9	C14	119.4(2)	C25	C24	C23	120.8(2)
C14	C9	C8	119.3(2)	C24	C25	C25 ¹	120.06(14)

Table A3.21. Torsion Angles for red-TPPB BDP 4.

A	B	C	D	Angle/°	A	B	C	D	Angle/°
P1	C1	C2	C3	64.9(3)	C8	N1	C1	C2	82.5(2)
P1	C1	C2	C7	-114.8(2)	C8	C9	C10	C11	178.5(2)
P1	C16	C17	C18	-41.8(3)	C8	C9	C14	C13	-177.8(2)
P1	C16	C17	C22	138.02(19)	C8	C9	C14	C15	4.8(4)
P1	C23	C24	C25	174.32(18)	C9	C10	C11	C12	-0.9(4)
N1	N2	C15	C14	54.2(2)	C9	C14	C15	N2	-20.3(3)
N1	N2	C16	P1	-46.61(19)	C10	C9	C14	C13	0.7(4)
N1	N2	C16	C17	-166.92(18)	C10	C9	C14	C15	-176.7(2)
N1	C1	C2	C3	-171.2(2)	C10	C11	C12	C13	1.2(4)
N1	C1	C2	C7	9.1(3)	C11	C12	C13	C14	-0.5(4)
N1	C8	C9	C10	156.8(2)	C12	C13	C14	C9	-0.4(4)
N1	C8	C9	C14	-24.7(3)	C12	C13	C14	C15	176.9(2)
N2	N1	C1	P1	-38.1(2)	C13	C14	C15	N2	162.4(2)
N2	N1	C1	C2	-165.18(17)	C14	C9	C10	C11	0.0(4)
N2	N1	C8	C9	58.2(2)	C15	N2	C16	P1	-161.32(15)
N2	C16	C17	C18	73.8(3)	C15	N2	C16	C17	78.4(2)
N2	C16	C17	C22	-106.4(2)	C16	P1	C1	N1	10.24(17)
C1	P1	C16	N2	20.36(16)	C16	P1	C1	C2	137.96(19)
C1	P1	C16	C17	139.25(17)	C16	P1	C23	C23 ¹	148.3(2)
C1	P1	C23	C23 ¹	-118.0(2)	C16	P1	C23	C24	-29.7(2)
C1	P1	C23	C24	64.0(2)	C16	N2	C15	C14	168.47(19)
C1	N1	N2	C15	172.05(18)	C16	C17	C18	C19	179.1(2)
C1	N1	N2	C16	56.0(2)	C16	C17	C22	C21	179.4(2)
C1	N1	C8	C9	169.9(2)	C17	C18	C19	C20	1.4(4)
C1	C2	C3	C4	-179.5(2)	C18	C17	C22	C21	-0.8(4)
C1	C2	C7	C6	-179.5(2)	C18	C19	C20	C21	-0.5(4)
C2	C3	C4	C5	-1.1(4)	C19	C20	C21	C22	-1.0(4)
C3	C2	C7	C6	0.8(4)	C20	C21	C22	C17	1.7(4)
C3	C4	C5	C6	0.8(4)	C22	C17	C18	C19	-0.7(4)
C4	C5	C6	C7	0.2(4)	C23	P1	C1	N1	-94.33(17)

C5	C6	C7	C2	-1.0(4)	C23	P1	C1	C2	33.4(2)
C7	C2	C3	C4	0.3(4)	C23	P1	C16	N2	125.55(15)
C8	N1	N2	C15	-74.1(2)	C23	P1	C16	C17	-115.55(16)
C8	N1	N2	C16	169.86(17)	C23 ¹	C23	C24	C25	-3.6(4)
C8	N1	C1	P1	-150.41(16)	C23	C24	C25	C25 ¹	0.1(4)

Table A3.22. Hydrogen Atom Coordinates ($\text{\AA}\times 10^4$) and Isotropic Displacement Parameters ($\text{\AA}^2\times 10^3$) for red-TPPB BDP **4**.

Atom	<i>x</i>	<i>y</i>	<i>z</i>	U(eq)
H1	7212.09	5245.9	736.26	22
H3	6890.66	4788.37	1023.8	28
H4	7634.55	4434.03	1834.96	33
H5	8801.49	4468.59	3409.58	34
H6	9173.77	4855.2	4178.53	32
H7	8391.4	5209.19	3406.79	28
H8A	8309.36	5528.86	532.79	27
H8B	8995.92	5439.09	1617.84	27
H10	10354.15	5764.82	1215.02	32
H11	10872.03	6172.19	1511.73	34
H12	9602.67	6471.38	2005.48	32
H13	7836.68	6356.6	2265.27	31
H15A	6784.16	5903.49	2960.26	25
H15B	6416.18	6043.62	1813.45	25
H16	5556.26	5620.99	2894.66	23
H18	4793.93	5553.65	-97.88	28
H19	3390.33	5758.41	-994.77	33
H20	2470.59	6068.54	-12.48	32
H21	2941.85	6169.35	1872.32	32
H22	4303.8	5951.28	2803.5	29
H24	6049.5	5356.14	4187.27	25
H25	5537.39	5176.19	5922.32	27

A3.2.4 Crystallographic Data for TNSB BDP 7

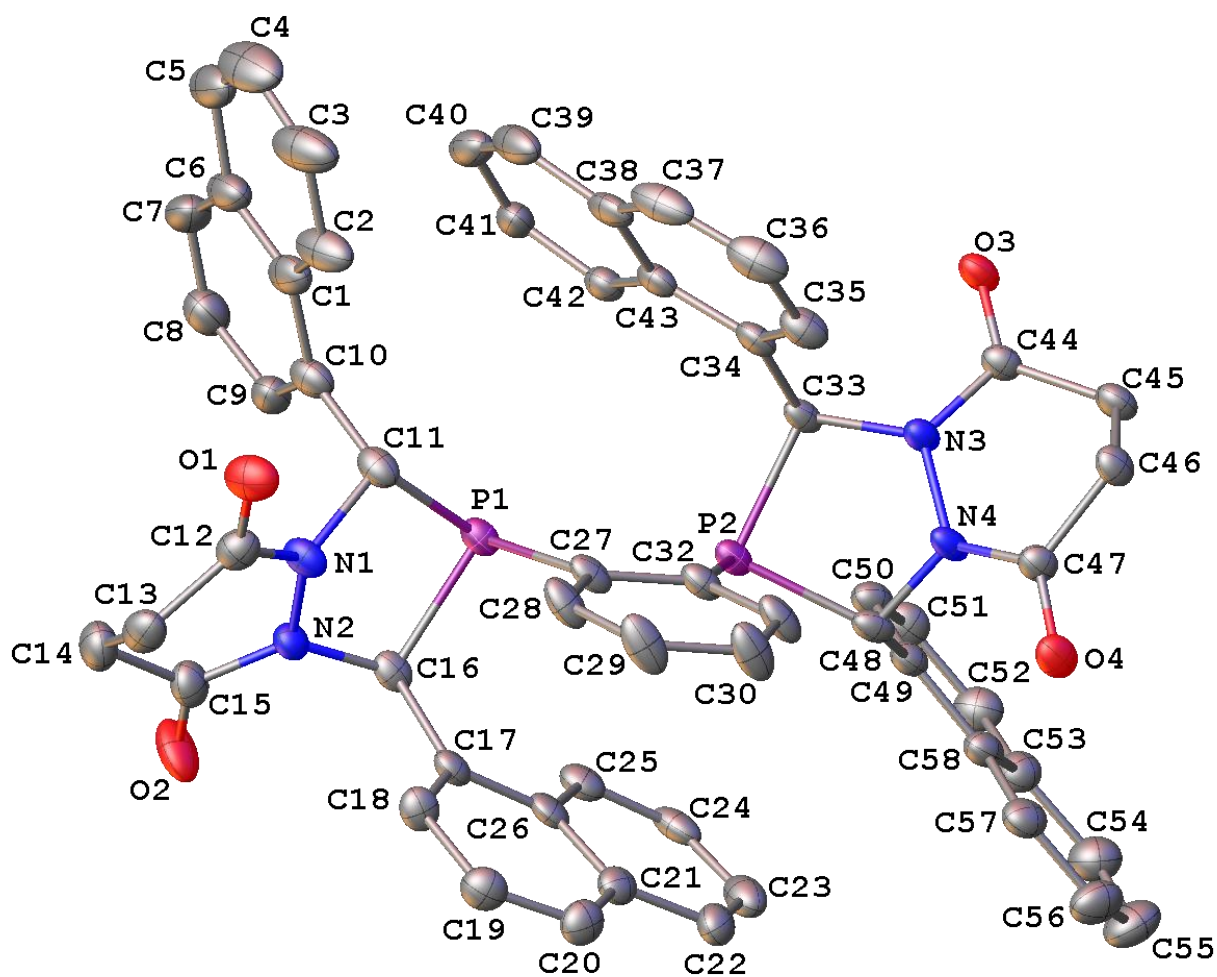


Figure A3.20. A molecular drawing of the first diposphine in TNSB BDP 7 shown with 40% probability ellipsoids. All H atoms are omitted.

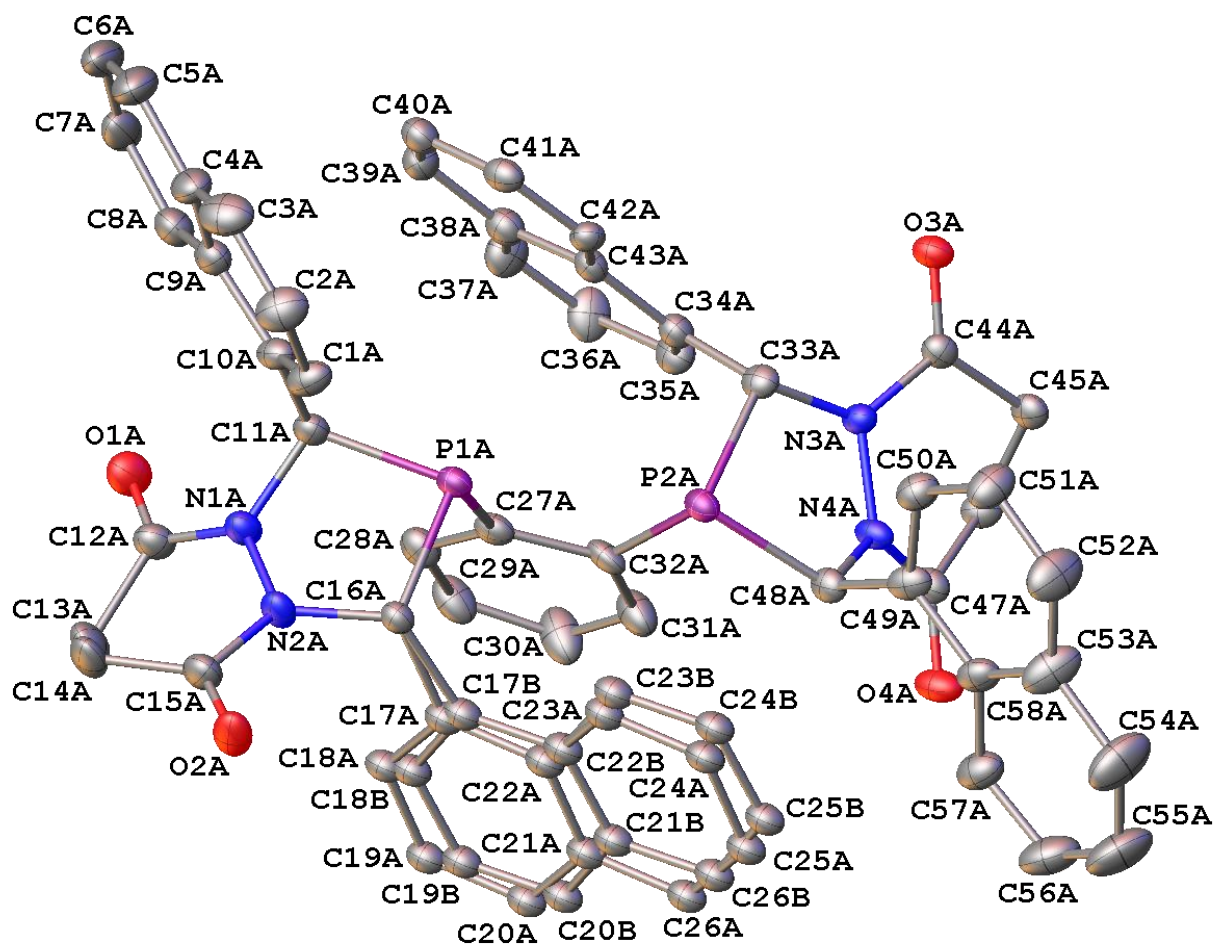


Figure A3.21. A molecular drawing of the second diphosphine in TNSB BDP 7 shown with 40% probability ellipsoids. All H atoms are omitted. Both disordered positions of the disordered naphthalenyl group are shown.

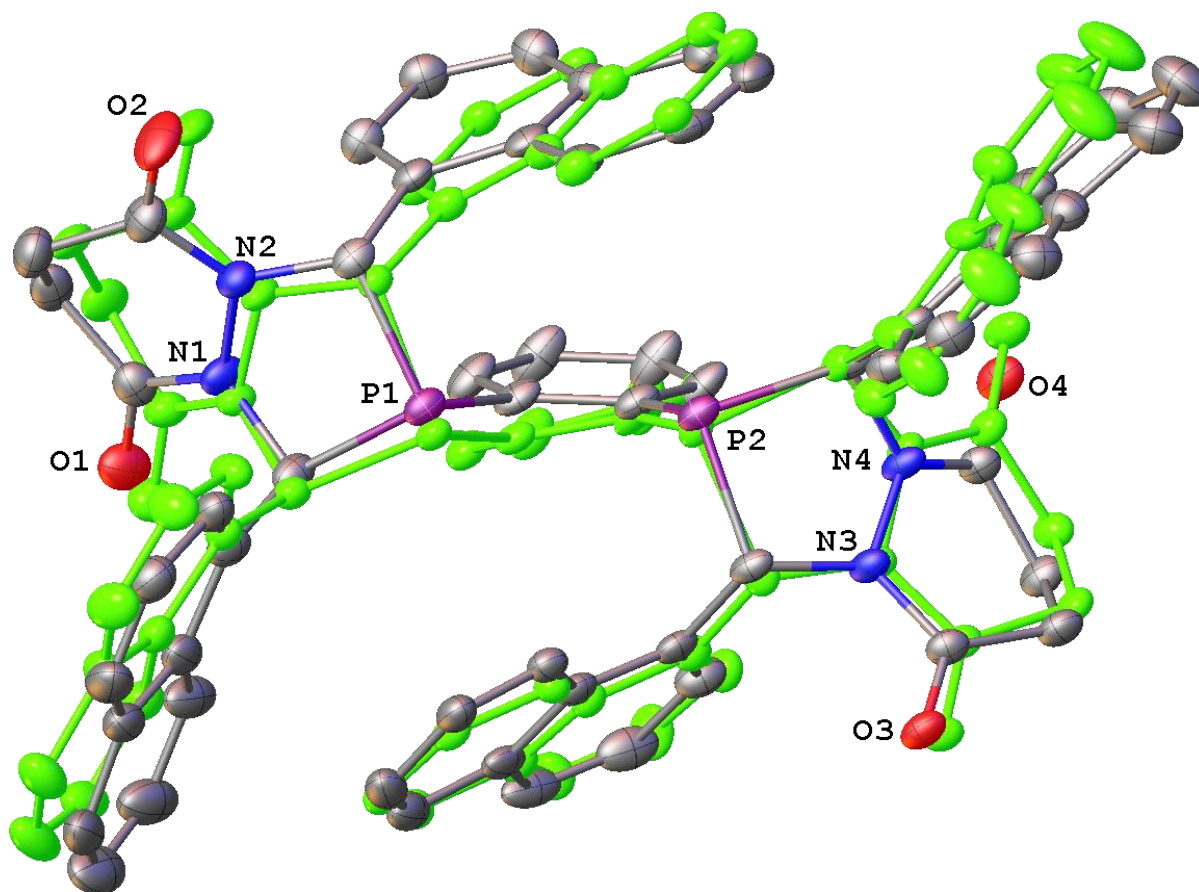


Figure A3.22. A superposition of the two symmetry-independent disphosphines. All H atoms are omitted.

Data Collection

A colorless crystal with approximate dimensions $0.248 \times 0.018 \times 0.016 \text{ mm}^3$ was selected under oil under ambient conditions and attached to the tip of a MiTeGen MicroMount®. The crystal was mounted in a stream of cold nitrogen at 100(1) K and centered in the X-ray beam by using a video camera.

The crystal evaluation and data collection were performed on a Bruker Quazar SMART APEXII diffractometer with Mo K_α ($\lambda = 0.71073 \text{ \AA}$) radiation and the diffractometer to crystal distance of 4.96 cm [1].

The initial cell constants were obtained from three series of ω scans at different starting angles. Each series consisted of 12 frames collected at intervals of 0.5° in a 6° range about ω with the exposure time of 10 seconds per frame. The reflections were successfully indexed by an automated indexing routine built in the APEXII program suite. The final cell constants were calculated from a set of 9945 strong reflections from the actual data collection.

The data were collected by using the full sphere data collection routine to survey the reciprocal space to the extent of a full sphere to a resolution of 0.82 \AA . A total of 155176 data were harvested by collecting 4 sets of frames with 0.5° scans in ω and ϕ with exposure times of 180 sec per frame. These highly redundant datasets were corrected for Lorentz and polarization effects. The absorption correction was based on fitting a function to the empirical transmission surface as sampled by multiple equivalent measurements. [2]

Structure Solution and Refinement

The systematic absences in the diffraction data were uniquely consistent for the space group $P2_1/c$ that yielded chemically reasonable and computationally stable results of refinement [3-8].

A successful solution by the direct methods provided most non-hydrogen atoms from the E -map. The remaining non-hydrogen atoms were located in an alternating series of least-squares cycles and difference Fourier maps. All non-hydrogen atoms were refined with anisotropic displacement coefficients. All hydrogen atoms were included in the structure factor calculation at idealized positions and were allowed to ride on the neighboring atoms with relative isotropic displacement coefficients.

There are two symmetry independent diphosphines in the asymmetric unit with identical composition but different conformations.

The C17a naphthalenyl group, equally disordered over two positions, was refined with constraints.

There were five or more fully or partially occupied molecules of CH₂Cl₂, pentane, and unidentifiable solvents present in the asymmetric unit. A significant amount of time was invested in identifying and refining the disordered molecules. Bond length restraints were applied to model the molecules but the resulting isotropic displacement coefficients suggested the molecules were mobile. In addition, the refinement was computationally unstable. Option SQUEEZE of program PLATON [9] was used to correct the diffraction data for diffuse scattering effects and to identify the solvent molecules. PLATON calculated the upper limit of volume that can be occupied by the solvent to be 2564 Å³, or 23% of the unit cell volume. The program calculated 762 electrons in the unit cell for the diffuse species. This approximately corresponds to two molecules of CH₂Cl₂ and 2.5 molecules of pentane in the asymmetric unit (756 electrons). However, this is an approximation because the diphosphine of interest has also been exposed to chloroform, ethyl acetate, and THF, and these solvents may also be present. Please note that all derived results in the following tables are based on the known contents. No data are given for the diffusely scattering species.

The final least-squares refinement of 1153 parameters against 20864 data resulted in residuals R (based on F^2 for $I \geq 2\sigma$) and wR (based on F^2 for all data) of 0.0874 and 0.2219, respectively. The final difference Fourier map was featureless.

Summary

Crystal data for C₅₈H₄₄N₄O₄P₂ (M = 922.91 g/mol): monoclinic, space group P2₁/c (no. 14), a = 18.883(5) Å, b = 35.438(9) Å, c = 16.404(4) Å, β = 90.815(10)°, V = 10976(5) Å³, Z = 8, T = 100.0 K, μ (MoK α) = 0.126 mm⁻¹, D_{calc} = 1.117 g/cm³, 155176 reflections measured ($2.156^\circ \leq 2\theta \leq 51.436^\circ$), 20864 unique (R_{int} = 0.1053, R_{sigma} = 0.0734) which were used in all calculations. The final R_1 was 0.0874 ($I > 2\sigma(I)$) and wR_2 was 0.2219 (all data).

References

- [1] Bruker-AXS (2016). *APEX3*. Version 2016.5-0. Madison, Wisconsin, USA.
- [2] Krause, L., Herbst-Irmer, R., Sheldrick, G. M. & Stalke, D. (2015). *J. Appl. Cryst.* 48, 3-10.
- [3] Sheldrick, G. M. (2013b). *XPREF*. Version 2013/1. Georg-August-Universität Göttingen, Göttingen, Germany.
- [4] Sheldrick, G. M. (2013a). The *SHELX* homepage, <http://shelx.uni-ac.gwdg.de/SHELX/>.
- [5] Sheldrick, G. M. (2015a). *Acta Cryst. A*, 71, 3-8.
- [6] Sheldrick, G. M. (2015b). *Acta Cryst. C*, 71, 3-8.
- [7] Dolomanov, O. V., Bourhis, L. J., Gildea, R. J., Howard, J. A. K. & Puschmann, H. (2009). *J. Appl. Crystallogr.* 42, 339-341.
- [8] Guzei, I. A. (2007-2013). Programs *Gn*. University of Wisconsin-Madison, Madison, Wisconsin, USA.
- [9] Spek, A. L. (2015). *Acta Cryst. C*, 71, 9-18.

Table A3.23. Crystal Data and Structure Refinement for TNSB BDP 7.

Empirical formula	C ₅₈ H ₄₄ N ₄ O ₄ P ₂ x solvents
Formula weight	922.91
Temperature/K	100.0
Crystal system	monoclinic
Space group	P2 ₁ /c
a/Å	18.883(5)
b/Å	35.438(9)
c/Å	16.404(4)
α/°	90
β/°	90.815(10)
γ/°	90
Volume/Å ³	10976(5)
Z	8
ρ _{calc} /g/cm ³	1.117
μ/mm ⁻¹	0.126
F(000)	3856.0
Crystal size/mm ³	0.248 × 0.018 × 0.016
Radiation	MoKα (λ = 0.71073)
2θ range for data collection/°	2.156 to 51.436
Index ranges	-23 ≤ h ≤ 23, -43 ≤ k ≤ 43, -20 ≤ l ≤ 20
Reflections collected	155176
Independent reflections	20864 [R _{int} = 0.1053, R _{sigma} = 0.0734]
Data/restraints/parameters	20864/2/1153
Goodness-of-fit on F ²	1.060
Final R indexes [I > 2σ (I)]	R ₁ = 0.0874, wR ₂ = 0.2071

Final R indexes [all data]
Largest diff. peak/hole / e Å⁻³

$R_1 = 0.1219$, $wR_2 = 0.2219$
0.77/-0.60

Table A3.24. Fractional Atomic Coordinates ($\times 10^4$) and Equivalent Isotropic Displacement Parameters ($\text{\AA}^2 \times 10^3$) for TNSB BDP **7**. U_{eq} is defined as 1/3 of the trace of the orthogonalised U_{ij} tensor.

Atom	x	y	z	U(eq)
P1	8842.4(6)	6684.2(4)	6988.5(7)	26.7(3)
P2	9561.5(6)	7429.4(4)	6195.1(7)	25.6(3)
O1	7564.4(19)	5611.4(11)	6513(3)	46.9(10)
O2	7390(2)	6504.7(12)	9122(2)	57.0(12)
O3	11650.4(16)	7487(1)	4769.7(19)	32.4(8)
O4	9183.4(17)	8160.6(10)	4029.8(19)	35.2(8)
N1	7887(2)	6131.7(12)	7206(2)	32.0(9)
N2	7761(2)	6391.3(11)	7844(2)	28.9(9)
N3	10484.9(19)	7590.0(11)	4986(2)	26.5(8)
N4	9903.4(19)	7834.4(12)	4890(2)	27.4(9)
C1	9349(3)	5561.2(15)	6947(4)	43.4(14)
C2	9132(3)	5431.8(16)	6181(4)	54.0(17)
C3	9394(4)	5107(2)	5843(5)	70(2)
C4	9905(4)	4898.5(19)	6267(6)	76(2)
C5	10126(3)	5002.9(17)	7021(5)	63(2)
C6	9838(3)	5332.5(16)	7387(4)	49.0(15)
C7	10063(3)	5441.2(18)	8185(5)	59.5(17)
C8	9818(3)	5762.6(18)	8533(4)	51.0(15)
C9	9346(3)	6003.4(16)	8089(3)	40.4(13)
C10	9113(3)	5908.9(15)	7319(3)	35.5(12)
C11	8613(3)	6166.9(14)	6875(3)	32.2(11)
C12	7459(3)	5831.9(15)	7073(3)	35.6(12)
C13	6885(3)	5790.1(16)	7695(3)	40.3(13)
C14	7161(3)	5885.3(16)	8542(3)	45.0(14)
C15	7451(3)	6284.2(16)	8556(3)	37.9(12)
C16	8028(2)	6765.8(14)	7672(3)	27.9(10)
C17	7485(2)	7025.6(14)	7286(3)	27.3(10)
C18	6839(2)	6888.2(15)	7006(3)	31.4(11)
C19	6373(3)	7120.3(15)	6543(3)	37.8(12)
C20	6562(3)	7474.7(15)	6331(3)	38.1(12)
C21	7208(3)	7633.2(14)	6631(3)	32.3(11)
C22	7397(3)	8009.1(15)	6455(3)	38.0(12)
C23	7986(3)	8170.8(16)	6794(3)	42.9(14)
C24	8418(3)	7956.9(15)	7318(3)	37.4(13)
C25	8272(3)	7586.2(15)	7480(3)	33.5(11)
C26	7660(2)	7410.6(14)	7138(3)	30.2(11)

C27	8508(2)	6868.9(15)	5996(3)	29.4(11)
C28	7912(3)	6713.8(17)	5624(3)	38.3(13)
C29	7598(3)	6873.7(19)	4938(3)	47.0(15)
C30	7911(3)	7187.6(18)	4594(3)	45.9(15)
C31	8519(2)	7336.4(17)	4934(3)	36.4(12)
C32	8827(2)	7190.3(14)	5644(3)	28.8(11)
C33	10389(2)	7296.1(14)	5604(3)	25.8(10)
C34	10338(2)	6903.5(14)	5255(3)	29.0(11)
C35	10106(3)	6841.2(16)	4475(3)	37.4(12)
C36	10031(3)	6473.0(19)	4163(4)	49.1(15)
C37	10192(3)	6171.5(18)	4644(4)	50.3(17)
C38	10454(3)	6219.1(15)	5448(3)	37.4(13)
C39	10686(3)	5910.1(16)	5936(4)	50.3(16)
C40	10971(3)	5965.5(16)	6700(4)	47.7(15)
C41	11019(3)	6331.7(15)	7026(3)	38.1(12)
C42	10795(2)	6633.0(14)	6577(3)	30.8(11)
C43	10524(2)	6591.8(14)	5769(3)	29.1(11)
C44	11108(2)	7666.3(14)	4612(3)	27.5(10)
C45	11036(2)	7966.7(15)	3962(3)	33.1(11)
C46	10319(2)	7937.4(15)	3533(3)	31.0(11)
C47	9741(2)	7981.7(14)	4151(3)	28.4(10)
C48	9535(2)	7901.8(14)	5663(3)	28.4(11)
C49	9886(2)	8219.6(14)	6133(3)	28.7(11)
C50	10437(2)	8141.4(15)	6669(3)	31.6(11)
C51	10788(3)	8429.7(15)	7093(3)	37.5(12)
C52	10597(3)	8798.2(16)	6989(3)	42.1(13)
C53	10045(3)	8893.2(15)	6449(3)	38.3(12)
C54	9848(3)	9275.7(18)	6329(4)	50.5(15)
C55	9286(4)	9369.2(18)	5824(4)	57.5(17)
C56	8911(3)	9084.6(17)	5409(4)	49.7(15)
C57	9089(3)	8713.2(16)	5498(3)	38.7(13)
C58	9666(3)	8602.9(15)	6019(3)	32.7(11)
P1A	4021.2(6)	6488.1(3)	4571.3(7)	23.8(3)
P2A	3652.5(6)	7234.3(3)	3675.7(7)	24.5(3)
O1A	4613.6(19)	5290.7(10)	4120(2)	40.2(9)
O2A	6039.8(19)	6233.9(10)	6075(2)	40.4(9)
O3A	1604.1(16)	7527.7(9)	2233.7(18)	28.2(7)
O4A	4249.6(17)	7930.4(10)	1524.5(19)	35.5(8)
N1A	4731.4(19)	5845.3(11)	4783(2)	27.9(9)
N2A	5168(2)	6114.2(11)	5157(2)	28.5(9)
N3A	2783.1(19)	7497.1(10)	2458(2)	23.9(8)
N4A	3461.3(18)	7662.9(11)	2359(2)	25.2(8)
C1A	3704(3)	6117.2(15)	6209(3)	33.4(11)
C2A	3346(3)	6055.9(17)	6950(3)	44.5(14)
C3A	2876(3)	5765.5(18)	7007(3)	46.6(14)

C4A	2757(3)	5515.5(15)	6361(3)	39.2(13)
C5A	2256(3)	5216.6(16)	6414(4)	50.5(15)
C6A	2140(3)	4980.5(16)	5786(4)	51.9(16)
C7A	2533(3)	5018.4(15)	5062(4)	45.8(14)
C8A	3021(3)	5298.5(15)	4992(3)	36.6(12)
C9A	3139(2)	5560.4(14)	5623(3)	31.1(11)
C10A	3607(2)	5878.2(14)	5559(3)	28.6(10)
C11A	3987(2)	5964.2(13)	4756(3)	26.8(10)
C12A	4986(3)	5511.6(14)	4503(3)	32.9(11)
C13A	5744(3)	5444.2(15)	4771(4)	42.6(13)
C14A	5851(3)	5586.3(15)	5643(4)	41.0(13)
C15A	5713(3)	6000.9(15)	5681(3)	35.2(12)
C16A	4977(2)	6509.5(12)	5000(3)	23.2(9)
C17A	5491(4)	6696.4(15)	4416(5)	26.5(7)
C18A	5896(4)	6469.9(12)	3911(5)	26.5(7)
C19A	6365(4)	6633.8(12)	3370(4)	26.5(7)
C20A	6429(3)	7024.1(12)	3334(3)	26.5(7)
C21A	6025(2)	7250.6(12)	3839(3)	26.5(7)
C22A	5556(3)	7086.8(15)	4380(3)	26.5(7)
C23A	5151(3)	7313.3(18)	4885(4)	26.5(7)
C24A	5216(3)	7703.6(18)	4849(4)	26.5(7)
C25A	5685(3)	7867.4(14)	4308(4)	26.5(7)
C26A	6089(3)	7641.0(12)	3803(3)	26.5(7)
C27A	4211(2)	6514.1(13)	3470(3)	25.6(10)
C28A	4464(3)	6212.4(15)	3011(3)	32.1(11)
C29A	4701(3)	6270.6(16)	2229(3)	38.7(13)
C30A	4705(3)	6629.2(17)	1898(3)	48.6(15)
C31A	4422(3)	6928.6(16)	2324(3)	40.3(13)
C32A	4152(2)	6876.7(14)	3103(3)	28(1)
C33A	2763(2)	7210.2(13)	3105(3)	26.5(10)
C34A	2615(2)	6816.0(13)	2792(3)	25.8(10)
C35A	2743(3)	6719.9(14)	1997(3)	32.0(11)
C36A	2671(3)	6339.4(15)	1740(3)	39.8(13)
C37A	2471(3)	6065.2(15)	2265(3)	38.3(12)
C38A	2323(2)	6153.0(14)	3085(3)	30.7(11)
C39A	2100(2)	5871.5(14)	3637(3)	31.3(11)
C40A	1956(2)	5959.2(14)	4427(3)	30.4(11)
C41A	2037(2)	6332.7(14)	4704(3)	28.4(10)
C42A	2239(2)	6613.1(13)	4188(3)	24(1)
C43A	2392(2)	6534.0(13)	3360(3)	24.2(10)
C44A	2199(2)	7638.7(13)	2069(3)	24.2(10)
C45A	2377(2)	7915.7(13)	1397(3)	26.9(10)
C46A	3075(2)	7800.7(14)	991(3)	27.4(10)
C47A	3652(2)	7803.6(13)	1625(3)	27(1)
C48A	3880(2)	7679.1(13)	3123(3)	25.9(10)

C49A	3712(2)	8026.6(14)	3614(3)	29.4(11)
C50A	3144(3)	8030.0(14)	4133(3)	32.0(11)
C51A	2973(3)	8347.0(15)	4604(3)	40.2(13)
C52A	3391(3)	8659.0(17)	4560(4)	53.0(16)
C53A	3971(3)	8677.4(17)	4036(3)	48.7(15)
C54A	4398(4)	9006.5(18)	3984(4)	64(2)
C55A	4944(4)	9027(2)	3446(4)	68(2)
C56A	5098(3)	8718.9(19)	2962(4)	54.5(17)
C57A	4715(3)	8392.9(16)	3015(3)	39.0(13)
C58A	4141(2)	8360.6(14)	3557(3)	31.3(11)
C17B	5429(4)	6759.0(14)	4447(5)	26.5(7)
C18B	5867(4)	6568.3(12)	3912(5)	26.5(7)
C19B	6319(3)	6769.4(12)	3410(4)	26.5(7)
C20B	6333(3)	7161.3(12)	3444(3)	26.5(7)
C21B	5895(2)	7352.0(12)	3979(3)	26.5(7)
C22B	5443(3)	7150.8(15)	4481(3)	26.5(7)
C23B	5005(3)	7341.5(19)	5016(4)	26.5(7)
C24B	5019(3)	7733.4(19)	5050(4)	26.5(7)
C25B	5471(3)	7934.5(15)	4548(4)	26.5(7)
C26B	5909(3)	7743.8(12)	4013(3)	26.5(7)

Table A3.25. Anisotropic Displacement Parameters ($\text{\AA}^2 \times 10^3$) for TNSB BDP 7. The Anisotropic displacement factor exponent takes the form: $-2\pi^2[h^2a^{*2}U_{11}+2hka^*b^*U_{12}+\dots]$.

Atom	U_{11}	U_{22}	U_{33}	U_{23}	U_{13}	U_{12}
P1	20.5(6)	38.1(7)	21.5(6)	-3.1(5)	-0.4(5)	-3.5(5)
P2	18.8(6)	40.7(7)	17.2(6)	0.2(5)	-0.8(4)	1.3(5)
O1	32(2)	46(2)	62(3)	-12(2)	-0.5(18)	-7.2(17)
O2	80(3)	62(3)	30(2)	-7(2)	21(2)	-22(2)
O3	21.9(17)	49(2)	26.9(17)	3.1(15)	2.7(13)	2.5(15)
O4	28.7(18)	52(2)	24.5(17)	5.9(16)	-5.3(14)	3.6(16)
N1	21(2)	41(2)	34(2)	-6.1(19)	3.0(17)	-5.8(18)
N2	29(2)	35(2)	22(2)	2.0(17)	3.7(16)	2.1(18)
N3	20.1(19)	38(2)	21.1(19)	4.3(17)	0.9(15)	6.1(17)
N4	18.8(19)	47(2)	16.8(19)	2.8(17)	1.0(15)	6.5(17)
C1	30(3)	33(3)	67(4)	1(3)	16(3)	-5(2)
C2	39(3)	40(3)	84(5)	-24(3)	20(3)	-14(3)
C3	45(4)	55(4)	112(6)	-27(4)	27(4)	-12(3)
C4	70(5)	39(4)	120(7)	-29(4)	35(5)	-15(4)
C5	49(4)	36(3)	104(6)	11(4)	34(4)	0(3)
C6	40(3)	35(3)	72(4)	2(3)	25(3)	1(3)
C7	45(4)	52(4)	83(5)	21(3)	24(3)	19(3)
C8	44(3)	60(4)	49(4)	7(3)	11(3)	4(3)
C9	32(3)	43(3)	46(3)	11(3)	10(2)	7(2)
C10	26(3)	40(3)	41(3)	-7(2)	8(2)	-6(2)

C11	31(3)	36(3)	29(3)	-9(2)	6(2)	-7(2)
C12	30(3)	35(3)	41(3)	1(2)	-7(2)	0(2)
C13	24(3)	40(3)	57(4)	7(3)	-2(2)	-3(2)
C14	44(3)	45(3)	46(3)	11(3)	6(3)	-5(3)
C15	39(3)	46(3)	29(3)	7(2)	0(2)	-1(2)
C16	26(2)	41(3)	17(2)	-3(2)	-2.7(18)	-3(2)
C17	24(2)	40(3)	19(2)	-1(2)	5.3(18)	1(2)
C18	28(3)	41(3)	24(2)	1(2)	-7(2)	-4(2)
C19	31(3)	47(3)	35(3)	-3(2)	-6(2)	0(2)
C20	43(3)	43(3)	28(3)	2(2)	-7(2)	3(2)
C21	37(3)	39(3)	21(2)	0(2)	4(2)	6(2)
C22	45(3)	39(3)	30(3)	4(2)	9(2)	3(2)
C23	48(3)	35(3)	47(3)	-7(3)	19(3)	-4(3)
C24	28(3)	44(3)	41(3)	-18(3)	15(2)	-7(2)
C25	30(3)	43(3)	27(3)	-11(2)	7(2)	1(2)
C26	27(2)	43(3)	21(2)	-5(2)	10.2(19)	1(2)
C27	23(2)	50(3)	15(2)	-5(2)	2.3(18)	0(2)
C28	33(3)	64(4)	18(2)	-4(2)	3(2)	-13(3)
C29	31(3)	87(5)	22(3)	2(3)	-7(2)	-20(3)
C30	31(3)	85(4)	22(3)	11(3)	-7(2)	-14(3)
C31	25(2)	66(4)	18(2)	-1(2)	2.4(19)	-8(2)
C32	21(2)	45(3)	20(2)	-4(2)	2.9(18)	0(2)
C33	19(2)	43(3)	16(2)	0(2)	-0.1(17)	4(2)
C34	18(2)	40(3)	29(3)	-4(2)	7.3(19)	-2(2)
C35	29(3)	54(3)	29(3)	-9(2)	1(2)	-1(2)
C36	31(3)	67(4)	50(4)	-27(3)	1(3)	-9(3)
C37	30(3)	51(4)	70(4)	-37(3)	14(3)	-14(3)
C38	23(2)	35(3)	55(3)	-10(3)	16(2)	-6(2)
C39	39(3)	31(3)	82(5)	-8(3)	28(3)	-8(2)
C40	32(3)	35(3)	77(5)	10(3)	16(3)	5(2)
C41	31(3)	40(3)	44(3)	10(2)	13(2)	7(2)
C42	24(2)	34(3)	35(3)	-1(2)	7(2)	1(2)
C43	20(2)	35(3)	32(3)	-5(2)	8.8(19)	-3(2)
C44	20(2)	37(3)	25(2)	-3(2)	-1.9(18)	1(2)
C45	22(2)	45(3)	32(3)	0(2)	5(2)	2(2)
C46	29(3)	45(3)	19(2)	2(2)	-0.6(19)	1(2)
C47	23(2)	38(3)	24(2)	1(2)	-2.9(19)	3(2)
C48	20(2)	45(3)	20(2)	-2(2)	-1.0(18)	8(2)
C49	24(2)	39(3)	23(2)	2(2)	3.9(19)	5(2)
C50	28(3)	41(3)	26(2)	1(2)	0(2)	9(2)
C51	31(3)	48(3)	33(3)	-2(2)	-6(2)	-1(2)
C52	39(3)	43(3)	44(3)	-8(3)	-2(2)	-1(3)
C53	42(3)	40(3)	33(3)	-2(2)	2(2)	5(2)
C54	49(4)	50(4)	53(4)	-5(3)	1(3)	7(3)
C55	71(4)	41(4)	60(4)	-4(3)	-6(3)	16(3)

C56	54(4)	53(4)	42(3)	2(3)	-7(3)	20(3)
C57	42(3)	48(3)	26(3)	-2(2)	5(2)	10(3)
C58	29(3)	43(3)	27(3)	3(2)	5(2)	9(2)
P1A	18.1(5)	31.1(6)	22.2(6)	2.8(5)	-1.7(4)	0.8(5)
P2A	20.6(6)	32.2(7)	20.6(6)	4.8(5)	-0.1(5)	2.8(5)
O1A	39(2)	37(2)	45(2)	-10.6(17)	-2.1(17)	0.4(17)
O2A	38(2)	33(2)	50(2)	0.4(17)	-24.8(17)	-2.3(16)
O3A	21.3(16)	38.2(19)	25.0(17)	0.8(14)	-1.0(13)	-1.2(14)
O4A	22.5(17)	56(2)	27.8(18)	8.0(16)	1.5(14)	-3.2(16)
N1A	23(2)	28(2)	33(2)	-3.1(17)	-5.0(17)	0.3(16)
N2A	24(2)	29(2)	33(2)	-1.2(17)	-11.6(17)	1.7(17)
N3A	20.2(19)	28(2)	23.7(19)	5.6(16)	-1.9(15)	-3.1(16)
N4A	17.4(18)	38(2)	20.0(19)	6.3(17)	-2.2(15)	-0.2(16)
C1A	32(3)	41(3)	27(3)	6(2)	-3(2)	-11(2)
C2A	48(3)	56(4)	30(3)	2(3)	1(2)	-10(3)
C3A	40(3)	68(4)	32(3)	8(3)	5(2)	-7(3)
C4A	30(3)	40(3)	48(3)	15(3)	6(2)	-4(2)
C5A	38(3)	41(3)	73(4)	10(3)	11(3)	-7(3)
C6A	33(3)	30(3)	93(5)	3(3)	12(3)	-4(2)
C7A	34(3)	28(3)	75(4)	-6(3)	-9(3)	-1(2)
C8A	27(3)	38(3)	45(3)	3(2)	-1(2)	5(2)
C9A	25(2)	34(3)	34(3)	6(2)	-4(2)	1(2)
C10A	21(2)	37(3)	27(2)	8(2)	-1.1(19)	-3(2)
C11A	20(2)	30(3)	30(3)	1(2)	-3.5(19)	-1.0(19)
C12A	26(2)	36(3)	37(3)	-3(2)	-4(2)	-1(2)
C13A	28(3)	35(3)	65(4)	-5(3)	-5(3)	11(2)
C14A	27(3)	35(3)	60(4)	2(3)	-21(3)	4(2)
C15A	24(2)	39(3)	42(3)	7(2)	-8(2)	0(2)
C16A	20(2)	27(2)	23(2)	0.4(19)	-1.7(17)	2.0(18)
C17A	20.2(13)	35.4(17)	24.0(12)	0.5(13)	1.0(7)	1.9(14)
C18A	20.2(13)	35.4(17)	24.0(12)	0.5(13)	1.0(7)	1.9(14)
C19A	20.2(13)	35.4(17)	24.0(12)	0.5(13)	1.0(7)	1.9(14)
C20A	20.2(13)	35.4(17)	24.0(12)	0.5(13)	1.0(7)	1.9(14)
C21A	20.2(13)	35.4(17)	24.0(12)	0.5(13)	1.0(7)	1.9(14)
C22A	20.2(13)	35.4(17)	24.0(12)	0.5(13)	1.0(7)	1.9(14)
C23A	20.2(13)	35.4(17)	24.0(12)	0.5(13)	1.0(7)	1.9(14)
C24A	20.2(13)	35.4(17)	24.0(12)	0.5(13)	1.0(7)	1.9(14)
C25A	20.2(13)	35.4(17)	24.0(12)	0.5(13)	1.0(7)	1.9(14)
C26A	20.2(13)	35.4(17)	24.0(12)	0.5(13)	1.0(7)	1.9(14)
C27A	19(2)	38(3)	20(2)	0(2)	-3.3(17)	1(2)
C28A	29(3)	39(3)	28(3)	-1(2)	-6(2)	5(2)
C29A	39(3)	51(3)	26(3)	-4(2)	1(2)	16(3)
C30A	59(4)	59(4)	28(3)	11(3)	12(3)	24(3)
C31A	37(3)	51(3)	33(3)	10(2)	6(2)	16(3)
C32A	18(2)	42(3)	24(2)	3(2)	-1.0(18)	10(2)

C33A	26(2)	33(3)	20(2)	5.7(19)	2.3(19)	-2(2)
C34A	23(2)	29(2)	26(2)	0.3(19)	-1.2(19)	2.4(19)
C35A	35(3)	38(3)	23(2)	6(2)	1(2)	1(2)
C36A	62(4)	38(3)	20(3)	-7(2)	4(2)	7(3)
C37A	48(3)	33(3)	34(3)	-8(2)	2(2)	-1(2)
C38A	27(2)	36(3)	28(3)	1(2)	-2(2)	3(2)
C39A	29(3)	29(3)	37(3)	1(2)	1(2)	2(2)
C40A	24(2)	34(3)	32(3)	2(2)	-1(2)	4(2)
C41A	22(2)	40(3)	23(2)	5(2)	-1.8(18)	0(2)
C42A	20(2)	26(2)	26(2)	1.0(19)	-1.3(18)	-2.9(18)
C43A	22(2)	27(2)	24(2)	0.7(19)	-2.8(18)	3.3(19)
C44A	24(2)	27(2)	22(2)	-3.2(19)	-3.1(18)	-0.6(19)
C45A	24(2)	34(3)	22(2)	3(2)	-5.9(19)	0(2)
C46A	28(2)	36(3)	19(2)	0(2)	0.3(19)	-4(2)
C47A	25(2)	36(3)	20(2)	2(2)	-0.9(18)	2(2)
C48A	24(2)	34(3)	19(2)	6.2(19)	-2.0(18)	1(2)
C49A	27(2)	43(3)	18(2)	4(2)	-5.0(19)	-8(2)
C50A	35(3)	36(3)	25(2)	2(2)	1(2)	-7(2)
C51A	51(3)	38(3)	32(3)	-3(2)	13(2)	-8(3)
C52A	69(4)	44(3)	46(4)	-17(3)	19(3)	-9(3)
C53A	66(4)	53(4)	27(3)	-8(3)	5(3)	-26(3)
C54A	93(5)	48(4)	53(4)	-14(3)	16(4)	-30(4)
C55A	72(5)	64(4)	68(5)	-4(4)	10(4)	-40(4)
C56A	46(4)	71(4)	47(4)	5(3)	4(3)	-26(3)
C57A	37(3)	47(3)	33(3)	9(2)	-3(2)	-11(2)
C58A	26(2)	41(3)	27(2)	4(2)	-6(2)	-9(2)
C17B	20.2(13)	35.4(17)	24.0(12)	0.5(13)	1.0(7)	1.9(14)
C18B	20.2(13)	35.4(17)	24.0(12)	0.5(13)	1.0(7)	1.9(14)
C19B	20.2(13)	35.4(17)	24.0(12)	0.5(13)	1.0(7)	1.9(14)
C20B	20.2(13)	35.4(17)	24.0(12)	0.5(13)	1.0(7)	1.9(14)
C21B	20.2(13)	35.4(17)	24.0(12)	0.5(13)	1.0(7)	1.9(14)
C22B	20.2(13)	35.4(17)	24.0(12)	0.5(13)	1.0(7)	1.9(14)
C23B	20.2(13)	35.4(17)	24.0(12)	0.5(13)	1.0(7)	1.9(14)
C24B	20.2(13)	35.4(17)	24.0(12)	0.5(13)	1.0(7)	1.9(14)
C25B	20.2(13)	35.4(17)	24.0(12)	0.5(13)	1.0(7)	1.9(14)
C26B	20.2(13)	35.4(17)	24.0(12)	0.5(13)	1.0(7)	1.9(14)

Table A3.26. Bond Lengths for TNSB BDP 7.

Atom	Atom	Length/Å	Atom	Atom	Length/Å
P1	C11	1.892(5)	O1A	C12A	1.221(6)
P1	C16	1.938(5)	O2A	C15A	1.212(6)
P1	C27	1.856(5)	O3A	C44A	1.223(5)
P2	C32	1.850(5)	O4A	C47A	1.228(5)
P2	C33	1.910(4)	N1A	N2A	1.396(5)

P2	C48	1.888(5)	N1A	C11A	1.467(6)
O1	C12	1.225(6)	N1A	C12A	1.359(6)
O2	C15	1.220(6)	N2A	C15A	1.390(6)
O3	C44	1.230(5)	N2A	C16A	1.469(6)
O4	C47	1.242(5)	N3A	N4A	1.420(5)
N1	N2	1.416(5)	N3A	C33A	1.470(6)
N1	C11	1.488(6)	N3A	C44A	1.362(6)
N1	C12	1.350(6)	N4A	C47A	1.357(6)
N2	C15	1.368(6)	N4A	C48A	1.473(6)
N2	C16	1.449(6)	C1A	C2A	1.417(7)
N3	N4	1.406(5)	C1A	C10A	1.371(7)
N3	C33	1.467(6)	C2A	C3A	1.364(8)
N3	C44	1.361(6)	C3A	C4A	1.397(8)
N4	C47	1.350(6)	C4A	C5A	1.424(7)
N4	C48	1.475(5)	C4A	C9A	1.427(7)
C1	C2	1.394(9)	C5A	C6A	1.343(9)
C1	C6	1.419(8)	C6A	C7A	1.414(9)
C1	C10	1.448(7)	C7A	C8A	1.360(7)
C2	C3	1.373(8)	C8A	C9A	1.405(7)
C3	C4	1.394(11)	C9A	C10A	1.436(7)
C4	C5	1.352(11)	C10A	C11A	1.540(6)
C5	C6	1.424(8)	C12A	C13A	1.510(7)
C6	C7	1.424(9)	C13A	C14A	1.528(8)
C7	C8	1.358(9)	C14A	C15A	1.494(7)
C8	C9	1.427(8)	C16A	C17A	1.525(5)
C9	C10	1.374(7)	C16A	C17B	1.535(5)
C10	C11	1.496(7)	C17A	C18A	1.3900
C12	C13	1.505(7)	C17A	C22A	1.3900
C13	C14	1.515(8)	C18A	C19A	1.3900
C14	C15	1.516(8)	C19A	C20A	1.3900
C16	C17	1.511(7)	C20A	C21A	1.3900
C17	C18	1.385(6)	C21A	C22A	1.3900
C17	C26	1.425(7)	C21A	C26A	1.3900
C18	C19	1.417(7)	C22A	C23A	1.3900
C19	C20	1.353(7)	C23A	C24A	1.3900
C20	C21	1.424(7)	C24A	C25A	1.3900
C21	C22	1.410(7)	C25A	C26A	1.3900
C21	C26	1.423(7)	C27A	C28A	1.396(7)
C22	C23	1.362(8)	C27A	C32A	1.423(7)
C23	C24	1.400(8)	C28A	C29A	1.379(7)
C24	C25	1.369(7)	C29A	C30A	1.382(8)
C25	C26	1.421(7)	C30A	C31A	1.383(8)
C27	C28	1.386(7)	C31A	C32A	1.393(7)
C27	C32	1.416(7)	C33A	C34A	1.513(6)
C28	C29	1.387(7)	C34A	C35A	1.372(6)

C29	C30	1.384(8)	C34A	C43A	1.434(6)
C30	C31	1.375(7)	C35A	C36A	1.418(7)
C31	C32	1.393(7)	C36A	C37A	1.356(7)
C33	C34	1.508(7)	C37A	C38A	1.412(7)
C34	C35	1.363(7)	C38A	C39A	1.416(7)
C34	C43	1.431(7)	C38A	C43A	1.429(7)
C35	C36	1.408(8)	C39A	C40A	1.363(7)
C36	C37	1.360(9)	C40A	C41A	1.408(7)
C37	C38	1.412(8)	C41A	C42A	1.364(6)
C38	C39	1.422(8)	C42A	C43A	1.421(6)
C38	C43	1.428(7)	C44A	C45A	1.518(6)
C39	C40	1.371(9)	C45A	C46A	1.539(6)
C40	C41	1.406(8)	C46A	C47A	1.496(6)
C41	C42	1.361(7)	C48A	C49A	1.507(7)
C42	C43	1.420(7)	C49A	C50A	1.380(6)
C44	C45	1.512(7)	C49A	C58A	1.438(7)
C45	C46	1.521(7)	C50A	C51A	1.404(7)
C46	C47	1.509(6)	C51A	C52A	1.361(8)
C48	C49	1.513(7)	C52A	C53A	1.403(8)
C49	C50	1.381(7)	C53A	C54A	1.422(8)
C49	C58	1.432(7)	C53A	C58A	1.411(8)
C50	C51	1.398(7)	C54A	C55A	1.369(9)
C51	C52	1.365(8)	C55A	C56A	1.384(9)
C52	C53	1.399(8)	C56A	C57A	1.367(8)
C53	C54	1.419(8)	C57A	C58A	1.416(7)
C53	C58	1.433(7)	C17B	C18B	1.3900
C54	C55	1.376(9)	C17B	C22B	1.3900
C55	C56	1.404(9)	C18B	C19B	1.3900
C56	C57	1.366(8)	C19B	C20B	1.3900
C57	C58	1.431(7)	C20B	C21B	1.3900
P1A	C11A	1.882(5)	C21B	C22B	1.3900
P1A	C16A	1.929(4)	C21B	C26B	1.3900
P1A	C27A	1.849(4)	C22B	C23B	1.3900
P2A	C32A	1.845(5)	C23B	C24B	1.3900
P2A	C33A	1.913(5)	C24B	C25B	1.3900
P2A	C48A	1.872(5)	C25B	C26B	1.3900

Table A3.27. Bond Angles for TNSB BDP 7.

Atom	Atom	Atom	Angle/°	Atom	Atom	Atom	Angle/°
C11	P1	C16	91.1(2)	N1A	N2A	C16A	115.5(3)
C27	P1	C11	100.4(2)	C15A	N2A	N1A	120.1(4)
C27	P1	C16	101.1(2)	C15A	N2A	C16A	124.2(4)
C32	P2	C33	104.6(2)	N4A	N3A	C33A	113.6(3)
C32	P2	C48	99.5(2)	C44A	N3A	N4A	121.4(3)

C48	P2	C33	90.1(2)	C44A	N3A	C33A	124.3(4)
N2	N1	C11	112.4(4)	N3A	N4A	C48A	113.2(3)
C12	N1	N2	121.6(4)	C47A	N4A	N3A	120.3(4)
C12	N1	C11	124.1(4)	C47A	N4A	C48A	126.5(4)
N1	N2	C16	112.9(3)	C10A	C1A	C2A	120.8(5)
C15	N2	N1	122.0(4)	C3A	C2A	C1A	119.6(5)
C15	N2	C16	125.1(4)	C2A	C3A	C4A	121.6(5)
N4	N3	C33	114.3(3)	C3A	C4A	C5A	121.6(5)
C44	N3	N4	120.4(4)	C3A	C4A	C9A	119.7(5)
C44	N3	C33	124.6(4)	C5A	C4A	C9A	118.6(5)
N3	N4	C48	112.4(3)	C6A	C5A	C4A	121.2(6)
C47	N4	N3	120.4(4)	C5A	C6A	C7A	120.2(5)
C47	N4	C48	127.2(4)	C8A	C7A	C6A	120.3(6)
C2	C1	C6	116.9(5)	C7A	C8A	C9A	121.4(5)
C2	C1	C10	124.9(6)	C4A	C9A	C10A	117.9(5)
C6	C1	C10	118.3(6)	C8A	C9A	C4A	118.3(5)
C3	C2	C1	122.5(7)	C8A	C9A	C10A	123.8(5)
C2	C3	C4	119.6(8)	C1A	C10A	C9A	120.3(4)
C5	C4	C3	121.0(7)	C1A	C10A	C11A	118.9(4)
C4	C5	C6	119.7(7)	C9A	C10A	C11A	120.8(4)
C1	C6	C5	120.3(7)	N1A	C11A	P1A	104.7(3)
C1	C6	C7	119.8(5)	N1A	C11A	C10A	112.0(4)
C7	C6	C5	119.9(6)	C10A	C11A	P1A	110.5(3)
C8	C7	C6	121.0(6)	O1A	C12A	N1A	121.9(4)
C7	C8	C9	120.1(6)	O1A	C12A	C13A	125.8(5)
C10	C9	C8	120.9(5)	N1A	C12A	C13A	112.2(4)
C1	C10	C11	120.7(5)	C12A	C13A	C14A	109.4(4)
C9	C10	C1	119.9(5)	C15A	C14A	C13A	110.0(4)
C9	C10	C11	119.4(5)	O2A	C15A	N2A	120.0(5)
N1	C11	P1	104.8(3)	O2A	C15A	C14A	127.2(4)
N1	C11	C10	110.5(4)	N2A	C15A	C14A	112.7(4)
C10	C11	P1	113.8(3)	N2A	C16A	P1A	104.7(3)
O1	C12	N1	121.3(5)	N2A	C16A	C17A	111.5(4)
O1	C12	C13	124.9(5)	N2A	C16A	C17B	121.0(4)
N1	C12	C13	113.8(5)	C17A	C16A	P1A	112.9(5)
C12	C13	C14	111.0(4)	C17B	C16A	P1A	109.5(4)
C13	C14	C15	109.9(4)	C18A	C17A	C16A	118.9(3)
O2	C15	N2	121.2(5)	C18A	C17A	C22A	120.0
O2	C15	C14	124.8(5)	C22A	C17A	C16A	121.1(3)
N2	C15	C14	113.8(5)	C17A	C18A	C19A	120.0
N2	C16	P1	104.9(3)	C20A	C19A	C18A	120.0
N2	C16	C17	113.8(4)	C19A	C20A	C21A	120.0
C17	C16	P1	112.8(3)	C20A	C21A	C26A	120.0
C18	C17	C16	120.9(4)	C22A	C21A	C20A	120.0
C18	C17	C26	119.1(4)	C22A	C21A	C26A	120.0

C26	C17	C16	119.8(4)	C21A	C22A	C17A	120.0
C17	C18	C19	120.7(5)	C21A	C22A	C23A	120.0
C20	C19	C18	120.8(5)	C23A	C22A	C17A	120.0
C19	C20	C21	120.4(5)	C24A	C23A	C22A	120.0
C22	C21	C20	121.3(5)	C25A	C24A	C23A	120.0
C22	C21	C26	119.5(5)	C26A	C25A	C24A	120.0
C26	C21	C20	119.1(5)	C25A	C26A	C21A	120.0
C23	C22	C21	121.4(5)	C28A	C27A	P1A	124.1(4)
C22	C23	C24	119.2(5)	C28A	C27A	C32A	119.2(4)
C25	C24	C23	121.5(5)	C32A	C27A	P1A	116.3(3)
C24	C25	C26	120.5(5)	C29A	C28A	C27A	120.3(5)
C21	C26	C17	119.4(4)	C28A	C29A	C30A	120.4(5)
C25	C26	C17	122.8(5)	C29A	C30A	C31A	120.2(5)
C25	C26	C21	117.8(5)	C30A	C31A	C32A	120.7(5)
C28	C27	P1	120.7(4)	C27A	C32A	P2A	116.2(3)
C28	C27	C32	119.1(4)	C31A	C32A	P2A	124.9(4)
C32	C27	P1	120.0(3)	C31A	C32A	C27A	118.7(4)
C27	C28	C29	122.1(5)	N3A	C33A	P2A	106.9(3)
C30	C29	C28	118.6(5)	N3A	C33A	C34A	113.6(4)
C31	C30	C29	120.1(5)	C34A	C33A	P2A	111.3(3)
C30	C31	C32	122.3(5)	C35A	C34A	C33A	121.2(4)
C27	C32	P2	119.2(3)	C35A	C34A	C43A	120.1(4)
C31	C32	P2	122.7(4)	C43A	C34A	C33A	118.5(4)
C31	C32	C27	117.7(4)	C34A	C35A	C36A	120.0(4)
N3	C33	P2	106.6(3)	C37A	C36A	C35A	121.3(5)
N3	C33	C34	113.6(4)	C36A	C37A	C38A	120.5(5)
C34	C33	P2	111.9(3)	C37A	C38A	C39A	121.2(5)
C35	C34	C33	121.6(5)	C37A	C38A	C43A	119.4(4)
C35	C34	C43	120.1(5)	C39A	C38A	C43A	119.4(4)
C43	C34	C33	118.3(4)	C40A	C39A	C38A	120.8(5)
C34	C35	C36	121.4(6)	C39A	C40A	C41A	120.0(5)
C37	C36	C35	119.8(5)	C42A	C41A	C40A	120.9(4)
C36	C37	C38	121.4(5)	C41A	C42A	C43A	120.9(4)
C37	C38	C39	122.3(5)	C38A	C43A	C34A	118.7(4)
C37	C38	C43	119.0(5)	C42A	C43A	C34A	123.3(4)
C39	C38	C43	118.5(5)	C42A	C43A	C38A	118.0(4)
C40	C39	C38	121.2(5)	O3A	C44A	N3A	121.2(4)
C39	C40	C41	120.1(5)	O3A	C44A	C45A	125.6(4)
C42	C41	C40	120.0(6)	N3A	C44A	C45A	113.1(4)
C41	C42	C43	121.9(5)	C44A	C45A	C46A	110.1(4)
C38	C43	C34	118.4(5)	C47A	C46A	C45A	108.5(4)
C42	C43	C34	123.6(4)	O4A	C47A	N4A	120.6(4)
C42	C43	C38	118.0(5)	O4A	C47A	C46A	124.8(4)
O3	C44	N3	121.7(4)	N4A	C47A	C46A	114.5(4)
O3	C44	C45	125.4(4)	N4A	C48A	P2A	104.8(3)

N3	C44	C45	112.8(4)	N4A	C48A	C49A	111.8(4)
C44	C45	C46	110.4(4)	C49A	C48A	P2A	112.2(3)
C47	C46	C45	109.3(4)	C50A	C49A	C48A	120.5(4)
O4	C47	N4	121.5(4)	C50A	C49A	C58A	118.5(5)
O4	C47	C46	124.4(4)	C58A	C49A	C48A	121.0(4)
N4	C47	C46	113.9(4)	C49A	C50A	C51A	122.2(5)
N4	C48	P2	104.2(3)	C52A	C51A	C50A	118.9(5)
N4	C48	C49	110.5(4)	C51A	C52A	C53A	121.9(5)
C49	C48	P2	114.6(3)	C52A	C53A	C54A	121.6(6)
C50	C49	C48	119.7(4)	C52A	C53A	C58A	119.4(5)
C50	C49	C58	119.2(5)	C58A	C53A	C54A	119.0(5)
C58	C49	C48	121.0(4)	C55A	C54A	C53A	121.1(6)
C49	C50	C51	121.2(5)	C54A	C55A	C56A	119.5(6)
C52	C51	C50	120.9(5)	C57A	C56A	C55A	121.1(6)
C51	C52	C53	120.2(5)	C56A	C57A	C58A	121.2(6)
C52	C53	C54	120.6(5)	C53A	C58A	C49A	119.0(4)
C52	C53	C58	120.1(5)	C53A	C58A	C57A	118.0(5)
C54	C53	C58	119.3(5)	C57A	C58A	C49A	123.0(5)
C55	C54	C53	120.8(6)	C18B	C17B	C16A	115.7(4)
C54	C55	C56	119.9(6)	C18B	C17B	C22B	120.0
C57	C56	C55	121.2(6)	C22B	C17B	C16A	124.2(4)
C56	C57	C58	120.8(5)	C19B	C18B	C17B	120.0
C49	C58	C53	118.4(4)	C18B	C19B	C20B	120.0
C57	C58	C49	123.7(5)	C21B	C20B	C19B	120.0
C57	C58	C53	118.0(5)	C20B	C21B	C26B	120.0
C11A	P1A	C16A	90.8(2)	C22B	C21B	C20B	120.0
C27A	P1A	C11A	102.4(2)	C22B	C21B	C26B	120.0
C27A	P1A	C16A	99.26(19)	C21B	C22B	C17B	120.0
C32A	P2A	C33A	99.9(2)	C23B	C22B	C17B	120.0
C32A	P2A	C48A	102.1(2)	C23B	C22B	C21B	120.0
C48A	P2A	C33A	90.4(2)	C22B	C23B	C24B	120.0
N2A	N1A	C11A	112.2(3)	C25B	C24B	C23B	120.0
C12A	N1A	N2A	122.2(4)	C24B	C25B	C26B	120.0
C12A	N1A	C11A	125.7(4)	C25B	C26B	C21B	120.0

Table A3.28. Torsion Angles for TNSB BDP 7.

A	B	C	D	Angle/°	A	B	C	D	Angle/°
P1	C16	C17	C18	109.1(4)	N1A	N2A	C15A	C14A	11.8(6)
P1	C16	C17	C26	-65.2(5)	N1A	N2A	C16A	P1A	15.8(4)
P1	C27	C28	C29	171.9(4)	N1A	N2A	C16A	C17A	-106.6(5)
P1	C27	C32	P2	-1.6(5)	N1A	N2A	C16A	C17B	-108.2(6)
P1	C27	C32	C31	-174.7(4)	N1A	C12A	C13A	C14A	38.2(6)
P2	C33	C34	C35	94.8(5)	N2A	N1A	C11A	P1A	36.6(4)
P2	C33	C34	C43	-83.8(4)	N2A	N1A	C11A	C10A	-83.1(5)

P2	C48	C49	C50	28.6(5)	N2A	N1A	C12A	O1A	-174.1(4)
P2	C48	C49	C58	-152.7(4)	N2A	N1A	C12A	C13A	9.7(7)
O1	C12	C13	C14	137.9(5)	N2A	C16A	C17A	C18A	21.1(5)
O3	C44	C45	C46	141.0(5)	N2A	C16A	C17A	C22A	-159.4(3)
N1	N2	C15	O2	174.9(5)	N2A	C16A	C17B	C18B	20.3(6)
N1	N2	C15	C14	-8.8(7)	N2A	C16A	C17B	C22B	-156.9(4)
N1	N2	C16	P1	-30.5(4)	N3A	N4A	C47A	O4A	-176.4(4)
N1	N2	C16	C17	93.3(4)	N3A	N4A	C47A	C46A	5.7(6)
N1	C12	C13	C14	-39.0(6)	N3A	N4A	C48A	P2A	36.2(4)
N2	N1	C11	P1	-31.9(4)	N3A	N4A	C48A	C49A	-85.6(4)
N2	N1	C11	C10	91.0(5)	N3A	C33A	C34A	C35A	21.9(6)
N2	N1	C12	O1	178.9(4)	N3A	C33A	C34A	C43A	-163.2(4)
N2	N1	C12	C13	-4.1(7)	N3A	C44A	C45A	C46A	33.3(5)
N2	C16	C17	C18	-10.3(6)	N4A	N3A	C33A	P2A	9.0(4)
N2	C16	C17	C26	175.4(4)	N4A	N3A	C33A	C34A	-114.3(4)
N3	N4	C47	O4	171.2(4)	N4A	N3A	C44A	O3A	-170.5(4)
N3	N4	C47	C46	-13.9(6)	N4A	N3A	C44A	C45A	13.7(6)
N3	N4	C48	P2	-38.0(4)	N4A	C48A	C49A	C50A	84.5(5)
N3	N4	C48	C49	85.5(5)	N4A	C48A	C49A	C58A	-95.9(5)
N3	C33	C34	C35	-25.9(6)	C1A	C2A	C3A	C4A	2.7(9)
N3	C33	C34	C43	155.6(4)	C1A	C10A	C11A	P1A	-36.6(5)
N3	C44	C45	C46	-34.7(6)	C1A	C10A	C11A	N1A	79.7(5)
N4	N3	C33	P2	-11.4(4)	C2A	C1A	C10A	C9A	-0.1(8)
N4	N3	C33	C34	112.2(4)	C2A	C1A	C10A	C11A	177.9(5)
N4	N3	C44	O3	170.1(4)	C2A	C3A	C4A	C5A	-178.8(6)
N4	N3	C44	C45	-14.0(6)	C2A	C3A	C4A	C9A	0.5(9)
N4	C48	C49	C50	-88.7(5)	C3A	C4A	C5A	C6A	179.2(6)
N4	C48	C49	C58	90.0(5)	C3A	C4A	C9A	C8A	178.4(5)
C1	C2	C3	C4	-1.0(9)	C3A	C4A	C9A	C10A	-3.4(7)
C1	C6	C7	C8	-0.3(9)	C4A	C5A	C6A	C7A	1.9(9)
C1	C10	C11	P1	-138.4(4)	C4A	C9A	C10A	C1A	3.2(7)
C1	C10	C11	N1	104.0(5)	C4A	C9A	C10A	C11A	-174.7(4)
C2	C1	C6	C5	4.6(8)	C5A	C4A	C9A	C8A	-2.3(7)
C2	C1	C6	C7	-177.8(5)	C5A	C4A	C9A	C10A	175.9(5)
C2	C1	C10	C9	178.1(5)	C5A	C6A	C7A	C8A	-1.2(9)
C2	C1	C10	C11	-1.6(8)	C6A	C7A	C8A	C9A	-1.3(8)
C2	C3	C4	C5	2.6(10)	C7A	C8A	C9A	C4A	3.0(7)
C3	C4	C5	C6	-0.5(10)	C7A	C8A	C9A	C10A	-175.1(5)
C4	C5	C6	C1	-3.2(9)	C8A	C9A	C10A	C1A	-178.7(5)
C4	C5	C6	C7	179.2(6)	C8A	C9A	C10A	C11A	3.3(7)
C5	C6	C7	C8	177.3(5)	C9A	C4A	C5A	C6A	-0.1(8)
C6	C1	C2	C3	-2.6(8)	C9A	C10A	C11A	P1A	141.3(4)
C6	C1	C10	C9	-2.0(7)	C9A	C10A	C11A	N1A	-102.4(5)
C6	C1	C10	C11	178.3(4)	C10A	C1A	C2A	C3A	-2.9(8)
C6	C7	C8	C9	-2.0(9)	C11A	P1A	C27A	C28A	-16.3(4)

C7	C8	C9	C10	2.3(8)	C11A	P1A	C27A	C32A	169.7(3)
C8	C9	C10	C1	-0.2(8)	C11A	N1A	N2A	C15A	139.8(4)
C8	C9	C10	C11	179.5(5)	C11A	N1A	N2A	C16A	-36.1(5)
C9	C10	C11	P1	41.9(6)	C11A	N1A	C12A	O1A	7.7(8)
C9	C10	C11	N1	-75.7(6)	C11A	N1A	C12A	C13A	-168.6(4)
C10	C1	C2	C3	177.4(5)	C12A	N1A	N2A	C15A	-38.7(6)
C10	C1	C6	C5	-175.3(5)	C12A	N1A	N2A	C16A	145.4(4)
C10	C1	C6	C7	2.3(8)	C12A	N1A	C11A	P1A	-144.9(4)
C11	P1	C27	C28	33.8(4)	C12A	N1A	C11A	C10A	95.3(5)
C11	P1	C27	C32	-151.3(4)	C12A	C13A	C14A	C15A	-61.5(6)
C11	N1	N2	C15	-133.6(5)	C13A	C14A	C15A	O2A	-140.4(6)
C11	N1	N2	C16	43.2(5)	C13A	C14A	C15A	N2A	35.7(6)
C11	N1	C12	O1	-18.4(8)	C15A	N2A	C16A	P1A	-160.0(4)
C11	N1	C12	C13	158.5(4)	C15A	N2A	C16A	C17A	77.6(6)
C12	N1	N2	C15	30.9(7)	C15A	N2A	C16A	C17B	76.0(7)
C12	N1	N2	C16	-152.3(4)	C16A	P1A	C11A	N1A	-22.4(3)
C12	N1	C11	P1	164.0(4)	C16A	P1A	C11A	C10A	98.4(3)
C12	N1	C11	C10	-73.0(6)	C16A	P1A	C27A	C28A	76.6(4)
C12	C13	C14	C15	57.8(6)	C16A	P1A	C27A	C32A	-97.4(4)
C13	C14	C15	O2	142.3(6)	C16A	N2A	C15A	O2A	3.9(7)
C13	C14	C15	N2	-33.8(6)	C16A	N2A	C15A	C14A	-172.6(4)
C15	N2	C16	P1	146.3(4)	C16A	C17A	C18A	C19A	179.6(7)
C15	N2	C16	C17	-89.9(5)	C16A	C17A	C22A	C21A	-179.6(7)
C16	P1	C11	N1	11.5(3)	C16A	C17A	C22A	C23A	0.4(7)
C16	P1	C11	C10	-109.3(4)	C16A	C17B	C18B	C19B	-177.3(6)
C16	P1	C27	C28	-59.4(4)	C16A	C17B	C22B	C21B	177.0(7)
C16	P1	C27	C32	115.6(4)	C16A	C17B	C22B	C23B	-3.0(7)
C16	N2	C15	O2	-1.5(8)	C17A	C18A	C19A	C20A	0.0
C16	N2	C15	C14	174.8(4)	C17A	C22A	C23A	C24A	180.0
C16	C17	C18	C19	-171.1(4)	C18A	C17A	C22A	C21A	0.0
C16	C17	C26	C21	167.3(4)	C18A	C17A	C22A	C23A	180.0
C16	C17	C26	C25	-12.9(6)	C18A	C19A	C20A	C21A	0.0
C17	C18	C19	C20	3.2(8)	C19A	C20A	C21A	C22A	0.0
C18	C17	C26	C21	-7.1(6)	C19A	C20A	C21A	C26A	180.0
C18	C17	C26	C25	172.7(4)	C20A	C21A	C22A	C17A	0.0
C18	C19	C20	C21	-5.7(8)	C20A	C21A	C22A	C23A	180.0
C19	C20	C21	C22	-176.4(5)	C20A	C21A	C26A	C25A	180.0
C19	C20	C21	C26	1.6(7)	C21A	C22A	C23A	C24A	0.0
C20	C21	C22	C23	174.6(5)	C22A	C17A	C18A	C19A	0.0
C20	C21	C26	C17	4.8(6)	C22A	C21A	C26A	C25A	0.0
C20	C21	C26	C25	-175.1(4)	C22A	C23A	C24A	C25A	0.0
C21	C22	C23	C24	1.0(7)	C23A	C24A	C25A	C26A	0.0
C22	C21	C26	C17	-177.2(4)	C24A	C25A	C26A	C21A	0.0
C22	C21	C26	C25	3.0(6)	C26A	C21A	C22A	C17A	180.0
C22	C23	C24	C25	1.7(7)	C26A	C21A	C22A	C23A	0.0

C23	C24	C25	C26	-2.0(7)	C27A	P1A	C11A	N1A	77.2(3)
C24	C25	C26	C17	179.8(4)	C27A	P1A	C11A	C10A	-162.0(3)
C24	C25	C26	C21	-0.3(6)	C27A	C28A	C29A	C30A	1.5(8)
C26	C17	C18	C19	3.2(7)	C28A	C27A	C32A	P2A	168.3(3)
C26	C21	C22	C23	-3.4(7)	C28A	C27A	C32A	C31A	-6.9(7)
C27	P1	C11	N1	-89.9(3)	C28A	C29A	C30A	C31A	-4.9(9)
C27	P1	C11	C10	149.3(3)	C29A	C30A	C31A	C32A	2.3(9)
C27	C28	C29	C30	3.1(9)	C30A	C31A	C32A	P2A	-171.2(4)
C28	C27	C32	P2	173.4(4)	C30A	C31A	C32A	C27A	3.6(8)
C28	C27	C32	C31	0.3(7)	C32A	P2A	C48A	N4A	75.2(3)
C28	C29	C30	C31	-0.4(9)	C32A	P2A	C48A	C49A	-163.3(3)
C29	C30	C31	C32	-2.4(9)	C32A	C27A	C28A	C29A	4.5(7)
C30	C31	C32	P2	-170.4(4)	C33A	P2A	C32A	C27A	-100.0(4)
C30	C31	C32	C27	2.4(8)	C33A	P2A	C32A	C31A	74.8(5)
C32	P2	C48	N4	-79.4(3)	C33A	P2A	C48A	N4A	-25.0(3)
C32	P2	C48	C49	159.7(3)	C33A	P2A	C48A	C49A	96.5(3)
C32	C27	C28	C29	-3.1(8)	C33A	N3A	N4A	C47A	152.6(4)
C33	P2	C32	C27	106.6(4)	C33A	N3A	N4A	C48A	-30.6(5)
C33	P2	C32	C31	-80.6(4)	C33A	N3A	C44A	O3A	-1.1(7)
C33	P2	C48	N4	25.4(3)	C33A	N3A	C44A	C45A	-176.9(4)
C33	P2	C48	C49	-95.5(3)	C33A	C34A	C35A	C36A	173.4(5)
C33	N3	N4	C47	-146.8(4)	C33A	C34A	C43A	C38A	-173.6(4)
C33	N3	N4	C48	33.7(5)	C33A	C34A	C43A	C42A	6.1(6)
C33	N3	C44	O3	0.4(7)	C34A	C35A	C36A	C37A	0.6(8)
C33	N3	C44	C45	176.2(4)	C35A	C34A	C43A	C38A	1.4(7)
C33	C34	C35	C36	-177.4(4)	C35A	C34A	C43A	C42A	-178.9(4)
C33	C34	C43	C38	178.0(4)	C35A	C36A	C37A	C38A	0.6(8)
C33	C34	C43	C42	-3.8(6)	C36A	C37A	C38A	C39A	178.7(5)
C34	C35	C36	C37	0.1(8)	C36A	C37A	C38A	C43A	-0.7(8)
C35	C34	C43	C38	-0.6(6)	C37A	C38A	C39A	C40A	-179.8(5)
C35	C34	C43	C42	177.6(4)	C37A	C38A	C43A	C34A	-0.3(7)
C35	C36	C37	C38	-1.9(8)	C37A	C38A	C43A	C42A	180.0(4)
C36	C37	C38	C39	-174.2(5)	C38A	C39A	C40A	C41A	-0.9(7)
C36	C37	C38	C43	2.4(7)	C39A	C38A	C43A	C34A	-179.7(4)
C37	C38	C39	C40	176.7(5)	C39A	C38A	C43A	C42A	0.5(6)
C37	C38	C43	C34	-1.1(6)	C39A	C40A	C41A	C42A	2.0(7)
C37	C38	C43	C42	-179.4(4)	C40A	C41A	C42A	C43A	-1.8(7)
C38	C39	C40	C41	1.9(8)	C41A	C42A	C43A	C34A	-179.2(4)
C39	C38	C43	C34	175.6(4)	C41A	C42A	C43A	C38A	0.5(6)
C39	C38	C43	C42	-2.7(6)	C43A	C34A	C35A	C36A	-1.5(7)
C39	C40	C41	C42	-1.3(8)	C43A	C38A	C39A	C40A	-0.4(7)
C40	C41	C42	C43	-1.4(7)	C44A	N3A	N4A	C47A	-37.0(6)
C41	C42	C43	C34	-174.8(4)	C44A	N3A	N4A	C48A	139.9(4)
C41	C42	C43	C38	3.4(7)	C44A	N3A	C33A	P2A	-161.2(3)
C43	C34	C35	C36	1.1(7)	C44A	N3A	C33A	C34A	75.6(5)

C43	C38	C39	C40	0.1(7)	C44A	C45A	C46A	C47A	-60.2(5)
C44	N3	N4	C47	42.4(6)	C45A	C46A	C47A	O4A	-137.5(5)
C44	N3	N4	C48	-137.0(4)	C45A	C46A	C47A	N4A	40.4(5)
C44	N3	C33	P2	158.9(4)	C47A	N4A	C48A	P2A	-147.2(4)
C44	N3	C33	C34	-77.5(5)	C47A	N4A	C48A	C49A	91.0(5)
C44	C45	C46	C47	58.9(5)	C48A	P2A	C32A	C27A	167.5(3)
C45	C46	C47	O4	140.3(5)	C48A	P2A	C32A	C31A	-17.7(5)
C45	C46	C47	N4	-34.4(6)	C48A	N4A	C47A	O4A	7.2(7)
C47	N4	C48	P2	142.6(4)	C48A	N4A	C47A	C46A	-170.7(4)
C47	N4	C48	C49	-93.8(5)	C48A	C49A	C50A	C51A	179.5(5)
C48	P2	C32	C27	-160.8(4)	C48A	C49A	C58A	C53A	-179.0(5)
C48	P2	C32	C31	11.9(4)	C48A	C49A	C58A	C57A	3.5(7)
C48	N4	C47	O4	-9.5(8)	C49A	C50A	C51A	C52A	-1.3(8)
C48	N4	C47	C46	165.4(4)	C50A	C49A	C58A	C53A	0.5(7)
C48	C49	C50	C51	177.9(4)	C50A	C49A	C58A	C57A	-176.9(5)
C48	C49	C58	C53	-176.6(4)	C50A	C51A	C52A	C53A	2.3(10)
C48	C49	C58	C57	3.2(7)	C51A	C52A	C53A	C54A	179.0(6)
C49	C50	C51	C52	0.0(8)	C51A	C52A	C53A	C58A	-1.9(10)
C50	C49	C58	C53	2.1(7)	C52A	C53A	C54A	C55A	-177.2(7)
C50	C49	C58	C57	-178.0(4)	C52A	C53A	C58A	C49A	0.4(8)
C50	C51	C52	C53	-0.4(8)	C52A	C53A	C58A	C57A	177.9(5)
C51	C52	C53	C54	-179.2(5)	C53A	C54A	C55A	C56A	-2.1(12)
C51	C52	C53	C58	1.7(8)	C54A	C53A	C58A	C49A	179.5(5)
C52	C53	C54	C55	-177.2(6)	C54A	C53A	C58A	C57A	-2.9(8)
C52	C53	C58	C49	-2.6(7)	C54A	C55A	C56A	C57A	-0.2(11)
C52	C53	C58	C57	177.6(5)	C55A	C56A	C57A	C58A	0.9(9)
C53	C54	C55	C56	-1.3(10)	C56A	C57A	C58A	C49A	178.1(5)
C54	C53	C58	C49	178.4(5)	C56A	C57A	C58A	C53A	0.7(8)
C54	C53	C58	C57	-1.5(7)	C58A	C49A	C50A	C51A	-0.1(7)
C54	C55	C56	C57	0.4(10)	C58A	C53A	C54A	C55A	3.7(11)
C55	C56	C57	C58	0.0(9)	C17B	C18B	C19B	C20B	0.0
C56	C57	C58	C49	-179.2(5)	C17B	C22B	C23B	C24B	180.0
C56	C57	C58	C53	0.6(7)	C18B	C17B	C22B	C21B	0.0
C58	C49	C50	C51	-0.9(7)	C18B	C17B	C22B	C23B	180.0
C58	C53	C54	C55	1.9(8)	C18B	C19B	C20B	C21B	0.0
P1A	C16A	C17A	C18A	-96.5(4)	C19B	C20B	C21B	C22B	0.0
P1A	C16A	C17A	C22A	83.1(5)	C19B	C20B	C21B	C26B	180.0
P1A	C16A	C17B	C18B	-101.4(3)	C20B	C21B	C22B	C17B	0.0
P1A	C16A	C17B	C22B	81.4(5)	C20B	C21B	C22B	C23B	180.0
P1A	C27A	C28A	C29A	-169.4(4)	C20B	C21B	C26B	C25B	180.0
P1A	C27A	C32A	P2A	-17.4(5)	C21B	C22B	C23B	C24B	0.0
P1A	C27A	C32A	C31A	167.4(4)	C22B	C17B	C18B	C19B	0.0
P2A	C33A	C34A	C35A	-98.9(5)	C22B	C21B	C26B	C25B	0.0
P2A	C33A	C34A	C43A	76.1(4)	C22B	C23B	C24B	C25B	0.0
P2A	C48A	C49A	C50A	-32.9(5)	C23B	C24B	C25B	C26B	0.0

P2A	C48A	C49A	C58A	146.7(4)	C24B	C25B	C26B	C21B	0.0
O1A	C12A	C13A	C14A	-137.9(5)	C26B	C21B	C22B	C17B	180.0
O3A	C44A	C45A	C46A	-142.3(4)	C26B	C21B	C22B	C23B	0.0
N1A	N2A	C15A	O2A	-171.7(4)					

Table A3.29. Hydrogen Atom Coordinates ($\text{\AA}\times 10^4$) and Isotropic Displacement Parameters ($\text{\AA}^2\times 10^3$) for TNSB BDP 7.

Atom	x	y	z	U(eq)
H2	8789.8	5573.7	5881.36	65
H3	9228.33	5025.23	5322.5	85
H4	10100.15	4679.6	6023.22	91
H5	10471.3	4857.05	7306.33	76
H7	10389.22	5286.61	8478.52	71
H8	9961.74	5827.1	9072.97	61
H9	9191.03	6232.3	8329.7	48
H11	8603.2	6099.22	6283.42	39
H13C	6706.9	5527.4	7687.42	48
H13D	6485.9	5959.6	7551.55	48
H14C	7539.22	5705.54	8701.99	54
H14D	6772.56	5862.49	8938.44	54
H16	8195.08	6881.61	8196.25	33
H18	6707.36	6635.67	7125.65	38
H19	5921.79	7025.89	6380.45	45
H20	6262.39	7618.61	5980.15	46
H22	7107.56	8152.71	6091.78	46
H23	8101.38	8425.74	6676.02	51
H24	8820.91	8071.52	7565.87	45
H25	8582.94	7445.38	7824.43	40
H28	7713.11	6490.92	5846.59	46
H29	7176.28	6769.83	4708.37	56
H30	7705.37	7300.52	4121.29	55
H31	8736.37	7545.89	4677.55	44
H33	10804.65	7304.34	5989.06	31
H35	9991.59	7050.47	4136.39	45
H36	9869.62	6435.36	3617.74	59
H37	10127.5	5923.74	4434.23	60
H39	10643.04	5660.72	5728.65	60
H40	11136.47	5755.99	7010.01	57
H41	11206.78	6368.91	7560.09	46
H42	10820.75	6878.07	6810.09	37
H45C	11417.06	7936.16	3558.95	40
H45D	11086.58	8219.28	4213.93	40
H46C	10274.27	8136.9	3112.88	37
H46D	10274.05	7689.28	3259.98	37

H48	9031.34	7970.93	5541.98	34
H50	10579.85	7887.07	6752	38
H51	11165.41	8368.36	7458.77	45
H52	10839.03	8990.7	7283.77	50
H54	10106.97	9469.64	6599.42	61
H55	9153.21	9625.94	5757.61	69
H56	8525.34	9151.7	5059.03	60
H57	8825.95	8525.85	5210.2	46
H1A	4015.44	6326.42	6160.63	40
H2A	3433.66	6216.06	7405.13	53
H3A	2621.79	5732.4	7497.66	56
H5A	1999.32	5183.62	6902.2	61
H6A	1793.53	4787.49	5827.02	62
H7A	2455.74	4847.62	4623.8	55
H8A	3287.73	5317.33	4507.34	44
H11A	3734.84	5836.88	4291.9	32
H13A	6068.23	5578.8	4401.71	51
H13B	5852.55	5171.24	4744.05	51
H14A	5524.42	5452.21	6010.26	49
H14B	6342.36	5533.53	5828	49
H16A	4980.01	6651.29	5526.72	28
H16B	4955.45	6638.29	5541.11	28
H18A	5851.77	6203.13	3935.83	32
H19A	6641.49	6478.95	3024.91	32
H20A	6750.11	7136.07	2964.02	32
H23A	4830.61	7201.27	5254.66	32
H24A	4939.22	7858.4	5193.8	32
H25A	5728.93	8134.23	4282.88	32
H26A	6410.03	7752.94	3432.83	32
H28A	4473.71	5965.83	3238.03	39
H29A	4862.19	6062.84	1916.49	46
H30A	4903.23	6670.04	1376.55	58
H31A	4410.69	7172.45	2083.94	48
H33A	2381.07	7280.18	3492.38	32
H35A	2879.14	6908.28	1618.37	38
H36A	2764.3	6275.61	1189.66	48
H37A	2430.67	5811.96	2080.18	46
H39A	2050.42	5618.22	3455.04	38
H40A	1800.19	5768.24	4789.04	36
H41A	1949.36	6390.26	5259.67	34
H42A	2277.07	6864.58	4384.26	29
H45A	2424.17	8172.69	1627.72	32
H45B	1989.56	7919.25	983.88	32
H46A	3028.08	7545.3	751.54	33
H46B	3187.85	7980.02	548.86	33

H48A	4395.79	7677.89	2993.12	31
H50A	2857.65	7810.35	4172.15	38
H51A	2572.68	8343.77	4948.11	48
H52A	3286.83	8870.42	4893.83	64
H54A	4303.86	9215.35	4329.12	77
H55A	5215.89	9252.11	3404.48	82
H56A	5475.89	8734.06	2587.09	65
H57A	4835.66	8183.96	2681.42	47
H18B	5857.6	6300.46	3888.42	32
H19B	6618.21	6639.08	3044.6	32
H20B	6641.51	7298.74	3101.67	32
H23B	4696.13	7204.06	5358.36	32
H24B	4719.4	7863.73	5415.46	32
H25B	5480	8202.36	4571.66	32
H26B	6217.34	7881.33	3670.75	32

Table A3.30. Atomic Occupancy for TNSB BDP 7.

Atom	Occupancy	Atom	Occupancy	Atom	Occupancy
H16A	0.5	H16B	0.5	C17A	0.5
C18A	0.5	H18A	0.5	C19A	0.5
H19A	0.5	C20A	0.5	H20A	0.5
C21A	0.5	C22A	0.5	C23A	0.5
H23A	0.5	C24A	0.5	H24A	0.5
C25A	0.5	H25A	0.5	C26A	0.5
H26A	0.5	C17B	0.5	C18B	0.5
H18B	0.5	C19B	0.5	H19B	0.5
C20B	0.5	H20B	0.5	C21B	0.5
C22B	0.5	C23B	0.5	H23B	0.5
C24B	0.5	H24B	0.5	C25B	0.5
H25B	0.5	C26B	0.5	H26B	0.5

A3.2.5 Crystallographic Data for red-TNSB BDP 8

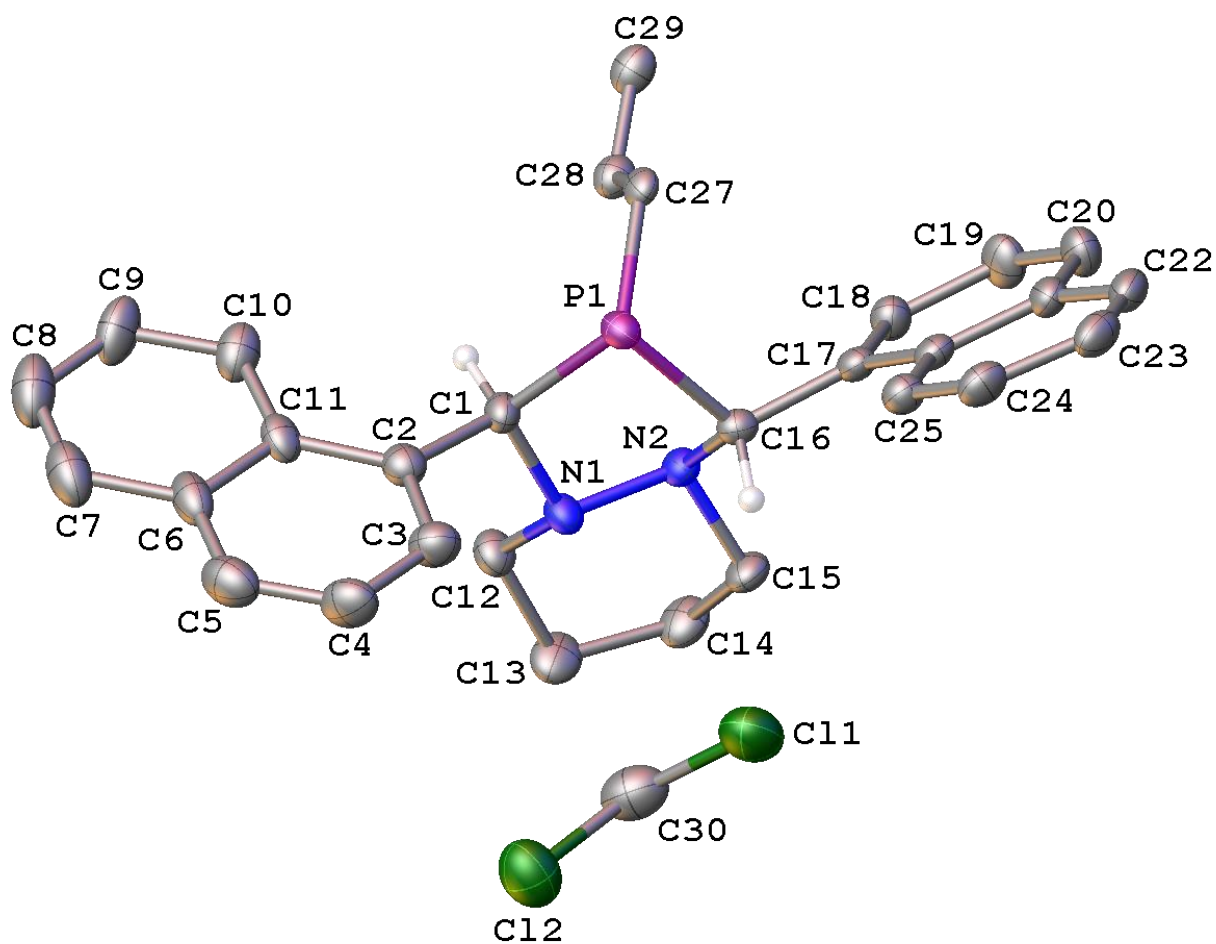


Figure A3.23. A molecular drawing of the content of the asymmetric unit of red-TNSB BDP 8 – half of the diphosphine and one dichloromethane – shown with 50% probability ellipsoids. All H atoms are omitted except the ones on anomeric carbons.

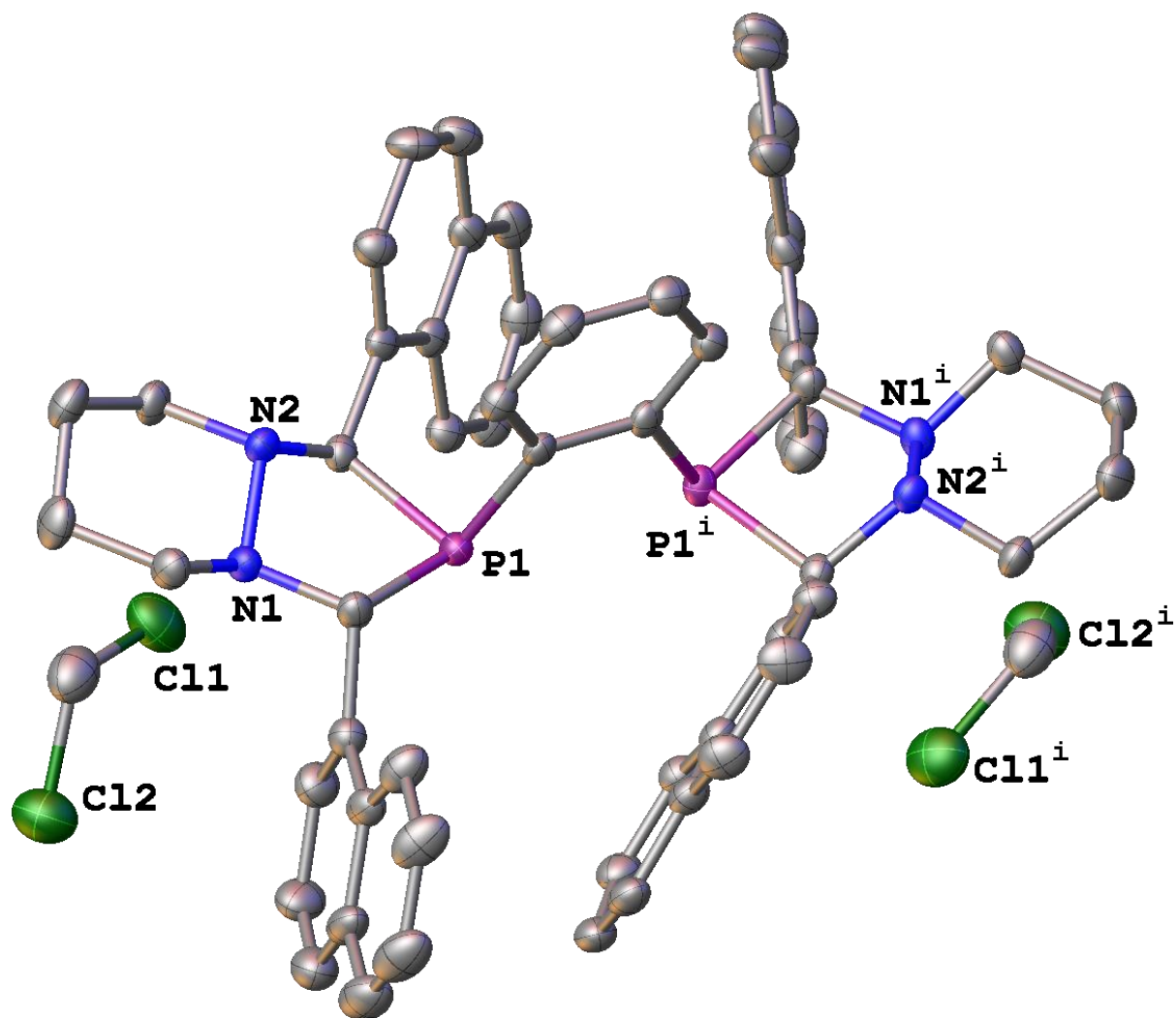


Figure A3.24. A molecular drawing of red-TNSB BDP **8** shown with 50% probability ellipsoids.

All H atoms are omitted. Symmetry code: $i = \frac{1}{2} - x, \frac{1}{2} - y, z$.

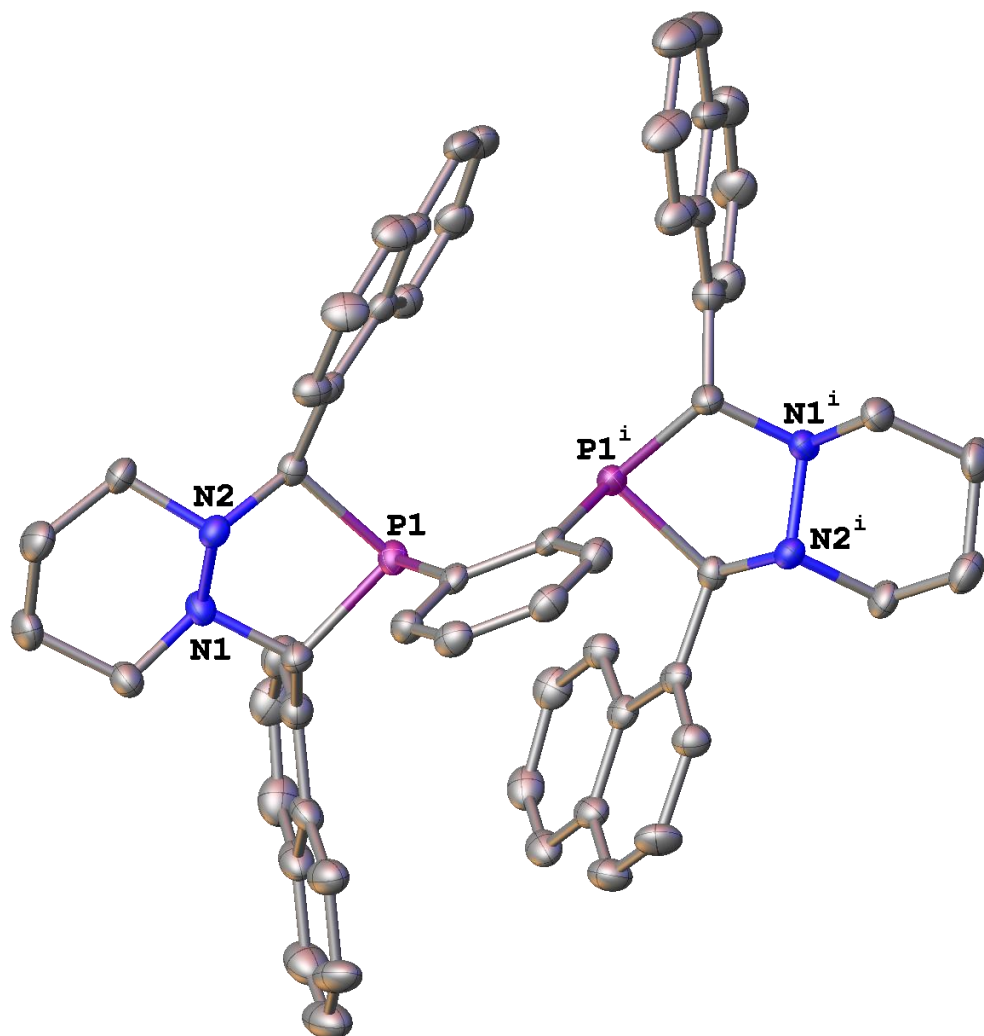


Figure A3.25. A molecular drawing of the diposphine in red-TNSB BDP **8** shown with 50% probability ellipsoids. All H atoms are omitted. Symmetry code: $i = \frac{1}{2} - x, \frac{1}{2} - y, z$.

Data Collection

A colorless crystal with approximate dimensions $0.281 \times 0.107 \times 0.01 \text{ mm}^3$ was selected under oil under ambient conditions and attached to the tip of a MiTeGen MicroMount©. The crystal was mounted in a stream of cold nitrogen at 100(1) K and centered in the X-ray beam by using a video camera.

The crystal evaluation and data collection were performed on a Bruker Quazar SMART APEXII diffractometer with Mo K α ($\lambda = 0.71073$ Å) radiation and the diffractometer to crystal distance of 4.96 cm [1].

The initial cell constants were obtained from three series of ω scans at different starting angles. Each series consisted of 12 frames collected at intervals of 0.5° in a 6° range about ω with the exposure time of 10 seconds per frame. The reflections were successfully indexed by an automated indexing routine built in the APEX3 program suite. The final cell constants were calculated from a set of 9870 strong reflections from the actual data collection.

The data were collected by using the full sphere data collection routine to survey the reciprocal space to the extent of a full sphere to a resolution of 0.80 Å. A total of 162027 data were harvested by collecting 4 sets of frames with 0.5° scans in ω and ϕ with exposure times of 90 sec per frame. These highly redundant datasets were corrected for Lorentz and polarization effects. The absorption correction was based on fitting a function to the empirical transmission surface as sampled by multiple equivalent measurements. [2]

Structure Solution and Refinement

The systematic absences in the diffraction data were uniquely consistent for the space group *Pccn* that yielded chemically reasonable and computationally stable results of refinement [3-8].

A successful solution by the direct methods provided most non-hydrogen atoms from the *E*-map. The remaining non-hydrogen atoms were located in an alternating series of least-squares cycles and difference Fourier maps. All non-hydrogen atoms were refined with anisotropic displacement coefficients. All hydrogen atoms were included in the structure factor calculation at idealized positions and were allowed to ride on the neighboring atoms with relative isotropic displacement coefficients.

The diphosphine molecule resides on a crystallographic two-fold axis.

There are also two molecules of solvent dichloromethane per one diphosphine in the lattice.

The only crystal large enough for the single-crystal X-ray diffraction experiment proved to be a three-component non-merohedral twin with an approximate 66:28:6 component ratio. The reported structure is based on the major component data only.

The final least-squares refinement of 316 parameters against 4514 data resulted in residuals R (based on F^2 for $I \geq 2\sigma$) and wR (based on F^2 for all data) of 0.0606 and 0.1754, respectively. The final difference Fourier map was featureless.

Summary

Crystal data for $C_{60}H_{56}Cl_4N_4P_2$ ($M = 1036.82$ g/mol): orthorhombic, space group Pccn (no. 56), $a = 21.860(6)$ Å, $b = 14.301(5)$ Å, $c = 16.479(5)$ Å, $V = 5152(3)$ Å³, $Z = 4$, $T = 100.0$ K, $\mu(\text{MoK}\alpha) = 0.337$ mm⁻¹, $D_{\text{calc}} = 1.337$ g/cm³, 4514 reflections measured ($3.404^\circ \leq 2\theta \leq 49.996^\circ$), 4514 unique ($R_{\text{int}} = 0.0725$, $R_{\text{sigma}} = 0.0303$) which were used in all calculations. The final R_1 was 0.0606 ($I > 2\sigma(I)$) and wR_2 was 0.1754 (all data).

References

- [1] Bruker-AXS (2016). *APEX3*. Version 2016.5-0. Madison, Wisconsin, USA.
- [2] Krause, L., Herbst-Irmer, R., Sheldrick, G. M. & Stalke, D. (2015). *J. Appl. Cryst.* 48, 3-10.
- [3] Sheldrick, G. M. (2013b). *XPREF*. Version 2013/1. Georg-August-Universität Göttingen, Göttingen, Germany.
- [4] Sheldrick, G. M. (2013a). The *SHELX* homepage, <http://shelx.uni-ac.gwdg.de/SHELX/>.
- [5] Sheldrick, G. M. (2015a). *Acta Cryst. A*, 71, 3-8.
- [6] Sheldrick, G. M. (2015b). *Acta Cryst. C*, 71, 3-8.
- [7] Dolomanov, O. V., Bourhis, L. J., Gildea, R. J., Howard, J. A. K. & Puschmann, H. (2009). *J. Appl. Crystallogr.* 42, 339-341.

[8] Guzei, I. A. (2007-2013). Programs *Gn*. University of Wisconsin-Madison, Madison, Wisconsin, USA.

Table A3.31. Crystal Data and Structure Refinement for red-TNSB BDP **8**.

Empirical formula	C ₆₀ H ₅₆ Cl ₄ N ₄ P ₂
Formula weight	1036.82
Temperature/K	100.0
Crystal system	orthorhombic
Space group	Pccn
a/Å	21.860(6)
b/Å	14.301(5)
c/Å	16.479(5)
α/°	90
β/°	90
γ/°	90
Volume/Å ³	5152(3)
Z	4
ρ _{calc} /g/cm ³	1.337
μ/mm ⁻¹	0.337
F(000)	2168.0
Crystal size/mm ³	0.281 × 0.107 × 0.01
Radiation	MoKα (λ = 0.71073)
2Θ range for data collection/°	3.404 to 49.996
Index ranges	-25 ≤ h ≤ 25, -16 ≤ k ≤ 16, -19 ≤ l ≤ 19
Reflections collected	162027
Independent reflections	4514 [R _{int} = 0.0725, R _{sigma} = 0.0303]
Data/restraints/parameters	4514/0/316
Goodness-of-fit on F ²	1.036
Final R indexes [>=2σ (I)]	R ₁ = 0.0606, wR ₂ = 0.1682
Final R indexes [all data]	R ₁ = 0.0694, wR ₂ = 0.1754
Largest diff. peak/hole / e Å ⁻³	0.75/-0.60

Table A3.32. Fractional Atomic Coordinates (×10⁴) and Equivalent Isotropic Displacement Parameters (Å²×10³) for red-TNSB BDP **8**. U_{eq} is defined as 1/3 of of the trace of the orthogonalised U_{ij} tensor.

Atom	x	y	z	U(eq)
Cl1	1132.7(5)	5078.4(7)	8908.6(6)	55.9(3)
Cl2	1815.1(5)	6757.8(7)	9314.3(6)	57.0(3)
C30	1391.3(18)	6185(3)	8570(2)	49.0(9)
P1	2384.9(3)	3595.8(5)	6852.7(4)	21.6(2)
N1	2038.7(11)	5392.1(15)	6658.7(14)	23.2(5)

N2	1553.7(10)	4815.4(16)	6284.6(14)	21.9(5)
C1	2606.2(12)	4836.2(19)	6620.5(18)	23.7(6)
C2	3053.2(13)	5238(2)	7239.0(18)	26.8(6)
C3	2890.2(15)	5267(2)	8041.5(19)	33.8(7)
C4	3255.4(16)	5684(2)	8639(2)	39.0(8)
C5	3795.1(16)	6083(2)	8425(2)	41.4(8)
C6	3998.1(14)	6067(2)	7603(2)	34.2(7)
C7	4567.8(16)	6452(2)	7394(2)	44.8(9)
C8	4770.6(17)	6400(3)	6613(3)	48.2(9)
C9	4413.1(15)	5973(3)	6017(2)	41.5(8)
C10	3858.2(14)	5591(2)	6197(2)	35.5(7)
C11	3622.4(14)	5621.9(19)	7006.0(19)	27.8(6)
C12	2103.7(14)	6256(2)	6175.6(19)	27.7(6)
C13	1525.9(15)	6836(2)	6223(2)	35.1(7)
C14	984.0(14)	6250(2)	5937(2)	34.2(7)
C15	973.9(13)	5333(2)	6406.2(19)	27.4(6)
C16	1557.1(12)	3968.8(18)	6798.6(16)	20.9(6)
C17	1138.1(12)	3206.1(19)	6513.8(17)	21.6(6)
C18	914.7(13)	3185(2)	5736.1(18)	26.7(6)
C19	510.3(14)	2470(2)	5481.1(19)	33.8(7)
C20	333.5(15)	1784(2)	6008(2)	33.9(7)
C21	558.1(13)	1773(2)	6815.7(18)	26.0(6)
C22	366.3(13)	1081(2)	7373.2(19)	30.7(7)
C23	582.8(14)	1070(2)	8152(2)	32.4(7)
C24	1011.3(14)	1739(2)	8401.8(19)	30.5(7)
C25	1197.8(13)	2432(2)	7879.9(17)	25.4(6)
C26	971.5(12)	2478(2)	7073.8(17)	22.6(6)
C27	2458.6(12)	2988.4(19)	5860.8(16)	20.6(6)
C28	2413.0(12)	3458(2)	5116.2(17)	25.0(6)
C29	2456.2(13)	2982(2)	4389.3(17)	28.3(6)

Table A3.33. Anisotropic Displacement Parameters ($\text{\AA}^2 \times 10^3$) for red-TNSB BDP **8**. The Anisotropic displacement factor exponent takes the form: $-2\pi^2[h^2a^{*2}U_{11}+2hka^*b^*U_{12}+\dots]$.

Atom	U_{11}	U_{22}	U_{33}	U_{23}	U_{13}	U_{12}
Cl1	62.2(7)	52.3(6)	53.2(6)	-14.5(4)	7.8(5)	-3.6(5)
Cl2	62.6(7)	56.4(6)	51.9(6)	-3.6(4)	-4.7(5)	-10.2(5)
C30	49(2)	58(2)	40.7(19)	-3.2(17)	-0.2(17)	12.9(18)
P1	20.5(4)	19.2(4)	25.1(4)	-2.1(3)	-4.5(3)	1.6(3)
N1	22.5(12)	17.7(11)	29.4(12)	-0.3(9)	-3.9(10)	-0.3(9)
N2	17.2(12)	22.5(12)	26.1(12)	-1.4(9)	-1.2(9)	2.0(9)
C1	17.9(14)	20.8(14)	32.4(15)	-1.2(12)	-0.3(11)	-0.8(11)
C2	25.8(15)	23.6(14)	30.9(15)	-0.8(12)	-1.9(12)	1.8(12)
C3	33.4(18)	36.8(17)	31.3(16)	-5.5(13)	0.1(13)	3.6(14)
C4	39.3(19)	47(2)	30.4(16)	-10.8(15)	-5.9(14)	3.6(16)

C5	42(2)	37.9(19)	44(2)	-8.9(15)	-11.8(16)	3.4(15)
C6	25.3(16)	24.2(15)	53(2)	1.0(14)	-12.1(14)	-2.0(12)
C7	36.5(19)	35.2(18)	63(2)	5.7(17)	-14.2(17)	-9.0(15)
C8	30.7(18)	45(2)	69(3)	18.8(19)	-7.6(18)	-10.0(16)
C9	27.7(17)	51(2)	46(2)	21.1(16)	3.1(14)	-5.9(15)
C10	26.4(17)	36.9(18)	43.0(18)	11.6(14)	-1.1(14)	-1.7(13)
C11	26.3(15)	18.8(14)	38.2(16)	3.3(12)	-6.9(13)	-2.9(11)
C12	26.6(15)	20.9(14)	35.6(16)	3.1(12)	-3.0(13)	-1.4(12)
C13	34.4(18)	23.4(15)	47.6(19)	10.1(13)	0.7(15)	5.9(13)
C14	25.1(16)	35.2(17)	42.1(18)	7.3(14)	-1.1(13)	8.4(13)
C15	19.6(14)	26.9(15)	35.6(16)	-0.7(12)	3.1(12)	5.9(12)
C16	21.2(14)	20.3(13)	21.1(13)	-1(1)	0.9(11)	2.9(11)
C17	17.1(13)	24.2(14)	23.5(14)	-4.7(11)	2.1(11)	2.5(11)
C18	24.0(15)	29.3(16)	26.9(15)	-2.2(12)	1.1(12)	-3.0(12)
C19	30.1(16)	42.8(18)	28.4(15)	-4.9(13)	-7.2(13)	-8.1(14)
C20	28.9(17)	35.0(17)	37.8(17)	-7.3(14)	-1.3(13)	-8.4(14)
C21	18.0(14)	27.4(15)	32.6(16)	-4.5(12)	2.9(11)	-0.5(11)
C22	21.4(15)	27.5(15)	43.2(18)	-2.9(13)	8.7(13)	-1.8(12)
C23	27.7(16)	30.4(16)	39.2(18)	5.5(13)	12.5(13)	1.8(13)
C24	28.2(16)	36.8(17)	26.6(15)	1.0(13)	7.5(12)	3.2(13)
C25	23.1(14)	27.8(15)	25.3(14)	-2.5(12)	2.6(11)	0.6(12)
C26	17.6(13)	25.3(14)	24.9(14)	-2.5(11)	4.4(11)	3.4(11)
C27	13.2(12)	21.7(14)	26.8(14)	-0.6(11)	-2.2(11)	1.9(10)
C28	21.9(15)	24.9(14)	28.3(15)	3.3(12)	0.5(11)	2.1(12)
C29	23.6(15)	35.8(16)	25.6(15)	5.2(12)	-0.9(12)	1.9(12)

Table A3.34. Bond Lengths for red-TNSB BDP 8.

Atom	Atom	Length/Å	Atom	Atom	Length/Å
Cl1	C30	1.771(4)	C10	C11	1.431(5)
Cl2	C30	1.741(4)	C12	C13	1.513(4)
P1	C1	1.878(3)	C13	C14	1.526(5)
P1	C16	1.889(3)	C14	C15	1.522(4)
P1	C27	1.858(3)	C16	C17	1.500(4)
N1	N2	1.478(3)	C17	C18	1.372(4)
N1	C1	1.475(4)	C17	C26	1.438(4)
N1	C12	1.476(4)	C18	C19	1.415(4)
N2	C15	1.481(3)	C19	C20	1.367(5)
N2	C16	1.478(3)	C20	C21	1.418(4)
C1	C2	1.524(4)	C21	C22	1.414(4)
C2	C3	1.370(4)	C21	C26	1.419(4)
C2	C11	1.413(4)	C22	C23	1.368(5)
C3	C4	1.401(5)	C23	C24	1.401(5)
C4	C5	1.357(5)	C24	C25	1.374(4)
C5	C6	1.425(5)	C25	C26	1.419(4)

C6	C7	1.405(5)	C27	C27 ¹	1.409(6)
C6	C11	1.432(4)	C27	C28	1.402(4)
C7	C8	1.363(6)	C28	C29	1.381(4)
C8	C9	1.396(5)	C29	C29 ¹	1.391(6)
C9	C10	1.363(5)			

Table A3.35. Bond Angles for red-TNSB BDP 8.

Atom	Atom	Atom	Angle/°	Atom	Atom	Atom	Angle/°
Cl2	C30	Cl1	111.6(2)	N1	C12	C13	110.5(2)
C1	P1	C16	88.30(12)	C12	C13	C14	109.3(3)
C27	P1	C1	103.89(13)	C15	C14	C13	109.1(3)
C27	P1	C16	100.00(12)	N2	C15	C14	110.4(2)
C1	N1	N2	106.5(2)	N2	C16	P1	105.26(17)
C1	N1	C12	110.3(2)	N2	C16	C17	114.4(2)
C12	N1	N2	108.1(2)	C17	C16	P1	113.23(18)
N1	N2	C15	106.2(2)	C18	C17	C16	121.7(3)
C16	N2	N1	102.39(19)	C18	C17	C26	119.5(3)
C16	N2	C15	109.6(2)	C26	C17	C16	118.7(2)
N1	C1	P1	106.49(18)	C17	C18	C19	121.1(3)
N1	C1	C2	107.9(2)	C20	C19	C18	120.4(3)
C2	C1	P1	112.6(2)	C19	C20	C21	120.4(3)
C3	C2	C1	119.3(3)	C20	C21	C26	119.6(3)
C3	C2	C11	118.6(3)	C22	C21	C20	120.9(3)
C11	C2	C1	122.0(3)	C22	C21	C26	119.4(3)
C2	C3	C4	122.9(3)	C23	C22	C21	121.0(3)
C5	C4	C3	119.4(3)	C22	C23	C24	119.9(3)
C4	C5	C6	120.7(3)	C25	C24	C23	120.5(3)
C5	C6	C11	118.8(3)	C24	C25	C26	121.1(3)
C7	C6	C5	120.2(3)	C21	C26	C17	118.9(3)
C7	C6	C11	120.9(3)	C21	C26	C25	118.0(3)
C8	C7	C6	119.9(3)	C25	C26	C17	123.1(3)
C7	C8	C9	120.4(3)	C27 ¹	C27	P1	118.34(9)
C10	C9	C8	121.3(3)	C28	C27	P1	122.7(2)
C9	C10	C11	120.8(3)	C28	C27	C27 ¹	118.96(16)
C2	C11	C6	119.4(3)	C29	C28	C27	121.2(3)
C2	C11	C10	124.0(3)	C28	C29	C29 ¹	119.87(17)
C10	C11	C6	116.6(3)				

Table A3.36. Torsion Angles for red-TNSB BDP 8.

A	B	C	D	Angle/°	A	B	C	D	Angle/°
P1	C1	C2	C3	-58.3(3)	C11	C2	C3	C4	1.8(5)
P1	C1	C2	C11	124.7(3)	C11	C6	C7	C8	-0.4(5)
P1	C16	C17	C18	-102.7(3)	C12	N1	N2	C15	-67.5(3)

P1	C16	C17	C26	77.0(3)	C12	N1	N2	C16	177.6(2)
P1	C27	C28	C29	-178.5(2)	C12	N1	C1	P1	-156.78(19)
N1	N2	C15	C14	65.3(3)	C12	N1	C1	C2	82.1(3)
N1	N2	C16	P1	-50.0(2)	C12	C13	C14	C15	52.6(3)
N1	N2	C16	C17	-174.9(2)	C13	C14	C15	N2	-58.5(3)
N1	C1	C2	C3	59.0(3)	C15	N2	C16	P1	-162.39(18)
N1	C1	C2	C11	-118.1(3)	C15	N2	C16	C17	72.7(3)
N1	C12	C13	C14	-56.8(3)	C16	P1	C1	N1	8.55(19)
N2	N1	C1	P1	-39.7(2)	C16	P1	C1	C2	126.7(2)
N2	N1	C1	C2	-160.8(2)	C16	P1	C27	C27 ¹	-111.7(3)
N2	N1	C12	C13	64.7(3)	C16	P1	C27	C28	65.9(2)
N2	C16	C17	C18	18.0(4)	C16	N2	C15	C14	175.2(2)
N2	C16	C17	C26	-162.4(2)	C16	C17	C18	C19	-178.8(3)
C1	P1	C16	N2	23.90(18)	C16	C17	C26	C21	177.8(2)
C1	P1	C16	C17	149.6(2)	C16	C17	C26	C25	-1.7(4)
C1	P1	C27	C27 ¹	157.6(3)	C17	C18	C19	C20	0.0(5)
C1	P1	C27	C28	-24.8(3)	C18	C17	C26	C21	-2.6(4)
C1	N1	N2	C15	173.9(2)	C18	C17	C26	C25	177.9(3)
C1	N1	N2	C16	59.0(2)	C18	C19	C20	C21	-0.6(5)
C1	N1	C12	C13	-179.1(2)	C19	C20	C21	C22	178.3(3)
C1	C2	C3	C4	-175.4(3)	C19	C20	C21	C26	-0.4(5)
C1	C2	C11	C6	174.2(3)	C20	C21	C22	C23	179.9(3)
C1	C2	C11	C10	-6.3(4)	C20	C21	C26	C17	2.0(4)
C2	C3	C4	C5	0.2(5)	C20	C21	C26	C25	-178.5(3)
C3	C2	C11	C6	-2.9(4)	C21	C22	C23	C24	-1.4(4)
C3	C2	C11	C10	176.6(3)	C22	C21	C26	C17	-176.8(2)
C3	C4	C5	C6	-1.1(5)	C22	C21	C26	C25	2.8(4)
C4	C5	C6	C7	-177.7(3)	C22	C23	C24	C25	2.6(5)
C4	C5	C6	C11	0.0(5)	C23	C24	C25	C26	-1.1(4)
C5	C6	C7	C8	177.3(3)	C24	C25	C26	C17	178.0(3)
C5	C6	C11	C2	2.0(4)	C24	C25	C26	C21	-1.6(4)
C5	C6	C11	C10	-177.5(3)	C26	C17	C18	C19	1.6(4)
C6	C7	C8	C9	0.6(5)	C26	C21	C22	C23	-1.4(4)
C7	C6	C11	C2	179.7(3)	C27	P1	C1	N1	108.43(19)
C7	C6	C11	C10	0.1(4)	C27	P1	C1	C2	-133.5(2)
C7	C8	C9	C10	-0.6(6)	C27	P1	C16	N2	-79.90(18)
C8	C9	C10	C11	0.4(5)	C27	P1	C16	C17	45.8(2)
C9	C10	C11	C2	-179.7(3)	C27 ¹	C27	C28	C29	-0.9(5)
C9	C10	C11	C6	-0.1(5)	C27	C28	C29	C29 ¹	0.3(5)

Table A3.37. Hydrogen Atom Coordinates ($\text{\AA} \times 10^4$) and Isotropic Displacement Parameters ($\text{\AA}^2 \times 10^3$) for red-TNSB BDP **8**.

Atom	x	y	z	U(eq)
H30A	1647	6102	8080	59

H30B	1034	6575	8420	59
H1	2786	4875	6064	28
H3	2513	4992	8200	41
H4	3126	5687	9190	47
H5	4040	6376	8827	50
H7	4811	6749	7796	54
H8	5158	6656	6474	58
H9	4560	5948	5474	50
H10	3625	5302	5780	43
H12A	2188	6092	5603	33
H12B	2454	6625	6383	33
H13A	1567	7398	5877	42
H13B	1458	7044	6789	42
H14A	598	6596	6030	41
H14B	1022	6122	5349	41
H15A	916	5463	6991	33
H15B	626	4945	6219	33
H16	1426	4156	7357	25
H18	1033	3657	5363	32
H19	361	2467	4940	41
H20	59	1310	5833	41
H22	83	617	7204	37
H23	443	608	8523	39
H24	1174	1714	8936	37
H25	1483	2887	8061	31
H28	2351	4116	5112	30
H29	2426	3311	3890	34

A3.2.6. Crystallographic Data for [Rh(acac)TPSB BDP 1]

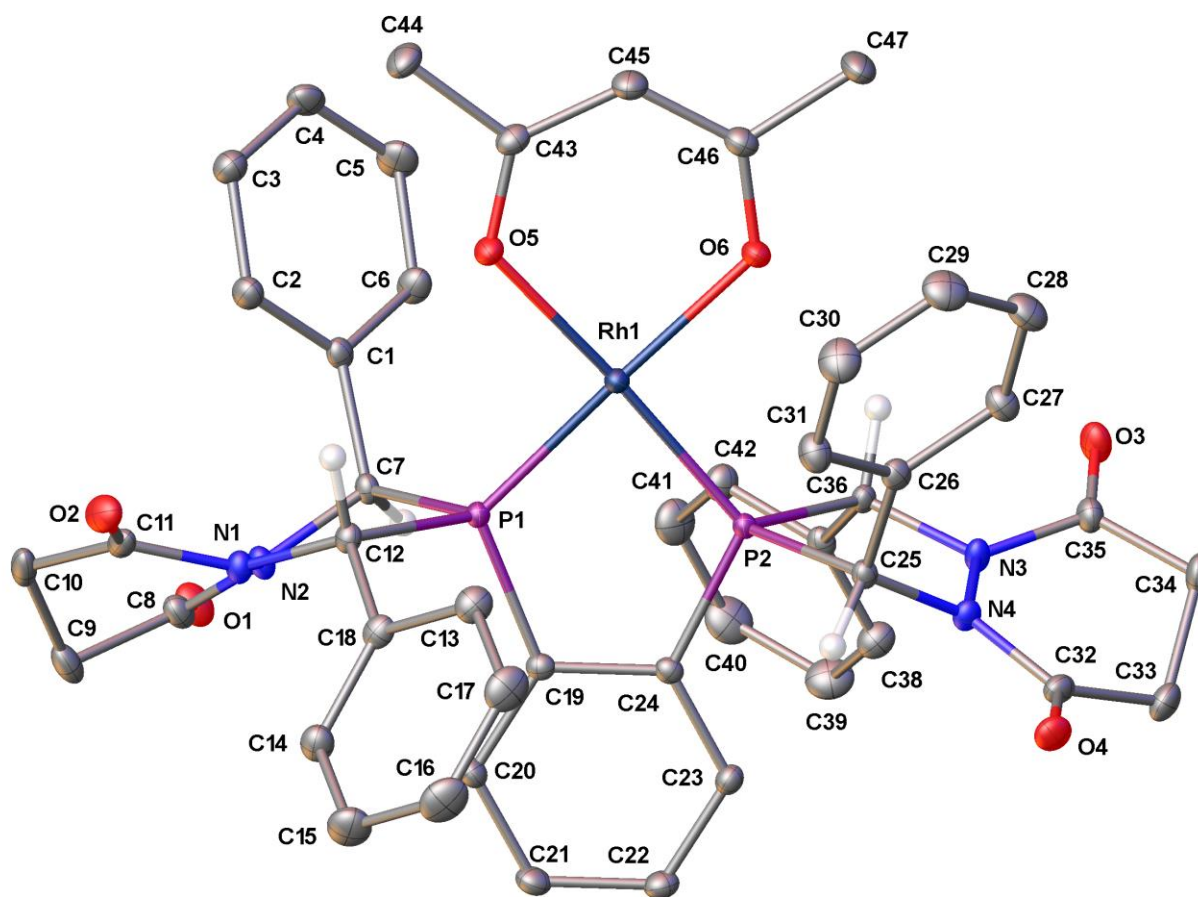


Figure A3.26. A molecular drawing of [Rh(acac)TPSB BDP 1] shown with 40% probability ellipsoids. All non stereoactive H atoms are omitted. All dichloromethane molecules are omitted.

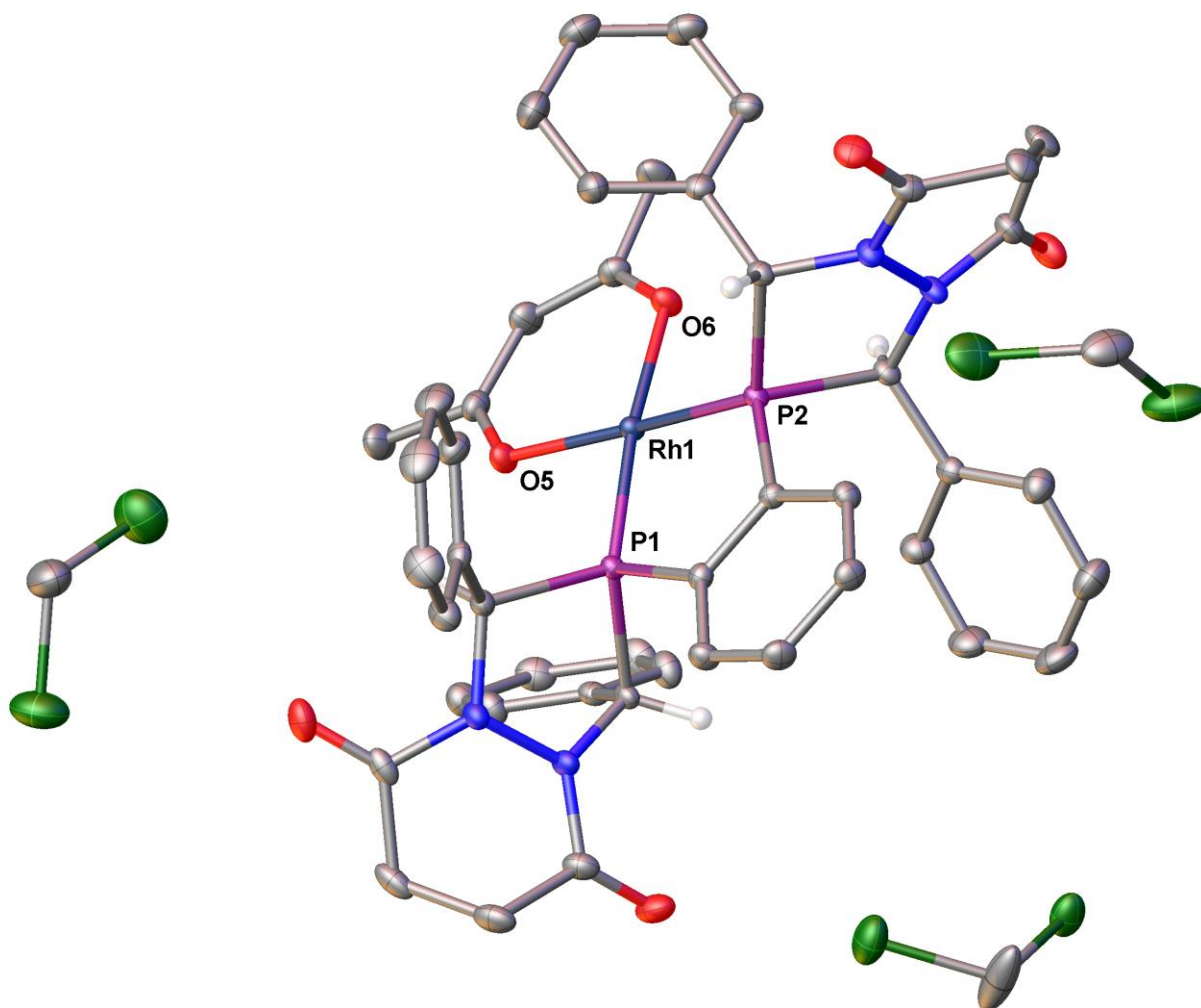


Figure A3.27. A molecular drawing of [Rh(acac)TPSB BDP 1] shown with 50% probability ellipsoids. All non stereoactive H atoms are omitted.

Data Collection

An orange crystal with approximate dimensions 0.204 x 0.172 x 0.124 mm³ was selected under oil under ambient conditions and attached to the tip of a MiTeGen MicroMount©. The crystal was mounted in a stream of cold nitrogen at 100(1) K and centered in the X-ray beam by using a video camera.

The crystal evaluation and data collection were performed on a Bruker Quazar SMART APEXII diffractometer with Mo K α ($\lambda = 0.71073 \text{ \AA}$) radiation and the diffractometer to crystal distance of 4.96 cm [1].

The initial cell constants were obtained from three series of ω scans at different starting angles. Each series consisted of 12 frames collected at intervals of 0.5° in a 6° range about ω with the exposure time of 5 seconds per frame. The reflections were successfully indexed by an automated indexing routine built in the APEX3 program suite. The final cell constants were calculated from a set of 9703 strong reflections from the actual data collection.

The data were collected by using the full sphere data collection routine to survey the reciprocal space to the extent of a full sphere to a resolution of 0.70 \AA . A total of 72109 data were harvested by collecting 6 sets of frames with 0.5° scans in ω and ϕ with exposure times of 25 sec per frame. These highly redundant datasets were corrected for Lorentz and polarization effects. The absorption correction was based on fitting a function to the empirical transmission surface as sampled by multiple equivalent measurements. [2]

Structure Solution and Refinement

The systematic absences in the diffraction data were consistent for the space groups $P\bar{1}$ and $P1$. The E -statistics strongly suggested the centrosymmetric space group $P\bar{1}$ that yielded chemically reasonable and computationally stable results of refinement [2-4].

A successful solution by the direct methods provided most non-hydrogen atoms from the E -map. The remaining non-hydrogen atoms were located in an alternating series of least-squares cycles and difference Fourier maps. All non-hydrogen atoms were refined with anisotropic displacement coefficients. All hydrogen atoms were included in the structure factor calculation at idealized positions and were allowed to ride on the neighboring atoms with relative isotropic displacement coefficients.

The chiral centers are C7-*R*, C12-*R*, C25-*R*, and C36-*R*. Both enantiomers are present in the crystal structure.

There are also three molecule of solvate dichloromethane in the asymmetric unit. Atom Cl6 is disordered over two positions with major component contribution equal to 61.3(1.9)%. The final least-squares refinement of 634 parameters against 14629 data resulted in residuals R (based on F^2 for $\geq 2\sigma$) and wR (based on F^2 for all data) of 0.0251 and 0.0675, respectively. The final difference Fourier map was featureless.

Summary

Crystal data for $C_{50}H_{49}Cl_6N_4O_6P_2Rh$ ($M=1179.48$ g/mol): triclinic, space group $P\bar{1}$ (no. 2), $a = 12.305(3)$ Å, $b = 13.540(4)$ Å, $c = 17.593(6)$ Å, $\alpha = 111.943(5)^\circ$, $\beta = 100.152(10)^\circ$, $\gamma = 94.594(14)^\circ$, $V = 2641.8(13)$ Å³, $Z = 2$, $T = 100.0$ K, $\mu(\text{MoK}\alpha) = 0.739$ mm⁻¹, $D_{\text{calc}} = 1.483$ g/cm³, 72109 reflections measured ($2.56^\circ \leq 2\theta \leq 58.976^\circ$), 14629 unique ($R_{\text{int}} = 0.0232$, $R_{\text{sigma}} = 0.0189$) which were used in all calculations. The final R_1 was 0.0251 ($I > 2\sigma(I)$) and wR_2 was 0.0675 (all data).

References

- [1] Bruker-AXS (2014). *APEX2*. Version 2014.11-0. Madison, Wisconsin, USA.
- [2] Krause, L., Herbst-Irmer, R., Sheldrick, G. M. & Stalke, D. (2015). *J. Appl. Cryst.* 48, 3-10.
- [3] Sheldrick, G. M. (2013b). *XPREF*. Version 2013/1. Georg-August-Universität Göttingen, Göttingen, Germany.
- [4] Sheldrick, G. M. (2013a). The *SHELX* homepage, <http://shelx.uni-ac.gwdg.de/SHELX/>.
- [5] Sheldrick, G. M. (2015a). *Acta Cryst. A*, 71, 3-8.
- [6] Sheldrick, G. M. (2015b). *Acta Cryst. C*, 71, 3-8.

- [7] Dolomanov, O. V., Bourhis, L. J., Gildea, R. J., Howard, J. A. K. & Puschmann, H. (2009). *J. Appl. Crystallogr.* 42, 339-341.
- [8] Guzei, I. A. (2007-2013). Programs *Gn*. University of Wisconsin-Madison, Madison, Wisconsin, USA.

Table A3.38. Crystal Data and Structure Refinement for [Rh(acac)TPSB BDP 1].

Empirical formula	C ₅₀ H ₄₉ Cl ₆ N ₄ O ₆ P ₂ Rh
Formula weight	1179.48
Temperature/K	100.0
Crystal system	triclinic
Space group	P $\bar{1}$
a/Å	12.305(3)
b/Å	13.540(4)
c/Å	17.593(6)
α /°	111.943(5)
β /°	100.152(10)
γ /°	94.594(14)
Volume/Å ³	2641.8(13)
Z	2
ρ_{calc} /g/cm ³	1.483
μ /mm ⁻¹	0.739
F(000)	1204.0
Crystal size/mm ³	0.204 × 0.172 × 0.124
Radiation	MoK α (λ = 0.71073)
2 θ range for data collection/°	2.56 to 58.976
Index ranges	-17 ≤ h ≤ 17, -18 ≤ k ≤ 18, -24 ≤ l ≤ 24
Reflections collected	72109
Independent reflections	14629 [R _{int} = 0.0232, R _{sigma} = 0.0189]
Data/restraints/parameters	14629/0/634
Goodness-of-fit on F ²	1.089
Final R indexes [$I \geq 2\sigma(I)$]	R ₁ = 0.0251, wR ₂ = 0.0663
Final R indexes [all data]	R ₁ = 0.0286, wR ₂ = 0.0675
Largest diff. peak/hole / e Å ⁻³	0.62/-0.45

Table A3.39. Fractional Atomic Coordinates ($\times 10^4$) and Equivalent Isotropic Displacement Parameters ($\text{\AA}^2 \times 10^3$) for [Rh(acac)TPSB BDP **1**]. U_{eq} is defined as 1/3 of the trace of the orthogonalised U_{ij} tensor.

Atom	x	y	z	U(eq)
Rh1	7459.6(2)	4691.6(2)	6609.4(2)	11.41(3)
P1	7485.6(3)	6000.9(2)	7777.0(2)	11.19(6)
P2	6780.7(3)	3688.9(2)	7167.5(2)	10.88(6)
O1	5781.8(9)	8837.3(8)	8850.4(7)	24.6(2)
O2	10083.0(9)	9024.3(9)	8863.8(6)	24.3(2)
O3	4057.2(9)	856.9(8)	5590.8(6)	23.0(2)
O4	7576.3(9)	872.3(8)	7824.2(6)	21.1(2)
O5	8250.3(8)	5688.4(7)	6158.6(6)	16.30(18)
O6	7240.2(8)	3412.4(7)	5470.5(5)	16.21(18)
N1	7256.9(9)	8008.0(8)	8560.3(7)	14.2(2)
N2	8439.2(9)	8046.2(9)	8741.7(7)	14.3(2)
N3	5485.8(9)	1775.6(8)	6699.6(7)	14.5(2)
N4	6528.5(9)	1748.5(9)	7189.6(7)	14.3(2)
C1	6567.7(11)	7312.2(10)	7002.5(8)	14.4(2)
C2	7373.5(12)	8008.5(11)	6907.2(8)	18.8(3)
C3	7288.9(12)	8129.6(11)	6148.7(9)	20.9(3)
C4	6407.2(13)	7541.5(12)	5475.4(9)	22.0(3)
C5	5593.6(13)	6850.3(13)	5566.2(9)	26.0(3)
C6	5669.3(12)	6736.7(11)	6326.6(9)	20.5(3)
C7	6656.5(10)	7106.6(10)	7798.1(7)	12.8(2)
C8	6788.5(12)	8841.7(11)	9018.4(8)	18.7(3)
C9	7643.1(13)	9753.1(11)	9676.5(9)	23.1(3)
C10	8554.8(13)	9980.8(11)	9252.7(9)	22.5(3)
C11	9110.5(12)	9008.2(11)	8921.8(8)	17.9(2)
C12	8787.8(10)	7001.5(10)	8336.2(8)	13.5(2)
C13	9568.9(10)	6655.8(11)	8923.2(8)	15.8(2)
C14	9833.1(12)	7218.4(11)	9788.0(9)	20.1(3)
C15	10556.2(13)	6860.7(13)	10300.5(10)	28.2(3)
C16	11000.2(13)	5932.9(14)	9952.0(11)	30.2(3)
C17	10731.5(13)	5359.8(13)	9086.9(11)	27.6(3)
C18	10026.3(12)	5720.0(12)	8572.1(9)	21.1(3)
C19	7025.8(10)	5558.8(10)	8546.7(7)	12.6(2)
C20	6985.4(11)	6222(1)	9365.6(8)	16.5(2)
C21	6565.7(12)	5772.6(11)	9868.8(8)	18.7(3)
C22	6190.4(11)	4669.0(11)	9563.5(8)	17.7(2)
C23	6225.5(11)	4006(1)	8748.4(8)	14.8(2)

C24	6648.2(10)	4449(1)	8239.4(7)	12.3(2)
C25	7456.7(10)	2527.9(10)	7249.3(7)	13.1(2)
C26	8165.8(11)	2103.2(10)	6611.0(8)	15.3(2)
C27	7790.3(12)	1167.3(11)	5886.2(8)	19.2(3)
C28	8472.7(13)	813.5(13)	5315.0(9)	25.5(3)
C29	9522.0(13)	1396.2(13)	5460.3(10)	28.4(3)
C30	9894.3(13)	2328.9(13)	6178.5(10)	28.1(3)
C31	9222.1(12)	2683.0(11)	6755.4(9)	21.3(3)
C32	6660.1(12)	925.8(11)	7451.0(8)	17.1(2)
C33	5609.3(12)	119.2(11)	7196.5(9)	21.6(3)
C34	5071.4(13)	-158.4(11)	6272.2(9)	22.5(3)
C35	4819.0(11)	833.5(10)	6127.8(8)	18.0(2)
C36	5408(1)	2793.1(10)	6601.8(7)	12.9(2)
C37	4432.7(10)	3326.9(10)	6886.9(8)	14.5(2)
C38	3759.2(12)	2966.8(12)	7317.8(9)	21.4(3)
C39	2904.4(13)	3521.1(14)	7593.3(10)	29.0(3)
C40	2720.6(14)	4436.2(14)	7444.1(11)	31.0(3)
C41	3383.1(13)	4793.5(13)	7010(1)	27.8(3)
C42	4230.5(12)	4239.1(11)	6728.1(9)	20.1(3)
C43	8403.9(11)	5405.4(11)	5417.4(8)	16.9(2)
C44	8996.5(13)	6274.1(12)	5224.0(9)	23.2(3)
C45	8082.4(12)	4369.7(11)	4775.2(8)	20.5(3)
C46	7550.0(11)	3457.4(11)	4828.6(8)	17.8(2)
C47	7289.9(14)	2405.9(12)	4067.3(9)	25.7(3)
Cl1	1140.0(3)	6750.6(3)	7318.5(2)	28.21(8)
Cl2	3337.5(3)	7991.6(4)	8299.1(3)	34.61(9)
C48	1938.8(15)	7638(2)	8313.7(12)	58.6(7)
Cl3	3803.6(5)	1359.4(4)	8943.5(3)	47.34(12)
Cl4	6238.3(5)	2000.6(4)	9525.1(3)	43.62(11)
C49	5045.0(16)	1188.3(15)	9533.4(12)	35.7(4)
Cl5	8988.9(5)	8467.6(4)	1784.6(3)	50.25(12)
Cl6	9515(2)	10718.2(16)	3029.0(16)	45.0(8)
Cl6A	9241(13)	10529(11)	3102(4)	101(2)
C50	9941.3(16)	9483.8(15)	2638.7(13)	42.0(4)

Table A3.40. Anisotropic Displacement Parameters ($\text{\AA}^2 \times 10^3$) for [Rh(acac)TPSB BDP 1]. The Anisotropic displacement factor exponent takes the form: $-2\pi^2[h^2a^{*2}U_{11}+2hka^*b^*U_{12}+\dots]$.

Atom	U_{11}	U_{22}	U_{33}	U_{23}	U_{13}	U_{12}
Rh1	13.35(5)	10.46(5)	10.29(5)	3.94(3)	2.85(3)	1.53(3)
P1	12.29(14)	9.71(14)	10.84(13)	3.74(11)	1.85(10)	0.95(11)

P2	12.45(14)	9.30(14)	10.22(13)	3.60(11)	1.51(10)	1.52(11)
O1	21.1(5)	22.4(5)	24.7(5)	2.6(4)	3.8(4)	9.0(4)
O2	20.6(5)	25.3(5)	22.6(5)	9.3(4)	-0.3(4)	-7.3(4)
O3	22.9(5)	17.2(5)	21.9(5)	5.6(4)	-5.3(4)	-1.3(4)
O4	24.2(5)	21.1(5)	21.6(5)	12.9(4)	2.2(4)	7.7(4)
O5	19.2(5)	14.8(4)	15.5(4)	6.3(3)	5.8(3)	0.2(3)
O6	21.4(5)	14.1(4)	11.6(4)	3.6(3)	4.2(3)	0.9(4)
N1	12.1(5)	11.9(5)	14.4(5)	2.2(4)	-0.5(4)	1.3(4)
N2	12.7(5)	12.0(5)	16.4(5)	5.2(4)	-0.1(4)	0.6(4)
N3	14.3(5)	10.8(5)	16.6(5)	5.8(4)	-2.0(4)	1.2(4)
N4	13.9(5)	13.3(5)	16.1(5)	7.6(4)	-0.1(4)	2.3(4)
C1	15.8(6)	11.3(5)	14.7(5)	4.3(4)	1.1(4)	4.0(4)
C2	20.2(6)	17.3(6)	16.0(6)	6.0(5)	-0.1(5)	-0.6(5)
C3	24.1(7)	19.7(6)	20.1(6)	9.7(5)	4.1(5)	2.3(5)
C4	28.1(7)	22.8(7)	16.2(6)	10.0(5)	1.0(5)	8.0(6)
C5	24.1(7)	29.7(8)	19.7(6)	10.6(6)	-6.7(5)	0.5(6)
C6	17.4(6)	21.0(7)	21.2(6)	10.0(5)	-2.8(5)	-1.0(5)
C7	11.7(5)	10.0(5)	13.7(5)	2.9(4)	0.2(4)	0.5(4)
C8	23.1(7)	15.1(6)	15.0(6)	3.4(5)	1.4(5)	5.5(5)
C9	27.9(7)	15.4(6)	17.3(6)	-0.2(5)	-3.1(5)	5.9(5)
C10	29.4(7)	11.8(6)	19.2(6)	5.2(5)	-7.3(5)	-2.4(5)
C11	21.7(6)	15.5(6)	12.9(5)	6.7(5)	-3.9(5)	-5.1(5)
C12	12.4(5)	12.3(5)	15.3(5)	5.5(4)	2.0(4)	0.8(4)
C13	10.5(5)	17.6(6)	19.8(6)	9.3(5)	1.1(4)	0.4(5)
C14	18.6(6)	19.0(6)	20.5(6)	8.1(5)	-1.3(5)	1.2(5)
C15	26.1(8)	33.0(8)	23.1(7)	13.4(6)	-4.8(6)	3.0(6)
C16	20.7(7)	39.5(9)	36.6(8)	24.4(7)	-0.5(6)	8.6(6)
C17	21.6(7)	30.3(8)	38.1(8)	19.1(7)	8.2(6)	12.8(6)
C18	17.6(6)	23.4(7)	24.6(7)	11.1(6)	5.6(5)	5.5(5)
C19	11.2(5)	14.4(6)	11.9(5)	5.4(4)	1.9(4)	1.7(4)
C20	19.4(6)	13.9(6)	13.7(5)	3.0(4)	3.3(5)	1.9(5)
C21	22.7(7)	19.9(6)	13.3(5)	4.9(5)	6.3(5)	5.0(5)
C22	19.7(6)	20.5(6)	16.1(6)	9.5(5)	6.7(5)	4.2(5)
C23	16.1(6)	13.4(6)	16.0(5)	7.2(5)	3.3(4)	1.8(5)
C24	11.8(5)	13.4(6)	11.0(5)	4.4(4)	1.3(4)	2.7(4)
C25	13.8(6)	11.2(5)	13.2(5)	4.5(4)	0.8(4)	2.2(4)
C26	16.2(6)	14.1(6)	16.4(6)	6.8(5)	2.7(4)	5.1(5)
C27	18.5(6)	18.1(6)	18.2(6)	4.2(5)	2.7(5)	4.2(5)
C28	28.1(8)	25.1(7)	19.3(6)	3.1(5)	6.4(6)	8.8(6)
C29	27.3(8)	33.0(8)	27.6(7)	9.9(6)	13.7(6)	12.6(6)
C30	19.8(7)	30.6(8)	34.9(8)	11.8(7)	10.6(6)	4.2(6)

C31	17.7(6)	18.5(6)	24.3(7)	5.3(5)	3.9(5)	2.0(5)
C32	23.7(7)	15.0(6)	15.9(6)	8.4(5)	5.8(5)	6.4(5)
C33	24.7(7)	16.7(6)	27.7(7)	13.4(5)	6.0(5)	2.9(5)
C34	26.2(7)	10.9(6)	27.7(7)	7.3(5)	1.1(6)	-0.1(5)
C35	19.3(6)	13.0(6)	18.6(6)	4.5(5)	2.4(5)	-0.8(5)
C36	14.9(6)	10.4(5)	12.9(5)	5.3(4)	0.5(4)	1.4(4)
C37	13.1(6)	13.8(6)	14.0(5)	4.2(4)	-0.6(4)	1.9(4)
C38	18.6(6)	23.8(7)	24.8(7)	12.6(6)	4.9(5)	4.2(5)
C39	21.4(7)	38.8(9)	31.8(8)	16.4(7)	11.5(6)	8.4(6)
C40	23.2(8)	35.1(9)	35.0(8)	10.9(7)	9.6(6)	15.0(7)
C41	26.2(8)	23.9(7)	34.8(8)	12.3(6)	5.9(6)	11.9(6)
C42	19.7(6)	18.6(6)	23.1(6)	9.5(5)	3.6(5)	5.1(5)
C43	15.7(6)	19.7(6)	19.5(6)	10.7(5)	6.9(5)	4.2(5)
C44	27.4(7)	21.4(7)	26.1(7)	12.7(6)	12.4(6)	2.0(6)
C45	25.3(7)	21.8(7)	16.5(6)	7.8(5)	9.0(5)	4.0(5)
C46	19.8(6)	18.9(6)	13.6(5)	4.7(5)	4.5(5)	4.0(5)
C47	37.4(8)	20.1(7)	16.2(6)	2.1(5)	10.9(6)	0.3(6)
Cl1	22.68(17)	38.4(2)	19.89(15)	7.25(14)	7.14(13)	0.41(15)
Cl2	21.17(18)	47.0(2)	31.06(19)	12.22(17)	4.43(14)	-1.03(16)
C48	20.8(8)	97.3(18)	24.6(8)	-9.3(10)	6.4(7)	-9.1(10)
Cl3	61.7(3)	48.0(3)	36.4(2)	15.7(2)	11.8(2)	34.5(2)
Cl4	65.3(3)	37.8(2)	45.3(2)	30.3(2)	22.3(2)	14.0(2)
C49	48.1(10)	35.5(9)	39.2(9)	24.9(8)	19.0(8)	22.5(8)
Cl5	53.7(3)	48.0(3)	38.6(2)	10.4(2)	2.7(2)	0.2(2)
Cl6	57.1(11)	30.6(9)	42.7(7)	9.6(4)	5.3(7)	18.3(8)
Cl6A	128(4)	99(4)	64.9(16)	2(2)	32(2)	77(3)
C50	33.0(9)	33.8(10)	53.0(11)	8.0(8)	13.2(8)	9.4(8)

Table A3.41. Bond Lengths for [Rh(acac)TPSB BDP 1].

Atom	Atom	Length/Å	Atom	Atom	Length/Å
Rh1	P1	2.1470(6)	C14	C15	1.3972(19)
Rh1	P2	2.1469(5)	C15	C16	1.380(2)
Rh1	O5	2.0635(10)	C16	C17	1.388(2)
Rh1	O6	2.0562(10)	C17	C18	1.390(2)
P1	C7	1.8707(13)	C19	C20	1.3964(17)
P1	C12	1.8631(14)	C19	C24	1.3994(18)
P1	C19	1.8259(13)	C20	C21	1.3906(18)
P2	C24	1.8238(13)	C21	C22	1.392(2)
P2	C25	1.8762(13)	C22	C23	1.3891(18)
P2	C36	1.8686(14)	C23	C24	1.3957(17)

O1	C8	1.2209(18)	C25	C26	1.5153(17)
O2	C11	1.2180(18)	C26	C27	1.3914(18)
O3	C35	1.2195(17)	C26	C31	1.3934(19)
O4	C32	1.2227(17)	C27	C28	1.3953(19)
O5	C43	1.2680(16)	C28	C29	1.387(2)
O6	C46	1.2743(16)	C29	C30	1.383(2)
N1	N2	1.4258(15)	C30	C31	1.393(2)
N1	C7	1.4548(16)	C32	C33	1.506(2)
N1	C8	1.3579(17)	C33	C34	1.532(2)
N2	C11	1.3808(17)	C34	C35	1.5029(19)
N2	C12	1.4645(16)	C36	C37	1.5148(18)
N3	N4	1.4255(15)	C37	C38	1.3901(18)
N3	C35	1.3765(17)	C37	C42	1.3956(18)
N3	C36	1.4592(16)	C38	C39	1.392(2)
N4	C25	1.4530(16)	C39	C40	1.386(2)
N4	C32	1.3652(16)	C40	C41	1.384(2)
C1	C2	1.3881(19)	C41	C42	1.388(2)
C1	C6	1.3961(18)	C43	C44	1.5099(18)
C1	C7	1.5136(17)	C43	C45	1.403(2)
C2	C3	1.3914(19)	C45	C46	1.3938(19)
C3	C4	1.385(2)	C46	C47	1.5080(19)
C4	C5	1.386(2)	Cl1	C48	1.7627(19)
C5	C6	1.391(2)	Cl2	C48	1.7565(19)
C8	C9	1.5047(19)	Cl3	C49	1.7725(19)
C9	C10	1.524(2)	Cl4	C49	1.768(2)
C10	C11	1.501(2)	Cl5	C50	1.761(2)
C12	C13	1.5143(17)	Cl6	C50	1.717(3)
C13	C14	1.3858(19)	Cl6A	C50	1.730(5)
C13	C18	1.3984(19)			

Table A3.42. Bond Angles for [Rh(acac)TPSB BDP 1].

Atom	Atom	Atom	Angle/°	Atom	Atom	Atom	Angle/°
P2	Rh1	P1	85.09(3)	C13	C14	C15	120.37(14)
O5	Rh1	P1	92.66(4)	C16	C15	C14	120.34(14)
O5	Rh1	P2	174.56(3)	C15	C16	C17	119.61(14)
O6	Rh1	P1	173.49(3)	C16	C17	C18	120.36(15)
O6	Rh1	P2	92.14(4)	C17	C18	C13	120.20(14)
O6	Rh1	O5	90.60(4)	C20	C19	P1	126.12(10)
C7	P1	Rh1	120.43(4)	C20	C19	C24	119.90(11)
C12	P1	Rh1	119.43(4)	C24	C19	P1	113.93(9)

C12	P1	C7	90.89(6)	C21	C20	C19	119.59(12)
C19	P1	Rh1	113.19(5)	C20	C21	C22	120.53(12)
C19	P1	C7	102.71(6)	C23	C22	C21	120.12(12)
C19	P1	C12	107.04(6)	C22	C23	C24	119.78(12)
C24	P2	Rh1	112.95(5)	C19	C24	P2	114.68(9)
C24	P2	C25	103.37(6)	C23	C24	P2	125.22(10)
C24	P2	C36	106.29(6)	C23	C24	C19	120.09(11)
C25	P2	Rh1	121.31(4)	N4	C25	P2	104.00(8)
C36	P2	Rh1	118.29(4)	N4	C25	C26	114.87(10)
C36	P2	C25	91.70(6)	C26	C25	P2	113.42(8)
C43	O5	Rh1	125.09(9)	C27	C26	C25	122.20(12)
C46	O6	Rh1	125.02(9)	C27	C26	C31	119.38(12)
N2	N1	C7	114.61(10)	C31	C26	C25	118.42(12)
C8	N1	N2	120.29(11)	C26	C27	C28	120.00(13)
C8	N1	C7	124.54(11)	C29	C28	C27	120.38(14)
N1	N2	C12	113.35(10)	C30	C29	C28	119.68(14)
C11	N2	N1	118.05(11)	C29	C30	C31	120.31(14)
C11	N2	C12	121.97(11)	C30	C31	C26	120.25(14)
N4	N3	C36	114.31(10)	O4	C32	N4	120.31(12)
C35	N3	N4	120.48(11)	O4	C32	C33	126.17(12)
C35	N3	C36	120.88(10)	N4	C32	C33	113.46(12)
N3	N4	C25	115.04(10)	C32	C33	C34	108.92(11)
C32	N4	N3	120.80(11)	C35	C34	C33	111.33(11)
C32	N4	C25	123.23(11)	O3	C35	N3	120.19(12)
C2	C1	C6	119.05(12)	O3	C35	C34	125.29(12)
C2	C1	C7	122.43(11)	N3	C35	C34	114.39(12)
C6	C1	C7	118.44(12)	N3	C36	P2	106.94(8)
C1	C2	C3	120.51(13)	N3	C36	C37	114.66(10)
C4	C3	C2	120.19(13)	C37	C36	P2	112.16(9)
C3	C4	C5	119.72(13)	C38	C37	C36	122.91(12)
C4	C5	C6	120.19(13)	C38	C37	C42	119.11(12)
C5	C6	C1	120.32(13)	C42	C37	C36	117.95(11)
N1	C7	P1	102.81(8)	C37	C38	C39	120.05(14)
N1	C7	C1	114.60(10)	C40	C39	C38	120.45(14)
C1	C7	P1	111.55(8)	C41	C40	C39	119.75(14)
O1	C8	N1	120.98(12)	C40	C41	C42	120.04(14)
O1	C8	C9	126.11(12)	C41	C42	C37	120.60(13)
N1	C8	C9	112.75(12)	O5	C43	C44	115.98(12)
C8	C9	C10	107.25(11)	O5	C43	C45	126.02(12)
C11	C10	C9	110.52(11)	C45	C43	C44	117.99(12)
O2	C11	N2	120.50(13)	C46	C45	C43	126.97(12)

O2	C11	C10	125.59(12)	O6	C46	C45	126.26(12)
N2	C11	C10	113.71(12)	O6	C46	C47	114.76(12)
N2	C12	P1	106.78(8)	C45	C46	C47	118.98(12)
N2	C12	C13	114.69(10)	Cl2	C48	Cl1	112.61(10)
C13	C12	P1	112.26(9)	Cl4	C49	Cl3	111.99(9)
C14	C13	C12	122.77(12)	Cl6	C50	Cl5	115.96(13)
C14	C13	C18	119.11(12)	Cl6A	C50	Cl5	108.6(4)
C18	C13	C12	118.12(12)				

Table A3.43. Torsion Angles for [Rh(acac)TPSB BDP 1].

A	B	C	D	Angle/°	A	B	C	D	Angle/°
Rh1	P1	C7	N1	-155.12(6)	C9	C10	C11	O2	-148.94(13)
Rh1	P1	C7	C1	-31.84(10)	C9	C10	C11	N2	25.82(15)
Rh1	P1	C12	N2	145.61(6)	C11	N2	C12	P1	-154.01(10)
Rh1	P1	C12	C13	-87.88(9)	C11	N2	C12	C13	80.95(14)
Rh1	P1	C19	C20	178.04(10)	C12	P1	C7	N1	-29.73(8)
Rh1	P1	C19	C24	-4.57(10)	C12	P1	C7	C1	93.55(9)
Rh1	P2	C24	C19	-1.32(10)	C12	P1	C19	C20	44.38(13)
Rh1	P2	C24	C23	179.49(9)	C12	P1	C19	C24	-138.23(9)
Rh1	P2	C25	N4	-148.84(6)	C12	N2	C11	O2	-11.07(18)
Rh1	P2	C25	C26	-23.36(10)	C12	N2	C11	C10	173.88(11)
Rh1	P2	C36	N3	140.86(7)	C12	C13	C14	C15	179.77(13)
Rh1	P2	C36	C37	-92.62(9)	C12	C13	C18	C17	-178.82(13)
Rh1	O5	C43	C44	179.56(9)	C13	C14	C15	C16	-1.1(2)
Rh1	O5	C43	C45	-0.92(19)	C14	C13	C18	C17	0.3(2)
Rh1	O6	C46	C45	-0.4(2)	C14	C15	C16	C17	0.5(2)
Rh1	O6	C46	C47	-179.89(9)	C15	C16	C17	C18	0.5(2)
P1	C12	C13	C14	-115.06(12)	C16	C17	C18	C13	-0.9(2)
P1	C12	C13	C18	64.05(14)	C18	C13	C14	C15	0.7(2)
P1	C19	C20	C21	177.05(10)	C19	P1	C7	N1	77.96(9)
P1	C19	C24	P2	3.58(12)	C19	P1	C7	C1	-158.76(9)
P1	C19	C24	C23	-177.18(9)	C19	P1	C12	N2	-84.16(9)
P2	C25	C26	C27	-101.83(13)	C19	P1	C12	C13	42.35(10)
P2	C25	C26	C31	77.34(13)	C19	C20	C21	C22	0.2(2)
P2	C36	C37	C38	-113.35(13)	C20	C19	C24	P2	-178.85(10)
P2	C36	C37	C42	64.69(13)	C20	C19	C24	C23	0.39(18)
O1	C8	C9	C10	-128.18(15)	C20	C21	C22	C23	-0.4(2)
O4	C32	C33	C34	-131.61(14)	C21	C22	C23	C24	0.6(2)
O5	C43	C45	C46	-0.8(2)	C22	C23	C24	P2	178.56(10)
N1	N2	C11	O2	-160.61(11)	C22	C23	C24	C19	-0.59(19)

N1	N2	C11	C10	24.33(15)	C24	P2	C25	N4	83.32(9)
N1	N2	C12	P1	-3.17(12)	C24	P2	C25	C26	-151.21(9)
N1	N2	C12	C13	-128.21(11)	C24	P2	C36	N3	-90.93(9)
N1	C8	C9	C10	47.22(15)	C24	P2	C36	C37	35.59(10)
N2	N1	C7	P1	34.74(11)	C24	C19	C20	C21	-0.20(19)
N2	N1	C7	C1	-86.48(13)	C25	P2	C24	C19	131.57(9)
N2	N1	C8	O1	177.31(12)	C25	P2	C24	C23	-47.62(12)
N2	N1	C8	C9	1.64(17)	C25	P2	C36	N3	13.53(9)
N2	C12	C13	C14	7.05(17)	C25	P2	C36	C37	140.05(9)
N2	C12	C13	C18	-173.84(11)	C25	N4	C32	O4	6.84(19)
N3	N4	C25	P2	29.99(12)	C25	N4	C32	C33	-170.44(11)
N3	N4	C25	C26	-94.56(13)	C25	C26	C27	C28	179.58(12)
N3	N4	C32	O4	175.27(11)	C25	C26	C31	C30	-179.10(13)
N3	N4	C32	C33	-2.02(17)	C26	C27	C28	C29	-0.7(2)
N3	C36	C37	C38	8.88(17)	C27	C26	C31	C30	0.1(2)
N3	C36	C37	C42	-173.08(11)	C27	C28	C29	C30	0.4(2)
N4	N3	C35	O3	-164.52(12)	C28	C29	C30	C31	0.1(2)
N4	N3	C35	C34	19.43(17)	C29	C30	C31	C26	-0.4(2)
N4	N3	C36	P2	1.09(12)	C31	C26	C27	C28	0.4(2)
N4	N3	C36	C37	-123.93(11)	C32	N4	C25	P2	-160.98(10)
N4	C25	C26	C27	17.61(17)	C32	N4	C25	C26	74.48(15)
N4	C25	C26	C31	-163.23(11)	C32	C33	C34	C35	-57.64(16)
N4	C32	C33	C34	45.49(15)	C33	C34	C35	O3	-150.24(14)
C1	C2	C3	C4	-1.1(2)	C33	C34	C35	N3	25.58(17)
C2	C1	C6	C5	0.9(2)	C35	N3	N4	C25	135.26(12)
C2	C1	C7	P1	-86.74(13)	C35	N3	N4	C32	-34.07(17)
C2	C1	C7	N1	29.56(17)	C35	N3	C36	P2	-155.63(10)
C2	C3	C4	C5	1.6(2)	C35	N3	C36	C37	79.36(15)
C3	C4	C5	C6	-0.8(2)	C36	P2	C24	C19	-132.61(9)
C4	C5	C6	C1	-0.4(2)	C36	P2	C24	C23	48.20(12)
C6	C1	C2	C3	-0.1(2)	C36	P2	C25	N4	-23.87(8)
C6	C1	C7	P1	89.96(13)	C36	P2	C25	C26	101.61(10)
C6	C1	C7	N1	-153.74(12)	C36	N3	N4	C25	-21.57(14)
C7	P1	C12	N2	19.43(8)	C36	N3	N4	C32	169.11(11)
C7	P1	C12	C13	145.94(9)	C36	N3	C35	O3	-9.23(19)
C7	P1	C19	C20	-50.55(12)	C36	N3	C35	C34	174.72(11)
C7	P1	C19	C24	126.85(9)	C36	C37	C38	C39	177.30(13)
C7	N1	N2	C11	130.19(12)	C36	C37	C42	C41	-176.88(13)
C7	N1	N2	C12	-21.88(14)	C37	C38	C39	C40	-0.3(2)
C7	N1	C8	O1	6.4(2)	C38	C37	C42	C41	1.2(2)
C7	N1	C8	C9	-169.29(12)	C38	C39	C40	C41	0.7(3)

C7	C1	C2	C3	176.53(12)	C39	C40	C41	C42	-0.2(3)
C7	C1	C6	C5	-175.94(13)	C40	C41	C42	C37	-0.8(2)
C8	N1	N2	C11	-41.59(16)	C42	C37	C38	C39	-0.7(2)
C8	N1	N2	C12	166.33(11)	C43	C45	C46	O6	1.6(2)
C8	N1	C7	P1	-153.87(11)	C43	C45	C46	C47	-178.94(14)
C8	N1	C7	C1	84.91(15)	C44	C43	C45	C46	178.68(14)
C8	C9	C10	C11	-61.47(14)					

Table A3.44. Hydrogen Atom Coordinates ($\text{\AA} \times 10^4$) and Isotropic Displacement Parameters ($\text{\AA}^2 \times 10^3$) for [Rh(acac)TPSB BDP 1].

Atom	<i>x</i>	<i>y</i>	<i>z</i>	U(eq)
H2	7987	8405	7363	23
H3	7838	8617	6092	25
H4	6360	7611	4953	26
H5	4983	6453	5108	31
H6	5107	6265	6387	25
H7	5889	6904	7862	15
H9A	7964	9548	10143	28
H9B	7293	10403	9907	28
H10A	8224	10177	8784	27
H10B	9119	10598	9663	27
H12	9188	7055	7902	16
H14	9521	7851	10034	24
H15	10743	7258	10892	34
H16	11487	5688	10302	36
H17	11031	4718	8845	33
H18	9854	5329	7980	25
H20	7243	6975	9578	20
H21	6535	6223	10425	22
H22	5910	4368	9913	21
H23	5963	3254	8538	18
H25	7951	2779	7824	16
H27	7069	769	5780	23
H28	8217	170	4824	31
H29	9983	1156	5068	34
H30	10612	2730	6279	34
H31	9485	3322	7249	26
H33A	5082	427	7553	26
H33B	5791	-541	7273	26
H34A	5584	-510	5917	27

H34B	4370	-675	6104	27
H36	5318	2641	5990	15
H38	3882	2342	7424	26
H39	2444	3271	7886	35
H40	2142	4816	7639	37
H41	3258	5419	6905	33
H42	4677	4483	6424	24
H44A	8459	6496	4862	35
H44B	9587	5993	4935	35
H44C	9328	6896	5749	35
H45	8245	4281	4247	25
H47A	7477	1819	4239	39
H47B	7732	2450	3666	39
H47C	6492	2265	3802	39
H48A	1599	8301	8511	70
H48B	1918	7293	8719	70
H49A	4975	1376	10121	43
H49B	5142	421	9297	43
H50A	10106	9229	3100	50
H50B	10649	9582	2462	50
H50C	10259	9191	3053	50
H50D	10563	9749	2440	50

Table A3.45. Atomic Occupancy for [Rh(acac)TPSB BDP 1]

Atom	Occupancy	Atom	Occupancy	Atom	Occupancy
Cl6	0.613(19)	Cl6A	0.387(19)	H50A	0.613(19)
H50B	0.613(19)	H50C	0.387(19)	H50D	0.387(19)

A3.3 NMR Spectra from Chapter 4

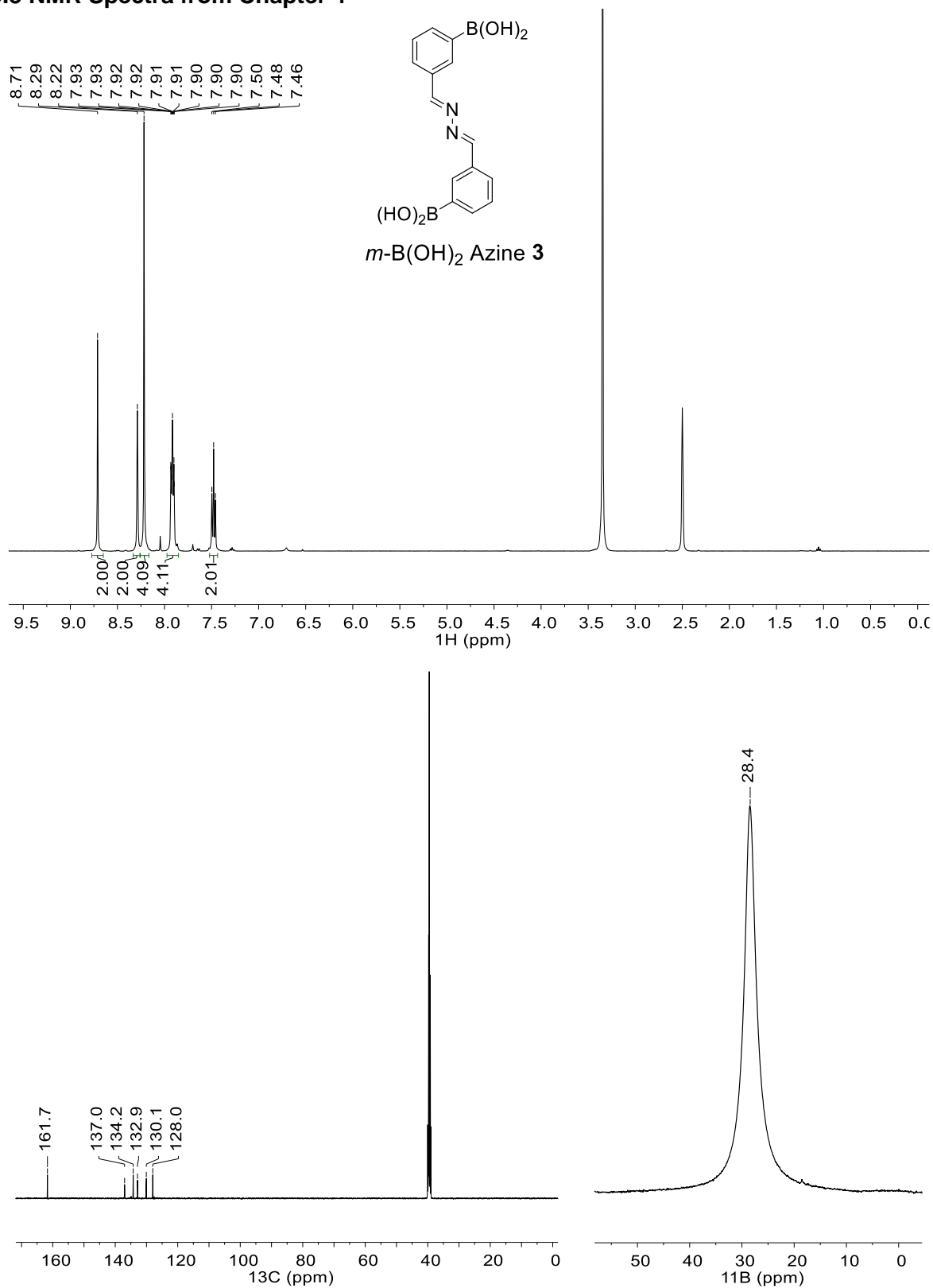


Figure A3.28. NMR spectra of *m*-B(OH)₂ Azine **3** (¹H, (top); ¹³C{¹H} and ¹¹B (bottom)).

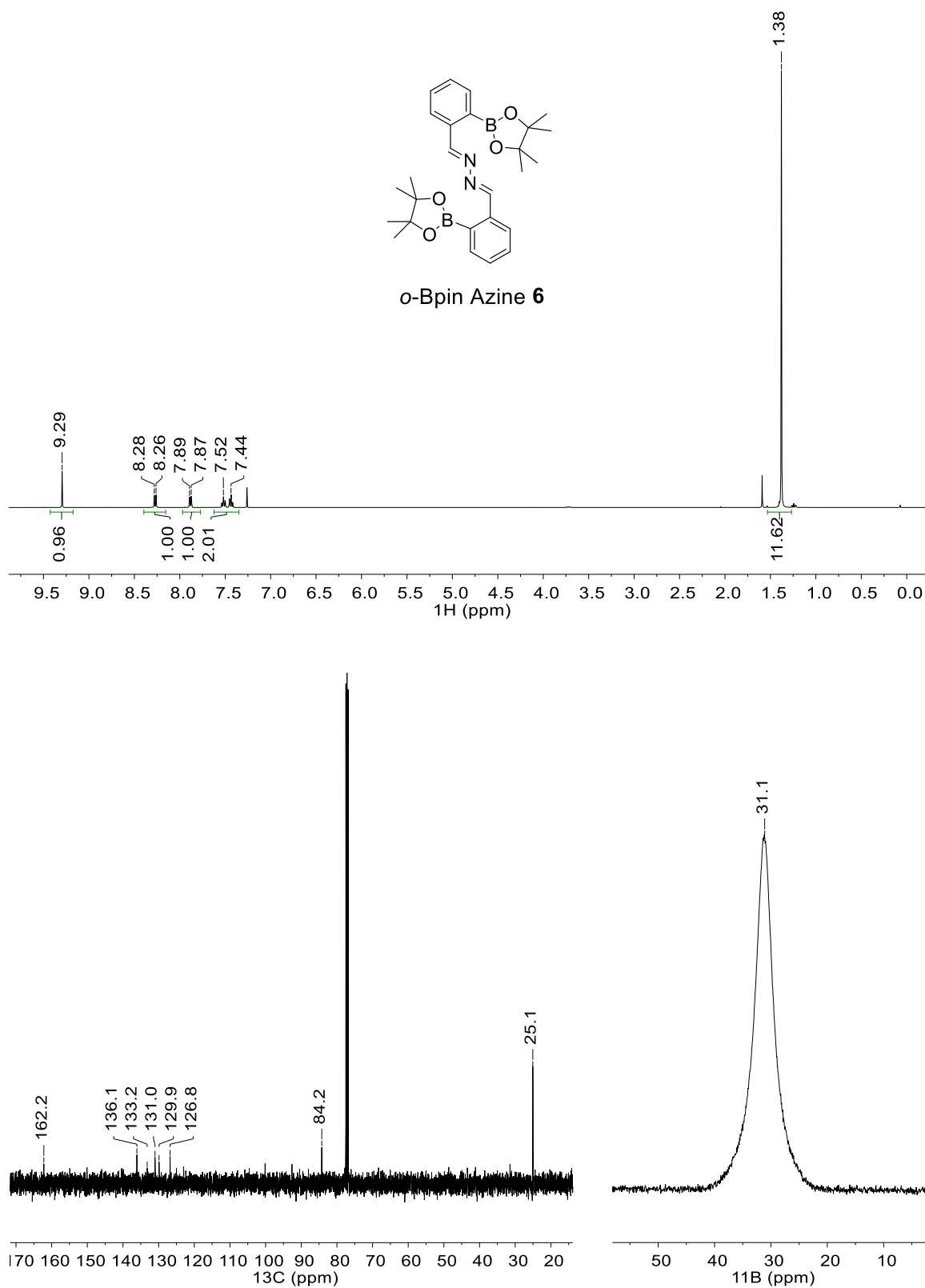


Figure A3.29. NMR spectra of o-Bpin Azine **6** (¹H, (top); ¹³C{¹H} and ¹¹B (bottom)).

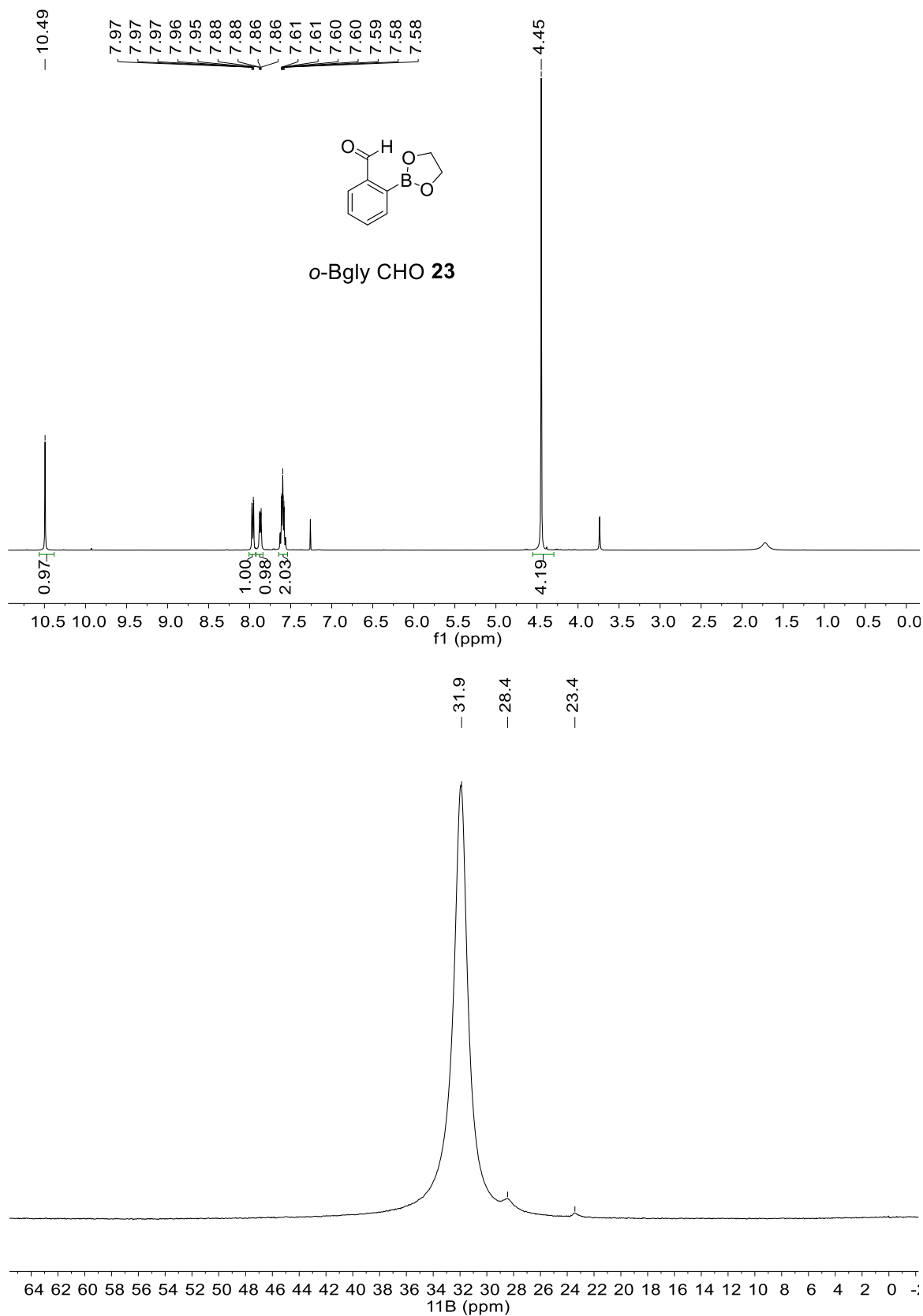


Figure A3.30. NMR spectra of *o*-Bgly CHO **23** (¹H, (top) and ¹¹B (bottom)).

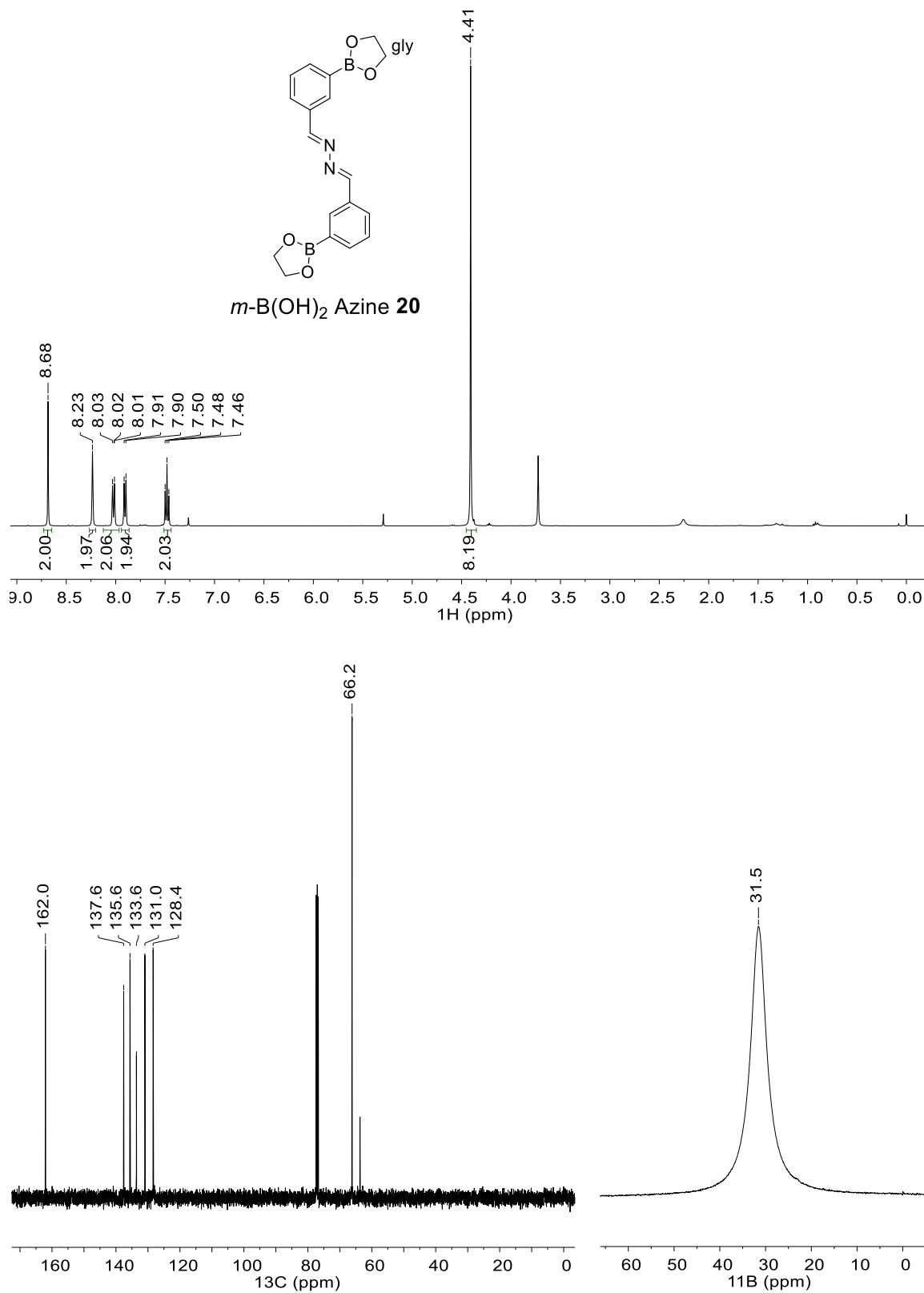


Figure A3.31. NMR spectra of *m*-Bpin Azine **20** (¹H, (top); ¹³C{¹H} and ¹¹B (bottom)).

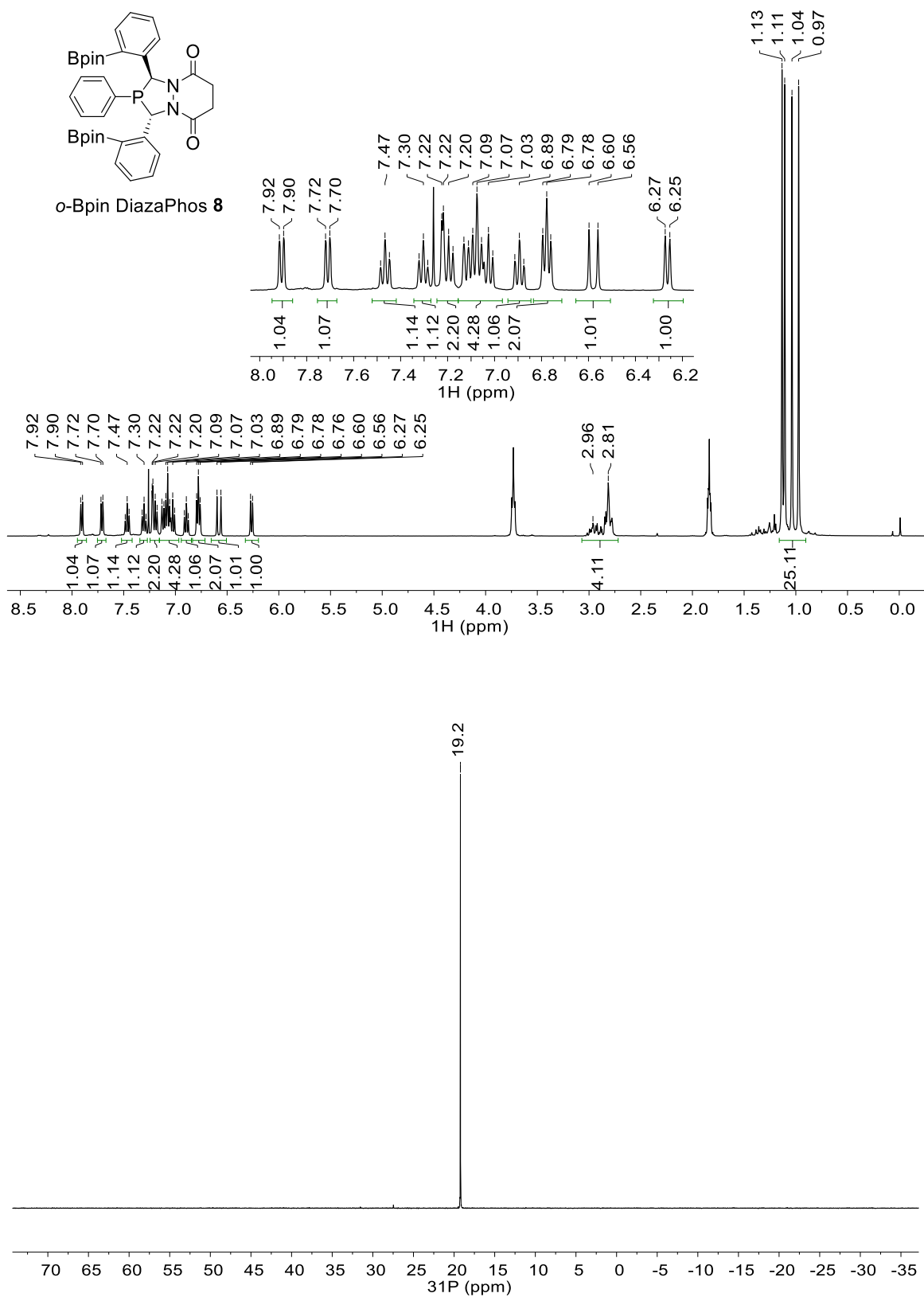


Figure A3.32. NMR spectra of *o*-Bpin DiazaPhos **8** (^1H , (top) and $^{31}\text{P}\{^1\text{H}\}$ (bottom)).

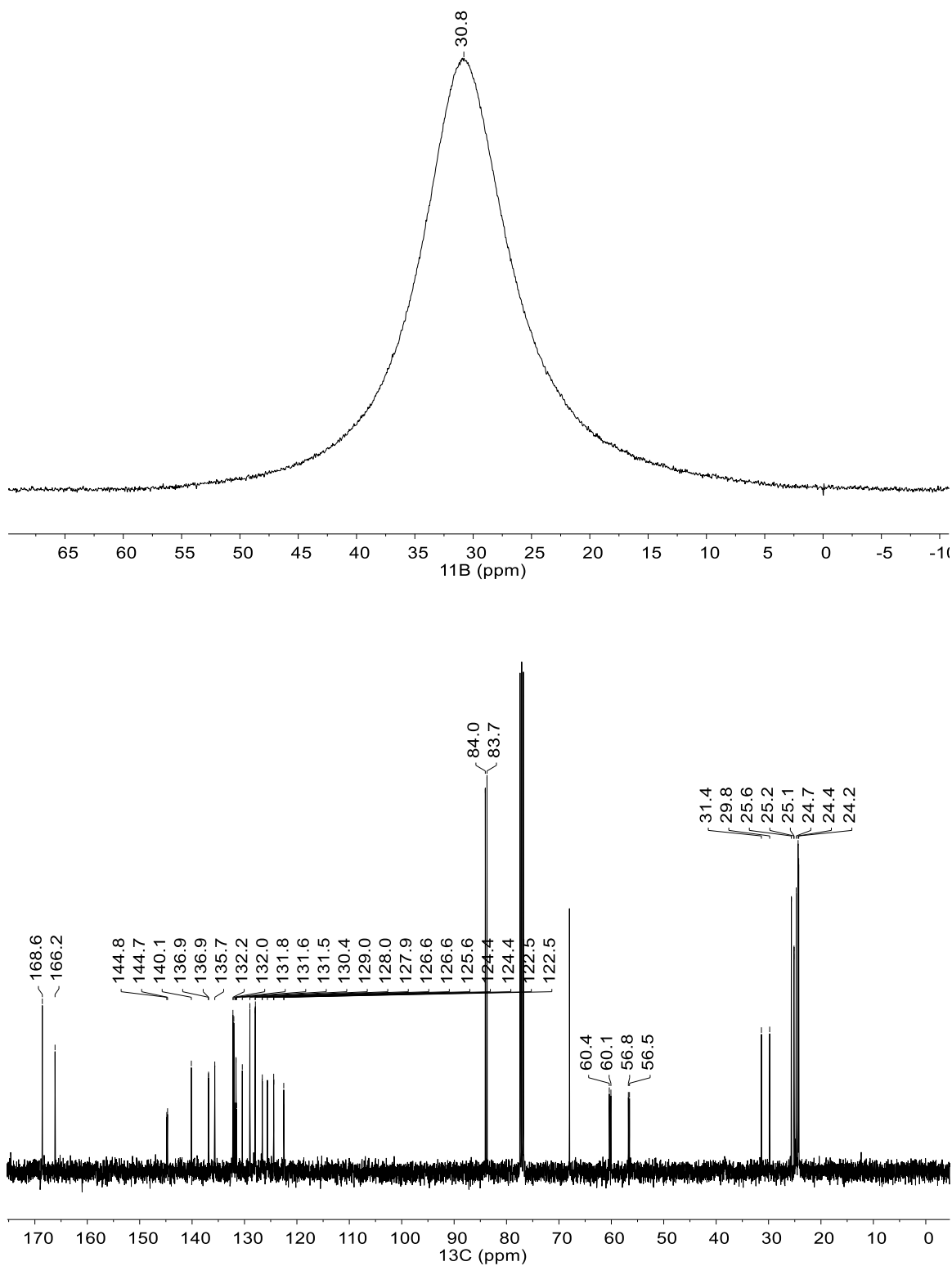


Figure A3.33. NMR spectra of *o*-Bpin DiazaPhos **8** (^{11}B , (top) and $^{13}\text{C}\{^1\text{H}\}$ (bottom)).

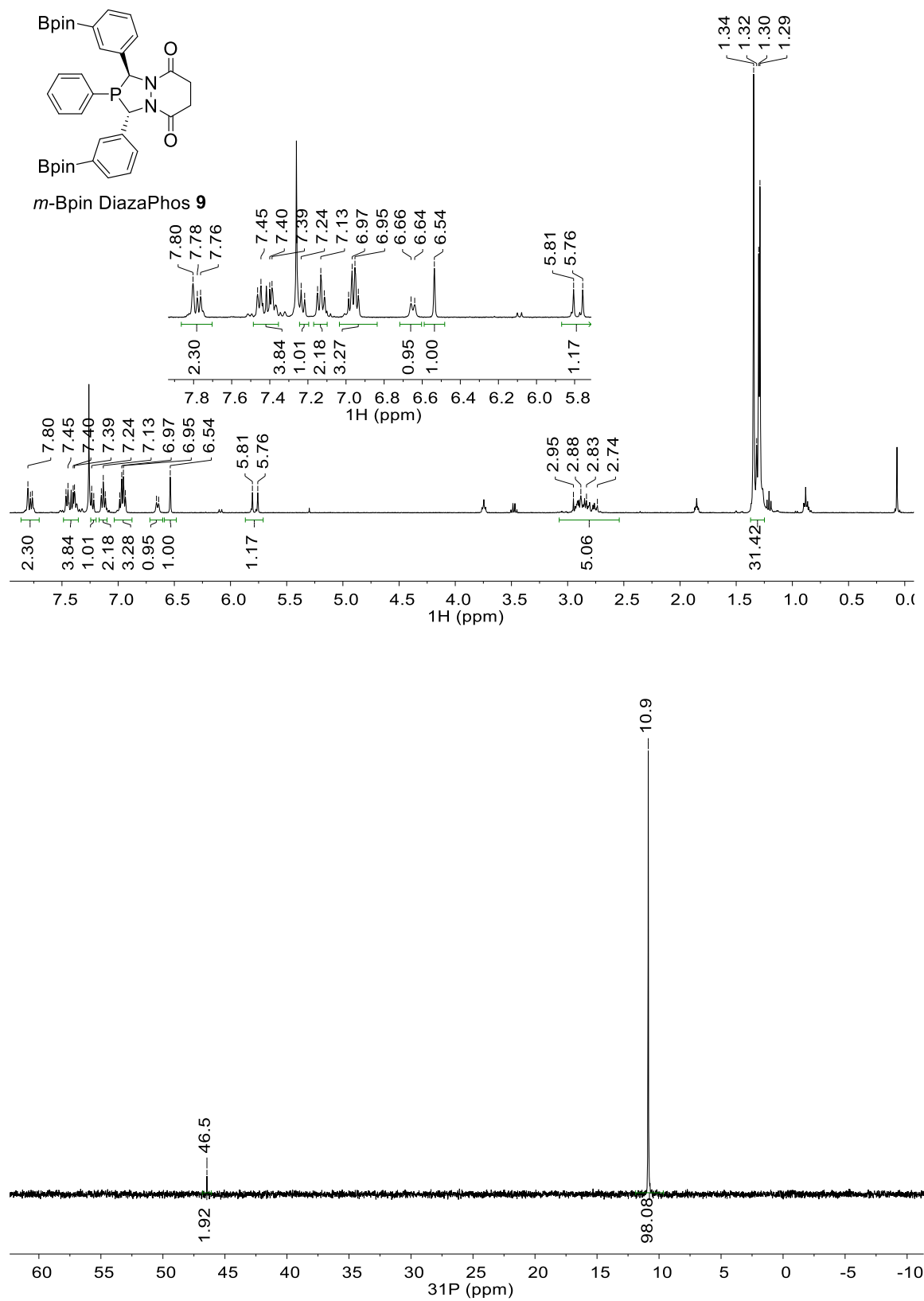


Figure A3.34. NMR spectra of *m*-Bpin DiaDiazaPhos **8** (¹H, (top) and ³¹P{¹H} (bottom)).

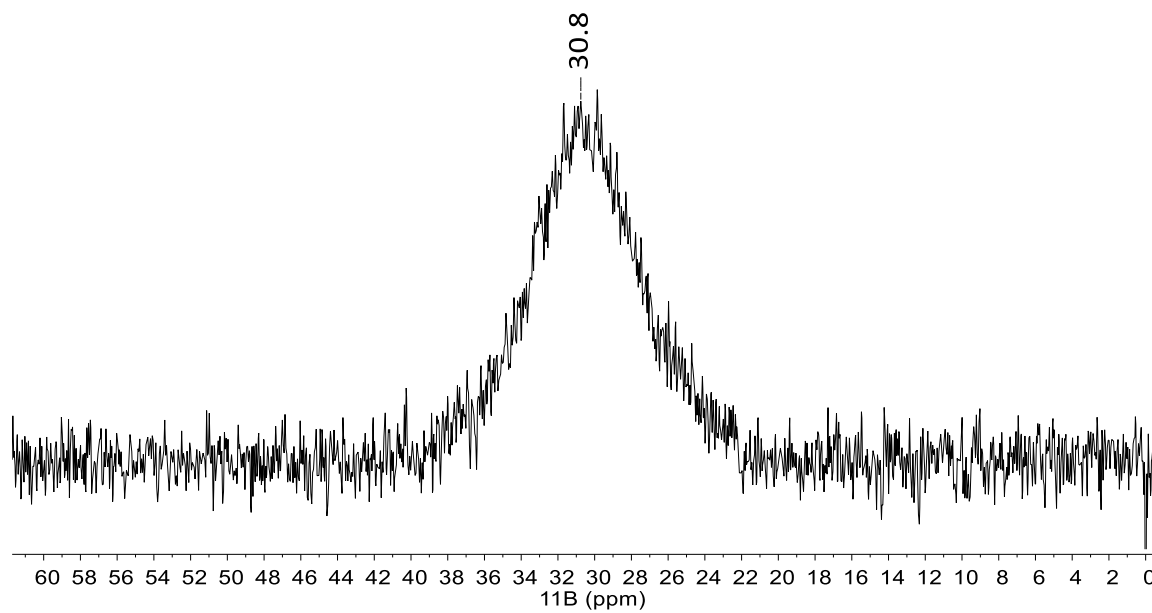


Figure A3.35. ^{11}B NMR spectrum of *m*-Bpin DiazaPhos **9**.

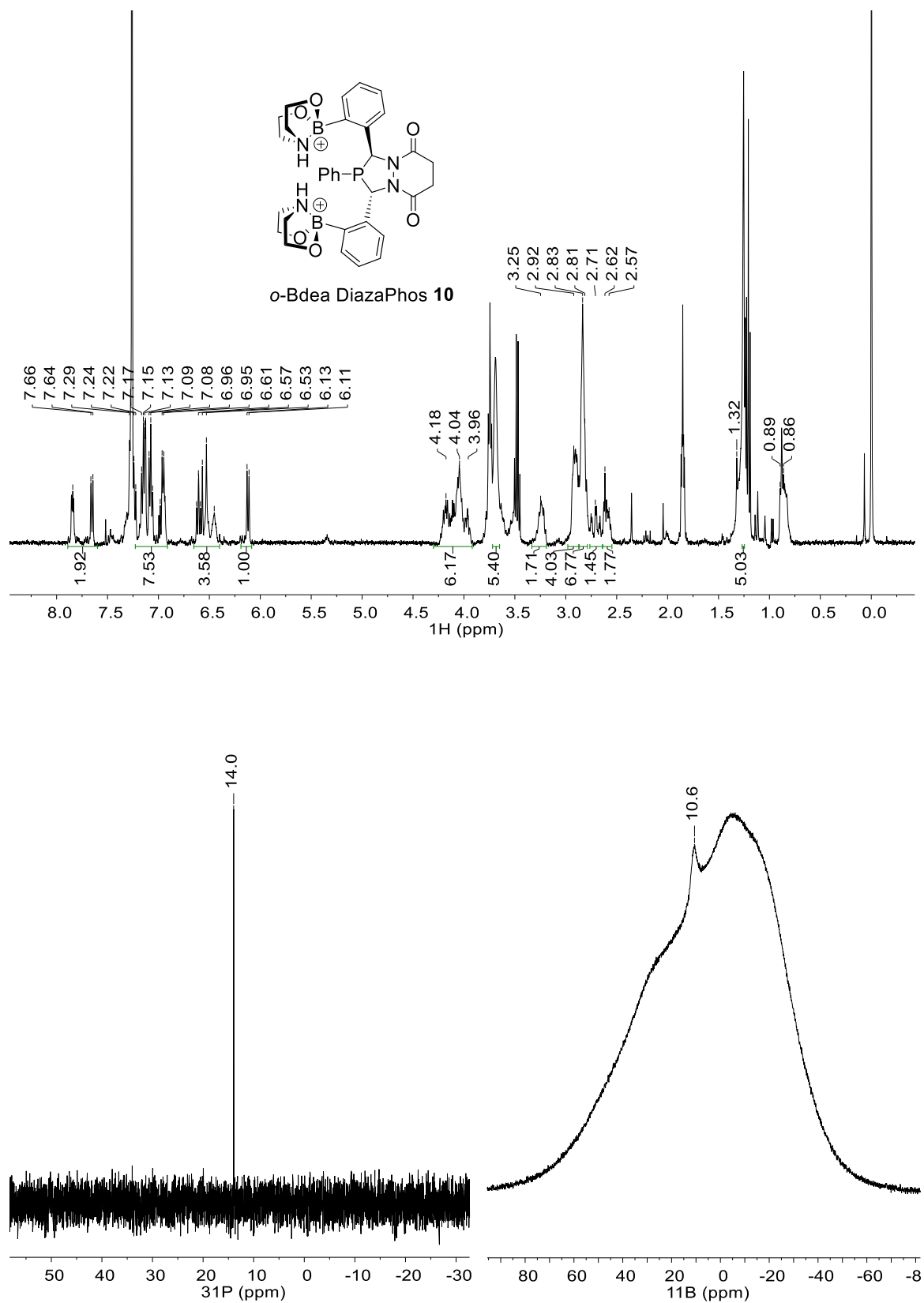


Figure A3.36. NMR spectra of o-Bdea Azine 10 (^1H , (top); $^{31}\text{P}\{^1\text{H}\}$ and ^{11}B (bottom)).

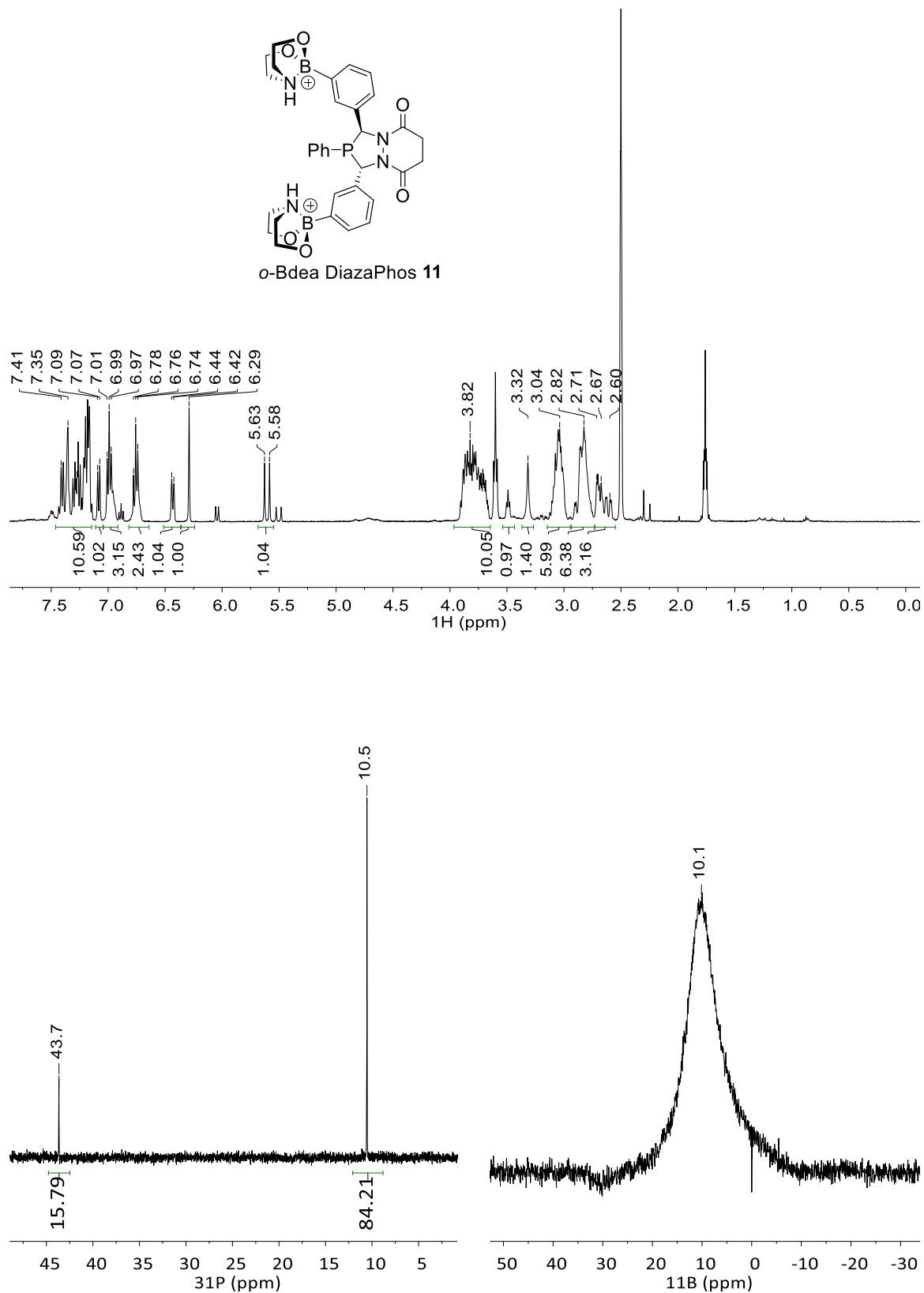


Figure A3.37. NMR spectra of *m*-Bdea Azine **11** (^1H , (top); $^{31}\text{P}\{^1\text{H}\}$ and ^{11}B (bottom)).

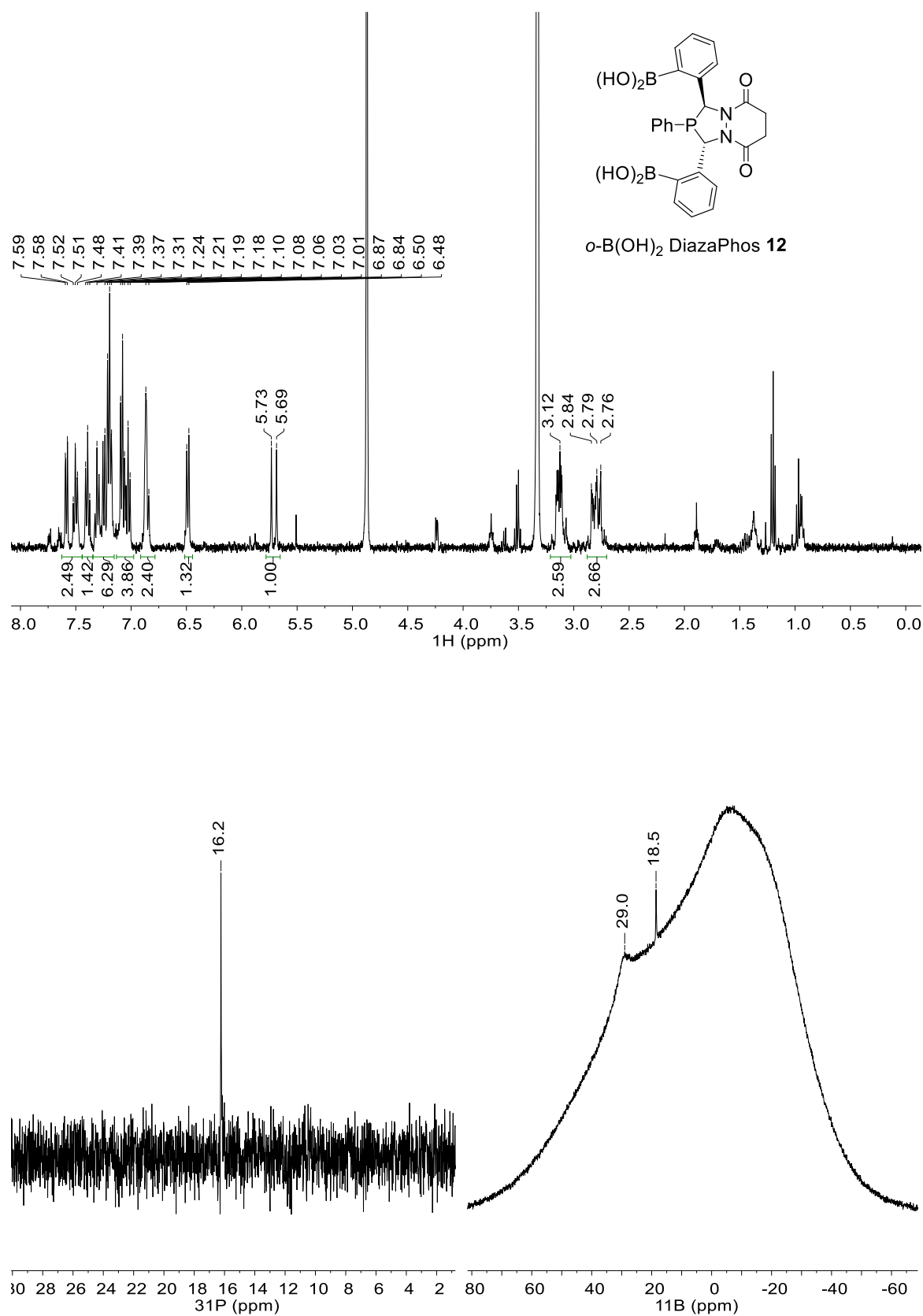


Figure A3.38. NMR spectra of *o*-B(OH)₂ DiazaPhos **12** (¹H, (top); ³¹P{¹H} and ¹¹B (bottom)).

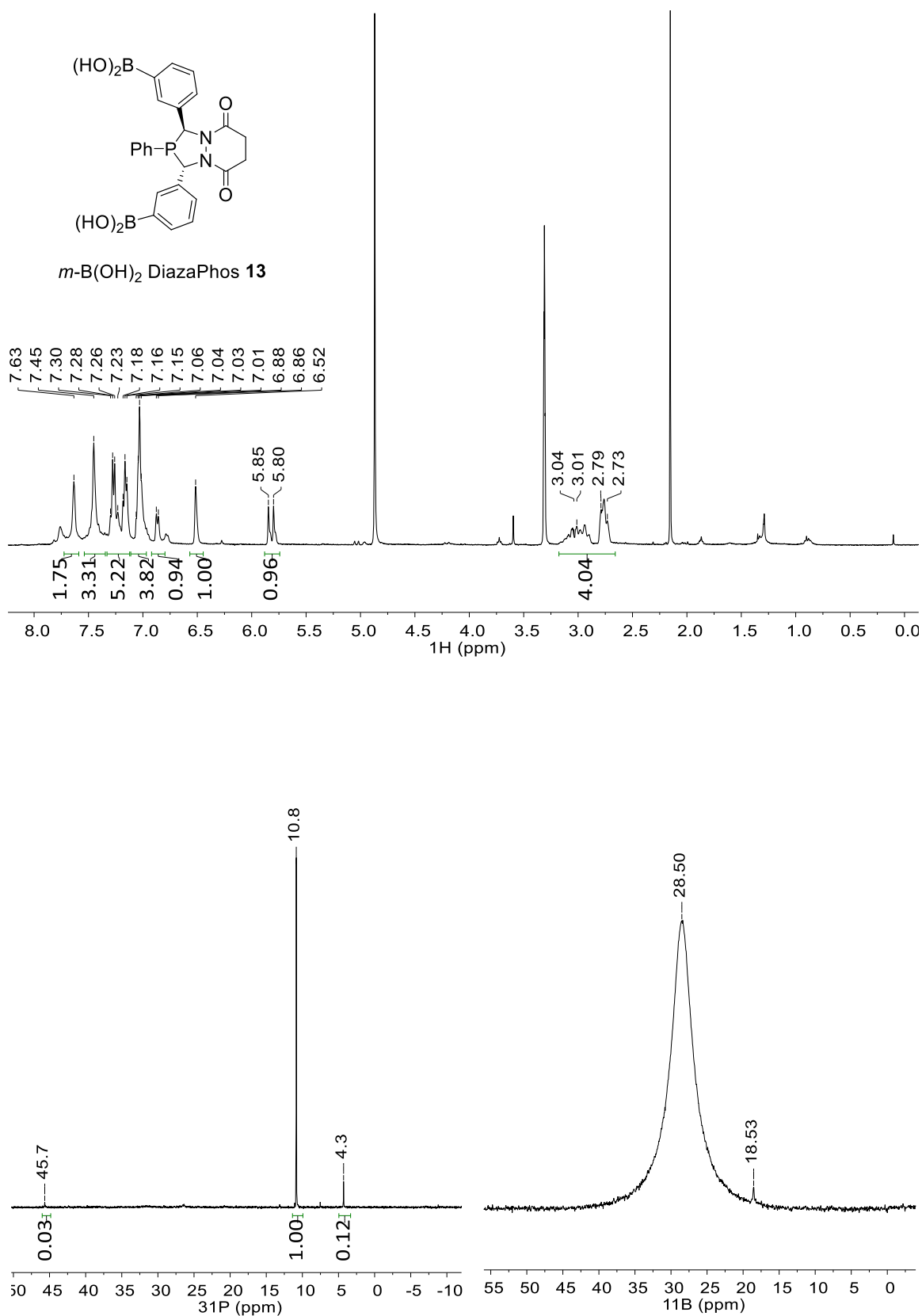


Figure A3.39. NMR spectra of *m*-B(OH)₂ DiazaPhos **13** (¹H, (top); ³¹P{¹H} and ¹¹B (bottom)).

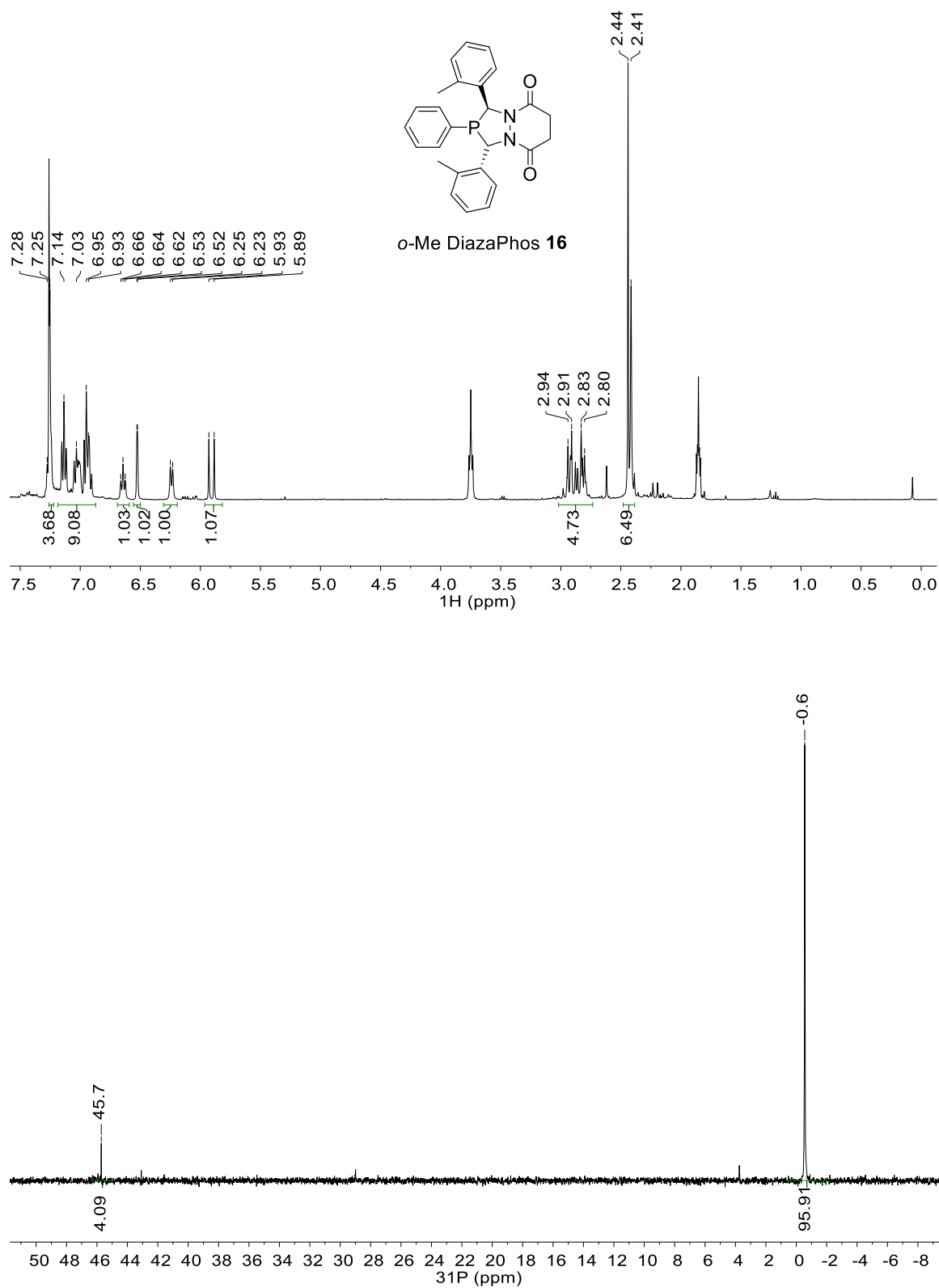


Figure A3.40. NMR spectra of o-Me DiazaPhos **16** (^1H , (top); $^{31}\text{P}\{^1\text{H}\}$ (bottom)).

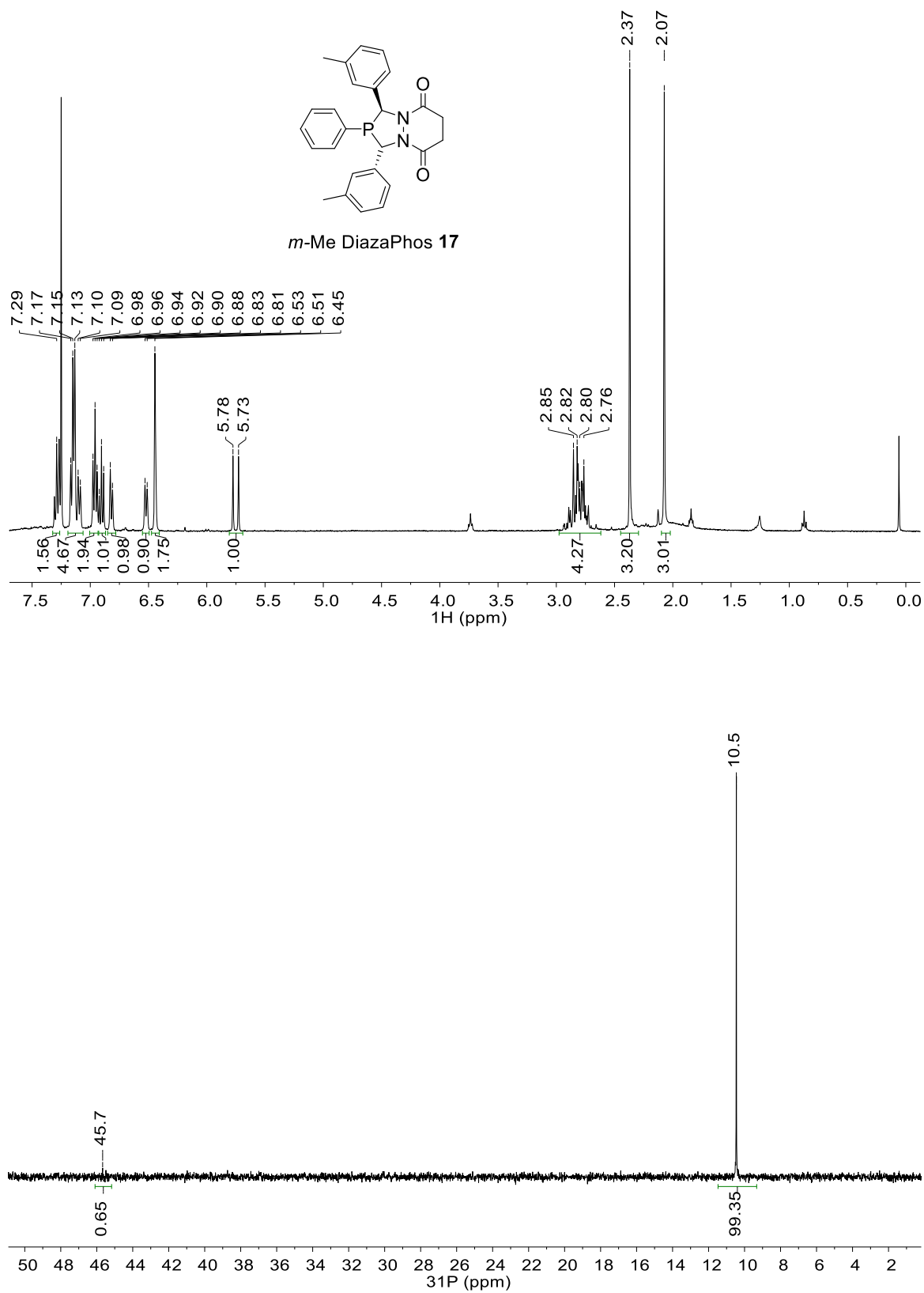


Figure A3.41. NMR spectra of *m*-Me DiazaPhos 17 (¹H, (top); ³¹P{¹H} (bottom)).

A3.4 Crystallographic Data from Chapter 4

A3.4.1 Crystallographic Data for Diazaborine 2

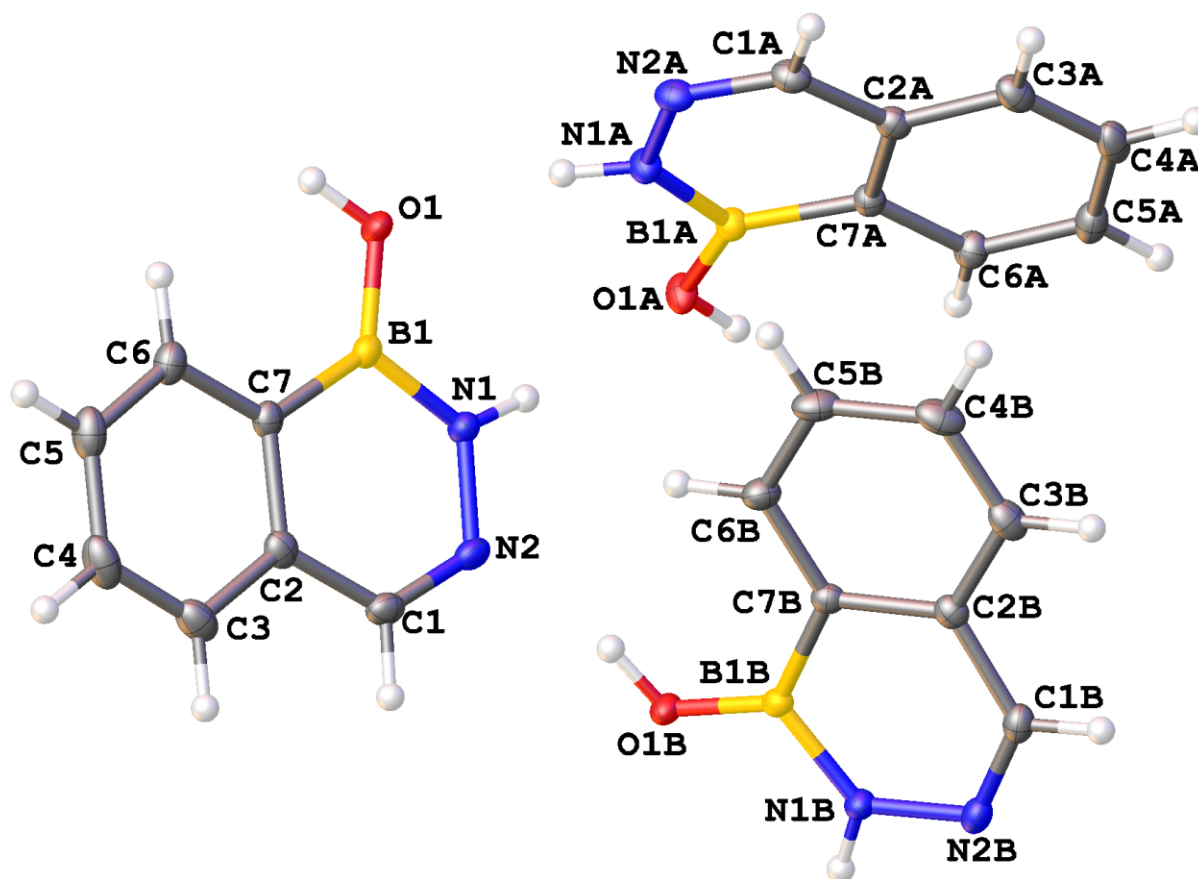


Figure A3.42. A molecular drawing of Diazaborine 2 shown with 50% probability ellipsoids.

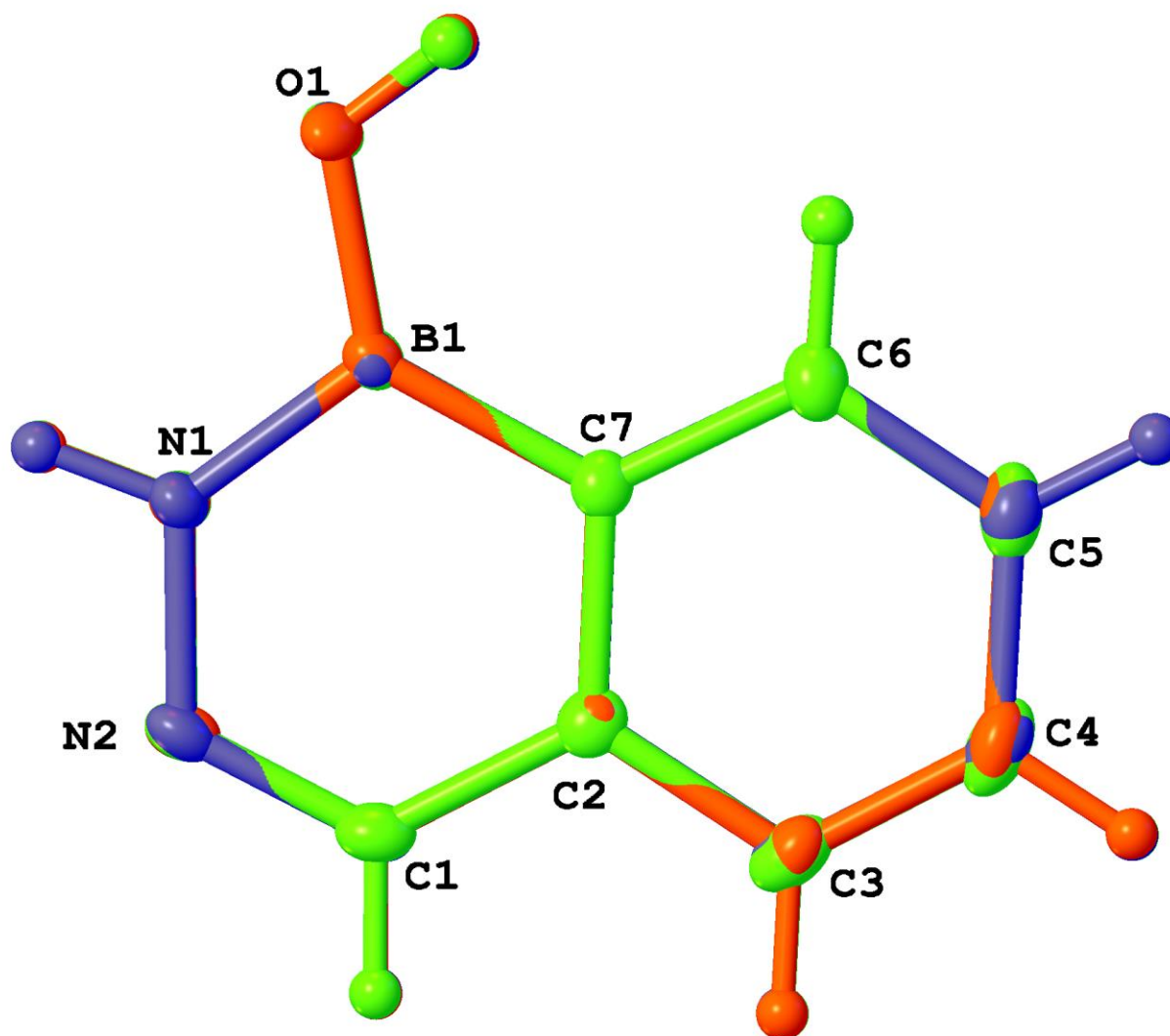


Figure A3.43. A molecular drawing of a superposition of the three symmetry-independent molecules of Diazaborine **2** shown with 50% probability ellipsoids. Each molecule is colored in one color, green, blue, or red.

Data Collection

A colorless crystal with approximate dimensions 0.25 x 0.20 x 0.20 mm³ was selected under oil under ambient conditions and attached to the tip of a MiTeGen MicroMount®. The crystal was mounted in a stream of cold nitrogen at 100(1) K and centered in the X-ray beam by using a video camera.

The crystal evaluation and data collection were performed on a Bruker Quazar SMART APEXII diffractometer with Mo K α ($\lambda = 0.71073$ Å) radiation and the diffractometer to crystal distance of 4.96 cm.

The initial cell constants were obtained from three series of ω scans at different starting angles. Each series consisted of 12 frames collected at intervals of 0.5° in a 6° range about ω with the exposure time of 10 seconds per frame. The reflections were successfully indexed by an automated indexing routine built in the APEXII program suite. The final cell constants were calculated from a set of 9981 strong reflections from the actual data collection.

The data were collected by using the full sphere data collection routine to survey the reciprocal space to the extent of a full sphere to a resolution of 0.70 Å. A total of 33740 data were harvested by collecting 5 sets of frames with 0.5° scans in ω and ϕ with exposure times of 30 sec per frame. These highly redundant datasets were corrected for Lorentz and polarization effects. The absorption correction was based on fitting a function to the empirical transmission surface as sampled by multiple equivalent measurements. [1]

Structure Solution and Refinement

The systematic absences in the diffraction data were uniquely consistent for the space group $P2_1/n$ that yielded chemically reasonable and computationally stable results of refinement [2-4].

A successful solution by the direct methods provided most non-hydrogen atoms from the E -map. The remaining non-hydrogen atoms were located in an alternating series of least-squares cycles and difference Fourier maps. All non-hydrogen atoms were refined with anisotropic displacement coefficients. All hydrogen atoms were included in the structure factor calculation at idealized positions and were allowed to ride on the neighboring atoms with relative isotropic displacement coefficients.

There are three symmetry-independent molecules of 1,2-dihydro-1-hydroxy-2,3,1-benzodiazaborine (Fig. 1) with essentially identical geometries (Fig.2) in the asymmetric unit. This crystal structure is a polymorph of another previously reported structure of 1,2-dihydro-1-hydroxy-2,3,1-benzodiazaborine determined at RT in which there is only one symmetry independent molecule. Structure Landis53 exhibits a different hydrogen-bonding pattern and does not undergo a phase change between 100-280 K.

The final least-squares refinement of 316 parameters against 5833 data resulted in residuals R (based on F^2 for $I \geq 2\sigma$) and wR (based on F^2 for all data) of 0.0404 and 0.1175, respectively. The final difference Fourier map was featureless.

Summary

Crystal data for $C_7H_7BN_2O$ ($M=145.96$ g/mol): monoclinic, space group $P2_1/n$ (no. 14), $a = 10.282(3)$ Å, $b = 19.686(5)$ Å, $c = 11.747(4)$ Å, $\beta = 115.314(12)^\circ$, $V = 2149.4(12)$ Å³, $Z = 12$, $T = 100$ K, $\mu(\text{MoK}\alpha) = 0.091$ mm⁻¹, $D_{\text{calc}} = 1.353$ g/cm³, 33740 reflections measured ($4.138^\circ \leq 2\theta \leq 58.494^\circ$), 5833 unique ($R_{\text{int}} = 0.0262$, $R_{\text{sigma}} = 0.0174$) which were used in all calculations. The final R_1 was 0.0404 ($I > 2\sigma(I)$) and wR_2 was 0.1175 (all data).

References

- [1] Bruker-AXS. (2007-2014) APEX2 (Ver. 2014.1-1), SADABS (2012-1), and SAINT+ (Ver. 8.32A) Software Reference Manuals. Bruker-AXS, Madison, Wisconsin, USA.
- [2] Sheldrick, G. M. (2008) SHELXL. *Acta Cryst.* **A64**, 112-122.
- [3] Dolomanov, O.V.; Bourhis, L.J.; Gildea, R.J.; Howard, J.A.K.; Puschmann, H. "OLEX2: a complete structure solution, refinement and analysis program". *J. Appl. Cryst.* (2009) **42**, 339-341.
- [4] Guzei, I.A. (2013). Internal laboratory computer programs Gn.

Table A3.46. Crystal data and structure refinement for Diazaborine **2**.

Empirical formula	C ₇ H ₇ BN ₂ O
Formula weight	145.96
Temperature/K	100
Crystal system	monoclinic
Space group	P2 ₁ /n
a/Å	10.282(3)
b/Å	19.686(5)
c/Å	11.747(4)
α/°	90
β/°	115.314(12)
γ/°	90
Volume/Å ³	2149.4(12)
Z	12
ρ _{calc} /g/cm ³	1.353
μ/mm ⁻¹	0.091
F(000)	912.0
Crystal size/mm ³	0.25 × 0.2 × 0.2
Radiation	MoKα (λ = 0.71073)
2θ range for data collection/°	4.138 to 58.494
Index ranges	-14 ≤ h ≤ 14, -27 ≤ k ≤ 26, -15 ≤ l ≤ 16
Reflections collected	33740
Independent reflections	5833 [R _{int} = 0.0262, R _{sigma} = 0.0174]
Data/restraints/parameters	5833/0/316
Goodness-of-fit on F ²	1.015
Final R indexes [I ≥ 2σ (I)]	R ₁ = 0.0404, wR ₂ = 0.1124
Final R indexes [all data]	R ₁ = 0.0463, wR ₂ = 0.1175
Largest diff. peak/hole / e Å ⁻³	0.45/-0.19

Table A3.47. Fractional Atomic Coordinates (×10⁴) and Equivalent Isotropic Displacement Parameters (Å²×10³) for Diazaborine **2**. U_{eq} is defined as 1/3 of the trace of the orthogonalised U_{ij} tensor.

Atom	x	y	z	U(eq)
O1	5997.2(9)	6245.5(4)	6612.1(7)	16.56(17)
N1	5834(1)	5781.4(5)	4696.3(8)	14.68(18)
N2	6085.0(11)	5325.3(5)	3930.4(9)	16.58(19)
C1	6886.2(12)	4805.1(6)	4457.0(11)	17.8(2)
C2	7585.0(12)	4669.5(6)	5790.6(11)	16.5(2)
C3	8495.7(13)	4100.4(6)	6242.0(13)	22.1(2)
C4	9226.4(13)	3995.9(7)	7517.9(13)	25.2(3)
C5	9070.2(13)	4450.1(7)	8363.6(12)	23.2(2)
C6	8151.9(12)	5002.0(6)	7929.9(11)	18.7(2)
C7	7388.9(11)	5123.5(5)	6632.6(10)	14.8(2)

B1	6387.6(13)	5734.8(6)	6034.0(11)	13.8(2)
O1A	4230.8(8)	7085.0(4)	3504.3(7)	16.64(17)
N1A	6184(1)	7523.2(5)	5305.4(8)	14.88(18)
N2A	7294.5(10)	7956.2(5)	5982.7(9)	16.01(19)
C1A	7470.8(12)	8483.9(6)	5407.9(10)	16.5(2)
C2A	6605.0(11)	8658.4(5)	4103.3(10)	15.1(2)
C3A	6908.5(12)	9253.2(6)	3601.6(11)	18.7(2)
C4A	6122.7(13)	9406.0(6)	2346.4(12)	20.1(2)
C5A	5044.6(13)	8964.8(6)	1568.3(11)	19.5(2)
C6A	4725.0(12)	8382.5(6)	2061.3(10)	16.5(2)
C7A	5486.5(11)	8218.9(5)	3341.5(10)	13.7(2)
B1A	5237.0(12)	7586.8(6)	4000.2(11)	13.4(2)
O1B	5589.7(9)	5434.8(4)	1470.9(7)	15.76(17)
N1B	6025.8(10)	5817.1(5)	-251.4(8)	14.53(18)
N2B	6528.8(10)	6240.6(5)	-898.1(9)	16.55(19)
C1B	7190.1(12)	6788.9(6)	-337.9(10)	16.7(2)
C2B	7490.0(11)	6984.0(5)	933.6(10)	14.5(2)
C3B	8237.5(12)	7591.8(6)	1436.1(12)	19.1(2)
C4B	8605.5(13)	7752.8(6)	2677.0(12)	21.8(2)
C5B	8261.1(13)	7312.5(6)	3439.0(11)	20.8(2)
C6B	7495.1(12)	6722.6(6)	2943.8(10)	16.9(2)
C7B	7075.4(11)	6548.4(5)	1674.7(10)	13.18(19)
B1B	6209.7(12)	5911.3(6)	1012.2(11)	12.7(2)

Table A3.48. Anisotropic Displacement Parameters ($\text{\AA}^2 \times 10^3$) for Diazaborine **2**. The Anisotropic displacement factor exponent takes the form: $-2\pi^2[h^2a^{*2}U_{11}+2hka^*b^*U_{12}+\dots]$.

Atom	U_{11}	U_{22}	U_{33}	U_{23}	U_{13}	U_{12}
O1	22.9(4)	16.5(4)	11.5(3)	1.2(3)	8.5(3)	2.8(3)
N1	17.7(4)	14.5(4)	12.5(4)	0.3(3)	7.2(3)	1.0(3)
N2	20.3(4)	18.1(4)	14.6(4)	-2.7(3)	10.5(4)	-3.3(4)
C1	20.2(5)	17.9(5)	19.7(5)	-3.3(4)	12.8(4)	-2.2(4)
C2	15.1(5)	16.0(5)	20.9(5)	1.5(4)	10.2(4)	-1.2(4)
C3	20.1(5)	16.7(5)	33.5(6)	1.4(5)	15.2(5)	2.0(4)
C4	18.1(5)	21.6(6)	36.2(7)	10.5(5)	12.0(5)	5.1(4)
C5	17.0(5)	26.5(6)	23.8(6)	10.4(5)	6.5(4)	1.5(4)
C6	17.3(5)	21.3(5)	17.7(5)	4.5(4)	7.7(4)	0.0(4)
C7	13.9(5)	15.7(5)	16.0(5)	2.6(4)	7.7(4)	-0.6(4)
B1	15.4(5)	14.7(5)	12.3(5)	1.2(4)	6.8(4)	-0.9(4)
O1A	15.7(4)	17.1(4)	12.1(3)	2.0(3)	1.2(3)	-3.3(3)
N1A	14.5(4)	14.9(4)	11.9(4)	0.5(3)	2.4(3)	-1.2(3)
N2A	13.4(4)	17.0(4)	13.7(4)	-3.6(3)	2.0(3)	-0.3(3)
C1A	13.9(5)	15.9(5)	16.8(5)	-3.5(4)	3.8(4)	-1.0(4)
C2A	14.0(5)	14.0(5)	17.6(5)	-0.6(4)	7.1(4)	0.8(4)
C3A	17.7(5)	14.6(5)	25.6(6)	-1.0(4)	11.2(4)	-1.7(4)

C4A	22.0(5)	16.6(5)	27.6(6)	5.5(4)	16.3(5)	2.4(4)
C5A	19.6(5)	21.7(5)	19.2(5)	6.0(4)	10.2(4)	4.0(4)
C6A	14.7(5)	18.0(5)	15.5(5)	1.8(4)	5.4(4)	1.1(4)
C7A	12.8(4)	13.8(5)	14.5(5)	0.8(4)	6.0(4)	1.0(4)
B1A	12.5(5)	14.4(5)	12.0(5)	0.9(4)	3.9(4)	0.7(4)
O1B	21.8(4)	14.7(4)	11.5(3)	-1.6(3)	7.8(3)	-3.2(3)
N1B	19.1(4)	13.0(4)	11.5(4)	-0.6(3)	6.5(3)	-1.0(3)
N2B	19.0(4)	18.3(4)	13.7(4)	3.2(3)	8.3(3)	2.8(3)
C1B	17.1(5)	17.8(5)	16.4(5)	4.0(4)	8.3(4)	1.4(4)
C2B	12.4(4)	13.8(5)	16.9(5)	0.4(4)	6.0(4)	1.1(4)
C3B	15.8(5)	15.0(5)	27.3(6)	0.6(4)	9.9(4)	-1.6(4)
C4B	17.4(5)	17.0(5)	30.6(6)	-8.0(4)	9.7(5)	-4.7(4)
C5B	18.8(5)	22.8(6)	20.6(5)	-9.3(4)	8.0(4)	-3.4(4)
C6B	17.6(5)	17.8(5)	16.6(5)	-3.4(4)	8.5(4)	-1.4(4)
C7B	12.3(4)	13.2(5)	14.2(5)	-1.0(4)	5.8(4)	0.8(4)
B1B	13.8(5)	12.5(5)	11.4(5)	-0.3(4)	5.1(4)	1.9(4)

Table A3.49. Bond Lengths for Diazaborine 2.

Atom	Atom	Length/Å	Atom	Atom	Length/Å
O1	B1	1.3660(14)	C2A	C7A	1.4113(15)
N1	N2	1.3714(13)	C3A	C4A	1.3779(17)
N1	B1	1.4273(15)	C4A	C5A	1.3972(17)
N2	C1	1.2940(15)	C5A	C6A	1.3857(16)
C1	C2	1.4419(16)	C6A	C7A	1.4041(15)
C2	C3	1.4101(16)	C7A	B1A	1.5436(16)
C2	C7	1.4100(16)	O1B	B1B	1.3677(14)
C3	C4	1.3749(19)	N1B	N2B	1.3696(13)
C4	C5	1.3958(19)	N1B	B1B	1.4259(15)
C5	C6	1.3858(17)	N2B	C1B	1.2954(15)
C6	C7	1.4046(16)	C1B	C2B	1.4421(16)
C7	B1	1.5438(16)	C2B	C3B	1.4080(15)
O1A	B1A	1.3675(14)	C2B	C7B	1.4116(15)
N1A	N2A	1.3735(13)	C3B	C4B	1.3772(18)
N1A	B1A	1.4275(15)	C4B	C5B	1.3961(18)
N2A	C1A	1.2933(15)	C5B	C6B	1.3839(16)
C1A	C2A	1.4466(16)	C6B	C7B	1.4058(15)
C2A	C3A	1.4047(16)	C7B	B1B	1.5422(16)

Table A3.50. Bond Angles for Diazaborine 2

Atom	Atom	Atom	Angle/°	Atom	Atom	Atom	Angle/°
N2	N1	B1	125.59(10)	C6A	C5A	C4A	120.30(11)
C1	N2	N1	117.67(9)	C5A	C6A	C7A	120.94(10)
N2	C1	C2	125.84(10)	C2A	C7A	B1A	116.19(9)

C3	C2	C1	119.86(11)	C6A	C7A	C2A	117.94(10)
C7	C2	C1	119.38(10)	C6A	C7A	B1A	125.86(10)
C7	C2	C3	120.72(11)	O1A	B1A	N1A	116.01(10)
C4	C3	C2	119.63(12)	O1A	B1A	C7A	128.78(10)
C3	C4	C5	120.30(11)	N1A	B1A	C7A	115.21(10)
C6	C5	C4	120.54(11)	N2B	N1B	B1B	125.79(9)
C5	C6	C7	120.60(11)	C1B	N2B	N1B	117.78(9)
C2	C7	B1	116.23(10)	N2B	C1B	C2B	125.56(10)
C6	C7	C2	118.18(10)	C3B	C2B	C1B	119.82(10)
C6	C7	B1	125.53(10)	C3B	C2B	C7B	120.81(10)
O1	B1	N1	115.87(10)	C7B	C2B	C1B	119.33(10)
O1	B1	C7	128.88(10)	C4B	C3B	C2B	119.54(11)
N1	B1	C7	115.21(10)	C3B	C4B	C5B	120.37(11)
N2A	N1A	B1A	125.74(9)	C6B	C5B	C4B	120.40(11)
C1A	N2A	N1A	117.61(9)	C5B	C6B	C7B	120.80(11)
N2A	C1A	C2A	125.71(10)	C2B	C7B	B1B	116.37(9)
C3A	C2A	C1A	119.73(10)	C6B	C7B	C2B	117.97(10)
C3A	C2A	C7A	120.79(10)	C6B	C7B	B1B	125.65(10)
C7A	C2A	C1A	119.46(10)	O1B	B1B	N1B	116.37(10)
C4A	C3A	C2A	119.81(11)	O1B	B1B	C7B	128.65(10)
C3A	C4A	C5A	120.17(11)	N1B	B1B	C7B	114.97(9)

Table A3.51. Hydrogen Bonds for Diazaborine 2

D	H	A	d(D-H)/Å	d(H-A)/Å	d(D-A)/Å	D-H-A/°
O1	H1O	N2B ¹	0.885(17)	1.861(17)	2.7361(16)	169.1(15)
N1	H1N	O1A	0.891(16)	2.180(16)	3.0480(14)	164.6(13)
O1A	H1OA	N2A ²	0.888(17)	1.899(17)	2.7751(15)	168.6(15)
N1A	H1NA	O1	0.899(15)	2.108(16)	2.9954(14)	168.9(13)
O1B	H1OB	N2	0.898(17)	1.836(17)	2.7193(15)	167.0(15)
N1B	H1NB	O1B ³	0.880(16)	2.109(16)	2.9750(14)	167.7(14)

Table A3.52. Torsion Angles for Diazaborine 2

A	B	C	D	Angle/°	A	B	C	D	Angle/°
N1	N2	C1	C2	-2.16(17)	C3A	C2A	C7A	C6A	2.24(16)
N2	N1	B1	O1	-179.80(9)	C3A	C2A	C7A	B1A	-179.08(10)
N2	N1	B1	C7	2.10(16)	C3A	C4A	C5A	C6A	2.17(17)
N2	C1	C2	C3	-176.46(11)	C4A	C5A	C6A	C7A	-0.92(17)
N2	C1	C2	C7	1.25(17)	C5A	C6A	C7A	C2A	-1.25(16)
C1	C2	C3	C4	176.14(11)	C5A	C6A	C7A	B1A	-179.79(10)
C1	C2	C7	C6	-176.14(10)	C6A	C7A	B1A	O1A	-2.29(19)
C1	C2	C7	B1	1.35(15)	C6A	C7A	B1A	N1A	178.10(10)
C2	C3	C4	C5	-0.03(18)	C7A	C2A	C3A	C4A	-1.05(17)
C2	C7	B1	O1	179.41(11)	B1A	N1A	N2A	C1A	2.90(16)

C2	C7	B1	N1	-2.79(14)	N1B	N2B	C1B	C2B	2.25(16)
C3	C2	C7	C6	1.55(16)	N2B	N1B	B1B	O1B	178.48(9)
C3	C2	C7	B1	179.04(10)	N2B	N1B	B1B	C7B	-0.85(15)
C3	C4	C5	C6	1.57(19)	N2B	C1B	C2B	C3B	179.15(11)
C4	C5	C6	C7	-1.54(18)	N2B	C1B	C2B	C7B	1.53(17)
C5	C6	C7	C2	-0.01(16)	C1B	C2B	C3B	C4B	-175.66(11)
C5	C6	C7	B1	-177.25(11)	C1B	C2B	C7B	C6B	174.43(10)
C6	C7	B1	O1	-3.30(19)	C1B	C2B	C7B	B1B	-4.75(14)
C6	C7	B1	N1	174.50(10)	C2B	C3B	C4B	C5B	0.99(18)
C7	C2	C3	C4	-1.54(17)	C2B	C7B	B1B	O1B	-174.85(10)
B1	N1	N2	C1	0.32(16)	C2B	C7B	B1B	N1B	4.37(14)
N1A	N2A	C1A	C2A	-0.52(17)	C3B	C2B	C7B	C6B	-3.17(15)
N2A	N1A	B1A	O1A	177.99(10)	C3B	C2B	C7B	B1B	177.65(10)
N2A	N1A	B1A	C7A	-2.35(16)	C3B	C4B	C5B	C6B	-2.62(18)
N2A	C1A	C2A	C3A	179.35(11)	C4B	C5B	C6B	C7B	1.31(18)
N2A	C1A	C2A	C7A	-2.20(17)	C5B	C6B	C7B	C2B	1.55(16)
C1A	C2A	C3A	C4A	177.37(10)	C5B	C6B	C7B	B1B	-179.35(10)
C1A	C2A	C7A	C6A	-176.19(10)	C6B	C7B	B1B	O1B	6.04(18)
C1A	C2A	C7A	B1A	2.50(15)	C6B	C7B	B1B	N1B	-174.74(10)
C2A	C3A	C4A	C5A	-1.18(17)	C7B	C2B	C3B	C4B	1.93(16)
C2A	C7A	B1A	O1A	179.15(11)	B1B	N1B	N2B	C1B	-2.49(16)
C2A	C7A	B1A	N1A	-0.46(14)					

Table A3.53. Hydrogen Atom Coordinates ($\text{\AA} \times 10^4$) and Isotropic Displacement Parameters ($\text{\AA}^2 \times 10^3$) for Diazaborine 2

Atom	x	y	z	U(eq)
H1O	6214(17)	6191(8)	7421(16)	25
H1N	5236(16)	6109(8)	4250(14)	18
H1D	7027	4484	3917	21
H3	8604	3791	5668	27
H4	9840	3613	7825	30
H5	9598	4380	9244	28
H6	8037	5301	8515	22
H1OA	3637(18)	7131(8)	2695(16)	25
H1NA	6138(16)	7177(8)	5785(14)	18
H1DA	8236	8783	5884	20
H3A	7653	9549	4126	22
H4A	6314	9812	2009	24
H5A	4528	9065	697	23
H6A	3980	8090	1525	20
H1OB	5755(18)	5468(8)	2284(16)	24
H1NB	5552(16)	5470(8)	-717(14)	17
H1BB	7504	7088	-804	20
H3B	8486	7889	923	23

H4B	9096	8166	3016	26
H5B	8554	7418	4303	25
H6B	7250	6432	3468	20

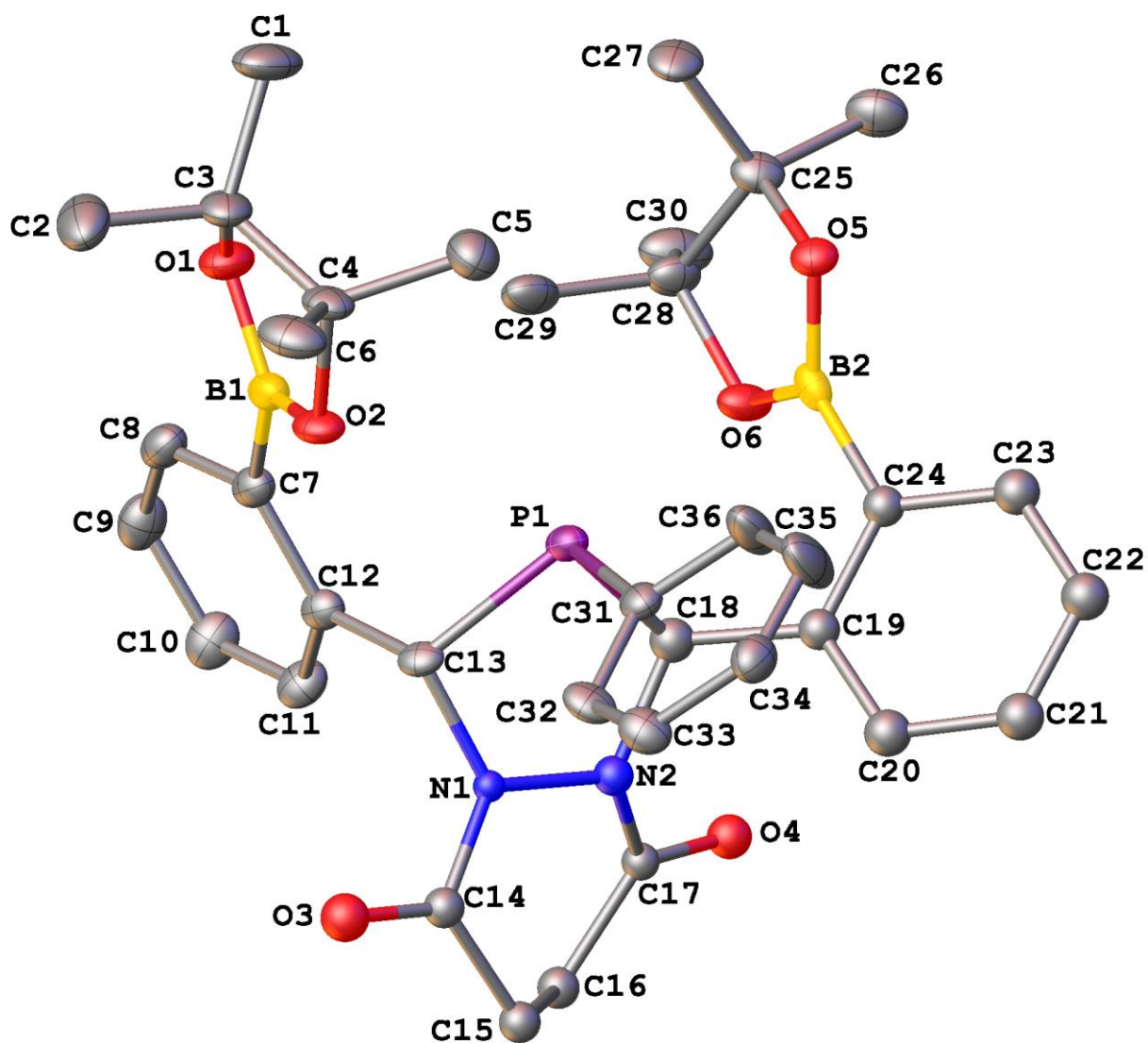
A3.4.2 Crystallographic Data for *o*-Bpin DiazaPhos 8

Figure A3.44. A molecular drawing of *o*-Bpin DiazaPhos 8 shown with 50% probability ellipsoids.

All H atoms, minor components of the disorder, and solvent molecule are omitted.

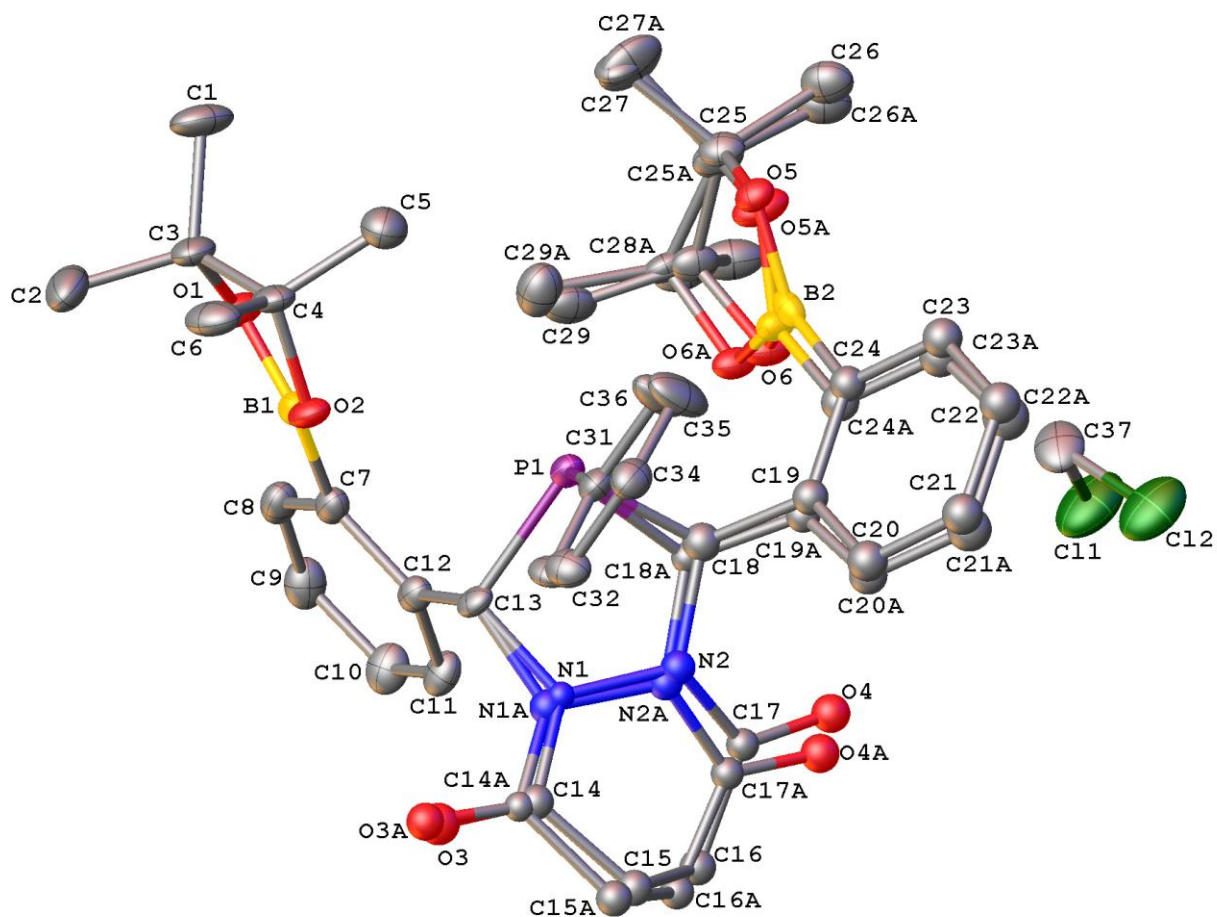


Figure A3.45. A molecular drawing of the content of the asymmetric unit of *o*-Bpin DiazaPhos **8** shown with 50% probability ellipsoids. All H atoms are omitted. Note that only $\frac{1}{2}$ of the solvent chloroform is present.

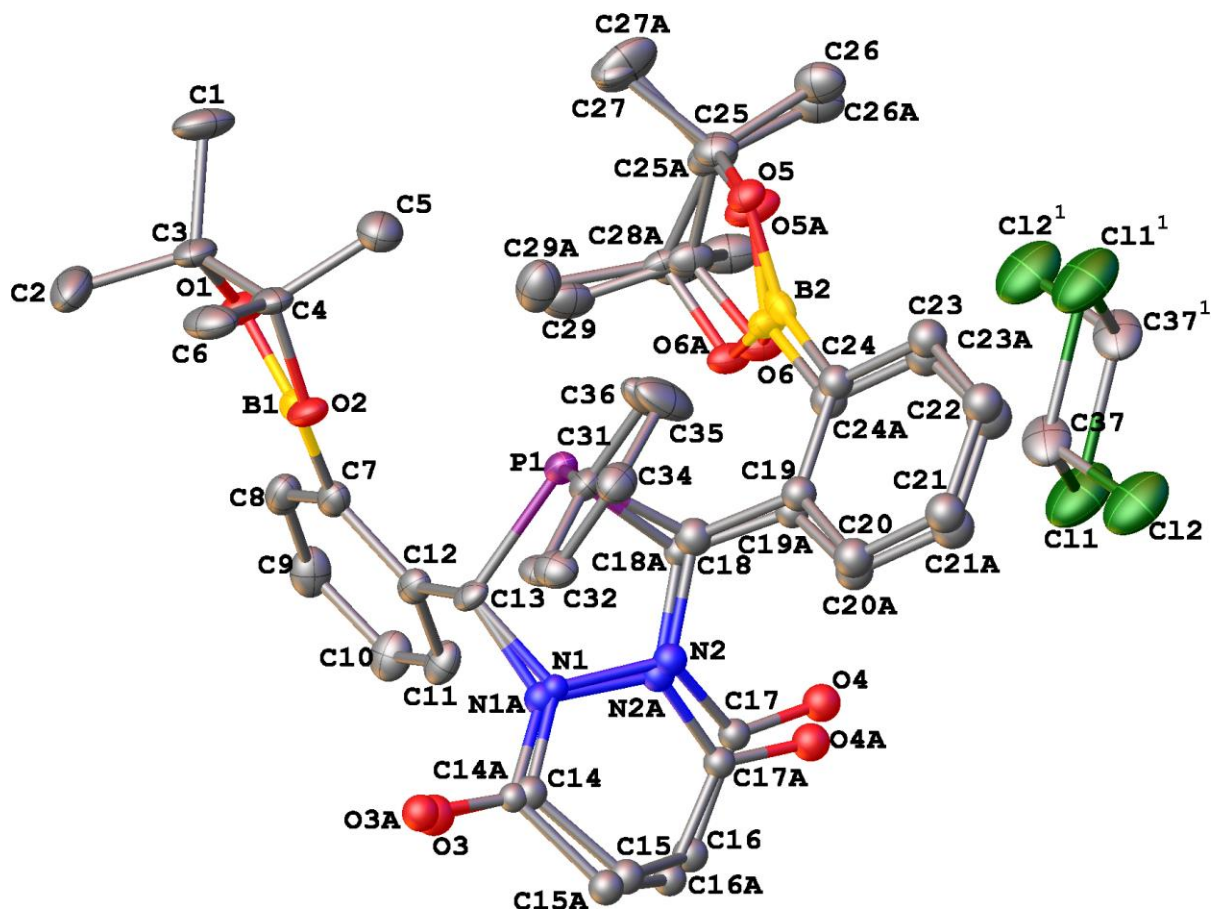


Figure A3.46. Completed fragments of *o*-Bpin DiazaPhos **8** shown with 50% probability ellipsoids. All H atoms are omitted. Both positions of the solvent chloroform molecule disordered over an inversion center are shown: in the crystal in their positions atom Cl1 is present 100% of time whereas atoms C37 and Cl2 50% of the time.

Data Collection

A colorless crystal with approximate dimensions $0.19 \times 0.097 \times 0.08 \text{ mm}^3$ was selected under oil under ambient conditions and attached to the tip of a MiTeGen MicroMount©. The crystal was mounted in a stream of cold nitrogen at 100(1) K and centered in the X-ray beam by using a video camera.

The crystal evaluation and data collection were performed on a Bruker Quazar SMART APEXII diffractometer with Mo K α ($\lambda = 0.71073$ Å) radiation and the diffractometer to crystal distance of 4.96 cm.

The initial cell constants were obtained from three series of ω scans at different starting angles. Each series consisted of 12 frames collected at intervals of 0.5° in a 6° range about ω with the exposure time of 3 seconds per frame. The reflections were successfully indexed by an automated indexing routine built in the APEXII program suite. The final cell constants were calculated from a set of 9909 strong reflections from the actual data collection.

The data were collected by using the full sphere data collection routine to survey the reciprocal space to the extent of a full sphere to a resolution of 0.75 Å. A total of 34846 data were harvested by collecting 6 sets of frames with 0.5° scans in ω and ϕ with exposure times of 20 sec per frame. These highly redundant datasets were corrected for Lorentz and polarization effects. The absorption correction was based on fitting a function to the empirical transmission surface as sampled by multiple equivalent measurements. [1]

Structure Solution and Refinement

The systematic absences in the diffraction data were consistent for the space groups $P\bar{1}$ and $P1$. The E -statistics strongly suggested the centrosymmetric space group $P\bar{1}$ that yielded chemically reasonable and computationally stable results of refinement [2-4].

A successful solution by the direct methods provided most non-hydrogen atoms from the E -map. The remaining non-hydrogen atoms were located in an alternating series of least-squares cycles and difference Fourier maps. All non-hydrogen atoms were refined with anisotropic displacement coefficients unless otherwise specified. All hydrogen atoms were included in the structure factor calculation at idealized positions and were allowed to ride on the neighboring atoms with relative isotropic displacement coefficients.

A part of the molecule exhibits positional disorder. Atoms N1, N2, O3-O6, B2, and C14-C36 are disordered over two positions with the major component contribution of 51.0(10)%. The disordered fragments were refined with geometry restraints and many of the atoms were refined isotropically. Attempts to refine all atoms anisotropically were unsuccessful.

There is also $\frac{1}{2}$ of a solvent chloroform in the asymmetric unit. This molecule is disordered over a crystallographic inversion center.

The final least-squares refinement of 529 parameters against 6355 data resulted in residuals R (based on F^2 for $I \geq 2\sigma$) and wR (based on F^2 for all data) of 0.0571 and 0.1622, respectively. The final difference Fourier map was featureless.

Summary

Crystal data for $C_{36.5}H_{43.5}B_2Cl_{1.5}N_2O_6P$ ($M=712.00$): triclinic, space group $P\bar{1}$ (no. 2), $a = 11.510(4)$ Å, $b = 11.672(3)$ Å, $c = 14.667(4)$ Å, $\alpha = 98.762(15)^\circ$, $\beta = 110.950(13)^\circ$, $\gamma = 92.485(15)^\circ$, $V = 1808.3(9)$ Å³, $Z = 2$, $T = 100.02$ K, $\mu(\text{Mo K}\alpha) = 0.235$ mm⁻¹, $D_{\text{calc}} = 1.308$ g/mm³, 34846 reflections measured ($3.022 \leq 2\theta \leq 49.996$), 6355 unique ($R_{\text{int}} = 0.0534$, $R_{\text{sigma}} = 0.0348$) which were used in all calculations. The final R_1 was 0.0571 ($I > 2\sigma(I)$) and wR_2 was 0.1622 (all data).

References

- [1] Bruker-AXS. (2007-2014) APEX2 (Ver. 2014.1-1), SADABS (2012-1), and SAINT+ (Ver. 8.32A) Software Reference Manuals. Bruker-AXS, Madison, Wisconsin, USA.
- [2] Sheldrick, G. M. (2008) SHELXL. *Acta Cryst.* **A64**, 112-122.
- [3] Dolomanov, O.V.; Bourhis, L.J.; Gildea, R.J.; Howard, J.A.K.; Puschmann, H. "OLEX2: a complete structure solution, refinement and analysis program". *J. Appl. Cryst.* (2009) **42**, 339-341.
- [4] Guzei, I.A. (2013). Internal laboratory computer programs Gn.

Table A3.54. Crystal data and structure refinement for *o*-Bpin DiazaPhos **8**.

Empirical formula	C ₃₆ H ₄₃ B ₂ N ₂ O ₆ P · ½ CHCl ₃
Formula weight	712.00
Temperature/K	100.02
Crystal system	triclinic
Space group	P $\bar{1}$
a/Å	11.510(4)
b/Å	11.672(3)
c/Å	14.667(4)
α/°	98.762(15)
β/°	110.950(13)
γ/°	92.485(15)
Volume/Å ³	1808.3(9)
Z	2
ρ _{calc} /mg/mm ³	1.308
m/mm ⁻¹	0.235
F(000)	750.0
Crystal size/mm ³	0.19 × 0.097 × 0.08
Radiation	Mo Kα (λ = 0.71073)
2θ range for data collection	3.022 to 49.996°
Index ranges	-13 ≤ h ≤ 13, -13 ≤ k ≤ 13, -17 ≤ l ≤ 17
Reflections collected	34846
Independent reflections	6355 [R _{int} = 0.0534, R _{sigma} = 0.0348]
Data/restraints/parameters	6355/211/529
Goodness-of-fit on F ²	1.072
Final R indexes [I >= 2σ (I)]	R ₁ = 0.0571, wR ₂ = 0.1555
Final R indexes [all data]	R ₁ = 0.0649, wR ₂ = 0.1622
Largest diff. peak/hole / e Å ⁻³	0.70/-0.70

Table A3.55. Fractional Atomic Coordinates (×10⁴) and Equivalent Isotropic Displacement Parameters (Å²×10³) for *o*-Bpin DiazaPhos **8**. U_{eq} is defined as 1/3 of the trace of the orthogonalised U_{ij} tensor.

Atom	x	y	z	U(eq)
P1	5895.7(5)	3233.4(5)	2716.0(4)	19.36(17)
O1	8279.1(15)	2568.2(15)	5643.5(11)	28.1(4)
O2	8233.7(14)	3867.7(14)	4614.3(11)	22.8(4)
C13	7307.1(19)	2777.1(18)	2480.8(15)	17.0(4)
C1	7976(3)	3767(3)	7019(2)	40.3(7)
C2	10029(3)	3837(3)	6811.1(19)	42.7(7)
C3	8628(2)	3720(2)	6281.6(17)	27.9(5)
C4	8173(2)	4561(2)	5522.0(16)	24.4(5)

C5	6818(2)	4791(2)	5288.8(19)	32.5(6)
C6	9002(3)	5689(2)	5773.7(19)	34.4(6)
C7	8115.6(19)	1662(2)	3903.1(16)	20.8(5)
C8	8477(2)	622(2)	4229.1(17)	25.6(5)
C9	8439(2)	-387(2)	3580.1(18)	28.7(5)
C10	8018(2)	-371(2)	2572.5(18)	28.3(5)
C11	7650(2)	649.9(19)	2225.3(17)	23.8(5)
C12	7702.4(19)	1663.5(18)	2873.1(15)	18.8(4)
C31	5889(2)	4731.9(19)	2475.4(15)	19.9(5)
C32	6779(2)	5300.7(19)	2223.3(16)	22.7(5)
C33	6763(2)	6474(2)	2152.1(17)	24.9(5)
C34	5843(2)	7091(2)	2317.3(17)	25.9(5)
C35	4940(3)	6524(3)	2542(2)	41.8(7)
C36	4966(2)	5367(3)	2637(2)	36.2(6)
B1	8197(2)	2726(2)	4717.5(18)	21.8(5)
N1	6874(5)	2674(5)	1399(3)	11(2)
C14	7617(7)	2913(6)	908(4)	18(3)
O3	8714(5)	3314(5)	1362(4)	25.0(19)
C15	6990(6)	2547(5)	-199(3)	18.4(15)
C16	6129(6)	1406(4)	-463(3)	18.7(12)
C17	5169(5)	1532(4)	7(3)	15.3(6)
O4	4110(4)	1053(3)	-336(3)	21.2(10)
N2	5568(5)	2341(5)	865(3)	17.1(19)
C18	4795(5)	2432(5)	1477(2)	22(2)
C19	3623(4)	3010(6)	1103(4)	18.2(16)
C20	3445(5)	3701(6)	383(4)	23.4(18)
C21	2396(4)	4279(6)	102(4)	23.9(14)
C22	1530(4)	4190(6)	546(4)	24.3(13)
C23	1710(4)	3518(6)	1276(4)	22.5(13)
C24	2748(4)	2911(6)	1563(3)	18.1(14)
B2	2878(11)	2120(9)	2358(7)	18(2)
O5	2762(11)	2500(7)	3251(6)	18.9(15)
C25	2741(9)	1478(8)	3716(6)	23(2)
C26	1370(10)	1095(10)	3486(11)	31(2)
C27	3428(13)	1830(13)	4829(6)	28(3)
C28	3386(9)	599(7)	3184(6)	25(2)
C29	4798(9)	697(10)	3683(8)	30(2)
C30	2839(9)	-660(7)	2978(8)	38(2)
O6	3117(8)	992(7)	2233(5)	23.2(15)
N1A	7051(5)	2628(6)	1413(4)	17(2)
C14A	7813(7)	3011(6)	982(4)	13(3)
O3A	8856(4)	3492(5)	1457(4)	20.1(18)
C15A	7262(6)	2746(5)	-140(4)	18.4(16)
C16A	6462(6)	1570(4)	-486(3)	16.8(12)
C17A	5449(5)	1563(4)	-74(3)	15.3(6)

O4A	4391(4)	1056(3)	-512(3)	21.3(11)
N2A	5747(5)	2258(5)	843(3)	16(2)
C18A	4990(5)	2302(5)	1473(2)	14.0(19)
C19A	3738(5)	2753(6)	1035(4)	16.9(17)
C20A	3463(5)	3419(6)	291(4)	20.9(18)
C21A	2345(5)	3908(7)	-33(4)	27.8(16)
C22A	1477(5)	3765(7)	421(4)	30.7(15)
C23A	1754(4)	3125(7)	1179(4)	25.9(15)
C24A	2861(5)	2602(6)	1494(4)	20.4(15)
B2A	3053(13)	1876(11)	2339(7)	21(3)
O5A	2729(14)	2273(8)	3140(7)	30(2)
C25A	2789(10)	1312(8)	3685(6)	28(3)
C26A	1453(10)	768(11)	3372(11)	34(3)
C27A	3296(17)	1815(15)	4789(7)	45(5)
C28A	3667(9)	524(7)	3331(6)	23(2)
C29A	5044(9)	871(12)	3954(9)	36(3)
C30A	3337(9)	-771(6)	3206(7)	33(2)
O6A	3470(8)	811(7)	2348(6)	20.7(15)
Cl1	418.2(9)	-800.4(7)	-646.1(6)	58.3(3)
Cl2	149.9(17)	1524.9(12)	-1025.9(11)	51.9(4)
C37	660(5)	655(5)	-103(4)	36.8(12)

Table A3.56. Anisotropic Displacement Parameters ($\text{\AA}^2 \times 10^3$) for o-Bpin DiazaPhos **8**. The Anisotropic displacement factor exponent takes the form: $-2\pi^2[h^2a^{*2}U_{11}+2hka^*b^*U_{12}+\dots]$.

Atom	U_{11}	U_{22}	U_{33}	U_{23}	U_{13}	U_{12}
P1	17.4(3)	26.0(3)	14.8(3)	4.6(2)	6.0(2)	-0.4(2)
O1	35.1(9)	34.4(9)	17.8(8)	4.4(7)	13.2(7)	5.8(7)
O2	25.9(8)	28.5(9)	14.2(7)	-1.8(6)	10.4(6)	-1.1(6)
C13	20.3(10)	17.2(10)	10.7(9)	-2.8(8)	5.0(8)	-3.2(8)
C1	59.1(18)	47.6(16)	29.3(14)	10.8(12)	31.4(13)	16.6(14)
C2	36.2(15)	62.9(19)	21.4(13)	-3.6(12)	4.9(11)	15.2(13)
C3	30.9(12)	38.8(14)	16.6(11)	0.2(10)	13.2(10)	7.5(10)
C4	27.0(12)	32.1(13)	16.2(11)	-2.0(9)	13.0(9)	2.1(10)
C5	30.5(13)	38.7(14)	29.8(13)	3.0(11)	13.7(11)	8.2(11)
C6	40.7(14)	36.8(14)	27.6(13)	-7.8(11)	21.2(11)	-4.9(11)
C7	16.4(10)	26.6(12)	18.2(11)	4.2(9)	5.5(8)	-2.1(8)
C8	21.9(11)	33.4(13)	20.5(11)	9.1(10)	5.4(9)	-0.2(9)
C9	27.3(12)	24.5(12)	31.9(13)	10.5(10)	6(1)	0.5(9)
C10	30.2(12)	20.0(11)	28.7(13)	2.7(10)	5.1(10)	-2.9(9)
C11	25.1(11)	21.2(11)	18.8(11)	1.1(9)	2.5(9)	-4.1(9)
C12	16.8(10)	20.6(11)	17.2(10)	2.0(9)	5.2(8)	-3.5(8)
C31	19.8(10)	25.2(11)	12.7(10)	1.1(8)	4.6(8)	1.7(9)
C32	27.0(11)	19.4(11)	23.5(11)	-4.9(9)	14.9(10)	1.3(9)
C33	27.5(12)	21.0(11)	25.9(12)	-2.5(9)	12.4(10)	-0.4(9)

C34	28.2(12)	25.9(12)	22.7(12)	3.6(9)	8.2(10)	9.2(9)
C35	39.3(15)	49.8(17)	58.6(18)	28.8(15)	34.3(14)	28.3(13)
C36	30.8(13)	48.1(16)	48.9(16)	28.4(13)	28.1(12)	18.3(12)
B1	15.4(11)	33.5(14)	16.7(12)	4.6(10)	6.2(9)	0.8(10)
B2	11(4)	16(4)	24(4)	-2(2)	6(2)	-1(3)
O5	23(3)	18(3)	15(3)	-1(2)	7.3(19)	-1(2)
C25	30(4)	19(3)	22(4)	-2(2)	13(3)	1(2)
C26	36(3)	29(5)	32(4)	5(4)	18(3)	-3(3)
C27	36(4)	32(7)	18(4)	-4(3)	14(3)	9(4)
C28	34(4)	22(3)	24(4)	9(2)	16(3)	5(2)
C29	42(5)	30(4)	29(5)	14(3)	22(4)	11(3)
C30	61(5)	26(3)	38(5)	7(3)	32(4)	7(3)
O6	34(4)	20(3)	22(2)	4.2(17)	17(3)	6(2)
B2A	22(4)	27(5)	15(3)	6(3)	9(3)	6(3)
O5A	50(4)	21(3)	22(3)	1(3)	19(3)	4(3)
C25A	40(4)	26(4)	23(4)	8(3)	16(3)	4(3)
C26A	41(4)	34(6)	33(5)	7(4)	23(3)	4(3)
C27A	74(9)	35(8)	28(5)	16(4)	17(4)	11(6)
C28A	34(4)	24(3)	15(3)	4(2)	13(3)	3(2)
C29A	34(4)	40(5)	32(5)	12(4)	7(3)	-1(3)
C30A	56(5)	19(3)	29(4)	4(2)	21(4)	7(3)
O6A	29(4)	19(3)	18(2)	4.0(16)	13(2)	6(2)
Cl1	87.1(6)	39.4(4)	36.0(4)	-7.7(3)	13.2(4)	11.5(4)
Cl2	79.7(11)	28.8(7)	36.4(8)	-6.7(6)	13.8(7)	3.7(7)
C37	39(3)	27(3)	35(3)	-13(2)	10(2)	8(2)

Table A3.57. Bond Lengths for o-Bpin DiazaPhos **8**.

Atom	Atom	Length/Å	Atom	Atom	Length/Å
P1	C13	1.860(2)	C22	C23	1.384(6)
P1	C31	1.836(2)	C23	C24	1.382(7)
P1	C18	1.875(3)	C24	B2	1.565(7)
P1	C18A	1.879(3)	B2	O5	1.373(7)
O1	C3	1.464(3)	B2	O6	1.355(8)
O1	B1	1.369(3)	O5	C25	1.464(6)
O2	C4	1.475(3)	C25	C26	1.522(6)
O2	B1	1.365(3)	C25	C27	1.519(6)
C13	C12	1.523(3)	C25	C28	1.565(7)
C13	N1	1.467(5)	C28	C29	1.516(8)
C13	N1A	1.467(6)	C28	C30	1.514(6)
C1	C3	1.517(3)	C28	O6	1.467(6)
C2	C3	1.508(4)	N1A	C14A	1.349(6)
C3	C4	1.563(3)	N1A	N2A	1.440(6)
C4	C5	1.518(3)	C14A	O3A	1.211(7)
C4	C6	1.507(3)	C14A	C15A	1.512(6)

C7	C8	1.398(3)	C15A	C16A	1.527(7)
C7	C12	1.413(3)	C16A	C17A	1.494(6)
C7	B1	1.561(3)	C17A	O4A	1.228(5)
C8	C9	1.385(4)	C17A	N2A	1.378(5)
C9	C10	1.384(3)	N2A	C18A	1.476(6)
C10	C11	1.391(3)	C18A	C19A	1.507(7)
C11	C12	1.384(3)	C19A	C20A	1.389(6)
C31	C32	1.384(3)	C19A	C24A	1.418(6)
C31	C36	1.389(3)	C20A	C21A	1.384(6)
C32	C33	1.389(3)	C21A	C22A	1.402(6)
C33	C34	1.376(3)	C22A	C23A	1.383(6)
C34	C35	1.371(4)	C23A	C24A	1.394(7)
C35	C36	1.380(4)	C24A	B2A	1.563(7)
N1	C14	1.345(6)	B2A	O5A	1.377(7)
N1	N2	1.428(6)	B2A	O6A	1.352(8)
C14	O3	1.228(7)	O5A	C25A	1.464(6)
C14	C15	1.505(6)	C25A	C26A	1.517(7)
C15	C16	1.537(7)	C25A	C27A	1.520(7)
C16	C17	1.498(6)	C25A	C28A	1.564(7)
C17	O4	1.212(5)	C28A	C29A	1.518(8)
C17	N2	1.368(5)	C28A	C30A	1.510(6)
N2	C18	1.468(7)	C28A	O6A	1.470(6)
C18	C19	1.496(7)	Cl1	C37 ¹	1.927(6)
C19	C20	1.389(6)	Cl1	C37	1.728(5)
C19	C24	1.408(6)	Cl2	C37	1.764(6)
C20	C21	1.371(6)	C37	Cl1 ¹	1.927(6)
C21	C22	1.381(5)			

Table A3.58. Bond Angles for *o*-Bpin DiazaPhos **8**.

Atom	Atom	Atom	Angle/°	Atom	Atom	Atom	Angle/°
C13	P1	C18	93.2(2)	C19	C24	B2	123.0(5)
C13	P1	C18A	85.2(2)	C23	C24	C19	118.2(4)
C31	P1	C13	101.47(10)	C23	C24	B2	118.8(5)
C31	P1	C18	100.4(2)	O5	B2	C24	123.3(7)
C31	P1	C18A	104.77(19)	O6	B2	C24	123.4(6)
B1	O1	C3	106.85(18)	O6	B2	O5	113.3(5)
B1	O2	C4	107.39(17)	B2	O5	C25	107.3(6)
C12	C13	P1	111.43(14)	O5	C25	C26	106.3(6)
N1	C13	P1	101.1(3)	O5	C25	C27	108.9(7)
N1	C13	C12	115.2(3)	O5	C25	C28	102.3(4)
N1A	C13	P1	109.2(3)	C26	C25	C28	113.8(6)
N1A	C13	C12	111.0(3)	C27	C25	C26	109.9(6)
O1	C3	C1	108.2(2)	C27	C25	C28	114.7(6)
O1	C3	C2	106.7(2)	C29	C28	C25	114.2(6)

O1	C3	C4	102.73(17)	C30	C28	C25	114.4(6)
C1	C3	C4	114.2(2)	C30	C28	C29	110.3(6)
C2	C3	C1	110.6(2)	O6	C28	C25	102.0(5)
C2	C3	C4	113.7(2)	O6	C28	C29	106.6(6)
O2	C4	C3	101.76(18)	O6	C28	C30	108.5(6)
O2	C4	C5	106.82(18)	B2	O6	C28	107.8(5)
O2	C4	C6	108.45(18)	C14A	N1A	C13	126.6(5)
C5	C4	C3	113.48(19)	C14A	N1A	N2A	120.9(5)
C6	C4	C3	114.8(2)	N2A	N1A	C13	111.0(4)
C6	C4	C5	110.7(2)	N1A	C14A	C15A	113.9(6)
C8	C7	C12	117.8(2)	O3A	C14A	N1A	122.6(5)
C8	C7	B1	116.7(2)	O3A	C14A	C15A	123.5(5)
C12	C7	B1	125.5(2)	C14A	C15A	C16A	109.5(4)
C9	C8	C7	122.3(2)	C17A	C16A	C15A	111.1(4)
C10	C9	C8	119.1(2)	O4A	C17A	C16A	125.1(4)
C9	C10	C11	120.0(2)	O4A	C17A	N2A	120.0(4)
C12	C11	C10	121.1(2)	N2A	C17A	C16A	114.8(4)
C7	C12	C13	119.85(19)	N1A	N2A	C18A	112.2(4)
C11	C12	C13	120.38(19)	C17A	N2A	N1A	117.4(5)
C11	C12	C7	119.8(2)	C17A	N2A	C18A	126.0(4)
C32	C31	P1	125.29(17)	N2A	C18A	P1	109.5(3)
C32	C31	C36	117.8(2)	N2A	C18A	C19A	114.4(4)
C36	C31	P1	116.71(17)	C19A	C18A	P1	108.9(4)
C31	C32	C33	121.0(2)	C20A	C19A	C18A	123.3(4)
C34	C33	C32	120.4(2)	C20A	C19A	C24A	118.7(5)
C35	C34	C33	118.8(2)	C24A	C19A	C18A	117.5(4)
C34	C35	C36	121.2(2)	C21A	C20A	C19A	121.9(5)
C35	C36	C31	120.8(2)	C20A	C21A	C22A	119.5(5)
O1	B1	C7	120.6(2)	C23A	C22A	C21A	119.0(5)
O2	B1	O1	113.6(2)	C22A	C23A	C24A	122.0(4)
O2	B1	C7	125.7(2)	C19A	C24A	B2A	124.0(6)
C14	N1	C13	124.0(4)	C23A	C24A	C19A	118.7(4)
C14	N1	N2	119.8(4)	C23A	C24A	B2A	117.3(5)
N2	N1	C13	116.1(4)	O5A	B2A	C24A	120.7(8)
N1	C14	C15	113.0(5)	O6A	B2A	C24A	125.5(6)
O3	C14	N1	120.7(5)	O6A	B2A	O5A	113.7(5)
O3	C14	C15	126.1(5)	B2A	O5A	C25A	107.2(6)
C14	C15	C16	110.8(4)	O5A	C25A	C26A	106.1(7)
C17	C16	C15	110.7(3)	O5A	C25A	C27A	108.4(7)
O4	C17	C16	126.1(4)	O5A	C25A	C28A	102.2(5)
O4	C17	N2	120.8(4)	C26A	C25A	C27A	109.6(7)
N2	C17	C16	112.9(4)	C26A	C25A	C28A	114.9(7)
N1	N2	C18	114.9(4)	C27A	C25A	C28A	114.8(7)
C17	N2	N1	120.1(5)	C29A	C28A	C25A	112.9(7)
C17	N2	C18	118.5(4)	C30A	C28A	C25A	115.1(6)

N2	C18	P1	103.6(3)	C30A	C28A	C29A	111.0(7)
N2	C18	C19	116.7(4)	O6A	C28A	C25A	102.3(5)
C19	C18	P1	111.7(4)	O6A	C28A	C29A	106.3(6)
C20	C19	C18	121.3(4)	O6A	C28A	C30A	108.4(6)
C20	C19	C24	120.7(5)	B2A	O6A	C28A	107.2(5)
C24	C19	C18	117.8(4)	C37	Cl1	C37 ¹	75.3(3)
C21	C20	C19	119.9(4)	Cl1	C37	Cl1 ¹	104.7(3)
C20	C21	C22	120.1(4)	Cl1	C37	Cl2	110.0(3)
C21	C22	C23	120.4(4)	Cl2	C37	Cl1 ¹	107.7(3)
C24	C23	C22	120.7(4)				

Table A3.59. Torsion Angles for *o*-Bpin DiazaPhos **8**.

A	B	C	D	Angle/°	A	B	C	D	Angle/°
C31	P1	C13	N1A_b	-70.9(3)	C18	P1	C31	C36	87.9(3)
P1	C13	C12	C7	-64.6(2)	C18	P1	C18A	N2A	132(2)
P1	C13	C12	C11	114.92(19)	C18	P1	C18A	C19A	6.1(18)
P1	C13	N1	C14	146.7(6)	C18	C19	C20	C21	-175.8(5)
P1	C13	N1	N2	-30.8(5)	C18	C19	C24	C23	175.0(5)
P1	C13	N1A	C14A	135.2(6)	C18	C19	C24	B2	-6.8(9)
P1	C13	N1A	N2A	-30.8(5)	C19	C20	C21	C22	1.1(10)
P1	C31	C32	C33	-173.52(17)	C19	C24	B2	O5	131.0(10)
P1	C31	C36	C35	175.6(2)	C19	C24	B2	O6	-49.0(13)
P1	C18	C19	C20	101.8(6)	C20	C19	C24	C23	0.1(9)
P1	C18	C19	C24	-73.1(6)	C20	C19	C24	B2	178.3(7)
P1	C18A	C19A	C20A	102.7(6)	C20	C21	C22	C23	-0.1(9)
P1	C18A	C19A	C24A	-69.6(6)	C21	C22	C23	C24	-1.0(9)
O1	C3	C4	O2	-27.1(2)	C22	C23	C24	C19	0.9(9)
O1	C3	C4	C5	87.3(2)	C22	C23	C24	B2	-177.3(7)
O1	C3	C4	C6	-143.96(19)	C23	C24	B2	O5	-50.8(13)
C13	P1	C31	C32	-2.0(2)	C23	C24	B2	O6	129.2(9)
C13	P1	C31	C36	-176.70(19)	C24	C19	C20	C21	-1.1(9)
C13	P1	C18	N2	-23.8(4)	C24	B2	O5	C25	171.1(8)
C13	P1	C18	C19	-150.3(3)	C24	B2	O6	C28	170.5(8)
C13	P1	C18A	N2A	-28.2(4)	B2	O5	C25	C26	-97.8(10)
C13	P1	C18A	C19A	-153.9(3)	B2	O5	C25	C27	143.7(9)
C13	N1	C14	O3	-4.8(10)	B2	O5	C25	C28	21.9(9)
C13	N1	C14	C15	170.4(5)	O5	B2	O6	C28	-9.5(12)
C13	N1	N2	C17	-136.8(5)	O5	C25	C28	C29	88.3(8)
C13	N1	N2	C18	14.6(7)	O5	C25	C28	C30	-143.2(7)
C13	N1A	C14A	O3A	3.7(11)	O5	C25	C28	O6	-26.3(7)
C13	N1A	C14A	C15A	-178.4(5)	C25	C28	O6	B2	22.2(8)
C13	N1A	N2A	C17A	-149.3(5)	C26	C25	C28	C29	-157.4(8)
C13	N1A	N2A	C18A	8.7(7)	C26	C25	C28	C30	-28.9(9)
C1	C3	C4	O2	-144.0(2)	C26	C25	C28	O6	88.0(8)

C1	C3	C4	C5	-29.6(3)	C27	C25	C28	C29	-29.5(9)
C1	C3	C4	C6	99.1(3)	C27	C25	C28	C30	99.0(9)
C2	C3	C4	O2	87.8(2)	C27	C25	C28	O6	-144.1(8)
C2	C3	C4	C5	-157.9(2)	C29	C28	O6	B2	-97.9(8)
C2	C3	C4	C6	-29.1(3)	C30	C28	O6	B2	143.3(8)
C3	O1	B1	O2	-10.9(2)	O6	B2	O5	C25	-8.9(12)
C3	O1	B1	C7	167.20(19)	N1A	C13	C12	C7	173.5(3)
C4	O2	B1	O1	-7.9(2)	N1A	C13	C12	C11	-7.0(3)
C4	O2	B1	C7	174.1(2)	N1A	C13	N1	C14	-33(3)
C7	C8	C9	C10	-0.7(3)	N1A	C13	N1	N2	150(3)
C8	C7	C12	C13	-179.57(19)	N1A	C14A	C15A	C16A	-35.0(7)
C8	C7	C12	C11	0.9(3)	N1A	N2A	C18A	P1	16.9(6)
C8	C7	B1	O1	-17.3(3)	N1A	N2A	C18A	C19A	139.4(5)
C8	C7	B1	O2	160.5(2)	C14A	N1A	N2A	C17A	43.8(9)
C8	C9	C10	C11	0.6(3)	C14A	N1A	N2A	C18A	-158.2(6)
C9	C10	C11	C12	0.3(3)	C14A	C15A	C16A	C17A	57.7(6)
C10	C11	C12	C13	179.5(2)	O3A	C14A	C15A	C16A	142.9(6)
C10	C11	C12	C7	-1.0(3)	C15A	C16A	C17A	O4A	144.3(5)
C12	C13	N1	C14	-93.1(6)	C15A	C16A	C17A	N2A	-31.0(6)
C12	C13	N1	N2	89.4(5)	C16A	C17A	N2A	N1A	-17.3(7)
C12	C13	N1A	C14A	-101.6(7)	C16A	C17A	N2A	C18A	-171.9(5)
C12	C13	N1A	N2A	92.4(5)	C17A	N2A	C18A	P1	172.5(5)
C12	C7	C8	C9	-0.1(3)	C17A	N2A	C18A	C19A	-64.9(7)
C12	C7	B1	O1	162.2(2)	O4A	C17A	N2A	N1A	167.0(5)
C12	C7	B1	O2	-19.9(3)	O4A	C17A	N2A	C18A	12.5(9)
C31	P1	C13	C12	166.08(14)	N2A	N1A	C14A	O3A	168.4(7)
C31	P1	C13	N1	-71.0(2)	N2A	N1A	C14A	C15A	-13.7(9)
C31	P1	C18	N2	78.5(4)	N2A	C18A	C19A	C20A	-20.2(8)
C31	P1	C18	C19	-48.0(4)	N2A	C18A	C19A	C24A	167.5(5)
C31	P1	C18A	N2A	72.5(4)	C18A	P1	C13	C12	-89.8(2)
C31	P1	C18A	C19A	-53.3(3)	C18A	P1	C13	N1	33.1(3)
C31	C32	C33	C34	-1.0(3)	C18A	P1	C13	N1A	33.2(3)
C32	C31	C36	C35	0.5(4)	C18A	P1	C31	C32	-90.0(3)
C32	C33	C34	C35	-0.7(4)	C18A	P1	C31	C36	95.3(3)
C33	C34	C35	C36	2.3(4)	C18A	P1	C18	N2	-43.7(19)
C34	C35	C36	C31	-2.2(5)	C18A	P1	C18	C19	-170(2)
C36	C31	C32	C33	1.1(3)	C18A	C19A	C20A	C21A	-174.1(6)
B1	O1	C3	C1	144.7(2)	C18A	C19A	C24A	C23A	172.7(5)
B1	O1	C3	C2	-96.3(2)	C18A	C19A	C24A	B2A	-7.3(10)
B1	O1	C3	C4	23.5(2)	C19A	C20A	C21A	C22A	2.2(10)
B1	O2	C4	C3	21.7(2)	C19A	C24A	B2A	O5A	138.5(11)
B1	O2	C4	C5	-97.6(2)	C19A	C24A	B2A	O6A	-45.2(16)
B1	O2	C4	C6	143.1(2)	C20A	C19A	C24A	C23A	0.1(9)
B1	C7	C8	C9	179.5(2)	C20A	C19A	C24A	B2A	-179.9(8)
B1	C7	C12	C13	0.9(3)	C20A	C21A	C22A	C23A	-0.7(10)

B1	C7	C12	C11	-178.6(2)	C21A	C22A	C23A	C24A	-1.1(10)
N1	C13	C12	C7	-178.9(3)	C22A	C23A	C24A	C19A	1.4(10)
N1	C13	C12	C11	0.6(3)	C22A	C23A	C24A	B2A	-178.6(8)
N1	C13	N1A	C14A	136(4)	C23A	C24A	B2A	O5A	-41.5(16)
N1	C13	N1A	N2A	-30(3)	C23A	C24A	B2A	O6A	134.8(11)
N1	C14	C15	C16	-36.3(7)	C24A	C19A	C20A	C21A	-1.9(10)
N1	N2	C18	P1	10.1(6)	C24A	B2A	O5A	C25A	169.1(10)
N1	N2	C18	C19	133.3(5)	C24A	B2A	O6A	C28A	172.6(11)
C14	N1	N2	C17	45.6(9)	B2A	O5A	C25A	C26A	-99.6(12)
C14	N1	N2	C18	-163.0(6)	B2A	O5A	C25A	C27A	142.7(12)
C14	C15	C16	C17	57.2(6)	B2A	O5A	C25A	C28A	21.2(12)
O3	C14	C15	C16	138.7(7)	O5A	B2A	O6A	C28A	-10.8(14)
C15	C16	C17	O4	147.3(5)	O5A	C25A	C28A	C29A	87.4(9)
C15	C16	C17	N2	-27.8(6)	O5A	C25A	C28A	C30A	-143.8(8)
C16	C17	N2	N1	-20.9(7)	O5A	C25A	C28A	O6A	-26.5(8)
C16	C17	N2	C18	-171.3(5)	C25A	C28A	O6A	B2A	23.0(9)
C17	N2	C18	P1	161.9(5)	C26A	C25A	C28A	C29A	-158.1(8)
C17	N2	C18	C19	-74.8(7)	C26A	C25A	C28A	C30A	-29.3(9)
O4	C17	N2	N1	163.7(5)	C26A	C25A	C28A	O6A	88.0(8)
O4	C17	N2	C18	13.3(8)	C27A	C25A	C28A	C29A	-29.6(10)
N2	N1	C14	O3	172.6(6)	C27A	C25A	C28A	C30A	99.2(9)
N2	N1	C14	C15	-12.2(9)	C27A	C25A	C28A	O6A	-143.5(8)
N2	C18	C19	C20	-17.2(7)	C29A	C28A	O6A	B2A	-95.6(9)
N2	C18	C19	C24	167.9(5)	C30A	C28A	O6A	B2A	145.0(8)
C18	P1	C13	C12	-92.7(2)	O6A	B2A	O5A	C25A	-7.6(15)
C18	P1	C13	N1	30.2(3)	C37 ¹	Cl1	C37	Cl1 ¹	0.003(0)
C18	P1	C13	N1A	30.3(3)	C37 ¹	Cl1	C37	Cl2	-115.4(4)
C18	P1	C31	C32	-97.4(3)					

Table A3.60. Hydrogen Atom Coordinates ($\text{\AA} \times 10^4$) and Isotropic Displacement Parameters ($\text{\AA}^2 \times 10^3$) for *o*-Bpin DiazaPhos **8**.

Atom	<i>x</i>	<i>y</i>	<i>z</i>	U(eq)
H13	8011	3415	2804	20
H13A	8009	3411	2832	20
H1A	7081	3525	6663	60
H1B	8095	4565	7386	60
H1C	8333	3241	7485	60
H2A	10263	3194	7178	64
H2B	10300	4581	7275	64
H2C	10434	3811	6324	64
H5A	6535	5173	4708	49
H5B	6745	5297	5860	49
H5C	6298	4050	5148	49
H6A	9850	5521	5834	52

H6B	9025	6134	6404	52
H6C	8671	6147	5247	52
H8	8758	606	4920	31
H9	8700	-1079	3823	34
H10	7979	-1059	2118	34
H11	7359	652	1532	29
H32	7412	4883	2097	27
H33	7390	6852	1988	30
H34	5835	7896	2277	31
H35	4284	6936	2633	50
H36	4346	5001	2816	43
H15A	7634	2438	-497	22
H15B	6494	3169	-480	22
H16A	5704	1196	-1192	22
H16B	6635	770	-229	22
H18	4560	1628	1554	26
H20	4048	3773	85	28
H21	2266	4741	-399	29
H22	805	4593	350	29
H23	1114	3474	1584	27
H26A	998	1727	3768	47
H26B	1305	404	3777	47
H26C	924	907	2766	47
H27A	4280	2169	4967	43
H27B	3462	1141	5142	43
H27C	2984	2406	5098	43
H29A	5136	1519	3838	45
H29B	5149	258	3236	45
H29C	5023	380	4297	45
H30A	2946	-915	3607	56
H30B	3272	-1150	2626	56
H30C	1947	-729	2568	56
H15C	7942	2724	-404	22
H15D	6741	3365	-394	22
H16C	6085	1407	-1220	20
H16D	6998	947	-269	20
H18A	4837	1493	1581	17
H20A	4059	3543	-4	25
H21A	2168	4337	-559	33
H22A	710	4102	212	37
H23A	1172	3040	1494	31
H26D	903	1384	3382	50
H26E	1407	257	3833	50
H26F	1185	311	2700	50
H27D	4112	2261	4971	67

H27E	3390	1179	5167	67
H27F	2714	2329	4941	67
H29D	5233	1715	4029	55
H29E	5553	463	3625	55
H29F	5232	659	4609	55
H30D	3375	-965	3843	50
H30E	3933	-1194	2984	50
H30F	2489	-994	2712	50
H37	1556	891	335	44

Table A3.61. Atomic Occupancy for o-Bpin DiazaPhos 8

Atom	Occupancy	Atom	Occupancy	Atom	Occupancy
H13	0.510(10)	H13A	0.490(10)	N1	0.510(10)
C14	0.510(10)	O3	0.510(10)	C15	0.510(10)
H15A	0.510(10)	H15B	0.510(10)	C16	0.510(10)
H16A	0.510(10)	H16B	0.510(10)	C17	0.510(10)
O4	0.510(10)	N2	0.510(10)	C18	0.510(10)
H18	0.510(10)	C19	0.510(10)	C20	0.510(10)
H20	0.510(10)	C21	0.510(10)	H21	0.510(10)
C22	0.510(10)	H22	0.510(10)	C23	0.510(10)
H23	0.510(10)	C24	0.510(10)	B2	0.510(10)
O5	0.510(10)	C25	0.510(10)	C26	0.510(10)
H26A	0.510(10)	H26B	0.510(10)	H26C	0.510(10)
C27	0.510(10)	H27A	0.510(10)	H27B	0.510(10)
H27C	0.510(10)	C28	0.510(10)	C29	0.510(10)
H29A	0.510(10)	H29B	0.510(10)	H29C	0.510(10)
C30	0.510(10)	H30A	0.510(10)	H30B	0.510(10)
H30C	0.510(10)	O6	0.510(10)	N1A	0.490(10)
C14A	0.490(10)	O3A	0.490(10)	C15A	0.490(10)
H15C	0.490(10)	H15D	0.490(10)	C16A	0.490(10)
H16C	0.490(10)	H16D	0.490(10)	C17A	0.490(10)
O4A	0.490(10)	N2A	0.490(10)	C18A	0.490(10)
H18A	0.490(10)	C19A	0.490(10)	C20A	0.490(10)
H20A	0.490(10)	C21A	0.490(10)	H21A	0.490(10)
C22A	0.490(10)	H22A	0.490(10)	C23A	0.490(10)
H23A	0.490(10)	C24A	0.490(10)	B2A	0.490(10)
O5A	0.490(10)	C25A	0.490(10)	C26A	0.490(10)
H26D	0.490(10)	H26E	0.490(10)	H26F	0.490(10)
C27A	0.490(10)	H27D	0.490(10)	H27E	0.490(10)
H27F	0.490(10)	C28A	0.490(10)	C29A	0.490(10)
H29D	0.490(10)	H29E	0.490(10)	H29F	0.490(10)
C30A	0.490(10)	H30D	0.490(10)	H30E	0.490(10)
H30F	0.490(10)	O6A	0.490(10)	Cl2	0.5
C37	0.5	H37	0.5		

A3.4.3 Crystallographic Data for *o*-Me DiazaPhos **16**

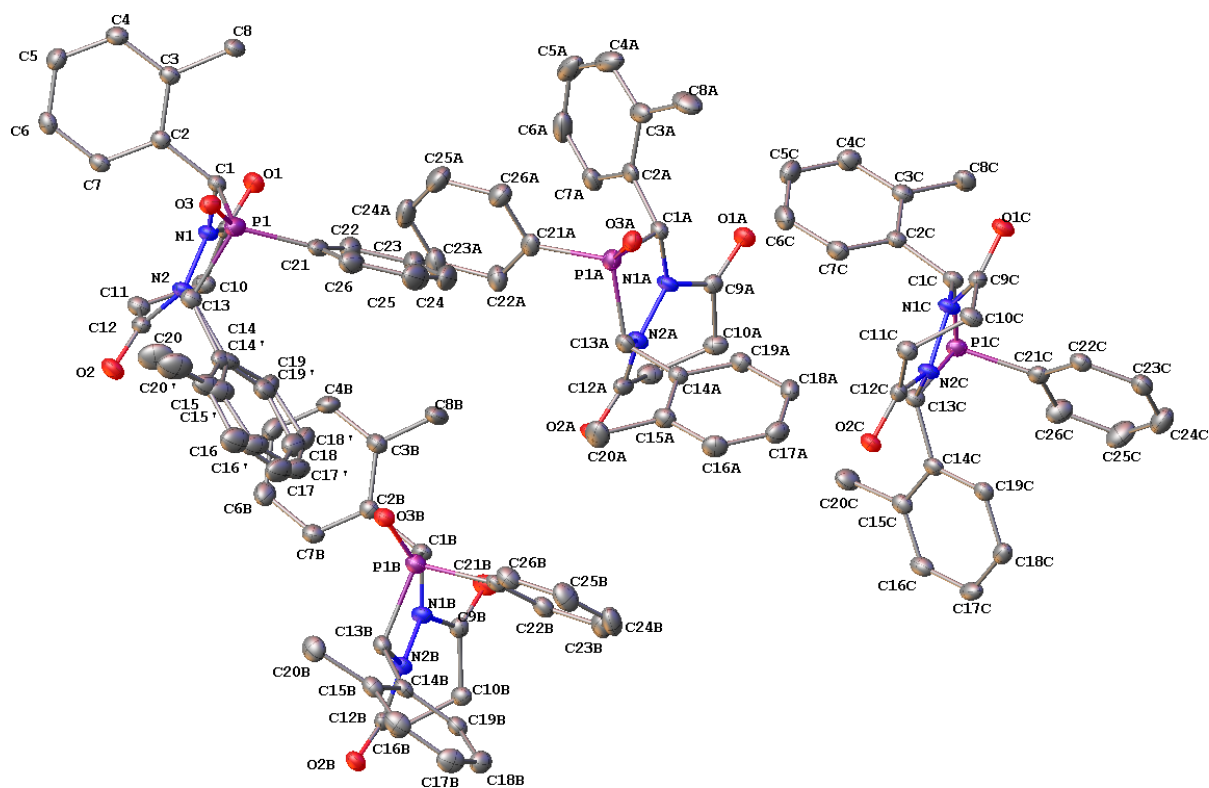


Figure A3.47. The asymmetric unit of *o*-Me DiazaPhos **16**, including all disordered components.

All atoms are drawn as 50% thermal probability ellipsoids. All H atoms are omitted for clarity.

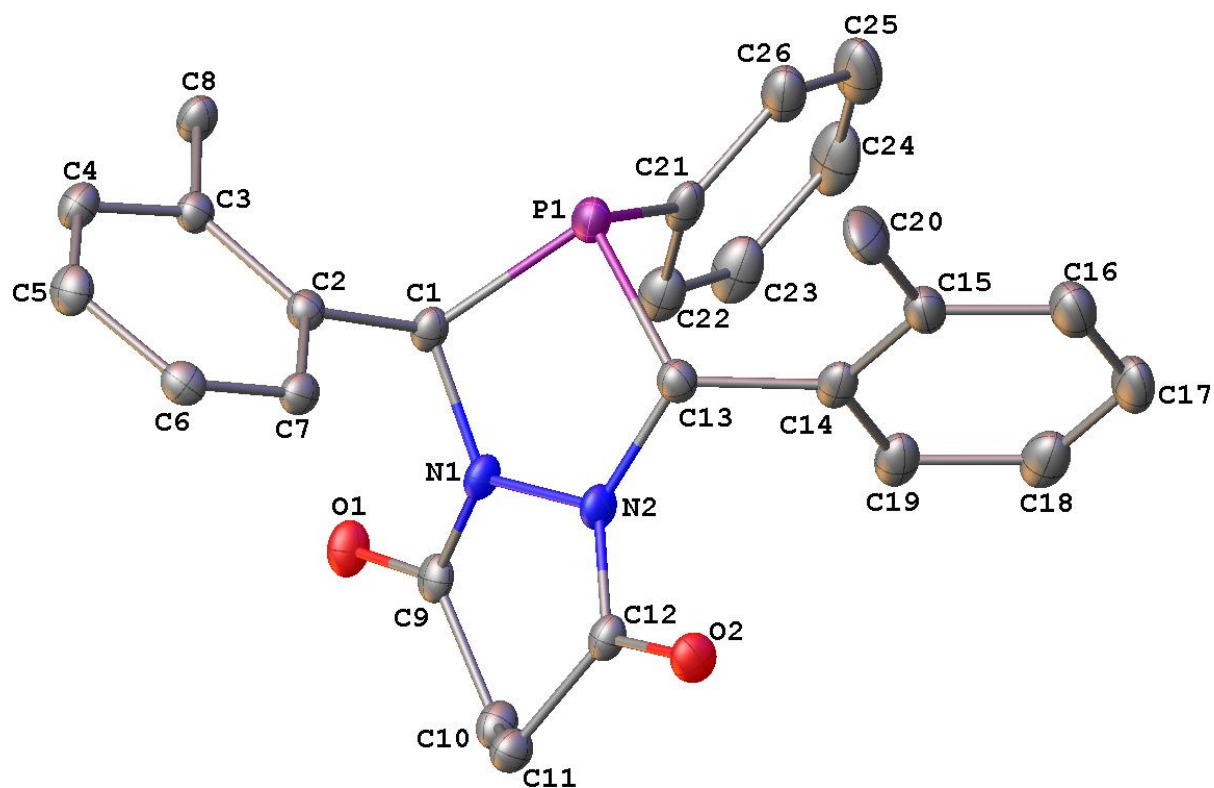


Figure A3.48. A molecular drawing of phosphine of *o*-Me DiazaPhos **16** shown with 50% thermal probability ellipsoids. All H atoms and minor disordered components are omitted for clarity.

Figure A3.49. The phosphine oxide of o-Me DiazaPhos **16**. All atoms are drawn as 50% thermal probability ellipsoids. All H atoms and minor disordered components are omitted for clarity.

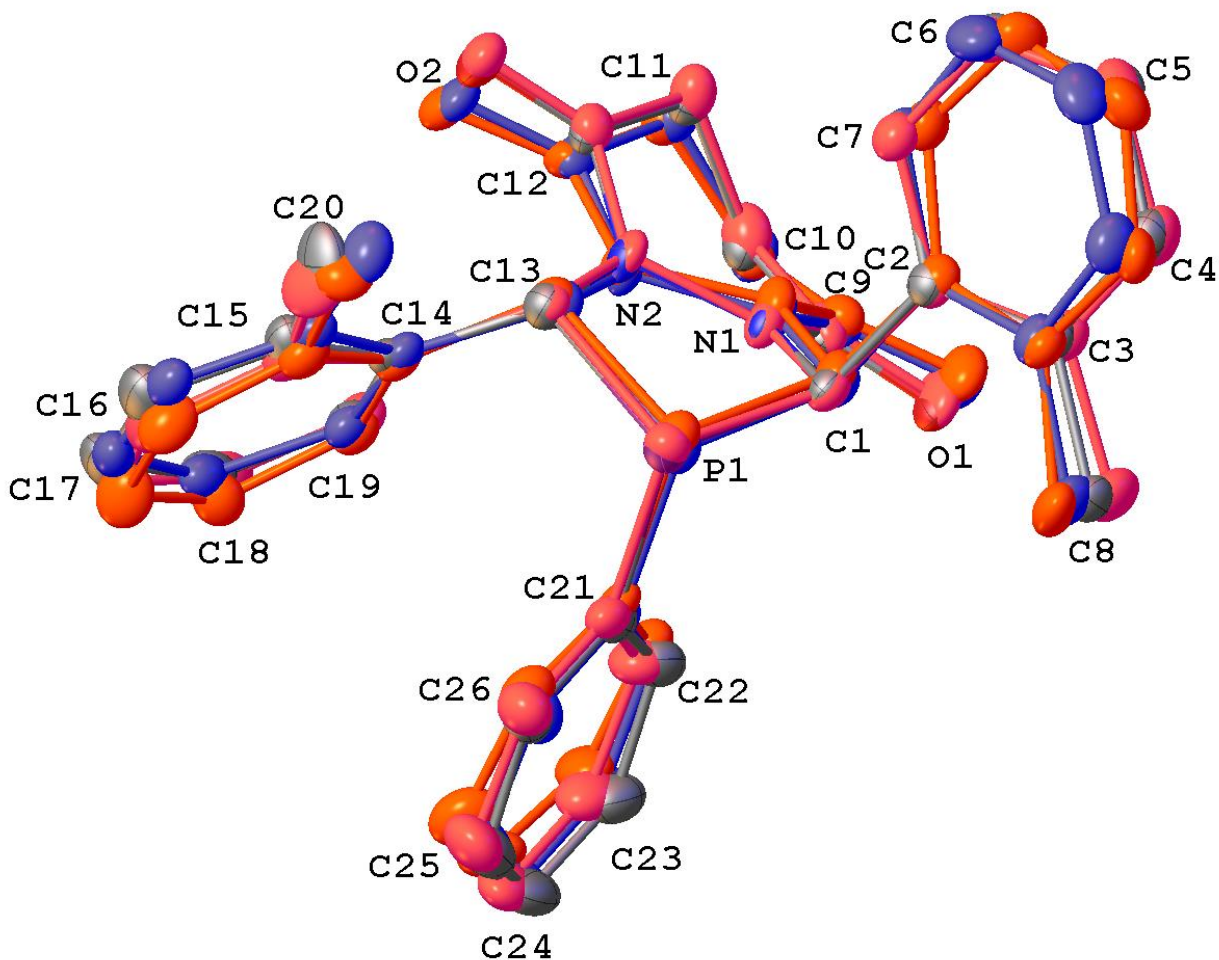


Figure A3.50. The overlay diagram of the phosphine moelcules of *o*-Me DiazaPhos **16**. All atoms are drawn as 50% thermal probability ellipsoids. All H atoms and disordered components are omitted for clarity.

Data Collection

A colorless crystal with approximate dimensions 0.494 x 0.138 x 0.110 mm³ was selected under oil under ambient conditions and attached to the tip of a MiTeGen MicroMount®. The crystal was mounted in a stream of cold nitrogen at 100(1) K and centered in the X-ray beam by using a video camera.

The crystal evaluation and data collection were performed on a Bruker SMART APEXII diffractometer with Cu K α ($\lambda = 1.54178 \text{ \AA}$) radiation and the diffractometer to crystal distance of 4.03 cm.

The initial cell constants were obtained from three series of ω scans at different starting angles. Each series consisted of 41 frames collected at intervals of 0.6° in a 25° range about ω with the exposure time of 10 seconds per frame. The reflections were successfully indexed by an automated indexing routine built in the APEXII program. The final cell constants were calculated from a set of 9683 strong reflections from the actual data collection.

The data were collected by using the full sphere data collection routine to survey the reciprocal space to the extent of a full sphere to a resolution of 0.82 \AA . A total of 150239 data were harvested by collecting 15 sets of frames with 0.6° scans in ω and ϕ with an exposure time 5-10 sec per frame. These highly redundant datasets were corrected for Lorentz and polarization effects. The absorption correction was based on fitting a function to the empirical transmission surface as sampled by multiple equivalent measurements. [1]

Structure Solution and Refinement

The systematic absences in the diffraction data were uniquely consistent for the space group $P2_1/n$ that yielded chemically reasonable and computationally stable results of refinement [2-4].

A successful solution by the direct methods provided most non-hydrogen atoms from the E -map. The remaining non-hydrogen atoms were located in an alternating series of least-squares cycles and difference Fourier maps. All hydrogen atoms were included in the structure factor calculation at idealized positions and were allowed to ride on the neighboring atoms with relative isotropic displacement coefficients.

The asymmetric unit (Figure 1) consists of four molecules of the phosphine shown in Figure 2. Three of these molecules are compositionally disordered with the corresponding

phosphine oxide (Figure 3) (oxide occupancy: O3 = 19.6(3)%, O3A = 14.3(3)%, O3B = 10.7(3)%). There is also positional disorder in tolyl group C14 (major component: 55(2)%). Bond distance and thermal parameter restraints were used to ensure a chemically reasonable and computationally stable refinement of the disordered components.

Figure 4 shows an overlay diagram of the four symmetry independent phosphine molecules of Landis49. Molecules P1A and P1B can be overlaid with molecule P1 (RMSD = 0.170 Å, 0.319 Å, respectively). Molecule P1C can be overlaid with molecule P1 with an inversion (RMSD = 0.299 Å). The molecules differ primarily in bond angle $\angle(\text{C9-C10-C11})$ and the conformation of their tolyl groups.

The final least-squares refinement of 1178 parameters against 17451 data resulted in residuals R (based on F^2 for $I \geq 2\sigma$) and wR (based on F^2 for all data) of 0.0414 and 0.1045, respectively. The final difference Fourier map was featureless.

Summary

Crystal data for $\text{C}_{104}\text{H}_{100}\text{N}_8\text{O}_{8.44595}\text{P}_4$ ($M=1720.93$): monoclinic, space group $P2_1/n$ (no. 14), $a = 14.190(3)$ Å, $b = 25.468(3)$ Å, $c = 25.267(2)$ Å, $\beta = 100.803(6)^\circ$, $V = 8969(2)$ Å³, $Z = 4$, $T = 100.0$ K, $\mu(\text{CuK}\alpha) = 1.288$ mm⁻¹, $D_{\text{calc}} = 1.274$ g/mm³, 150239 reflections measured ($4.972 \leq 2\theta \leq 146.546$), 17451 unique ($R_{\text{int}} = 0.0527$, $R_{\text{sigma}} = 0.0287$) which were used in all calculations. The final R_1 was 0.0414 ($I > 2\sigma(I)$) and wR_2 was 0.1045 (all data).

References

- [1] Bruker-AXS. (2007-2013) APEX2 (Ver. 2013.2-0), SADABS (2012-1), and SAINT+ (Ver. 8.30C) Software Reference Manuals. Bruker-AXS, Madison, Wisconsin, USA.
- [2] Sheldrick, G. M. (2008) SHELXL. *Acta Cryst.* **A64**, 112-122.

- [3] Dolomanov, O.V.; Bourhis, L.J.; Gildea, R.J.; Howard, J.A.K.; Puschmann, H. "OLEX2: a complete structure solution, refinement and analysis program". *J. Appl. Cryst.* (2009) **42**, 339-341.
- [4] Guzei, I.A. (2013). Internal laboratory computer programs Gn.

Table A3.62. Crystal data and structure refinement for *o*-Me DiazaPhos **16**.

Empirical formula	3.55 C ₂₆ H ₂₅ N ₂ O ₂ P, 0.45 C ₂₆ H ₂₅ N ₂ O ₃ P
Formula weight	1720.93
Temperature/K	100(1)
Crystal system	monoclinic
Space group	<i>P</i> 2 ₁ / <i>n</i>
<i>a</i> /Å	14.190(3)
<i>b</i> /Å	25.468(3)
<i>c</i> /Å	25.267(2)
α /°	90
β /°	100.803(6)
γ /°	90
Volume/Å ³	8969(2)
<i>Z</i>	4
ρ_{calc} mg/mm ³	1.274
μ /mm ⁻¹	1.288
<i>F</i> (000)	3630.0
Crystal size/mm ³	0.494 × 0.138 × 0.11
Radiation	CuK α (λ = 1.54178)
2 θ range for data collection	4.972 to 146.546°
Index ranges	-15 ≤ <i>h</i> ≤ 17, -31 ≤ <i>k</i> ≤ 30, -31 ≤ <i>l</i> ≤ 30
Reflections collected	150239
Independent reflections	17451 [<i>R</i> _{int} = 0.0527, <i>R</i> _{sigma} = 0.0287]
Data/restraints/parameters	17451/195/1178
Goodness-of-fit on <i>F</i> ²	1.022
Final <i>R</i> indexes [<i>I</i> ≥ 2 σ (<i>I</i>)]	<i>R</i> ₁ = 0.0414, <i>wR</i> ₂ = 0.0974
Final <i>R</i> indexes [all data]	<i>R</i> ₁ = 0.0544, <i>wR</i> ₂ = 0.1045
Largest diff. peak/hole / e Å ⁻³	0.68/-0.45

Table A3.63. Fractional Atomic Coordinates ($\times 10^4$) and Equivalent Isotropic Displacement Parameters ($\text{\AA}^2 \times 10^3$) for *o*-Me DiazaPhos **16**. U_{eq} is defined as 1/3 of the trace of the orthogonalised U_{ij} tensor.

Atom	<i>x</i>	<i>y</i>	<i>z</i>	$U(\text{eq})$
P1	5149.4(3)	4899.2(2)	2977.4(2)	23.79(10)
O1	3731.6(9)	6371.6(5)	2321.4(5)	25.9(3)
O2	7525.4(9)	6071.5(5)	2815.5(5)	25.8(3)
O3	5327(4)	4354.3(17)	2856(2)	23.79(10)
N1	5027.5(10)	5851.1(6)	2549.4(6)	19.5(3)
N2	6009.4(10)	5806.6(6)	2798.6(6)	20.5(3)
C1	4538.6(12)	5348.9(7)	2436.0(7)	20.3(3)
C2	4553.1(12)	5146.0(7)	1873.0(7)	18.7(3)
C3	3764.5(12)	4869.8(7)	1585.7(7)	19.3(3)
C4	3779.4(13)	4724.5(7)	1057.4(7)	24.1(4)
C5	4559.0(13)	4832.5(7)	816.4(7)	25.0(4)
C6	5347.3(12)	5091.2(7)	1106.2(7)	21.3(4)
C7	5341.7(12)	5248.2(7)	1630.7(7)	20.2(3)
C8	2896.0(13)	4746.0(7)	1830.0(7)	24.5(4)
C9	4599.2(12)	6329.8(7)	2472.7(6)	20.0(4)
C10	5301.7(13)	6777.1(7)	2567.2(7)	23.8(4)
C11	6226.2(13)	6630.6(7)	2374.3(7)	23.3(4)
C12	6667.2(12)	6150.6(7)	2667.4(7)	20.3(4)
C13	6281.7(13)	5305.2(7)	3063.5(7)	21.8(4)
C21	4606.0(13)	5091.0(8)	3550.4(7)	27.3(4)
C22	4115.4(14)	5556.9(9)	3594.5(8)	32.2(4)
C23	3707.6(15)	5650.9(10)	4045.5(8)	39.8(5)
C24	3785.0(17)	5282.9(11)	4452.6(8)	46.9(6)
C25	4264.0(17)	4820.1(11)	4411.3(9)	47.0(6)
C26	4677.2(15)	4720.3(9)	3963.4(8)	36.1(5)
C14	6799(9)	5332(5)	3636(3)	25.3(13)
C15	7441(8)	4938(4)	3843(3)	30.5(12)
C16	7900(6)	4953(4)	4379(3)	40.5(17)
C17	7717(6)	5363(4)	4709(3)	39.3(18)
C18	7075(7)	5757(4)	4503(3)	38.7(15)
C19	6616(8)	5742(4)	3966(3)	30.7(13)
C20	7715(11)	4505(5)	3494(5)	40(2)
C14'	6732(11)	5389(6)	3664(3)	26.2(17)
C15'	7362(10)	5020(5)	3938(4)	36.0(17)
C16'	7731(7)	5086(4)	4484(4)	34.0(18)
C17'	7471(8)	5521(5)	4755(3)	36.5(18)

C18'	6842(9)	5891(5)	4481(4)	36.9(17)
C19'	6472(10)	5825(5)	3936(4)	31.5(15)
C20'	7654(14)	4542(8)	3658(6)	47(3)
P1A	1343.3(3)	6940.5(2)	4786.8(2)	21.48(10)
O1A	-723.1(9)	8265.6(5)	5000.7(5)	23.9(3)
O2A	3107.3(9)	8350.1(6)	5375.7(5)	31.7(3)
O3A	1168(6)	6408(2)	4956(3)	21.48(10)
N1A	715.8(10)	7915.0(6)	4966.2(6)	20.2(3)
N2A	1716.2(10)	7905.7(6)	5168.7(6)	20.5(3)
C1A	317.3(12)	7426.1(7)	4717.2(7)	19.1(3)
C2A	-206.1(12)	7494.5(7)	4142.5(7)	21.5(4)
C3A	-908.7(13)	7127.5(8)	3923.5(8)	28.0(4)
C4A	-1318.1(16)	7165.2(10)	3379.2(9)	40.3(5)
C5A	-1070.8(16)	7564.2(10)	3064.2(8)	44.1(6)
C6A	-416.3(16)	7940.8(10)	3287.0(8)	39.6(5)
C7A	24.5(13)	7901.7(8)	3824.7(8)	28.5(4)
C8A	-1250.9(15)	6710.3(8)	4266.1(9)	38.1(5)
C9A	148.2(12)	8299.0(7)	5115.7(7)	19.5(4)
C10A	705.6(13)	8757.3(7)	5390.4(7)	24.6(4)
C11A	1619.8(14)	8842.5(7)	5163.3(8)	26.8(4)
C12A	2233.8(13)	8357.9(7)	5241.7(7)	22.8(4)
C13A	2114.0(12)	7380.3(7)	5283.3(7)	21.1(4)
C14A	2140.1(12)	7216.0(7)	5863.9(7)	20.1(3)
C15A	2937.0(13)	6948.2(7)	6154.2(7)	24.1(4)
C16A	2928.7(14)	6811.3(8)	6686.0(8)	29.0(4)
C17A	2150.4(14)	6923.8(8)	6928.9(7)	27.8(4)
C18A	1368.0(13)	7185.9(7)	6639.5(7)	24.4(4)
C19A	1367.7(13)	7333.2(7)	6112.9(7)	22.9(4)
C20A	3796.9(14)	6814.7(9)	5905.5(8)	35.6(5)
C21A	1812.2(13)	7044.8(8)	4168.0(7)	24.8(4)
C22A	2334.7(14)	7481.5(8)	4055.2(8)	31.4(4)
C23A	2651.2(15)	7515.9(9)	3569.4(8)	37.0(5)
C24A	2457.1(16)	7117.4(10)	3193.1(8)	40.0(5)
C25A	1933.6(17)	6685(1)	3297.4(8)	41.9(5)
C26A	1614.5(15)	6648.3(9)	3784.2(8)	32.5(4)
P1B	6968.3(3)	7031.4(2)	5613.9(2)	21.1(1)
O1B	5883.3(9)	8657.7(5)	5645.6(5)	26.6(3)
O2B	9571.0(8)	8091.2(5)	6230.0(5)	21.6(3)
O3B	6850(8)	6574(3)	5265(4)	21.1(1)
N1B	7094(1)	8082.0(6)	5653.5(6)	19.2(3)
N2B	8010.3(10)	7894.4(5)	5934.8(6)	18.0(3)

C1B	6465.6(12)	7681.0(7)	5364.0(7)	19.2(3)
C2B	6356.7(12)	7707.1(7)	4754.5(7)	19.7(3)
C3B	5535.4(13)	7484.9(8)	4434.6(7)	25.6(4)
C4B	5442.0(14)	7510.6(8)	3877.3(8)	29.0(4)
C5B	6141.5(15)	7736.5(8)	3636.3(8)	28.9(4)
C6B	6956.6(14)	7942.7(8)	3953.6(8)	29.0(4)
C7B	7058.7(13)	7931.2(7)	4511.5(7)	24.0(4)
C8B	4769.7(15)	7226.8(10)	4686.3(8)	37.3(5)
C9B	6721.8(12)	8540.2(7)	5811.8(7)	20.4(4)
C10B	7441.7(12)	8876.0(7)	6174.2(7)	20.7(4)
C11B	8440.9(12)	8806.7(7)	6040.6(7)	20.0(3)
C12B	8748.3(12)	8243.8(7)	6074.3(6)	17.9(3)
C13B	8181.5(12)	7335.6(7)	5859.0(7)	19.2(3)
C14B	8682.2(12)	7057.7(7)	6366.0(7)	18.9(3)
C15B	9154.7(13)	6579.2(7)	6324.6(7)	23.0(4)
C16B	9535.5(14)	6314.0(7)	6799.7(8)	28.3(4)
C17B	9463.6(14)	6510.9(8)	7299.6(8)	30.3(4)
C18B	9003.9(14)	6985.7(7)	7335.9(7)	26.3(4)
C19B	8613.6(12)	7257.1(7)	6871.8(7)	20.8(4)
C20B	9277.0(14)	6354.0(7)	5790.1(8)	28.6(4)
C21B	6557.2(12)	6950.7(7)	6251.2(7)	21.0(4)
C22B	6267.4(13)	7353.2(7)	6559.6(7)	24.0(4)
C23B	6054.4(14)	7244.0(8)	7064.1(8)	29.9(4)
C24B	6139.6(15)	6735.9(9)	7260.3(9)	35.5(5)
C25B	6412.6(15)	6333.9(8)	6954.0(9)	34.8(5)
C26B	6614.7(13)	6440.6(7)	6451.0(8)	27.4(4)
P1C	250.2(3)	5248.9(2)	7973.7(2)	19.87(10)
O1C	-971.1(9)	3637.2(5)	7970.6(5)	24.2(3)
O2C	2771.4(8)	4100.0(5)	8465.3(5)	22.1(3)
N1C	266.8(10)	4195.6(6)	7994.2(6)	19.9(3)
N2C	1218.9(10)	4346.1(6)	8253.4(6)	18.7(3)
C1C	-307.8(12)	4615.1(7)	7702.2(7)	19.5(3)
C2C	-337.9(12)	4609.9(7)	7097.7(7)	19.5(3)
C3C	-1099.0(12)	4855.8(7)	6749.5(7)	21.5(4)
C4C	-1071.2(14)	4873.7(8)	6203.1(7)	28.1(4)
C5C	-307.3(15)	4668.2(8)	5998.4(8)	32.1(4)
C6C	441.5(14)	4431.5(8)	6345.0(8)	31.4(4)
C7C	418.4(13)	4397.2(7)	6889.6(7)	25.6(4)
C8C	-1922.0(13)	5098.6(8)	6957.7(7)	26.9(4)
C9C	-121.5(12)	3735.7(7)	8131.5(7)	20.1(4)
C10C	591.6(12)	3375.4(7)	8461.0(7)	22.8(4)

C11C	1565.5(12)	3418.6(7)	8286.8(7)	21.5(4)
C12C	1928.5(12)	3973.3(7)	8338.0(6)	18.9(3)
C13C	1431.1(12)	4901.5(6)	8172.0(7)	18.5(3)
C14C	2038.2(12)	5164.9(7)	8655.5(7)	18.8(3)
C15C	2599.7(12)	5601.2(7)	8578.8(7)	20.4(4)
C16C	3122.8(13)	5849.0(7)	9031.0(7)	23.4(4)
C17C	3093.5(13)	5677.2(7)	9547.2(7)	25.5(4)
C18C	2529.7(13)	5247.4(7)	9620.2(7)	23.9(4)
C19C	2002.4(12)	4993.6(7)	9175.9(7)	20.4(3)
C20C	2668.5(14)	5801.7(8)	8025.0(8)	27.9(4)
C21C	-146.5(12)	5332.3(7)	8616.8(7)	21.5(4)
C22C	-498.6(12)	4938.6(7)	8910.0(7)	22.6(4)
C23C	-795.4(13)	5056.4(8)	9390.5(7)	27.3(4)
C24C	-738.5(16)	5566.7(9)	9582.2(8)	35.0(5)
C25C	-380.6(17)	5961.7(9)	9299.8(8)	38.3(5)
C26C	-92.5(15)	5845.7(8)	8816.7(8)	30.4(4)

Table A3.64. Anisotropic Displacement Parameters ($\text{\AA}^2 \times 10^3$) for o-Me DiazaPhos **16**. The Anisotropic displacement factor exponent takes the form: $-2\pi^2[h^2a^{*2}U_{11}+2hka^*b^*U_{12}+\dots]$.

Atom	U_{11}	U_{22}	U_{33}	U_{23}	U_{13}	U_{12}
P1	21.9(2)	29.7(2)	19.0(2)	0.91(18)	1.77(17)	-4.86(18)
O1	14.6(7)	38.0(8)	24.6(6)	-2.0(5)	2.4(5)	3.6(5)
O2	14.5(7)	33.0(7)	29.5(7)	2.6(5)	3.0(5)	-0.2(5)
O3	21.9(2)	29.7(2)	19.0(2)	0.91(18)	1.77(17)	-4.86(18)
N1	11.5(7)	26.3(8)	19.7(7)	-3.0(6)	-0.2(5)	-1.7(5)
N2	11.8(8)	26.3(8)	21.7(7)	1.0(6)	-1.5(6)	-0.7(6)
C1	13.9(9)	27.6(9)	19.0(8)	-0.9(7)	2.3(6)	-3.3(7)
C2	15.9(9)	20.5(8)	19.2(8)	1.2(7)	1.9(6)	1.3(6)
C3	15.3(9)	21.4(8)	20.2(8)	1.7(7)	0.9(7)	0.2(6)
C4	19.7(10)	26.8(9)	24.3(9)	-3.9(7)	0.4(7)	-2.4(7)
C5	25(1)	29.9(10)	20.7(9)	-3.5(7)	5.5(7)	1.2(7)
C6	18.0(9)	23.1(9)	24.1(9)	2.1(7)	7.2(7)	3.0(7)
C7	14.3(9)	22.7(9)	22.7(9)	0.6(7)	1.1(7)	-0.2(6)
C8	17.8(10)	33.3(10)	21.8(9)	-0.5(7)	2.2(7)	-7.2(7)
C9	17.8(10)	28.5(9)	13.9(8)	-3.5(7)	3.7(7)	1.0(7)
C10	19.8(10)	25.4(9)	24.7(9)	-3.5(7)	0.0(7)	2.6(7)
C11	17.9(10)	25.0(9)	26.1(9)	0.4(7)	1.5(7)	-1.8(7)
C12	15.4(10)	26.7(9)	18.4(8)	-3.5(7)	2.2(7)	-1.7(7)
C13	18.6(9)	25.4(9)	21.0(9)	2.3(7)	2.5(7)	-1.5(7)
C21	19.8(10)	41.7(11)	19.6(9)	-1.2(8)	1.9(7)	-13.1(8)

C22	27.0(11)	45.8(12)	24.8(10)	-2.2(8)	7.6(8)	-9.8(9)
C23	27.6(12)	63.6(15)	30.5(11)	-8.3(10)	11.0(9)	-9.6(10)
C24	36.7(14)	83.9(19)	22.7(10)	-5.2(11)	12.1(9)	-17.6(12)
C25	41.4(14)	74.9(18)	24.2(11)	11.4(11)	5.0(9)	-18.8(12)
C26	30.3(12)	51.8(13)	24.9(10)	4.5(9)	2.0(8)	-12.5(9)
C14	22(3)	37(3)	18(2)	1(2)	6(2)	-12(2)
C15	28(2)	35(3)	25(3)	8(2)	-2(2)	-8(2)
C16	39(3)	51(4)	29(3)	11(3)	0(2)	-10(2)
C17	41(3)	54(4)	21(2)	8(3)	1(2)	-14(3)
C18	36(4)	54(4)	27(2)	-1(3)	8(2)	-18(3)
C19	23(3)	44(3)	24(2)	1(2)	4(2)	-11(2)
C20	42(3)	34(3)	39(5)	9(4)	-11(4)	10(2)
C14'	16(3)	37(4)	23(3)	7(3)	-3(3)	-8(3)
C15'	33(3)	44(4)	28(3)	9(3)	-3(3)	-12(3)
C16'	34(3)	41(4)	23(3)	8(3)	-3(3)	-13(3)
C17'	34(4)	53(5)	20(2)	6(3)	-1(3)	-20(3)
C18'	37(4)	52(4)	23(3)	-10(3)	12(3)	-16(3)
C19'	25(3)	50(4)	20(3)	-9(3)	7(2)	-12(3)
C20'	43(4)	53(5)	39(7)	14(5)	-10(5)	-1(4)
P1A	20.3(2)	25.3(2)	19.1(2)	-0.87(17)	4.55(17)	2.89(17)
O1A	15.3(7)	31.3(7)	24.2(6)	-1.0(5)	1.0(5)	3.1(5)
O2A	16.4(8)	45.1(8)	31.3(7)	1.2(6)	-1.2(5)	-8.5(6)
O3A	20.3(2)	25.3(2)	19.1(2)	-0.87(17)	4.55(17)	2.89(17)
N1A	10.3(7)	24.3(8)	24.4(8)	-1.8(6)	-1.0(6)	-0.9(5)
N2A	12.6(8)	25.8(8)	21.8(7)	1.4(6)	-0.1(6)	-0.3(6)
C1A	13.9(9)	23.1(9)	20.5(8)	-1.8(7)	4.1(7)	-1.8(6)
C2A	11.9(9)	31.8(10)	21.3(9)	-3.5(7)	4.6(7)	3.7(7)
C3A	17(1)	35.1(11)	31.1(10)	-11.2(8)	2.3(8)	3.5(7)
C4A	26.6(12)	53.4(14)	37.0(12)	-19.2(10)	-4.3(9)	6.3(9)
C5A	32.6(13)	74.7(17)	21.7(10)	-8.5(10)	-3.4(9)	19.2(11)
C6A	30.8(12)	63.7(15)	26.8(10)	10.4(10)	12.1(9)	13.8(10)
C7A	17(1)	44.0(12)	25.3(9)	3.8(8)	5.9(7)	1.2(8)
C8A	27.3(12)	34.0(11)	51.6(13)	-10.3(10)	3.6(10)	-9.8(9)
C9A	19(1)	22.5(9)	16.3(8)	2.1(6)	1.7(7)	0.8(7)
C10A	23.1(10)	23.6(9)	25.0(9)	-2.1(7)	-1.4(7)	0.5(7)
C11A	27.6(11)	25.0(9)	25.8(9)	1.9(7)	0.0(8)	-6.8(7)
C12A	20(1)	32.1(10)	15.6(8)	0.7(7)	1.8(7)	-7.6(7)
C13A	13.1(9)	27.8(9)	22.2(9)	0.5(7)	2.7(7)	1.6(7)
C14A	16.2(9)	23.4(9)	20.2(8)	-0.8(7)	2.1(7)	-0.7(6)
C15A	18.9(10)	28.1(10)	24.1(9)	-0.9(7)	0.9(7)	2.7(7)
C16A	24.0(11)	34.5(11)	25.9(10)	3.6(8)	-2.3(8)	4.5(8)

C17A	31.5(11)	31.2(10)	19.5(9)	2.9(7)	1.8(8)	-3.0(8)
C18A	21.9(10)	29.3(10)	23.5(9)	-4.7(7)	8.1(7)	-3.7(7)
C19A	17.7(9)	27.1(9)	23.2(9)	-0.5(7)	2.1(7)	1.4(7)
C20A	22.5(11)	51.9(13)	31.7(11)	4.7(9)	3.7(8)	13.4(9)
C21A	17.9(10)	36.6(10)	20.1(9)	1.9(7)	4.2(7)	8.3(7)
C22A	26.0(11)	41.2(12)	29.5(10)	-0.8(8)	11.9(8)	1.8(8)
C23A	28.7(12)	52.6(13)	32.6(11)	7(1)	13.4(9)	5.6(9)
C24A	31.4(12)	69.8(16)	20.7(10)	3.8(10)	9.6(9)	10.4(10)
C25A	40.7(14)	60.7(15)	24.3(10)	-11.3(10)	5.9(9)	3.1(11)
C26A	29.6(11)	42.6(12)	25.4(10)	-6.3(8)	5.1(8)	1.6(9)
P1B	17.2(2)	23.2(2)	22.4(2)	-0.30(17)	2.31(17)	-1.13(16)
O1B	17.0(7)	29.4(7)	31.3(7)	-2.3(5)	-0.8(5)	5.7(5)
O2B	14.0(7)	27.4(6)	23.2(6)	2.7(5)	3.1(5)	-0.3(5)
O3B	17.2(2)	23.2(2)	22.4(2)	-0.30(17)	2.31(17)	-1.13(16)
N1B	13.7(7)	21.9(7)	20.4(7)	-1.5(6)	-1.2(6)	2.4(5)
N2B	12.1(7)	21.2(7)	19.6(7)	0.5(6)	0.3(5)	2.1(5)
C1B	13.9(9)	23.4(9)	19.7(8)	-1.8(7)	1.2(6)	-0.3(6)
C2B	16.6(9)	22.3(9)	19.9(8)	-1.1(7)	2.5(7)	1.4(6)
C3B	16.9(10)	34.4(10)	25.2(9)	-4.0(8)	3.4(7)	-2.3(7)
C4B	21.1(10)	40.8(11)	23.0(9)	-7.1(8)	-1.2(7)	-5.5(8)
C5B	34.1(11)	33.4(10)	19.7(9)	-4.0(8)	6.2(8)	-3.3(8)
C6B	31.5(11)	29.7(10)	27.8(10)	-2.0(8)	10.5(8)	-8.3(8)
C7B	20(1)	27.0(9)	24.0(9)	-2.8(7)	1.8(7)	-4.3(7)
C8B	20.8(11)	63.6(15)	26.7(10)	-4.9(10)	2.4(8)	-15.3(9)
C9B	19.3(10)	24.1(9)	17.8(8)	1.4(7)	3.3(7)	2.2(7)
C10B	17.5(9)	22.4(9)	21.3(8)	-1.9(7)	1.5(7)	2.5(7)
C11B	18.6(9)	22.7(9)	18.6(8)	0.6(7)	3.0(7)	-1.6(7)
C12B	15.4(9)	24.4(9)	14.4(8)	0.8(6)	4.6(6)	-0.8(6)
C13B	16.0(9)	21.5(8)	20.8(8)	-1.3(7)	5.4(7)	-0.3(6)
C14B	12.1(9)	21.1(8)	23.4(9)	2.2(7)	3.5(7)	-1.5(6)
C15B	17.6(9)	22.9(9)	28.7(9)	0.9(7)	5.1(7)	-1.3(7)
C16B	23.5(10)	21.9(9)	38.3(11)	5.5(8)	3.1(8)	2.5(7)
C17B	31.6(11)	28.3(10)	29(1)	10.4(8)	0.1(8)	-0.6(8)
C18B	27.3(11)	29.5(10)	22.1(9)	2.6(7)	4.3(8)	-3.6(8)
C19B	15.6(9)	23.3(9)	23.8(9)	1.4(7)	4.2(7)	-1.8(7)
C20B	27.2(11)	25.1(10)	34.4(10)	-1.9(8)	8.3(8)	5.0(7)
C21B	11.4(9)	27.4(9)	23.7(9)	1.1(7)	1.7(7)	-1.8(7)
C22B	16.0(9)	28.8(10)	26.9(9)	1.2(7)	3.6(7)	0.8(7)
C23B	19.2(10)	42.0(12)	29.6(10)	-0.1(8)	7.5(8)	5.3(8)
C24B	24.8(11)	52.3(13)	32.2(11)	11.0(9)	12.3(9)	3.3(9)
C25B	29.5(12)	34.6(11)	41.6(12)	12.5(9)	10.1(9)	-1.3(8)

C26B	21.1(10)	26.8(10)	34.4(10)	0.9(8)	5.2(8)	-2.4(7)
P1C	16.8(2)	23.0(2)	18.5(2)	1.10(16)	0.00(16)	-0.13(16)
O1C	14.7(7)	31.1(7)	25.9(6)	0.3(5)	1.5(5)	-5.5(5)
O2C	12.5(7)	28.3(7)	24.9(6)	-1.0(5)	2.3(5)	-0.7(5)
N1C	11.4(7)	23.9(7)	22.1(7)	2.0(6)	-2.5(6)	-2.3(5)
N2C	11.3(7)	21.9(7)	21.1(7)	-0.1(6)	-1.5(5)	-2.4(5)
C1C	13.6(9)	23.5(9)	20.3(8)	0.6(7)	0.0(6)	0.7(6)
C2C	14.8(9)	22.7(9)	20.0(8)	-1.4(7)	1.0(7)	-3.2(6)
C3C	16.5(9)	23.8(9)	23.1(9)	0.7(7)	1.1(7)	-2.6(7)
C4C	25.1(11)	34.1(10)	23.1(9)	4.0(8)	-0.4(7)	-1.2(8)
C5C	34.1(12)	43.6(12)	19.8(9)	-1.6(8)	8.5(8)	-6.9(9)
C6C	23.7(11)	40.5(11)	32.9(11)	-7.2(9)	12.4(8)	-1.3(8)
C7C	16.2(10)	32.5(10)	26.9(9)	-3.7(8)	1.3(7)	1.5(7)
C8C	17.1(10)	37.2(11)	24.9(9)	3.2(8)	0.1(7)	4.4(7)
C9C	17.2(10)	26.0(9)	17.1(8)	-2.7(7)	3.2(7)	-3.6(7)
C10C	17.5(9)	24.6(9)	25.2(9)	2.9(7)	1.4(7)	-3.2(7)
C11C	18.1(9)	23.4(9)	22.5(9)	0.2(7)	2.2(7)	1.0(7)
C12C	16.3(9)	25.9(9)	14.5(8)	0.2(6)	3.2(6)	0.0(7)
C13C	15.8(9)	20.0(8)	19.1(8)	1.7(6)	1.7(6)	-1.8(6)
C14C	12.3(9)	21.7(9)	21.6(8)	-0.8(7)	1.0(6)	1.9(6)
C15C	15.7(9)	20.0(8)	25.2(9)	0.0(7)	3.0(7)	1.9(6)
C16C	17.1(9)	21.0(9)	31.1(10)	-4.5(7)	2.1(7)	-0.2(7)
C17C	18.6(10)	30.6(10)	25.6(9)	-10.5(8)	-0.3(7)	2.0(7)
C18C	19.4(10)	33.5(10)	18.6(8)	-1.9(7)	2.9(7)	5.7(7)
C19C	14.2(9)	24.7(9)	21.7(8)	0.4(7)	2.3(7)	1.6(6)
C20C	24.7(10)	29.9(10)	28.3(10)	4.5(8)	2.7(8)	-7.4(8)
C21C	15.0(9)	28.3(9)	19.4(8)	-0.5(7)	-1.5(7)	2.6(7)
C22C	14.8(9)	27.3(9)	24.4(9)	-1.1(7)	0.5(7)	0.3(7)
C23C	17.4(10)	38.5(11)	25.6(9)	0.3(8)	2.9(7)	-0.3(8)
C24C	36.9(12)	44.9(12)	23.3(10)	-4.6(9)	6.0(8)	5.1(9)
C25C	50.8(14)	32.1(11)	30.6(11)	-9.0(9)	4.3(10)	2.9(9)
C26C	36.0(12)	26.1(10)	27.5(10)	-0.5(8)	1.9(8)	0.6(8)

Table A3.65. Bond Lengths for *o*-Me DiazaPhos **16**.

Atom	Atom	Length/Å	Atom	Atom	Length/Å
P1	O3	1.453(4)	C22A	C23A	1.387(3)
P1	C1	1.8682(18)	C23A	C24A	1.383(3)
P1	C13	1.8888(18)	C24A	C25A	1.381(3)
P1	C21	1.8297(19)	C25A	C26A	1.391(3)
O1	C9	1.223(2)	P1B	O3B	1.451(5)

O2	C12	1.222(2)	P1B	C1B	1.8642(18)
N1	N2	1.422(2)	P1B	C13B	1.8836(18)
N1	C1	1.458(2)	P1B	C21B	1.8242(18)
N1	C9	1.360(2)	O1B	C9B	1.222(2)
N2	C12	1.366(2)	O2B	C12B	1.223(2)
N2	C13	1.460(2)	N1B	N2B	1.4414(19)
C1	C2	1.517(2)	N1B	C1B	1.459(2)
C2	C3	1.403(2)	N1B	C9B	1.371(2)
C2	C7	1.397(2)	N2B	C12B	1.369(2)
C3	C4	1.389(2)	N2B	C13B	1.462(2)
C3	C8	1.511(2)	C1B	C2B	1.520(2)
C4	C5	1.387(3)	C2B	C3B	1.407(2)
C5	C6	1.384(3)	C2B	C7B	1.387(2)
C6	C7	1.386(2)	C3B	C4B	1.391(3)
C9	C10	1.503(2)	C3B	C8B	1.509(3)
C10	C11	1.529(2)	C4B	C5B	1.383(3)
C11	C12	1.504(2)	C5B	C6B	1.382(3)
C13	C14	1.497(7)	C6B	C7B	1.390(3)
C13	C14'	1.548(8)	C9B	C10B	1.504(2)
C21	C22	1.391(3)	C10B	C11B	1.528(2)
C21	C26	1.397(3)	C11B	C12B	1.496(2)
C22	C23	1.392(3)	C13B	C14B	1.518(2)
C23	C24	1.381(3)	C14B	C15B	1.404(2)
C24	C25	1.374(4)	C14B	C19B	1.396(2)
C25	C26	1.392(3)	C15B	C16B	1.395(3)
C14	C15	1.3900	C15B	C20B	1.507(3)
C14	C19	1.3900	C16B	C17B	1.381(3)
C15	C16	1.3900	C17B	C18B	1.385(3)
C15	C20	1.508(12)	C18B	C19B	1.384(2)
C16	C17	1.3900	C21B	C22B	1.396(3)
C17	C18	1.3900	C21B	C26B	1.391(3)
C18	C19	1.3900	C22B	C23B	1.392(3)
C14'	C15'	1.3900	C23B	C24B	1.383(3)
C14'	C19'	1.3900	C24B	C25B	1.382(3)
C15'	C16'	1.3900	C25B	C26B	1.381(3)
C15'	C20'	1.505(17)	P1C	C1C	1.8707(18)
C16'	C17'	1.3900	P1C	C13C	1.8782(18)
C17'	C18'	1.3900	P1C	C21C	1.8290(18)
C18'	C19'	1.3900	O1C	C9C	1.224(2)
P1A	O3A	1.458(4)	O2C	C12C	1.222(2)
P1A	C1A	1.8931(18)	N1C	N2C	1.439(2)

P1A	C13A	1.8734(18)	N1C	C1C	1.458(2)
P1A	C21A	1.8298(18)	N1C	C9C	1.366(2)
O1A	C9A	1.219(2)	N2C	C12C	1.371(2)
O2A	C12A	1.222(2)	N2C	C13C	1.469(2)
N1A	N2A	1.416(2)	C1C	C2C	1.520(2)
N1A	C1A	1.460(2)	C2C	C3C	1.406(2)
N1A	C9A	1.364(2)	C2C	C7C	1.390(2)
N2A	C12A	1.360(2)	C3C	C4C	1.389(3)
N2A	C13A	1.460(2)	C3C	C8C	1.501(2)
C1A	C2A	1.512(2)	C4C	C5C	1.388(3)
C2A	C3A	1.403(3)	C5C	C6C	1.382(3)
C2A	C7A	1.388(3)	C6C	C7C	1.385(3)
C3A	C4A	1.392(3)	C9C	C10C	1.498(2)
C3A	C8A	1.507(3)	C10C	C11C	1.531(2)
C4A	C5A	1.376(4)	C11C	C12C	1.501(2)
C5A	C6A	1.380(3)	C13C	C14C	1.513(2)
C6A	C7A	1.389(3)	C14C	C15C	1.402(2)
C9A	C10A	1.505(2)	C14C	C19C	1.395(2)
C10A	C11A	1.529(3)	C15C	C16C	1.392(2)
C11A	C12A	1.502(3)	C15C	C20C	1.510(2)
C13A	C14A	1.519(2)	C16C	C17C	1.384(3)
C14A	C15A	1.404(2)	C17C	C18C	1.388(3)
C14A	C19A	1.394(2)	C18C	C19C	1.387(2)
C15A	C16A	1.390(3)	C21C	C22C	1.394(3)
C15A	C20A	1.512(3)	C21C	C26C	1.399(3)
C16A	C17A	1.390(3)	C22C	C23C	1.390(3)
C17A	C18A	1.382(3)	C23C	C24C	1.384(3)
C18A	C19A	1.382(3)	C24C	C25C	1.384(3)
C21A	C22A	1.396(3)	C25C	C26C	1.390(3)
C21A	C26A	1.392(3)			

Table A3.66. Bond Angles for *o*-Me DiazaPhos **16**.

Atom	Atom	Atom	Angle/°	Atom	Atom	Atom	Angle/°
O3	P1	C1	120.4(2)	C26A	C21A	P1A	115.59(15)
O3	P1	C13	111.7(3)	C26A	C21A	C22A	118.78(17)
O3	P1	C21	122.5(2)	C23A	C22A	C21A	120.2(2)
C1	P1	C13	90.95(8)	C24A	C23A	C22A	120.4(2)
C21	P1	C1	102.07(9)	C25A	C24A	C23A	119.93(19)
C21	P1	C13	103.79(8)	C24A	C25A	C26A	119.9(2)
N2	N1	C1	114.07(14)	C25A	C26A	C21A	120.7(2)

C9	N1	N2	120.62(14)	O3B	P1B	C1B	120.8(4)
C9	N1	C1	125.10(15)	O3B	P1B	C13B	121.6(4)
N1	N2	C13	115.21(13)	O3B	P1B	C21B	115.3(4)
C12	N2	N1	119.94(14)	C1B	P1B	C13B	90.83(8)
C12	N2	C13	122.56(15)	C21B	P1B	C1B	103.51(8)
N1	C1	P1	104.81(11)	C21B	P1B	C13B	100.36(8)
N1	C1	C2	113.18(14)	N2B	N1B	C1B	115.17(13)
C2	C1	P1	113.07(12)	C9B	N1B	N2B	119.96(14)
C3	C2	C1	120.40(15)	C9B	N1B	C1B	120.62(14)
C7	C2	C1	120.01(15)	N1B	N2B	C13B	114.50(13)
C7	C2	C3	119.56(16)	C12B	N2B	N1B	119.17(13)
C2	C3	C8	121.70(15)	C12B	N2B	C13B	121.90(14)
C4	C3	C2	118.43(16)	N1B	C1B	P1B	107.00(11)
C4	C3	C8	119.83(16)	N1B	C1B	C2B	114.44(14)
C5	C4	C3	121.76(17)	C2B	C1B	P1B	109.98(11)
C6	C5	C4	119.63(16)	C3B	C2B	C1B	118.72(15)
C5	C6	C7	119.64(16)	C7B	C2B	C1B	121.42(16)
C6	C7	C2	120.92(16)	C7B	C2B	C3B	119.85(16)
O1	C9	N1	121.29(16)	C2B	C3B	C8B	121.17(16)
O1	C9	C10	125.61(16)	C4B	C3B	C2B	118.31(17)
N1	C9	C10	113.04(15)	C4B	C3B	C8B	120.51(17)
C9	C10	C11	110.34(14)	C5B	C4B	C3B	121.68(18)
C12	C11	C10	110.13(15)	C6B	C5B	C4B	119.63(18)
O2	C12	N2	120.49(16)	C5B	C6B	C7B	119.81(17)
O2	C12	C11	125.72(16)	C2B	C7B	C6B	120.69(17)
N2	C12	C11	113.63(15)	O1B	C9B	N1B	120.76(16)
N2	C13	P1	106.24(12)	O1B	C9B	C10B	125.18(16)
N2	C13	C14	116.3(5)	N1B	C9B	C10B	114.00(15)
N2	C13	C14'	110.7(5)	C9B	C10B	C11B	110.63(14)
C14	C13	P1	112.9(6)	C12B	C11B	C10B	111.76(14)
C14'	C13	P1	112.0(7)	O2B	C12B	N2B	120.94(16)
C22	C21	P1	125.64(15)	O2B	C12B	C11B	124.97(16)
C22	C21	C26	118.95(18)	N2B	C12B	C11B	114.04(14)
C26	C21	P1	115.37(16)	N2B	C13B	P1B	106.22(11)
C21	C22	C23	120.2(2)	N2B	C13B	C14B	113.97(14)
C24	C23	C22	120.4(2)	C14B	C13B	P1B	109.88(11)
C25	C24	C23	119.8(2)	C15B	C14B	C13B	119.75(15)
C24	C25	C26	120.5(2)	C19B	C14B	C13B	120.08(15)
C25	C26	C21	120.1(2)	C19B	C14B	C15B	120.01(16)
C15	C14	C13	119.9(5)	C14B	C15B	C20B	122.27(16)
C15	C14	C19	120.0	C16B	C15B	C14B	118.01(17)

C19	C14	C13	120.1(5)	C16B	C15B	C20B	119.71(17)
C14	C15	C20	122.1(6)	C17B	C16B	C15B	121.88(18)
C16	C15	C14	120.0	C16B	C17B	C18B	119.63(17)
C16	C15	C20	117.7(6)	C19B	C18B	C17B	119.89(17)
C15	C16	C17	120.0	C18B	C19B	C14B	120.58(17)
C16	C17	C18	120.0	C22B	C21B	P1B	125.92(14)
C19	C18	C17	120.0	C26B	C21B	P1B	114.78(14)
C18	C19	C14	120.0	C26B	C21B	C22B	119.13(17)
C15'	C14'	C13	120.2(6)	C23B	C22B	C21B	120.12(17)
C15'	C14'	C19'	120.0	C24B	C23B	C22B	119.72(18)
C19'	C14'	C13	119.7(6)	C25B	C24B	C23B	120.50(19)
C14'	C15'	C16'	120.0	C26B	C25B	C24B	119.85(19)
C14'	C15'	C20'	121.4(8)	C25B	C26B	C21B	120.65(18)
C16'	C15'	C20'	118.6(8)	C1C	P1C	C13C	89.23(8)
C17'	C16'	C15'	120.0	C21C	P1C	C1C	104.26(8)
C16'	C17'	C18'	120.0	C21C	P1C	C13C	103.04(8)
C19'	C18'	C17'	120.0	N2C	N1C	C1C	115.06(13)
C18'	C19'	C14'	120.0	C9C	N1C	N2C	120.11(14)
O3A	P1A	C1A	117.7(3)	C9C	N1C	C1C	122.87(14)
O3A	P1A	C13A	118.1(3)	N1C	N2C	C13C	113.12(13)
O3A	P1A	C21A	119.6(3)	C12C	N2C	N1C	119.08(14)
C13A	P1A	C1A	90.80(8)	C12C	N2C	C13C	121.65(14)
C21A	P1A	C1A	102.84(8)	N1C	C1C	P1C	106.78(11)
C21A	P1A	C13A	103.02(9)	N1C	C1C	C2C	114.19(14)
N2A	N1A	C1A	114.98(13)	C2C	C1C	P1C	107.83(11)
C9A	N1A	N2A	121.05(14)	C3C	C2C	C1C	119.90(15)
C9A	N1A	C1A	121.96(14)	C7C	C2C	C1C	120.34(16)
N1A	N2A	C13A	114.27(13)	C7C	C2C	C3C	119.59(16)
C12A	N2A	N1A	120.95(15)	C2C	C3C	C8C	121.41(16)
C12A	N2A	C13A	124.78(15)	C4C	C3C	C2C	118.35(16)
N1A	C1A	P1A	106.73(11)	C4C	C3C	C8C	120.24(16)
N1A	C1A	C2A	113.35(14)	C5C	C4C	C3C	121.83(18)
C2A	C1A	P1A	113.29(12)	C6C	C5C	C4C	119.32(18)
C3A	C2A	C1A	119.14(16)	C5C	C6C	C7C	119.90(17)
C7A	C2A	C1A	121.01(16)	C6C	C7C	C2C	120.97(18)
C7A	C2A	C3A	119.80(17)	O1C	C9C	N1C	120.69(16)
C2A	C3A	C8A	121.66(17)	O1C	C9C	C10C	125.43(16)
C4A	C3A	C2A	118.5(2)	N1C	C9C	C10C	113.81(15)
C4A	C3A	C8A	119.76(19)	C9C	C10C	C11C	110.38(14)
C5A	C4A	C3A	121.2(2)	C12C	C11C	C10C	110.89(14)
C4A	C5A	C6A	120.2(2)	O2C	C12C	N2C	120.81(16)

C5A	C6A	C7A	119.6(2)	O2C	C12C	C11C	125.04(16)
C2A	C7A	C6A	120.5(2)	N2C	C12C	C11C	114.09(15)
O1A	C9A	N1A	120.60(16)	N2C	C13C	P1C	107.15(11)
O1A	C9A	C10A	125.88(16)	N2C	C13C	C14C	114.49(14)
N1A	C9A	C10A	113.40(15)	C14C	C13C	P1C	110.54(11)
C9A	C10A	C11A	110.28(15)	C15C	C14C	C13C	119.48(15)
C12A	C11A	C10A	110.22(15)	C19C	C14C	C13C	120.42(15)
O2A	C12A	N2A	121.19(18)	C19C	C14C	C15C	120.02(16)
O2A	C12A	C11A	125.64(17)	C14C	C15C	C20C	122.24(16)
N2A	C12A	C11A	113.12(15)	C16C	C15C	C14C	118.38(16)
N2A	C13A	P1A	105.05(11)	C16C	C15C	C20C	119.37(16)
N2A	C13A	C14A	112.49(14)	C17C	C16C	C15C	121.66(17)
C14A	C13A	P1A	112.79(12)	C16C	C17C	C18C	119.64(17)
C15A	C14A	C13A	120.65(15)	C19C	C18C	C17C	119.79(17)
C19A	C14A	C13A	119.84(16)	C18C	C19C	C14C	120.51(16)
C19A	C14A	C15A	119.51(16)	C22C	C21C	P1C	126.12(14)
C14A	C15A	C20A	121.72(16)	C22C	C21C	C26C	118.78(17)
C16A	C15A	C14A	118.35(17)	C26C	C21C	P1C	115.10(14)
C16A	C15A	C20A	119.93(17)	C23C	C22C	C21C	120.42(17)
C15A	C16A	C17A	121.76(18)	C24C	C23C	C22C	120.07(18)
C18A	C17A	C16A	119.48(17)	C25C	C24C	C23C	120.33(18)
C17A	C18A	C19A	119.72(17)	C24C	C25C	C26C	119.67(19)
C18A	C19A	C14A	121.18(17)	C25C	C26C	C21C	120.72(19)
C22A	C21A	P1A	125.63(15)				

Table A3.67. Torsion Angles for *o*-Me DiazaPhos **16**.

A	B	C	D	Angle/°	A	B	C	D	Angle/°
P1	C1	C2	C3	96.41(17)	C16A	C17A	C18A	C19A	0.0(3)
P1	C1	C2	C7	-85.64(17)	C17A	C18A	C19A	C14A	0.8(3)
P1	C13	C14	C15	85.5(6)	C19A	C14A	C15A	C16A	-0.4(3)
P1	C13	C14	C19	-92.5(6)	C19A	C14A	C15A	C20A	-179.55(18)
P1	C13	C14'	C15'	86.6(8)	C20A	C15A	C16A	C17A	-179.59(19)
P1	C13	C14'	C19'	-90.7(7)	C21A	P1A	C1A	N1A	-90.43(12)
P1	C21	C22	C23	178.04(15)	C21A	P1A	C1A	C2A	35.02(14)
P1	C21	C26	C25	-178.17(16)	C21A	P1A	C13A	N2A	79.47(12)
O1	C9	C10	C11	-141.02(17)	C21A	P1A	C13A	C14A	-157.67(12)
O3	P1	C1	N1	-141.8(3)	C21A	C22A	C23A	C24A	-0.3(3)
O3	P1	C1	C2	-18.1(3)	C22A	C21A	C26A	C25A	0.2(3)
O3	P1	C13	N2	139.3(3)	C22A	C23A	C24A	C25A	0.9(3)
O3	P1	C13	C14	-92.1(5)	C23A	C24A	C25A	C26A	-0.9(3)

O3	P1	C13	C14'	-99.7(5)	C24A	C25A	C26A	C21A	0.4(3)
O3	P1	C21	C22	-156.3(3)	C26A	C21A	C22A	C23A	-0.2(3)
O3	P1	C21	C26	21.5(3)	P1B	C1B	C2B	C3B	82.79(17)
N1	N2	C12	O2	-169.09(15)	P1B	C1B	C2B	C7B	-95.43(17)
N1	N2	C12	C11	15.3(2)	P1B	C13B	C14B	C15B	80.80(17)
N1	N2	C13	P1	-1.32(17)	P1B	C13B	C14B	C19B	-94.51(16)
N1	N2	C13	C14	-127.9(6)	P1B	C21B	C22B	C23B	-173.98(14)
N1	N2	C13	C14'	-123.1(7)	P1B	C21B	C26B	C25B	173.85(15)
N1	C1	C2	C3	-144.61(16)	O1B	C9B	C10B	C11B	-145.85(17)
N1	C1	C2	C7	33.3(2)	O3B	P1B	C1B	N1B	-149.4(5)
N1	C9	C10	C11	36.2(2)	O3B	P1B	C1B	C2B	-24.5(5)
N2	N1	C1	P1	30.69(15)	O3B	P1B	C13B	N2B	150.4(5)
N2	N1	C1	C2	-92.95(17)	O3B	P1B	C13B	C14B	-85.9(5)
N2	N1	C9	O1	-170.80(15)	O3B	P1B	C21B	C22B	-155.4(5)
N2	N1	C9	C10	11.9(2)	O3B	P1B	C21B	C26B	29.4(5)
N2	C13	C14	C15	-151.3(4)	N1B	N2B	C12B	O2B	-167.63(14)
N2	C13	C14	C19	30.7(8)	N1B	N2B	C12B	C11B	14.9(2)
N2	C13	C14'	C15'	-155.1(6)	N1B	N2B	C13B	P1B	-19.02(16)
N2	C13	C14'	C19'	27.7(9)	N1B	N2B	C13B	C14B	-140.14(14)
C1	P1	C13	N2	15.88(12)	N1B	C1B	C2B	C3B	-156.75(16)
C1	P1	C13	C14	144.5(4)	N1B	C1B	C2B	C7B	25.0(2)
C1	P1	C13	C14'	136.9(5)	N1B	C9B	C10B	C11B	31.4(2)
C1	P1	C21	C22	-17.75(18)	N2B	N1B	C1B	P1B	14.50(16)
C1	P1	C21	C26	160.05(14)	N2B	N1B	C1B	C2B	-107.60(16)
C1	N1	N2	C12	143.19(15)	N2B	N1B	C9B	O1B	-166.91(15)
C1	N1	N2	C13	-20.08(19)	N2B	N1B	C9B	C10B	15.8(2)
C1	N1	C9	O1	3.7(3)	N2B	C13B	C14B	C15B	-160.14(15)
C1	N1	C9	C10	-173.64(15)	N2B	C13B	C14B	C19B	24.6(2)
C1	C2	C3	C4	175.39(16)	C1B	P1B	C13B	N2B	22.69(11)
C1	C2	C3	C8	-2.4(2)	C1B	P1B	C13B	C14B	146.41(12)
C1	C2	C7	C6	-176.48(16)	C1B	P1B	C21B	C22B	-21.26(18)
C2	C3	C4	C5	1.8(3)	C1B	P1B	C21B	C26B	163.57(14)
C3	C2	C7	C6	1.5(3)	C1B	N1B	N2B	C12B	160.07(14)
C3	C4	C5	C6	0.1(3)	C1B	N1B	N2B	C13B	3.23(19)
C4	C5	C6	C7	-1.2(3)	C1B	N1B	C9B	O1B	-11.2(2)
C5	C6	C7	C2	0.4(3)	C1B	N1B	C9B	C10B	171.48(14)
C7	C2	C3	C4	-2.6(2)	C1B	C2B	C3B	C4B	-179.98(17)
C7	C2	C3	C8	179.63(16)	C1B	C2B	C3B	C8B	0.3(3)
C8	C3	C4	C5	179.67(17)	C1B	C2B	C7B	C6B	178.72(17)
C9	N1	N2	C12	-41.8(2)	C2B	C3B	C4B	C5B	1.5(3)
C9	N1	N2	C13	154.98(15)	C3B	C2B	C7B	C6B	0.5(3)

C9	N1	C1	P1	-144.10(14)	C3B	C4B	C5B	C6B	0.1(3)
C9	N1	C1	C2	92.25(19)	C4B	C5B	C6B	C7B	-1.3(3)
C9	C10	C11	C12	-58.88(19)	C5B	C6B	C7B	C2B	1.0(3)
C10	C11	C12	O2	-142.81(17)	C7B	C2B	C3B	C4B	-1.7(3)
C10	C11	C12	N2	32.5(2)	C7B	C2B	C3B	C8B	178.55(19)
C12	N2	C13	P1	-164.11(13)	C8B	C3B	C4B	C5B	-178.8(2)
C12	N2	C13	C14	69.3(6)	C9B	N1B	N2B	C12B	-42.9(2)
C12	N2	C13	C14'	74.1(7)	C9B	N1B	N2B	C13B	160.23(14)
C13	P1	C1	N1	-25.76(12)	C9B	N1B	C1B	P1B	-142.33(13)
C13	P1	C1	C2	97.95(13)	C9B	N1B	C1B	C2B	95.57(18)
C13	P1	C21	C22	76.25(18)	C9B	C10B	C11B	C12B	-56.23(19)
C13	P1	C21	C26	-105.94(15)	C10B	C11B	C12B	O2B	-144.86(16)
C13	N2	C12	O2	-7.1(3)	C10B	C11B	C12B	N2B	32.46(19)
C13	N2	C12	C11	177.29(15)	C12B	N2B	C13B	P1B	-175.15(12)
C13	C14	C15	C16	-178.0(10)	C12B	N2B	C13B	C14B	63.7(2)
C13	C14	C15	C20	6.1(10)	C13B	P1B	C1B	N1B	-21.11(12)
C13	C14	C19	C18	178.0(10)	C13B	P1B	C1B	C2B	103.75(12)
C13	C14'	C15'	C16'	-177.2(13)	C13B	P1B	C21B	C22B	72.13(17)
C13	C14'	C15'	C20'	2.5(12)	C13B	P1B	C21B	C26B	-103.04(14)
C13	C14'	C19'	C18'	177.2(13)	C13B	N2B	C12B	O2B	-12.6(2)
C21	P1	C1	N1	78.55(12)	C13B	N2B	C12B	C11B	169.99(14)
C21	P1	C1	C2	-157.73(12)	C13B	C14B	C15B	C16B	-174.64(16)
C21	P1	C13	N2	-86.80(13)	C13B	C14B	C15B	C20B	6.6(3)
C21	P1	C13	C14	41.8(4)	C13B	C14B	C19B	C18B	174.97(16)
C21	P1	C13	C14'	34.2(5)	C14B	C15B	C16B	C17B	-0.4(3)
C21	C22	C23	C24	-0.1(3)	C15B	C14B	C19B	C18B	-0.3(3)
C22	C21	C26	C25	-0.2(3)	C15B	C16B	C17B	C18B	-0.2(3)
C22	C23	C24	C25	-0.3(3)	C16B	C17B	C18B	C19B	0.5(3)
C23	C24	C25	C26	0.4(3)	C17B	C18B	C19B	C14B	-0.3(3)
C24	C25	C26	C21	-0.1(3)	C19B	C14B	C15B	C16B	0.7(3)
C26	C21	C22	C23	0.3(3)	C19B	C14B	C15B	C20B	-178.05(16)
C14	C13	C14'	C15'	-12(10)	C20B	C15B	C16B	C17B	178.33(18)
C14	C13	C14'	C19'	171(11)	C21B	P1B	C1B	N1B	79.76(12)
C14	C15	C16	C17	0.0	C21B	P1B	C1B	C2B	-155.39(12)
C15	C14	C19	C18	0.0	C21B	P1B	C13B	N2B	-81.20(12)
C15	C16	C17	C18	0.0	C21B	P1B	C13B	C14B	42.51(13)
C16	C17	C18	C19	0.0	C21B	C22B	C23B	C24B	0.6(3)
C17	C18	C19	C14	0.0	C22B	C21B	C26B	C25B	-1.7(3)
C19	C14	C15	C16	0.0	C22B	C23B	C24B	C25B	-1.5(3)
C19	C14	C15	C20	-175.8(10)	C23B	C24B	C25B	C26B	0.9(3)
C20	C15	C16	C17	176.0(10)	C24B	C25B	C26B	C21B	0.7(3)

C14'	C13	C14	C15	170(11)	C26B	C21B	C22B	C23B	1.0(3)
C14'	C13	C14	C19	-8(10)	P1C	C1C	C2C	C3C	-84.11(17)
C14'	C15'	C16'	C17'	0.0	P1C	C1C	C2C	C7C	91.15(17)
C15'	C14'	C19'	C18'	0.0	P1C	C13C	C14C	C15C	-84.28(17)
C15'	C16'	C17'	C18'	0.0	P1C	C13C	C14C	C19C	92.32(17)
C16'	C17'	C18'	C19'	0.0	P1C	C21C	C22C	C23C	-178.71(14)
C17'	C18'	C19'	C14'	0.0	P1C	C21C	C26C	C25C	179.44(16)
C19'	C14'	C15'	C16'	0.0	O1C	C9C	C10C	C11C	142.19(17)
C19'	C14'	C15'	C20'	179.7(13)	N1C	N2C	C12C	O2C	166.67(14)
C20'	C15'	C16'	C17'	-179.7(13)	N1C	N2C	C12C	C11C	-16.2(2)
P1A	C1A	C2A	C3A	81.84(17)	N1C	N2C	C13C	P1C	19.86(16)
P1A	C1A	C2A	C7A	-95.65(18)	N1C	N2C	C13C	C14C	142.82(14)
P1A	C13A	C14A	C15A	102.66(17)	N1C	C1C	C2C	C3C	157.40(15)
P1A	C13A	C14A	C19A	-77.55(18)	N1C	C1C	C2C	C7C	-27.3(2)
P1A	C21A	C22A	C23A	-179.90(15)	N1C	C9C	C10C	C11C	-34.8(2)
P1A	C21A	C26A	C25A	179.91(17)	N2C	N1C	C1C	P1C	-19.79(16)
O1A	C9A	C10A	C11A	-143.54(17)	N2C	N1C	C1C	C2C	99.29(16)
O3A	P1A	C1A	N1A	135.7(4)	N2C	N1C	C9C	O1C	169.90(15)
O3A	P1A	C1A	C2A	-98.8(4)	N2C	N1C	C9C	C10C	-12.9(2)
O3A	P1A	C13A	N2A	-146.2(4)	N2C	C13C	C14C	C15C	154.60(15)
O3A	P1A	C13A	C14A	-23.4(4)	N2C	C13C	C14C	C19C	-28.8(2)
O3A	P1A	C21A	C22A	-154.9(4)	C1C	P1C	C13C	N2C	-25.90(11)
O3A	P1A	C21A	C26A	25.4(4)	C1C	P1C	C13C	C14C	-151.27(12)
N1A	N2A	C12A	O2A	-174.17(15)	C1C	P1C	C21C	C22C	19.00(18)
N1A	N2A	C12A	C11A	8.2(2)	C1C	P1C	C21C	C26C	-160.13(14)
N1A	N2A	C13A	P1A	30.50(16)	C1C	N1C	N2C	C12C	-152.97(14)
N1A	N2A	C13A	C14A	-92.56(17)	C1C	N1C	N2C	C13C	-0.07(19)
N1A	C1A	C2A	C3A	-156.33(15)	C1C	N1C	C9C	O1C	6.6(3)
N1A	C1A	C2A	C7A	26.2(2)	C1C	N1C	C9C	C10C	-176.23(15)
N1A	C9A	C10A	C11A	32.5(2)	C1C	C2C	C3C	C4C	175.81(16)
N2A	N1A	C1A	P1A	1.84(17)	C1C	C2C	C3C	C8C	-3.7(3)
N2A	N1A	C1A	C2A	-123.57(15)	C1C	C2C	C7C	C6C	-174.19(17)
N2A	N1A	C9A	O1A	-169.83(15)	C2C	C3C	C4C	C5C	-1.6(3)
N2A	N1A	C9A	C10A	13.9(2)	C3C	C2C	C7C	C6C	1.1(3)
N2A	C13A	C14A	C15A	-138.73(17)	C3C	C4C	C5C	C6C	1.0(3)
N2A	C13A	C14A	C19A	41.1(2)	C4C	C5C	C6C	C7C	0.6(3)
C1A	P1A	C13A	N2A	-23.91(12)	C5C	C6C	C7C	C2C	-1.7(3)
C1A	P1A	C13A	C14A	98.95(13)	C7C	C2C	C3C	C4C	0.5(3)
C1A	P1A	C21A	C22A	72.35(18)	C7C	C2C	C3C	C8C	-178.97(17)
C1A	P1A	C21A	C26A	-107.34(15)	C8C	C3C	C4C	C5C	177.92(18)
C1A	N1A	N2A	C12A	157.66(15)	C9C	N1C	N2C	C12C	42.5(2)

C1A	N1A	N2A	C13A	-22.11(19)	C9C	N1C	N2C	C13C	-164.62(14)
C1A	N1A	C9A	O1A	-6.7(2)	C9C	N1C	C1C	P1C	144.28(14)
C1A	N1A	C9A	C10A	177.00(15)	C9C	N1C	C1C	C2C	-96.64(19)
C1A	C2A	C3A	C4A	-173.78(17)	C9C	C10C	C11C	C12C	57.71(19)
C1A	C2A	C3A	C8A	8.5(3)	C10C	C11C	C12C	O2C	145.47(17)
C1A	C2A	C7A	C6A	175.74(17)	C10C	C11C	C12C	N2C	-31.5(2)
C2A	C3A	C4A	C5A	-2.5(3)	C12C	N2C	C13C	P1C	171.97(12)
C3A	C2A	C7A	C6A	-1.7(3)	C12C	N2C	C13C	C14C	-65.1(2)
C3A	C4A	C5A	C6A	-0.9(3)	C13C	P1C	C1C	N1C	25.67(12)
C4A	C5A	C6A	C7A	3.0(3)	C13C	P1C	C1C	C2C	-97.46(12)
C5A	C6A	C7A	C2A	-1.7(3)	C13C	P1C	C21C	C22C	-73.55(17)
C7A	C2A	C3A	C4A	3.7(3)	C13C	P1C	C21C	C26C	107.32(15)
C7A	C2A	C3A	C8A	-174.02(18)	C13C	N2C	C12C	O2C	16.2(2)
C8A	C3A	C4A	C5A	175.3(2)	C13C	N2C	C12C	C11C	-166.71(14)
C9A	N1A	N2A	C12A	-38.1(2)	C13C	C14C	C15C	C16C	177.55(15)
C9A	N1A	N2A	C13A	142.10(15)	C13C	C14C	C15C	C20C	-3.7(2)
C9A	N1A	C1A	P1A	-162.21(13)	C13C	C14C	C19C	C18C	-177.49(15)
C9A	N1A	C1A	C2A	72.4(2)	C14C	C15C	C16C	C17C	-0.5(3)
C9A	C10A	C11A	C12A	-58.91(19)	C15C	C14C	C19C	C18C	-0.9(3)
C10A	C11A	C12A	O2A	-139.51(18)	C15C	C16C	C17C	C18C	-0.1(3)
C10A	C11A	C12A	N2A	38.0(2)	C16C	C17C	C18C	C19C	0.1(3)
C12A	N2A	C13A	P1A	-149.26(14)	C17C	C18C	C19C	C14C	0.4(3)
C12A	N2A	C13A	C14A	87.7(2)	C19C	C14C	C15C	C16C	0.9(2)
C13A	P1A	C1A	N1A	13.12(12)	C19C	C14C	C15C	C20C	179.69(16)
C13A	P1A	C1A	C2A	138.57(13)	C20C	C15C	C16C	C17C	-179.26(17)
C13A	P1A	C21A	C22A	-21.52(19)	C21C	P1C	C1C	N1C	-77.59(12)
C13A	P1A	C21A	C26A	158.80(15)	C21C	P1C	C1C	C2C	159.28(11)
C13A	N2A	C12A	O2A	5.6(3)	C21C	P1C	C13C	N2C	78.56(12)
C13A	N2A	C12A	C11A	-172.08(15)	C21C	P1C	C13C	C14C	-46.81(13)
C13A	C14A	C15A	C16A	179.38(17)	C21C	C22C	C23C	C24C	-0.3(3)
C13A	C14A	C15A	C20A	0.2(3)	C22C	C21C	C26C	C25C	0.2(3)
C13A	C14A	C19A	C18A	179.59(16)	C22C	C23C	C24C	C25C	-0.4(3)
C14A	C15A	C16A	C17A	1.3(3)	C23C	C24C	C25C	C26C	1.1(3)
C15A	C14A	C19A	C18A	-0.6(3)	C24C	C25C	C26C	C21C	-1.0(3)
C15A	C16A	C17A	C18A	-1.1(3)	C26C	C21C	C22C	C23C	0.4(3)

Table A3.68. Hydrogen Atom Coordinates ($\text{\AA} \times 10^4$) and Isotropic Displacement Parameters ($\text{\AA}^2 \times 10^3$) for *o*-Me DiazaPhos **16**.

Atom	<i>x</i>	<i>y</i>	<i>z</i>	U(eq)
H1	3855	5392	2477	24

H4	3241	4546	856	29
H5	4552	4729	454	30
H6	5889	5161	946	26
H7	5882	5428	1828	24
H8A	3096	4547	2164	37
H8B	2440	4537	1575	37
H8C	2589	5074	1909	37
H10A	5450	6863	2956	29
H10B	5014	7092	2371	29
H11A	6083	6561	1982	28
H11B	6685	6927	2441	28
H13	6721	5127	2854	26
H13A	6758	5126	2879	26
H22	4058	5812	3316	39
H23	3374	5970	4073	48
H24	3508	5349	4760	56
H25	4313	4566	4691	56
H26	5008	4400	3939	43
H16	8339	4684	4520	49
H17	8031	5374	5076	47
H18	6950	6037	4728	46
H19	6177	6011	3825	37
H20A	7136	4319	3317	61
H20B	8146	4257	3718	61
H20C	8042	4655	3220	61
H16'	8162	4833	4671	41
H17'	7724	5566	5128	44
H18'	6664	6188	4667	44
H19'	6041	6078	3749	38
H20D	7080	4365	3462	70
H20E	8012	4302	3925	70
H20F	8060	4649	3403	70
H1A	-154	7290	4933	23
H4A	-1776	6911	3222	48
H5A	-1351	7580	2692	53
H6A	-268	8225	3074	48
H7A	488	8156	3976	34
H8AA	-704	6497	4438	57
H8AB	-1723	6486	4039	57
H8AC	-1548	6877	4544	57
H10C	876	8690	5783	30

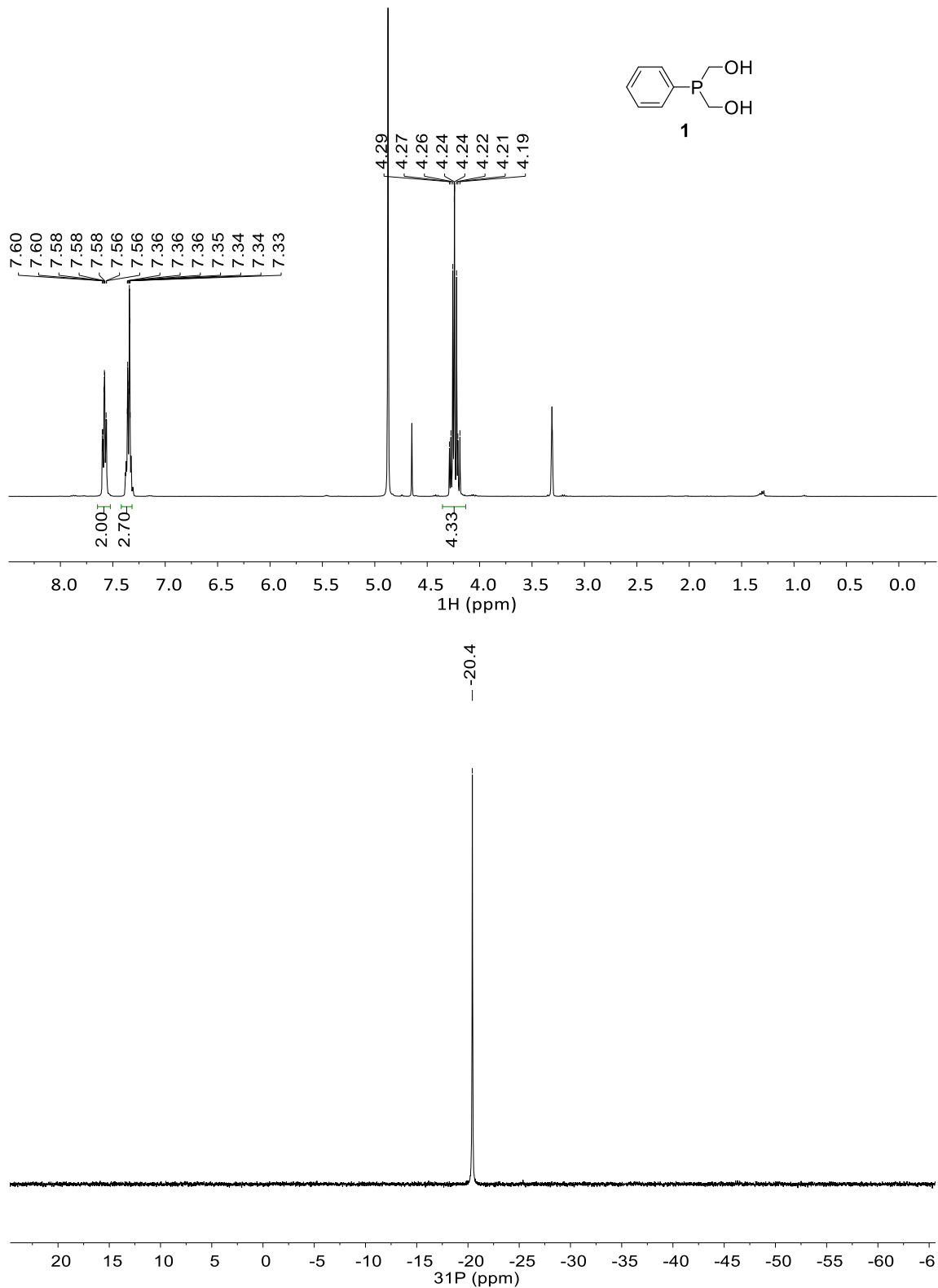
H10D	304	9078	5335	30
H11C	1449	8926	4774	32
H11D	1983	9143	5348	32
H13B	2782	7374	5210	25
H16A	3469	6636	6889	35
H17A	2157	6821	7291	33
H18A	832	7265	6802	29
H19A	832	7517	5917	27
H20G	3595	6588	5591	53
H20H	4276	6631	6171	53
H20I	4077	7138	5794	53
H22A	2474	7756	4312	38
H23A	3004	7815	3495	44
H24A	2684	7141	2863	48
H25A	1792	6413	3037	50
H26A	1258	6349	3855	39
H1B	5816	7719	5459	23
H4B	4884	7369	3657	35
H5B	6062	7750	3255	35
H6B	7446	8092	3791	35
H7B	7615	8078	4729	29
H8BA	5059	6949	4932	56
H8BB	4279	7075	4403	56
H8BC	4474	7489	4887	56
H10E	7456	8777	6555	25
H10F	7248	9249	6129	25
H11E	8440	8939	5672	24
H11F	8908	9017	6295	24
H13C	8578	7295	5573	23
H16B	9854	5988	6779	34
H17B	9728	6322	7617	36
H18B	8957	7125	7679	32
H19B	8296	7582	6898	25
H20J	8656	6350	5543	43
H20K	9524	5995	5842	43
H20L	9731	6570	5637	43
H22B	6215	7702	6425	29
H23B	5851	7517	7273	36
H24B	6010	6663	7608	43
H25B	6461	5985	7089	42
H26B	6795	6163	6239	33

H1C	-977	4594	7773	23
H4C	-1589	5031	5963	34
H5C	-299	4690	5624	38
H6C	971	4293	6210	38
H7C	927	4226	7124	31
H8CA	-2244	4829	7136	40
H8CB	-2378	5249	6657	40
H8CC	-1681	5376	7216	40
H10G	357	3009	8415	27
H10H	663	3468	8847	27
H11G	2033	3185	8514	26
H11H	1502	3302	7908	26
H13D	1780	4925	7864	22
H16C	3510	6144	8984	28
H17C	3457	5852	9850	31
H18C	2505	5128	9973	29
H19C	1614	4701	9226	24
H20M	3001	5542	7840	42
H20N	3027	6133	8059	42
H20O	2022	5861	7817	42
H22C	-536	4587	8781	27
H23C	-1037	4786	9587	33
H24C	-946	5646	9909	42
H25C	-332	6311	9435	46
H26C	144	6118	8620	36

Table A3.69. Atomic Occupancy for o-Me DiazaPhos **16**.

Atom	Occupancy	Atom	Occupancy	Atom	Occupancy
O3	0.196(3)	H13	0.55(2)	H13A	0.45(2)
C14	0.55(2)	C15	0.55(2)	C16	0.55(2)
H16	0.55(2)	C17	0.55(2)	H17	0.55(2)
C18	0.55(2)	H18	0.55(2)	C19	0.55(2)
H19	0.55(2)	C20	0.55(2)	H20A	0.55(2)
H20B	0.55(2)	H20C	0.55(2)	C14'	0.45(2)
C15'	0.45(2)	C16'	0.45(2)	H16'	0.45(2)
C17'	0.45(2)	H17'	0.45(2)	C18'	0.45(2)
H18'	0.45(2)	C19'	0.45(2)	H19'	0.45(2)
C20'	0.45(2)	H20D	0.45(2)	H20E	0.45(2)
H20F	0.45(2)	O3A	0.143(3)	O3B	0.107(3)

A3.5 NMR Spectra of Appendix 1

Figure A3.51. NMR spectra of **1** (¹H (top) and ³¹P{¹H} (bottom)).

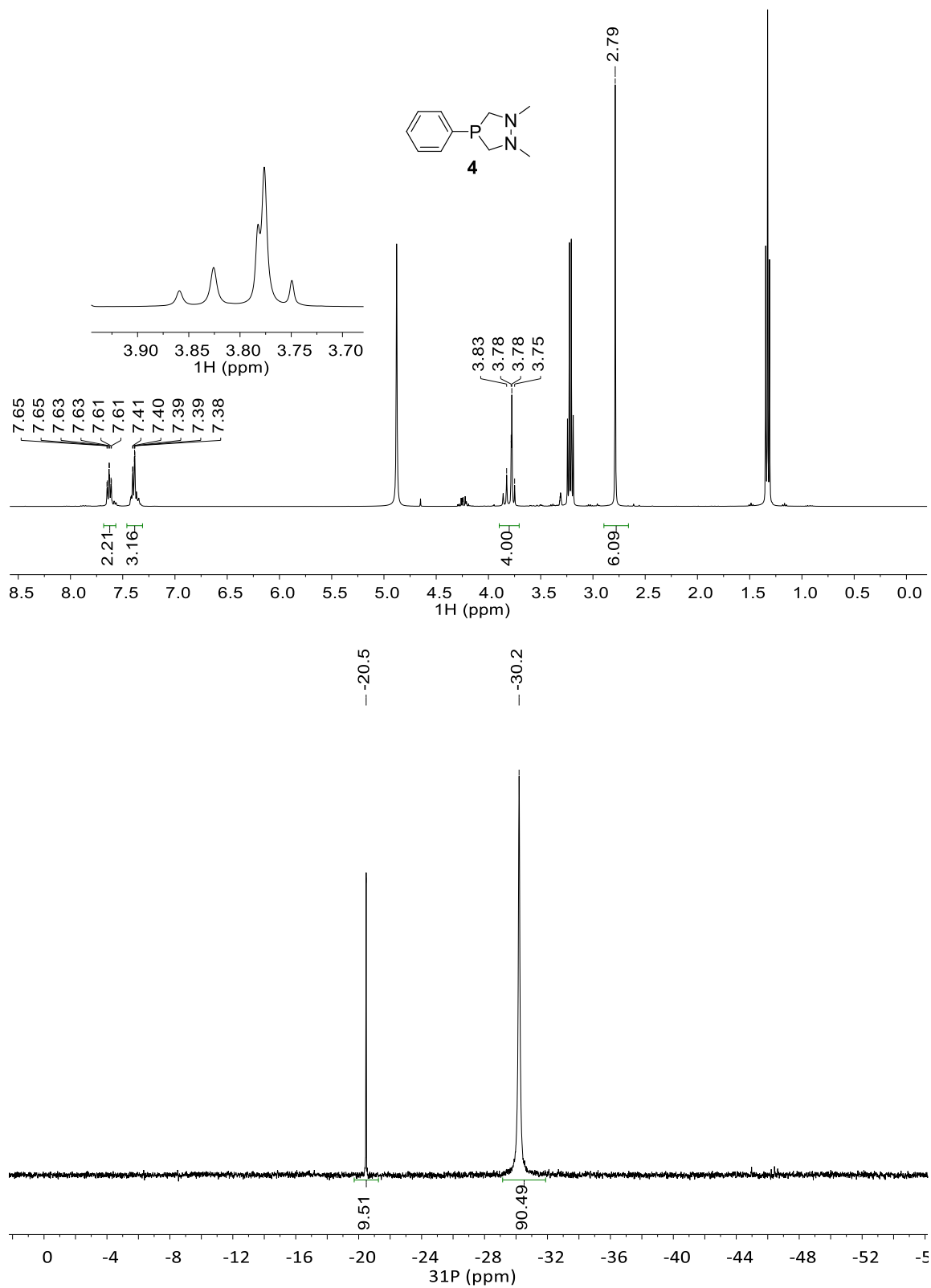


Figure A3.52. NMR spectra of crude **4** (^1H (top) and $^{31}\text{P}\{^1\text{H}\}$ (bottom)).

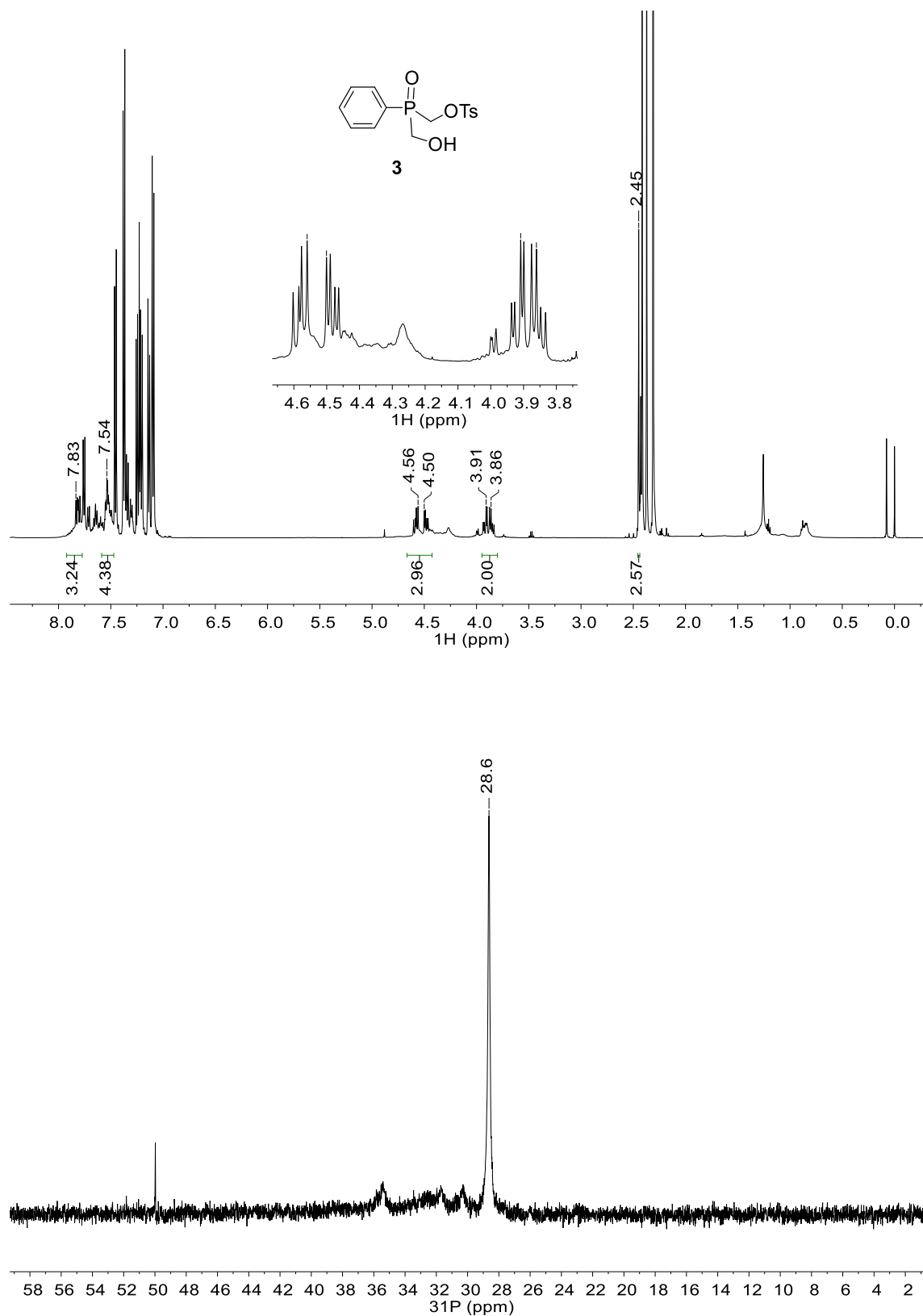


Figure A3.53. NMR spectra of crude **3** (^1H (top) and $^{31}\text{P}\{^1\text{H}\}$ (bottom)).

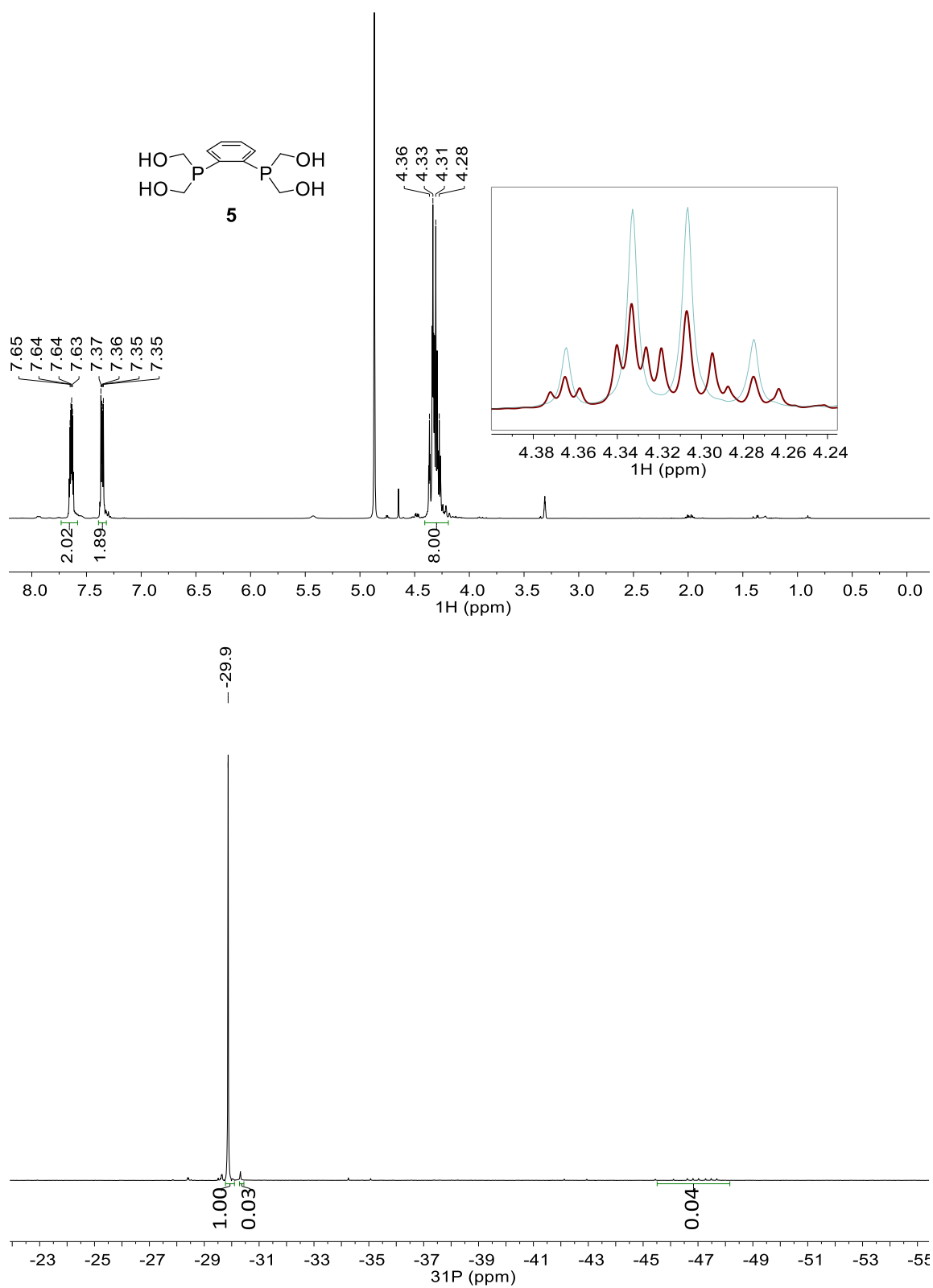


Figure A3.54. NMR spectra of **5** (^1H (top, red: ^1H , blue: $^1\text{H}\{^{31}\text{P}\}$) and $^{31}\text{P}\{^1\text{H}\}$ (bottom)).

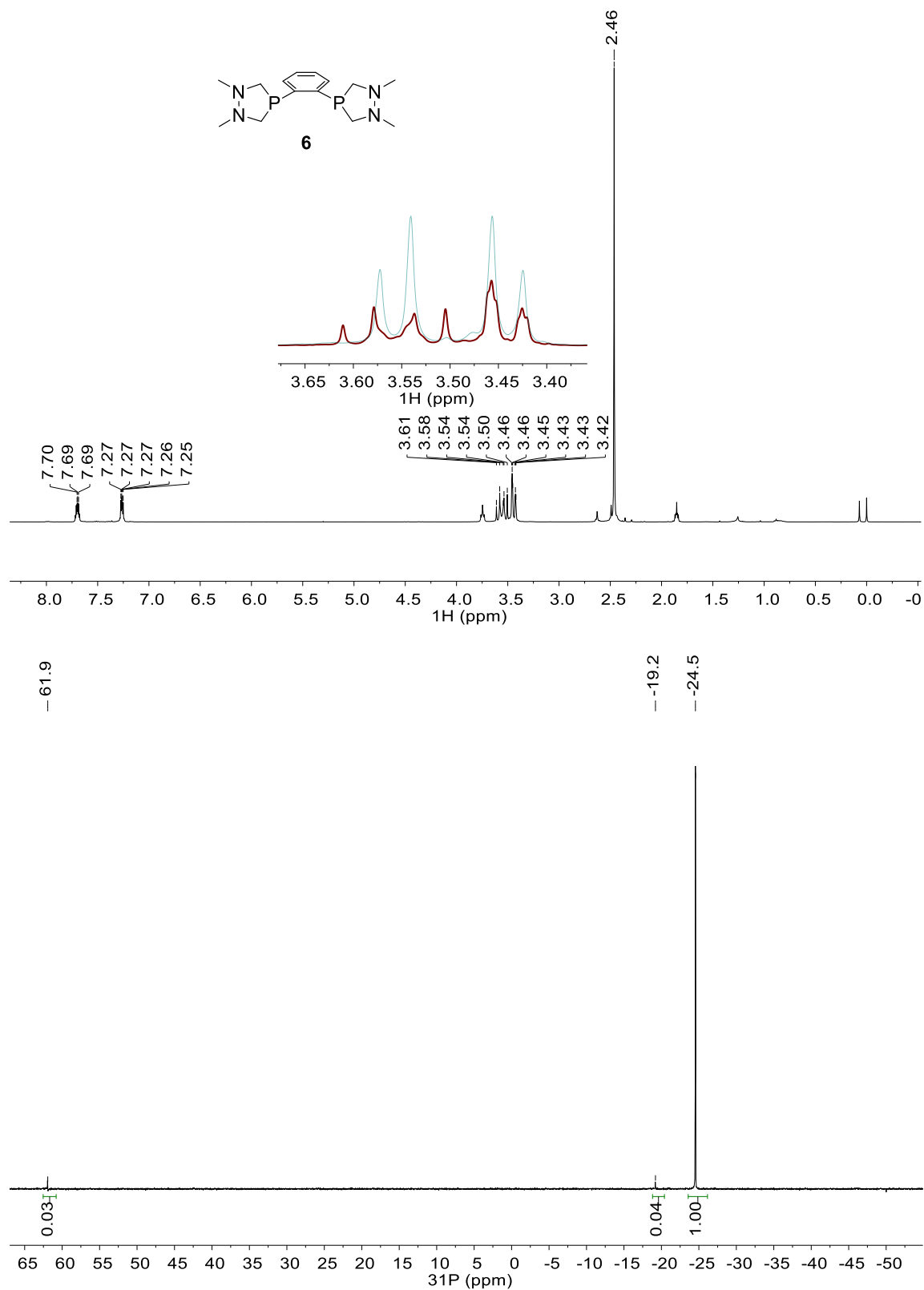


Figure A3.55. NMR spectra of **6** (^1H (top, red: ^1H , blue: $^1\text{H}\{^{31}\text{P}\}$) and $^{31}\text{P}\{^1\text{H}\}$ (bottom)).

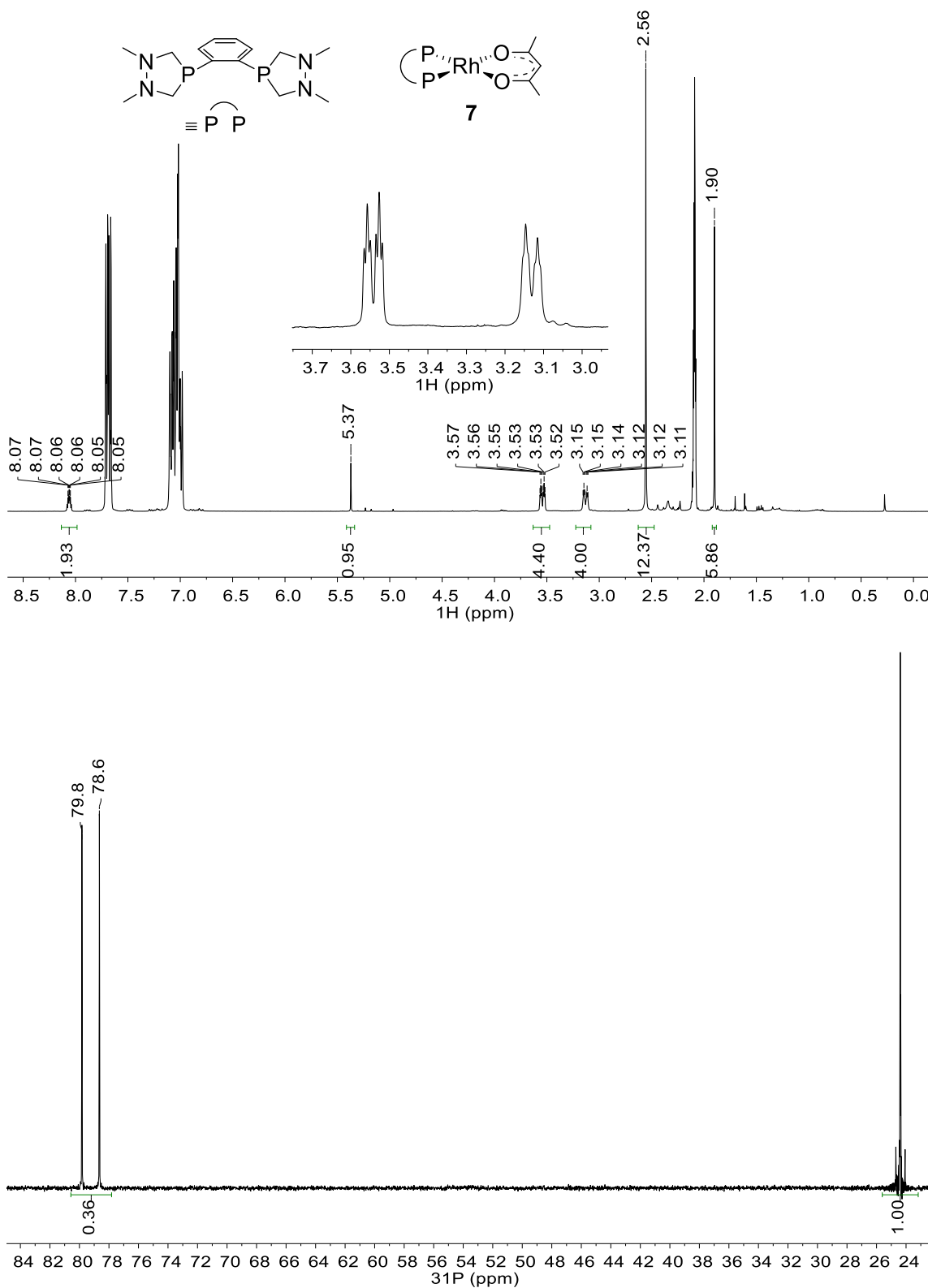


Figure A3.56. NMR spectra of **7** with Ph₃PO internal standard (¹H (top) and ³¹P{¹H} (bottom)).

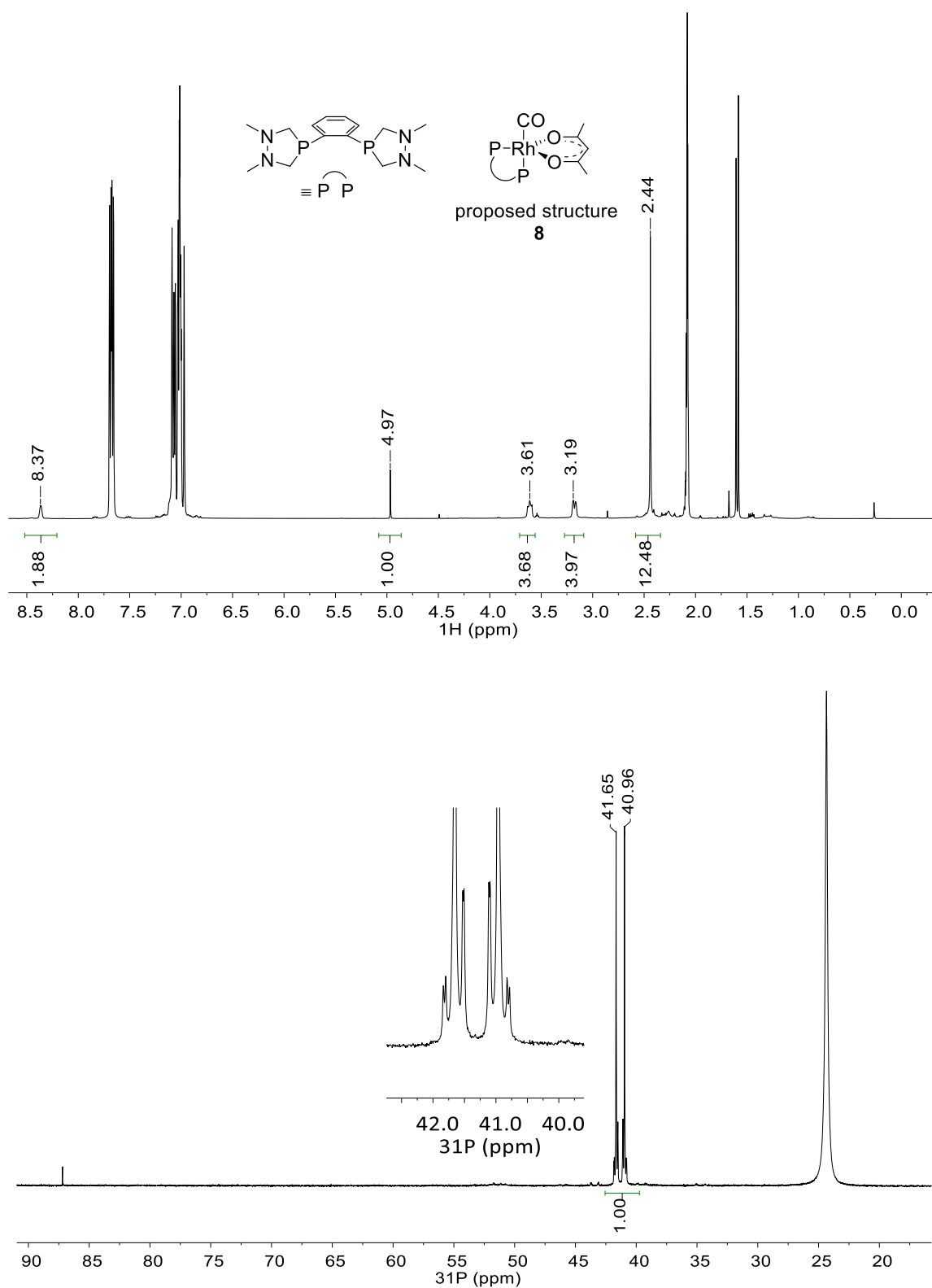


Figure A3.57. NMR spectra of **7** after preactivation with syngas and formation of **8** (with Ph_3PO internal standard) (^1H (top) and $^{31}\text{P}\{^1\text{H}\}$ (bottom)).

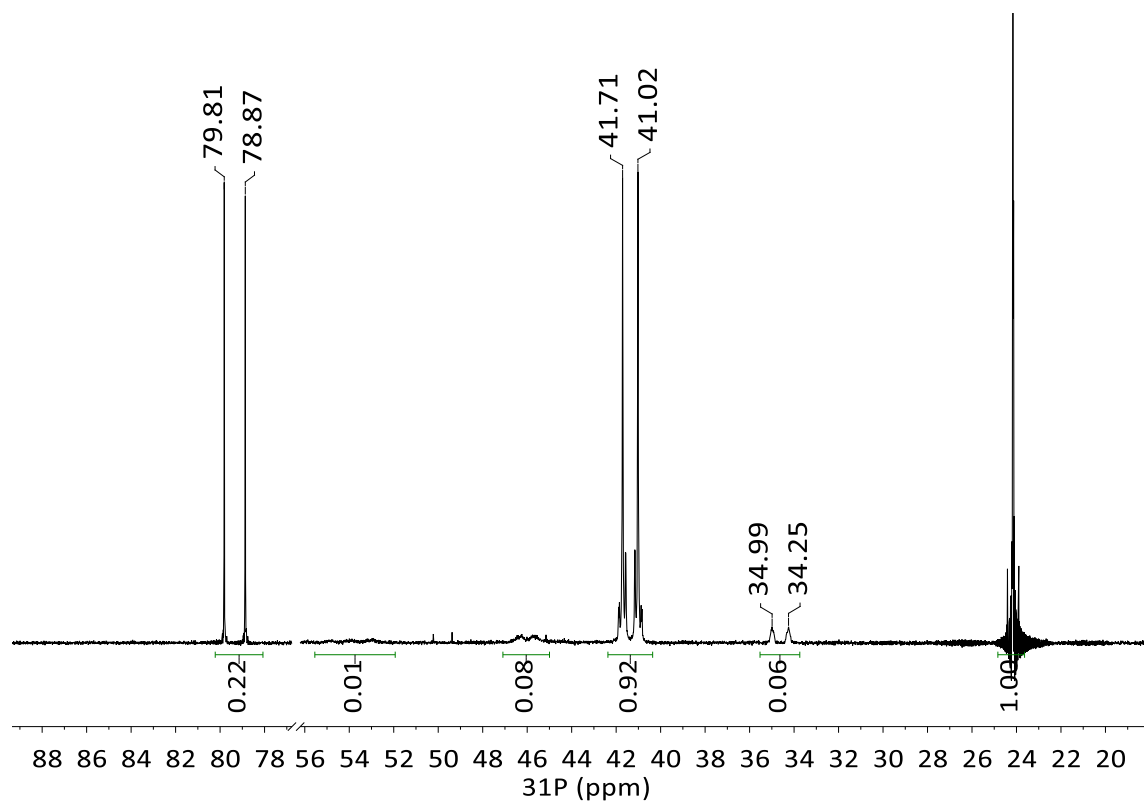


Figure A3.58. $^{31}\text{P}\{^1\text{H}\}$ NMR spectra of a mixture of **7** and **8** with Ph_3PO internal standard.

A3.6 NMR Spectra of Appendix 2

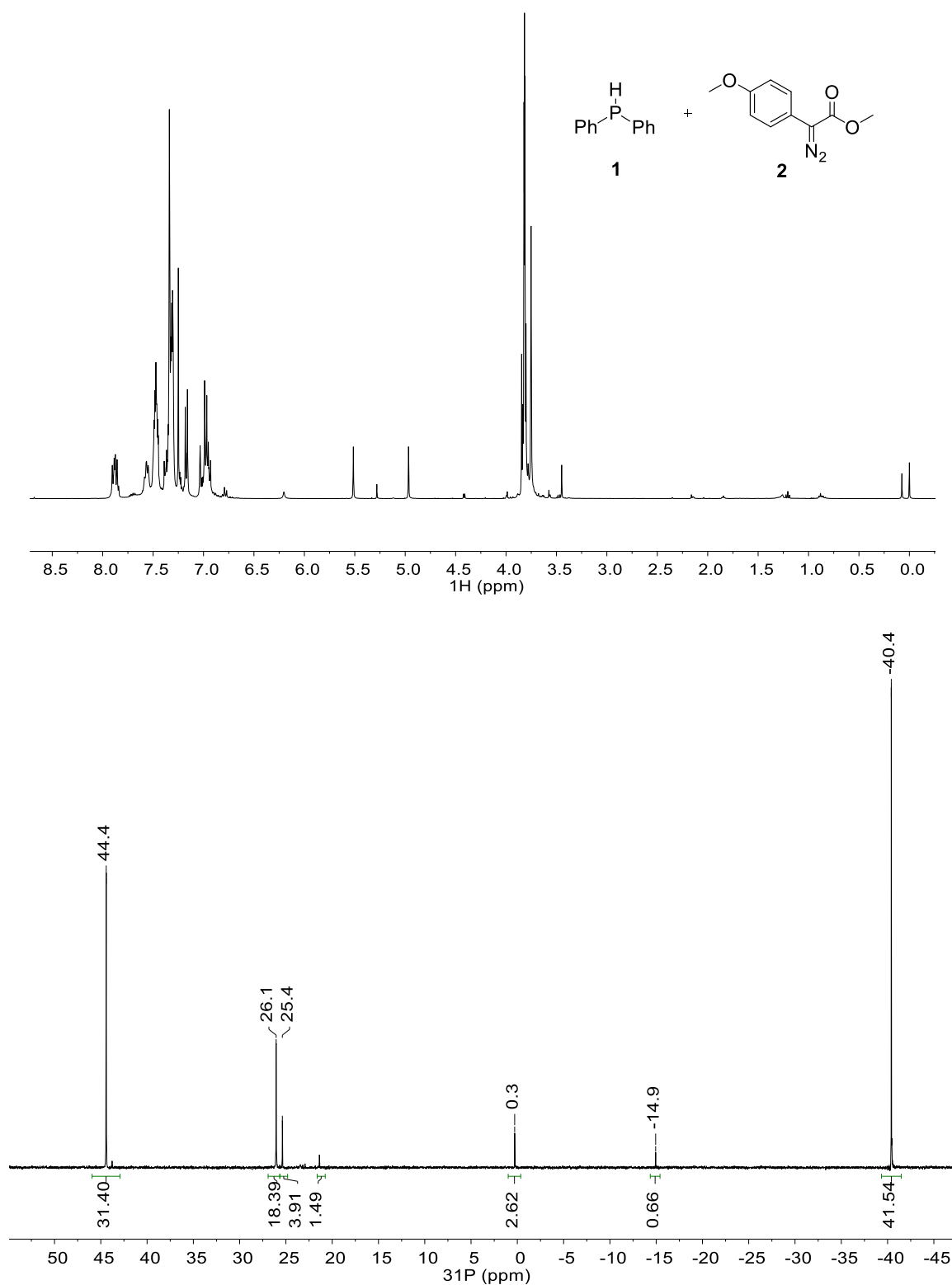


Figure A3.59. NMR spectra of the reaction mixture of **1** and **2** (^1H (top) and $^{31}\text{P}\{^1\text{H}\}$ (bottom)).

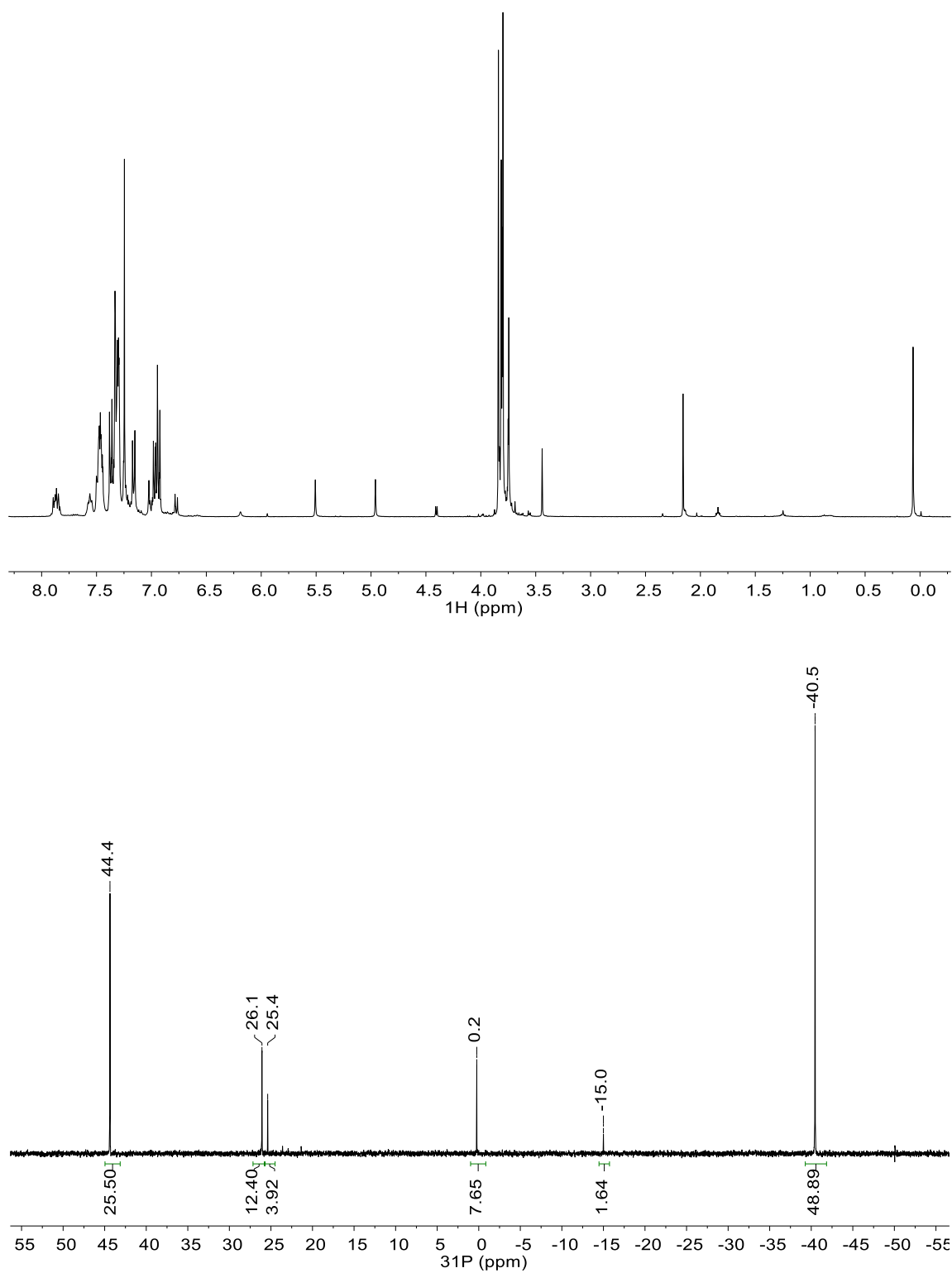


Figure A3.60. Reaction mixture NMR spectra of **1** and **2** with catalyst (^1H (top) and $^{31}\text{P}\{^1\text{H}\}$ (bottom)).

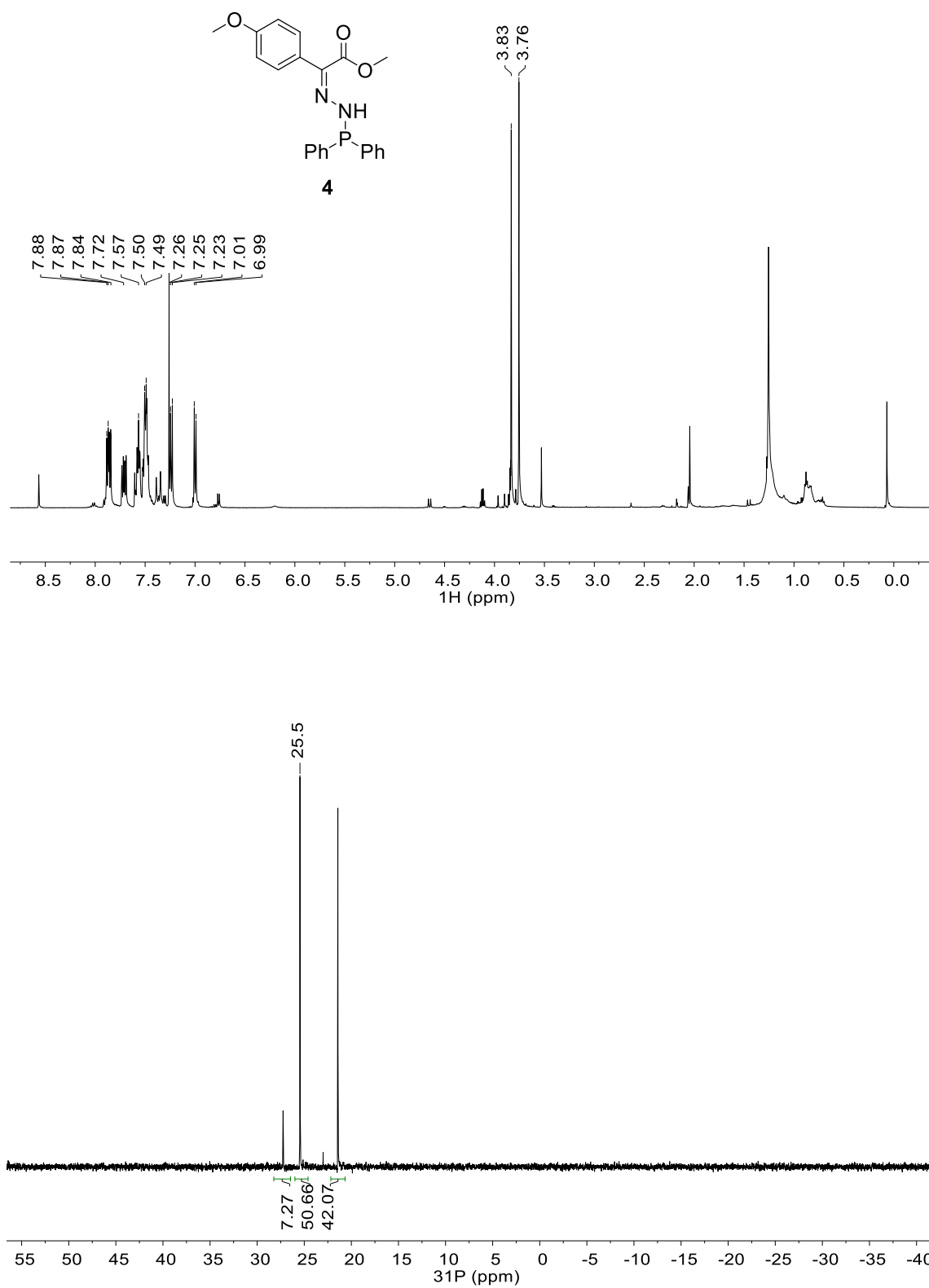


Figure A3.61. NMR spectra of **4** contaminated with Ph₃P(O)H (¹H (top) and ³¹P{¹H} (bottom)).

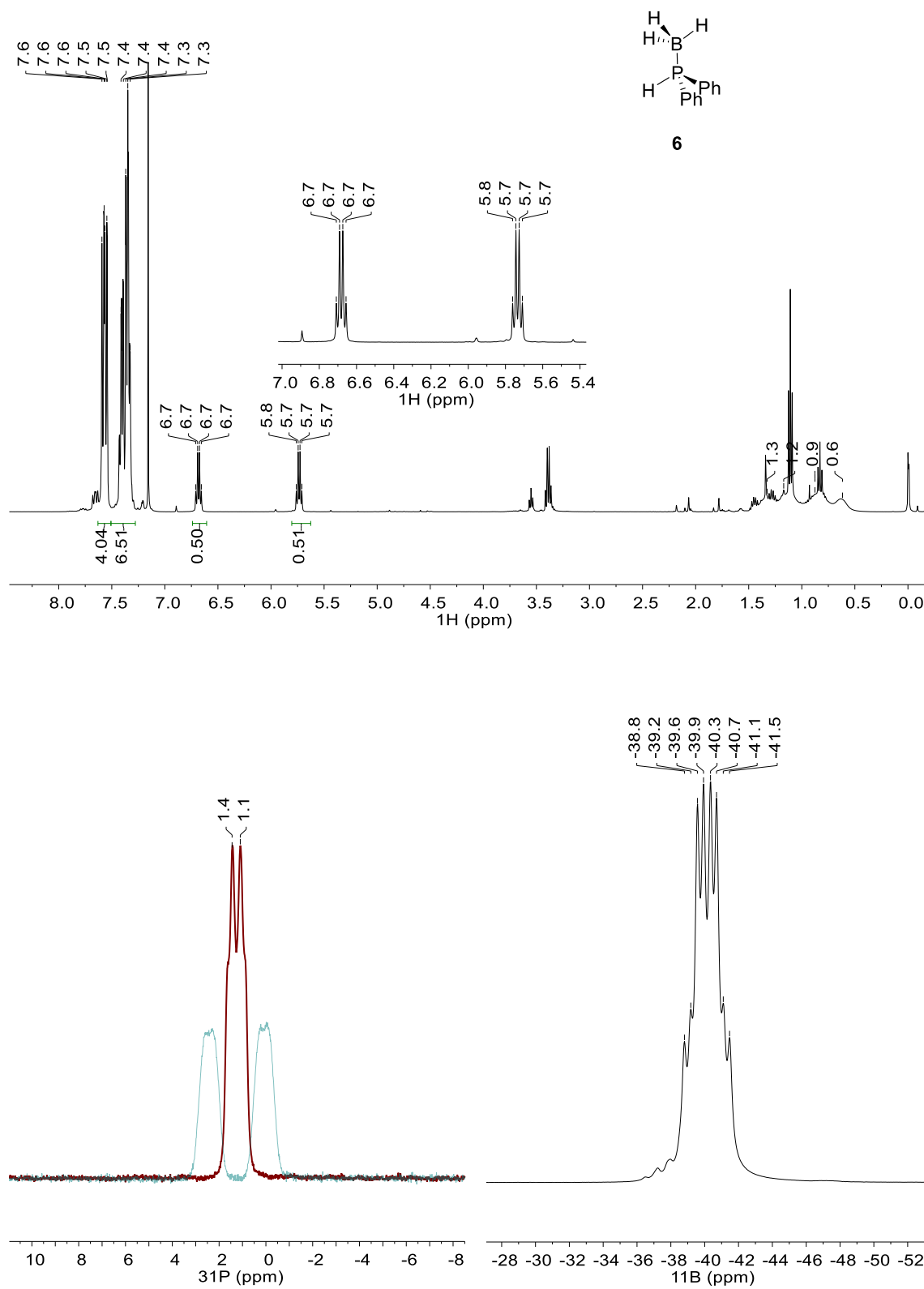


Figure A3.62. NMR spectra of **7** (^1H (top) and ^{31}P ($^{31}\text{P}\{^1\text{H}\}$ (bottom left; red: $^{31}\text{P}\{^1\text{H}\}$, blue: ^{31}P)), ^{11}B (bottom right)).

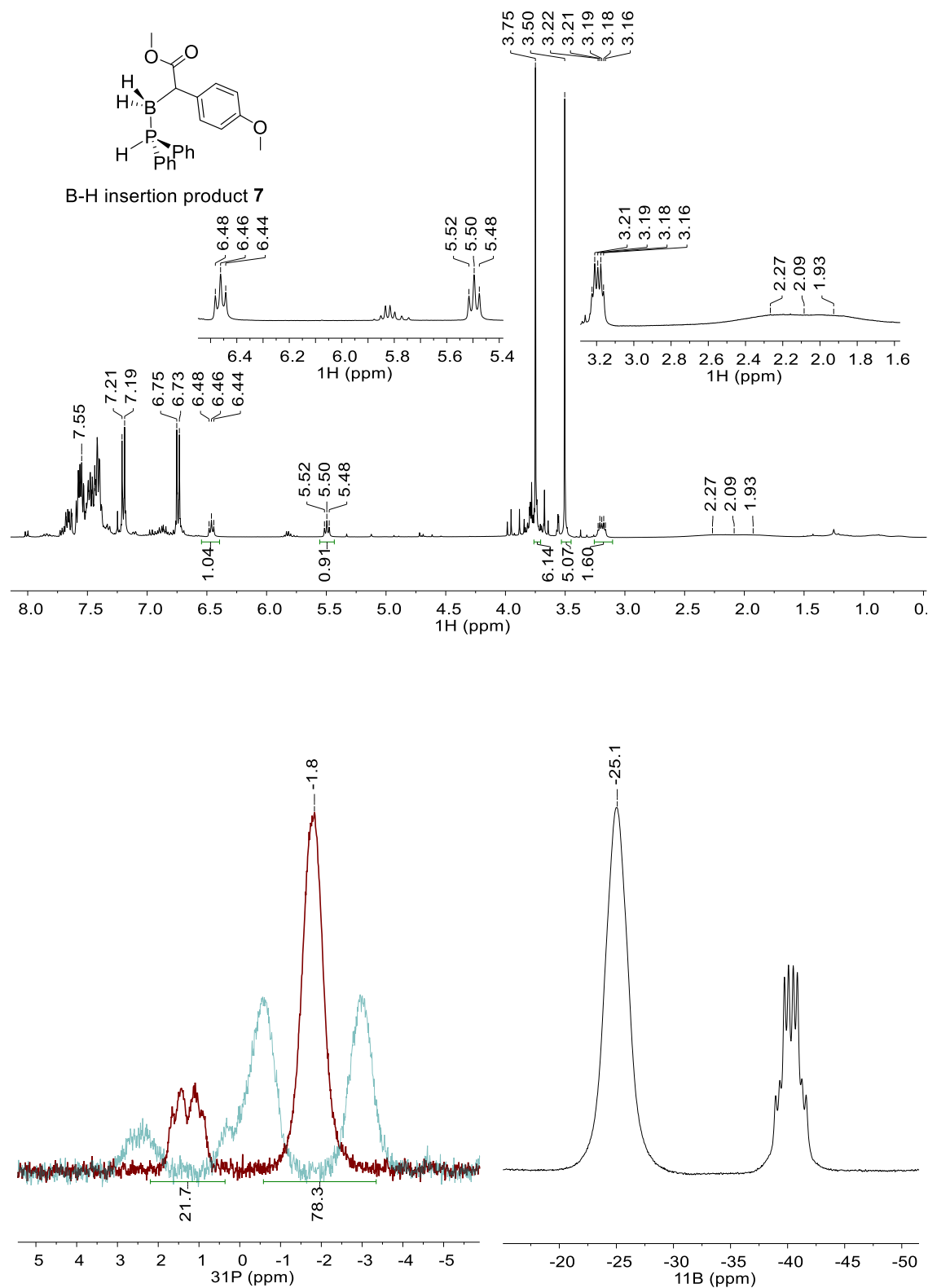


Figure A3.63. NMR spectra of the reaction of **6** and **2** to give B-H insertion product **7** in 78% NMR yield (^1H (top) and ^{31}P ($^{31}\text{P}\{^1\text{H}\}$ (bottom left; red: $^{31}\text{P}\{^1\text{H}\}$, blue: ^{31}P), ^{11}B (bottom right).

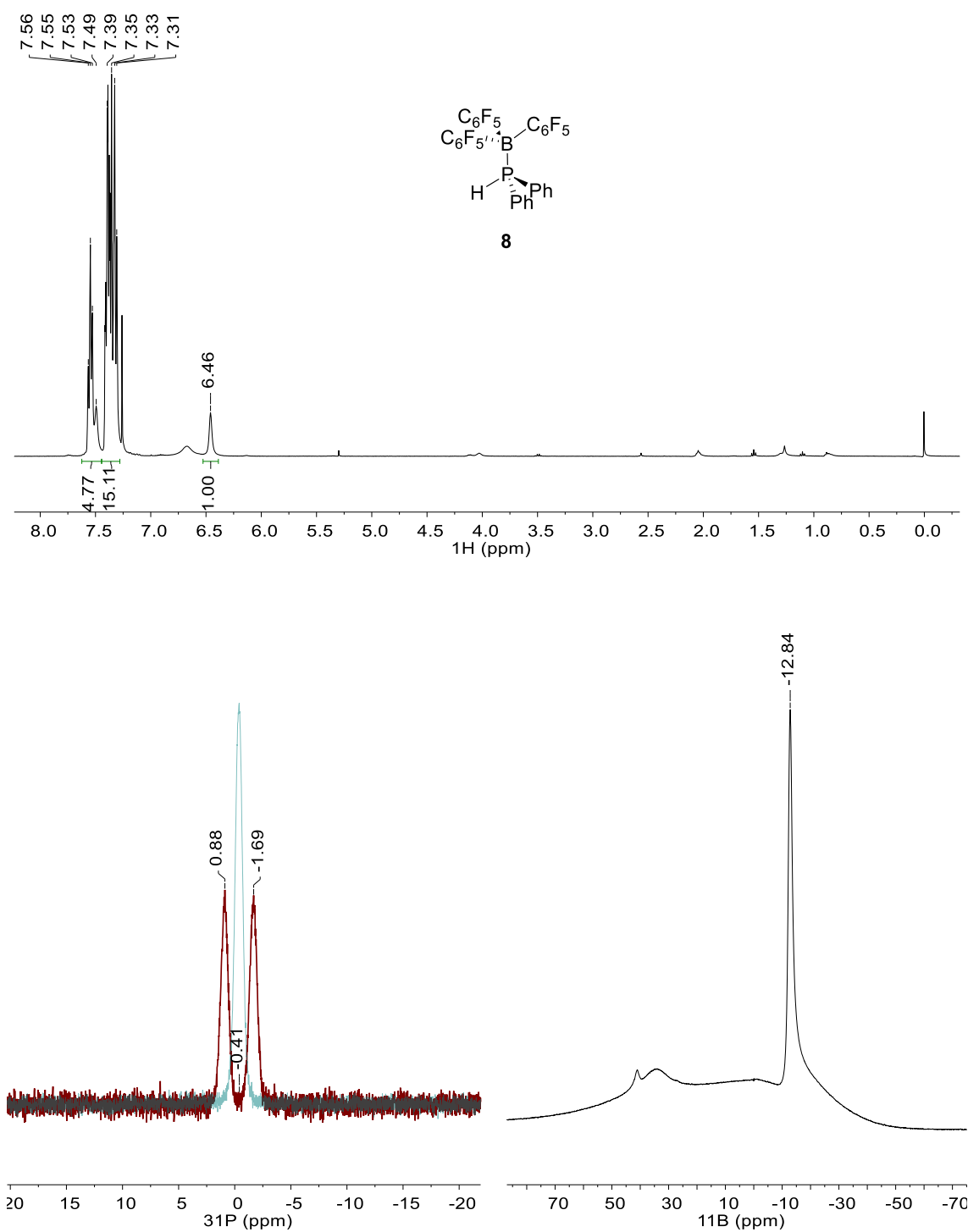


Figure A3.64. NMR spectra of $\text{Ph}_2\text{PH}\cdot\text{B}(\text{C}_6\text{F}_5)_3$ **8** (^1H (top) and ^{31}P ($^{31}\text{P}\{^1\text{H}\}$ (bottom left; red: $^{31}\text{P}\{^1\text{H}\}$, blue: ^{31}P), ^{11}B (bottom right)).

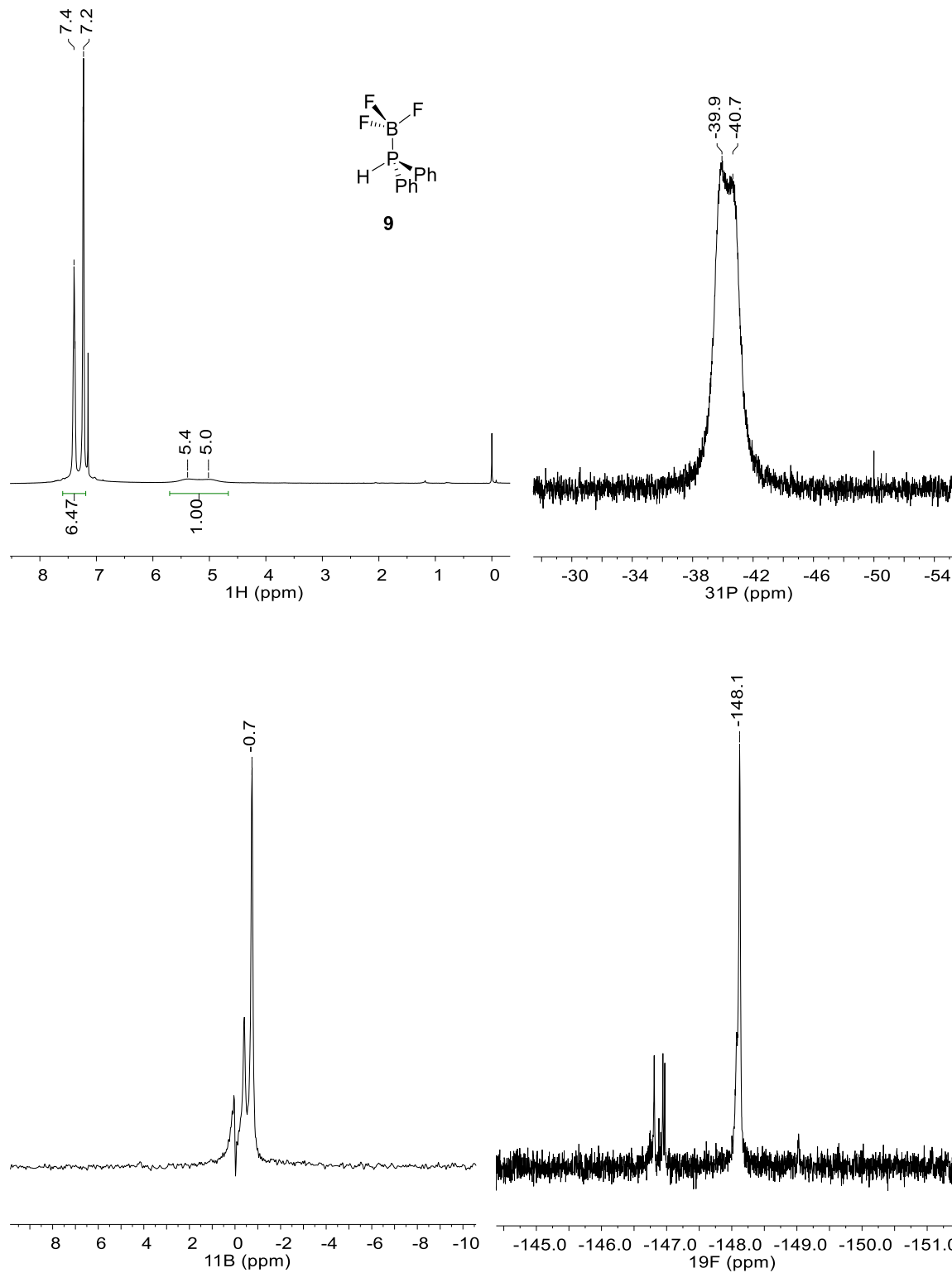


Figure A3.65. NMR spectra of $\text{Ph}_2\text{PH}\cdot\text{BF}_3$ **9** with leftover BF_3 starting material (^1H (top left), ^{31}P (top right), ^{11}B (bottom left) and ^{19}F (bottom right)).

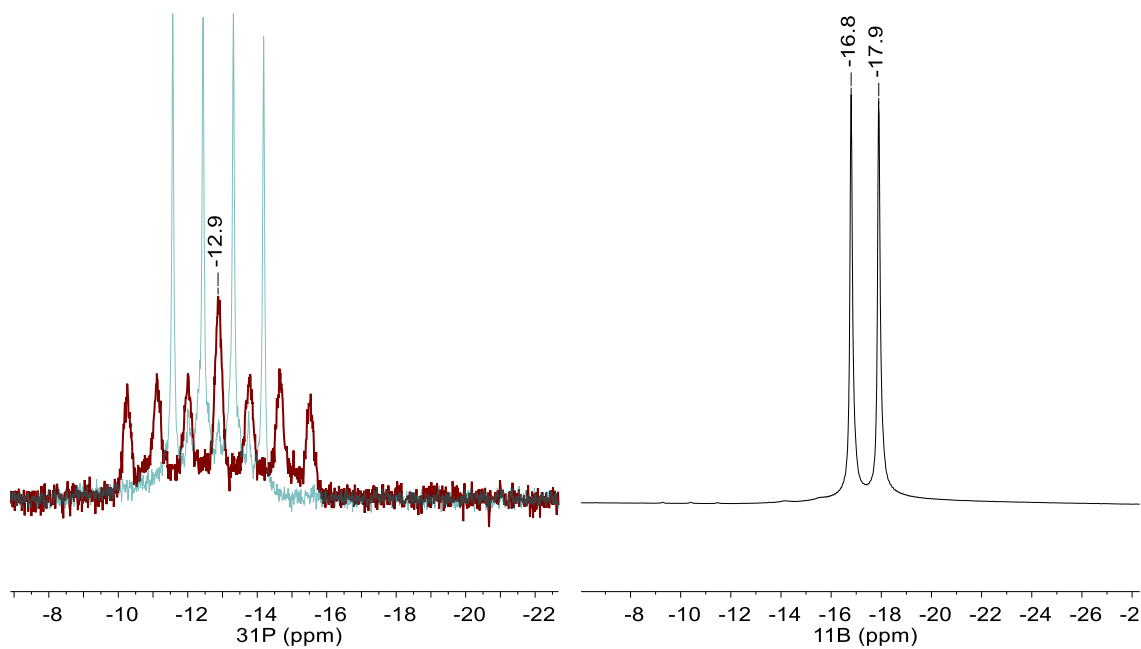
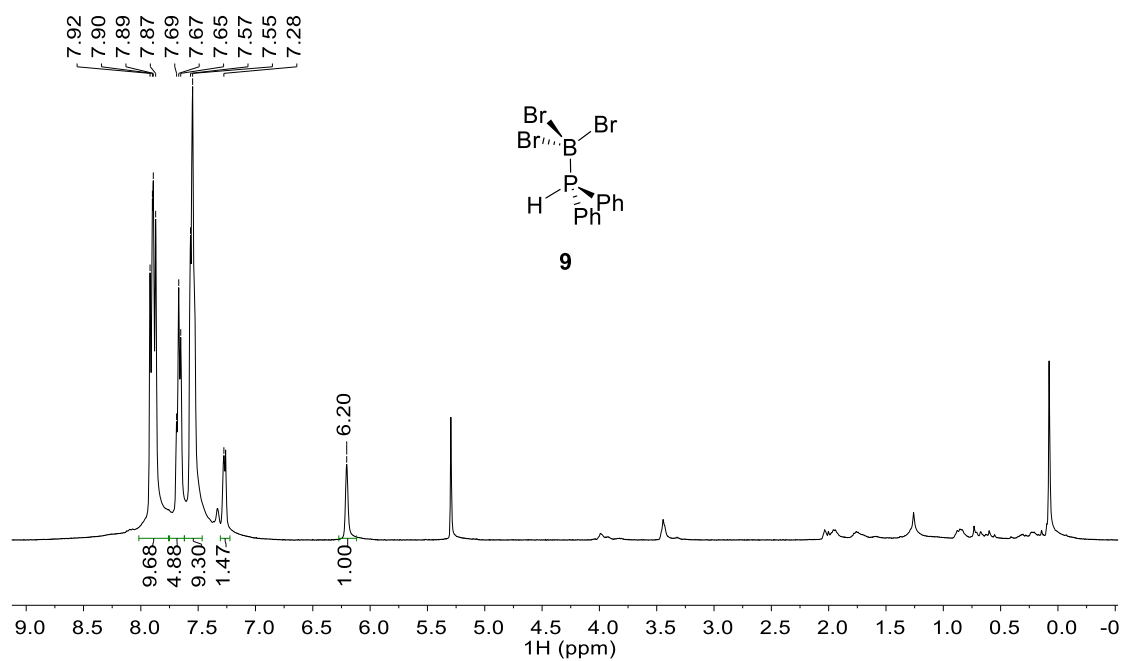


Figure A3.66. NMR spectra of **10** $\text{Ph}_2\text{PH}\cdot\text{BBr}_3$ (^1H (top) and ^{31}P ($^{31}\text{P}\{^1\text{H}\}$) (bottom left; red: $^{31}\text{P}\{^1\text{H}\}$, blue: ^{31}P), ^{11}B (bottom right)).

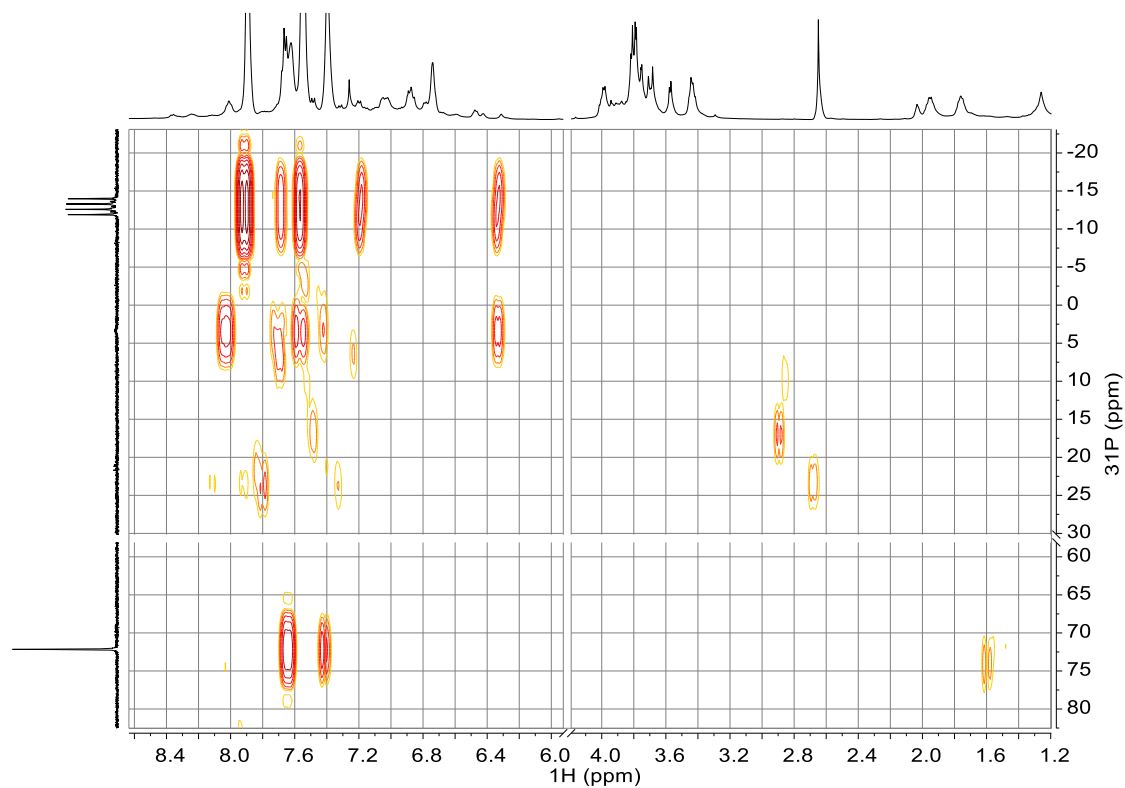


Figure A3.67. Spectrum for reaction of $\text{Ph}_2\text{PH}\cdot\text{BBr}_3$ **10**, diazo **2** and $\text{Rh}_2(\text{tpa})_4$ (^1H - ^{31}P HMBC).

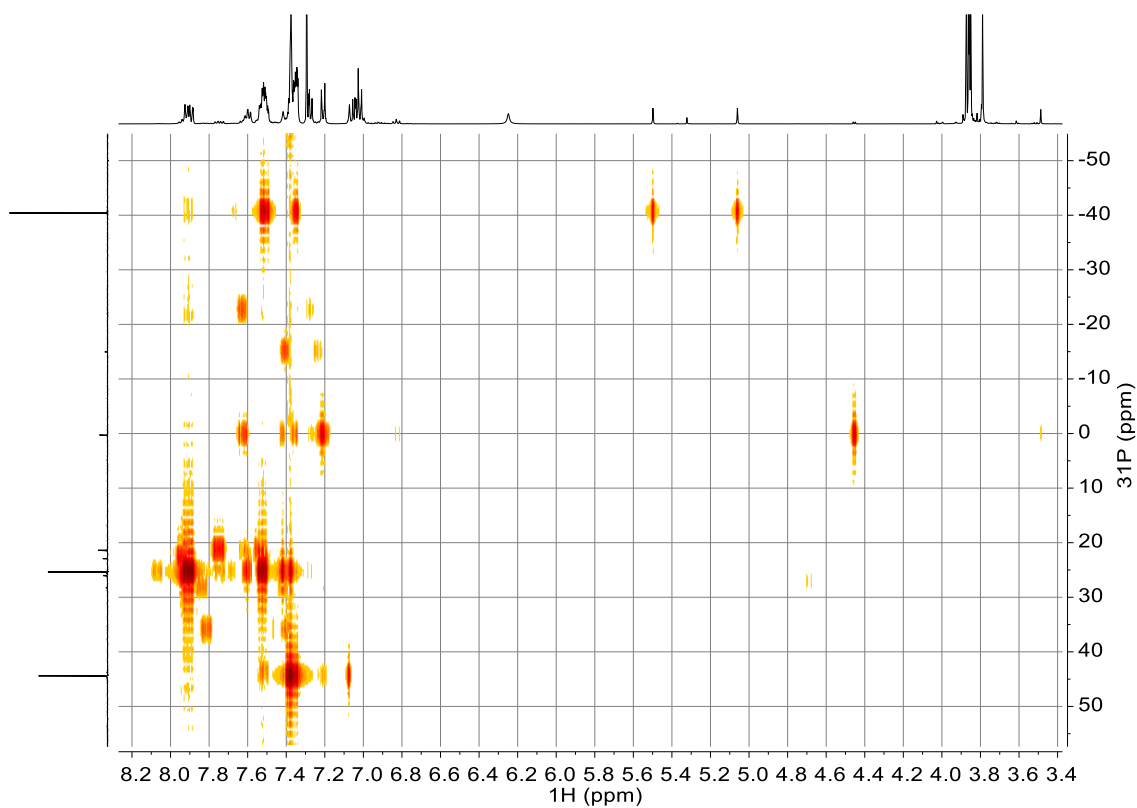


Figure A3.68. ^1H - ^{31}P HMBC of reaction mixture of **1** and **2** in CDCl_3